IAEA-207

DIFFERENTIAL AND INTEGRAL NUCLEAR DATA REQUIREMENTS FOR SHIELDING CALCULATIONS

PROCEEDINGS OF A SPECIALISTS' MEETING
ON DIFFERENTIAL AND INTEGRAL NUCLEAR DATA REQUIREMENTS
FOR SHIELDING CALCULATIONS
JOINTLY ORGANIZED BY THE
INTERNATIONAL ATOMIC ENERGY AGENCY
AND THE
OECD NUCLEAR ENERGY AGENCY
AND HELD IN
VIENNA, 12–15 OCTOBER 1976

A TECHNICAL DOCUMENT ISSUED BY THE
INTERNATIONAL ATOMIC ENERGY AGENCY, VIENNA, 1978

Printed by the IAEA in Austria
February 1978

PLEASE BE AWARE THAT
ALL OF THE MISSING PAGES IN THIS DOCUMENT
WERE ORIGINALLY BLANK

CONTENTS

SESSION C: APPLICATION OF SENSITIVITY AND UNCERTAINTY ANALYSIS TO DESIGN SITUATIONS: FISSION AND FUSION REACTOR SYSTEMS

SESSION D: STATUS OF THEORETICAL METHODS AND DATA

SESSION E: REVIEW OF PROGRESS WITH BENCHMARK EXPERIMENTS:

FISSION AND FUSION SOURCE SPECTRUM

SUMMARY REPORT

Dr. J. Butler, UKAEA, Winfrith, UK.

1 The Vienna meeting on Differential and Integral Nuclear Data Requirements for Shielding Calculations was the fourth in the series of meetings initiated by the EACRP in June 1973 with the aim, initially, of co-ordinating work on the assessment of data, and the intercomparison of benchmark experiments. It was envisaged that the experimental and theoretical programmes reviewed at these meetings would, ultimately, lead to a revised data request list covering the broad area of shield design for fast and thermal reactors which includes energy-deposition calculations for in-core gamma heating.

2 The first two meetings in this series were held at Ispra (1) in April 1974 and AEE Winfrith in March 1975 (2), sponsored by the NEA with the assistance of staff from the ESIS Centre. The IAEA was invited to co-sponsor the third meeting held in Paris in October 1975 (3) because the Agency had proposed an international meeting on differential data requirements for shielding as long ago as April 1972, but this was subsequently postponed until the necessary groundwork could be carried out which would enable the accuracy requirements to be properly identified, thereby avoiding the subjective judgements underlying so many of the items in the current WRENDA list.

3 Each of these meetings has proved to be a milestone in the development of both experimental and theoretical capabilities in the participating European and Japanese laboratories. At the Ispra meeting, procedures were agreed for the conduct and reporting of benchmark experiments; the Winfrith meeting afforded an opportunity to co-ordinate benchmark programmes, to clarify issues concerned with inter-calibration of detectors and to reach agreement on a standard calculational route for the analysis of the first series of single-material experiments which were to be conducted in iron. By the time of the Paris meeting, all the participating laboratories had implemented the ANISN/SWANLAKE sensitivity codes; although difficulties had been encountered with convergence, and with the normalisation of forward and adjoint calculations. Two theoretical benchmarks were accordingly proposed which were intended not only to validate the methods, but also to check the effects of using different in-house data-sets to calculate sensitivity profiles. The emphasis in the exploitation of sensitivity analysis at this stage was on the interpretation of benchmark experiments: but some preliminary assessments were made of data requirements, notably for fusion experiments and water reactor shields.

4 The first assessments of data requirements for sodium-cooled fast reactors to emerge from this collaborative programme were made at the Vienna meeting, based on the study of the theoretical benchmarks which reproduced the essential features of generic design problems. The most important issue raised by these assessments was the treatment of error-correlations in the cross-section data and the role of the variance-covariance matrices now being established in the ENDF/B files. In contrast to the considerable progress being made on this topic in the US, there was no indication of any significant work for shielding applications in Europe and elsewhere, although the importance of error-correlations had been recognised in the studies of theoretical benchmark problems. Moreover, there appeared to be no doubt that the practical solution to the problem of treating the effects of these correlations would be sought, initially, by adjusting multigroup data on the basis of integral benchmark experiments.

5 The recognition of the importance of errors in the basic cross-section data together with partial and energy-dependent correlations has achieved prominence in the shielding community outside the USA at this time, because of the marked increase in the use of transport codes with multigroup sets derived from the basic data libraries to predict design parameters which cannot usually be measured directly in experiments. Traditionally, the European role of transport calculations has been relegated to that of checking the physics approximations made in simplified design methods using the same - albeit inaccurate - data-sets. The simplified methods were, in turn, checked against a range of mock-up experiments and used for extrapolation to the practical design. Alternatively, when transport methods were used directly in the design calculations - principally Monte Carlo for complicated geometries - data-sets of long standing were used, and the bias factors observed in mock-up experiments carried over to the design predictions. The change in the role of transport methods which has taken place during the last five years reflects the development of sodium-cooled fast reactor shields which, owing to their size and complexity, cannot be adequately mocked-up in bulk shield facilities; moreover, the range of extrapolation from feasible experiments to practical shields has greatly increased so that it is no longer practicable to rely exclusively on simplified design methods without the support of transport calculations. Whilst the transition in thermal reactor shield design has been less marked, the more stringent target accuracies specified for PWR shields, with the emphasis on cavity streaming, for example, are resulting in the more widespread use of transport methods for design calculations.

6 The collaborative programme has now reached a turning point: realistic estimates can be made of the data requirements for energy-deposition and shielding calculations on all reactor systems; but it remains to be seen how these requests will be met in practice. The answer to this question depends initially on two criteria which will be specified for individual reactor projects, namely the target accuracies for shield designs and the time scales for construction of the plant. In spite of the current uncertainties about the scope and timing of fast reactor programmes in all the participating countries, however, the objectives of the continuing programme, now sponsored jointly by the NEA and the IAEA have clearly emerged. Firstly, the established techniques for the assessment of data requirements must now be applied to the wide range of design problems which have already been identified, and the results correlated in a revised version of the WRENDA compilation. Secondly, the information which can be derived from the analysis of benchmark experiments must be clearly established in order to reach agreement on the strategy for meeting these requests, which may involve new differential measurements, new evaluations, and the adjustment of multigroup data-sets. The framework of collaboration on benchmark experiments, which is already well established within the European and Japanese communities, affords an excellent opportunity to define the capabilities of integral measurements in this regard; when their findings are taken in conjunction with the available information from the US, and any results which may be contributed by laboratories in the IAEA community, it should be possible to reach firm conclusions about the role of benchmark experiments. With these two broad aims in view the next joint IAEA/NEA meeting has been provisionally proposed for the Autumn of 1978.

ORGANISATION AND SCOPE OF THE MEETING

7 A total of 27 papers was tabled at the meeting which was attended by 44 participants, and 7 observers including shielding representatives from 11 NEA countries, the USSR, Israel and the IAEA. For the first time in this series, representatives of the evaluators were present from the USA, the UK, the NEA Neutron Data Compilation Center at Saclay and the IAEA Nuclear Data Section in Vienna.

8 Initially the participants addressed themselves to the question of target accuracies for design calculations and then they examined in detail the analyses of the two theoretical benchmarks prepared by M Barre (FBR) and Dr Hehn (PWR) as proposed at the previous meeting in Paris. These had been specified in such a way that they represented one-dimensional models of generic design problems and thereby furnished not only the tests of methods and data-sets for which they had originally been intended, but also preliminary estimates of accuracy requirements, highlighting the problem of error-correlations. The meeting split up into three sub-groups to consider in more detail the issues raised by the theoretical benchmarks and to draw preliminary conclusions from the available sensitivity and uncertainty analyses of practical design problems. Following the practice established at previous meetings, state-of-the-art reviews were presented by members of the Editorial Panel.

METHODOLOGY OF SENSITIVITY ANALYSIS

9 The standard method for sensitivity analysis adopted for this programme is the ANISN/SWANLAKE route. These codes have been well tested in the US and can be obtained from the RSIC Code Library at Oak Ridge. Most of the benchmark experiments required a two-dimensional analysis, however, and until the VIP (4) code becomes more generally available, with supporting documentation, it had been agreed at the Paris meeting that two alternative approaches should be followed. For the analysis of the iron benchmarks, fictitious absorption cross-sections derived from DOT calculations could be used to represent lateral leakage in the one-dimensional codes. At the same time, the development of a three-dimensional Monte Carlo sensitivity code employing correlated tracking was initiated at Ispra based on the well-known TIMOC code. The progress made with this work will be reviewed by Dr Rief in a paper to be presented at the Knoxville Conference (5).

TARGET ACCURACIES

10 In contrast to the position at the beginning of this series of meetings when there were no clearly agreed target accuracies laid down for shield design, a compilation of approximately 30 design requirements has been broadly agreed by the participants covering a wide range of PFR, FBR and CTR problems. In order to avoid any misinterpretation, the estimates have all been reduced to one standard deviation leaving aside the choice of confidence limits for specific problems, which is clearly a matter for the design engineer. These target accuracies embrace all possible sources of calculational error including, for example, geometric modelling of the shield, uncertainties in composition, dimensional changes with temperature and irradiation, errors in the sources derived from reactor physics calculations, and approximations in the method, in addition to the errors attributable to the basic nuclear data. It was accordingly proposed that the last of these components, namely the errors due to nuclear data, should be arbitrarily limited to one-half of the designer's target accuracy. There will be an opportunity to refine these arguments at a later stage in the programme but, in the light of experience at the meeting, this proposal is not unrealistic for the design of thick shields.

THE NEA THEORETICAL SENSITIVITY BENCHMARKS

11 The calculational benchmark exercises comprised a one-dimensional steel/sodium radial shield for a fast reactor and a two-dimensional model of a PWR radial shield together with its one-dimensional representation. It had been agreed at the Paris meeting that the analysis should be undertaken using the

standard ANISN/SWANLAKE route with the various multigroup sets normally employed for in-house shield design and performance assessment calculations since these data-sets would provide the starting point for the assessments of accuracy requirements for individual project design calculations, ultimately to be included in the revised WRENDA compilation.

The PWR Radial Shield Benchmark

12 Significant differences were found in the prediction of the specified "design parameters" (atomic displacements, nuclear heating, biological dose, component activation etc) which were not unexpected in view of the different in-house data-sets employed. The sensitivities of these integral quantities to the total cross-sections used in the calculations, however, were all very similar. The cross-sections which most influenced the calculation of the design parameters for the PWR problem were, in decreasing order of importance, Hydrogen, Oxygen and Iron. The energy range of interest for these cross-sections was 6 MeV to 8 MeV, with inelastic scattering in oxygen between 8 MeV and 12 MeV also of importance for the predictions of iron-displacements in the pressure vessel region.

The (Sodium-Cooled) Fast Reactor Radial Shield Benchmark

13 Differences in the predictions of the design parameters were rather more serious in the case of the sodium/iron shield for an FBR, and it was apparent that they could not be adequately accounted for by differences between the data-sets and flux-to-dose conversion factors. It was accordingly agreed that a further study should be made of these results in order to establish the origin of the discrepancies. Meanwhile, they clearly indicate the importance of continued collaboration at the working level on the generation and application of multigroup data. Substantial progress in this area has already been achieved in the NEA Collaborative programme.

14 Only two contributors (EURATOM/Ispra and UKAEA, Winfrith) calculated sensitivity profiles for the fast reactor problem and the behaviour noted above in paragraph 12 was again observed: similar sensitivity profiles were achieved despite significant discrepancies between the predictions of the design parameters. These profiles indicated the considerable importance of the iron and sodium total cross-sections near the minimum in the latter at 300 keV and, to a lesser extent, near the minimum at 500 keV. For the prediction of sodium activation in the region corresponding to an intermediate heat exchanger the total cross-section of sodium from thermal energies up to approximately 3 keV was also of importance.

15 It was clearly impracticable for participants to specify the variance-covariance matrix of the group data used in their calculations, and it was not intended that the theoretical benchmarks should serve as a basis for assessing the influence of data errors on the prediction of design parameters. Nevertheless, the specifications were sufficiently close to generic design models to permit conclusions of practical significance to be drawn provided some allowance were made for the correlations which exist between components of a given total cross-section and between values of this cross-section at different energies. For this purpose it was necessary to modify the output of the standard SWANLAKE package which prints out the so-called problem-sensitivity: this can only be applied directly to problems in which every item of data correlates perfectly with every other item of data used in the calculation.

16 The effects of treating correlations realistically were clearly illustrated in the paper by McCracken (UKAEA, Winfrith) who obtained upper and lower bounds on the estimated standard deviation of the predicted "secondary sodium" activity of 71% and 25% respectively depending on whether full or zero correlation was assumed between values of a given cross-section at different energies. In the absence of more definite information on these correlations, the designer intent on guaranteeing a confidence level of 99.5% (ie 3 standard deviations) in the sodium activation-rate would need to multiply the calculated reaction-rate by 3.1 to cover nuclear data errors alone. Standard deviations of 5 to 7% had been assumed for the total cross-sections of sodium in the important energy range: whilst it is undoubtedly possible to measure these data to much greater precision - accuracies of better than 2 or 3% have been claimed - the error attributable to the method of averaging group cross-sections could easily amount to 5% (1sd).

17 In order to provide more useful pointers for the evaluators, the conventional sensitivity profiles in this paper were modified by differentiation with respect to the cross-section uncertainties to obtain so-called measurement profiles. These give directly the fractional improvement in the standard deviation of the predicted design parameter per unit fractional improvement in the standard deviations of the measured cross-sections. This artifice sharpens the profile by taking due account of the accuracies with which the data are already known (or are believed to be known).

THE CURRENT POSITION ON ERROR CORRELATION FILES

18 The derivation of full variance-covariance files which is now under way for the ENDF/B compilations is clearly a long term task. The partial correlations of a given cross-section at each energy-point are relatively easy to establish since elastic cross-sections may be derived as the difference between independent measurements of the non-elastic and total cross-sections, in which case they correlate negatively with the non-elastic and positively with the total cross-sections. It is the energy-dependent correlations which prove to be more difficult to establish: they may be inherent in the basic experimental technique, for example, the measurement of source strength with the same standard counter may introduce a systematic error over a wide energy range; alternatively, correlations may be introduced by the evaluator fitting either by eye or with the parametric adjustment of a nuclear model. In the latter case the production of a 'best' curve through a selection of measured points introduces correlations, generally positive, which extend over the whole range of the fit. Short range correlations, on the other hand, may be similarly introduced by the evaluator's judgement that measurements have resolved structure in the cross-section and that interpolation between points, rather than fitting through them is required - albeit using a nuclear model.

19 At ORNL a start has been made on the production of error files for the ENDF/B libraries and those for N, O and C have been already produced in ENDF/BIV (4). At LASL many files have been produced for reactions of relevance to CTR calculations. These files have been assembled relatively quickly on the grounds that any file is better than none; they are admittedly less full and less definitive that those of ENDFB/IV and are regarded as temporary expedients to be replaced in the long term (6). Similar work on the evaluation of data for penetration calculations in shield materials does not appear to be taking place in Europe, or, indeed, anywhere else in the world.

NUCLEAR DATA REQUIREMENTS FOR FUSION REACTOR SHIELDING

20 The nuclear data requirements for shielding fusion reactors (and fusion reactor experiments) were reviewed, in accordance with the proposals made at the Paris meeting (Paragraph 19 of the Summary Report) and subsequently endorsed by the NEACRP. A similar approach is being adopted in the USA and elsewhere

involving sensitivity analysis and benchmark experiments. The provisional variance-covariance files mentioned in the preceding paragraph which have been prepared at LASL, are being used for the study of the Tokamak Fusion Test Reactor (TFTR). The findings of the uncertainty analysis for the shield design have shown upper bounds to activation dose uncertainties of -50% which is considered to be acceptable. No urgent cross-section measurement or evaluation needs have been identified for fusion devices presently undergoing engineering design (7).

21 In the absence of definitive design proposals for power producing fusion reactor plant, it would be impracticable to draw up a detailed request list for shielding data; the primary objective of the meeting was to identify areas of common ground between fission and fusion reactor requirements. A preliminary list of the important materials was put forward with provisional data requirements and an indication of priorities. When these have been subjected to the standard procedures for sensitivity and uncertainty analysis it will be appropriate to include the findings in the request lists.

22 Attention was drawn to what was seen by some participants as a point of departure from fission reactor sensitivity and uncertainty analysis, namely the requirement for more multi-dimensional analyses in the design of fusion plant to handle streaming in large vacuum channels. Streaming is, however, now proving to be a problem on all types of power reactor shields, and there seemed to be no doubt that multi-dimensional codes would be applied to fission reactor designs when they became more generally available.

FUTURE IAEA/NEA PROGRAMME OF WORK FOR THE REVISION OF WRENDA SHIELDING REQUESTS

23 It was agreed that the laboratories and other organisations in the reactor industry represented at the meeting, having implemented the ANISN, DOT and SWANLAKE codes, were now in a position to compile a revised list of shielding requests for inclusion in WRENDA. These could be based on their own in-house data-sets using a calculational route which did not depend, initially, on a specific knowledge of energy-dependent correlations in the data. The procedure which is conveniently described in Paper (13) can be summarised as follows:-

(i) In consultation with design engineers ascribe target accuracies at the 1σ level to all reaction-rate parameters of current design interest. One-half of these target accuracies must be greater than the total uncertainties caused purely by data. (See paragraph 10)

(ii) Where possible, make one-dimensional models of the above situations which must be realistic with regard to material compositions. Where necessary a two-dimensional calculation with DOT can be transformed into a one-dimensional ANISN calculation either by the use of geometric bucklings or by the use of fictitious energy-dependent absorbers after the method described in (9).

(iii) Carry out forward and adjoint calculations with ANISN. Separate the scattering matrices used in ANISN into elastic and inelastic components and perform two separate SWANLAKE calculations: in the first of these, the absorption and inelastic cross-sections are suppressed to obtain the sensitivity to the elastic scattering matrix; in the second, the total scattering matrix is used with the total cross-sections to obtain the sensitivity to the total and absorption cross-sections. These two runs allow separation of the sensitivities to the absorption, elastic and inelastic scattering cross-sections.

(iv) Ascribe standard deviations at all energies to all the measured cross-sections used in ANISN (the uncertainties may be difficult to determine for some data-sets in common use but the compilation of Dr Schmidt (KFK 120 (EANCD-E-35U)) will provide a convenient first estimate if more up-to-date information is not readily available).

(v) Fold the standard deviations calculated in stage (iv) with the sensitivities from stage (iii) to obtain upper bounds (full correlations between groups at all energies) and lower bounds (no energy-dependent correlation) for the standard deviations on the calculation of the integral quantities of (i).

(vi) Where the criterion of (i) is not satisfied by an upper bound calculated in (v) the calculation of measurement sensitivities (defined in paragraph 17) will identify the energy range and accuracy requirements of cross-sections required to satisfy the criterion for incorporation into WRENDA.

CONCLUSIONS ABOUT THE ROLE OF BENCHMARK EXPERIMENTS

24 Whilst it was generally agreed that future requests for new measurements in WRENDA should be accompanied by an evaluation request for correlations - or at least the standard deviation on the measurements - in the same energy range, the consensus expressed at the meeting was in favour of adjusting multigroup cross-sections on the basis of integral experiments in order to meet short term requirements. In adopting this course, the shielding community would be following the practice of fast reactor physics but there were important differences in the nature of the problems which would necessitate some modification of the adjustment techniques to incorporate transport methods, and the results might prove to be valid only for a restricted range of shield configurations.

25 The most significant difference between fast reactor physics and shield penetration experiments was that almost all the quantities of interest could be measured in zero-energy core mock-ups to a high accuracy and, moreover, such experiments achieved a close simulation of the power reactor core environment. The degree of extrapolation accomplished with diffusion methods and adjusted multigroup data-sets was relatively small, embracing the effects of temperature, burn-up and the presence of fission products.

26 This is in marked contrast to the situation encountered in shielding: of the four main parameters required for shield design, namely nuclear heating, atomic-displacement, biological dose and component activation, only the last of these could be conveniently measured with sufficient precision for adjustments in mock-up experiments. Measurements of the leakage dose-rates could be made with adequate precision behind a given shield configuration but each experiment would then yield only one (or a few coarse-group Bonner-Ball type) integral measurement(s) at one penetration distance and this limitation would greatly increase the number of experiments required for the adjustment procedure. A much greater premium would therefore be placed on the measurement of spectra in shielding as opposed to reactor physics experiments. Secondly, the range of extrapolation from feasible experiments to practical designs of fast reactor shields was so large that it could not be spanned adequately using simplified diffusion methods without the support of transport calculations. These, in turn, called for validated multigroup data-sets, which could not be truncated below P_7, and variance-covariance matrices to estimate the accuracy of the predictions at deep penetration beyond the range of experiment.

27 The sensitivity profiles calculated for the key design parameters of typical fast reactor cores were slowly varying with energy; the range of interest was limited to the region below about 2 MeV. In deriving the adjustments, it had generally been possible to use simplified correlation functions because the results did not appear to be very sensitive to the nature of these assumptions. On the present evidence this might not be true for adjustments in deep penetration experiments.

28 The most serious reservations expressed by participants in the discussion of adjustment procedures concerned the range of validity of adjusted cross-sections based initially on benchmarks with single-materials and simple combinations of materials. Whilst they might reasonably be expected to lead to better predictions in shields containing these materials as heterogeneous components, it remained to be seen to what extent these data could be successfully applied to homogeneous mixtures where the spectral effects of group-averaging would be different. It would clearly be necessary to test these adjustments in as wide a range of design-orientated experiments as possible, and the NEA Benchmark Programme afforded an excellent opportunity to undertake the formidable amount of work involved on a collaborative basis.

29 An important advantage of this approach from the point of view of the participants representing laboratories outside the USA, was that it appeared to circumvent, at least in the short term, the problem of evaluating and processing error-correlation files of basic cross-section data. In certain cases, such as the 300 KeV region in sodium, for example, it might be possible to meet the requirement by assuming full positive correlation over the complete energy range of the problem and requesting a new differential measurement to within about 2%. Such requests could now be incorporated in the WRENDA compilation.

THE NEA COLLABORATIVE PROGRAMME OF BENCHMARK EXPERIMENTS

Progress to Date

30 The results of the first three single-material experiments in iron from Winfrith, Karlsruhe and the University of Tokyo have been published in a standard format, together with the original ORNL iron experiment (8). This format has been chosen to be consistent with that laid down by the CSEWG for the reporting of benchmark experiments in the US. Single-material experiments in iron and sodium have been carried out at HARMONIE, and the ESIS iron experiment is now in progress using the new fission-plate facility EURACOS II which has been set up by EURATOM on the reactor at the University of Pavia. Studies of iron have also been made (or are in progress) on TAPIRO and in the facility at MOL.

31 The objective in studying the same material in each facility to begin with was to investigate possible systematic errors between different laboratories and to demonstrate the effects of the different source spectra. Further information will be forthcoming on this latter point from HARMONIE and TAPIRO where fission converter-plates have been set up between the shield and the breeder/reflector regions to harden the input spectrum. In principle, all energy ranges of interest can be covered in one experiment with a fission source provided the measurements can be made over a sufficiently large depth of penetration: in practice source strengths are not usually adequate for this objective to be achieved in one facility; although the recent ORNL measurements, in which the TSF collimator has been opened out and the reactor power raised to 1 MW, afford an attenuation range of some 10^{12}, the detectors used, however, are necessarily low-resolution devices such as Bonner balls with the requisite high sensitivity (10).

32 The NEA collaborative experiments differ from the US reactor-source benchmarks in two respects: considerable effort is expended on the measurement of reaction-rate distributions through the shield using a common range of threshold, resonance and 1/V reactions; in some experiments simultaneous maximum-likelihood unfoldings of the spectrum are also obtained with multiple-probe spectrometers within the shield employing small (~5 ml) NE213 scintillators, and hydrogen-filled proportional counters supplemented by resonance sandwich foils. The experimental data are therefore complementary to those accumulated on the TSF at Oak Ridge, for example, and they should prove to be of value to the CSEWG benchmark programme.

Proposals for Further Work

33 It is proposed that a second NEA meeting of specialists who have completed single-material benchmarks in iron should be held at OECD Headquarters in Paris later this year in order to draw up the detailed programme for the theoretical analysis of the measurements. If all the experiments are to be analysed separately by the participating laboratories using the EURLIB 100-group scheme then the procedure might be as follows:

(i) Carry out sensitivity studies and seek adjustments of the scalar values of Σ absorption, Σ elastic and Σ inelastic to give maximum likelihood agreement with measurements assuming that the ratios of the down-scatter components of Σ inelastic remain constant.

(ii) For this purpose no energy-dependent correlations need be assumed ($r = o$) but the best available evaluations of partial cross-section data (including "vertical" correlations) will be required.

(iii) Each experiment will then furnish an adjusted multigroup set with the corresponding variance-covariance matrix, ie a complete (multigroup) error file; all these individually adjusted sets should then be tested against each of the experiments and the results compared.

34 There will be two courses open for dealing with any inadequacies in the data suggested by the intercomparisons of individually adjusted sets: the 'measurement sensitivity profile' could be utilised to identify a limited range for improved evaluations and/or differential measurements; but in the short term, a multi-material benchmark including appropriate regions of the material could be specifically designed to optimise the sensitivity to the cross-sections in question with a suitable choice of input spectrum and detector responses. This latter course would provide the designer with a full variance-covariance matrix for error estimation in project calculations performed with the adjusted data-set.

35 It is accepted that a considerable amount of work remains to be done in order to achieve these objectives, and the advantages of tackling this on a collaborative basis has been recognised by all participants. In particular, a new or modified EURLIB data-set will be required in which the multigroup scattering matrices are resolved into elastic and inelastic components, guidance will also be needed on the 'best' available estimates of the variances of the partial cross-sections and the covariances which exist between them. It will also be necessary to study in more detail the problem of multigroup spectral averaging: the present procedure with collision density weighting in 100 groups was devised specifically for iron; further tests with up to (say) 1000 groups may be required to establish a suitable procedure for choosing and averaging the group structure for other materials. In this connection the recent development of multigroup sets incorporating the Bondarenko approach to averaging should be taken into account (11).

SUMMARY AND CONCLUSIONS

36 Although substantial progress has been made by all the participating laboratories towards the objectives laid down originally by the NEACRP, and subsequently endorsed by the IAEA co-sponsors, a considerable amount of further work remains to be done before a properly revised list of shielding data requests can be formulated. In the meantime the following conclusions can be drawn:

(i) Techniques for sensitivity analysis have now been established which will enable proper assessments of the data requirements for shield design to be included in the WRENDA compilation.

(ii) New high accuracy requests have already been made for sodium and iron data although it appears that the latter may have been met by recent measurements. The preliminary nature of these findings is reflected in the present assignment to Category II.

(iii) With the present rate of progress on the application of sensitivity and uncertainty analysis to design problems it will be unlikely that a substantial body of results will be available before the Autumn of 1978 which is the earliest time at which the IAEA and NEA could convene a further meeting to co-ordinate the requests for inclusion in WRENDA.

(iv) Significant discrepancies were observed in the calculations submitted for the theoretical sensitivity benchmark on a typical sodium/iron shield for a fast reactor, and these could not be adequately accounted for by differences between data-sets and flux-to-dose conversion factors. It was agreed that a further study should be made of these results, preferably by a central laboratory, and Dr Nicks of the EURATOM group at Ispra was invited to undertake this task.

(v) Good progress is being made with the NEA Collaborative Programme of Benchmark Experiments, which has been given a new impetus by the importance attributed to the role of such experiments for the adjustment of cross-section data.

REFERENCES

1. J Butler and R Nicks, "Sensitivity Studies and Shielding Benchmark Experiments", Report of a Joint NEA/EURATOM Specialist Meeting held at Ispra, April 1974, NEACRP-L-1.

2. J Butler and A K McCracken, The NEA/EURATOM Restricted Meeting of Specialists on Shielding Benchmark Experiments held at AEE Winfrith, April 1975, NEACRP-L-121.

3. J Butler, R Nicks and N Tubbs, Joint NEA/IAEA Specialists Meeting on Sensitivity Studies and Shielding Benchmarks held at OECD Headquarters Paris, 7-10 October 1975.

4. E Oblow, "The Sensitivity Analysis Development and Application Programme at ORNL", Paper A1 presented at the Joint IAEA/NEA Specialists Meeting in Paris, ibid (3).

5. H Rief, "Three Dimensional Effects on Sensitivity Studies", Paper B4 to be presented at the 5th International Conference on Shielding, Knoxville, USA, April 1977.

6. S W Gerstl, "The Application of Sensitivity Analysis to Nuclear Data Assessments", Paper A18 presented at the Joint IAEA/NEA Specialist Meeting in Paris, ibid (3).

7. D J Dudziak, "Application of the Sensitivity and Uncertainty Analysis System LASS to Fusion Neutronics".

8. R Nicks, The NEA Co-ordinated Programme of Shielding Benchmark Experiments - Results of the First Four Single-Material Experiments in Iron (Issue 1) - NEACRP-U-73.

9. A K McCracken and M J Grimstone, Page 175 Proceedings of the Specialist Meeting on Sensitivity Studies and Shielding Benchmarks, Paris, 1975.

10. R E Maerker and F J Muckenthaler, Paper 111.3 to be published at the 5th International Shielding Conference, Knoxville, April 18-23, 1977.

11. I I Bondrenko et al, "Group Constants for Nuclear Reactor Calculations, published by Consultants Bureau, New York, 1964.

EDITORIAL PANEL

Dr J Butler	United Kingdom (Chairman)
Dr V Hernberger	Switzerland
Dr G Hehn	Federal Republic of Germany
Dr Khairallah	France
Dr T C Beynon	United Kingdom
Dr R Nicks	EURATOM, Ispra
Dr F Perey	United States of America
Dr J Schmidt	IAEA, Vienna

CHAIRMEN OF SUB-GROUPS

Sensitivity and Uncertainty Analysis of Fast Breeder Reactor Shields

Dr M Salvatores — Italy

Sensitivity and Uncertainty Analysis of PWR Shields

Dr C Devillers — France

Sensitivity and Uncertainty Analysis of Fusion Reactor Shields

Dr D Dudziak — United States of America

SCIENTIFIC SECRETARIES

Dr N Tubbs, NEA — Dr J A Larrimore, IAEA

REPRESENTATIVES FROM THE DATA COMPILATION CENTRES

Dr J Schmidt	Head of IAEA Nuclear Data Section
Dr L Edvardson	NEA Neutron Data Compilation Centre, Saclay

STATE-OF-THE-ART

REPORTS BY PANEL MEMBERS

TARGET ACCURACIES

V. Herrnberger

Meaning of Target Accuracies

Target accuracies or design criteria may concern calculational or experimental quantities such as radiation damage, nuclear heating, material activation and biological dose rate.

They can be divided into two different classes.

1. "Physical target accuracies" (PTA), which are determined in integral eyperiments by the comparison of experimental with calculational results or by direct error estimation.

2. "Required target accuracies" (RTA), which are required by people who are not directly concerned with shielding problems but need the results of the shield designer for their project work.

The first class is evaluated by the shield researcher or designer and should, in principle be only problem and method dependent.

The second class is essentially subjectively assessed and is time, design and cost dependent. A cost benefit analysis would in principle give a more objective basis for RTA determination. However, in practice this is not normally done due to the complexity of the analysis.

Both classes of accuracies are subject to uncertainties not only in cross-sections but also in

- source data
- modelling of the shield
- approximation in the method
- conversion factors.

The role of target accuracies for cross-section examination and request

Reactor benchmarks and integral experiments can be defined and performed in such a way that the PTA due to all other factors than that of cross-section data are negligible.

Then it can be assessed, by the use of cross-section accuracies and sensitivity profiles, whether the latest cross-section files satisfy the RTA. This assessment process leads to the definition of a request list for cross-sections as is drawn up by the sub-group of this meeting.

This process was applied in only two papers for PWR-shields, the papers for FBR-non-hydrogeneous shields and one contribution for TFTR-shields. It is quite astonishing that no more contributions were made to this, in our opinion, central problem of this meeting. The reason for this may be the lack of sufficiently complete error files of the cross-section libraries and/or the lack of a generally accepted list of reasonable RTA.

In the case of too severe accuracy requests for cross-sections (e.g. hydrogen to 0.5%), which result from high sensitivities and severe RTA (e.g. ±10% for damage), the requested accuracy for the cross-sections may be never achieved by new measurements and evaluations.

Then the PTA, as they are determined in reactor benchmarks, will indicate to the shield designer, how conservative he must be to fulfill the RTA, if he does not use adjusted cross-sections.

To avoid too severe requests, the shield designer should encourage relaxation of the RTA to be consistent with the other uncertainties in a design situation, in which the cross-section data is only one of many sources of inaccuracies.

At a later stage the requests can be made progressively more severe as the other uncertainties are reduced. This may be done in an iterative way.

The influence of partial uncertainties on the target accuracies

Beyond the uncertainties mentioned above the target accuracies are influenced by the inaccuracies of a lot of partial cross-sections. This is taken into account by summing properly over all cross-section accuracies weighted with the corresponding sensitivities.

The relationship between the RTA and the partial cross-section accuracies is used to define the cross-section requests. The influence of the uncertainties, other than in cross-sections (particularly that due to the applied method), is mostly taken arbitrarily as 50% of the RTA.

Status of target accuracy requirements

The now available compilation of ∿30 RTA covers those from Avery et al., and Devillers et al. for PWR shields, recent ones from Dudziak for TFTR shields and recent Russian and American requirements for non-hydrogeneous FBR shields. The definition of accuracy is in general not unique for the different requirements and should be specified as 2 standard deviations in future. Due to the lack of knowledge of the probability distribution of the calculated target quantities a Gaussian is generally assumed resulting in a confidence limit of ∿96%.

Generally acceptable RTA

We propose to consider as generally acceptable RTA those values which are most often required, because the wide spread and variable definition of accuracies make a calculated mean pointless. The values can be found in Table 1 for different targets, and table 2 contains a condensation giving a general overview.

Table 1

No.	Target		Generally acceptable RTA (%)
1	Gamma-ray heating in materials testing rigs	Without fissile heaters	20
		With fissile heaters	20
2	Gamma-ray heating in	sub-assemblies	10
		thermal shield	20
		biol. shield	20
3	Control and shutoff rod heating		10
4	Displacement rates in the	diagrid	10
		reflector region	20
5	LP instrument response		15
6	Displacement rates in the	supporting struct.	20
		int.shield system	30
7	Activation in the	heat exchangers	50
		cooling circuits	30
		turbines	30
8	External biological dose rate		Factor 2

Table 2

Target	Generally acceptable RTA (%)
Radiation heating	10 - 20
LP instrument response	15
Displacement rates	10 - 30
Activation	30 - 50
External biological dose rate	factor 2

Future aspects

The compilation of required target accuracies should be completed.

- Severe requirements should be checked for consistency with other inaccuracies and be progressively tightened only in step with reduction in other error sources.
- The compilation may be more useful if the "physical" target accuracies are indicated too. This allows the shield designer the determination of security margins.
- The accuracy definition of 2 standard deviations should be commonly used.

Conclusions from the sensitivity benchmark results of a PWR shield

by G. Hehn

1. Contributions came from 7 institutions. Papers were presented from

   AEE, Winfrith
   CEA, Saclay
   CEE, Mol
   EURATOM, Ispra
   JAERI, Japan

   Additional calculations are in progress and had been performed at IKE, Stuttgart and KWU, Erlangen having partial results available for comparison.

2. A comparison of the integral quantities calculated like radiation damage in the pressure vessel (interval 120), heating rate in the concrete shield (interval 147), and biological dose outside the shield (interval 202) is shown in table 1 :

institution	damage $dpa.s^{-1}$	heat Wcm^{-3}	total dose $mrem.h^{-1}$
AEE, Winfrith	1.39 (-12)[x]	9.71 (-6)	14.8
CEA, Saclay	1.98 (-12)	8.24 (-6)	41.1
CEE, Mol	6.99 (-13)	6.15 (-6)	13.0
[Sabine	2.82 (-13)	5.18 (-6)	5.5]
EURATOM, Ispra	1.12 (-12)	-	10.1 (with EL4 library)
	1.87 (-12)	10.22(-6)	27.0 (with EURLIB-3 library)
IKE, Stuttgart	1.90 (-12)	9.69 (-6)	25.5
KWU, Erlangen	1.01 (-12)	8.29 (-6)	8.34

[x] read 10^{-12}

Tab. 1 PWR benchmark - comparison of damage, heat and biological dose

3. The differences in the integral quantities reported are due to

   a) different cross section bases like ENDF/B-IV, ENDF/B-III, UKNDL, POPOP-IV,
   b) different group structures,
   c) different conversion factors used.

   A comparison with the programme SABINE, often used for design calculations, shows the methodical limitations of the removal-diffusion method.

   Comparisons between direct and adjoint solutions indicate that the methodical error of the one-dim ensional S_n-calculations are relatively small. The differences in the results of the atomic displacement rate is caused primarily by the displacement cross sections used. Old displacement cross sections are often incomplete and do not include all neutron interactions or aren't based on Lindhard theory.

   The second reason for differences in the damage quantity calculated can be attributed to the group structure of the cross sections used. Too few energy groups normally give an underestimation of the fast neutron flux in the pressure vessel. Different representation of the neutron resonances and last not least different data bases like ENDF/B-III, ENDF/B-IV and UKNDL are the other reasons.

   For calculating the heating rate in concrete the effects of different group cross sections are smaller and there are obviously no problems on conversion factors. Differences in the gamma production data have a greater influence on the biological dose.

4. In the benchmark specification the iron density in the stainless steel region ist 10.2% too high. The real iron content is 5.7903×10^{-2} instead of 6.4478×10^{-2}. An S_8/P_3 - calculation by Koban with a condensed version of the EL4 library containing 22 neutron groups and 19 gamma groups gives the following correction factors = right/false.

   a) for damage = 1.17
   b) for heating = 1.22
   c) for dose = 1.17

Since the corrections are small, the specification of the benchmark has not been changed.

So much for the results of the integral target quantities and now to the results of the sensitivity calculations.

5. The classification of the nuclides in regard to the damage in the pressure vessel is identical in all contributions as shown by the total sensitivities in the following table:

6. The sensitivity profiles of damage to the total cross section of the different nuclides show the importance of a narrow energy range between 5 and 7 MeV for all nuclides.

   So we presently know the relative importance of the nuclides in a given energy range. What is still unknown, are absolute values of importance.

7. Therefore, we need additionally the sensitivity profiles of the partial cross section between 5 and 7 MeV which should be calculated next. Since the energy region of interest is relatively narrow we can hope that a hand made correlation analysis will produce the results needed. Otherwise, we have to wait for the availability of the ENDF/B error files needed.

8. The sensitivity results for heating and dose show, that the requirements of neutron cross sections are less stringent. Nevertheless, the sensitivity profiles of partial cross sections like gamma production data should be calculated. We hope that a detailed correlation analysis will not be necessary.

9. At the end we want to propose that institutions who want to join the benchmark exercise in the future should make their sensitivity calculations for other important target quantities or other local positions like heat and damage near the core to enlarge the general overview of data requirements.

institution / Data Base / Element	CEA,Saclay ENDF/B-III	EURATOM,Ispra ENDF/B-III	AEA,Winfrith UKNDL	JAERI,Japan ENDF/B-IV	IKE,Stuttgart ENDF/B-IV
H	-5.67	-5.25	-5.02	-5.13	-5.02
O	-2.0	-1,89	-1.66	-1.89	-1.90
FE	-1.6	-1.51	-1.5	-1.58	-1.55
CR	-0.46	-0.42	-0.36	-0.39	-0.38
U- 38	-0.3	-0.31	-0.30	-0.23	-0.31
Ni	-0.23	-0.21	-0.21	-0.21	-0.20
ZR	-0.11	-0.13	-0.12	-0.12	-0.12
MN	-	-0.03	-0.27	-0.03	-0.03
AL,Si,Ca, U- 35	-	-0.01	-0.01	-	-0.01
TOTAL	-10.37	-9.76	-9.46	-9.58	-9.52

Tab. 2 PWR benchmark -
total sensitivity to damage

CONCLUSIONS CONCERNING THE "BENCHMARK PROBLEM FOR FAST REACTOR SHIELDING".

A. Khairallah

Four laboratories have contributed to this exercise:

- JAERI [1]
- UKAEA/Winfrith [2]
- EUR/Ispra [3]
- CEA/Cadarache [4]

Three of the laboratories have presented the results of calculations related to the integral parameters specified in the benchmark problem and two have presented the results of sensitivity calculations for the two parameters of importance in practice: damage rate in iron and activation rate of the secondary sodium.

From the two types of result we can draw interesting conclusions, which are, however, essentially qualitative as only a limited time could be devoted to their analysis during the meeting.

1. Comparison of integral parameters

Comparison will be confined to the following three parameters:

the total flux, the activation rate of the secondary sodium and the damage rate in iron. It is worth recalling that the calculations were performed with neutron data of various origins:

- JAERI: 100 groups, from ENDF/B4;
- UKAEA: 42 groups, from UKNDL;
- CEA: 26 groups, from DLC2 set (ENDF/B2).

The most striking feature is the large scatter of the results, which can be seen from Table 1 (in this table, the CEA results were taken as a reference since generally they lie between the other results).

The extreme results differ by a factor of 10-20 for the sodium activation at the heat exchanger and 1-4 for the damage rate in iron in the shielding.

More detailed analysis of these discrepancies and of their origins would certainly be very instructive, but one needs more time and more data (especially the cross-sections used for sodium capture and for damage in iron).

Even now, however, it can be seen that we are far from the target accuracies, quoted in Herrnberger's paper [5]:

- 30-50% for sodium activation;
- 10-30% for the damage rate.

In my opinion, this should help to convince those of us who are still sceptical of the practical importance of propagation integral experiments and of adjustments of the cross-sections used in design calculations on the basis of the results of such integral experiments. Besides a long-term effort aimed at more precise evaluations and microscopic measurements, we must be able to reduce considerably the observed discrepancies by:

(a) Performing more integral measurements, designed in the light of a precise aim and with the help of sensitivity studies,

(b) Adjusting the cross-sections on the basis of the results of these integral measurements. Despite its apparent weaknesses, this pragmatic approach has already proved itself very useful in other areas of reactor physics.

2. Sensitivity calculations

Through special studies of the activation rate of secondary sodium and of the damage rate in the shield, two contributors (UKAEA/Winfrith and EUR/Ispra) have arrived at qualitatively converging conclusions. They have identified the total cross-sections of iron and sodium in the ranges 0.1-0.7 MeV and 200-500 eV (for sodium) as those to which a particular effort must be devoted. The sensitivity values which they find differ slightly. This is not surprising since they use different data (EURLIB 100 gr for Ispra), and that does not constitute a problem since one needs above all orders of magnitude.

By introducing the interesting concept of "sensitivity to measurements", Dr. McCracken even manages to limit the important energy range to the interval 100-300 keV.

These sensitivity studies appear to be well established, despite difficulties reported by Dr. McCracken in the case of the Benchmark (shell-source). They are necessary whether it is a question of adjusting cross-sections or of quantifying cross-section precision requirements. It should be noted that the latter precisions are overall ones which must cover not only experimental uncertainties but also the uncertainties due to the subsequent treatment of the cross-sections.

TABLE 1

	UKAEA/CEA	IAERI/CEA	UKAEA/CEA	IAERI/CEA	UKAEA/CEA	JAERI/CEA
Start of shielding	1	.9	1	1	.4	1.1
Middle of shielding	1.4	.8	.7	.4	1.2	1.8
End of shielding	3.5	.8	1.5	.4	4	2.5
Middle of Na drum	5.1	.8	4.1	.8		
Start of heat exchanger	5	.4	5	.5	10	.6
End of heat exchanger	4	.1	2	.1		
	Total flux		Na activation		Fe damage	

REFERENCES.

111. Neutrone Induce Gamma-Ray Sources in Shielding Benchmark Calculations.
Shun-ichi Miyasaka, Kinji Koyoma, Kazuyoshi Minami and Satoshi Tsuzuki

121. Contribution to the Exercise on Sensitivity Studies for the NEA Theoretical Fast Reactor Benchmark
S. D. Lympany, A. K. McCracken, A. Packwood.

131. Two NEA Sensitivity, 1-D Benchmark Calculations.
Part II: Sensitivity of the Secondary Sodium Activation in the FBR Configuration.
U. Canali, G. Gonano, R. Nicks.

141. Probleme de reference pour les protections d'un reacteur a neutrons rapides.
J. C. Estiot, J. P. Trapp.

151. Target Accuracies Required in Radiation Shielding
V. Herrnberger, G. Hehn, R. Nicks

Methodology of Sensitivity Analysis (Dr T.D. Beynon, U.K.)

The main impression we must all have gained from this meeting is that of the increased use of the one dimensional ANISN SWANLAKE code compared with our previous meetings. Moreover, I think we have established firmly the importance of the covariance matrix in all our analyses. We have heard very elegantly from Dr Perey how the construction of a covariance matrix is a nice admixture of science, art and insight and we have had demonstrated to us very vividly by Mr McCracken the importance of allowing for error correlation in the final uncertainty that we should attach to a particular error evaluation. We have seen the elegant technique which Dr Oblow presented for giving an insight into the effects of streaming in space and energy. So we should really ask ourselves where should we go from here in sensitivity analysis and in particular is there any more development work to be done? I believe we still have areas where we can make some valuable contribution towards sensitivity study, and I would like to presume to list one or two of these. I am sure people can add some of their own.

An obvious question which should be asked is to what degree can we trust a first order perturbation analysis that produces in certain energy groups an uncertainty of .100%? In other words, should we be looking at higher order perturbation theory? I might add that if we look at the sensitivity profiles for certain threshold detectors in shields, we can very easily obtain uncertainties of a hundred percent. This was demonstrated at a meeting at Winfrith not long ago. I also believe that there is a good argument for having an intermediate step of data presentation which lies somewhere between the portrayal of a sensitivity profile and a final estimate of an error. One of the disadvantages of the sensitivity profile is that it tells you at which energies the particular parameter is most sensitive. What it does not tell you is whether or not the cross section in that particular energy range is well known. We can have a situation where we could see a very large peak in the profile and, without going to covariance

analysis, we could come to some fairly erroneous conclusions. It would be interesting to convolute a sensitivity profile with, say, a probability distribution that the errors should be greater than 10%. I think in some cases we would find that the profile would be altered. Or more simply we could perhaps multiply the profile by the diagonal of the covariance matrix.

Now a second area where we are bound to see an increase in the use of sensitivity analysis is in two dimensional analysis. We have already had an indication of this in some of the papers here. Now we all know that, in principle, we do not require any great extension to the analysis for first order perturbation theory for two dimensional work, but we do require a very large extension to the computer programmes and to the data handling of output. I think we should ask ourselves whether or not there may be a good case for looking at some approximation methods for two dimensional sensitivity analysis. We have seen the approximation technique that the USSR has used, using asymptotic theory, and this has been demonstrated to be quite useful. One wonders whether in two dimensional problems the pioneering work of the Russians in flux synthesis may not be a useful technique. I do not suggest it should in any way replace proper two dimensional transport calculations, but we should bear in mind that we could easily be overcalculating some of those quantities.

Now this leads naturally to the use of Monte Carlo codes in sensitivity analyses, and we have had contributions from Professor Rief and Mr Dubi which could throw some light on the use of Monte Carlo. I am not entirely convinced that the meeting has fully appreciated the future demands that fusion reactor work will make on Monte Carlo codes. I think that almost without exception what arguments have been put forward for data requirements for fusion reactors are based on approximations in which the toroidal geometry of the Tokamak system is replaced by an infinite cylinder, with no streaming and very little realistic structure. I would therefore argue that there is a a very good case for analytical development work for Monte Carlo sensitivity.

Next, we should ask ourselves what are the other areas in which sensitivity analysis in its present state can be used. I would suggest that the effects of the uncertainties of the energy distribution of emitted neutrons is an area which could be studied with some reward. I also suggest that the effects of anisotropic scattering, possibly characterized by $\bar{\mu}$, the average scattering cosine, could also be used as an integral handle for looking at this problem. We have seen the very nice results of Dr Perey for the anisotropy of elastic scattering in iron; I say nice in the sense of being a nice experiment but rather frightening in the sense of the amount of analysis which may be required. Nevertheless these data do exist and they must be looked at. Another possible area in which sensitivity analysis could be useful is for looking at this question of space-energy weighting of data. I always feel surprised when I go to shielding meetings that no one ever talks in much detail about this. I used to think at first it is because it is a non-problem and that this is why people use one data set for deep penetrations studies into materials. Why aren't spatially dependent sets constructed? One could think of a fairly straightforward application of the ANISN-SWANLAKE code, in which one arbitrarily divided the material into regions which have different cross sections, and looked at the sensitivity of some integral parameter on the cross sections in each of these artificial regions.

What can we conclude from a look at the sensitivity studies? I think we can conclude that by and large they are in good shape and that the analytical methods and computer codes, for one dimensional cases at least are now available, or appear to be to anyone who wants to use them. I believe that we can look forward to further significant developments of sensitivity analysis, particularly in the areas I have indicated.

Rewiew of the experimental benchmark programme (R. Nicks)

The present review, as well as stating the progress of the experimental activities since the Paris Meeting in October 1975, is also intended to give some information on future experiments planned in the different laboratories. The characteristics of the various shielding facilities available have been reported in the proceedings of the above mentioned meeting and shall not be repeated here.

Initially, it should be noted that the experimental programme for the source reactor HARMONIE has been reduced in the framework of a joint French-Italian Cooperation agreement in the fast reactor field, so that TAPIRO at Casaccia will be fully occupied with specific project orientated mock-up measurements. The joint French-Italian group is also analysing the neutron propagation results obtained at Harmonie concerning iron and pure sodium as well as iron-sodium layers, with the view of making a PROPANE calculational scheme adjustment. At the moment a new measurement is being undertaken at Harmonie; a configuration with an interface neutron source providing a harder spectrum has been installed by putting a convertor between the vertical iron reflector of Harmonie and the sodium column to be investigated.

As far as TAPIRO is concerned, the facility contains for the moment a model of the PEC diagrid; measurements are being performed with the view of checking radiation damage calculations made in 2 and 3 dimensions.

The future TAPIRO programme foresees neutron propagation studies in sodium-steel shields (25/75, 50/50, 75/25). Also in this experiment a fissile zone provides a neutron source with a harder spectrum; this zone is located between the copper reflector and the steel and/or sodium block under investigation.
According to forecasts the experimental programme should be finished by July 1977. Information on the neutron field in the models is obtained by conventional techniques using resonance and threshold activation detectors.

Neutron propagation studies in the iron block (1.9 x 1.8 x 1.2 m 3) housed by the ASPIS irradiation facility are virtually concluded; some supplementary refinements concerning the neutron spectra at various penetration depths are still underway. The future

utilization of ASPIS will be design orientated, a fast reactor shield model already being under preparation; the mock-up includes a fast breeder zone and a series of sodium-steel laminations . According to planning, this experiment will be finished early in 1977.

It should also be mentioned that during the period in question (October 1975 - October 1976) the ASPIS source power has been raised from 7 Watts to about 15 Watts; a supplementary power increase up to about 2 5 Watts is possible.

The energy range between a few KeV and several MeV will be covered by proton recoil spectroscopy and activation techniques.

Another convertor source was put into operation some months ago. At Pavia the EURACOS II facility (power: 30 Watts) is being used for neutron propagation studies in iron (block of 1.5 x 1.5 x 1.5 m^3). The geometrical lay-out of this facility is rather similar to the ASPIS one. Besides the activations detectors agreed upon at the Ispra meeting in 1975, gas counters and liquid organic scintillators are to be used. Therefore, the know-how in neutron spectrometry acquired by the Winfrith group is being transferred to Ispra. After the iron measurements, the fission disk power will be raised to 300 Watts.

The orientation of the future experimental programme strongly depends on the recommendations in terms of benchmark proposals issued by the present and possible future meetings.

Further computing efforts will be invested into the interpretation of the Winfrith (and Ispra) deep penetration measurements in iron in order to shed some light on the discrepancies between calculations and measurements in the high energy region.

As far as the ORNL-TSF measurements are concerned, one outstanding experiment may be identified in the study of the CRBR upper axial shield mock-up. The basic materials are stainless steel, iron and sodium, which are used in different geometrical combinations so as to create a dozen or more deep penetration experimental configurations. The maximum overall-thickness realized is about 7 metres. Bonner Balls, NE-213 - and proton recoil counters were and are being used as neutron detectors. The interpretation proceeds according to the classical scheme ANISN-DOT-ENDFB.

The CRBR radial shield mock-up measurement is specifically concerning gamma heating. This configuration comprises iron, uranium-oxide, stainless steel and concrete, making up a thickness of

approximately 2 meters. Gamma spectra and gamma heating are measured respectively with NAI - and TLD - detectors.

Finally, 2 benchmarks relating to the neutron propagation in stainless steel and in nickel slabs are under preparation. The maximum thickness is about 60 cm. Bonner Balls and liquid organic scintillators serve as detectors.

In the United States, increasing efforts are being invested in fusion experiments. CTR experiments with a 14 MeV source are being planned at ORNL as a preliminary shield study for a fusion reactor. Neutron transmission measurements will be performed on a stainless steel-water-carbon configuration eventually achieving an attenuation equal to seven (7) orders of magnitide.

Cf 252 fission and 14 MeV sources have been extensively used at Karlsruhe with the purpose of studying neutron transmission through iron spheres with radii up to 20 cm. These measurements have been thoroughly analyzed by the IKE-group of Stuttgart in order to ascertain the validity of ENDFB/3 and ENDFB/4. The experimental devices remain available for future shielding benchmark experiments.

Measurements at the fast neutron source reactor "YAYOI" concerned two dimensional distributions of the neutron flux and the gamma dose rates across a 70 cm thick iron shield. This iron shield was housed in the vertical experimental column located above the lead reflector surrounding the "YAYOI"core. The detection techniques were based on the use of threshold and sandwich resonance foils for neutrons and TLD's for the gamma dose rates. The analysis of the experimental results is still being undertaken with ANISN, TWOTRAN, ENDFB/4 and POPOP/4.

In the future programme, improvements of analytical methods and measuring techniques are planned.

A new experimental programme concerning neutron propagation in a NA-block is to be performed in the vertical column of the YAYOI source reactor. Measurements will start within some months and will extend up to middle 1977. Furthermore, the University of Tokyo envisages streaming experiments in ducts surrounded by concrete to be performed at the YAYOI facility.

In conclusion, I think it is important to state that quite a large amount of experimental data on iron is available now in the various laboratories; to sum up the situation, neutron propagation measurements in iron have been performed or are in the course

of execution on ASPIS, HARMONIE, TAPIRO, YAYOI, TSF, EURACOS II, and at Karlsruhe and MOL.

Results on the First Four Single Material Experiments in iron have been compiled in a first issue and distributed as a NEACRP document. It is very important to update and complete this issue with the new data which has become available in the meantime.

STATUS OF EVALUATIONS

F. G. Perey

I shall briefly review what we have learned about the status of evaluations in this meeting and also inject some comments on the meeting as an evaluator.

We have all agreed that there is only one way to look at the status of evaluations and it is provided by the answer to the question: are they adequate in providing the needed accuracies?. With almost no exception it is generally agreed that there is a way of answering in a credible way this question. One proceeds to obtain the sensitivity coefficients and fold in the covariance matric of the data. At this meeting we have heard a lot about these two aspects. The ability to generate sensitivity coefficients has been demonstrated by many different groups but on the subject of covariance matrixes you have only deplored the unavailability of the information in most evaluations. Having expanded myself a considerable amount of effort in this area of evaluation in the last few years I agree wholeheartedly with you. Within CSEWG I am happy to report that the concept of incorporating covariance data is a well accepted and we hope that ENDF/B.V will represent a large step forward. I can only recommend to you that you go back to your evaluations and request this new kind of information in the future. In defense of past evaluators, we cannot blame them for not having generated the information since you have only now acquired the capabilities of using this information.

At this meeting we have addressed the question of adequacy of evaluations in the now usual way, that is by comparing measurements on benchmark experiments to calculations. We have had the usual discussion on accuracy of the methods used and noted the failures of some evaluations in predicting the results properly. You have shown some surprise in seeing my interest in integral results, since you said you were used to receiving a deaf ear from evaluators. Let me assure you that I do not know of any evaluator who is not interested in understanding your problems and improving the evaluations. However, you must learn to communicate more effectively and I suggest that the common ground is the cross-section data. You must try to be as explicit as you can be. By definition an integral experiment result is a function of many cross-sections and unless you can point out in a convincing manner which cross-sections, in what energy range, are likely to give you problems, you will attract the attention of evaluators. You are now in possession of the tools to perform this analysis and I suggest that you use them to analyze the likely sources of the discrepancies and they communicate with evaluators.

Several summary reports indicate areas of perceived deficiencies in evaluation and I am sure that many of the evaluators will be interested in these findings. In the comparison of the various libraries which we have seen we have noted a great amount of honouring which goes on. I have found it most interesting but somewhat distrubing since it is difficult to judge whether these evaluations represent independent evaluations of the same data or new data. In particular, I have noted some curves which are more than 10 years old and certainly do not represent the current data situation. I, therefore, wonder how many of the statements claiming deficiencies in the data are actually well known deficiencies of past data and/or evaluations.

Design Sensitivity and Uncertainty Analysis of Fast Breeder Reactor Shields

A Subgroup Report. M. Salvatores

From the papers presented on this subject at the meeting, a number of preliminary conclusions can be drawn on areas of general agreement.

For what concerns the data requirements for the main elements of interest, Na and Fe, a number of sensitivity studies were presented, or related to the benchmark sensitivity study exercise proposed in Paris, (7, 2, 3) or to specific design oriented experiments (4), or related to specific reactor design (5).

The integral responses of interest taken into account in these papers were the activation-rate of sodium in the heat exchanger, the iron displacement rate in the Fe/Na shield, the heat generation in the shield. Not all of these responses were taken simultaneously into account in each paper, and in the Oblow paper the response was actually a total flux; but, however, a fairly significant range of overlapping information was presented.

From the sensitivity studies, and from the discussions on the result implications, the following main areas of high sensitivity for sodium and iron neutron cross-sections were pointed out:

a) Na total cross-section from 0.1 to 0.7 MeV, with special emphasis on the 0.3 and 0.5 MeV peaks.

   Na total cross-section from 200 to 500 eV.

b) Fe total cross-section from 0.1 to 0.35 MeV.

It is to be stressed at this point that these results reflect the situation that emerged at this meeting and are certainly not exhaustive of all the needs for shielding.

In the assessment of the relevance of the knowledge of the indicated cross-sections in these energy ranges, the notional target accuracy proposed by Herrnberger et al. (6) were considered, namely:

- Radiation heating: 10 ÷ 30% accuracy
- Activation rate: 30 ÷ 50% "
- Displacement rate: 10 ÷ 30% "
- External bio.dose: 200% "

It is important to stress that these target accuracies should be interpreted as comprehensive of any uncertainty arising not only from basic data, but also from source, methods and modeling uncertainties (8). This means that any request for accuracy in basic data that will make the uncertainty in data meet the quoted accuracies, should be interpreted as maximum allowable uncertainties in the hypothesis that no other source of uncertainties are relevant.

It is worth noting in this respect that from the data of ref. 1, if the iron total cross-sections in the energy-range near 300 KeV (the total cross-section near the 500 KeV antiresonance is of less importance but is also worth inspection) were known to approximately 3%, the uncertainty quoted for the sodium activation (last figure of Table 12 (Ref. 1), would fall from 71% to 50% exactly at the of the overall target accuracy.

In conclusion, from the qualitative results of the sensitivity analysis and the quantitative, even if to be used as broad indications, values of the target accuracy, new WRENDA request list values were proposed for sodium and iron, namely a 3÷8% accuracy request with priority 1 for the total cross-section in the energy ranges indicated above, and it is worth to note the complete lack of request in these areas in the present WRENDA list. It was considered also of interest to add at the present WRENDA format the possibility of introducing explicative comments on the requests, in particular of their implications in terms of design parameters.

One of the main difficulties encountered in the attempt to draw quantitative conclusions from the sensitivity analysis, was indicated (1,4) to be the existence of correlations among partial cross-sections of the same isotope and/or energy correlations in the same reaction cross-sections. The presence of correlations can strongly affect any statement on the relation of basic data uncertainty and integral design parameters uncertainty. It was indicated in (1) a factor of 3 uncertainty simply making use of two extreme hypothesis in introducing energy correlations (i.e. no correlations at all, or full energy correlation). By far larger effects can be found introducing partial cross-sections correlations.

The work on the definitions of the covariance matrices, which include the correlation information, is highly developed at ORNL, and LASL, but no indication was found of similar work going on in Europe. Due to the substantial contribution that the covariance matrices can give even in the adjustment procedures, it was generally agreed that any new request for a measurement in WRENDA should be put together with an evaluation request of correlations in the same energy range.

From the discussion emerged a proposal for the practical format of such requests, proposed by E. Oblow, according to the experience in this field at ORNL.

A significant point in the subgroup discussions was the attempt to foresee, even very generally, how the new requirements can be met. The opinion is that probably in the long range we could rely on very accurate new measurements, but that for the time being a more flexible approach can be sought, making a rational use of the cross-sections adjustments with integral experiments, in particular

in the framework of a two-step approach. Namely, if a design problem with the help of sensitivity analysis, indicates the need for new data requirements, these needs can be met or by performing a very accurate and representative mock-up experiment, which is fairly unlikely, or adjustment procedures can be successfully used as an immediate improvement tool which will give as output a data set, the applicability of which will be limited to the range of the integral experiments used and so will be useful for only one class of problems.

If now it is necessary to extrapolate from that class of problems, for a specific design requirement, it is necessary to have a second step in this procedure in terms of a better understanding of data. This second step implies an interaction with evaluators and experimentalists, for a better exploitation of the information obtained by the adjustment procedure. The new situation that can result from this interaction, will produce new evaluated data which can be used with more confidence and on a broader range of problems.

For what concerns production cross-sections, a number of indications were presented concerning the sensitivity of the heat generation to γ-production cross-section (3) and the present situation of the knowledge of the capture γ-ray yield data for nickel and chormium in stainless steel and sodium was indicated to be unsatisfactory, in view of the mentioned target accuracy ($10 \div 30\%$ accuracy on heating near the core).

Kulakovski pointed out the relevance of the correct energy dependence of the γ-emission spectra, for problems where small transport paths are involved. Finally, a sensitivity analysis (7) performed on the equivalent thermal flux on the heat exchanger, indicated significant effects of the neutron source distribution in the blanket, and as a consequence the high sensitivity of this quantity to the uncertainties that can arise in the source distribution and in the source spectra (smaller effects).

REFERENCES

1. Contribution to the Exercise on Sensitivity Studies for the NEA Theoretical Fast Reactor Benchmark.
   S. D. Lympony, A. K. McCracken, A. Pochwood.

2. Two NEA Sensitivity, 1-D Benchmark Calculation. Part II: Sensitivity of the Secondary Sodium Activation in the F.B.R Configuration.
   U. Canali, G. Gonano, R. Nicks.

3. Neutron Induce Gamma-Ray Sources in Shielding Benchmark Calculation.
   Shun-ichi Miyasaka, Kinji Koyoma, Kazuyoshi Minami and Satashi Tsuzuki.

4. Recent Progress at ORNL in Determining Nuclear Data Requirements for Fast Reactor Shield Design Using Advanced Sensitivity Techniques.
   E. M. Oblow and C. R. Weisbin

5. Investigation of cross-section requirements for shielding of power reactors.
   G. Hehn, J. Rataj.

6. Target Accuracies Required in Radiation Shielding.
   V. Herrnberger, G. Hehn, R. Nicks.

7. Etude spatio energetique de la sensibilite du flux termique equivalent sur l'echangeur dans un cas type de reacteur rapide refroidi ou sodium (1ére partie).
   A. Boioli, L. Fiorini, J. Moreau, G. Suntinger.

8. Target accuracies and sensitivity studies in the assessment data requirements for practical shield design.
   A. F. Avery, S. D. Lympany.

Summary of the conclusions of the Subgroup on

"Sensitivity studies and data requirements for thermal reactor shielding"

C. Devillers.

1. All papers presented at this meeting dealing with thermal reactors are in fact devoted to PWR shielding problems.

2. Conclusions are mainly based upon the contribution of different laboratories to the 1300 MW PWR benchmark exercise specified by Hehn and Koban.

3. Benchmark calculations include sensitivity studies of the following design parameters:
   - neutron damage rate in the pressure vessel
   - gamma heating rate of the concrete shield
   - dose rate outside the concrete shield.

4. Most of the sensitivity calculations have been performed by the two codes ANISN - SWANLAKE using coupled neutron-gamma or independent multigroup libraries coming from different evaluations.

5. Target accuracies on design parameters were agreed as follows:

   - 20% for damage in pressure vessel
   - 50% for γ-ray heating in concrete
   - factor 2 for dose rate outside the shield

   Half of these target accuracies are allowed to come from uncertainties in nuclear data: neutron and gamma source data as well as differential neutron and gamma cross sections.

6. Calculations of the sensitivity to total cross sections which have been mostly performed should be completed by further sensitivity calculations to partial cross sections because the errors on partial cross sections (ie elastic and non-elastic) may be correlated as pointed out in McCracken and Suvorov papers.

7. No complete error estimate, starting from sensitivity profiles, error files and covariance matrixes has yet been attempted - It is, therefore, not possible today to assess by this way if the target accuracies are met or not when using presently available data.

8. The inverse task consisting of the derivation of accuracy requirements for individual nuclides from target accuracy assessments is even more difficult. Sharing the allowed uncertainty equally between the nuclides involved and then between total and anisotropy cross sections as in Devillers paper is a starting guess which, of course, does not take into account the practical feasibility of such accuracies. This can be used, however, to identify which nuclides should have accurate cross sections. In a paper from Avery the sensitivity of the design parameters to improvements in the accuracy of cross section measurements is also shown.

9. For the radiation damage problem, nuclear data uncertainties should induce less than 10% uncertainty - Appendix 1 summarizes the sensitivity results obtained. All the contributors agree that the most important nuclides are hydrogen, oxygen and iron with the relative importances quoted in appendix 1. The important energy range lays above 4 MeV with a sharp peak around 6 MeV for all the nuclides. The important cross sections are those which affect the removal cross section, that is to say, total cross section of hydrogen, elastic and non-elastic cross sections of oxygen, non-elastic cross section of iron chromium and nickel. The high sensitivity of the calculations to the Legendre expansion of the scattering cross section shows that anisotropy distributions should be sufficiently accurate to generate Legendre moments up to the third order for oxygen and iron. It is believed that the uncertainty in the absolute value of the displacement response function due to uncertainty in the cross sections used to derive this function is of no practical importance today; this is because it only serves in extrapolating neutron damage in samples irradiated in experimental irradiation facilities to neutron damage which will occur in operating conditions -

The importance of the U235 fission neutron energy spectrum above 4 MeV has been pointed out. An increase as large as 14% occurs when using the EURLIB (ENDF/B IV) instead of the CRANBERG spectrum. The CRANBERG spectrum was found to be more consistent with recent measurements and, therefore, can be recommended.

10 As concerns the γ-heating problem for which an accuracy of 25% should be obtained, similar conclusions can be drawn as concerns the important nuclides, the important energy ranges and the important cross-section as is shown in Appendix 2. However, sensitivities to fast neutron

cross-sections are much lower than in the case of neutron damage. This results from the fact that important γ sources come from neutron captures in steel structures close to the core which are, therefore, not sensitive to high energy neutron transport. Sensitivity to high energy neutron cross-sections comes only from small contributions of capture γ rays

In addition it is shown that 80% of the capture gamma-rays come from thermal neutron capture and that the thermal capture cross section of iron is the only important data to know. No problem of neutron energy dependence of capture gamma-ray spectra is therefore detected and inelastic γ -rays are unimportant here. Due to the fact that γ -rays that contribute to the heating of concrete have to be transmitted through the pressure vessel, the high energy gamma yields are important; to this respect, an energy resolution of 1 MeV is quite sufficient. For the same reason, the γ interaction cross sections are important in the energy range 3 to 8 MeV. It is the subgroup's feeling that errors coming from the gamma yields and gamma interaction cross sections are consistant with the target accuracy.

11. The neutron cross-section sensitivities of the dose problem are quite similar to those obtained in the γ -heating problem, the total dose outside the biological concrete shield being dominated by high energy capture γ -rays coming from internal steel structures. A new feature, however, comes from the concrete material as it plays a role in generating supplementary γ -ray sources and attenuating neutrons and γ -rays. However, the uncertainty on those parameters coming from nuclear data errors is far below the errors coming from the imperfect knowledge of the actual composition of this material: density, water content, impurities, such as boron, lithium and rare earths

12. In conclusion, the predominant nuclear data which are likely to affect the accuracy of the predictions are neutron cross sections: total, non-elastic and differential scattering cross sections at energies between 4 and 10 MeV. For hydrogen, oxygen and iron which are the predominant nuclides, the accuracy requirements cannot yet be exactly assessed. It is therefore recommended that further and more detailed sensitivity analysis be pursued, in particular by taking into account energy and partial cross section correlations. In addition, it appears that the transmission type Broomstick experiments should be more extensively used to check the status of data used in design calculations. Given the narrow energy region involved (high channeling effect) it should be possible to use such experiments to directly adjust cross-sections of interest in this energy range.

Appendix I

Summary of sensitivity calculations for neutron damage

X -Sec

Element	Important X-sec	Sensitivity to σ_t	Deviation from p3 to p1(%)	Important energy range(MeV)
H	total	-5.5	Conversion from center of mass to laboratory	5-7
O	non-elastic elastic	-2.0	-9.	"
Fe	inelastic absorption	-1.5	-16.	"
Cr	"	-0.4	-4.	"
U238	"	-0.3	-1.	"
Ni	"	-0.2	-2	"
Zr	"	-0.1	neglig.	"

Appendix 2

Summary of sensitivity analysis for gamma heating

X-Sec

Element	Sensitivity to σ_t neutron	Sensitivity to σ_ϵ neutron	Sensitivity to σ_t gamma	Important energy range(MeV) neutron	gamma
H	-1.2	neglig	-0.1	4-10 +thermal	3-8
O	-0.3	"	-1.	4-10	"
Fe	-0.7	0.55 (thermal0.43)	-5.5	4-10 + thermal	"
Cr	-0.1			"	"
U238	-0.1		-1	"	"
Ni	-0.1		-2	"	"

REPORT OF SUB-GROUP ON FUSION REACTORS

Dr. D. J. Dudziak

INTRODUCTION

The sub-group participants were,

Dr. D. J. Dudziak, Chairman
Dr. T. Beynon
Mr. A. Dubi
Dr. J. Guasp
Dr. M. Mattes
Dr. R. Pannetier
Dr. R. Perey

The fusion reactor blanket and shield design field being embryonic, very little substantive analysis exists to document cross section measurement requests. Preliminary sensitivity analyses of EPRs in the U.S.A. have mainly verified the strong sensitivity of several critical response functions to Fe cross-sections, in support of previously qualitative judgements. Similar results apply to ^{10}B capture and high energy scattering. However, no comprehensive and realistic uncertainty analyses have yet been undertaken for power reactors. The reasonably complete uncertainty analysis for a low-power Tokamak Fusion Test Reactor (TFTR) showed upper bounds to activation dose uncertainties of -50%, considered to be an acceptable value. Thus, no urgent cross-section measurement or evaluation needs have been identified for fusion devices presently undergoing engineering design.

The sub-group confined its discussions as much as possible to measurement needs, in view of the Meeting Chairman's charge for it to crystallize its deliberations into a WRENDA request list. As to the question of whether any such requests can be met by existing data, the sub-group (including an experimentalist/evaluator) is not aware of measurements which can assuredly fulfill the requirements. In the natural manner discussed below we have conformed to the Chairman's charge to restrict ourselves to a few materials of highest priority. Some few comments on the status of evaluations for key fusion reactor materials are included.

The identified fusion reactor cross-section data requirements can in many cases be met by nuclear model calculations in conjunction with a few differential measurements. In the case of gas (H, He) production in structural materials, for example, simple integral measurements in well defined spectra may be sufficient to provide cross-section data for some materials damage analysis.

MEASUREMENT NEEDS

Careful consideration has been given by this Sub-Group to the question of the timeliness of proposing a data request list for fusion reactor design. Whilst it is not difficult to list several dozen nuclides which could be expected to be of interest to fusion reactor designers, it was nevertheless felt that in the absence of a definite design proposal for a power-producing fusion reactor, either of the Tokamak type, the reverse-field pinch or other concept, we should limit ourselves to those properties of a few important materials which could significantly affect the viability of a conceptual design. On the other hand the definite design of the American Experimental Power Reactor (EPR) requires some definite neutronic information: we know of no other definite design proposals which could have influenced our conclusions. We feel, therefore, that the following request list should be regarded as the minimal one which is consistent with the important needs of future conceptual fusion reactor designs and with the design requirements of the EPR.

* Priority I Recommendations

a. neutron emission spectra (5 angles, E_n, 500 keV)

^{7}Li $Nem(0°E_n')$ Accuracy = 10%, E_n = 11, 14 MeV

^{11}B " " " "

C " " " "

Fe " " " "

b. gas production

^{7}Li $^{o}n, n't$ (E_n) Accuracy = 10% E_n = thres. - 15 MeV (1-MeV increments)

^{11}B $^{o}n,xp(E)_n$ $n,xa(E)_n$ Accuracy = 15%, E_n = 14 MeV

^{12}C $^{o}n,xa(E)_n$

^{56}Fe $^{o}n,xp(E)_n$ $n,xa(E)_n$ " "

Priority II Recommendations

a. neutron emission spectra (5 angles, $E_n' > 500$ keV)

^{6}Li $on,$ Nem $(^{o}n\ 'E_n')$ Accuracy = 10%, E_n = 11, 14 MeV

AL " " "

Mo " " "

** Ni " " "

Cr " " "

b. gas production

Al $\sigma_{n,xp}(E_n)$ and $\sigma_{n,xa}(E_n)$ Accuracy = 15%, E_n = 14 MeV

No " " " "

** Ni " " " "

Cr " " " "

^{6}Li $\sigma_{n,t}(E_n)$ Accuracy = 15% E_n = 1-15 MeV (a few energies)

Priority II Recommendations

a. neutron emission spectra for Be, Cu, Ti, V, Nb

b. gas production cross-sections for Be, Cu, Ti, V, Nb

c. proton and alpha spectrum measurements at E_n = 14 MeV for Fe, Ni, Cr.

d. selected measurements on isotopic data (for nuclear heating and activation calculations) for important elements; e.g. Ni, Cr, and Mo.

* If an intense (D, Li) source is built, a value of En above 14 MeV may be required for materials other than Li.

** If high-nickel-content stainless steel (i.e. PE 16) is to be considered, Ni will require a higher priority number.

EVALUATION NEEDS

The most important materials being considered for conceptual experimental power reactor designs are B, C, Si, Fe, Ni, Cr and Cu. In addition, conceptual commercial power reactor designs employ ^{6}Li, ^{7}Li, Be, F, Ti, V, Nb and No. Data evaluation requirements for the latter class of reactors are clearly not stringent if the anticipated errors in nuclear performance parameters do not impact the very viability of the reactor concept. An important exception exists where radiation damage experiments are planned for such materials in the near future. These experiments are important in a materials selection screening process, and some nuclear data deficiencies could influence conclusions from such experiment (confined almost exclusively to H and He production cross-sections). A notorious example is Mo, where charged particle reactions are completely absent from the ENDF-4 files.

As a general statement, the fusion reactor applications require special evaluator attention to reactions such as (n, n^{1}), (n, 2n), (n, n^{1}x) and (n, x) at neutron energies up to ~15 MeV, some of which may be of limited interest in fission reactor applications.

Specific recommendations are as follows:

1) A new ^{11}B evaluation, including gamma-ray production, is badly needed. Realistic representation of secondary neutron spectra is important.

2) Recent new experimental data for secondary neutron spectra from ^{7}Li and ^{9}Be should be incorporated in new evaluations, again with realistic representations.

3) Gas production cross-sections for all the materials listed above should be carefully reviewed for adequacy.

4) Correlated error files for the above materials are of prime importance, in order to allow quantitative assessment of the impact of remaining uncertainties on nuclear performance.

5) It now appears likely that a (D-Li) neutron source will be constructed for fusion reactor materials irradiation studies. The source spectrum is a broad (HMHW-3 MeV) Gaussian about 15 MeV, with neutrons up to ~30 MeV. The impact of this device on nuclear data needs was discussed, but requires much more detailed assessment than our Sub-Group can provide in the time available. All we can do here is alert those involved to the potentially large impact on evaluation as well as measurement needs.

CONCLUSION

At least from the fusion reactor community's viewpoint, the exchange of views and data concerning sensitivity and uncertainty studies have proved valuable. The commonality and contrasts in shielding problems between fission and fusion were brought into sharper focus. When pressured to quantify target accuracies the fusion shielding engineers respond similarly to fission shielders, with regard to biological dose and activation outboard of the shield.* Only for damage to components such as superconducting coils and neutral beam intectors, (and possibly afterheat from activation in the blanket) are extremely stringent demands placed on cross-section data. Intermediate demands (10-20% target accuracy) apply to s/c coils anticipated-optimistically-to require shield design in the early 1980's. Such shields require energy attenuation factors of $\sim 10^{6}$. These, sensitivity and uncertainty studies are urgently needed to define the target cross-section accuracies required to, in turn, satisfy the target response accuracies. It appears highly unlikely that target response accuracies can be met on this time scale by refinement of microscopic data, so confirming prototypic shield experiments will be required.

* Cf. Herrnberger's summary of target accuracies.

Several observations can be made regarding the relevance of this meeting to fusion shielding. Firstly, it re-emphasizes the fact that a major hurdle lies ahead for fusion and fission alike - that of producing covariance data for numberous materials of interest. Extraction of useful information on design uncertainties and their feedback to measurement programmes depends strongly on a concerted effort to acquire covariance data.* A point of departure from fission reactor sensitivity and uncertainty analyses appears to occur in the requirement by fusion for more multi-dimensional analysis. This need is based upon the dominance of fusion reactor primary shield design by streaming in large vacuum channels. Another major caveat which must be attached to any fusion reactor request list is evoked by the ephermeral nature of the reactor concepts. Close attention must be paid to up-dating request lists as different concepts and material selections change in popularity. Finally, secondary energy and angular distributions may be more important for fusion, the former for blanker calculations vice shielding; the latter for streaming and scattering from duct walls.

It is worth adding to our recommendation the statement that we feel that many of the data measurements we propose contain a good deal of interesting basic nuclear physics. This interest should be used as an incentive to encourage the participation of low energy nuclear physicists outside the usual laboratories and data evaluation centres and to concentrate selected parts of the request list in University groups.

* This meeting, or its successor meeting, should give serious consideration to defining a limited list of materials, for which an ad hoc effort may evolve to produce the data prior to a formal ENDF-5, (3-5V)

Summary remarks from the IAEA Nuclear Data Section (J. Schmidt).

The major outcome of this meeting was to pinpoint the cross section areas of major importance to shielding. The open problem is what energy and angular detail is needed by shield designers? Must shield designers have more of Perey-type measurements?

At this moment it seems not yet possible to draw up a request list for shielding data. From the papers presented it would be useful to excerpt a few pages summary on cross section needs.

The following five general requirements seem to emerge from this meeting:

1. A better documentation of evaluated data files modelled on the ENDF/B data documentation.

2. The major evaluated nuclear data libraries should be updated and the reasons for remaining discrepancies be investigated in detail.

3. Uncertainty files should be added to evaluated nuclear data files.

4. In the preparation of next meeting measurers and evaluators should have a close look at and should improve the data required for shielding as apparent from this meeting.

5. Sensitivity and benchmark studies should be pursued simultaneously, particularly in order to find out about the importance of detailed Perey-type cross section structure to be taken into account in shielding calculations.

The next meeting on nuclear data for shielding should be held in about 1978. In preparation of this meeting there should be a better interaction between the shielding and data communities. In particular should the shielding experts communicate their updated requirements early enough to the data specialists so that they could find out about the status of the required data well before the meeting. The meeting itself could then devote more time to reach decisions on future work needed.

SESSION A

TARGET ACCURACIES

TARGET ACCURACIES REQUIRED IN RADIATION SHIELDING

by

V. Herrnberger[1], G. Hehn[2], R. Nicks[3]

1) Swiss Federal Institute for Reactor Research, 5303 Würenlingen, Switzerland

2) Institut für Kernenergetik, University of Stuttgart, Federal Republic of Germany

3) CCR, Euratom, Ispra, Italy

Abstract

The specification of target accuracies is shown to be central to the philosophy of shield design and basic to the definition of a cross-section data request list.

An inquiry on target accuracies was circulated to nuclear energy establishments in 6 countries. A compilation of the responses is presented, subdivided into three categories: 1) power reactors; 2) research and test reactors; 3) irradiation facilities.

The different possibilities for error interpretation are discussed.

INTORDUCTION

One of the envisaged objectives of today's meeting is to review the experimental and theoretical programmes, which would lead, ultimately, to a revised data request list covering the broader area of shield design for fast and thermal reactors (and perhaps other irradiation plants with isotopic and accelerator sources too). This includes calculations for in-core gamma heating and breeder diagrid and accelerator target damage studies. The current reactor data request lists do not adequately reflect the needs of shield designers. This can be attributed, among other reasons, to the very well known difficulty in arriving at a generally agreed statement of design criteria quantifying the requirements on target accuracies.

This difficulty arises from the fact that the nature of shielding problems is more diverse and complex and the target accuracies are more closely related to specific design issues than those of reactor physics. The specification of target accuracies is central to basic philosophy of shield design and is primarily a matter of individual commercial judgement.

These target accuracies are essentially subjectives. They are time and design dependent

THE ROLE OF TARGET ACCURACY REQUIREMENTS

The accuracy of practical shield design calculations is subject to uncertainties from the following factors:

1. source data,
2. modelling of the shield,
3. approximation in the method,
4. cross-section data,
5. conversion factors.

Their importance is discussed to some extent in (1). As the main interest of our meeting is focused to the relationship between target accuracy and cross section accuracy requirements, it is assumed that the uncertainties due to all other factors than that of the cross-section data are negligible. This seems to be a reasonable approach for well defined reactor benchmarks which are studied with the most advanced transport methods even if they are very expensive.

Data on required accuracies for practical shield design calculations have been collected by the authors and are presented in this paper. It is now necessary to assess whether the latest data files can satisfy the accuracy requirements. This is a task not only for the evaluators, but also for the benchmark experimentalists since it is their results analysed with the aid of sensitivity calculations which will provide the important

confirmation or otherwise of the accuracies quoted in the evaluations (2). The assessment should lead to definition of a request list for cross-sections for shielding as a function of the required target accuracies determined by the practical need.

There are two further reasons for well known target accuracy requirements:

- They are an important starting point for automated energy group boundary selection schemes designes to minimize the overall calculational effort in shield design, as was described by Oblow et al., in (3) and by one of the authors in (4).

- They permit the formulation of some recommendations concerning the preferred calculational methods for given targets. Shield design can then be optimized with respect to the invested work as Bouteau et al. proposed in (5).

THE PROBLEM OF ACCURACY INTERPRETATION

The term accuracy is commonly used in several ways (6). It may refer to

1. boundary values indicating the maximum permissible errors on the quantity of interest

2. probable or mean error defining the range for a certain confidence level

3. standard deviation (S.D.) of the probability distribution of the quantity of interest, or a multiple thereof.

The major part of the required target accuracies are quoted without any indication as to which definition is being used. In some few cases they may correspond to definition 1, specifying

asymetric accuracy limits of for example +50, -0 %. Or they are defined in units of S.D. in some cases (definition 3). Sometimes the confidence limits are given, too, indicating that normal probability distributions of the target quantities are supposed.

This is valid for most measured quantities like basic microscopic cross-section data, dose-rate, displacement rate and nuclear heating. But the major part of the required target quantities are calculated and are not normally distributed for the following reasons:

By a transport calculation the cross-section data are transformed into target quantities such as reaction rates for example. A transport solution for deep penetration problems is in general of exponential type. In this the cross-sections appear as multiplying factors or in the exponents. Therefore it is evident that the probability distribution of the reaction rate is quite different from that of a normal one.(Following the central limit theorems of statistics only the sum of a great number of arbitrarily distributed random variables is normally distributed). For relatively simple but mostly unrealistic problems the probability distribution and the confidence limit for 1 S.D. may be calculated with relatively little effort either analytically or by statistical variation of the cross-section data.

For the more general and realistic case with some hundred basic cross-section values the distribution can only be determined with a large amount of calculational effort by statistical variation of each cross-section value independently. Therefore the probability distribution of calculated quantities is unknown a priori, and it makes no sense to specify confidence limits and S.D. corresponding to those of a normal distribution. This would be equivalent to forcing symetry upon probability distributions, which are not necessarily symetric, leading to quoted errors of more than ±100 % for quantities that cannot get negative!

Unfortunately neither the shield designer nor the project staff realize the problem of accuracy and confidence limit interpretation; although they want to be sure that the calculated results stay within the required limits.

There seems to be a strong need for unifying the definition of accuracy and clarifying the possible confidence limits that can be required, if some problem-specific probability distributions have been determined. The few target accuracies specified in units of S.D. were normalized for the purpose of better comparison to 2 S.D. corresponding to a confidence limit of 95.5 % if the target quantities were normally distributed. All other accuracies correspond to the original requirements.

STATUS OF INFORMATION

Apart from the publication of Butler et al. in 1974 (7) concerning initial target accuracies for the British sodium cooled fast reactors, a compilation of actually required target accuracies did not exist to our knowledge until to the Paris meeting in 1975. There the authors published a preliminary list. It was the result of an inquiry on target accuracies circulated in central Europe to reactor and accelerator constructors, to users of power and test reactors and accelerators, to safety boards, and to radiation protection experts. 29 replies from 6 countries were received. Recent indications from the U.S. were also included and are presented in 3 different tables concerning

- power reactors (table 1)
- research and test reactors (table 2)
- irradiation facilities with isotopic and accelerator sources including transport containers for radioactive fission products (FP) (table 3).

SOME COMMENTS OF THE ACCURACIES

Power reactors (Table 1)

A1/J1 : These are respectively the English values mentioned above and the French values for pool-type sodium fast reactors. They are specified in terms of standard

deviation, on the assumption that normal design practice will acommodate 2 S.D.
Further they are considered as "initial" accuracies, recognizing that in the later stages of the design work higher accuracy may be needed for some key problems. In other design cases the accuracy of the calculation can be relaxed. Concerning J1, target No.1, the γ heating is considered as a core problem. An accuracy of ±2 % is required for the axially integrated power per assembly, leading to ±20% for the γ-heating for example.

B1 : The values of targets No.4, 6, and 7 are for a sodium loop fast reactor.

C1,K1,L1 : These values concern LWRs. The indicated accuracies for displacement rates actually relate to fast neutron fluxes above 0.1 MeV and not to displacement rates.

D1 : These values are for the HTGR.
The first value of target No.3 concerns the B_4C-α-heating, when the rods are introduced into the core. The second value concerns their Co-activation, if the rods are withdrawn. The values of target No.6 are dependent on the systems used and may be considerably relaxed, when the plateout is more important.

G1 : The accuracies concern particularly measurements. The extremely high relative accuracy of ±5 % of the target No.7 is required to detect time-dependent changes of loop activities.
The extremely high accuracies requested for target No.8 are perhaps unrealistic. They stem from the fact that in nuclear power plants the maximum personal dose is quickly achieved and the number of qualified personal for maintenance work is rather limited.
A well known radiation field can help to minimize the personal dose.

H1 includes the activation of pressure vessels.

I1 : Here target No.8 does not concern to dose rate outside the biological shield but in the gap between the pressure vessel and the biological shield. The required accuracy of 20 % is severe. On the other hand this region should remain accessible for personal to perform regular control examinations of the pressure vessel. The accuracy, that can be really achieved, will depend strongly upon the source configuration and on whether fuel or thermal shield are still in the vessel.

M1 is typical for safety boards asking for safety limits for design engineer targets. The accuracies requirements for dose rates depend upon their magnitude.

O1 : The requested target accuracies in the 2-6 % range are justified on the basis of actual core and fuel design considerations for LMFBR in the US because the actually attainable accuracies (10-20 % in heating and fission rates and 4-10 % in fast neutron environmental parameters such as fluence and displacement rates) lead to a high degree of conservation in the allowed operating power and a significant increase in breeding time.

Maximum/Minimum : These columns indicate the lowest/highest required accuracies per target. They represent a few extreme requirements.

Generally acceptable? : This column shows certain typical values which are most commonly required.
Numbers enclosed by brackets indicate that they are based on less than three requirements and may not be reconsidered as generally acceptable.

RESEARCH AND TEST REACTORS (Table 2)

A2 refers to a sodium cooled fast reactor for testing fuel elements and materials.

C2 concerns particularly collimators, shutters and parts of spectrometers.

D2 is for a swimming-pool reactor

E2 concerns a heavy water reactor with graphite reflector. It is one of the rare example, for which we obtained detailed comments.

IRRADIATION FACILITIES (Table 3)

C3 : The values for target No.4 concern the irradiation samples of Al, Fe and Cu with protons and neutrons up to 600 MeV.

The value for target No.6 is meant for a normal concrete shield.

D3 : The higher value is required for shielding of experiments. The lower value is required for the shielding of therapeutic γ- and Betatron-irradiation installations in hospitals.

E3 : Only gamma irradiation plants are concerned.

F3 : The values are meant for heavy metal shields. The accuracy may be questionable because the uncertainties in the radioactive sources, such as fuel elements or ion exchangers, are not very well known.

GENERALLY ACCEPTABLE ACCURACIES ?

We have already proposed considering as generally acceptable those values which appeared most often in the tables. Is this inter-

pretation meaningful in radiation shielding work? For target accuracies of power reactor shielding in table 1 sufficient material is available to calculate more arithmetic mean values. But the wide spread and the variable definition of accuracies makes the determination of precise mean values pointless. Accordingly we retain the above solution criteria for generally acceptable accuracies and condense them in the following table:

Target	Generally acceptable accuracy (%)
Radiation heating	10 - 20
LP instrument response	15
Displacement rates	10 - 30
Activation	30 - 50
External biological dose rate	factor 2

These accuracies are obviously subject to change as the requirements are better defined and more exactly stated. Exceptions to the general agreement with these mean values concerned particularly some severe accuracy request of 2-5 % for displacement rates and dose rates mentioned above.

For research and test reactors and irradiation facilities (tables 2 and 3) much less requirements are available. Therefore they cannot be representative nor generally acceptable apart from the targets γ-heating and biological dose rate.

FUTURE ASPECTS

This collection of required target accuracies represents further progress but it is not yet complete and the definition of accuracy is not evident in most requirements. The collection should be continued and coordinated in all interested countries

and unified to the same accuracy definition so as to arrive ultimately at generally accepted and clearly defined "mean" target accuracies. These would be very useful for the definition of request lists for basic shielding data and for the recommendation of properly chosen calculational methods and multigroup sets.

REFERENCE LIST

(1) A.F. Avery et al.
Target accuracies and sensitivity studies in the assessment of data requirements for practical shield design
(see ref. (4) please)

(2) J. Butler and R. Nicks
Specialist Meeting on Nuclear Data Uncertainties in Shielding Calculations
September 1975

(3) E. Oblow et al.,
Selection of group energy boundaries using sensitivity theory
Trans. ANS 17 (1) 1973

(4) V. Herrnberger
Application of Sensitivity Theory to Energy Group Structure Definition
Paper presented at the Specialists' Meeting on Sensitivity Studies and Shielding Benchmarks at Paris,
October 7-10, 1975

(5) F. Bouteau et al.,
Experiences intégrales de propagation de neutrons dans des milieux acier-sodium.
(see ref.(4) please)

(6) D.R. Marr et al.
Accomodation of uncertainties in shield design
WANL - TME - 1214

(7) J. Butler et al.
The UK Programme of DATAM Experiments on Energy-Deposition and Radiation Penetration
EACRP-L-100, May 1974

Table 1. Some Required Target Accuracies in Power Reactor Shielding

No.	Target		Required accuracies (%)																	
1	Gamma-ray heating in materials testing rigs	Without fissile heaters	±5	±5	±20	•	20	20-50	Factor 10	-	-	-	+20	-	Safety limits	-		Factor 10	±5	20
		With fissile heaters	20	20	-	-	-	10-20	-			20	+50		"	±20		+50 -20	+10 -2	20
2	Gamma-ray heating in	sub-assemblies *	±10	±10	20	±10	-	10-20		-	-	±20	+30	-	"	-		+30 -20	±10	10
		thermal shield	-	-	20	-	20	10-20				-	+30							20
		biol. shield	-	-	-	-	30	20-30	Factor 10			-	+20			±20		Factor 10		20
3	Control and shut-off rod heating		±10	±10	-	±10 (±15)	-	10-20	-	-	-	±10	+30	-	"			+30 -10	±10	10
4	Displacement rates in the	diagrid	±15	±50	±10	-	-	10-20	-	-	-	±20	-	-	"	-	2-6	±50	±2	10
		reflector region						20-30					+50							2
5	LP instrument response		±15	±15	-	±15	-	10-20	-	-	-	±20	-	±5	"	-		±10	±5	15
6	Displacement rates in the	supporting struct.	-	-			40	10-20	Factor 10	-	-	±20	+30	-	"	±10% nvt>1 MeV		Factor 10	±10	20
		int. shield system	±25	±(50-100)			30		-				+50					±100		30
7	Activation in the	heat exchangers	±50	Fact.2-3			30	20-50	±20 abs.	±50	-	Factor 3	+30	±20	50			Factor 3	±20	20
		cooling circuits	-	-	-	±25	30	10-20	± 5 relat.			-	+50			30		+50 -25		30
		turbines	-	-			50	20-50	-			-	+30			-		+50		30
8	External biological dose rate		Fact. 2-3	Factor 2-3	Factor 2-3	±50	40	20-30	± 5 abs. ± 2 relat.	±50	20	Factor 3	+30	-	20%, D>1 mrem/h Factor 2, D<1 "	Factor 2		Factor 3	±5	Factor 2
	Response from		A1	B1	C1	D1	E1	F1	G1	H1	I1	J1	K1	L1	M1	N1	O1	Minimum	Maximum	General acc. Aerab.

* sub-assemblies including barrels too.

Table 2. Some Required Target Accuracies in Research and Test Reactor Shielding

No.	Target		Required accuracies (%)							
1	Gamma-ray heating in materials testing rigs	Without fissile heaters	-	± 10	10	10	(C-mod.: 50)	50	±10	10
		With fissile heaters			-		10-20 (H_2O-mod ($q>70$ W/cm² ±10))	20		
2	Gamma-rig heating in	sub-assemblies	20	± 10	-	20				
		thermal shields	-	-	-	20	10-20	20	10	10
		biological shields	-	-	10	20	20			
3	Control and shut-off rod heating		30	-	-	10	-	30	10	(20)
4	Displacements rates in	diagrid	30	± 20	-		-	30	±20	(20)
		reflector region	-					±20		
5	LP instrument response		-	-	-	<10	±20 in watt region	±20	<10	(10)
6	Displacements	supporting structures		± 20	-			±20	±20	(20)
		int. shield system	30	-				30	30	(30)
7	Activation in the	sec.heat exchanger	50				no accuracy	50	50	(50)
		cooling circuits	-	-	-		but	-	-	-
		turbine	-				upper limit	-	-	-
8	External biological dose rate		Factor 2-3	± 50	10	20	Factor 2 in mrem/h-region	Factor 3	10	Factor 2
	Response from		A2	B2	C2	D2	E2	Minimum	Maximum	Generally acceptable?

Table 3. Some Required Target Accuracies (%) in Irradiation Plant Shielding

No.	Target		Accelerator				Isotopic source	F.P. transport container	Radiation waste installation	Medical irradiation plants			
1'	Gamma ray heating in structures		-	-	-	-	± 20	-	-	-	±20	±20	(20)
2'	Heating by particle beams	targets	10	-	-	-	-	-	-	-	10	10	(10)
		structures											
3'	Displacement rates in	targets	-	20	± 50	-	-	-	-	-	±50	±50	(50)
		structures		-	-						-	-	-
4'	Activation of	heat exchangers	-	20	-	-	-	-	-	-	20	20	(20-30)
		circuits			± 30						±30		
5'	External biological dose rate		±20 % Factor 2-3	20	± 10	{+ 50 - 0 / + 25 - 0}	± 10	-	-	≤ Factor 2	Factor 3	+10	20% - Factor 2
6'	Thickness of biological shield		-	-	-	-	-	± 3-5	10-20	-	±20	±3-5	(5-10)
	Response from		A3	B3	C3	D3	E3	F3	G3	H3	Minimum	Maximum	Generally accepted

TARGET ACCURACIES AND SENSITIVITY STUDIES IN THE ASSESSMENT OF DATA REQUIREMENTS FOR PRACTICAL SHIELD DESIGN

A F Avery
S D Lympany *

Radiation Physics and Shielding Group
Reactor Physics Division
AEE Winfrith Dorset

* Imperial College of Science and Technology, London

Sensitivity calculations are described which relate the accuracy of data requirements to the target accuracies specified by designers for various quantities in three practical shields. The importance of partial cross-sections and the need for evaluators to assign accuracies to data in the libraries are both underlined as a result of these studies.

1. Target Accuracies

The aim of a shield designer is to achieve levels of gamma-ray and neutron fluxes which are acceptable in their production of such effects as radiation damage, nuclear heating, instrument response, material activation and biological dose-rate. The calculations involved in design work are subject to uncertainties from the following factors:-

(a) Source data,
(b) Modelling of the shield,
(c) Approximations in the method,
(d) Cross-section data, and
(e) The conversion factors relating flux levels to the effects of interest.

The designer must assess the accuracy of his calculations and make allowances for them when specifying his final shield configuration. These assessments are made from the evidence of comparisons between predictions and experiment, from the accuracies estimated from cross-sections and from the possible errors in source distributions, using repeated calculations or sensitivity studies to predict their effect, and from supporting calculations which indicate the uncertainties due to modelling or method approximations. Having obtained an estimate of the accuracies of his calculations the designer must then make allowances for them. Usually this means including safety margins which increase his confidence that the target levels will be attained. Alternatively he can admit the possibility that the levels may not be reached and will be prepared to accept the consequent restrictions or make provisions for the shield to be changed during the testing and commissioning stage. The course which he adopts will depend upon the penalties involved in additional costs either directly in manufacture or indirectly in reduced performance and operational limitations. In most cases, however, subsequent modification will not be feasible and restricted operation will be unacceptable, so that the shield will have to be built to meet the specified target levels and will be made more expensive by the addition of safety margins.

The extra costs due to uncertainties in shielding calculations vary markedly from reactor to reactor. For example if the biological dose-rate is dominated by gamma-rays, as frequently occurs in a thick shield of light concrete then a large uncertainty in the neutron dose-rate can be accepted with no need for extra concrete. Alternatively the cost of including safety margins may be trivial. If in the case of the light concrete shield cited above there were an uncertainty of a factor of 2 in the gamma-ray dose-rate then this could be covered by adding a further 120 mm of concrete, and this could typically be less than 6% of the original shield thickness. In these cases there is little incentive to reduce the errors in the design calculations.

Other situations arise, however, in which the costs of uncertainties in shielding calculations produce severe penalties. If in a fast reactor, for example, the length of the fuel sub-assemblies is increased to provide material to shield the support grid from excessive radiation damage then the effects of uncertainties are reflected not only in the extra costs of the sub-assemblies but also in pumping power and the extra capacity needed in the fuel handling route including transport falsks. Similarly when internal shielding affects the diameter of the pressure vessel be it steel or concrete then the costs become large. Other situations arise where the uncertainties in shielding calculations can influence decisions about the acceptability of a certain engineering situation and this may necessitate the adoption of a much more expensive alternative. Such an example could arise for instance, in nuclear instrumentation monitoring power levels in a fast reactor where the site with convenient access might give borderline values for the flux conditions, whilst an alternative arrangement giving better levels would lead to much more expensive engineering for access and cooling of the chambers. In these situations there is an incentive to improve the accuracy of calculations in order to reduce the costs of allowing for uncertainties.

For many years in shielding calculations the accuracy was limited by approximations made in the method and in the representation of the geometry. The cross-section data were frequently chosen empirically to fit predictions of the method to measurements made in an experimental array. With the increase in the use of multi-dimensional Monte Carlo methods and two dimensional discrete co-ordinate codes the errors due to method and modelling can be reduced particularly in the important situations where high computing costs can be justified. The errors in sources are usually small, especially for neutrons where the distribution of fissions is accurately obtained for predictions of reactivity and power output, so that the pressure for improvement falls upon the cross-section data and conversion factors listed as items (d) and (e) above. The accuracy of conversion factors is another situation-dependent quantity. For biological dose-rate the acceptable levels are coupled with well-defined flux-to-dose conversion factors. For radiation damage the relationship between flux levels and their effects, such as embrittlement or swelling, is not always well known. In the case of nuclear heating the conversion factors from flux to heat deposition are well known, but frequently the required design condition is specified as a temperature distribution and this further 'conversion factor' includes uncertainties in heat transfer and diffusion calculations. The incentive to improve the other phases of the calculation is reduced if the conversion factors are inaccurately known.

Thus the advantage to be gained by improving the accuracy of any stage in the calculation of radiation penetration depends very much upon the shield situation and the output quantity of interest. One way in which the designer can express his assessment of the benefits to be gained from a reduction in uncertainties is to specify a target accuracy for the penetration calculation.

It is convenient for the calculator that this target accuracy should cover only stages (a) - (d) listed above since item (e) usually involves disciplines other than radiation transport. The uncertainty in (e) will, however, be taken into account when the designer specifies the target accuracy so that the two will be consistent, and fluxes will not be requested with an accuracy far in excess of that of the conversion factors. The assessment is thus a subjective judgement based upon the possible cost savings, the accuracy with which the results can be applied and to some extent an opinion of what improvement is reasonable. (If it were derived solely on the needs of the designer of the reactor the target accuracy would be zero uncertainty since this would give minimum additional costs. On the other hand it is not reasonable to attempt a strict cost-benefit analysis since improvements to methods and data apply to many reactors and to disciplines other than shield design.) The specification of target accuracies can then be translated into a requirement for more accurate cross-sections if examination of the uncertainties from source data, model and method approximations indicate that a target accuracy could be met by such an improvement.

2. Sensitivity Calculations for Total Cross-Sections

Sensitivity calculations give the changes in predictions of a particular effect following from changes in the cross-sections. A repeat calculation with a changed cross-section is the most straightforward way of determining such a sensitivity. Perturbation theory provides a much more powerful approach since the sensitivity of a particular data-set to small changes in any of its cross-section parameters can be determined. The code SWANLAKE(1) has been written by Bartine et al to perform such calculations in one dimension in conjunction with the multigroup discrete ordinates programme ANISN(2). Correlated tracking Monte Carlo codes have also been proposed for sensitivity calculations in complicated geometries(3). Such calculations can be used together with estimated accuracies of cross-sections in order to assess the errors in prediction of a particular response which come from data uncertainties. Conversely they can be used to define the conditions governing the accuracy of cross-section data which will give a specified accuracy in the predicted response. Thus sensitivity calculations can be used to interpret target accuracies in terms of data requirements.

As examples of the application of sensitivity calculations in the assessment of data needs for neutrons, three situations have been examined for total cross-section dependence with the SWANLAKE code. The first was a typical PWR with three iron thermal shields in front of the pressure vessel which in turn was surrounded by a large tank of water. The dimensions are given in Table I. The quantities of interest here are radiation damage to the inner surface of the pressure vessel and neutron capture at its outer surface since the latter is the dominant source for gamma-ray dose-rate outside of the shield. The 33 group condensation of the EURLIB library based on ENDF/B3 was used. Adjoint ANISN calculations were performed for each of these quantities and SWANLAKE was applied to the results togetherwith those from the forward ANISN calculations to provide the sensitivities. It is possible with SWANLAKE to assess the effects of partial cross-section changes with various constraints on other parameters. The results listed in Table III are for the effect of a 1% increase in all partial cross-sections which is thus a 1% increase in the total cross-section also. In these two cases the SWANLAKE sensitivity of the iron data in the column headed 'Fe' does not include the effects of cross-section

changes on the conversion factors for generating displacement and capture rates. Thus if the reaction rate is given by

$$R = \sum_i \phi_i \times f(\sigma_i) \qquad 2.1$$

Where ϕ_i are the group fluxes, f (σ_i) are the response functions and σ_i the cross-section, then

$$\frac{\partial R}{\partial \sigma_j} = \sum_i f(\sigma_i) \frac{\partial \phi_i}{\partial \sigma_j} + \phi_j \frac{\partial f}{\partial \sigma_j} \qquad 2.2$$

$$\frac{\partial R}{\partial \sigma_j} \frac{\sigma_j}{R} = \frac{\sigma_j}{R} \sum_i f(\sigma_i) \frac{\partial \phi_i}{\partial \sigma_j} + \frac{\sigma_j \phi_j}{R} \frac{\partial f}{\partial \sigma_j} \qquad 2.3$$

The first term on the RHS is that calculated by SWANLAKE and the second is the factor which must be added to take account of the sensitivity of the reaction rate to changes in the response function. For both capture and displacement rates when the partial cross-sections are proportionally increased the response function is linearly related to the total cross-section and therefore the additional term becomes the fraction of the response due to the j^{th} group. This extra term is added to the sensitivities in the column headed 'Fe*' in Table III.

The configuration of Table I was also investigated when the water shield outside of the pressure vessel was replaced by an iron-water mixture. In this case the gamma-ray attenuation properties are improved and neutron dose at the outside of the shield becomes a significant quantity. The sensitivities of this quantity to changes in the group total cross-section with corresponding increases in the partials are shown in Table IV.

The second configuration examined was a fuel transport flask in which the bulk of the shield was iron to attenuate the fission product gamma-rays. A 76.2 mm water jacket surrounds the iron in order to reduce the dose-rate due to neutrons emitted from spontaneous fission and alpha-n reactions due to Curium decay. The configuration is given in Table II. The neutron quantities of interest are the external dose-rate and the capture rate in the tank wall as significant gamma-ray dose-rates arise from this source. The adjoint ANISN cases were run for these two response functions and the sensitivities are listed in Table V again for 1% increases in all partial cross-sections.

As might be expected the sums of the sensitivities for each response in Tables III, IV and V increase with increasing attenuation. Of more interest is the variation of the important energy range. For capture rates the thermal cross-sections are very important although the sensitivity to the iron value is reduced or even reversed in sign by the inclusion of the response function change. For the flask shield with its small amount of moderator it is the intermediate energy cross-sections which influence the results most strongly. For the damage and neutron capture rates in the pressure vessel of the PWR shield the important range is transferred to the energy group around 3 MeV both by the presence of moderator and by the nature of the

response functions. The similarity of the sensitivities for both quantities reflects the fact that the capture rates at the outer surface of the pressure vessel are determined by fast neutrons incident on its inner surface. The problem with the greatest attenuation is the dose outside of the iron-water shield for which the sensitivities are given in Table IV. The feature of these results is the dominance of the energy range above 8 MeV. Only 20% of the leakage dose is due to neutrons at these high energies but the large sensitivity indicates that many of the neutrons which escape at lower energies will have penetrated through much of the shield in the higher energy range.

3. Data Requirements

The requirements for improvements in nuclear data arise from the identification of shortcomings in the available cross-sections. These in turn result from the specification of target accuracies. For the five response functions for which sensitivity calculations were carried out, a set of target accuracies can be postulated. These are ± 20% on pressure vessel damage and ± 50% for neutron dose-rates or for the sources leading to external gamma-ray dose-rates. It is assumed that the errors due to source, method and modelling are insignificant for the present exercise. The adequacy of the cross-section sets can then be assessed if one takes the assigned accuracies. These are often very difficult to obtain from evaluations, although this situation should be improved in future with the inclusion of error estimates in the data files. The error in the hydrogen cross-section has been assumed to be negligible. The accuracies of the total cross-sections for oxygen and iron which were suggested by Schmidt[4] in his evaluation have been adopted to illustrate their application, although other evaluations were used in the compilation of the ENDF/B3 files from which the EURLIB library was prepared. The accuracies of the total cross-section of iron were estimated to be better than 4% below 1 KeV, 5% from 1-400 KeV, better than 5% for 400 KeV to 1.5 MeV and 5% for the range 1.5-10 MeV. Accordingly 3% is adopted for the lower range and 4% for 1-400 KeV with 5% accuracy elsewhere. For oxygen the values taken from reference 4 were 3% for 0-1 KeV, 15% for 1-300 KeV, 4% for 300 KeV to 3.4 MeV and 5% for 3.4-10 MeV. (The difficulties of obtaining values for the accuracies can be appreciated and their scarcity understood when one is faced with several measurements which are discrepant by amounts exceeding many standard deviations as estimated by the measurers In this situation there is a doubt about the likely errors and it is one of the functions of benchmark experiments to check that the evaluators assignments of accuracies are consistent with any differences observed between integral measurements and calculations.)

If the accuracy for a particular group cross-section is multiplied by the corresponding sensitivity then the resulting error in the design calculation can be estimated. If the errors in the group cross-sections were independent then their combined effect could be obtained by deriving the square root of the sum of the squares of the individual contributions. In practice it is likely that errors in cross-sections will be positively correlated since the shape is usually better known than the absolute values. The effect of the individual errors are therefore added by a straightforward summation which should be a pessimistic assumption when the signs of the sensitivities are similar. Occasionally the signs change with energy range and in these cases the sum of the moduli is taken to ensure pessimism again, although this is less justifiable. Such a situation occurs infrequently, however, and the effect is usually unimportant.

The result of applying this procedure for the examples chosen above together with the assumed accuracies gives the following results:-

(a) PWR Shield Radiation Damage. Oxygen ± 11% Iron ± 9% Total ± 20%

(b) PWR Shield Neutron Capture. Oxygen ± 11% Iron ± 15% Total ± 26%

(c) Iron/Water Shield Neutron Dose-Rate. Oxygen ± 17% Iron ± 61% Total ± 78%

(d) Flask Shield Neutron Capture. Oxygen ± 1% Iron ± 8% Total ± 9%

(e) Flask Shield Neutron Dose-Rate. Oxygen ± 3% Iron ± 12% Total ± 15%

It can be seen that the only case which does not meet the target accuracy is the neutron dose-rate outside of the iron-water shield. This is as might be expected since the attenuation is largest. The flask shield has a considerable thickness of iron but as the penetration is at intermediate energies where the migration lengths are long one finds that the sensitivities are small. (If the thickness of the water shield were to be increased then the spectrum would be weighted toward the higher energies and the attenuation and the sensitivities would be much greater for iron.)

For the case where the target accuracy is not met then there is a requirement for improved data. The equation which must be satisfied is

$$\sum_i U_i \xi_i \leq \xi_T \qquad 3.1$$

where U_i is the sensitivity of the response to the cross-section for the i^{th} parameter

ξ_i is the accuracy of the cross-section for the i^{th} parameter, and

ξ_T is the target accuracy.

The summation over i is taken for all the materials and cross-sections under consideration.

This equation needs the addition of constraints before it can be solved. One simple approach would be to make all values of ξ_i equal

Thus

$$\xi_i = \frac{\xi_T}{\sum_i U_i} \qquad 3.2$$

This expression can however, lead to values of ξ_i which are greater than the current accuracy q_i, with an unnecessary penalty resulting on other values of ξ_i. If the expression is rewritten in terms of changes to the cross-section, then

$$c_i = q_i - \xi_i \qquad 3.3$$

$$\sum_i U_i c_i = \sum_i U_i q_i - \sum_i U_i \xi_i = q_T - \xi_T = c_T \qquad 3.4$$

where C_i is the change in accuracy of the i^{th} parameter

q_i is the current accuracy of the i^{th} parameter

and the subscript T indicates the summations.

Then if the change is constant for all parameters

$$C_i = \frac{C_T}{\sum U_i} \qquad 3.5$$

This expression will give the required positive values of C_i but it will lead to improvements in the cross-section which have little influence on the response function and it can be improved if C_i is made proportional to U_i so that

$$C_i = K U_i \qquad 3.6$$

where K is a constant of proportionality leading to

$$C_i = \frac{C_T U_i}{\sum U_i^2} \qquad 3.7$$

This approach can be further modified to take account of the present accuracy and the difficulty of measurement by adding extra factors so that the fractional change is given by

$$\frac{C_i}{q_i} = \frac{K U_i}{\eta_i} \qquad 3.8$$

Where η_i is an index of the difficulty of measurement. This would concentrate the improvements in the parameters which are most easy to measure. If, however, one adopts q_i as an estimate of η_i, which is reasonable especially when it is based upon the results of many experimentalists, then the expression for C_i again reduces to equation 3.6.

More generally this can be expressed as finding a solution to equation 3.1 with the constraint that

$$\sum_i C_i^2 \quad \text{is a minimum} \qquad 3.9$$

This approach can be extended to the situation where there is more than one response function for which cross-sections require improvement, and thus the values of C_i will simultaneously satisfy several equations similar to 3.1.

The above equations have been applied to the iron-water mixture and the resulting requirements for improvements in total cross-sections are listed in Table VI. It can be seen that the use of equation 3.7 leads to the most reasonable of the requirements obtained by analysis. These however, can be modified by further examination. The improvements required for oxygen are seen to be small and therefore it would be reasonable to accept the current accuracy of the oxygen cross-section and ask for a slightly greater improvement in the iron data. Similarly the iron data are required to a very high accuracy

over the narrow energy range 8.19 - 10.0 MeV for this particular problem. For general application it would be preferable to spread the improvement over a slightly wider energy range. Examination of the results in Table VI suggests that uniform improvements in the iron data from 8 MeV to 15 MeV with an accuracy requirement of $\pm$ 2% would be the best way of meeting the target accuracy in the dose-rate.

Thus although analysis can indicate the ways in which the uncertainties in the data need to be reduced, it will frequently be necessary to modify the analytic results in the preparation of data request lists.

In the cases examined above only the accuracies of group averaged total cross-sections were considered. There is another step needed to relate the group averaged value to the differential data needs. The adequacy of the averaging process is a feature of the method and no error was assumed to arise from this cause. It is prudent to note, however, that the difference between averaging with $1/E$ and $1/E\mathcal{L}_T$ weighting can lead to differences in excess of 50% for the group averaged cross-sections in the KeV energy range of the 33 group scheme and that neither assumption is correct for shielding calculations. Fortunately at the important high energies the differences with the two weightings are less than 0.1% so that the effect is negligible but there would obviously be little to be gained in improving the differential cross-section if the energy treatment in the method were to introduce a much greater uncertainty. The process of averaging a cross-section might be expected to reduce the uncertainty but this is not true for a smoothly varying parameter when the shape is well known and the error is most probably in its absolute value. For energy ranges with resonances the errors on the mean will be less than those of the maximum and minimum of the fine structure, but in this case uncertainty will probably be introduced by the weighing function used in the averaging process. Thus there is no point in requesting very well defined structures in cross-section unless the method is capable of treating them, and it is unlikely that any reduction in uncertainty can be claimed for the group-averaging process.

4. Sensitivity Analysis and Data Requirements for Partial Cross-Sections

The data requirements which were derived in Section 3 were for improvements in the total cross-section only. This is a simplification since the uncertainties in the division of a total cross-section between its contributing processes may be of more significance. The sensitivities of the neutron dose-rate outside of the iron/water shield to the partial cross-sections are given in Table VII for group 3 which was the most important. The sensitivity of the cross-sections listed in the table are not compensated by changes in other cross-sections, except for the values for the total elastic and the total inelastic scatter which do include the effects of corresponding changes in the transfer cross-sections. Thus the sensitivity due to the total cross-sections is for a change which no alteration to the transfer cross-section and is thus equivalent to a large increase in the absorption. The effect of an increase in the total cross-section with the partials remaining in proportion is obtained by adding the sensitivities for capture, elastic scatter and inelastic scatter giving the value of -4.01 listed previously in Table IV.

The angular expansion coefficients can change independently since this can be interpreted as a different angular distribution of scatter with no change in the scattering cross-section. In the case of elastic scatter the energy loss laws depend upon the angular distribution so that there

should also be a change in the transfer cross-sections. More explicitly the energy loss is proportional to $(1 - \bar{\mu})$ where $\bar{\mu}$ is the mean cosine of scatter in the laboratory system. For group 3, however, 97% of the elastically scattered neutrons remain within the group and thus one can consider small changes to $\bar{\mu}$ without altering the transfer cross-sections. The effect of changes in the coefficients above P_1 is less, but still significant although they are omitted from the subsequent examination.

In practice the elastic scatter cross-section is equated to the difference between the total and the non-elastic cross-sections. Thus an increase of 1% in the latter is compensated by an 0.8% decrease in the former. The effect of uncertainty in the non-elastic cross-section is thus the sum of the sensitivities of inelastic scatter and capture less the sensitivity to elastic scatter multiplied by 0.8 giving -2.573. This is obviously less than the sensitivity of the total cross-section but the contribution from uncertainties in the partials may have a considerable influence. Thus if the total and non-elastic scatter cross-sections and the mean cosine of elastic scatter are treated as independent parameters then their combined effect on the required response is given by the square root of the sum of the squares of the individual constributions. The error in the non-elastic cross-section and the mean cosine are given by Schmidt[4] as $\pm$ 10%, and $\pm$ 5% respectively, and the combined effect is given by

$$U_q = \sqrt{U_1^2 q_1^2 + U_2^2 q_2^2 + U_3^2 q_3^2}$$

where subscripts 1 and 2 and 3 refer to total, P_0 inelastic, and P_1 elastic parameters respectively. As

$U_1 = -4.01 \quad q_1 = \pm 5\%$
$U_2 = -2.57 \quad q_2 = \pm 10\%$
$U_3 = 1.27 \quad q_3 = \pm 5\%$

the calculated uncertainty due to group 3 parameters is $\pm$ 33.2% compared with the contribution of 20% from the total cross-section alone. The uncertainty arising from the required accuracy of $\pm$ 2% in the total cross-section is $\pm$ 8% in the response. This obviously cannot be met unless the accuracy of the partial cross-sections is also improved. If one postulates that the factor by which the uncertainty is reduced should be the same for each parameter then the required accuracy is $\pm$ 1.2% for the total cross-section and the mean cosine with $\pm$ 2.4% for the non-elastic. Thus consideration of the partial cross-sections can lead to more stringent requirements for the accuracy of data. (The above figures should not be taken as definite needs since the target accuracy of 50% in the neutron dose-rate is quoted as an example which might not necessarily be economically defensible.)

The strong sensitivity of group 3 to changes in the non-elastic cross-sections is not found in all cases. If the parameters for group 8 which is the most important group for the PWR neutron capture are examined then the cross-section and sensitivities are as follows:-

Parameter	Cross-Section (Barns/Atom)	Sensitivity
Absorption	4.8, -3	-2.41, -3
Total	3.37	-0.326
Elastic	2.40	-0.179
Inelastic	0.97	-0.147

In this case if the non-elastic is increased by 1% with a constant total cross-section then the elastic parameter is decreased by 0.4%. The corresponding sensitivity is thus -0.088 which is only 27% of that of the total cross-section compared with the value of 64% found for group 3.

However group 3 does show the need to examine the effects of partial cross-sections and this is usually difficult to achieve as transfer cross-sections in processed libraries are the combination of elastic and inelastic events. The investigation does also stress again the need for accuracy assessments of the data in the files.

5. Summary

The incentive to improve the accuracy of shielding calculations can be expressed subjectively by the designer in terms of target accuracies. By means of sensitivity calculations these can be related to requirements for improvement in cross-section data, but it is essential that partial cross-sections should be included in these considerations. Possible ways of performing these steps have been examined, but it is suggested that any analytic method needs to be supplemented by considerations of the practical implications when preparing a request list for future differential measurements. It is necessary in studies of this type to have accuracy assessments for the cross-sections available in the data files, and it is to be hoped that this situation will be improved in future. There will also be a need to support the assignment of accuracies by measurements in benchmark experiments to check the evaluators assessment. The need for partial cross-sections suggests that data sets will have to be expanded to include them if calculators are to be able to assess the effects of data uncertainties. Finally it is prudent to stress that the error in cross-section data is only one of many sources of inaccuracies and the shield designer must be confident that any requests for improved data are consistent with the uncertainties arising from the other causes.

REFERENCES

1. Bartine D. E., Mynatt F. R and Oblow E M. SWANLAKE. A Computer Code Utilising ANISN Radiation Transport Calculations for Cross-Section Sensitivity Analysis. ORNL-TM-3809.

2. Engle W. W. A Users' Manual for ANISN. K-1693.

3. Nicks R and Perlini G. Report of a Restricted Meeting on Iron Shielding Benchmark Experiments held at Winfrith on 24 and 25 April 1975. ESIS Newsletter No 14, Ispra July 1975.

4. Schmidt J. J. Neutron Cross-Sections for Fast Reactor Materials. Part 1: Evaluation. KFK 120 (EANDC-E-35-U).

TABLE I

PWR Shield Configuration

Region	Material	Thickness (mm)
1	Core	221.0
2	Water	381.0
3	Iron	19.05
4	Water	25.40
5	Iron	25.40
6	Water	25.40
7	Iron	76.20
8	Water	25.40
9	Iron (P.V.)	253.20
10*	Water	900.00
11	Iron	25.4

*For the second example region 10 was changed to an iron/water mixture of 40%/60% by volume.

TABLE II

Transport Flask Configuration

Region	Material	Thickness (mm)
1	Fuel Element	150.0
2	Iron	490.0
3	Water	76.2
4	Iron	25.4

TABLE III

Sensitivities in PWR Shield

(Percentage change in P.V. Damage Rate and Neutron Capture Rate in Outer Region of P.V. for 1% Change in Group Averaged Total Cross-Section and Partials.)

Group	Upper Energy MeV	Pressure Vessel Damage				Neutron Capture in Pressure Vessel			
		H	O	Fe	Fe*	H	O	Fe	Fe*
1	14.92	-0.025	-0.025	-0.009	-0.009	-0.029	-0.028	-0.014	-0.014
2	12.21	-0.092	-0.073	-0.024	-0.023	-0.098	-0.078	-0.035	-0.035
3	10.00	-0.378	-0.217	-0.090	-0.085	-0.392	-0.224	-0.120	-0.120
4	8.19	-0.626	-0.289	-0.130	-0.125	-0.643	-0.296	-0.160	-0.160
5	6.70	-1.074	-0.365	-0.200	-0.192	-1.092	-0.370	-0.241	-0.241
6	5.49	-1.082	-0.358	-0.222	-0.213	-1.097	-0.364	-0.254	-0.254
7	4.49	-0.702	-0.336	-0.214	-0.189	-0.684	-0.332	-0.211	-0.211
8	3.33	-1.325	-0.256	-0.390	-0.295	-1.248	-0.248	-0.326	-0.326
9	2.35	-0.410	-0.096	-0.162	-0.114	-0.424	-0.101	-0.187	-0.187
10	1.83	-0.226	-0.054	-0.100	-0.063	-0.240	-0.060	-0.146	-0.146
11	1.50	-0.196	-0.055	-0.109	-0.045	-0.187	-0.054	-0.170	-0.170
12	1.11	-0.139	-0.037	-0.069	-0.009	-0.161	-0.046	-0.148	-0 148
13	8.21,-1	-0.174	-0.029	-0.010	0.063	-0.158	-0.031	-0.122	-0.122
14	6.08,-1	-0.332	-0.070	-0.042	0.240	-0.180	-0.040	-0.178	-0.176
15	3.02,-1	-0.259	-0.017	-0.028	0.180	-0.160	-0.008	-0.178	-0.145
16	1.11,-1	-0.039	-0.002	-0.004	0.025	-0.039	-	-0.054	-0.051
17	6.74,-2	-0.053	-0.002	-0.013	0.031	-0.038	0.003	-0.038	-0.037
18	3.18,-2	-0.003	-	-0.002	0.001	-0.022	0.001	-0.001	-0.001
19	2.61,-2	-0.001	-	-0.001	0.002	-0.020	-	-0.066	-0.065
20	2.19,-2	-	-	-	-	-0.039	0.002	-0.083	-0.083
21	1.17,-2	-	-	-	-	0.012	0.003	-0.018	-0.017
22	7.10,-3	-	-	-	-	0.012	0.003	-0.024	-0.024
23	4.31,-3	-	-	-	-	0.021	0.004	-0.038	-0.038
24	2.03,-3	-	-	-	-	0.024	0.004	-0.033	-0.033
25	9.61,-4	-	-	-	-	0.027	0.004	-0.024	-0.024
26	4.54,-4	-	-	-	-	0.029	0.004	-0.023	-0.021
27	2.14,-4	-	-	-	-	0.030	0.004	-0.023	-0.020
28	1.01,-4	-	-	-	-	0.050	0.006	-0.042	-0.034
29	2.90,-5	-	-	-	-	0.049	0.006	-0.042	-0.027
30	8.32,-6	-	-	-	-	0.035	0.004	-0.029	-0.011
31	3.06,-6	-	-	-	-	0.028	0.004	-0.024	-0.002
32	1.13,-6	-	-	-	-	0.021	0.002	-0.020	0.016
33	4.17,-7	-	-	-	-	-0.860	-0.015	-0.295	0.577
Totals		-7.14	-2.28	-1.81	-0.81	-7.48	-2.24	-3.36	-2.36

Fe* = Iron sensitivities with sensitivity of response function included

TABLE IV

Sensitivities in PWR Shield with Iron/Water Mixture

Percentage change in dose-rate at shield boundary for a 1% change in group-averaged total cross-section and its partials

Group	Upper Energy Limit (MeV)	H	O	Fe
1	14.92	-0.903	-0.812	-2.377
2	12.21	-1.238	-0.872	-2.689
3	10.00	-1.980	-1.036	-4.011
4	8.19	-0.625	-0.271	-1.175
5	6.70	-0.558	-0.183	-0.908
6	5.49	-0.255	-0.080	-0.373
7	4.49	-0.151	-0.063	-0.187
8	3.33	-0.260	-0.041	-0.213
9	2.35	-0.130	-0.025	-0.084
10	1.83	-0.090	-0.019	-0.050
11	1.50	-0.076	-0.019	-0.046
12	1.11	-0.059	-0.016	-0.025
13	8.21,-1	-0.050	-0.010	-0.014
14	6.08,-1	-0.045	-0.011	-0.012
15	3.02,-1	-0.027	-0.003	-0.006
16	1.11,-1	-0.005	-	-0.001
17	6.74,-2	-0.003	-	-0.001
18	3.18,-2	-	-	-
19	2.61,-2	-0.001	-	-
20	2.19,-2	-0.002	-	-
21	1.17,-2	-	-	-
22	7.10,-3	-	-	-
23	4.31,-3	-	-	-
24	2.03,-3	-	-	-
25	9.61,-4	-	-	-
26	4.54,-4	-	-	-
27	2.14,-4	-	-	-
28	1.01,-4	-0.001	-	-
29	2.90,-5	-0.001	-	-
30	8.32,-6	-0.001	-	-
31	3.06,-6	-0.001	-	-
32	1.13,-6	-	-	-
33	4.17,-7	-0.004	-	-0.008
Totals		-6.47	-3.46	-12.23

TABLE V

Sensitivities in Flask Shield

(Percentage changes in neutron dose rate and capture rate in the tank wall for a 1% change in the group averaged total cross-section and its partials.)

Group	Upper Energy Limit (MeV)	Capture Rate in Tank Wall				External Neutron Dose		
		H	O	Fe	Fe*	H	O	Fe
1	14.92	-	-	-	-	-	-	-
2	12.21	-	-	-	-	-	-	-
3	10.00	-	-	-	-	-	-	-
4	8.19	-	-	-	-	-	-	-0.002
5	6.70	-	-	-	-	-	-	-0.004
6	5.49	-	-	-	-	-	-	-0.005
7	4.49	-	-	-0.003	-0.003	-	-	-0.012
8	3.33	-	-	-0.008	-0.008	-	-	-0.032
9	2.35	-	-	-0.010	-0.010	-0.002	-	-0.039
10	1.83	-	-	-0.012	-0.012	-0.004	-0.001	-0.055
11	1.50	-	-	-0.022	-0.022	-0.008	-0.003	-0.068
12	1.11	-	-	-0.039	-0.039	-0.027	-0.011	-0.150
13	8.21,-1	-	-	-0.085	-0.085	-0.151	-0.038	-0.380
14	6.08,-1	-0.007	-0.006	-0.268	-0.267	-0.379	-0.130	-0.531
15	3.02,-1	-0.034	-0.011	-0.323	-0.323	-0.361	-0.066	-0.421
16	1.11,-1	-0.017	-0.004	-0.096	-0.096	-0.073	-0.011	-0.077
17	6.74,-2	-0.022	-0.004	-0.050	-0.050	-0.069	-0.010	-0.045
18	3.18,-2	-0.004	-0.001	-0.004	-0.004	-0.011	-0.001	-0.002
19	2.61,-2	-0.055	-0.010	-0.390	-0.390	-0.059	-0.009	-0.262
20	2.19,-2	-0.065	-0.011	-0.226	-0.226	-0.084	-0.012	-0.150
21	1.17,-2	-0.039	-0.007	-0.017	-0.016	-0.048	-0.007	-0.012
22	7.10,-3	-0.034	-0.005	-0.021	-0.021	-0.041	-0.008	-0.014
23	4.31,-3	-0.050	-0.008	-0.027	-0.026	-0.061	-0.008	-0.019
24	2.03,-3	-0.049	-0.007	-0.016	-0.015	-0.059	-0.007	-0.012
25	9.61,-4	-0.048	-0.007	-0.010	-0.010	-0.057	-0.007	-0.008
26	4.54,-4	-0.048	-0.007	-0.007	-0.007	-0.056	-0.007	-0.007
27	2.14,-4	-0.048	-0.007	-0.006	-0.006	-0.055	-0.006	-0.007
28	1.01,-4	-0.080	-0.011	-0.008	-0.006	-0.091	-0.010	-0.012
29	2.90,-5	-0.082	-0.011	-0.005	-0.002	-0.088	-0.009	-0.013
30	8.32,-6	-0.067	-0.009	-0.003	0.002	-0.065	-0.007	-0.011
31	3.06,-6	-0.068	-0.008	-0.005	0.005	-0.060	-0.006	-0.013
32	1.13,-6	-0.069	-0.006	-0.012	0.005	-0.051	-0.004	-0.015
33	4.17,-7	-1.098	-0.025	-0.804	0.152	-0.634	-0.014	-0.464
Totals		-1.98	-0.168	-2.49	-1.49	-2.60	-0.393	-2.842

Fe* includes the sensitivity of the response function

TABLE VI

Accuracies for Data Requirements for the Iron-Water Shield Derived with the Equation of Section 3

Group	Iron				Oxygen			
	Current Accuracy q_i (%)	Target Accuracy			Current Accuracy q_i (%)	Target Accuracy		
		ξ (%) Eqn. 3.2	ξ (%) Eqn. 3.5	ξ (%) Eqn. 3.7		ξ (%) Eqn. 3.2	ξ (%) Eqn. 3.5	ξ (%) Eqn. 3.7
1	5.0	3.2	3.2	3.1	5.0	3.2	3.2	4.3
2	5.0	3.2	3.2	2.8	5.0	3.2	3.2	4.3
3	5.0	3.2	3.2	1.7	5.0	3.2	3.2	4.2
4	5.0	3.2	3.2	4.0	5.0	3.2	3.2	4.8
5	5.0	3.2	3.2	4.3	5.0	3.2	3.2	4.8
6	5.0	3.2	3.2	4.7	5.0	3.2	3.2	4.9
7	5.0	3.2	3.2	4.8	5.0	3.2	3.2	5.0
8	5.0	3.2	3.2	4.8	4.0	3.2	2.2	4.0
9	5.0	3.2	3.2	4.9	4.0	3.2	2.2	4.0
10	5.0	3.2	3.2	5.0	4.0	3.2	2.2	4.0
11	4.0	3.2	2.2	4.0	4.0	3.2	2.2	4.0
12	4.0	3.2	2.2	4.0	4.0	3.2	2.2	4.0
13	4.0	3.2	2.2	4.0	4.0	3.2	2.2	4.0
14	4.0	3.2	2.2	4.0	4.0	3.2	2.2	4.0
15	4.0	3.2	2.2	4.0	15.0	3.2	13.2	15.0
16	5.0	3.2	3.2	5.0	15.0	3.2	13.2	15.0
17-23	5.0	3.2	3.2	5.0	15.0	3.2	13.2	15.0
24	5.0	3.2	3.2	5.0	3.0	3.2	1.2	3.0
25-33	3.0	3.2	1.2	3.0	3.0	3.2	1.2	3.0

TABLE VII

Partial Cross-Sections for Group 3 in Iron
With Sensitivities for the Neutron Dose-Rate in the Iron/Water Shield

Parameter	Cross-Section (barns/atom)	Sensitivity
Σ_{tot}	3.260	-7.827
Σ_{abs}	0.112	-0.269
Elastic Scatter		
Σ_{el}	1.809	-0.797
Elastic Transfer		
P_0		
3-3	1.753	1.267
3-4	0.056	0.018
P_1		
3-3	4.501	1.472
3-4	0.029	0.004
P_2		
3-3	6.325	0.651
3-4	0.085	0.003
P_3		
3-3	6.818	0.151
3-4	0.030	-
Inelastic Scatter		
Σ_{inel}	1.339	-2.944
Inelastic Transfer P_0		
(a) Discrete Levels		
3-3	0.035	0.025
3-4	0.078	0.026
3-5	0.039	0.010
3-6	0.058	0.009
3-7	0.020	0.002
(b) Continuum		
3-3	0.019	0.014
3-4	0.146	0.048
3-5	0.254	0.062
3-6	0.204	0.033
3-7	0.135	0.016
3-8	0.164	0.017
3-9	0.085	0.007
3-10	0.046	0.003
3-11	0.042	0.002
3-12	0.012	0.001
3-13	0.001	-
3-14	0.001	-

SESSION B

REVIEW OF NEA SENSITIVITY BENCHMARK CALCULATIONS: PWR AND FBR SHIELD CONFIGURATION

CALCUL DE REFERENCE POUR UN REACTEUR A EAU PRESSURISEE DE 1300 MWe - ETUDE DE SENSIBILITE DES CALCULS DE PROTECTION

G. BRANDICOURT - C. DEVILLERS *

C.E.A. - SACLAY

Papier présenté à la réunion AIEA-OCDE (AEN) du Comité Technique sur : la qualité requise pour les valeurs de constantes nucléaires différentielles et intégrales utilisées dans les calculs de protection.

(Vienne, 12 - 16 Octobre 1976)

Département des Réacteurs à Eau

Service d'Etudes de Réacteurs et Mathématiques Appliquées

Abstract

The paper concerns the study of neutron transport, gamma-ray production and transport in the shield of a pressurized water reactor as defined in reference [1].

The following quantities have been considered: 1) the neutron-induced damage rate on the inner surface of the pressure vessel; 2) the gamma heating of the biological concrete shield; 3) the dose rate at the external surface of the concrete shield.

The neutron flux distribution is obtained by the discrete ordinate code ANISN in infinite cylindrical geometry. The energy transfer cross-sections are expanded to the third order (P_3), the angular quadrature is S_4. The 100-group DLC-2D library derived from ENDF/B-III has been used in these calculations.

Gamma transport calculations are performed by ANISN in the same conditions as neutron calculations, using an 18-group library derived from the evaluation ISRAEL.

Sensitivity studies utilizing direct and adjoint ANISN calculations and the perturbation code SWANLAKE have been done.

1 - INTRODUCTION

Les études de sensibilité ont une importance primordiale dans les études de protection par suite du manque de référence expérimentale en vraie grandeur.

Elles jouent un double rôle :

- mettre en évidence les données nucléaires importantes
- évaluer l'incertitude des calculs théoriques résultant des imprécisions des données nucléaires.

Les imprécisions des données nucléaires, telles qu'elles sont utilisées dans les calculs, ont deux origines : d'une part les erreurs dans les mesures de sections efficaces, d'autre part les distorsions introduites au niveau du traitement de ces données. Il ne sera possible de quantifier l'influence des premières que lorsque des fichiers d'erreurs accompagneront systématiquement les données évaluées. Par contre, les erreurs "volontaires" introduites par exemple par la condensation des sections efficaces à peu de groupes, ayant pour but de réduire le coût des calculs ou (et) l'encombrement en mémoire peuvent être analysées et minimisées grâce aux études de sensibilité.

Ce papier présente les résultats d'une étude de sensibilité dans le cas de la protection radiale d'un réacteur à eau pressurisée de 1300 MWe. Les quantités étudiées sont :

- la production de dommages par irradiation neutronique de la cuve
- l'échauffement du béton de protection par les gamma
- la dose biologique à l'extérieur de la protection.

2 - DESCRIPTION DU PROBLEME

Les données sont extraites de la référence [1]. La figure 1 représente une coupe horizontale du réacteur ; les dimensions principales et les compositions des matériaux sont rappelées dans les tableaux I et II de l'annexe 1.

La distribution radiale de puissance dans les trois rangées d'éléments périphériques est reportée dans le tableau III de l'annexe 2.

3 - METHODE ET CODES DE CALCUL

Les distributions de flux neutronique et de gamma sont déterminées à l'aide du programme de transport aux ordonnées discrètes ANISN [2] [3]. L'approximation du problème en géométrie monodimensionnelle cylindrique infinie est en effet acceptable pour l'étude de sensibilité.

Les calculs de neutrons utilisent la bibliothèque multigroupe à 100 groupes d'énergie DLC-2 D [4] basée sur ENDF/BIII. Les calculs gamma sont effectués indépendamment à partir d'une bibliothèque [5] à 17 groupes d'énergie générée d'après l'évaluation [7]. La structure multigroupe est reportée dans le tableau IV en annexe 3.

Les sources de gamma de capture sont déterminées à partir des taux de capture fournis par ANISN et des émissions gamma par capture de la référence [6]. Les spectres de gamma de capture sont supposés indépendant de l'énergie des neutrons. Les gamma des autres réactions sont négligés.

Dans les calculs neutron et gamma le flux angulaire est décrit suivant 8 directions (quadrature S 4), le développement de Legendre des sections efficaces est limité à l'ordre 3. Le maillage spatial est celui proposé dans [1], sauf cas particulier précisé par la suite. Les profils de sensibilité sont établis par une méthode de perturbation à l'aide du programme SWANLAKE [8] à partir des flux angulaires direct et adjoint calculés par ANISN.

4 - SENSIBILITE DU TAUX DE PRODUCTION DE DOMMAGES

Le taux de dommage dans la cuve (intervalle $I_o = 120$) s'obtient à partir des flux scalaires directs par l'expression :

$$R_D = \sum_G \phi(I_o, G)\, R_D(G) \qquad \text{(déplacements par atome x s)}$$

Les flux ϕ résultant d'un calcul direct où la source a la forme :

$$S(I, G) = S_1(I) * S_2(G)$$

$S_1(I)$ étant proportionnelle à la distribution de puissance et $S_2(G)$ le spectre de fission calculé par la formule de CRANBERG :

$$S_2(E) = 0.4527 \exp(-1.03627\, E)\, \mathrm{sh}\ (\sqrt{2.29\, E})$$

La section efficace de production de dommages R_D est tirée de [9].

Le même résultat peut être obtenu à l'aide d'un calcul adjoint avec source localisée à l'entrée de la cuve, dans l'intervalle I_o de volume $\Delta V(I_o)$

$$S^+(I, G) = \frac{R_D(G)}{\Delta V(I_o)}$$

Le taux de dommage s'écrit alors :

$$R_D = \sum_I S_1(I)\, \Delta V(I) \sum_G \phi^+(I, G)\, S_2(G)$$

Les deux expressions donnent effectivement le même résultat :

$$R_D = 1.975\ 10^{-12} \text{ déplacement/at.s}$$

qui correspondrait à un dommage intégré de 0.0015 déplacement par atome en 30 ans de fonctionnement avec un facteur de charge de 80%.

SENSIBILITE AUX SECTIONS EFFICACES TOTALES

Les profils de sensibilité du taux de dommage aux sections efficaces totales ont été déterminés par SWANLAKE pour les éléments : 238 U, Zr, H, O, Cr, Fe, Ni.

Les sensibilités par unité de léthargie sont reportées dans l'annexe 4.a à 4.g. On peut constater que pour tous les éléments, les sections efficaces importantes se situent dans le domaine 4 à 10 MeV avec un pic aigu à 5 - 6 MeV.

A un ensemble $\left(\frac{\Delta\sigma_t}{\sigma_t}\right)_G$ de variation des sections efficaces totales d'un élément donné, les courbes de l'annexe 4 permettent d'associer une variation du taux de dommage :

$$\frac{\Delta R}{R} = \sum_G s\ (U_G)\ \Delta U\ (G)\ \left(\frac{\Delta\sigma_t}{\sigma_t}\right)_G$$

où $s\ (U_G)$ est la sensibilité par unité de léthargie dans le groupe G.

L'intégrale sur l'énergie de la sensibilité :

$$S = \sum_G s\ (U_G)\ \Delta U\ (G)$$

permet de classer les éléments par ordre d'importance décroissante, pour ce problème, comme le montre le tableau V ci-dessous :

TABLEAU V - Sensibilité du taux de dommage aux sections efficaces totales

Elément	Sensibilité
Hydrogène	- 5.67
Oxygène	- 2.00
Fer	- 1.60
Chrome	- 0.46
238 U	- 0.30
Nickel	- 0.23
Zirconium	- 0.11

Une erreur systématique de 5 % par exemple sur la section efficace totale du fer entre 4 et 10 MeV se traduirait donc par une erreur de 8 % sur le taux de dommage ; de même, une imprécision de 1 % sur la densité de l'eau a pour conséquence une imprécision de 8 % sur le taux de dommage.

SENSIBILITE AU DEVELOPPEMENT DE LEGENDRE DE L'ANISOTROPIE DE LA DIFFUSION

L'importance des données nucléaires dans le domaine rapide mise en évidence plus haut incite à penser que la description fine des fortes anisotropies à haute énergie est nécessaire.

C'est en effet ce que montrent les résultats de SWANLAKE reportés dans le tableau VI suivant :

TABLEAU VI - SENSIBILITE DU TAUX DE DOMMAGE A LA DESCRIPTION DE L'ANISOTROPIE

	Erreur (%) par rapport à un calcul P3		
Elément	P_0	P_1	P_2
H	-116.2	- 30.4	- 4.9
Fe	- 68.8	- 21.3	- 6.1
O	- 47.2	- 11.6	- 2.2
Cr	- 18.0	- 4.6	- 0.8
Ni	- 10.2	- 2.6	- 0.4
^{238}U	- 4.9	1.4	0.1
Zr	- 2.0	0.5	0

Ce tableau confirme que l'approximation P_o est inadéquate dans les calculs de protection et que l'approximation P_1 est insuffisante.

Le développement P_3, le plus souvent utilisé dans les calculs monodimensionnels est donc justifié.

Rappelons que la précision souhaitée pour l'évaluation du taux de dommage est de l'ordre de 15 %.

5 - *SENSIBILITE DE L'ECHAUFFEMENT DU BETON*

Appelons q_k (I) l'échauffement ($W.cm^{-3}$) à l'entrée de la protection en béton (intervalle I_0 = 147) résultant des gamma émis par une capture neutronique dans l'intervalle I.

L'échauffement partiel résultant des captures dans l'élément k s'écrit alors :

$$Q_k = \sum_I q_k (I)\ \Delta V (I)\ N_k (I) \sum_G \sigma_k^c (G)\ \phi(I, G)$$

où N_k (I) est la concentration de l'élément k

σ_k^c (G) sa section efficace de capture radiative.

La quantité q_k, ou importance, est obtenue par un calcul gamma adjoint dont la source :

$$S^+ (G') = \frac{1.6\ 10^{-13} \mu_a (G')\ \overline{E}\ (G')}{\Delta V\ (I_0)}$$

est placée dans l'intervalle I_o, de volume $\Delta V\ (I_o)$, où l'on cherche l'échauffement; μ_a (G') est la section efficace d'absorption d'énergie du béton (cm^{-1}) et $\overline{E}$ (G') l'énergie moyenne (MeV) du groupe G'.

L'importance s'écrit :

$$q_k (I) = \sum_{G'} \phi^+(I, G')\ S_k (G')$$

où S_k (G') représente le nombre de gamma émis dans le groupe G' par capture dans l'élément k.

TABLEAU VII - ECHAUFFEMENT ($W.cm^{-3}$) DU BETON PAR LES GAMMA DE CAPTURE ET LES GAMMA DU COEUR

Origine des gamma	Coeur	Baffle	Eau	Ecran thermique	Eau	Gaine inox	Cuve	Béton	Total (%)
H	2.08^{-9}	-	2.15^{-7}	-	3.39^{-8}	-	-	5.27^{-8}	3.04^{-7} (3.7)
Al	-	-	-	-	-	-	-	7.25^{-8}	7.25^{-8} (0.9)
Si	-	-	-	-	-	-	-	2.40^{-7}	2.40^{-7} (2.9)
Ca	-	-	-	-	-	-	-	4.08^{-7}	4.08^{-7} (5.0)
Cr	-	7.06^{-7}	-	5.14^{-8}	-	8.1^{-10}	-	-	7.58^{-7} (9.2)
Fe	7.63^{-8}	2.81^{-6}	-	2.02^{-7}	-	3.1^{-9}	1.49^{-6}	-	4.58^{-6} (55.6)
Ni	-	8.05^{-7}	-	5.74^{-8}	-	8.3^{-10}	-	-	8.63^{-7} (10.5)
Coeur	1.01^{-6}	-	-	-	-	-	-	-	1.01^{-6} (12.2)
Total (%)	1.09^{-6} (13.2)	4.32^{-6} (52.4)	2.15^{-7} (2.6)	3.11^{-7} (3.8)	3.39^{-8} (0.4)	4.74^{-9} (0.1)	1.49^{-6} (18.1)	7.73^{-7} (9.4)	8.24^{-6} (100)

Un traitement analogue est appliqué pour les gamma de fission et de produits de fission émis dans le coeur.

Le tableau VII ci-dessous montre les contributions des diverses sources de gamma à l'échauffement du béton qui vaut au total $8.24\ 10^{-6}$ W.cm^{-3}.
On constate que 56 % de l'échauffement provient des captures dans le fer, principalement dans le baffle (34 %) et dans la cuve (18 %).

SENSIBILITE AUX SECTIONS EFFICACES DE CAPTURE NEUTRONIQUE

La sensibilité de l'échauffement total :

$$Q = \sum_k Q_k$$

aux sections efficaces de capture σ_k^c d'un élément k s'écrit :

$$\frac{\frac{\partial Q}{Q}}{\frac{\partial \sigma_k^c(G)}{\sigma_k^c(G)}} = \frac{1}{Q} \sum_I q_k(I)\,\Delta V(I)\,N_k(I)\,\sigma_k^c(G)\,\phi(I,G)$$

qui est simplement la contribution à l'échauffement total des gamma produits par les captures dans le groupe G.

Cette formulation, appliquée aux gamma de capture du fer, responsables de 60 % environ de l'échauffement donne les résultats du tableau VIII suivant :

TABLEAU VIII - SENSIBILITE DE L'ECHAUFFEMENT AUX SECTIONS EFFICACES DE CAPTURE DU FER

Domaine d'énergie	Sensibilité
E > 100 eV	0.05
0.4 < E < 100 eV	0.07
thermiques	0.43
total	0.55

La section efficace de capture thermique est donc pratiquement la seule importante; ceci justifie par ailleurs l'hypothèse de l'indépendance du spectre de gamma de capture vis à vis de l'énergie des neutrons.

SENSIBILITE AUX SECTIONS EFFICACES TOTALES DES NEUTRONS

Le calcul adjoint neutron devant fournir l'échauffement Q_k dû aux captures dans un élément k utilise une source :

$$S^+ (I, G) = N_k (I) \sigma_k^c (I) q_k (I)$$

qui est le taux de capture par atome d'élément k pondéré par la fonction d'importance q_k (I).

Les flux angulaires de ce calcul, exploités par SWANLAKE, ainsi que les flux angulaires du calcul direct, dans le cas des captures dans le fer, ont donné les profils de sensibilité reportés dans l'annexe 5.a à 5.g.

Le tableau IX donne la sensibilité totale aux sections efficaces des éléments considérés, par ordre d'importance décroissante.

TABLEAU IX - SENSIBILITE DE L'ECHAUFFEMENT DU BETON AUX SECTIONS EFFICACES TOTALES

Elément	Sensibilité totale	Sensibilité dans le groupe thermique
Hydrogène	- 1.25	- 0.24
Fer	- 0.68	- 0.22
Oxygène	- 0.35	- 0.01
238 U	- 0.14	- 0.00
Chrome	- 0.13	- 0.05
Nickel	- 0.08	- 0.03
Zirconium	- 0.03	- 0.00

Remarquons que les valeurs du tableau IX sont légèrement sous-estimées puisqu'elles ne traduisent l'influence des sections efficaces que à travers une fraction de l'échauffement, celle due aux gamma du fer.

Il apparaît cependant que le problème de l'échauffement est moins sensible à la précision des sections efficaces à haute énergie que celui de la prévision des dommages. L'hydrogène est l'élément le plus important, surtout dans le domaine rapide 2-10 MeV mais aussi dans le groupe thermique. Le fer vient en seconde position, son importance provenant essentiellement de ses sections efficaces thermiques.

SENSIBILITE AU DEVELOPPEMENT DE LEGENDRE DE L'ANISOTROPIE DE LA DIFFUSION

Des conclusions analogues à celles du paragraphe 4. peuvent être tirées quoique l'influence des troncatures soit moins marquée ; le passage de P3 à P1 entraîne une variation de 13 % de l'échauffement, surtout dans l'hydrogène et dans le fer.

Une partie notable de l'échauffement provenant du coeur (13 %) et des captures dans les structures proches du coeur (52 %) il n'est pas étonnant que cette composante soit peu sensible, à la fois aux sections efficaces totales et à l'anisotropie dans le domaine rapide, ce qui diminue la sensibilité de l'échauffement total à ces données.

Rappelons que la précision souhaitée des calculs d'échauffement est en général de 20 %.

6 - SENSIBILITE DE LA DOSE BIOLOGIQUE

La dose biologique à l'extérieur de la protection de béton comporte deux composantes : une composante neutron faible qui est fournie par un calcul direct et vaut :

$$D_n = 1.1 \text{ mrem/h}$$

et une composante gamma déterminée d'une manière analogue à celle exposée au paragraphe 5 relatif au problème de l'échauffement :

$$D_{\gamma k} = \sum_I q'_k (I)\ \Delta V (I)\ N_k (I) \sum_G \sigma_k^C (G)\ \phi (I, G)$$

TABLEAU X - DOSE BIOLOGIQUE ($mremh^{-1}$) DUE AUX GAMMA

Origine des gamma	Coeur	Baffle	Eau	Ecran thermique	Eau	Gaine inox	Cuve	Béton	Total (%)
H	2.5^{-6}	-	2.7^{-4}	-	4.7^{-5}	-	-	0.085	0.085 (0.2)
Al	-	-	-	-	-	-	-	2.65	2.65 (6.5)
Si	-	-	-	-	-	-	-	5.80	5.80 (14.3)
Ca	-	-	-	-	-	-	-	8.05	8.05 (19.8)
Cr	-	2.78	-	0.22	-	0.004	-	-	3.0 (7.4)
Fe	0.32	12.1	-	0.95	-	0.016	3.06	-	16.4 (40.3)
Ni	-	3.80	-	0.31	-	0.005	-	-	4.1 (10.1)
Coeur	0.50	-	-	-	-	-	-	-	0.5 (1.2)
Total (%)	0.82 (2.0)	18.7 (45.9)	$\sim$0 (0)	1.48 (3.6)	$\sim$0 (0)	0.025 (0)	3.06 (7.5)	16.6 (40.8)	40.7

où q'_k est l'importance d'une capture dans l'intervalle I pour la dose biologique. La détermination de cette importance, par un calcul adjoint ANISN a nécessité un maillage plus fin que celui proposé dans [1] à cause de la convergence des groupes de basse énergie. La dose gamma est égale à 40 mrem/h, le détail des contribution est reporté dans le tableau X.

Il n'est pas nécessaire d'étudier la sensibilité de la dose neutron qui représente moins de 3 % de la dose totale. Pour ce qui concerne la dose gamma, on retrouve une contribution importante des captures dans l'acier inoxydable du baffle (45.9 %) et une contribution totale due au fer de 40.3 %. La sensibilité aux sections efficaces neutroniques sera donc semblable à celle établie au paragraphe 5 sur les échauffements. Cependant il y aurait lieu de lui ajouter un complément qui représenterait l'influence des sections efficaces neutroniques à travers la dose due aux captures dans le béton (qui représente 40 % de la dose totale.)

La précision visée dans l'estimation de la dose est de l'ordre d'un facteur 2.

7 - *EFFET DE LA CONDENSATION DES SECTIONS EFFICACES ET VERIFICATION DE L'EFFET D'ANISOTROPIE*

Il est économique en temps de calcul et parfois indispensable pour des questions d'encombrement en mémoire de limiter le plus possible le nombre de groupes et l'ordre d'anisotropie, en particulier pour les calculs à deux dimensions.

Se pose alors le problème du choix du découpage multigroupe optimum permettant d'obtenir la précision désirée dans le temps minimum.

Dans l'exemple suivant, on a considéré un découpage à 15 groupes d'énergie dont les bornes sont reportées dans le tableau XI suivant.

TABLEAU XI - STRUCTURE MULTIGROUPE NEUTRON CONDENSEE

Groupe	Energie supérieure
1	14.918 MeV
2	6.065 "
3	3.68 "
4	2.23 "
5	1.35 "
6	821. KeV
7	302. "
8	86.5 "
9	24.8 "
10	19.3 "
11	1.58 "
12	78.9 eV
13	5.0 "
14	1.13 "
15	0.414"

Une bibliothèque condensée a été générée sur cette structure dans le cas de référence PWR-1300 MWe traité précédemment : le spectre de pondération est le spectre moyen par région fourni par ANISN dans la structure fine à 100 groupes.

Le calcul du taux de dommage a été repris à l'aide de cette bibliothèque condensée, en approximation P3.

L'écart par rapport au calcul de référence à 100 groupes reporté au paragraphe 4 est de -10 %. L'analyse de cet écart à l'aide des profils de sensibilité montre qu'il est imputable essentiellement aux groupes 1 et 2 qui sont trop larges.

L'effet d'anisotropie a également été étudié en comparant les résultats de deux calculs à 15 groupes, l'un en P3, l'autre en P1. L'écart obtenu : - 39 % est important et confirme les tendances annoncées par SWANLAKE dans les calculs à 100 groupes. Les courbes de l'annexe 6 illustrent ces effets. Il est intéressant parallèlement de comparer les coûts des différents calculs :

100 g - P3	:	16 m 21 s
15 g - P3	:	2 m 07 s
15 g - P1	:	1 m 46 s

Le gain le plus sensible est obtenu par la condensation à peu de groupes. Les études de sensibilité sont donc particulièrement intéressantes de ce point de vue si elles permettent d'optimiser la condensation.

8 - CONCLUSION

De ces études de sensibilité se dégagent les conclusions suivantes, qui sont propres aux calculs de protection radiale des PWR :

1. très grande importance des sections efficaces totales dans le domaine 4 à 10 MeV ; les précisions souhaitées sur σ_t seraient :
   hydrogène 0.5 % - oxygène 1.5 % - fer 2 % -
   uranium 238, chrome, nickel : 10 % - zirconium 30 % -
2. importance des sections efficaces de capture thermique de chrome, fer, nickel : précision requise 4 %.
3. importance modérée des sections efficaces de capture épithermique de chrome, fer, nickel : précision requise 15 %.
4. nécessité de traiter l'anisotropie de la diffusion jusqu'à l'ordre P3.
5. intérêt des profils de sensibilité dans le choix des structures à peu de groupes pour bibliothèques condensées.

REFERENCES

[1] G. HEHN - J. KOBAN
Reactor Shield Benchmark n°2 - ESIS Newsletter, Special Issue n° 4 (January 1976)

[2] C. DEVILLERS
Système ANISN - Description et mode d'utilisation du programme aux ordonnées discrètes ANISN et des programmes auxiliaires -
Note CEA.N.13[illegible] (Octobre 1970)

[3] W.W. ENGLE
A users manual for ANISN - A one dimensional discrete ordinates transport code with anisotropic scattering
AEC Research and Development Report K.1693

[4] RSIC Data Library Collection : DLC-2, 100 group neutron cross section data based on ENDF/B

[5] C. DEVILLERS - C. DUPONT
Création de la bibliothèque multigroupe gamma BIP/G1
Note CEA.N.1424 (mars 1971)

[6] R.E. MAERKER, F.J. MUCKENTHALER
Gamma-Ray spectra arising from thermal-neutron capture in elements found in soils, concretes, and structural materials
ORNL-4382 (August 1969)

[7] E. STORM - H. ISRAEL
Photon cross sections from 0.001 to 100 MeV for elements 1 through 100
LA-3753 (1967)

[8] D.E. BARTINE - F.R. MYNATT - E. OBLOW
SWANLAKE - A computer code utilizing ANISN transport calculations for cross section sensitivity analysis
ORNL-TM-3809 (1973)

[9] M. LOTT et autres
Sections efficaces de création de dommages
IAEA-SM-170/65
Nuclear Data in Science and Technology - Vol. I - Vienna (1973)

FIGURE 1

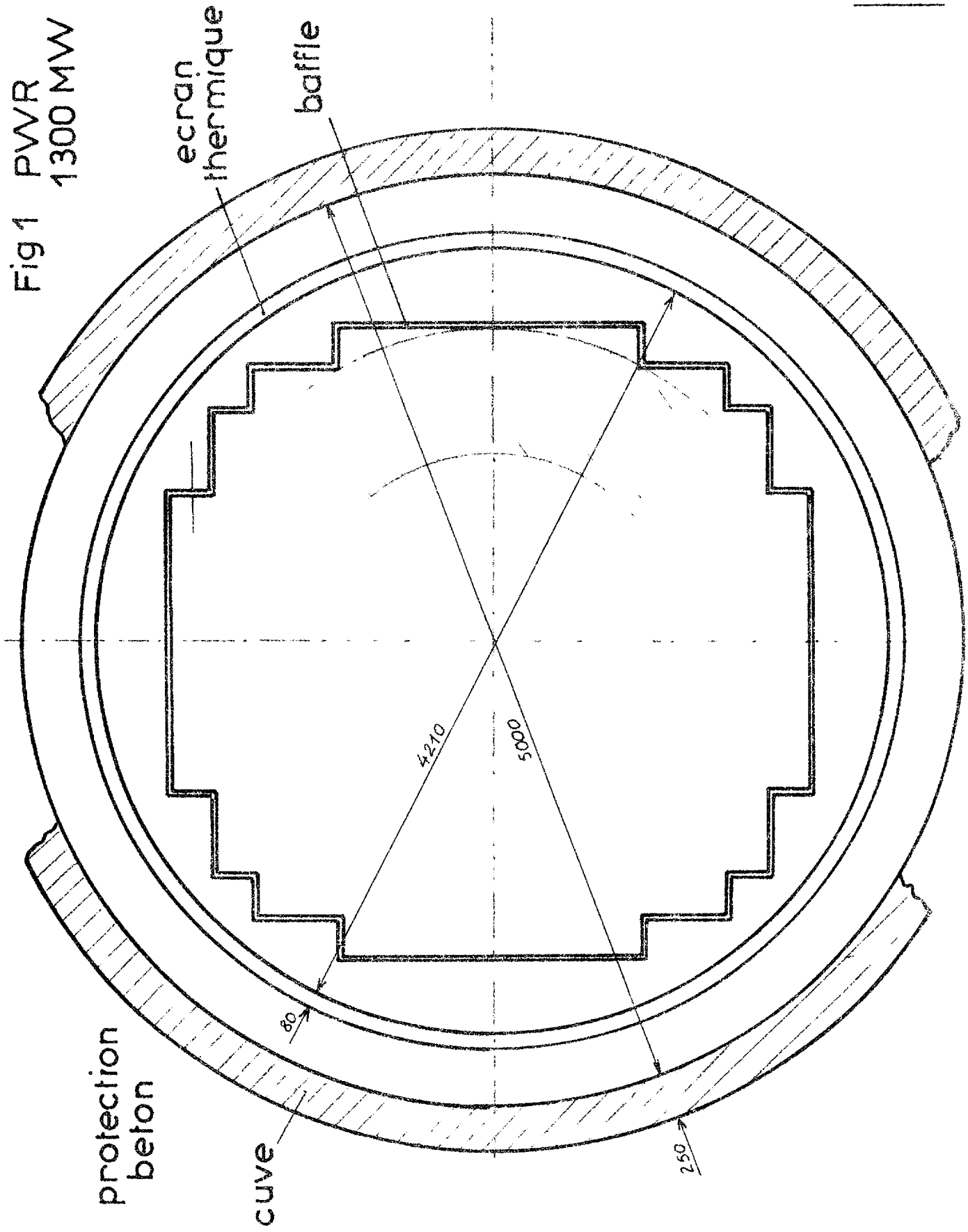
Fig 1 PWR 1300 MW
ecran thermique
baffle
4210
5000
80
250
protection beton
cuve

TABLEAU I - DIMENSIONS RADIALES SUIVANT UN AXE PRINCIPAL

Région	rayon extérieur (cm)	épaisseur (cm)
Coeur	172.5	-
Baffle	175.0	2.5
Eau 1	210.5	35.5
Ecran thermique	218.5	8.0
Eau 2	250.0	31.5
Gainage inox	250.6	0.6
Cuve	275.6	25.0
Protection béton	475.6	200.0

TABLEAU II - COMPOSITION DES MATERIAUX (10^{24} cm^{-3})

Elément \ Région	Coeur	Baffle Ecran Gainage	Cuve	Eau 1 et 2	Béton
H	2.8226^{-2}	-	-	5.0556^{-2}	4.4126^{-3}
O	2.7154^{-2}	-	-	2.5278^{-2}	4.7751^{-2}
Al	-	-	-	-	2.4553^{-3}
Si	-	-	-	-	9.4350^{-3}
Ca	-	-	-	-	6.6115^{-3}
Cr	-	1.6913^{-2}	-	-	-
Mn	-	1.1187^{-3}	-	-	-
Fe	9.8235^{-4}	6.4478^{-2}	8.4650^{-2}	-	-
Ni	-	8.5357^{-3}	-	-	-
Zr	4.3246^{-3}	-	-	-	-
^{235}U	2.1040^{-4}	-	-	-	-
^{238}U	6.3087^{-3}	-	-	-	-

TABLEAU III - DISTRIBUTION RADIALE DE PUISSANCE

Rayon (cm)	Distribution (unité arbitraire)
105.8	1.03
110.4	0.965
115.0	0.92
119.6	0.88
124.2	0.855
128.5	0.878
132.5	0.842
136.0	0.818
139.0	0.797
142.0	0.783
145.0	0.79
148.0	0.81
150.5	0.998
152.5	0.995
154.5	0.99
156.5	0.98
158.5	0.95
160.25	0.916
161.75	0.881
163.25	0.842
164.5	0.805
165.85	0.756
167.2	0.697
168.2	0.65
169.2	0.595
170.1	0.537
170.9	0.478
171.55	0.427
172.0	0.388
172.35	0.357

1 unité équivaut à 92.23 $W.cm^{-3}$

TABLEAU IV - STRUCTURE MULTIGROUPE GAMMA

Groupe	Energie supérieure (MeV
1	8.5
2	7.5
3	6.5
4	5.5
5	4.5
6	3.5
7	2.75
8	2.25
9	1.75
10	1.25
11	0.75
12	0.5066
13	0.3423
14	0.2312
15	0.1562
16	0.1055
17	0.07127
-	(0.04815)

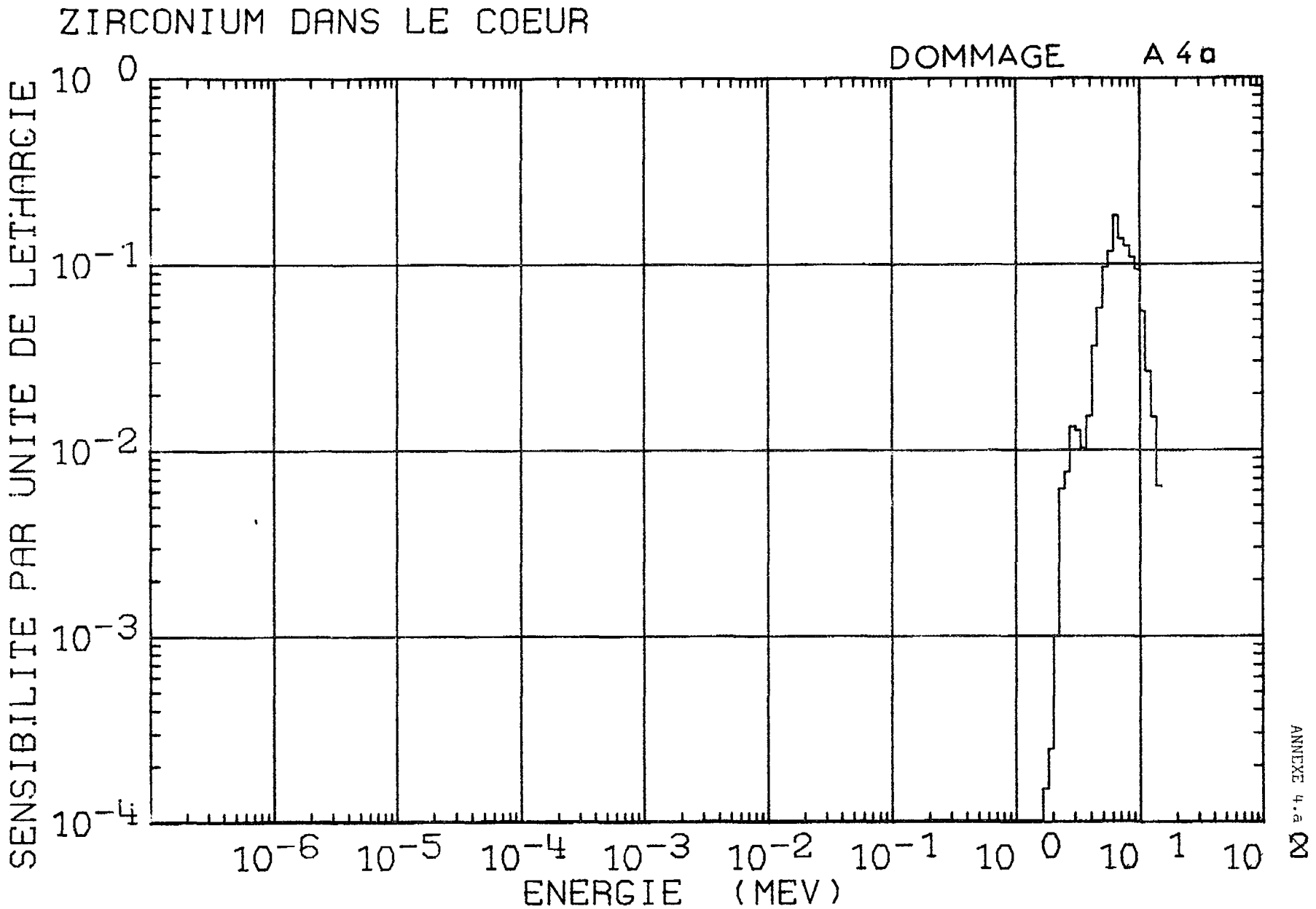
ZIRCONIUM DANS LE COEUR
DOMMAGE A 4a
SENSIBILITE PAR UNITE DE LETHARGIE
10 0
10-1
10-2
10-3
10-4
10-6 10-5 10-4 10-3 10-2 10-1 10 0 10 1 10
ENERGIE (MEV)

ANNEXE 4.a

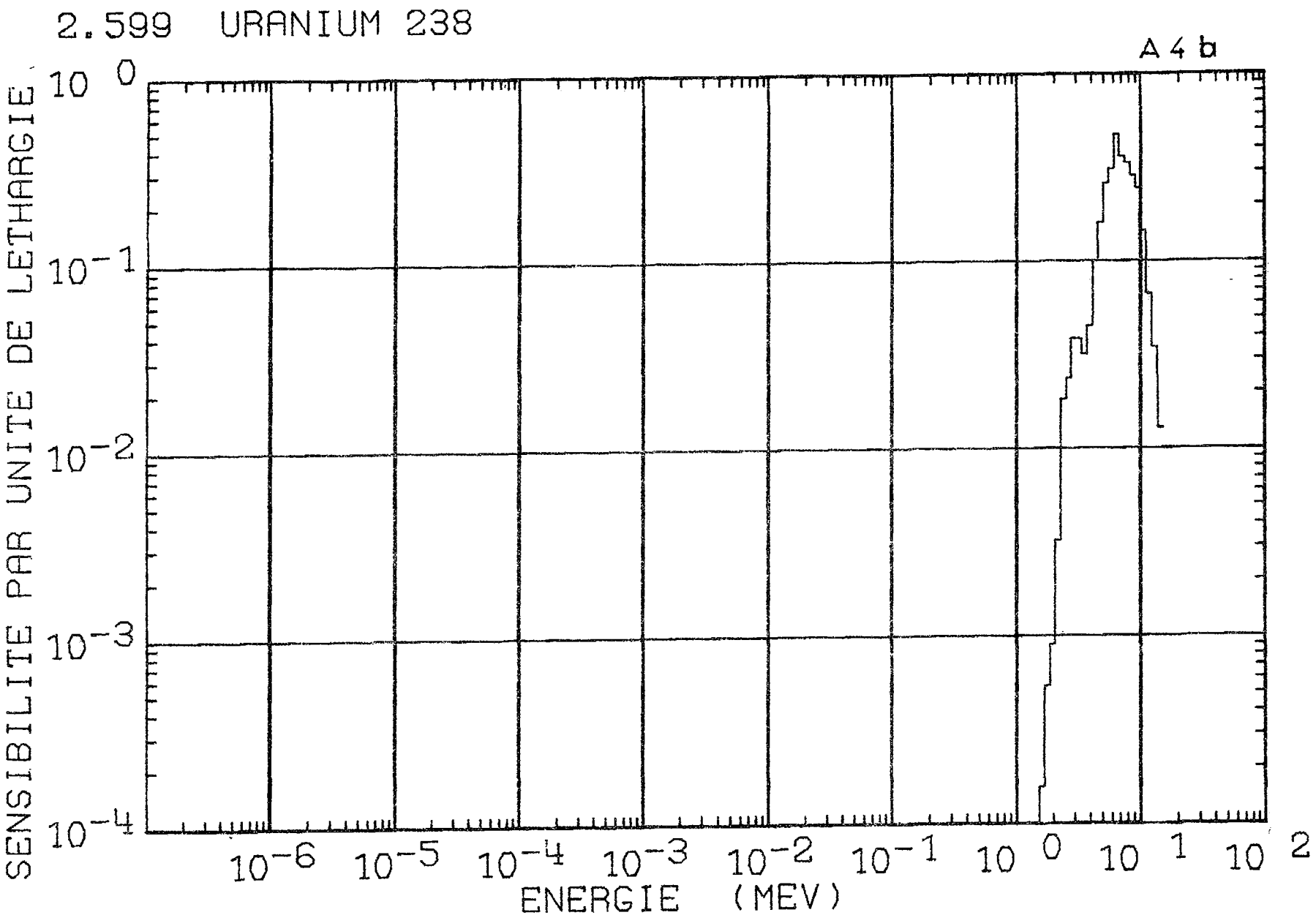

ANNEXE 4-b

III

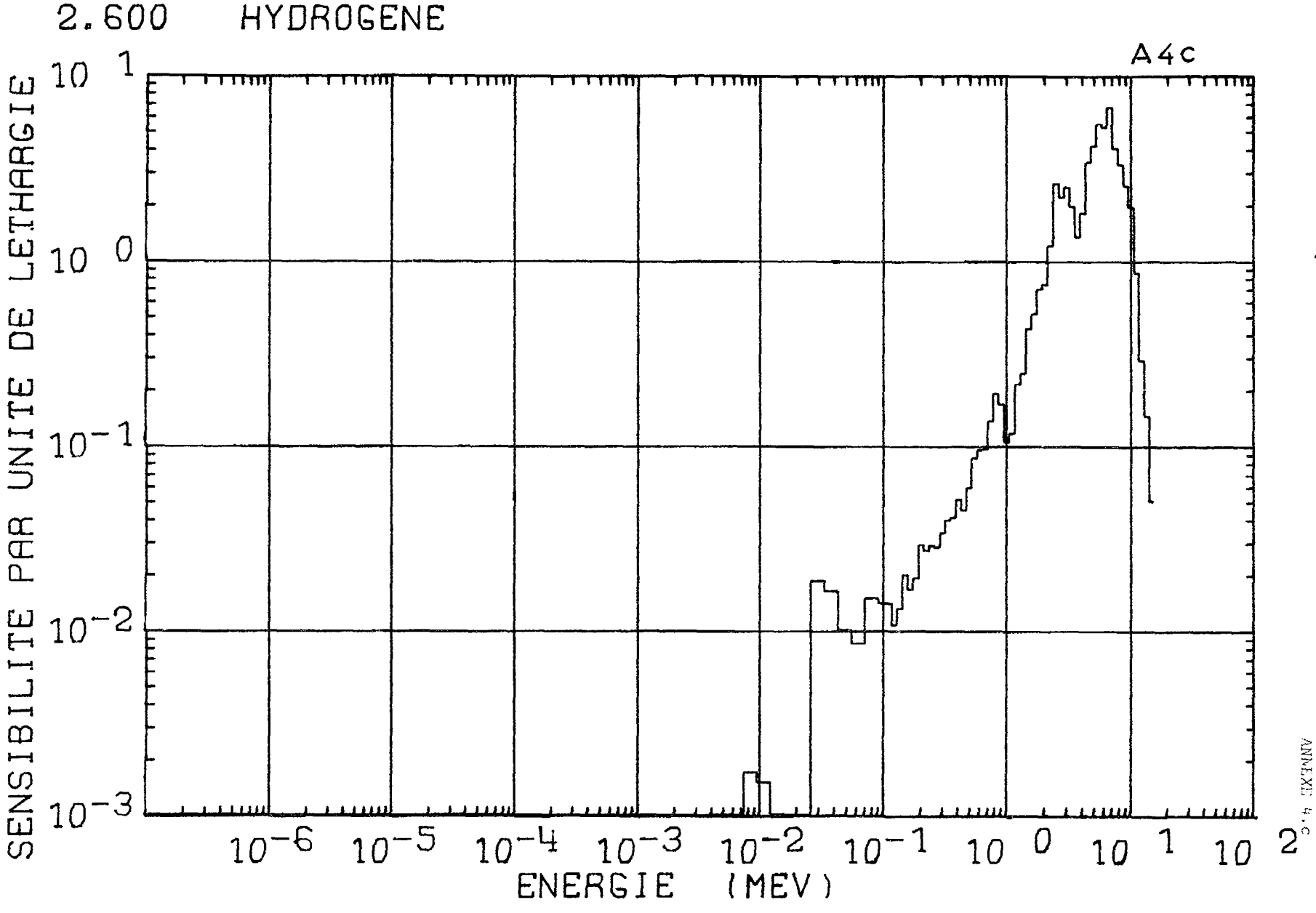
2.600 HYDROGENE
A4c
SENSIBILITE PAR UNITE DE LETHARGIE
10 1
10 0
10-1
10-2
10-3
10-6 10-5 10-4 10-3 10-2 10-1 10 0 10 1 10 2
ENERGIE (MEV)

ANNEXE 4.c

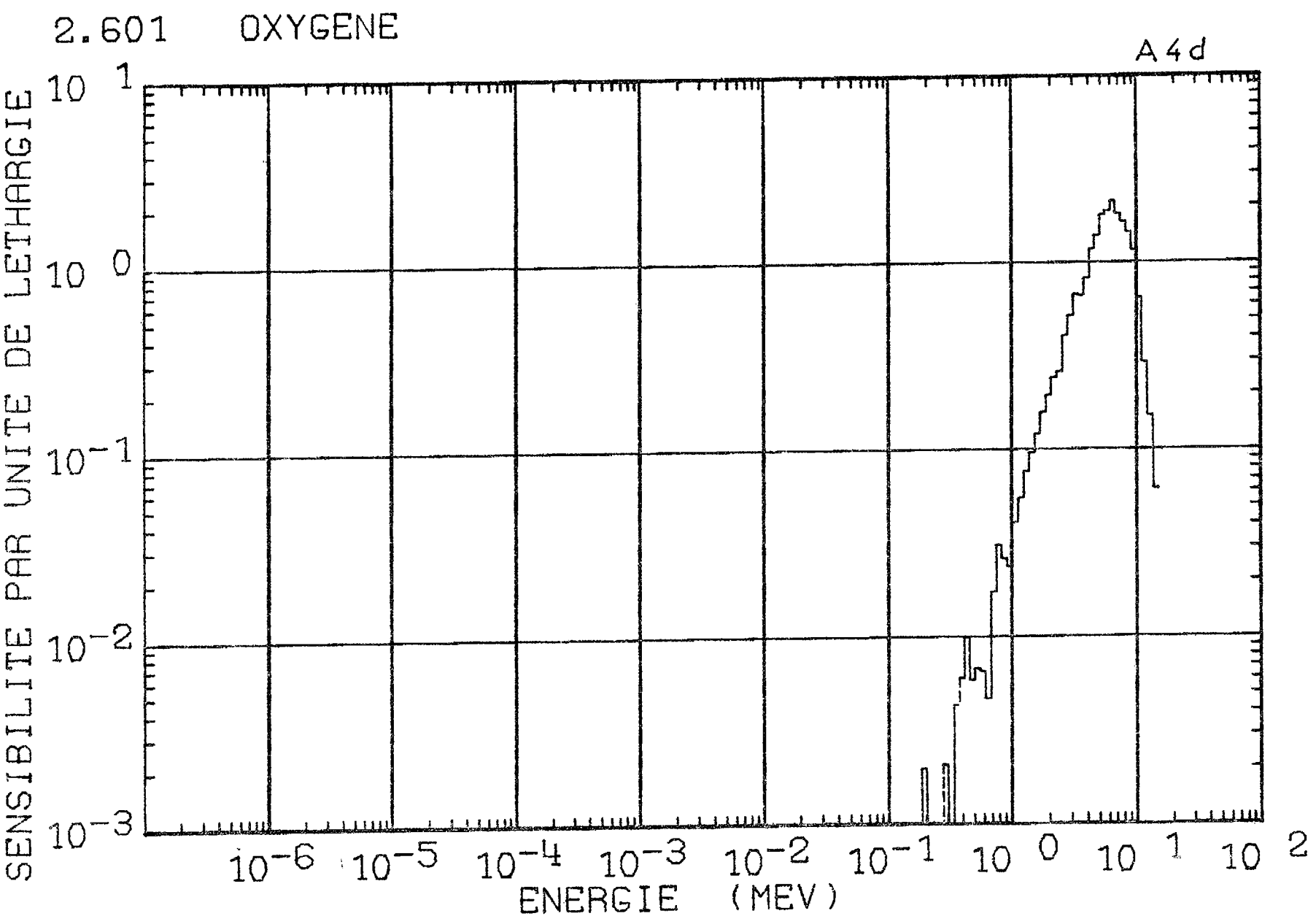
2.601 OXYGENE
A4d
SENSIBILITE PAR UNITE DE LETHARGIE
10 1
10 0
10-1
10-2
10-3
10-6 10-5 10-4 10-3 10-2 10-1 10 0 10 1 10 2
ENERGIE (MEV)

ANNEXE 4.d

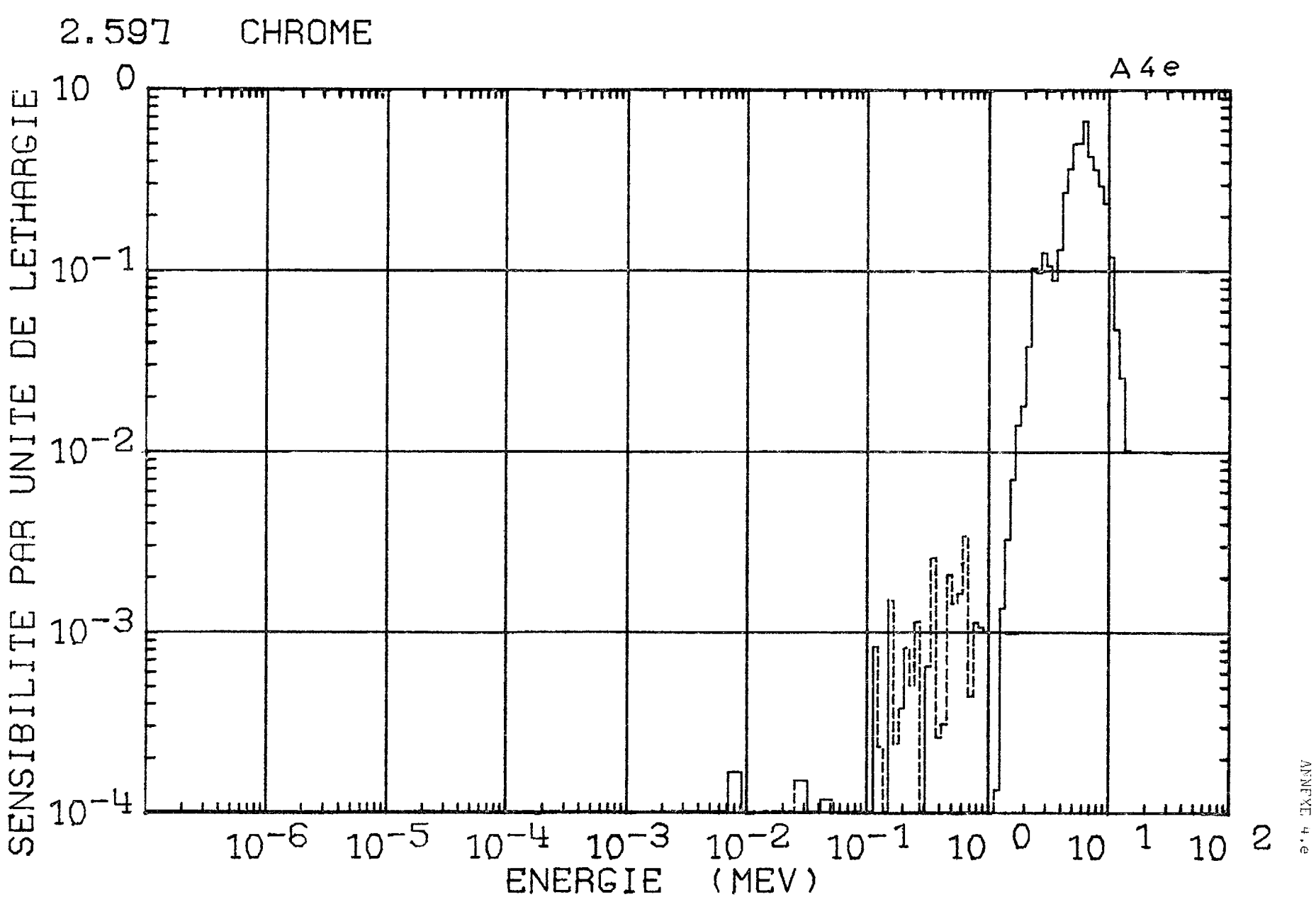
2.597 CHROME
A 4e
SENSIBILITE PAR UNITE DE LETHARGIE
10 0
10-1
10-2
10-3
10-4
10-6 10-5 10-4 10-3 10-2 10-1 10 0 10 1 10 2
ENERGIE (MEV)

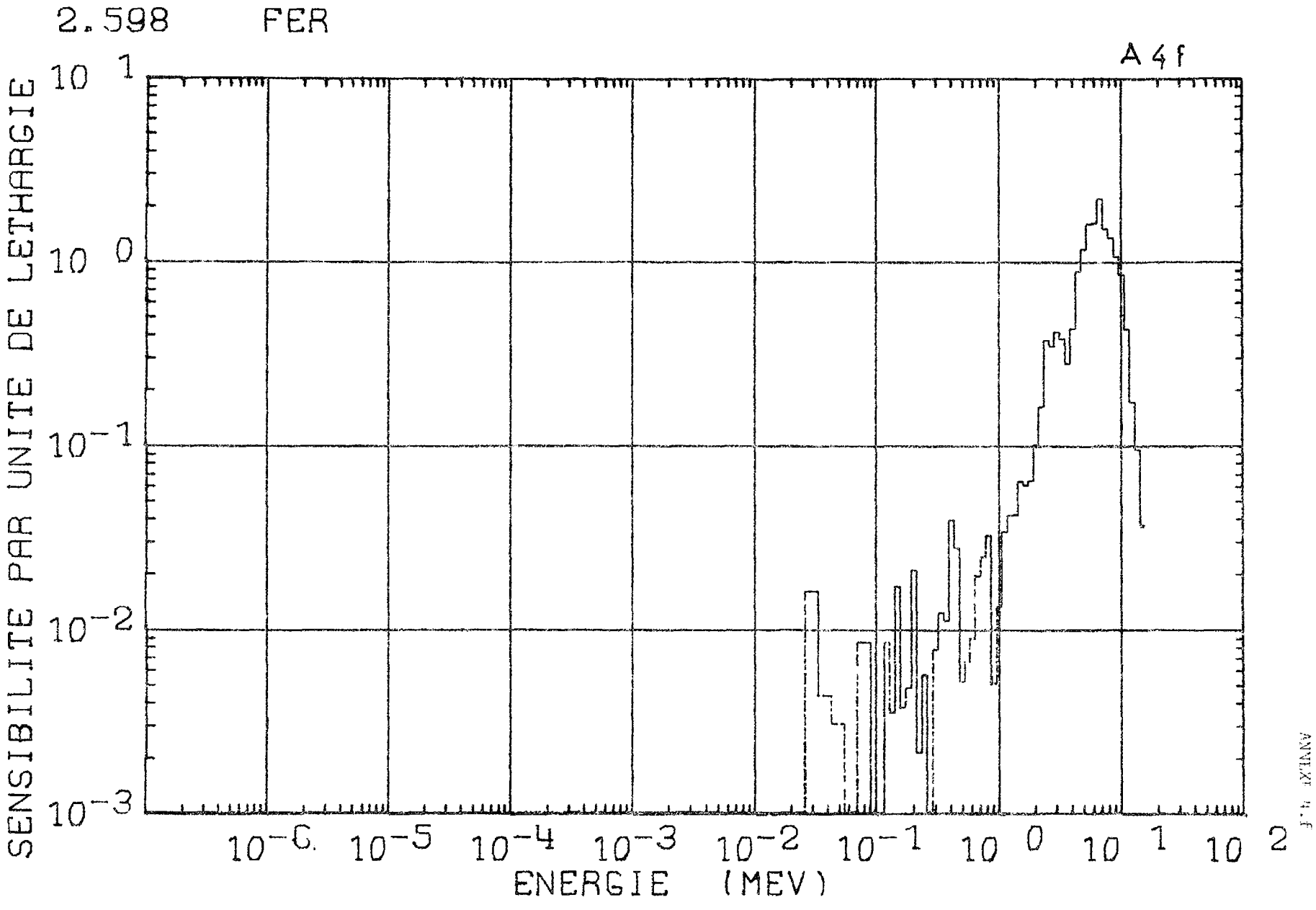
2.598 FER
A 4 f
SENSIBILITE PAR UNITE DE LETHARGIE
10 1
10 0
10-1
10-2
10-3
10-6 10-5 10-4 10-3 10-2 10-1 10 0 10 1 10 2
ENERGIE (MEV)

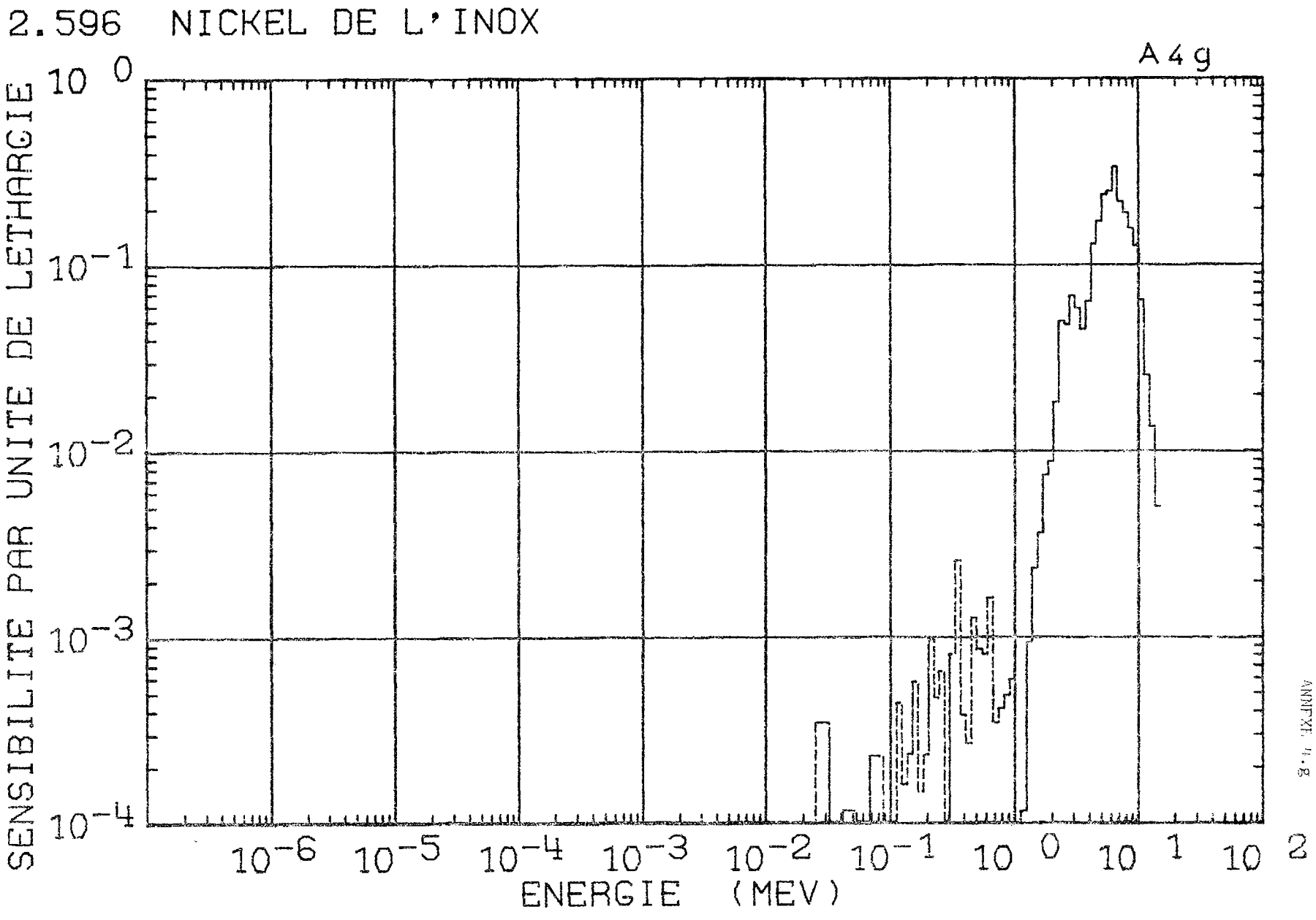
2.596 NICKEL DE L'INOX
A4g
SENSIBILITE PAR UNITE DE LETHARGIE
10 0
10-1
10-2
10-3
10-4
10-6 10-5 10-4 10-3 10-2 10-1 10 0 10 1 10 2
ENERGIE (MEV)

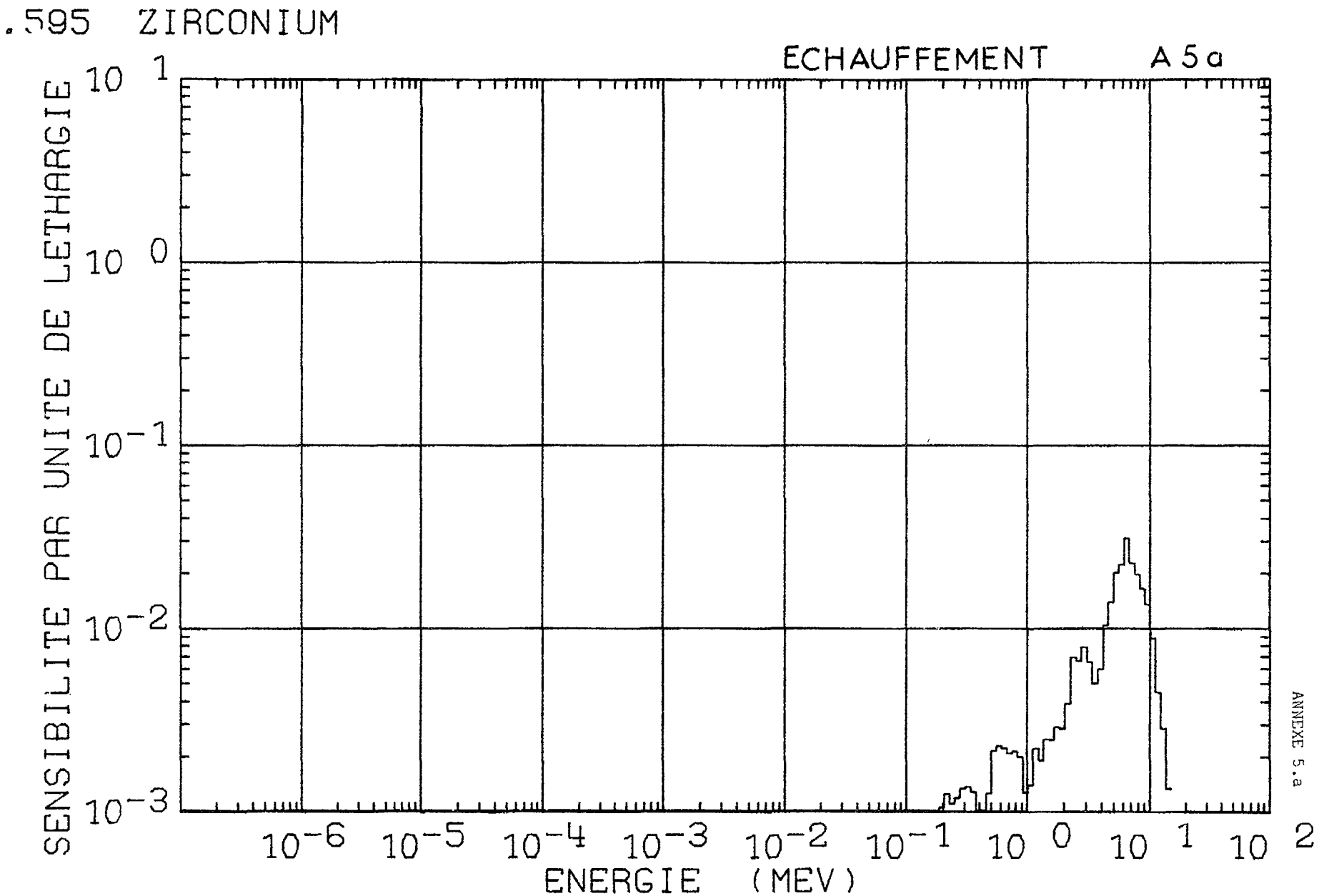
.595 ZIRCONIUM
ECHAUFFEMENT
A 5a
SENSIBILITE PAR UNITE DE LETHARGIE
10 1
10 0
10-1
10-2
10-3
10-6 10-5 10-4 10-3 10-2 10-1 10 0 10 1 10 2
ENERGIE (MEV)

ANNEXE 5.a

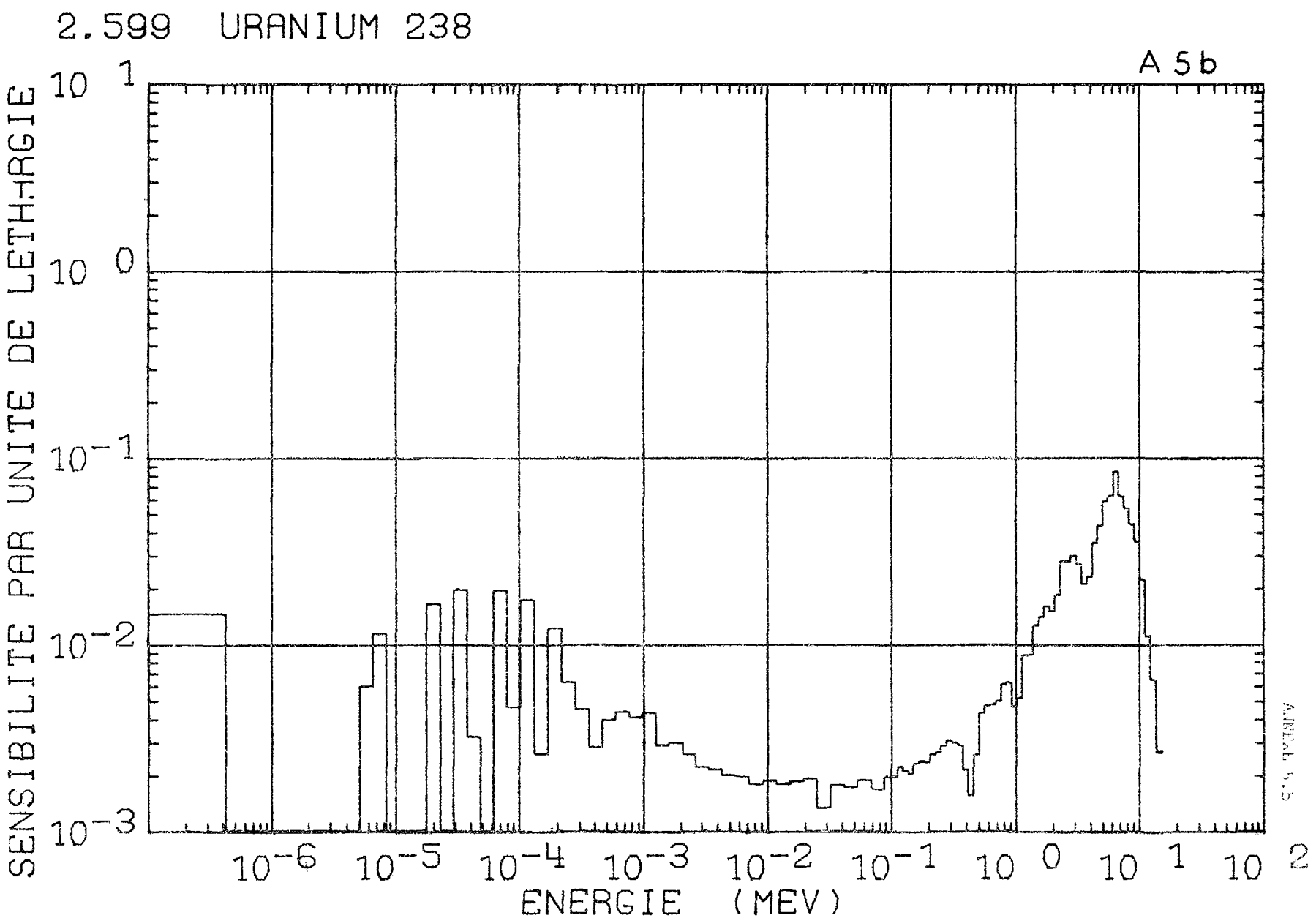
2.599 URANIUM 238
A 5b
SENSIBILITE PAR UNITE DE LETHARGIE
10 1
10 0
10-1
10-2
10-3
10-6 10-5 10-4 10-3 10-2 10-1 10 0 10 1 10 2
ENERGIE (MEV)
AMREAL 5.5

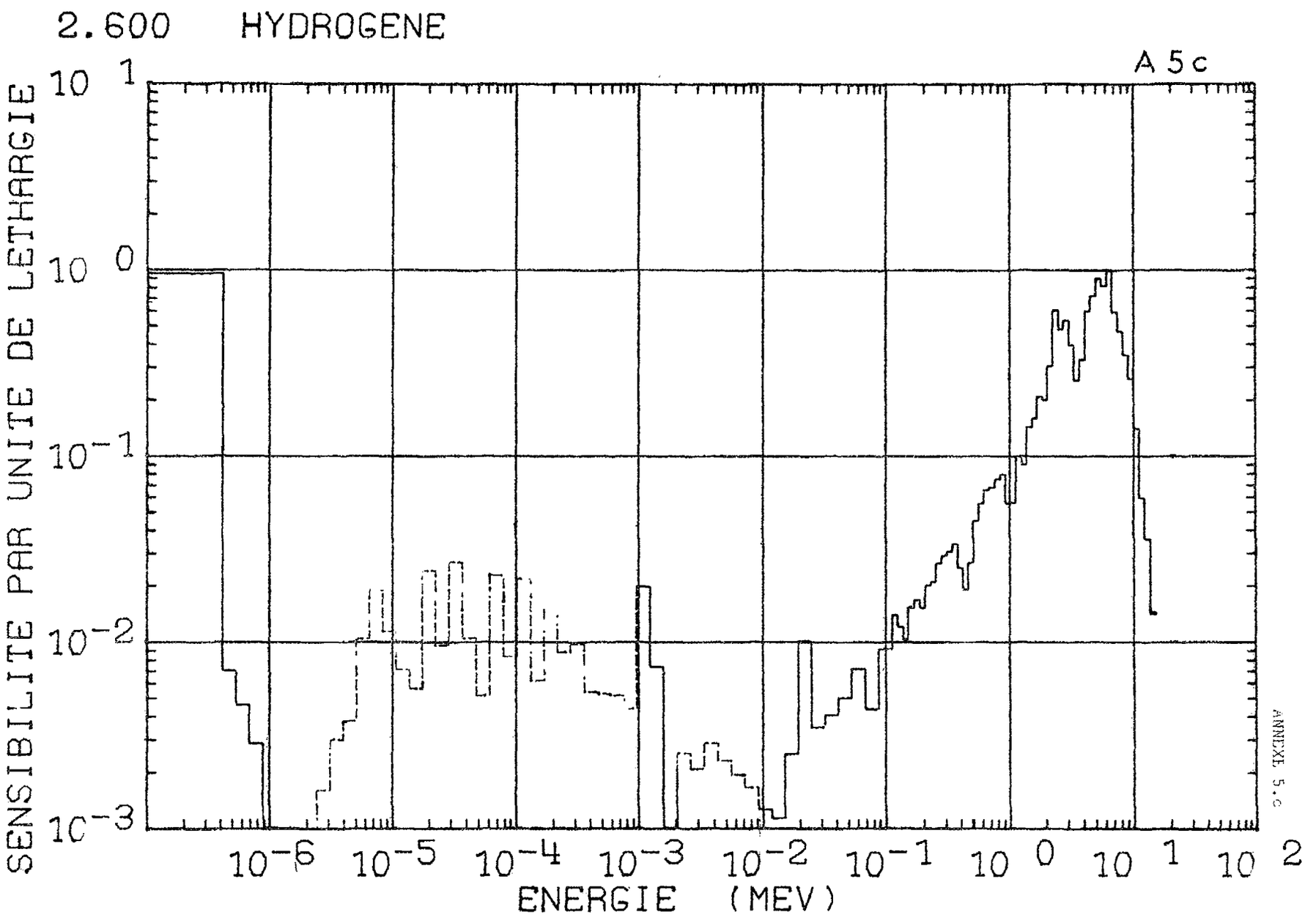
2.600 HYDROGENE
A 5c
SENSIBILITE PAR UNITE DE LETHARGIE
10 1
10 0
10 -1
10 -2
10 -3
10 -6 10 -5 10 -4 10 -3 10 -2 10 -1 10 0 10 1 10 2
ENERGIE (MEV)

ANNEXE 5.c

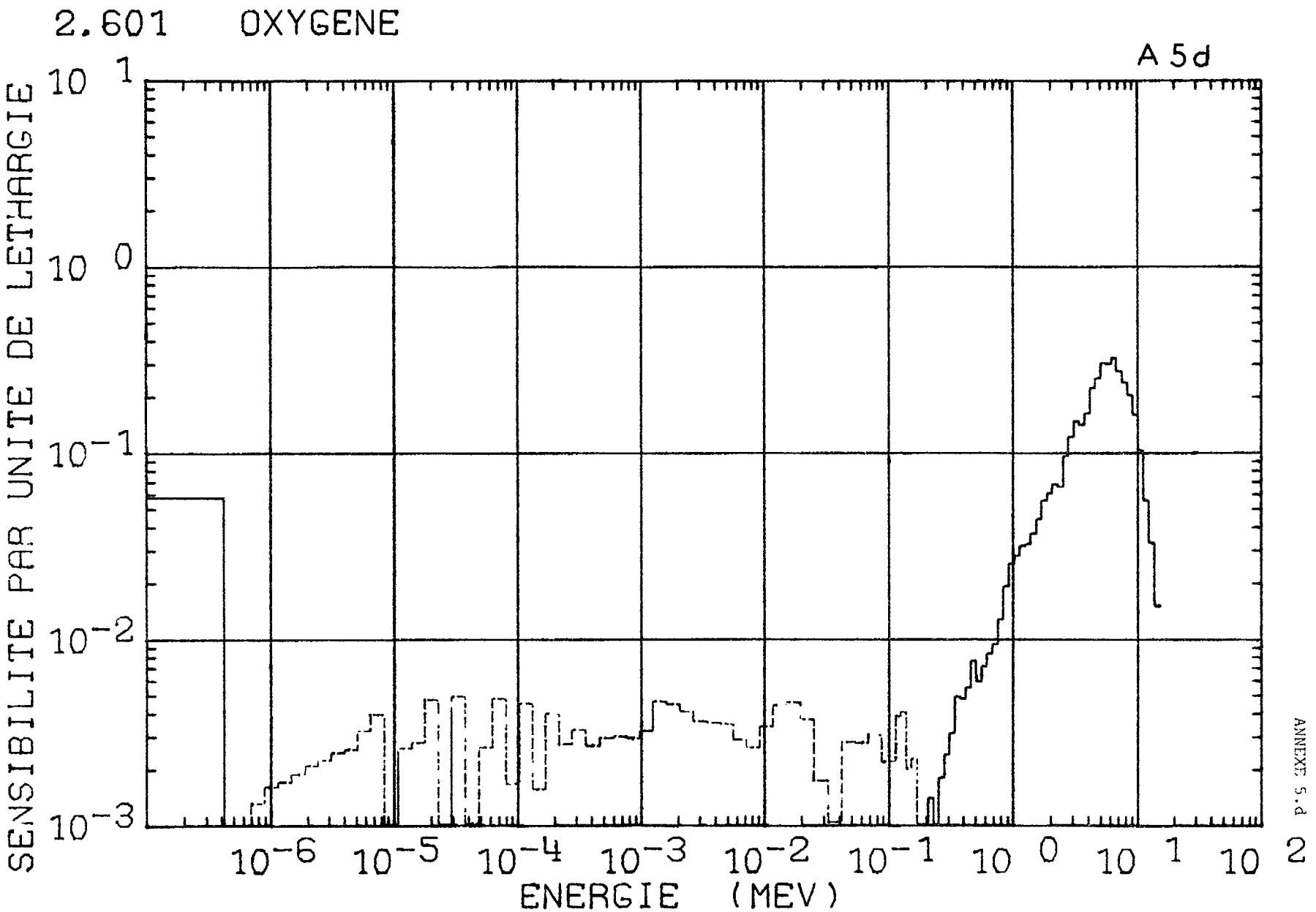
2.601 OXYGENE
A 5d
SENSIBILITE PAR UNITE DE LETHARGIE
10 1
10 0
10-1
10-2
10-3
10-6 10-5 10-4 10-3 10-2 10-1 10 0 10 1 10 2
ENERGIE (MEV)

ANNEXE 5.d

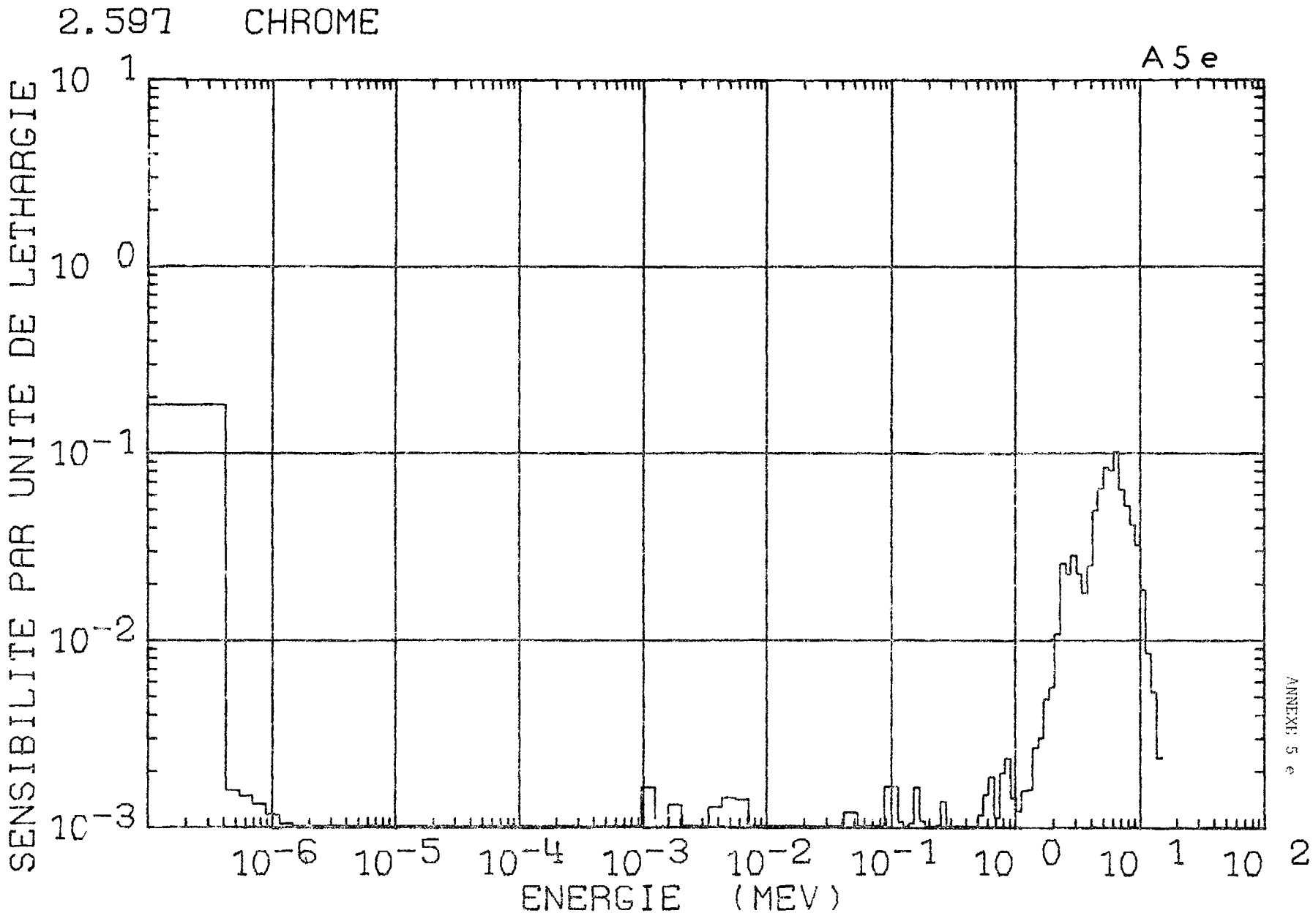
2.597 CHROME
A 5 e
SENSIBILITE PAR UNITE DE LETHARGIE
10 1
10 0
10-1
10-2
10-3
10-6 10-5 10-4 10-3 10-2 10-1 10 0 10 1 10 2
ENERGIE (MEV)

ANNEXE 5 e

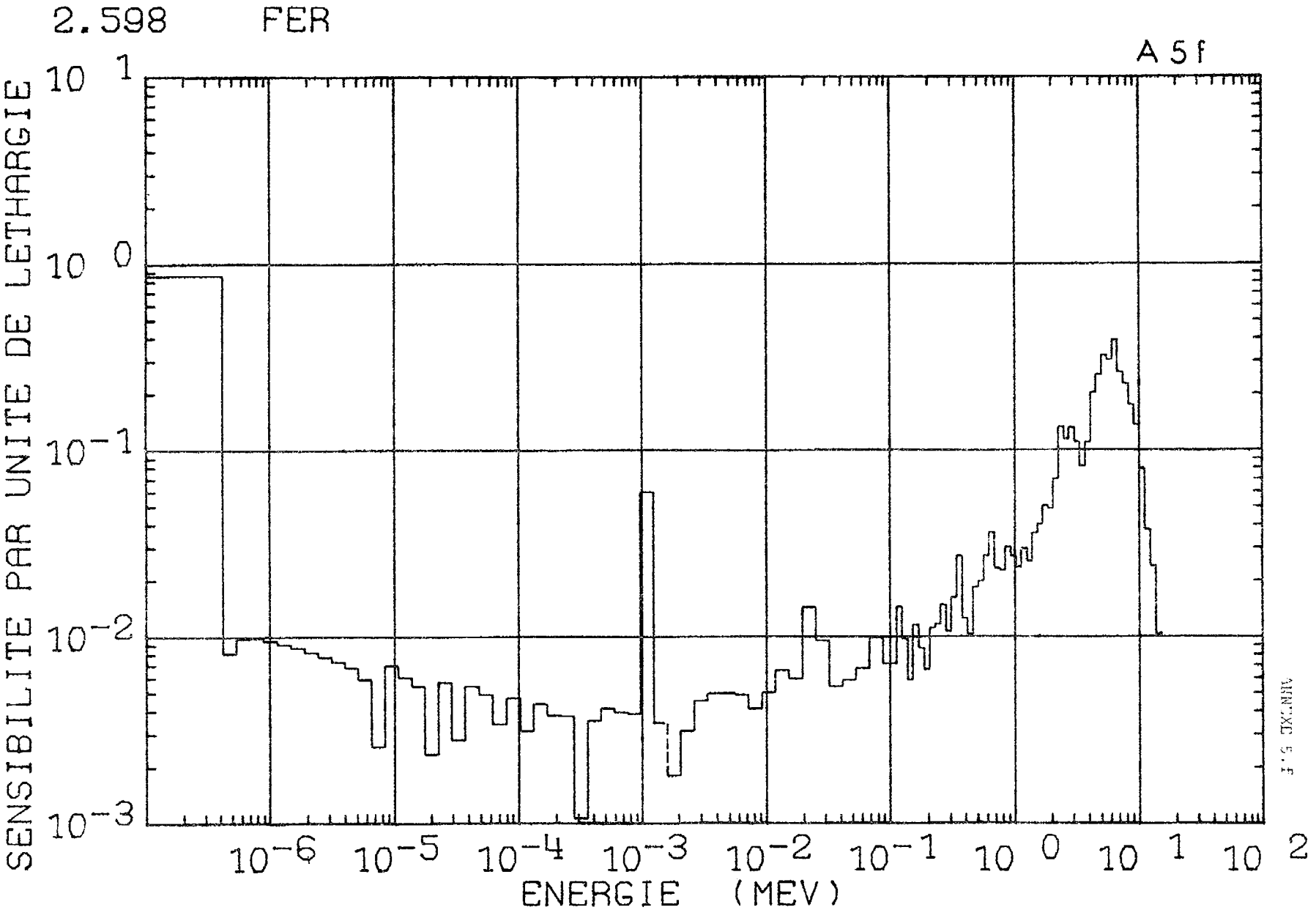
2.598 FER
A 5 f
SENSIBILITE PAR UNITE DE LETHARGIE
10 1
10 0
10-1
10-2
10-3
10-6 10-5 10-4 10-3 10-2 10-1 10 0 10 1 10 2
ENERGIE (MEV)

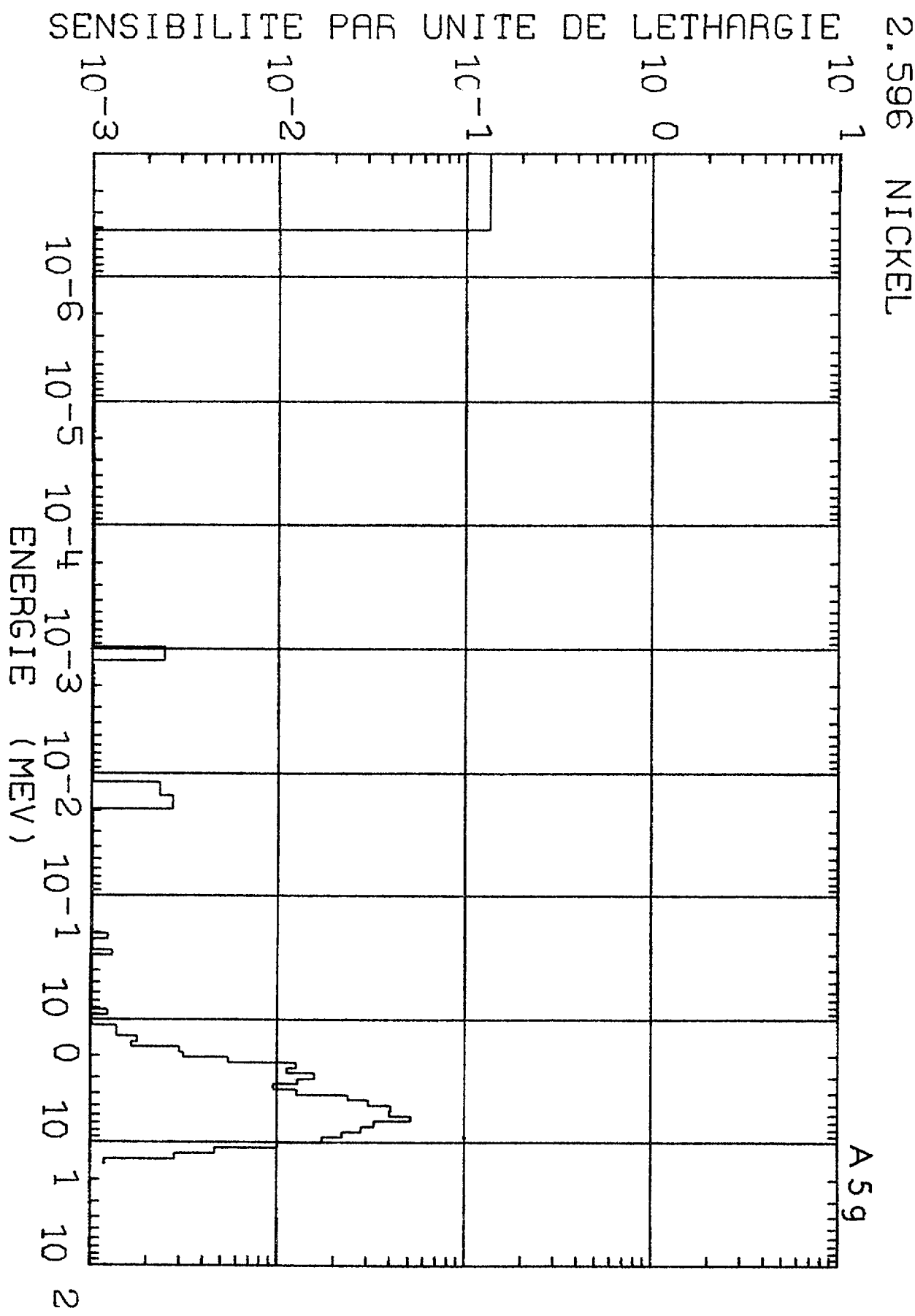
SENSIBILITE PAR UNITE DE LETHARGIE
2.596 NICKEL
10-3
10-2
10-1
10 0
10 1
10-6
10-5
10-4
10-3
10-2
10-1
10 0
10 1
10 2
ENERGIE (MEV)
A 5g

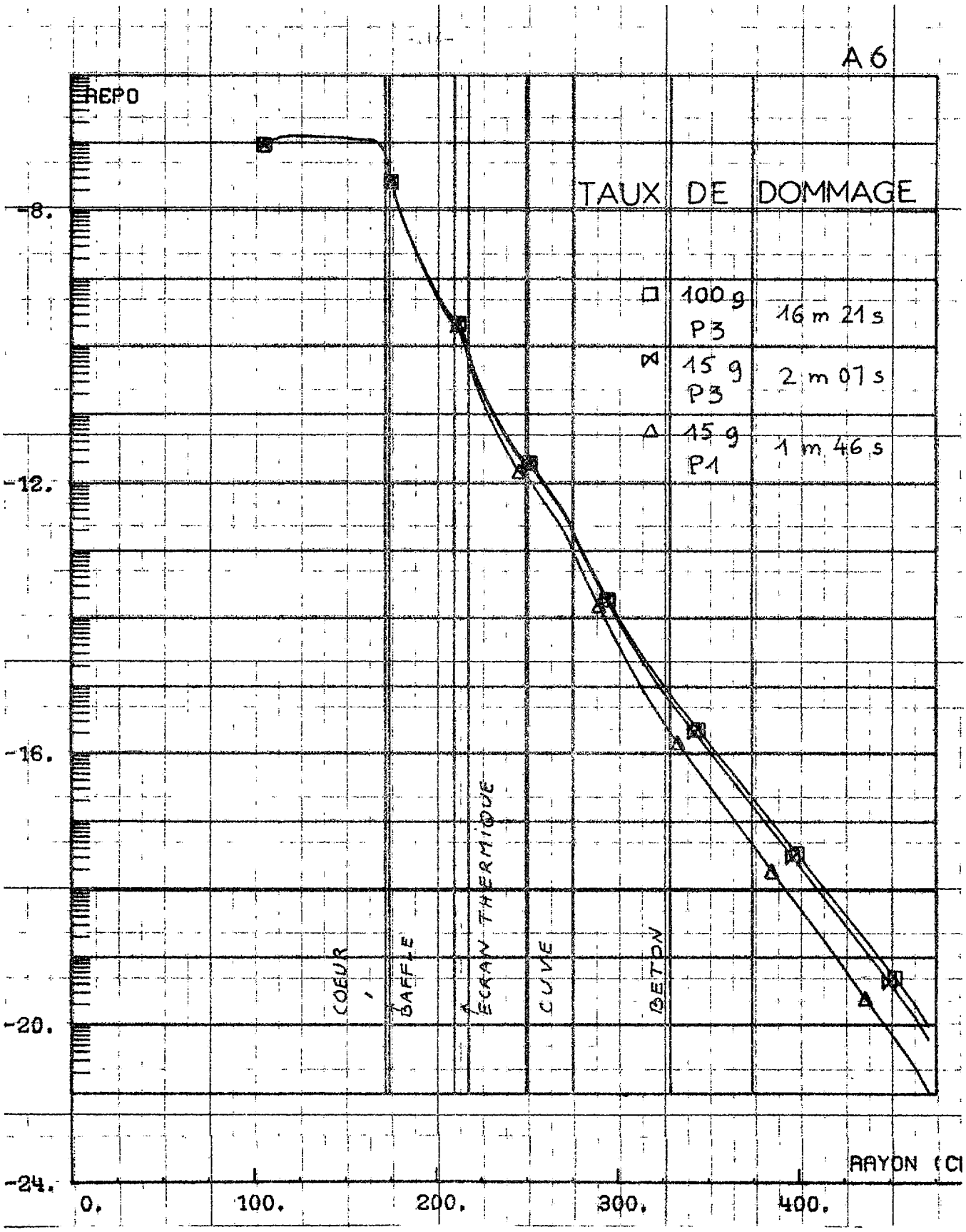
A 6
REPO
TAUX DE DOMMAGE
□ 100 g P3 16 m 21 s
⊠ 15 g P3 2 m 07 s
△ 15 g P1 1 m 46 s
-8.
-12.
-16.
-20.
-24.
0.
100.
200.
300.
400.
RAYON (C
COEUR
BAFFLE
ECRAN THERMIQUE
CUVE
BETON

Two NEA Sensitivity, 1-D Benchmark Calculations. Part I: Sensitivity of the dose rate at the outside of a PWR configuration and of the vessel damage.

(U.Canali, G.Gonano, R.Nicks)

Abstract

Within the framework of the coordinated programme of sensitivity analysis studies, the reactor shielding benchmark calculation concerning the shield of a typical Pressurized Water Reactor, as proposed by I.K.E. (Stuttgart)and K.W.U.(Erlangen) has been performed.

The direct and adjoint fluxes were calculated using ANISN, the cross-section sensitivity using SWANLAKE. The cross-section library used was EL4, 100 neutron + 19 gamma groups.
The following quantities were of interest:
- neutron damage in the pressure vessel
- dose rate outside the concrete shield

SWANLAKE was used to calculate the sensitivity of the above mentioned results to variations in the density of each nuclide present. The contributions of the different cross-section Legendre components are also given.

Sensitivity profiles indicate the energy ranges in which a cross-section variation has a greater influence on the results.

Introduction

The present work was performed within the framework of the Common Shielding Benchmark Calculations programme; it refers to the calculation proposed by G.Hehn and J. Koban /3/ for a typical Pressurized Water Reactor, the objective being the assessment of cross-section data needs.

The ANISN /1/ and SWANLAKE /2/ codes were used for the execution of this study.

Table 1 Radial dimensions along a main axis with simplified concrete shield.

Zone	Zone radius (cm)	Zone thickness (cm)
Reactor core	172.5	-
Core baffle	175.0	2.5
1. Water layer	210.5	35.5
Core barrel	218.5	8.0
2. Water layer	250.0	31.5
Austenitic cladding	250.6	0.6
Pressure vessel	275.6	25.0
Concrete shield	475.6	200.0

Table 2 Material composition (10^{24} cm^{-3})

Zone / Nuclide	Reactor core	Core baffle core barrel aust.cladding	Pressure vessel	1.and 2. water layer	Concrete shield
H	2.8226E-02	-	-	5.0556E-2	4.4126E-3
O	2.7154E-02	-	-	2.5278E-2	4.7751E-2
Al	-	-	-	-	2.4553E-3
Si	-	-	-	-	9.4350E-3
Ca	-	-	-	-	6.6115E-3
Cr	-	1.6913E-2	-	-	-
Mn	-	1.1187E-3	-	-	-
Fe	9.8235E-4	6.4478E-2	8.465E-2	-	-
Ni	-	8.5357E-3	-	-	-
Zr	4.3246E-3	-	-	-	-
^{235}U	2.1040E-4	-	-	-	-
^{238}U	6.3087E-3	-	-	-	-

Summary on the configuration

The geometrical configuration is an infinite cylinder. The different zones and compositions are reproduced from /3/ in Tables 1 and 2. The space intervals adopted were the same as those suggested in /3/ apart from in the outer part of the concrete zone.

The angular quadrature used was S6 and the cross-section expansion P3. As far as the library is concerned the EL4 (ESIS Library 4) /4/ /5/ coupled 100 - neutron + 19 - gamma group library was used.

Dose calculation and sensitivity

The response taken was the dose rate in rem/h multiplied by the volume of the last mesh interval, whose thickness was 0.4 cm, outer radius 475.6 cm, and area 1194.5 cm^2. The flux-to-dose-rate conversion factors for neutrons and for photons were interpolated for the EL4 structure from the values published in the report ANSI - N 666.
The responses calculated were:
(from a forward ANISN run) 5.97 (rem/h) cm^3
(from an adjoint ANISN run) 6.37 (rem/h) cm^3
the discrepancy being 7%
The SWANLAKE calculation provided sensitivity integrals per zone, element, etc. The most significant of these were represented as histograms in the following figures.

Figures 1 and 2 represent the dose sensitivity to neutron and gamma cross-sections, in the various zones respectively resulting from the variation of both. The sensitivity values for the different elements are referred to the horizontal axis.

Neutron and Photon dose conversion factors.

(REM/H)/(NEUT/SQCM*SEC), EL 4, ANSI N666

2.087E-04	1.902E-04	1.716E-04	1.548E-04	1.470E-04	1.470E-04
1.470E-04	1.470E-04	1.494E-04	1.521E-04	1.548E-04	1.532E-04
1.484E-04	1.437E-04	1.392E-04	1.348E-04	1.306E-04	1.265E-04
1.255E-04	1.262E-04	1.270E-04	1.277E-04	1.285E-04	1.293E-04
1.300E-04	1.308E-04	1.316E-04	1.289E-04	1.224E-04	1.163E-04
1.105E-04	1.050E-04	9.976E-05	9.479E-05	8.818E-05	8.058E-05
7.363E-05	6.728E-05	6.148E-05	5.618E-05	5.133E-05	4.691E-05
4.287E-05	3.918E-05	3.580E-05	3.271E-05	2.990E-05	2.732E-05
2.496E-05	2.137E-05	1.756E-05	1.443E-05	1.186E-05	9.745E-06
8.009E-06	6.582E-06	5.409E-06	4.444E-06	3.653E-06	3.578E-06
3.600E-06	3.621E-06	3.643E-06	3.664E-06	3.686E-06	3.708E-06
3.730E-06	3.752E-06	3.789E-06	3.832E-06	3.877E-06	3.922E-06
3.967E-06	4.013E-06	4.059E-06	4.106E-06	4.154E-06	4.197E-06
4.235E-06	4.273E-06	4.311E-06	4.350E-06	4.389E-06	4.429E-06
4.469E-06	4.509E-06	4.538E-06	4.529E-06	4.520E-06	4.512E-06
4.503E-06	4.494E-06	4.486E-06	4.477E-06	4.468E-06	4.457E-06
4.364E-06	4.273E-06	4.183E-06	3.670E-06		

(REM/H)/(PHOT/SQCM*SEC), EL 4, ANSI N666

8.076E-06	7.282E-06	6.546E-06	5.780E-06	5.007E-06	4.281E-06
3.710E-06	3.192E-06	2.608E-06	1.934E-06	1.380E-06	1.009E-06
7.068E-07	4.663E-07	3.275E-07	2.702E-07	2.755E-07	4.042E-07
7.211E-07					

Figure 4 shows the sensitivity per zone summed over the various elements and split up into neutron and gamma contributions, whereas figure 5 represents the dose sensitivity for the various elements integrated over all zones and clearly shows the importance of oxygen and hydrogen.

Table 3 illustrates the sensitivity of the dose R to the cross-sections of each element; the separate contributions for neutrons and gamma rays are given. The contributions of the higher order terms of the Legendre expansions of the angular distributions of the scattering are given as % changes of the dose rate with decreasing Legendre order.

TABLE 3

Element		Sensitivity of the dose to each X - section		Predicted % change from P(3) calculation to:		
		neutrons	gammas	P(0)	P(1)	P(2)
1	H	- 5.40	- 0.13	- 89	- 19	- 2
2	O	- 3.13	- 4.94	-112	- 24	- 4
3	Al	- 0.16	- 0.41	- 8	- 2	- 0
4	Si	- 0.57	- 1.71	- 31	- 8	- 1
5	Ca	- 0.62	- 1.86	- 33	- 8	- 1
6	Cr	- 0.31	- 0.15	- 12	- 3	- 0
7	Mn	- 0.02	- 0.01	- 1	- 0	- 0
8	Fe	- 2.33	- 2.83	-114	- 30	- 5
9	Ni	- 0.13	- 0.10	- 7	- 2	- 0
10	Zr	- 0.10	- 0.01	- 2	+ 0	+ 0
11	U5	+ 0.01	- 0	- 0	+ 0	+ 0
12	U8	- 0.31	- 0.06	- 5	+ 1	+ 0
Sum		-13.08	-12.23	-414	-100	-13

Figures 6 to 17 are the sensitivity profiles for the 12 elements occurring in the configuration, Figure 18 represents their sum.

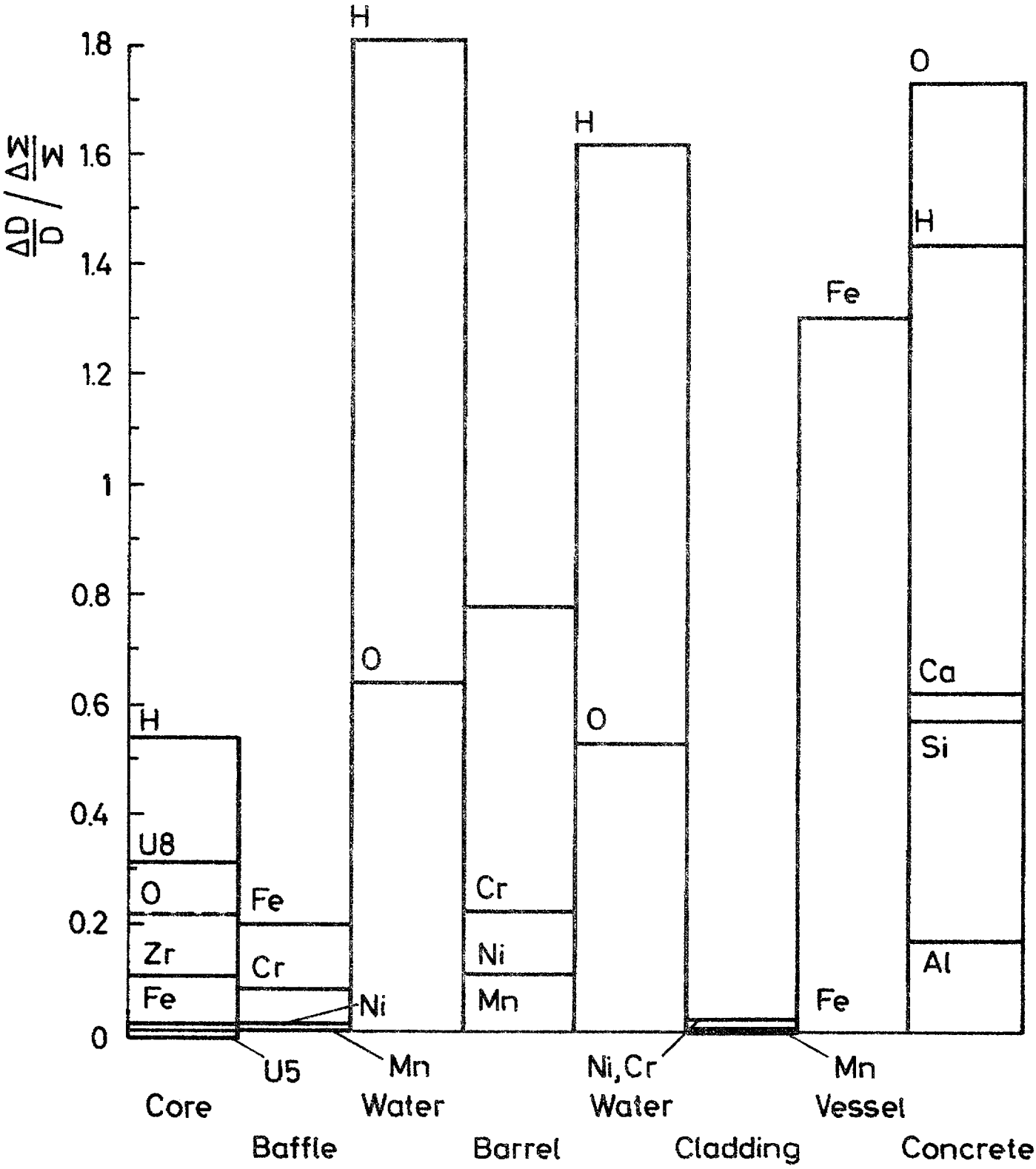

Dose Sensitivity to neutron cross sections in a PWR.

Library: EL-4

Fig. 1

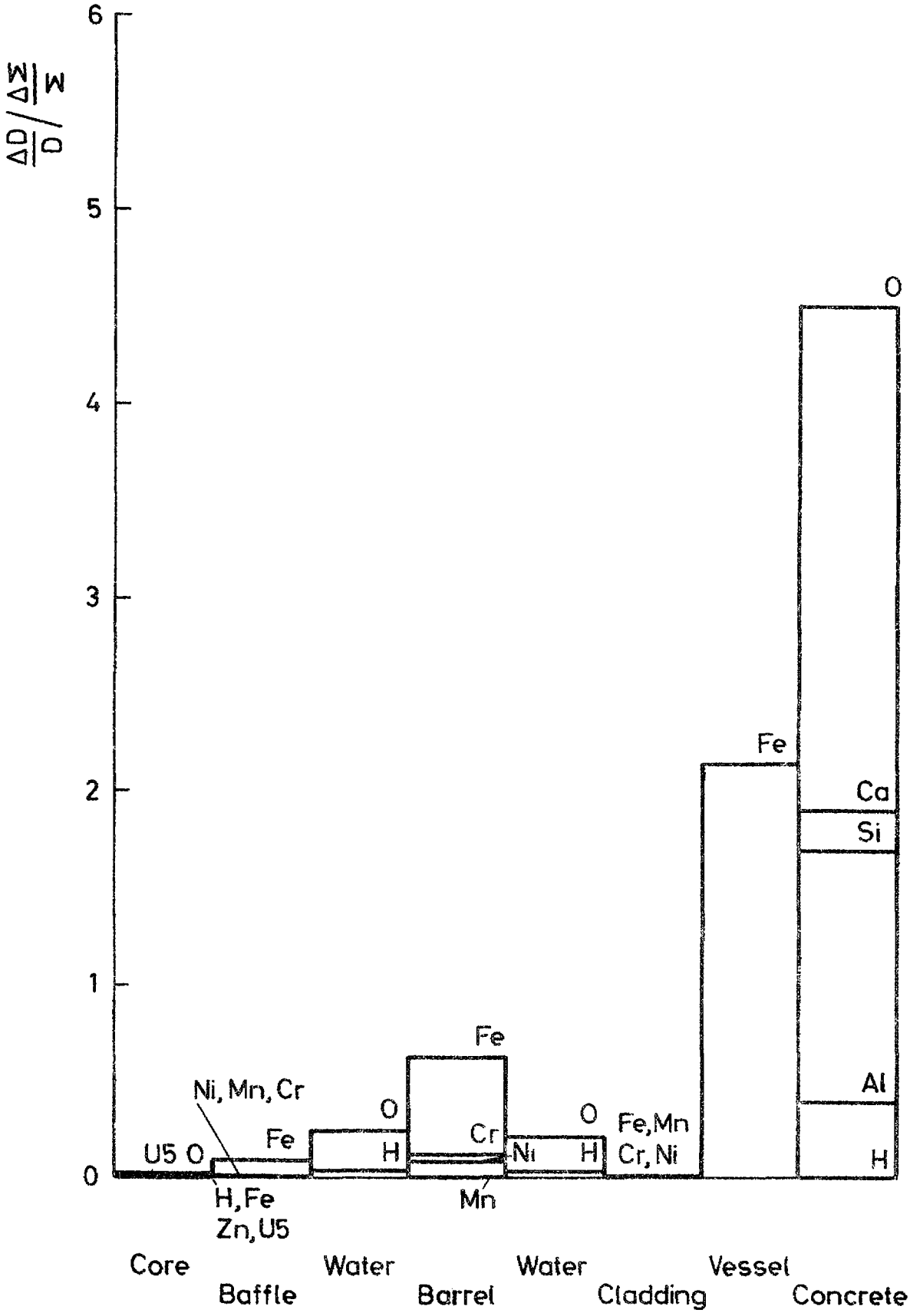

Dose Sensitivity to gamma cross sections in a PWR

Library : EL-4

Fig. 2

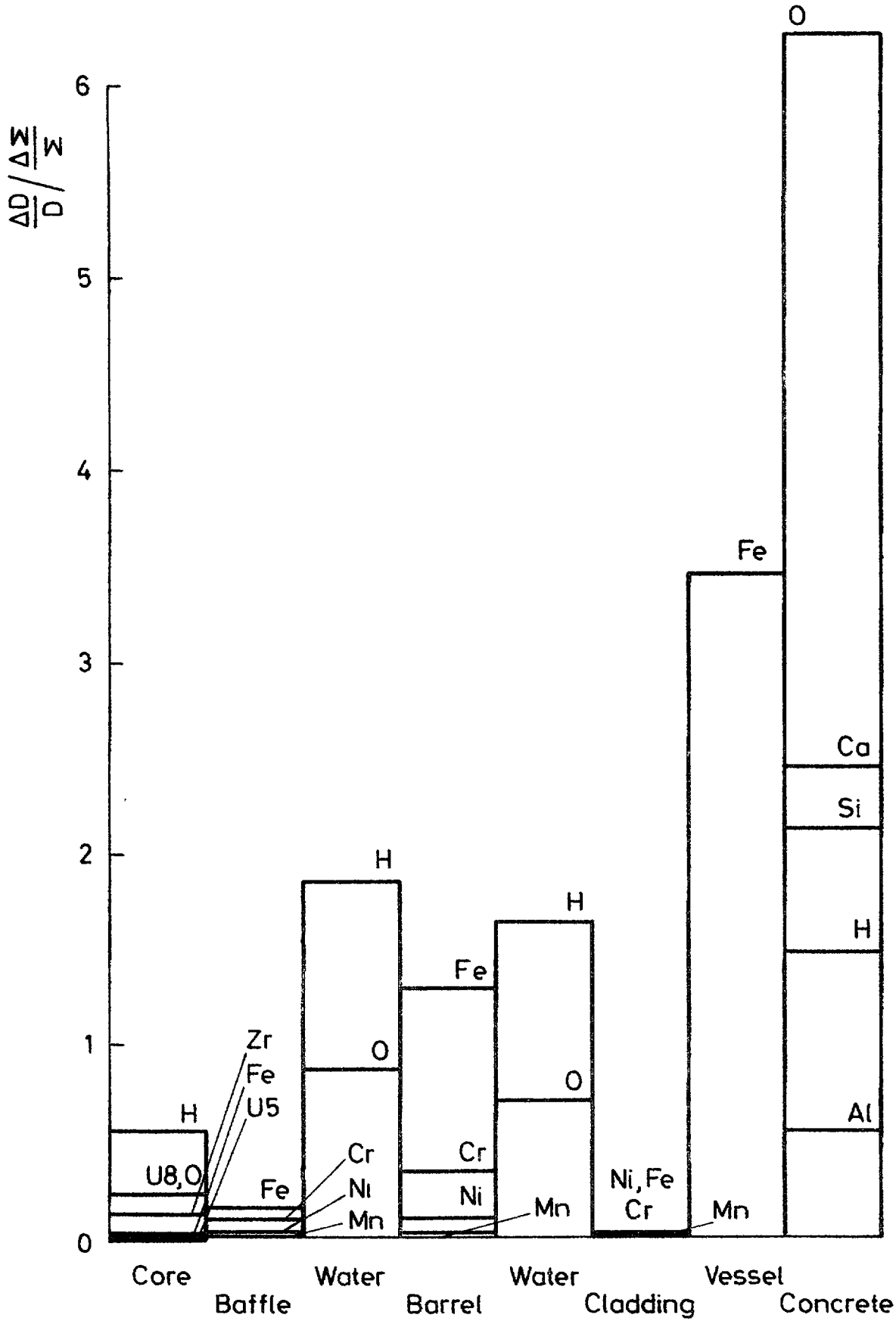

Dose sensitivity to cross sections in a PWR
Library : EL-4

Fig. 3

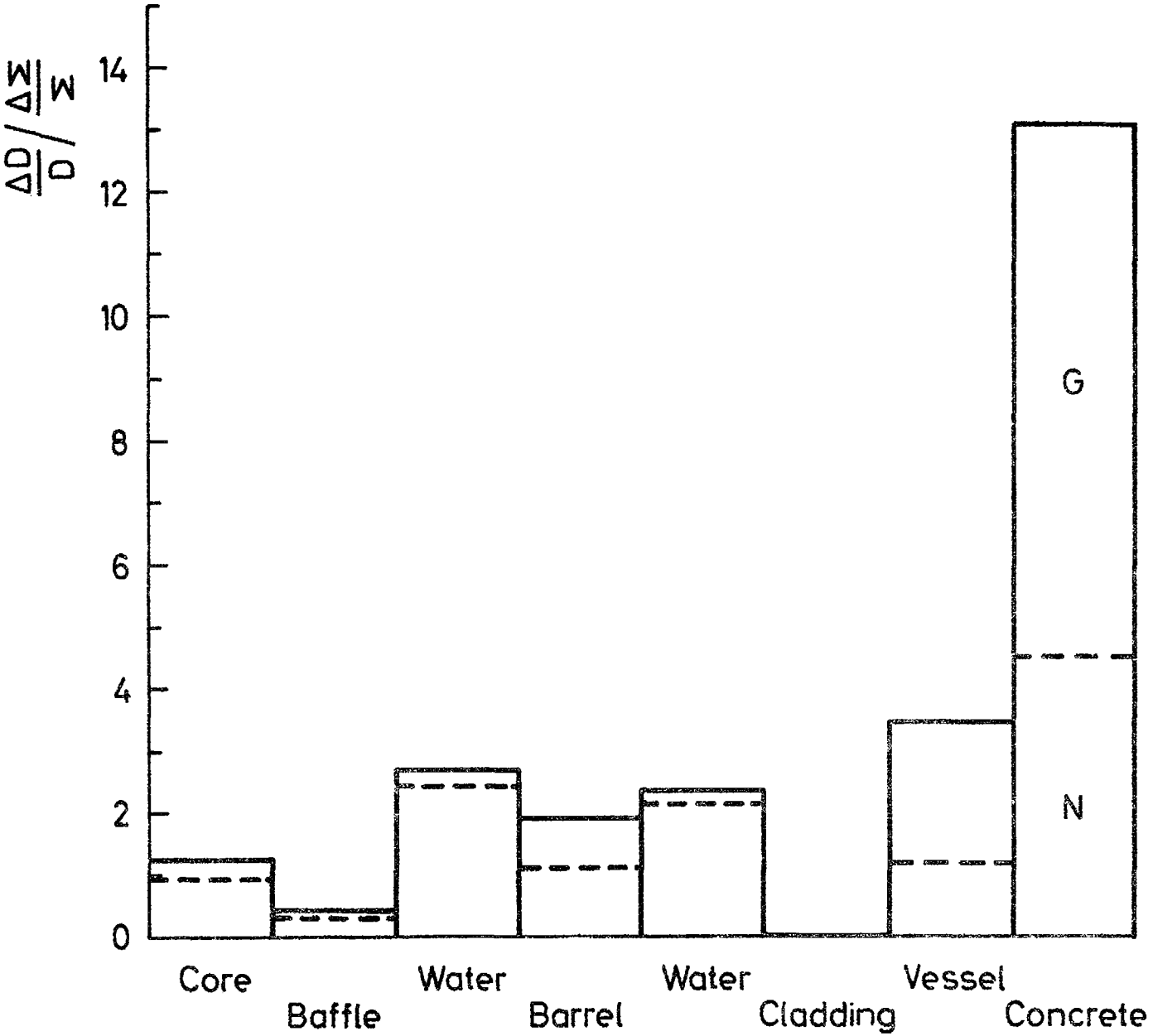

Dose sensitivity: * neutron summation
* gamma summation

Fig. 4

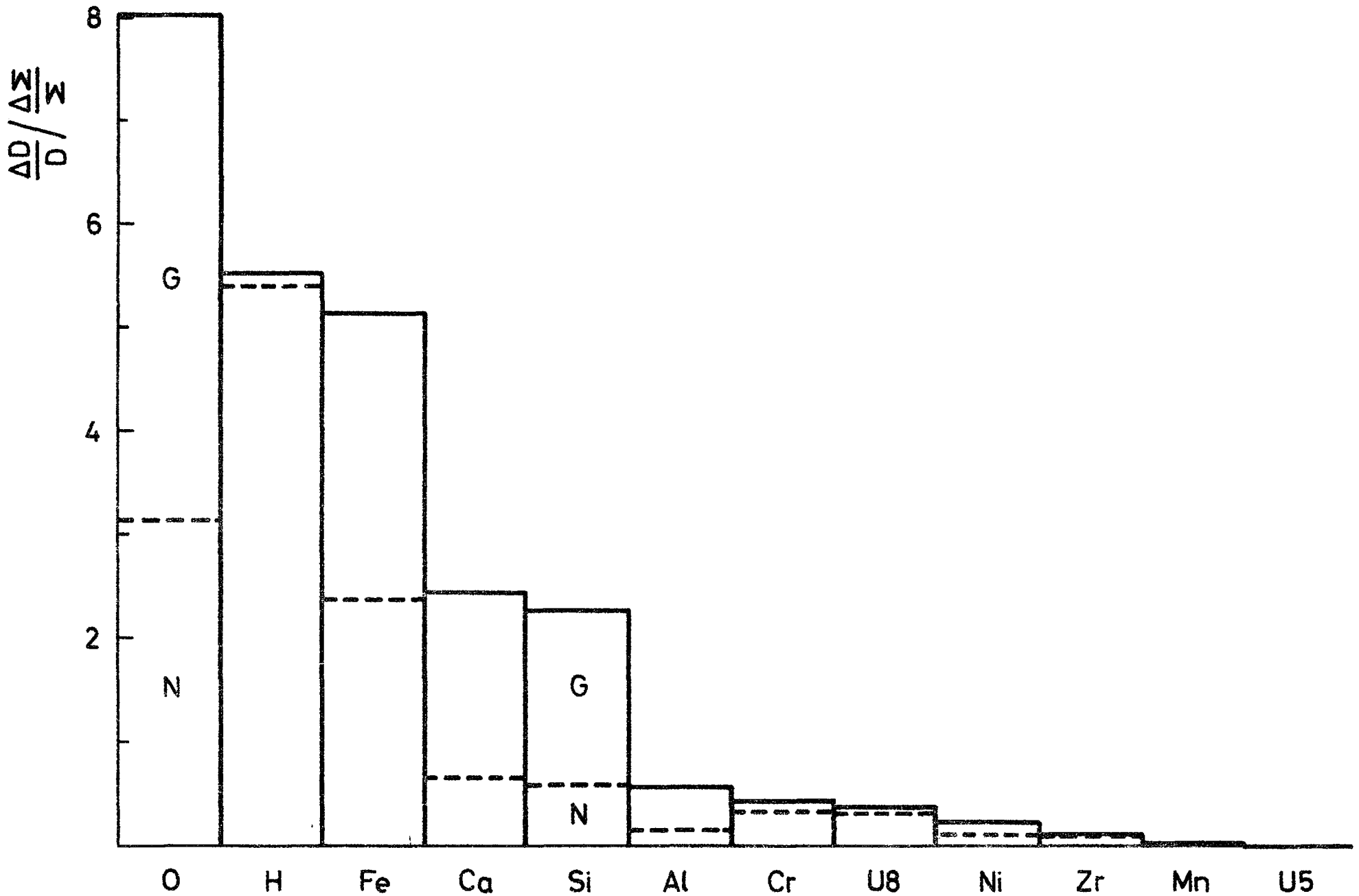

Dose Sensitivity for the various elements integrated over all zones
Total area: 22

Fig. 5

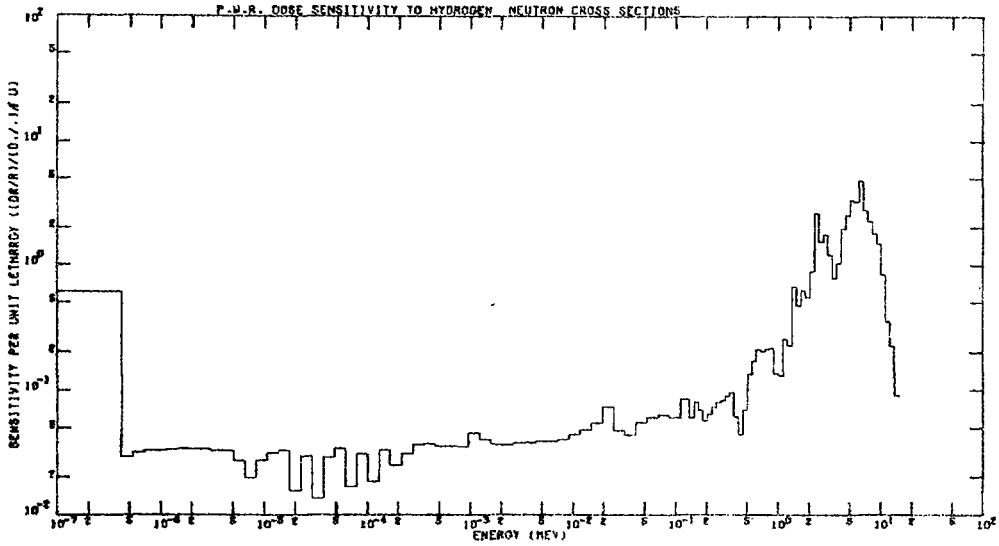

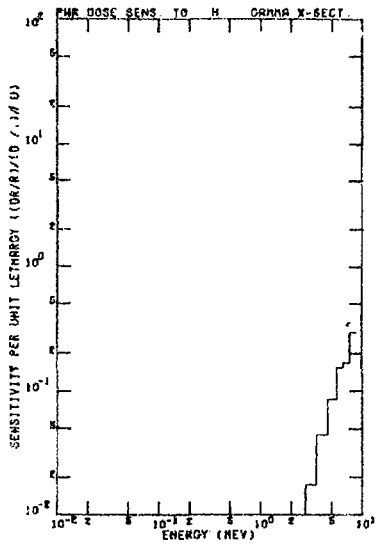

FIG. 6

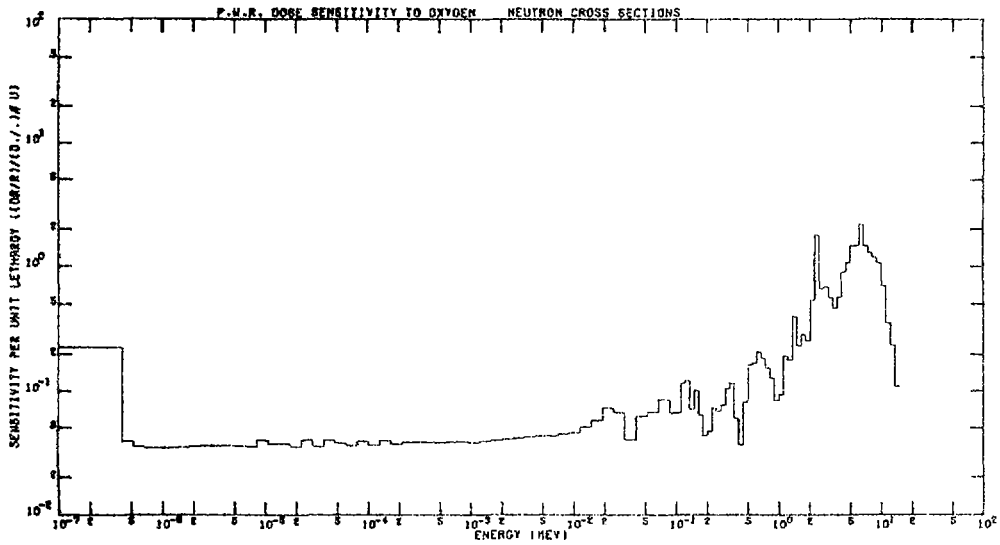

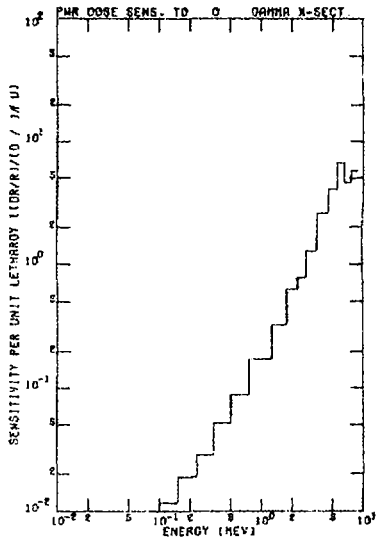

FIG. 7

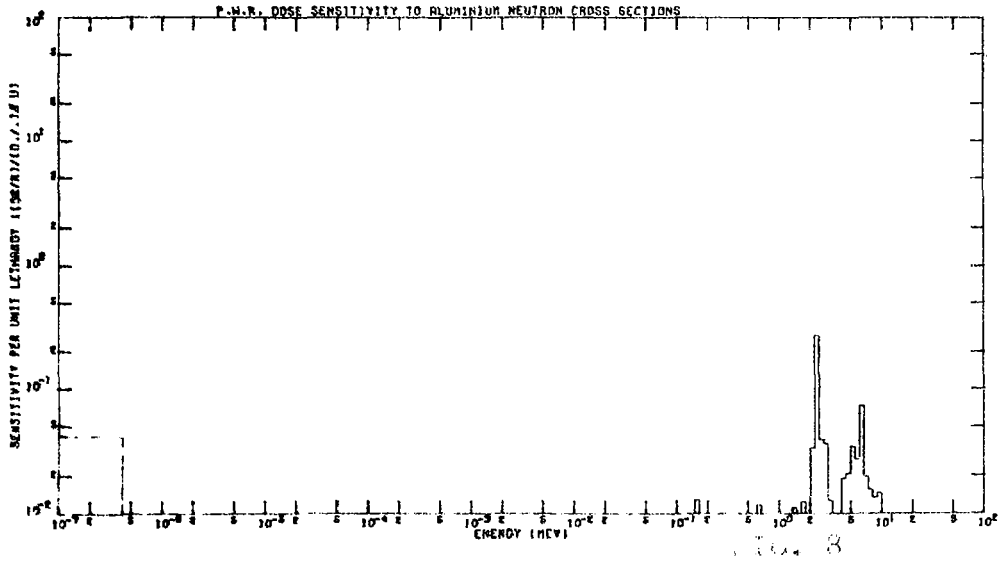

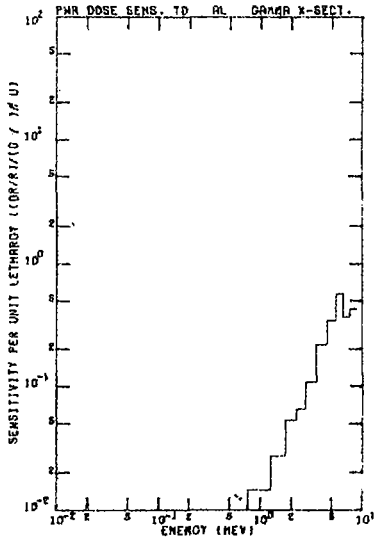

FIG. 8

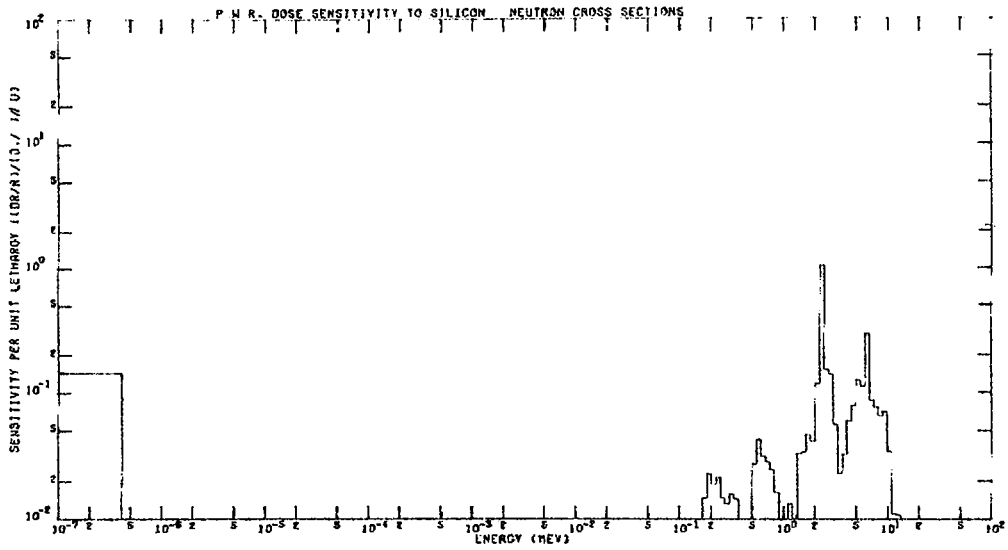

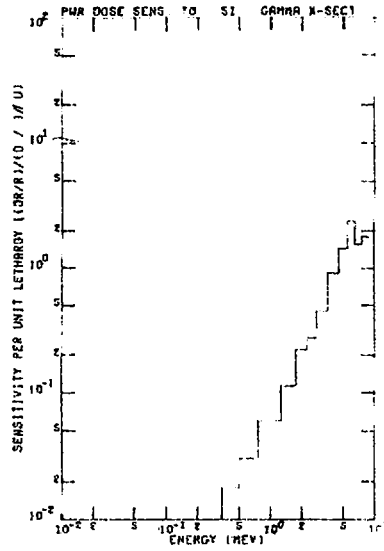

FIG. 9

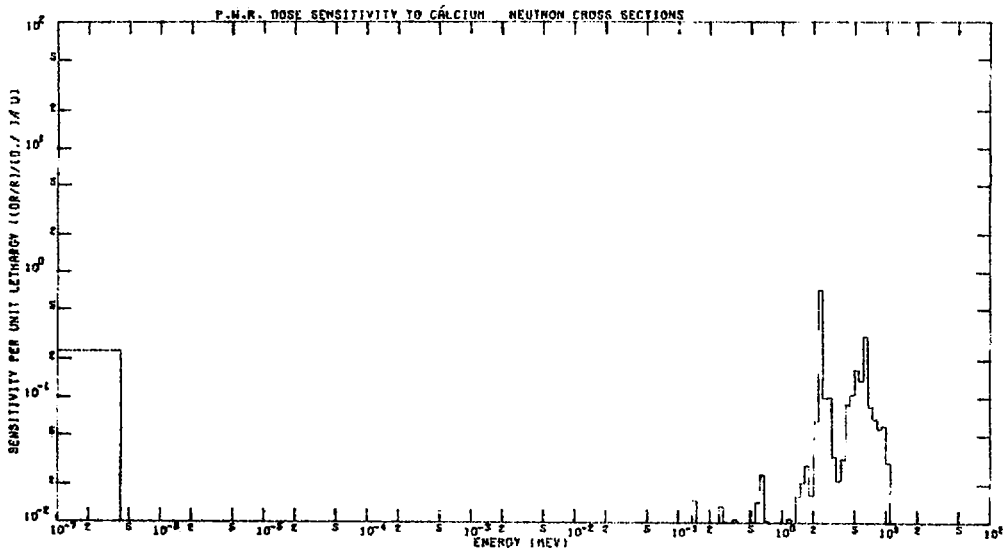

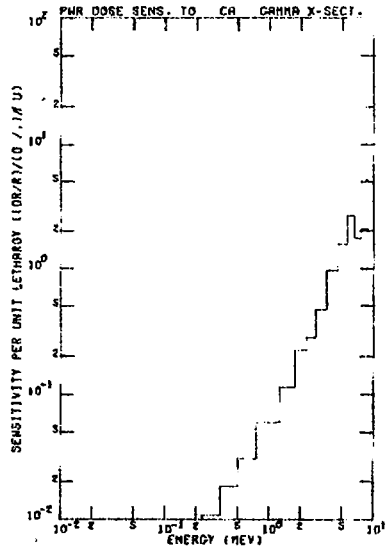

FIG. 10

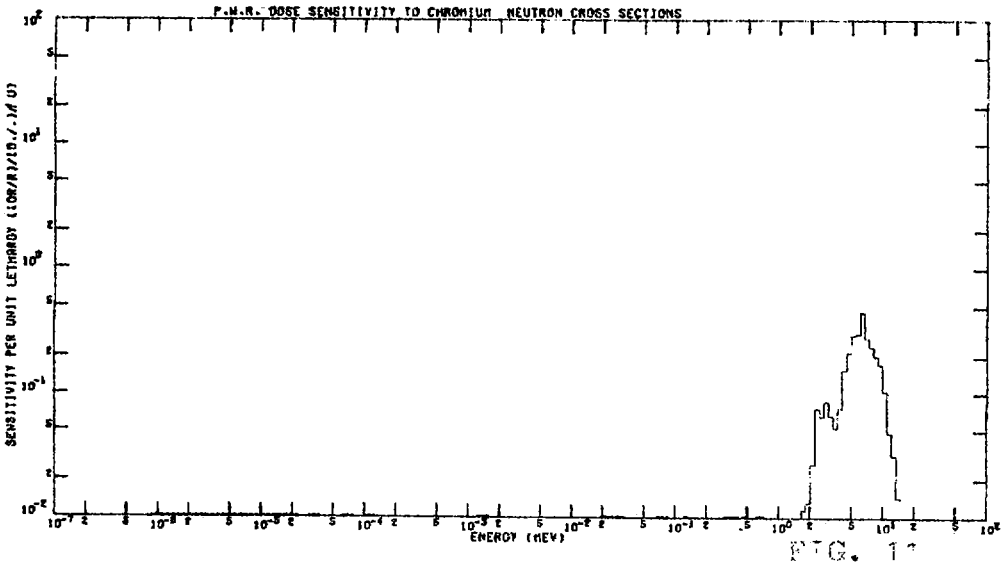

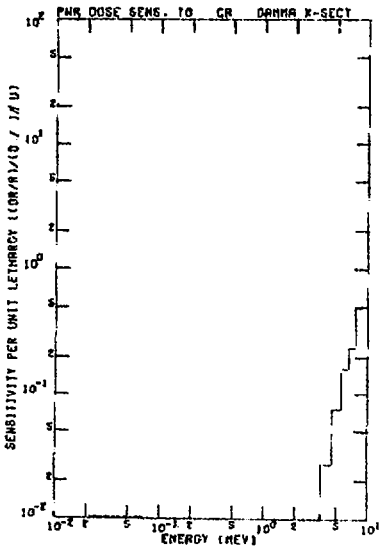

FIG. 11

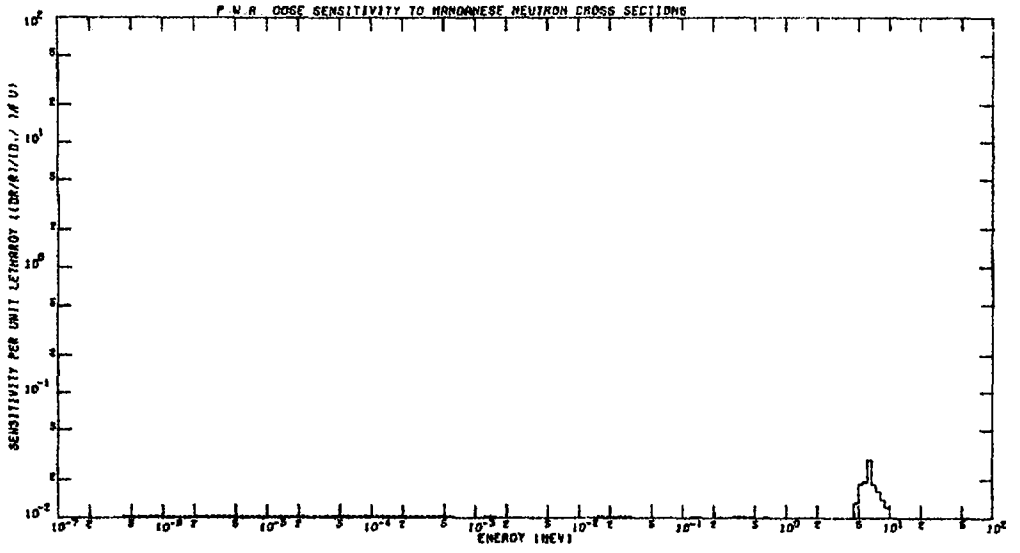

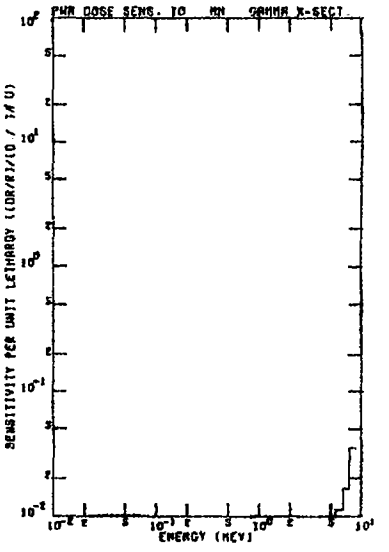

FIG. 12

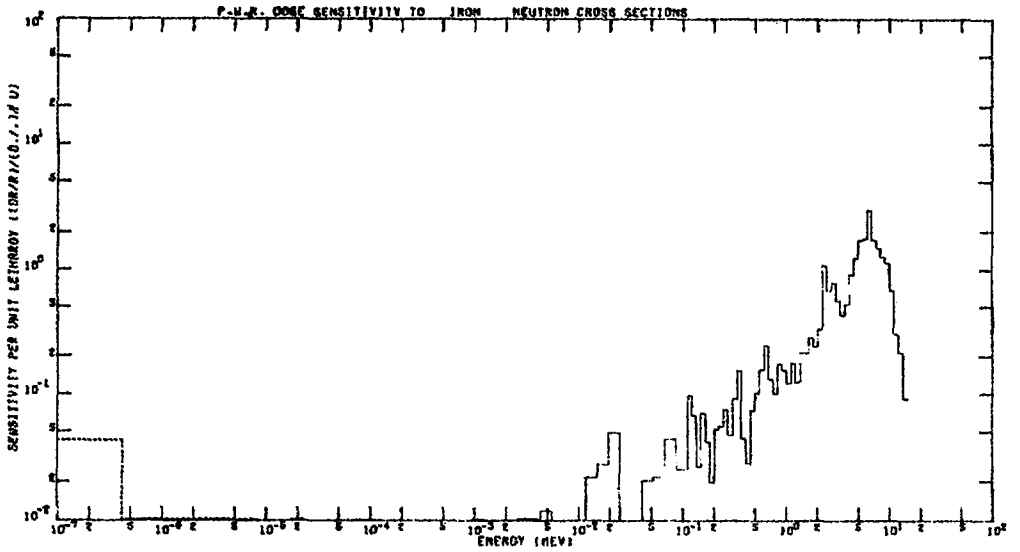

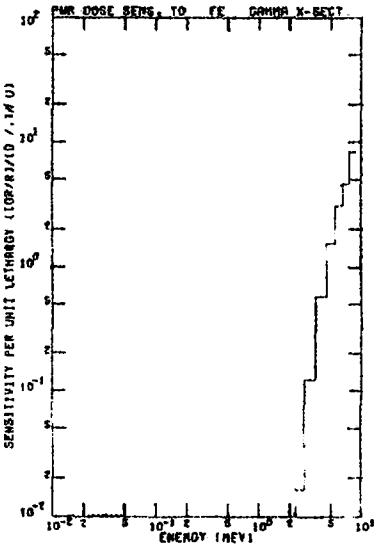

FIG. 13

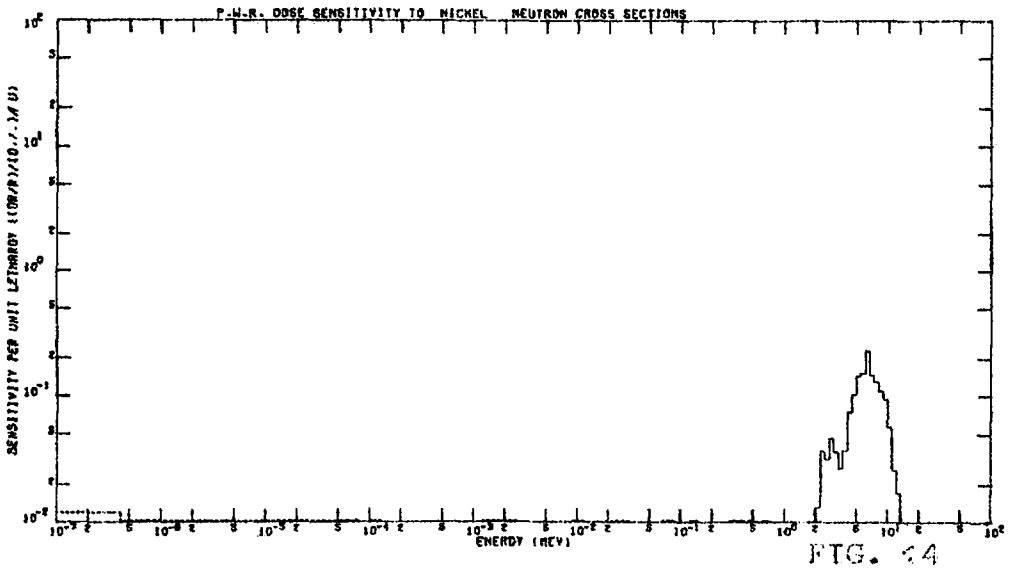

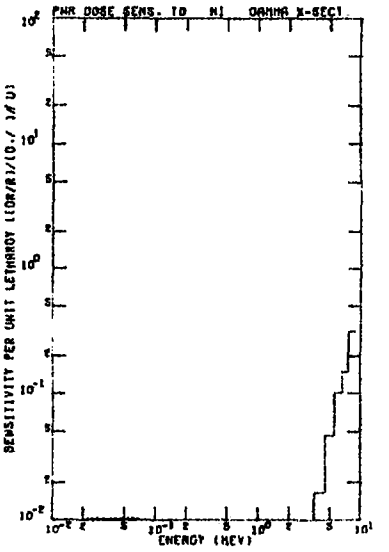

FIG. 14

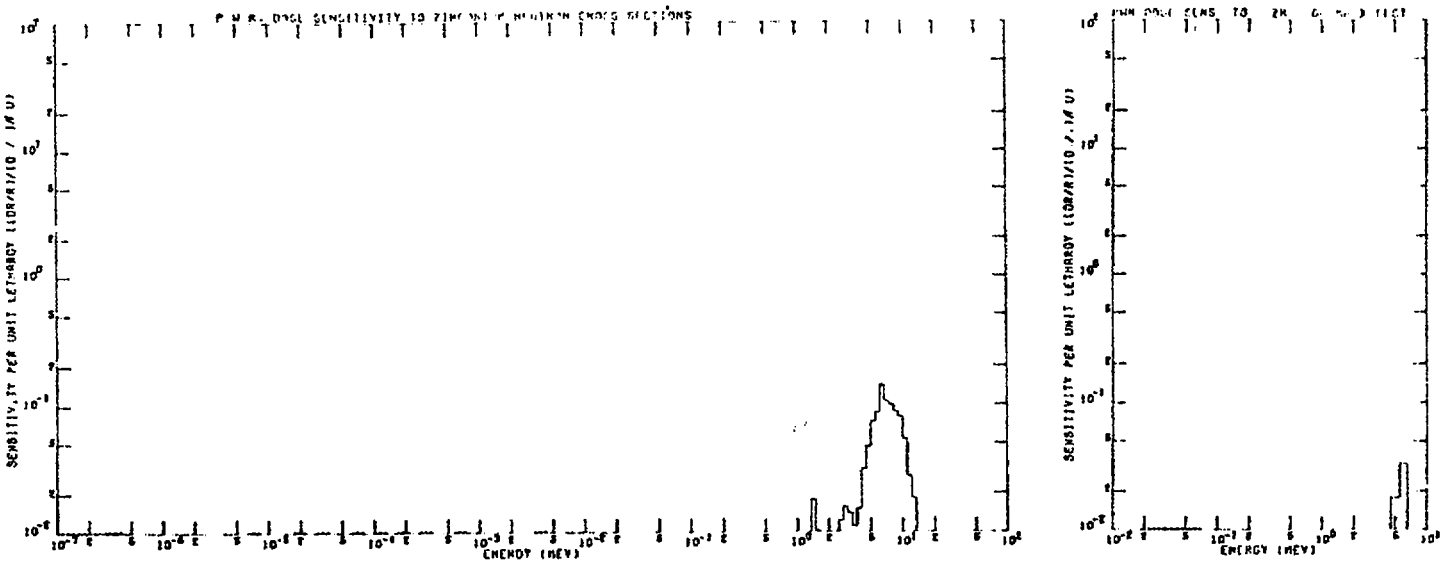

FIG. 15

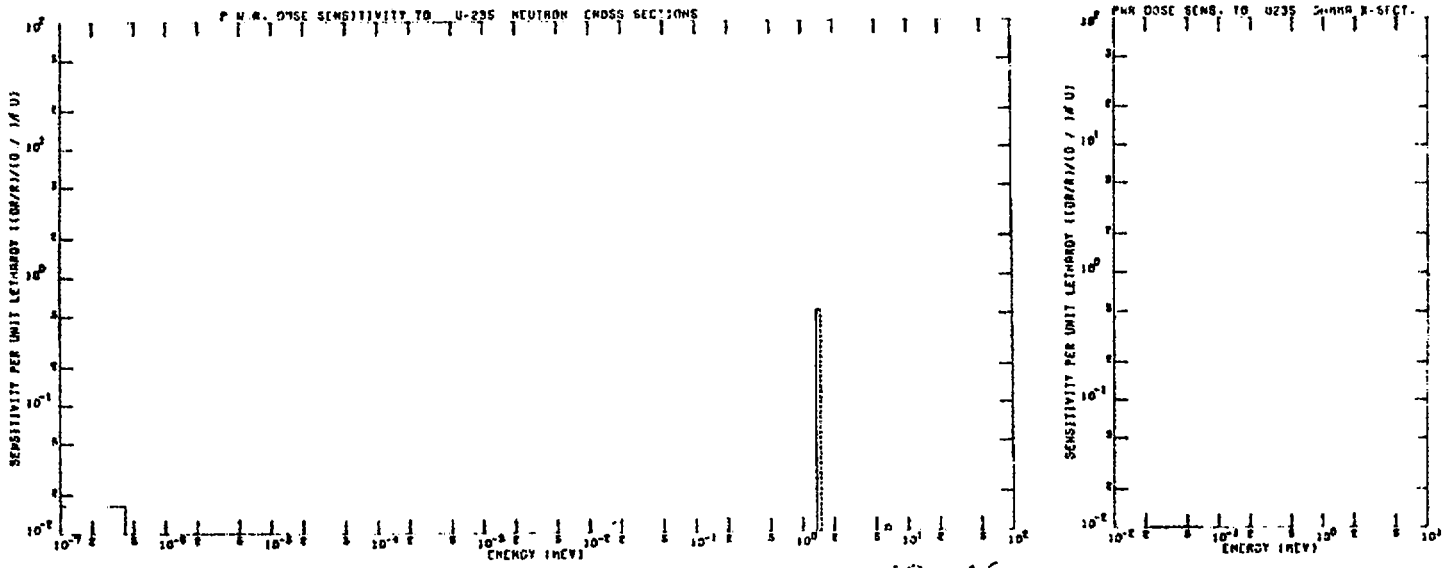

FIG. 16

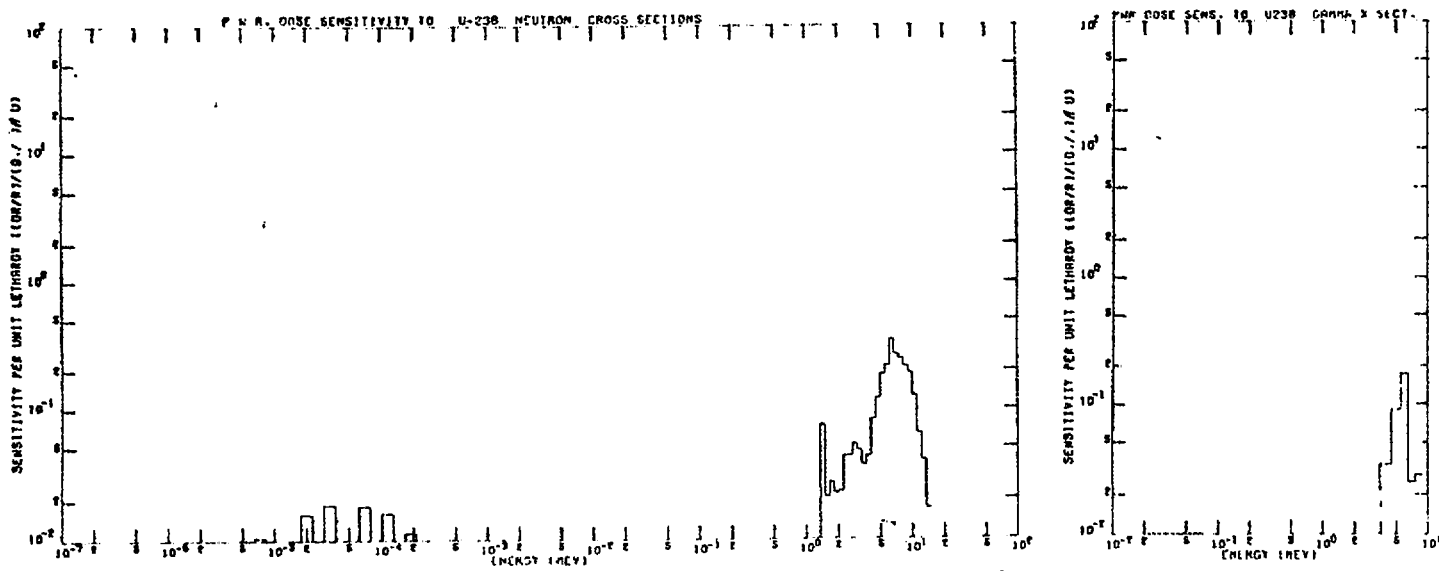

FIG. 17

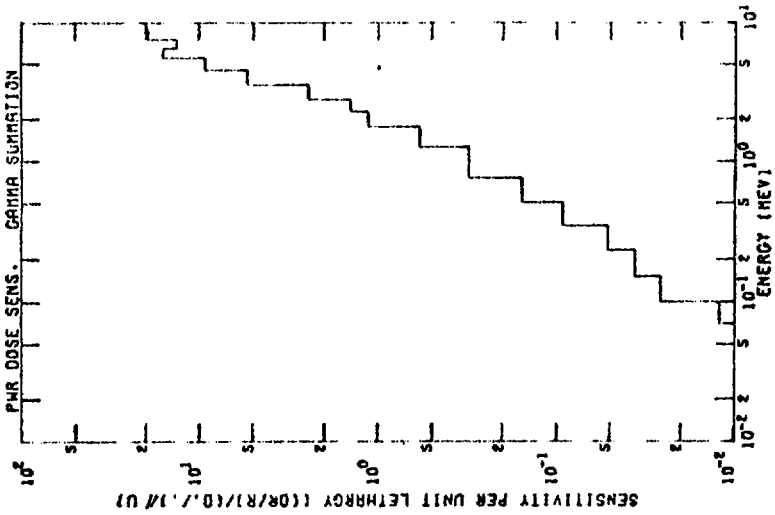
PWR DOSE SENS. GAMMA SUMMATION
ENERGY (MEV)
SENSITIVITY PER UNIT LETHARGY ((DR/R)/(D./.)// U)

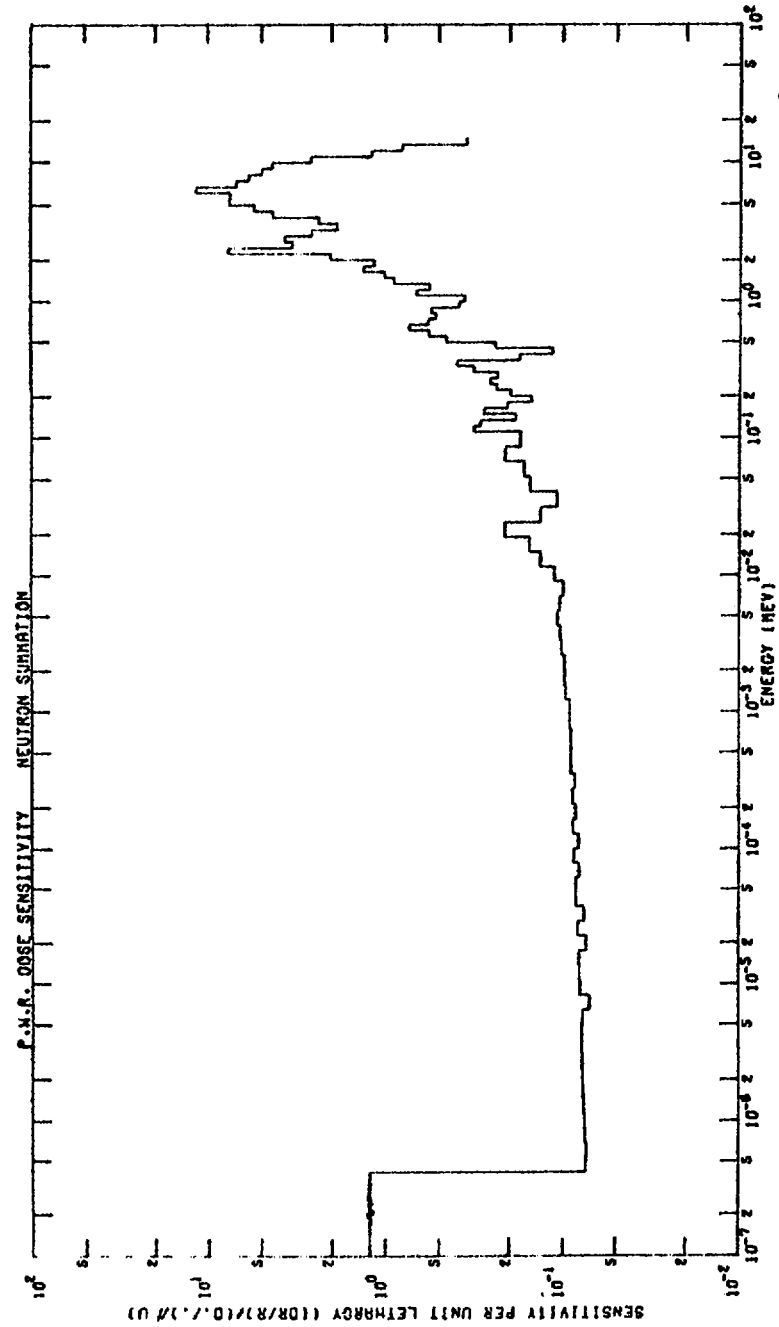
P.W.R. DOSE SENSITIVITY NEUTRON SUMMATION
ENERGY (MEV)
SENSITIVITY PER UNIT LETHARGY ((DR/R)/(D./.)// U)

FIG. 18

Discussion of the sensitivity results for the dose rate

It appears from the bulk of the sensitivity results that the particles having the longer mean free paths in this shield are the gammas (the overall sensitivity is greater for them than for the neutrons).

The most important of the gammas are those generated and being transported in the concrete: the gamma sensitivity of Fe, which only occurs in shells between the core and the concrete, is a small part of the total gamma sensitivity.

Antiresonances in the neutron cross-section of an element appear as sensitivity maxima not only for that element, but also for the other elements or isotopes in the material under investigation; thus the windows in the oxygen cross-section at 300 KeV and at 500 KeV may be detected for instance as maxima in the iron profile and also in the overall profile made up of the summation of the profiles of all elements present in the configuration.

The question that arise is to what extent the present results may be used for fixing cross-section priority requests of interest to the particular reactor type and the particular response function.

In the view of traditional dose rate exposure thinking a dose rate known with a precision of 100% is certainly acceptable. We also anticipate that the gamma cross-sections are known with a high enough precision, so that the resulting error may be neglected.

To the total neutron sensitivity of 13, oxygen contributes 3.13 so that a maximum error of 30% in the total cross-section leads to a 100% error in the response supposing the linear perturbation model still holds. The situation changes if one takes into account tha ALAP requirements established in the light of economic operation and maintenance of future power stations.
A valuable error limit might then be 10% which would lead to a 3% precision for the total cross-section.

Radiation Damage and Sensitivity

The response was the number of displacements (Frenkel pairs) produced per gram per second multiplied by the volume of the first mesh interval of the vessel, the thickness of which was 0.3 cm, the inner radius 250.6 cm and the volume 472.656 cm^3.

The damage coefficients are given in Table 4; they are based on the Wisconsin data /6/. The resulting response was:

from the forward ANISN calculation	5.704E12
from the adjoint ANISN calculation	5.849E12
the discrepancy being	2.5%

The sensitivity calculations were performed using the SWANLAKE code. The histogram in Fig. 19 shows the contribution of each element to the total sensitivity, whereas in Fig. 20 each column corresponds to a particular zone, and the contribution of each element in that zone is given (all the levels are measured from the horizontal axis).

Table 5 shows the vessel damage sensitivity and the P(L) contributions for each element, summed over groups and zones. Sensitivity profiles are given in Fig. 21.

Discussion of the Sensitivity Results for the Radiation damage.

As far as the fine structure of the sensitivity profile is concerned, the same observations made for the dose-rate hold also for the damage. The relatively high importance of the oxygen seems rather surprising. It could be explained by the fact that water is the most abundant material in the intervening zones and that the fast neutron propagation is strongly influenced by the antiresonances of the oxygen in the core and in the water zones. Supposing that the target accurancy of damage is about 20%, and attributing to oxygen and iron a sensitivity of 1.5 each (assuming that the hydrogen cross-section precision is high) an upper limit of the error allowed for the total oxygen and iron cross-sections should be about 7%.

TABLE 4

DISPLACEMENT CROSS SECTIONS FOR STAINLESS STEEL IN CM2/GR
WISCONSIN DATA N=1.C8+22ATOMS PER GRAM CHANGE ABOVE ENERGY GROUP 15

0.2862+02	C.2604+02	0.2446+02	0.2352+02	0.2259+02	0.2204+02
0.2173+02	C.2103+02	0.1990+02	0.1896+02	0.1844+02	0.1752+02
0.1729+02	C.1623+02	0.1530+02	0.1497+02	0.1410+02	0.1378+02
0.1269+02	C.1139+02	0.1082+02	0.8940+01	C.8571+C1	0.8224+01
0.7887+01	0.7041+01	C.5598+01	0.4980+01	0.4719+01	0.5544+01
C.5305+01	0.4144+01	0.3396+01	0.3786+01	0.3971+01	0.4502+01
0.4589+01	0.2647+01	0.2430+01	0.2159+01	0.2137+01	0.2094+01
C.1953+01	C.2604+01	0.1888+01	0.1747+01	C.2408+01	0.1747+01
0.9742+00	C.1389+01	0.1595+01	0.8083+00	0.7703+00	0.7280+00
0.2061+01	C.1942+00	0.3244+00	0.3146+00	0.2050+00	0.3428+00
0.2191+00	C.1671+0C	0.1226+00	0.7822-01	0.5511-01	0.3168-01
0.3450-01	C.6249-01	0.2126-01	0.1714-01	C.1302-01	0.1367-02
0.1378-02	0.1551-02	0.1725-02	0.1942-02	0.2202-02	0.2474-02
0.2777-02	C.3135-02	C.3558-02	0.4025-02	0.4567-02	0.5175-02
0.5869-02	0.6683-02	C.7475-02	0.8451-02	0.9591-02	0.1084-01
0.1226-01	C.1389-01	0.1584-01	0.1812-01	0.2072-01	0.2289-01
0.2571-01	C.2929-01	0.3320-01	0.5761-01		

TABLE 5

Element		Vessel damage sensitivity	Predicted % change passing from P(0) to: P(0)	P(1)	P(2)
1	H	-5.25	-99%	-21	-1
2	C	-1.98	-42	- 8	-1
3	Al	+0	+0	- 0	+0
4	Si	+0	+0	- 0	+0
5	Ca	-0	+0	- 0	+0
6	Cr	-0.42	-15	- 3	-0
7	Mn	-0.03	-11	- 0	-0
8	Fe	-1.51	-58	-15	-3
9	Ni	-0.21	- 9	- 2	-0
10	Zr	-0.13	- 2	+ 0	+0
11	U5	-0.01	- 0	+ 0	+0
12	U8	-0.31	- 6	+ 1	+0
Sum		-9.77	-242	-48	-5

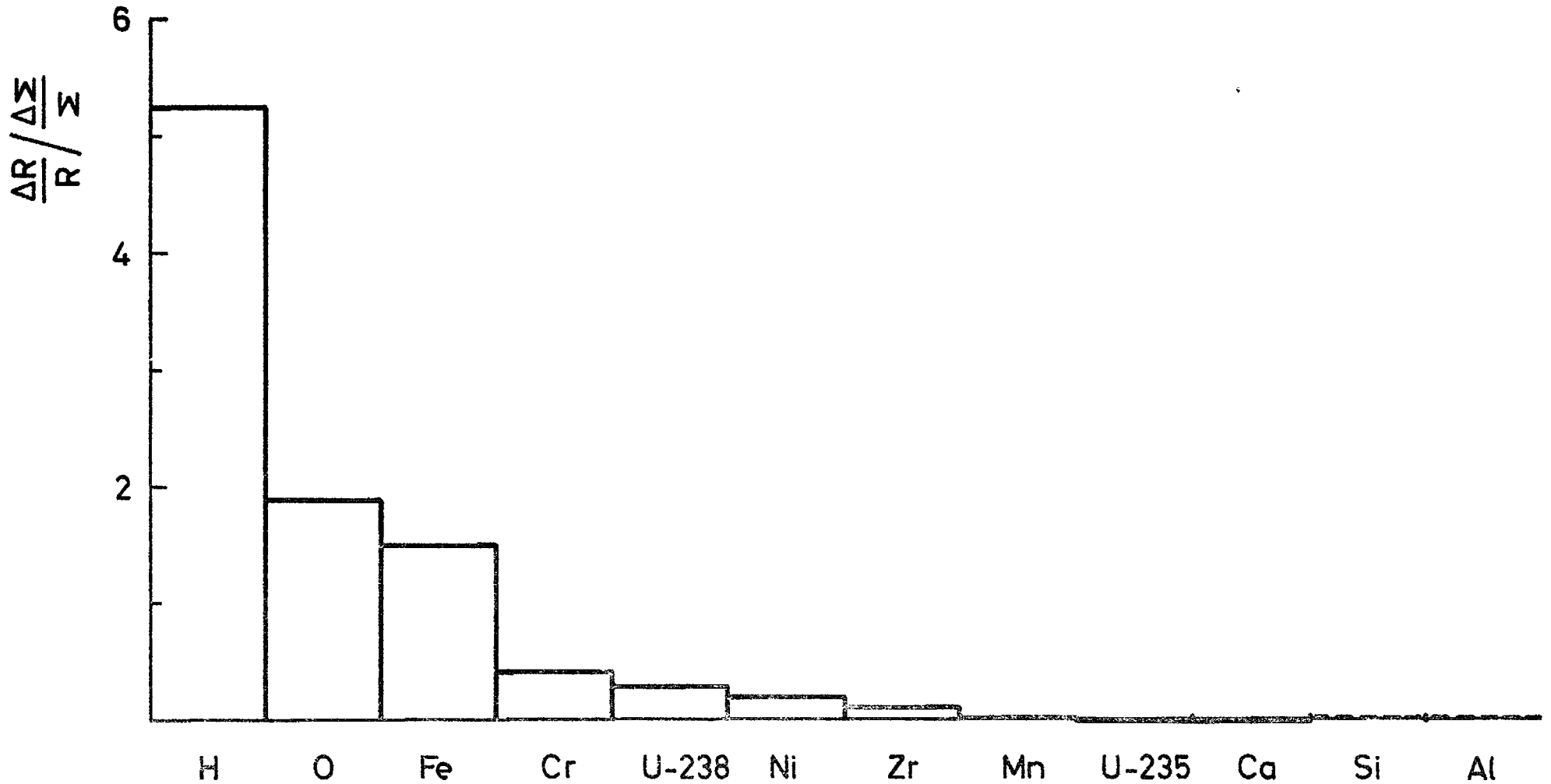

Radiation damage sensitivity for the various elements integrated over all zones

Fig. 19

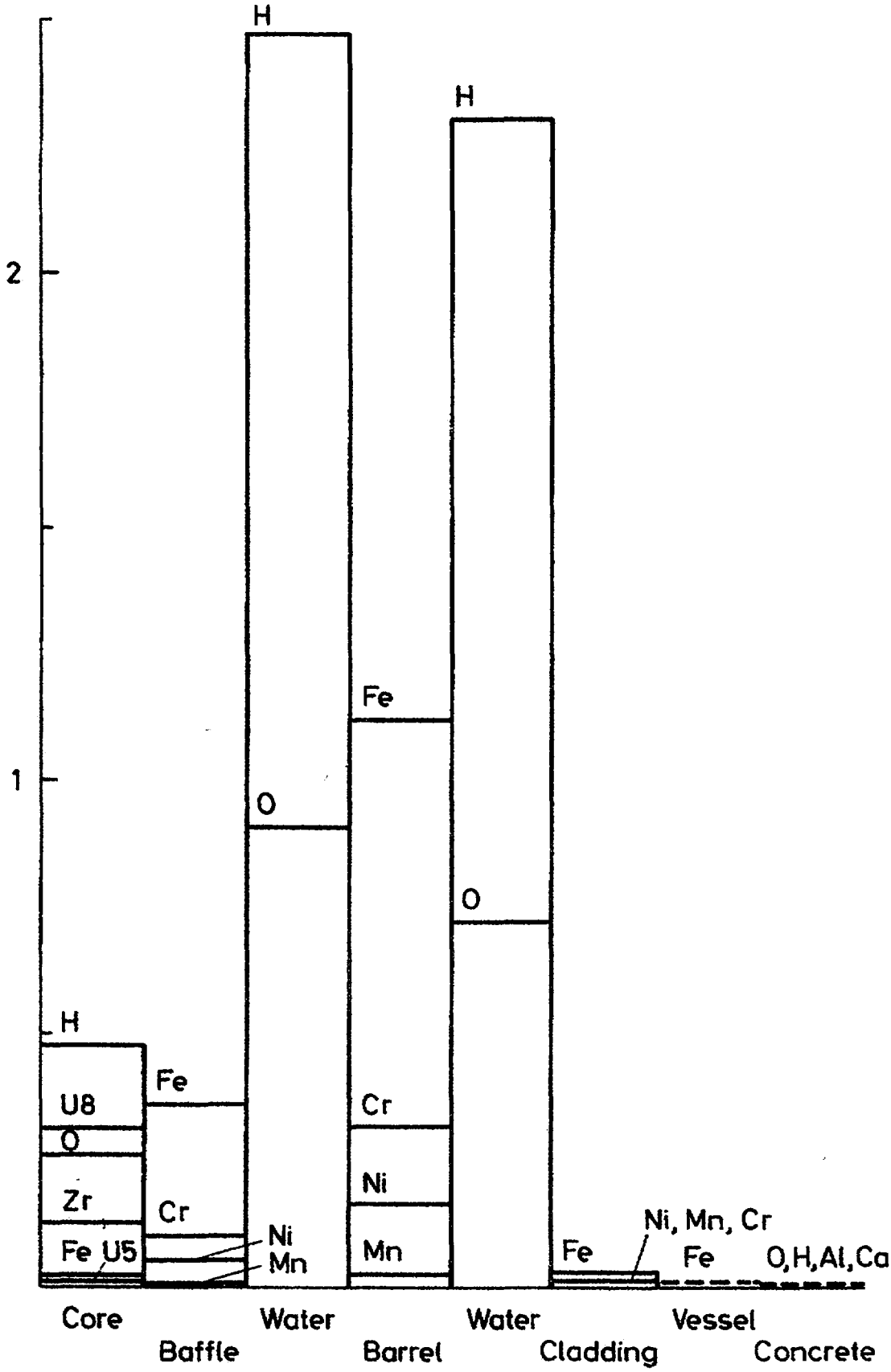

Radiation damage Sensitivity to neutron cross sections in a PWR
Library EL-4 Fig. 20

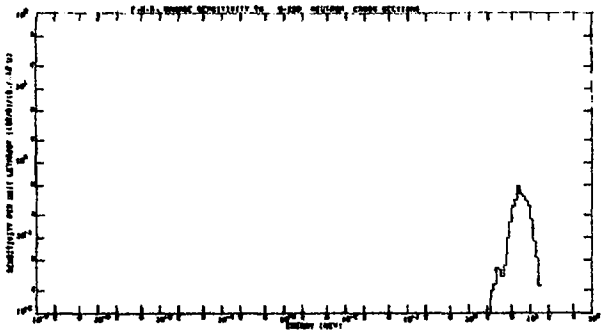
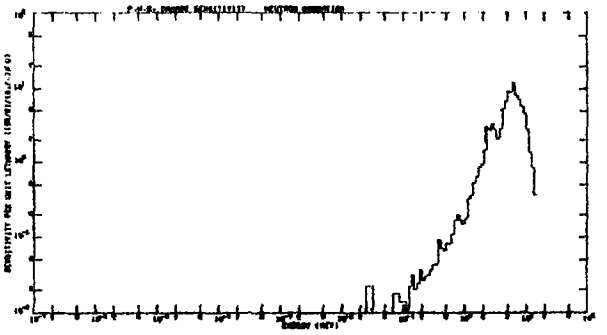
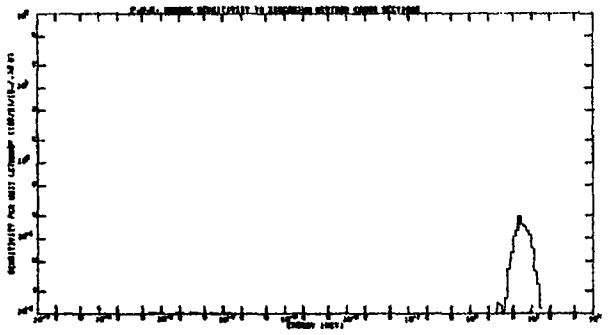
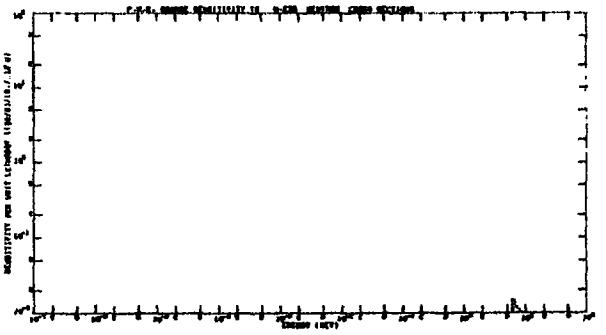
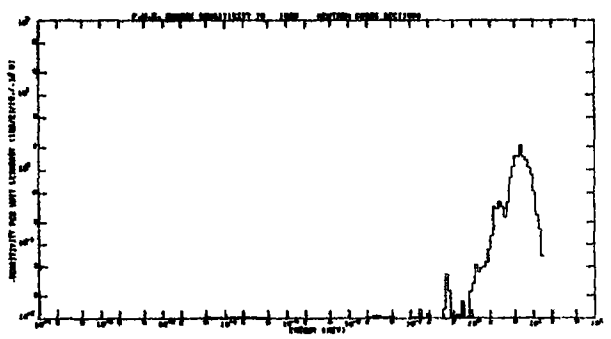
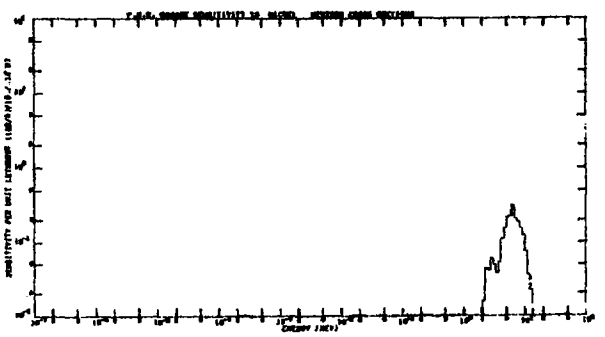
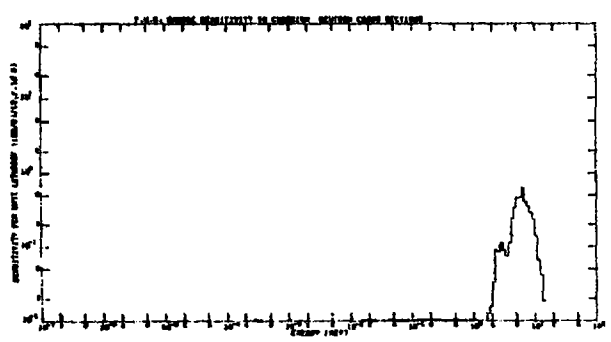
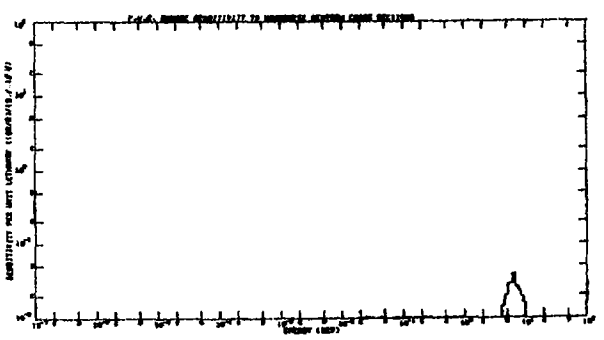
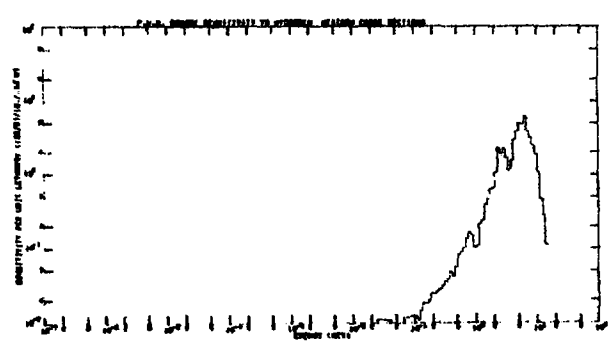
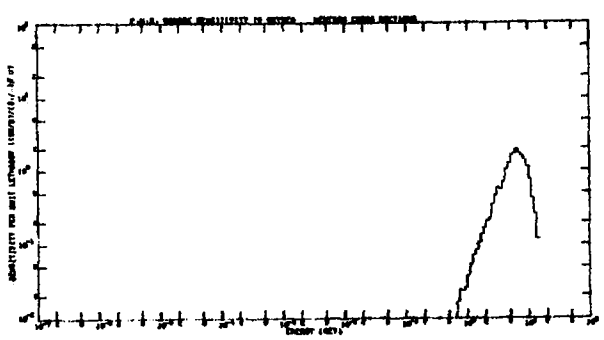

REFERENCES

/1/ W.W. ENGLE : " A User's Manual for ANISN", K-1693, 1973

/2/ D.E. BARTINE et al. : "SWANLAKE, A Computer Code for Cross Section Sensitivity Analysis", ORNL-TM-3809

/3/ G.HEHN, J.KOBAN : "Reactor Shielding Benchmark", N°2 ESIS Newsletter, Special Issue N° 4, Ispra, Jan. 1976

/4/ H. PENKUHN, G. GONANO : "The Coupled Neutron-Gamma Library EL4 with 119 Particle Groups", ESIS Newsletter N° 12, Jan. 1965, p.6

/5/ H. PENKUHN, G. GONANO: " An Enlargement of EL4 and its Retrieval Code PREL4", ESIS Newsletter N°14, July 1975, p.9

/6/ K. BURN : Private Communication.

Two NEA Sensitivity, 1-D Benchmark Calculations.

Part II: Sensitivity of the secondary sodium activation in the FBR configuration. (U.Canali, G.Gonano, R.Nicks).

Abstract

In the framework of the coordinated programme of sensitivity analysis studies, the reactor shielding benchmark calculation concerning the shield of a typical Fast Breeder Reactor, as proposed by J.Y. Barré (Cadarache), has been performed.

The direct and adjoint fluxes were calculated using ANISN, the cross-section sensitivity using SWANLAKE.
The cross-section library used was EURLIB-3 100 neutron + 20 gamma groups. The target quantity is the activation in the sodium of the secondary cooling circuit.

SWANLAKE was used to calculate the sensitivity of the sodium activation to variations in the density of each nuclide present.
Sensitivity profiles indicate the energy ranges in which a cross-section variation has a greater influence on the result.

The cross-section variation includes also that of the response function, viz. the absorption cross-section in the secondary sodium; therefore, a supplementary term was added to the SWANLAKE sensitivity for this zone.

Introduction

The present calculation is based on the configuration proposed by J.Y. Barré /3/ for the shield of a fast sodium reactor, in the framework of a collaborative international effort. The target quantity considered here is the activation of the secondary sodium.

The forward and adjoint transport calculations were made with ANISN /1/ and the sensitivity of this activation to variations in the different cross-section was calculated by SWANLAKE /2/.

Summary of the problem data /3/

As proposed by J.Y. Barré, a spherical geometry has been adopted, the inner radius being 236.5 cm.
The zones are described in Table 1.

TABLE 1. Configuration

Region	Thickness cm	% by volume sodium	steel
1 Source	0.1	47%	53%
2 Lateral Shield	200	47%	53%
3 Sodium tank	500	100%	--
4 Heat exchanger	50	85%	15%
5 Secondary sodium	50	100%	--

The steel is standard stainless steel with proportions by weight of about 70% Fe, 18% Cr, 12% Ni.
The suggested /3/ angular quadrature is S4. The cross-section expansion chosen is P1.
The source is defined by giving the forward angular fluxes at the inner radius of the configuration /3/.
As far as the cross-section library is concerned the recently produced EURLIB-3 /4/ library has been used.
Only the neutron part was of interest.

Activation, calculation and sensitivity

The number of captures per second in the secondary sodium was taken as response; in the steady state this is equal to the number of radioactive disintegrations per sec. In the forward ANISN calculation the macroscopic absorption cross-section of sodium was used as response function; the result was 1.4997 E 8 captures/sec in the secondary sodium (if one adopts the microscopic cross-section, the result is 6.7464 E 9).

The adjoint flux was also calculated with ANISN; the computation of the above mentioned response using the adjoint flux and the source is not yet finished. The main sensitivity results produced by SWANLAKE, are summarized in Table 2.

TABLE 2. Sensitivity

	Na	Cr	Fe	Ni	all elements
Lateral shield	- 4.30	-2.30	-6.06	-3.75	-16.41
Sodium tank	-15.18				-15.18
Heat exchanger	- 1.17	-0.33	-2.12	-0.96	- 4.59
Secondary sodium	- 0.16				- 0.16
Tot. system	-20.81	-2.63	-8.18	-4.71	-36.34
% P1 to P0	- 66%	- 29%	-67%	- 23%	-185%

Sensitivity profiles for each element, summed over all zones, and also for each zone, summed over all elements, are given in figures 1 to 9.

Discussion of the sensitivity results

From Table 2. one observes that the sensitivity of the number of absorptions/sec. in the secondary sodium to the secondary sodium cross-section itself is negative.
But clearly an increase in secondary sodium cross-section (equivalent to an increase in sodium density and also equivalent in plane geometry to an increase in the sodium zone thickness) must lead to an increase in the neutron absorption (the leakage is decreased); the sensitivity being the ratio of the two increments, must be positive.

However it can be shown that the overall sensitivity resulting from the same relative change in the transport cross-sections and the response function is

$$\frac{dR}{d\Sigma/\Sigma} = 1 + \frac{\partial R/R}{\partial \Sigma/\Sigma} \qquad (1)$$

where $\frac{\partial R/R}{\partial \Sigma/\Sigma}$ is the partial derivative corresponding to the variation of transport cross-section only (the response function remaining constant).
In our case this sensitivity of secondary sodium activation is equal to (see Table 2.)

$$1 + (-0.16) = 0.84$$

Besides being positive, this value must also be ≤ 1; in fact 1 would be the sensitivity due to an increase in σ_p without a decrease in the average fluxes ϕ in the zone (σ_x being the response function).

Examining the sensitivity profiles, one observes a minimum at about 3 KeV, corresponding to the large scattering resonance of Na. Comparison of Fig.1, 2 and 3 shows the influence of neutron slowing down in the system.

It is interesting to observe that the sodium activation of zone 5 is sensitive to the cross-section of the whole energy range throughout the system (Fig. 5); the lateral shield (zone 2) and the tank (zone 3) are the major contributors to sensitivity, according to Table 2.

Figure 6 (Na), 7 (Fe), 8 (Ni) and 9 (Cr) show the sensitivity of the various elements.

REFERENCES

1. W.W. Engle , "A User's Manual for ANISN", K-1693, 1973
2. D.E. Bartine et al. "SWANLAKE, a Computer Code .... for Cross-section Sensitivity Analysis", ORNL-TM-3809
3. J.Y.Barré, "Definition d'une configuration étalon pour les comparaison des calculs de protection", REF/SPNR/76/350, Cadarache, le 29 mars 1976
4. The EURLIB-III library is described in ESIS Newsletter N° 19, October 1976, page 5

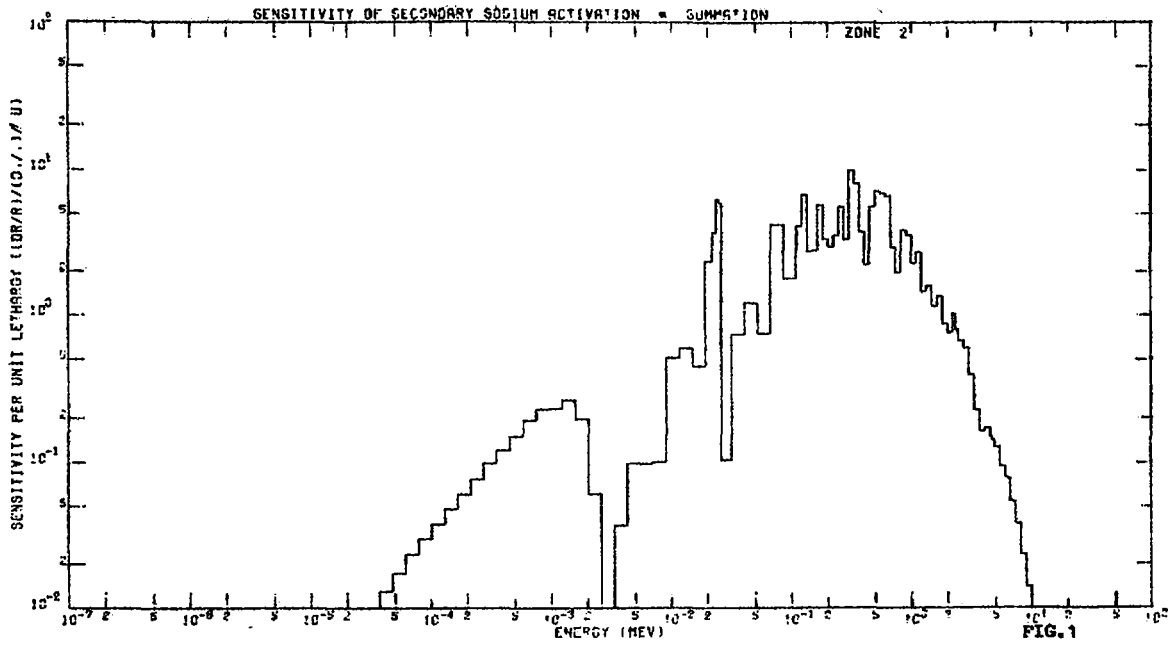
SENSITIVITY OF SECONDARY SODIUM ACTIVATION - SUMMATION
ZONE 2
SENSITIVITY PER UNIT LETHARGY ((DR/R)/(D./.)/MU)
ENERGY (MEV)

FIG. 1

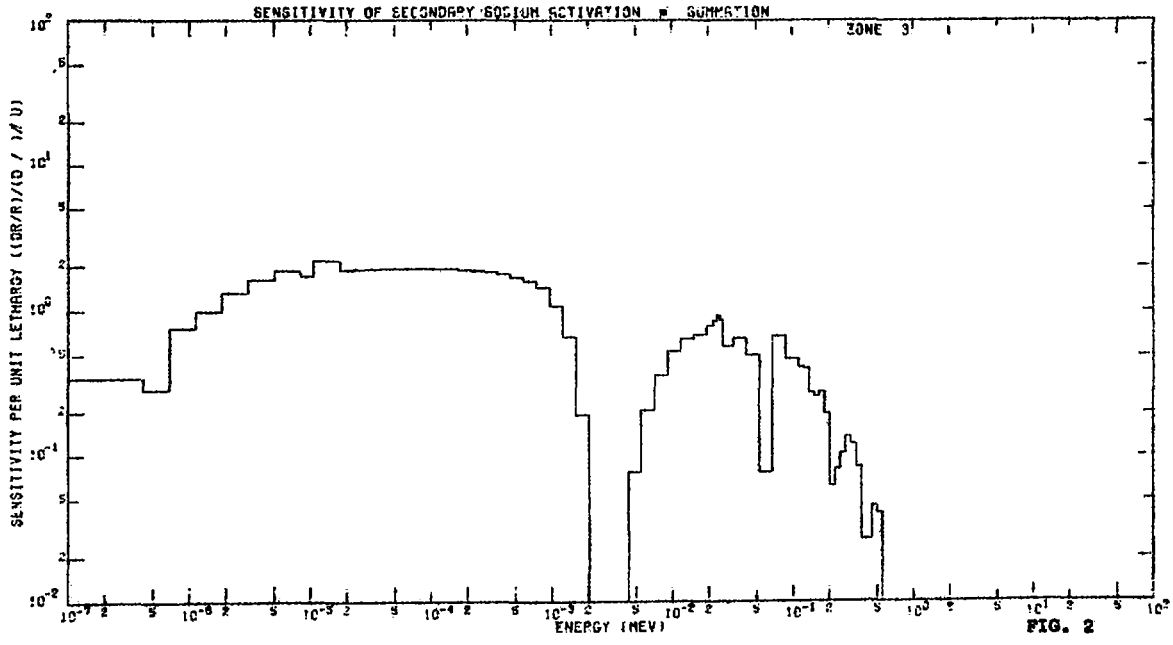
SENSITIVITY OF SECONDARY SODIUM ACTIVATION - SUMMATION
ZONE 3
SENSITIVITY PER UNIT LETHARGY ((DR/R)/(D / MU)
ENERGY (MEV)

FIG. 2

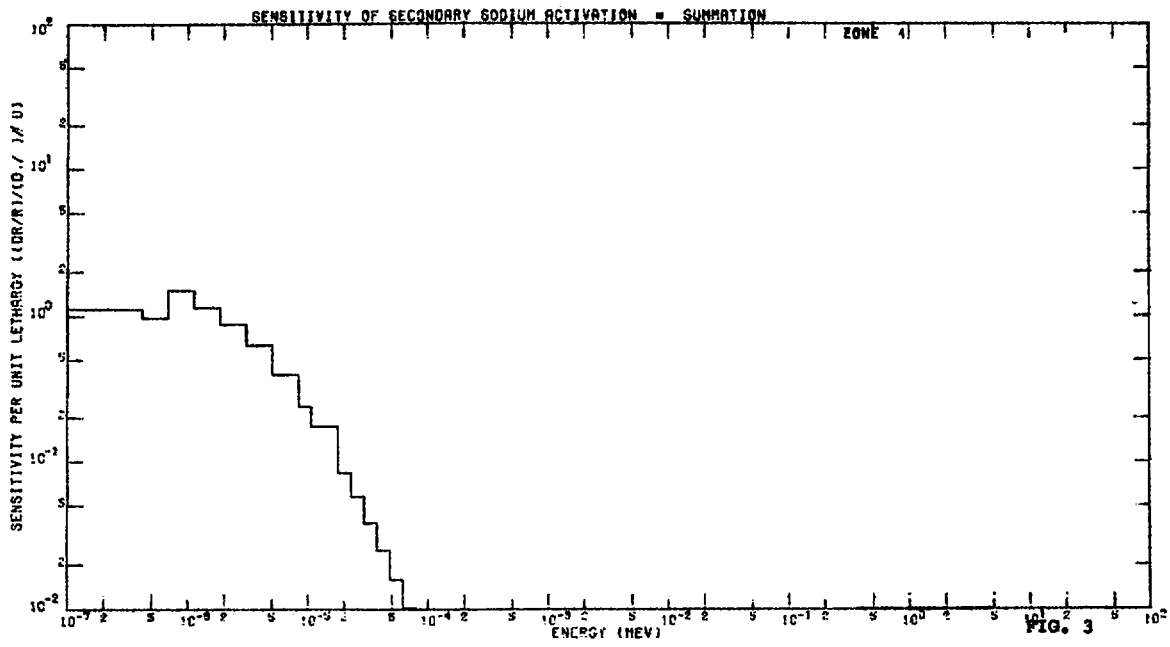
SENSITIVITY OF SECONDARY SODIUM ACTIVATION = SUMMATION
ZONE 4
SENSITIVITY PER UNIT LETHARGY ((DR/R)/(D./)
ENERGY (MEV)

FIG. 3

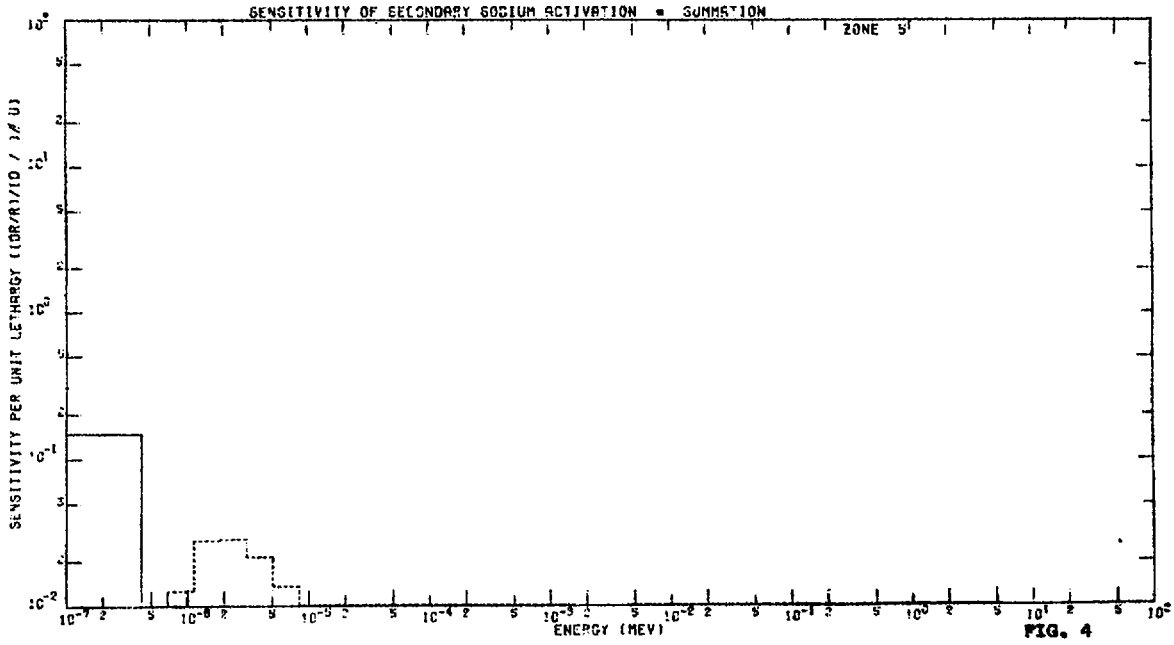
SENSITIVITY OF SECONDARY SODIUM ACTIVATION = SUMMATION
ZONE 5
SENSITIVITY PER UNIT LETHARGY ((DR/R)/(D /)
ENERGY (MEV)

FIG. 4

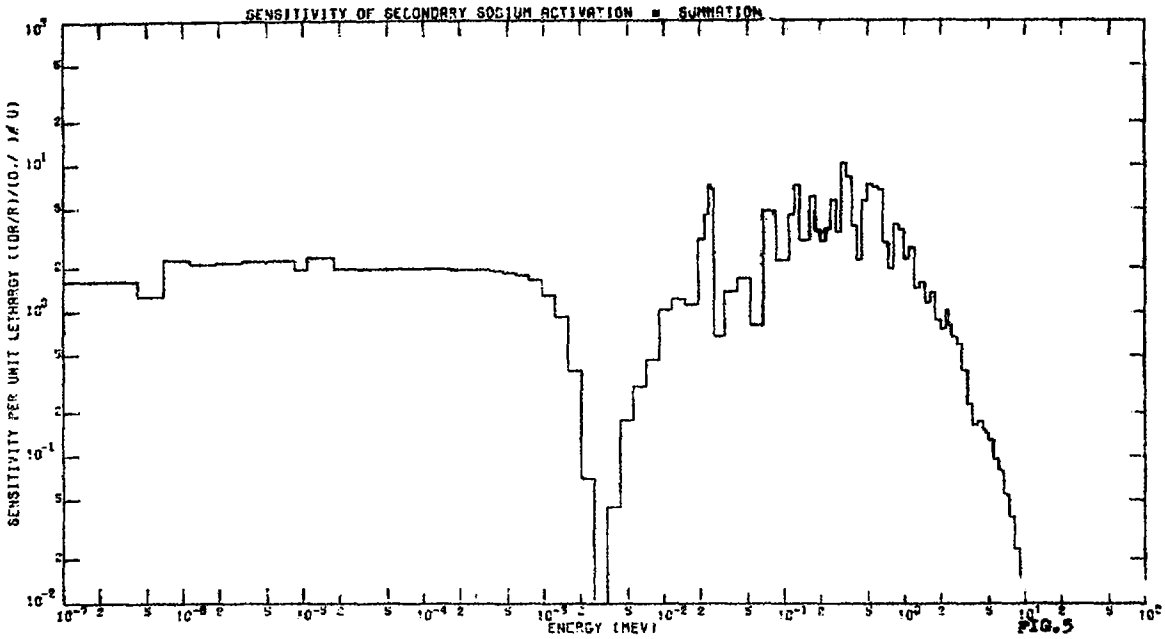
SENSITIVITY OF SECONDARY SODIUM ACTIVATION = SUMMATION
SENSITIVITY PER UNIT LETHARGY ((DR/R)/(D./ μ U)
ENERGY (MEV)

FIG.5

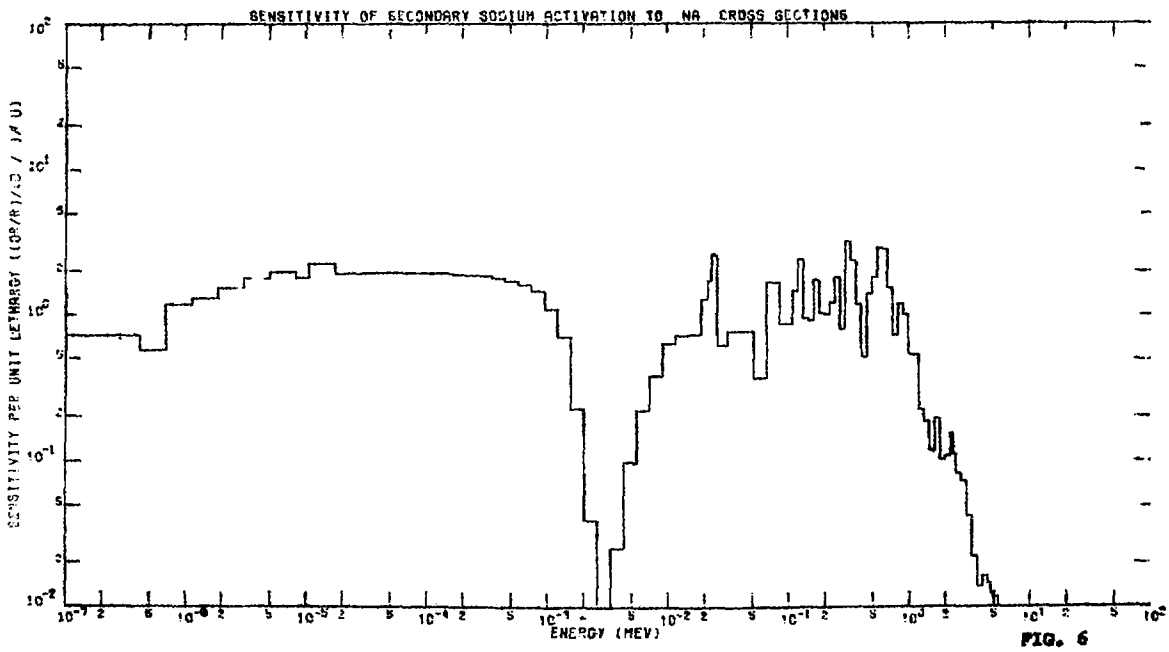
SENSITIVITY OF SECONDARY SODIUM ACTIVATION TO NA CROSS SECTIONS
ENERGY (MEV)

FIG. 6

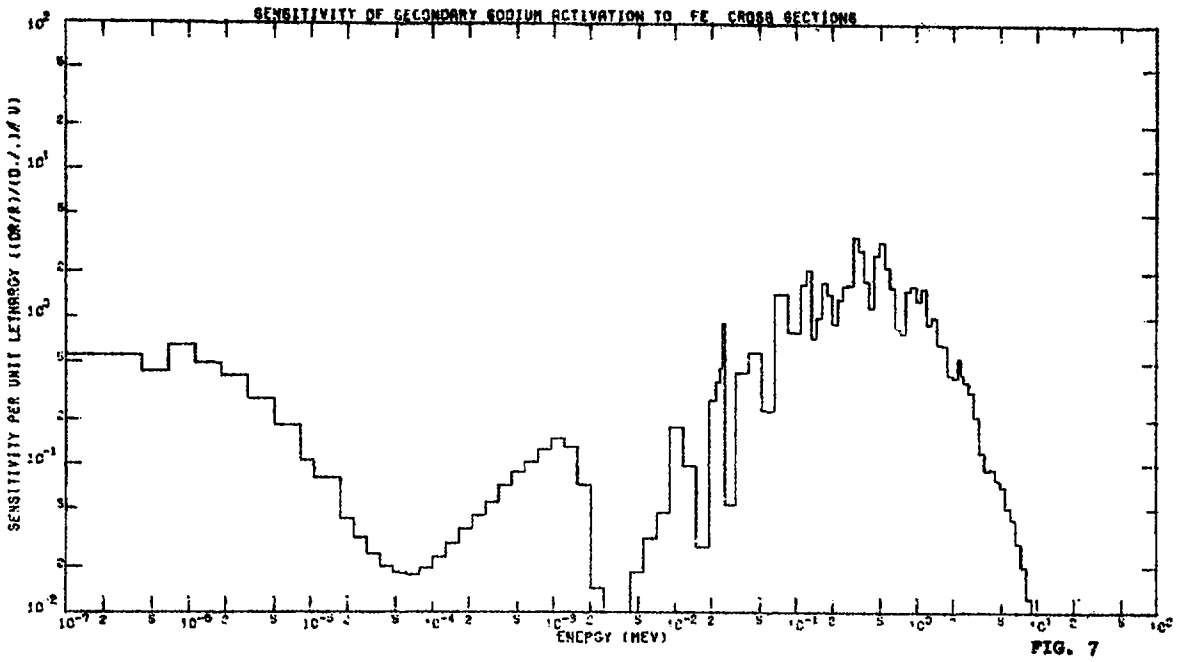

FIG. 7

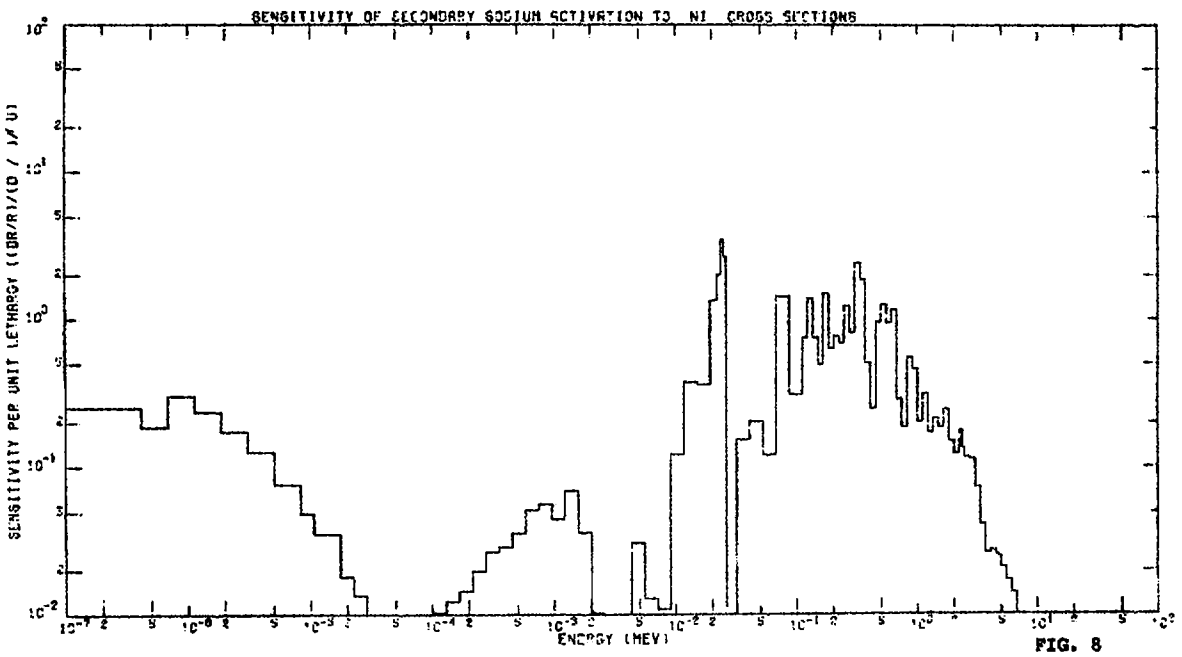

FIG. 8

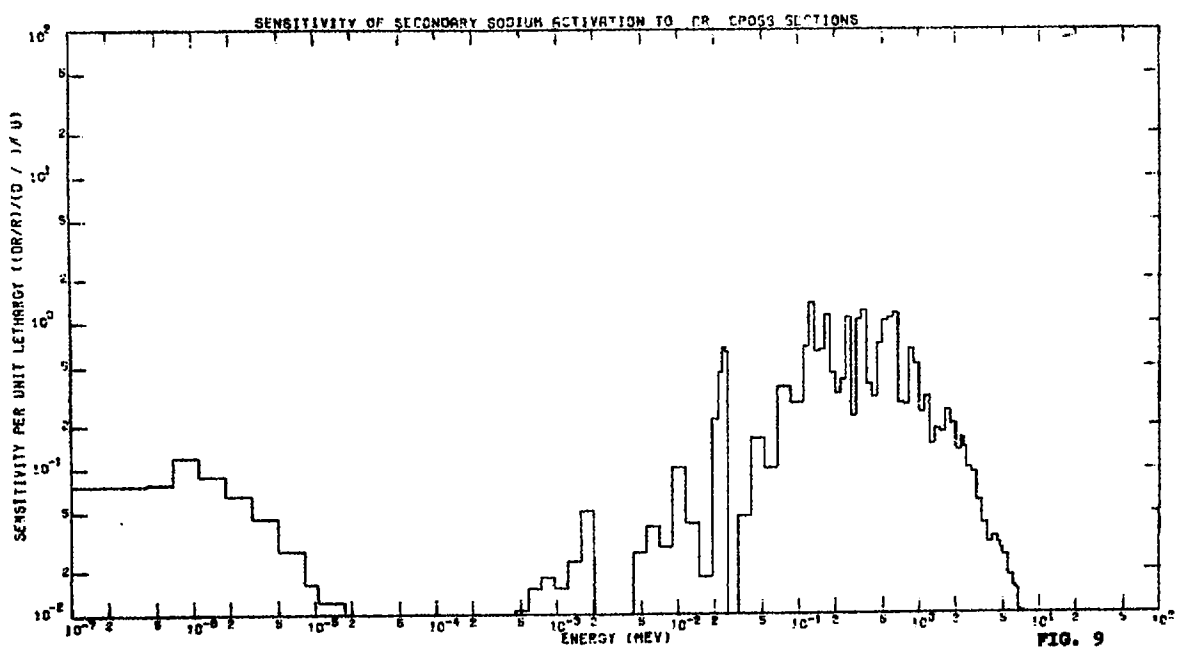

FIG. 9

CONTRIBUTION TO THE STUDY OF THE REACTOR SHIELDING BENCHMARK n° 2 (PWR) PROPOSED BY THE NEA

G. MINSART, C. VAN BOSSTRAETEN*

Centre d'Etude de l'Energie Nucléaire,
*Contrôle-Radioprotection

Mol, Belgium

ABSTRACT

The reactor shielding benchmark n° 2 (PWR) described in the note NEACRP-L-151 has been computed in two ways : first, using the shielding code SABINE-3; second, using an improved version of the criticality transport code DTF-IV. For both methods, a one-dimensional cylindrical model has been adopted; the code SABINE-3 has been applied with its own library (26 neutron energy groups, 7 groups for gammas) and with the standard recommended numerical constants and limits; with DTF-IV coupled to a 40-group library, only neutron calculations have been performed.

The results of both methods are compared : displacements per atom in the baffle, in the barrel and in the pressure vessel, flux intensity and spectrum at these locations and in the concrete shielding; in addition, γ-heating and biological dose rates are computed for mesh points specified in the NEACRP document.

Sensitivity of results to cross section changes is investigated for iron. Cross sections have been modified simultaneously in the core baffle, in the core barrel, in the austenitic cladding and in the pressure vessel; several sets of modifications have been applied and the results are analyzed.

1. INTRODUCTION

When the NEACRP issued his paper on the shielding benchmark n° 2 for a PWR[1], it was considered at the C.E.N./S.C.K. that it should be useful to perform the calculations in two different ways :

- first, with the reactor codes and cross section libraries currently used for the study of reactor cells and cores, and for the detailed analysis of irradiation loops in BR2,
- secondly, with a shielding code widely used in shielding studies.

One could then compare the results of both approaches and check them against those obtained in other institutions with different programs and cross section libraries, in order to get more confidence in the methods used, particularly in the frame of the campaign of pressure vessel monitoring undertaken in Belgium for the PWR's and, later, for the fast breeders.

Concerning sensitivity calculations, it was not possible to cover a broad set of nuclides without developing adapted computer tools such as sophisticated flux perturbation codes. As experiments are now being performed at C.E.N./S.C.K. to study fast neutron penetration through thick steel structures, more particularly iron, the sensitivity analysis has been focused on the iron cross sections, mainly the capture cross sections.

2. CALCULATIONAL METHODS

Two different methods have been applied in order to compute neutron damage in iron and steel and leakage fluxes at the outer surface of the concrete shield.

First, a multigroup neutron transport code (DS_n approximation) coupled to a 40-group library; secondly, the shielding code SABINE-3 with its own cross section library. In both cases, for calculating reaction rates, the code DETAN 74 has been used.

For both methods, the one-dimensional geometrical model described in [1] has been adopted, but with different numbers of mesh intervals for SABINE. The axial leakage was accounted for by introducing a buckling component deduced from the physical height of the core. Fig.1

A. The neutron transport code DTF-IV and the 40-group library

Since many years, the US multigroup transport code DTF-IV [2] has been incorporated in the C.E.N./S.C.K. code system MULCOS [3] ; it has been modified and improved in many respects; several of these changes were already reported at a previous IAEA Conference [4] .

It has been applied with the DS 4 approximation and the fixed source option. The power profile given in [1] for the outer core region has been used as the fixed source distributed in energy according to the fission spectrum. The inner core region has been filled with the same composition as the outer one, in order to preserve roughly the capture and scattering properties of this region. The fission source itself has been put equal to zero in the whole core.

The 40-group neutron library available in the MULCOS system [5] has been selected because it is able to yield a good representation of the entire energy range; its group structure is given in Appendix 1. The scattering matrices contain upscattering cross sections for group 29 and the following ones; as it is well known, this coupling between thermal groups markedly slows down the convergence rate of the fluxes mainly in the outer reflector zones, and this is reflected in the long computer times required to attain a good stabilization of the flux map. The macroscopic cross sections were prepared by the preprocessing part of MULCOS, whose formalism is similar to the one to be used with the ABBN and GROUCO/GfK 26-group libraries; furthermore, most of the microscopic cross sections above about 2 eV were taken from these libraries.

B. The shielding code SABINE-3

SABINE-3 [6], an improved version of the well known and widely applied shielding code SABINE [7] has been used.

It computes the neutron fluxes in 26 energy groups by the removal diffusion method. The group structure is shown in Appendix 1. Furthermore it provides energy fluxes in 7 groups, energy deposition and dose rate, due to primary and secondary gamma rays. Gamma ray sources include

neutron capture and inelastic scattering. The gamma energy fluxes are obtained by numerical integration over the source volume of the product of a kernel for uncollided flux and a build-up factor.

The data were prepared according to the recommendations of [6] and [7] :

- All calculations (removal flux, diffusion equation and gamma flux) were executed in cylindrical geometry.
- At the core-shield interface, the neutron flux was set equal to the one calculated with the transport code DTF-IV as described in the previous paragraph. Since the latter code uses 40 energy groups instead of 26, the flux values to be introduced in SABINE were interpolated from the curve $\Psi(u) = \int_0^u \Phi(u)\, du$, obtained from DTF-IV for the outer core mesh interval.
- The mesh distribution proposed in [1] could not be used since it requires a prohibitive number of regions and since the proposed thicknesses of the intervals are out of the range of recommended mesh paths for SABINE. Instead, the following mesh distribution was adopted :

Zone	Thickness (cm)	Number of intervals
- Core baffle	2.5	4
- 1. water layer	3.	10
	24.5	80
	3.	10
- Core barrel	8.	16
- 2. water layer	3.	10
	25.5	64
	3.	10
- Cladding	0.6	4
- Pressure vessel	3.	6
	19.	24
	3.	6
- Concrete shield	15.	10
	155.	80
	30.	10

- The parameters M_θ, M_R, M_φ and η were set equal to the standard recommended values (1 for M_x and 0.001 for η).
- The second gamma library (B) has been used. It contains complete (n,Y) matrices for 10 elements (Li, C, Na, Al, Si, Fe, Ni, Cr, Cu, Pb).

- The gamma build-up factor was computed according to Kitazume's formula.
- ^{235}U fission spectrum has been assumed for the neutron source in the core.

C. The DETAN code and the DPA cross sections

The code DETAN 74 performs the following operations : starting from cross sections given in a fine group structure and from spectra provided either in analytical form or in multigroup structure, average group cross sections, response functions, fluxes per unit lethargy and per unit energy and cumulative fluxes are computed in any group structure. The cross sections are read in a library (up to 621 groups) or given on cards; the spectrum is selected by options in the data (analytical forms) or given on cards; the final group structure is given on cards. The combination of group structures is based on linear interpolations; a reasonably large number of group should thus be adopted in order to keep a good accuracy of the results.

This code seems well adapted to the needs of the present study, for which we have to combine different group structures in order to compute reaction rates (rate of Displacements Per Atom) in iron and steel zones.

The DPA cross sections used in the present study are those reported in [8][9] (NRT standard); they are reprinted in Appendix 2. Below 10^{-4}MeV, the group structure has been extended as indicated ($\Delta u \approx 0.25$) down to about 2.10^{-2}eV, yielding a set of 83-group cross sections for the DETAN computations.

3. NOMINAL CASE

The following results are asked for in the NEACRP paper :

3.1. Neutron damage at the inner side of the pressure vessel

The SABINE-3 code yields 26-group fluxes at mesh points; the DTF-IV results are 40-group fluxes for each mesh interval; the DETAN code is then used for neutron damage calculations.

Since only additional DETAN runs were needed, neutron damage has been computed also for the core barrel and the baffle, using the DPA cross sections corresponding to the steel composition (Fe + Cr + Ni); these cross sections are reproduced in Appendix 2.

The results are displayed in the table hereafter and illustrated in Fig. 2 to 4 : neutron flux spectra and response functions for the damage production at several locations. In addition, effective microscopic iron capture cross-sections (40-group scheme) and group averaged iron and steel DPA cross-sections resulting from DETAN runs with the DTF-IV spectrum corresponding to the inner vessel side location are plotted in Fig. 5 and 6.

The values obtained for average DPA cross sections ($\bar{\sigma}$) and production rates of DPA clearly indicate that the two computation models differ not only by the flux level at the selected location but also by spectral shapes of these fluxes. Since the SABINE starts from DTF-IV fluxes at core boundary, results for core baffle are nearly the same; the discrepancy increases with the penetration into the reflector and the shield regions. From the neutronic point of view, a discrepancy of roughly a factor 2.5 as obtained at the inner side of the pressure vessel is not surprising over a range of 5 decades : very different methods (transport against removal diffusion) and different cross sections in the libraries have indeed been used. From the engineering point of view however, a remaining uncertainty of a factor 2.5 would be unacceptable; it would strongly influence the expected service lifetime of the vessel.

3.2. Gamma heating at the inner side of the concrete shield

The gamma heating at the inner side of the concrete shield as calculated by SABINE, equals $5.18\ 10^{-6} W/cm^3$. This value is obtained directly from the output listing.

69 % of this deposited energy come from the gamma rays originating in the baffle, 17 % come from the core, the remaining part coming mainly from the barrel and the pressure vessel.

When the contribution of each region to the gamma heating is weighted with the ratio of the average thermal fluxes in that region, computed with DTF-IV and with SABINE, a value of $6.15\ 10^{-6} W/cm^3$ is found for DTF-IV results. This is about the result that should be obtained if the gamma attenuation part of SABINE were applied with the neutron flux map of DTF-IV as input data. It is not completely exact since the gamma rays are partly produced by inelastic scattering and by epithermal captures, and since the ratios of fast and epithermal fluxes are not necessarily the same as the ratio of the thermal fluxes.

PRODUCTION RATE OF DISPLACEMENTS PER ATOM (DPA/s.)

	Inner surface of core baffle (SS)	Inner surface of core barrel (SS)	Inner surface of pressure vessel (Fe)	Inner mesh interval of pressure vessel (mesh "120") (Fe)
SABINE-3 :				
$\bar{\sigma}$ (barns)	$3.043\ 10^{2}$	$2.053\ 10^{2}$	$3.047\ 10^{2}$	-
DPA/s (x 10^{24})	$3.312\ 10^{16}$	$7.503\ 10^{13}$	$2.821\ 10^{11}$	-
$\frac{(DPA) > 1.35\ MeV}{DPA}$ (%)	65.51	77.77	78.25	-
$\frac{(DPA) > 821\ keV}{DPA}$ (%)	77.60	85.24	85.09	-
$\frac{(DPA) > 214\ eV}{DPA}$ (%)	99.716	98.24	99.33	-
DTF-IV :				
$\bar{\sigma}$ (barns)	$3.032\ 10^{2}$	$1.575\ 10^{2}$	$2.290\ 10^{2}$	$2.375\ 10^{2}$
DPA/s (x 10^{24})	$3.186\ 10^{16}$	$1.172\ 10^{14}$	$6.994\ 10^{11}$	$6.9265\ 10^{11}$
$\frac{(DPA) > 1.4\ MeV}{DPA}$ (%)	63.28	70.84	70.85	70.2[illegible]
$\frac{(DPA) > 800\ keV}{DPA}$ (%)	77.76	81.49	80.505	80.07
$\frac{(DPA) > 215\ eV}{DPA}$ (%)	99.68	97.14	98.842	98.946

3.3. Biological dose rate at the outer side of the shield

The results are shown in the following table :

Method	Dose rate (mrem/h)		
	Neutron	Gamma	Total
SABINE	0.5	5.	5.5
DTF-IV	3.	10.	13.

The neutron dose rate (dose equivalent) and also the gamma dose rate are again a part of the output listing of SABINE. The neutron dose rate is almost totally due to thermal neutrons. The gamma dose rate is caused mainly by gamma rays produced in the baffle (72 %), while the concrete contributes to 19 % of the dose rate. The remaining part comes from the core, the barrel and the pressure vessel.

DTF-IV provides no dose rates, but the neutron dose rate can be derived from the thermal flux. The last flux value corresponds to a mesh interval of 8.2 cm, and not to the outer side of the shield. The thermal flux at the border has been obtained by extrapolation. This was facilitated by the fact that in the outer part of the shield the ratio of the thermal fluxes calculated with SABINE and DTF-IV showed to be constant. The factor used to convert flux to dose equivalent was taken from the SABINE library. When comparing both values, one should bear in mind that the total attenuation of the thermal flux throughout the shield equals about eleven decades !

The gamma dose rate listed in the table for DTF-IV has been obtained in the same way as the gamma heating, i.e. by weighting the contribution from each region, as computed by SABINE, with the ratio of the average thermal fluxes obtained with DTF-IV and SABINE. The difference with respect to the SABINE result is due to the increased contribution from the gamma rays produced in the concrete shield by the higher thermal flux.

4. SENSITIVITY COMPUTATIONS

As already mentioned in the introduction, sensitivity of the results to cross section changes has been investigated only for iron. Since it is not easy to introduce temporary modifications in the SABINE library,

a variation of all the Fe cross sections has been simulated by a reduction of 10 % of the atomic density of this material in the three zones : core baffle, barrel and pressure vessel; since this procedure also changes the gamma ray attenuation coefficient of iron, the results for γ distributions were corrected by hand calculations with the aid of the results for the nominal case in order to get values corresponding to the correct γ attenuation factor.

It is easier to selectively modify cross sections in the MULCOS system. Four DTF-IV problems were run :

- all Fe cross sections reduced by 10 %, in order to enable comparisons with SABINE results,
- Fe capture cross sections reduced by 10 % in all groups,
- Fe capture cross sections reduced by 10 % in groups 1 - 17 ($E \geq 100$ eV),
- Fe capture cross sections reduced by 10 % in groups 1 - 8 ($E \geq 100$ keV).

When capture alone was to be changed, self scattering cross section was modified by the same amount in order to keep the total cross sections constant. The three last runs give an indication of the energy profile of the effect of $\Delta \sigma_{c\,Fe}$.

The relative variations of production rates of DPA for the various cases are given in the following tables. First, the SABINE-3 and DTF-IV results are compared for a reduction by 10 % of all the Fe cross sections.

	Inner baffle (SS)	Inner barrel (SS)	Inner pressure vessel (Fe)
SABINE	($\approx$ - 0.6 %)	+ 2.01 %	+ 14.62 %
DTF-IV	- 0.6 %	+ 2.71 %	+ 14.55 %

The SABINE values for the inner baffle side are not relevant, since this location is close to the imposed boundary fluxes, which were kept the same as in the unperturbed case; the other SABINE values have been shifted by about 0.6 % in order to take this fact into account. The agreement between SABINE and DTF-IV relative DPA variations is very good.

The reduction by 10 % of the Fe capture cross sections for the three energy range yields the following results $\left(\frac{\Delta DPA}{DPA}\right)$; only DTF-IV computations have been performed.

	Inner baffle (SS)	Inner barrel (SS)	Inner pressure vessel (Fe)
with $\Delta\sigma_c$ above 100 keV (groups 1 - 8)	$1.404\ 10^{-4}$	$6.417\ 10^{-4}$	$2.0705\ 10^{-3}$
with $\Delta\sigma_c$ above 100 eV (groups 1 - 17)	$1.515\ 10^{-4}$	$6.524\ 10^{-4}$	$2.167\ 10^{-3}$
with $\Delta\sigma_c$ in the whole energy range (groups 1-40)	$2.556\ 10^{-4}$	$1.402\ 10^{-3}$	$2.7945\ 10^{-3}$

From this table, one sees that modifications of $\sigma_{c\,Fe}$ in the energy range 100 eV - 100 keV contributes very little to the change in DPA. Furthermore, comparison with the previous table clearly indicates that modifications of the scattering cross sections have by far a larger effect than the Fe capture alone.

The results for gamma heating and dose rates are given in the next table (all Fe neutron cross sections reduced by 10 %). The figures between brackets indicate the difference with respect to the nominal case.

Method	Gamma heating (W/cm^3)	Dose rate (mrem/h)		
		neutron	gamma	total
SABINE	$5.0\ 10^{-6}$ (- 3 %)	0.63 (+ 26 %)	5. (-)	5.6 (+ 12 %)
DTF-IV	$6.07\ 10^{-6}$ (- 1 %)	3.7 (+ 23 %)	10. (-)	11.8 (+ 5 %)

The relative increase in neutron dose rate compared to the nominal case is about the same for both methods.

The gamma dose rate and the gamma heating are influenced by two effects : a decreasing effect due to the smaller cross sections in the iron and an increasing effect due to the higher flux densities. The

net effect is found to be zero for the gamma dose rate and very small for the gamma heating.

ACKNOWLEDGEMENTS

The authors wish to express their thanks to Mr. J. Lacroix who has carefully prepared the numerous input data for the DETAN problems and for the plotting routines, and to Mrs. Andries whose care has ensured the good presentation of this paper.

REFERENCES

[1] HEHN G., KOBAN J. - Reactor shielding benchmark n° 2 for a PWR - NEACRP-L-151.

[2] LATHROP K.D. - DTF-IV, a Fortran-IV program for solving the multigroup transport equation with anisotropic scattering - LA-3373 (1965).

[3] MINSART G. et al. - The MULtipurpose COde System MULCOS C.E.N./S.C.K. reports (1971-1975).

[4] MINSART G., QUENON J. - Some improvements to the stability and the convergence of the reactor codes DTF-IV, EXTERMINATOR and TREPAN - TRIBU - IAEA-SM-154/58 (Jan. 1972).

[5] VANDEPLAS P., SCHEPERS J.-C. - A 40-group cross section library for the calculation of fast-thermal systems - C.E.N./S.C.K. internal report (1971).

[6] PONTI C., VAN HEUSDEN R. - SABINE-3, an improved version of the shielding code SABINE - EUR-5159 (1974).

[7] PONTI C., PREUSCH H., SCHUBART H. - SABINE, a one-dimensional bulk shielding program - EUR-3636 e (1967).

[8] NORGETT M.J., ROBINSON M.T., TORRENS I.M. - A proposed method of calculating displacement dose rates - Nuclear Engineering and Design 33, 1 (1975).

[9] McELROY W.N. et al. - Damage function analysis - HEDL-SA-755 (1974).

APPENDIX 1

LIBRARY GROUP STRUCTURE

MOL-BR2-40 GROUP

GROUP	ENERGY RANGE	E_o = 10.5 MeV UPPER LETHARGY LIMIT u	Δu	χ FISSION SPECTRUM
1	10.5-6.5 MeV	0.47957	0.47957	0.018
2	6.5-4.0	0.96508	0.485508	0.095
3	4.0-2.5	1.43508	0.470004	0.188
4	2.5-1.4	2.01490	0.579818	0.269
5	1.4-0.8 MeV	2.57452	0.559615	0.198
6	800-400 keV	3.26767	0.693148	0.137
7	400-200	3.96081	0.693148	0.059
8	200-100	4.65396	0.693148	0.023
9	100-46.5	5.41968	0.765718	0.009
10	46.5-21.5	6.19108	0.771400	0.003
11	21.5-10.0	6.95654	0.765467	0.001
12	10.0-4.65	7.72226	0.765718	
13	4.65-2.15	8.49366	0.771400	
14	2.15-1.00 keV	9.25913	0.765467	
15	1000-465 eV	10.02485	0.765718	
16	465-215	10.79625	0.771400	
17	215-100	11.56171	0.765467	
18	100-46.5	12.32743	0.765718	
19	46.5-21.5	13.09883	0.771400	
20	21.5-10.0	13.86430	0.765467	
21	10.0-4.65	14.63002	0.765718	
22	4.65-2.15	15.40142	0.771400	
23	2.15-1.29999	15.90452	0.503100	
24	1.29999-1.15	16.02712	0.122600	
25	1.15-1.08	16.08992	0.062800	
26	1.08-1.03	16.13733	0.047410	
27	1.03-1.00	16.16688	0.02955	
28	1.0-0.95	16.21818	0.051300	
29	0.95-0.5	16.86003	0.641850	
30	0.5-0.414	17.04875	0.18872	
31	0.414-0.34	17.24570	0.19695	
32	0.34-0.278	17.44702	0.20132	
33	0.278-0.227	17.64969	0.202670	
34	0.227-0.152	18.05076	0.401070	
35	0.152-0.0923999	18.54851	0.497750	
36	0.0923999-0.056	19.04929	0.500780	
37	0.056-0.034	19.5483	0.499010	
38	0.034-0.0206	20.04935	0.501050	
39	0.0206-0.0125	20.54891	0.499560	
40	0.0125-0.001 eV	-	(1.0)	

ENERGY STRUCTURE OF THE NEUTRON GROUPS IN THE PRESENT SABINE-3 LIBRARY

i	E_H	Δu
0	18. MeV	
1	14.918	.9
2	6.065	.5
3	3.68	.5
4	2.23	.5
5	1.35	.5
6	821. keV	.5
7	498.	.5
8	302.	.5
9	183.	.75
10	86.5	1.00
11	31.8	1.00
12	11.7	1.00
13	4.31	1.00
14	1.58	1.00
15	583. eV	1.00
16	214.	1.00
17	78.9	1.00
18	29.0	1.00
19	10.7	.75
20	5.04	.5
21	3.06	.5
22	1.85	.5
23	1.12	.5
24	.682	.5
25	.414	.728
26	.200	-

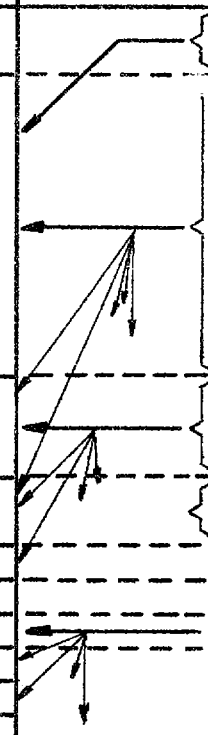

n	E_H (MeV)	χ_i
1	18.	3.359,-6
2	16.5	1.348,-5
3	14.918	5.062,-5
4	14.	5.080,-5
5	13.	1.160,-4
6	12.	2.630,-4
7	11.	5.89 ,-4
8	10.	1.310,-3
9	9.	2.86 ,-3
10	8.	6.15 ,-3
11	7.	1.18 ,-2
12	6.065	2.10 ,-2
13	5.2	3.18 ,-2
14	4.4	5.22 ,-2
15	3.68	7.69 ,-2
16	3.00	1.337,-1
17	2.23	2.310,-1
18	1.35	1.802,-1
19	.821	1.147,-1

i index of the diffusion groups

E_H upper energy of the groups

Δu lethargy width

n removal groups' index

χ_i fraction of fission neutrons emitted into the i^{th} group

APPENDIX 2

(reprinted from HEDL-SA-755)

DISPLACEMENT CROSS SECTIONS FOR DAMAGE FUNCTION ANALYSIS

Group	Energy, MeV* (group lower bound)	Displacement Cross Section, Barns			
		Iron	Chromium	Nickel	18/10 Stainless Steel
1	7.79 +00	1.99 +03	1.76 +03	1.54 +03	1.80 +03
2	6.05 +00	1.90 +03	1.70 +03	1.51 +03	1.62 +03
3	4.72 +00	1.71 +03	1.62 +03	1.44 +03	1.67 +03
4	3.68 +00	1.55 +03	1.54 +03	1.42 +03	1.54 +03
5	2.87 +00	1.35 +03	1.43 +03	1.35 +03	1.37 +03
6	2.23 +00	1.23 +03	1.24 +03	1.12 +03	1.22 +03
7	1.74 +00	9.70 +02	9.65 +02	1.01 +03	9.69 +02
8	1.35 +00	7.93 +02	6.69 +02	8.81 +02	7.70 +02
9	1.05 +00	6.08 +02	5.32 +02	8.87 +02	6.20 +02
10	8.21 -01	4.15 +02	5.43 +02	5.93 +02	4.56 +02
11	6.39 -01	4.78 +02	5.01 +02	4.85 +02	4.83 +02
12	4.98 -01	3.17 +02	3.47 +02	4.05 +02	3.31 +02
13	3.88 -01	3.97 +02	4.09 +02	4.55 +02	4.05 +02
14	3.02 -01	2.25 +02	2.37 +02	3.81 +02	2.42 +02
15	2.35 -01	1.82 +02	1.57 +02	3.62 +02	1.94 +02
16	1.83 -01	2.02 +02	1.66 +02	3.04 +02	2.05 +02
17	1.43 -01	1.55 +02	2.32 +02	2.29 +02	1.78 +02
18	1.11 -01	1.17 +02	1.79 +02	1.68 +02	1.34 +02
19	8.65 -02	1.14 +02	2.04 +02	1.46 +02	1.35 +02
20	6.74 -02	1.01 +02	4.02 +01	1.75 +02	1.39 +02
21	5.25 -02	6.91 +01	7.60 +01	1.63 +02	7.64 +01
22	4.09 -02	6.55 +01	7.39 +01	7.01 +01	6.74 +01
23	3.18 -02	8.15 +01	2.75 +01	8.54 +01	7.15 +01
24	2.48 -02	2.45 +02	2.74 +01	1.23 +02	1.92 +02
25	1.93 -02	4.68 +00	1.82 +01	1.02 +02	1.64 +01
26	1.50 -02	9.25 +00	1.34 +01	2.56 +02	3.33 +01
27	1.17 -02	1.13 +01	1.62 +01	1.56 +02	2.59 +01
28	9.12 -03	1.42 +01	2.01 +01	4.80 +01	1.86 +01
29	7.10 -03	3.40 +01	3.12 +01	2.13 +01	3.23 +01
30	5.55 -03	1.56 +01	2.80 +01	3.04 +01	1.94 +01
31	4.31 -03	7.59 +00	2.39 +01	5.68 +01	1.54 +01
32	3.35 -03	7.22 +00	1.70 +01	2.64 +01	1.09 +01
33	2.61 -03	5.38 +00	8.60 +00	1.47 +01	6.83 +00
34	2.03 -03	4.66 +00	3.93 +00	8.96 +00	4.92 +00
35	1.58 -03	4.00 +00	2.11 +00	5.98 +00	3.83 +00
36	1.23 -03	3.35 +00	1.45 +00	4.18 +00	3.08 +00
37	9.61 -04	7.35 +00	9.30 -01	2. 7 +00	5.70 +00
38	7.49 -04	2.24 +00	6.53 -01	2.05 +00	1.92 +00
39	5.83 -04	1.67 +00	4.34 -01	1.35 +00	1.54 +00
40	4.54 -04	1.32 +00	2.57 -01	7.59 -01	1.00 -01
41	3.54 -04	8.91 -02	1.62 -01	3.23 -01	1.15 -01
42	2.75 -04	1.00 -01	1.57 -01	2.08 -01	1.27 -01
43	2.14 -04	1.14 -01	1.78 -01	2.83 -01	1.42 -01
44	1.67 -04	1.28 -01	2.00 -01	2.99 -01	1.58 -01
45	1.30 -04	1.47 -01	2.27 -01	3.18 -01	1.78 -01
45	1.01 -04	1.66 -01	2.60 -01	3.41 -01	2.01 -01
**	E_L	$\frac{0.0016}{\sqrt{E_L}}$	$\frac{0.0025}{\sqrt{E_L}}$	$\frac{0.0028}{\sqrt{E_L}}$	$\frac{0.0020}{\sqrt{E_L}}$

* Group-averaged; one-quarter lethargy structure. Upper bound of highest group is 10 MeV. A 620 group set of values was collapsed to produce this 42 group set. Because of differences in the collapsing procedures, some differences appear in the values presented here as compared to those reported elsewhere [39].

** Below 1 x 10^{-4} MeV, the displacement cross section (σ_d) is proportional to $E^{-1/2}$; hence the group averaged values are expressed as $\bar{\sigma}_d$ = constant/$\sqrt{E_L}$, where E_L is the lower bound of each one-quarter lethargy group.

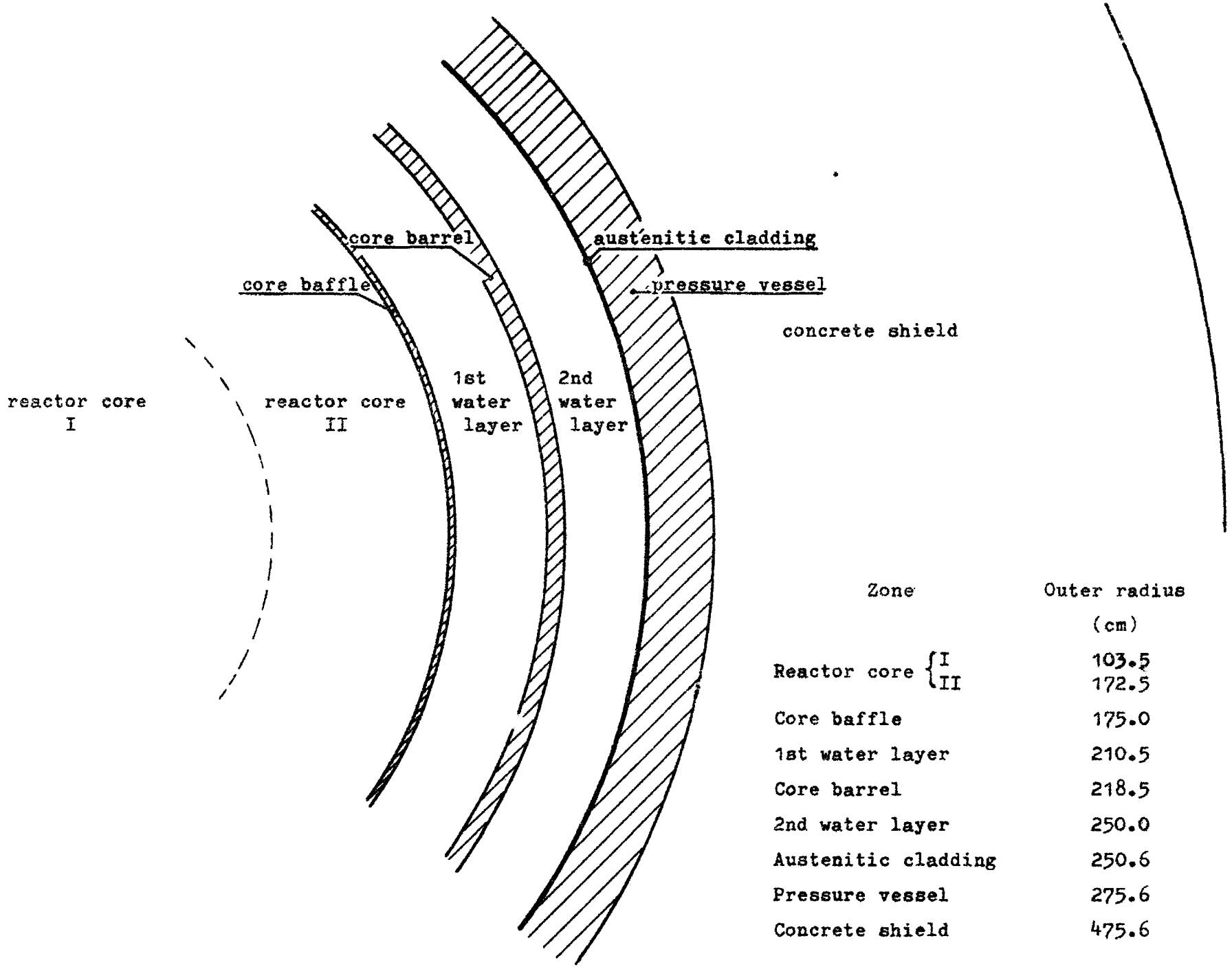

Zone	Outer radius (cm)	Zone thickness (cm)
Reactor core I	103.5	103.5
Reactor core II	172.5	69.0
Core baffle	175.0	2.5
1st water layer	210.5	35.5
Core barrel	218.5	8.0
2nd water layer	250.0	31.5
Austenitic cladding	250.6	0.6
Pressure vessel	275.6	25.0
Concrete shield	475.6	200.0

Fig. 1. Geometrical model of the reactor

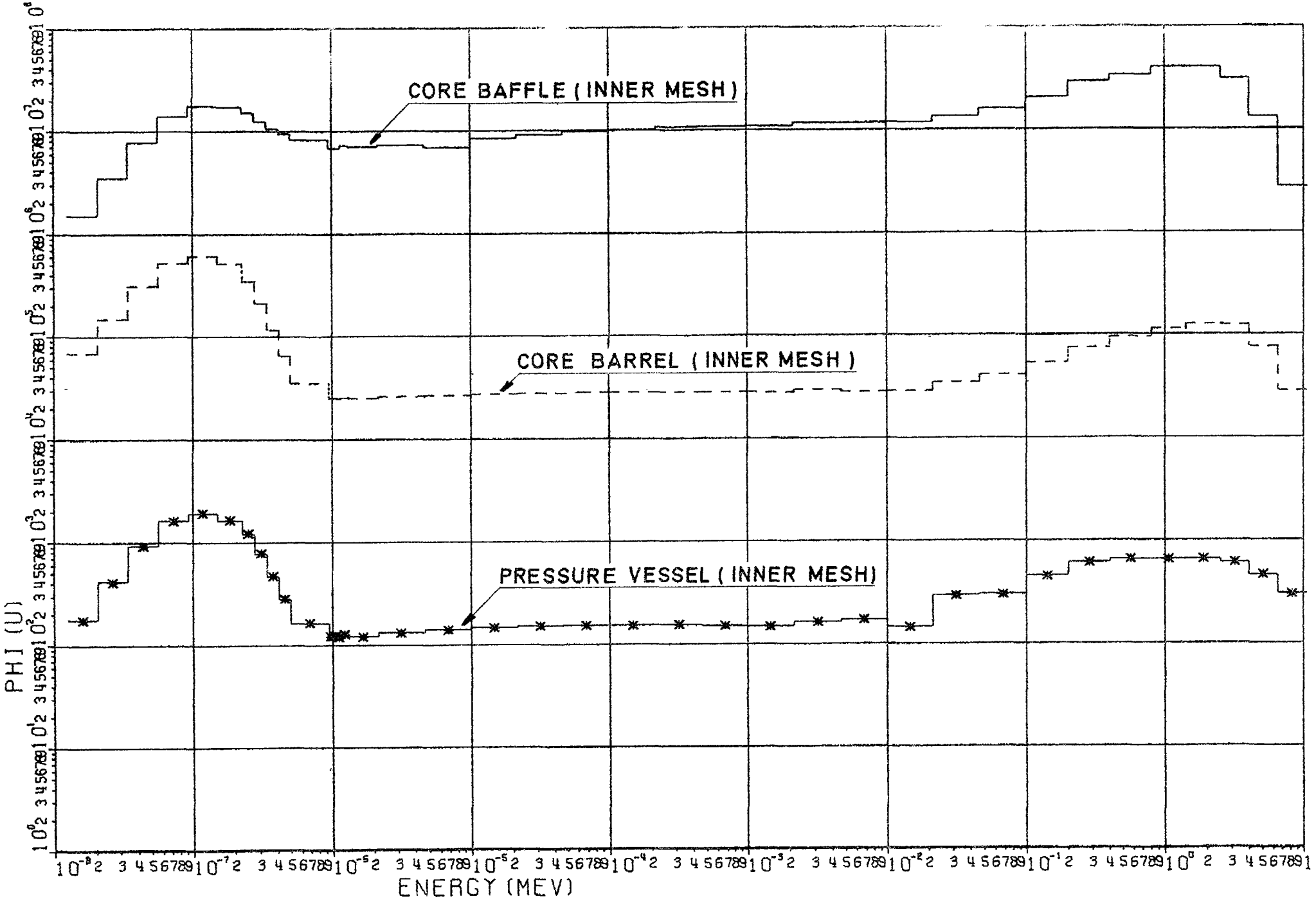

Fig. 2. 40-group (DTF-IV) neutron fluxes (arbitrary units)

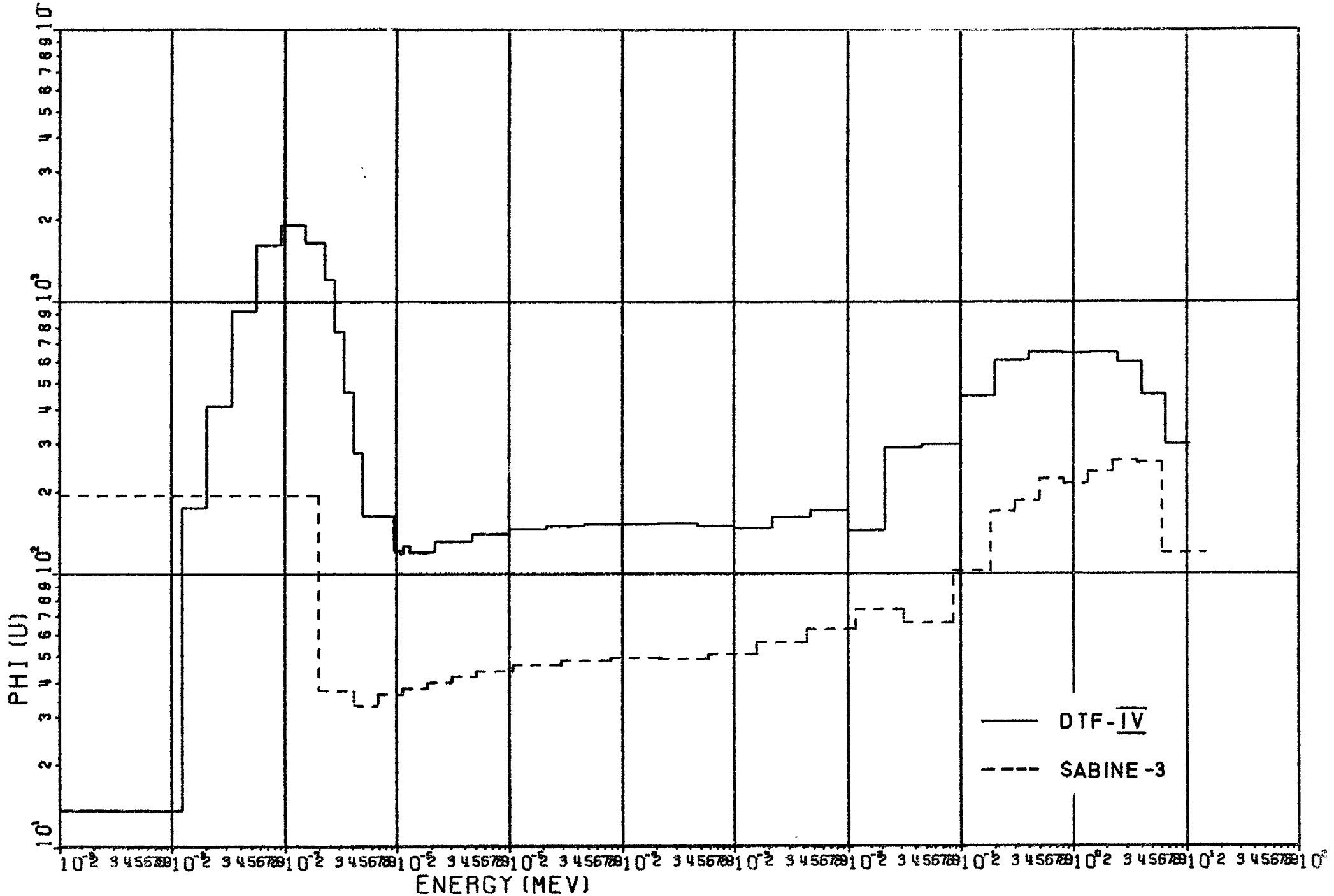

Fig. 3. Fluxes at inner mesh of pressure vessel (arbitrary units)

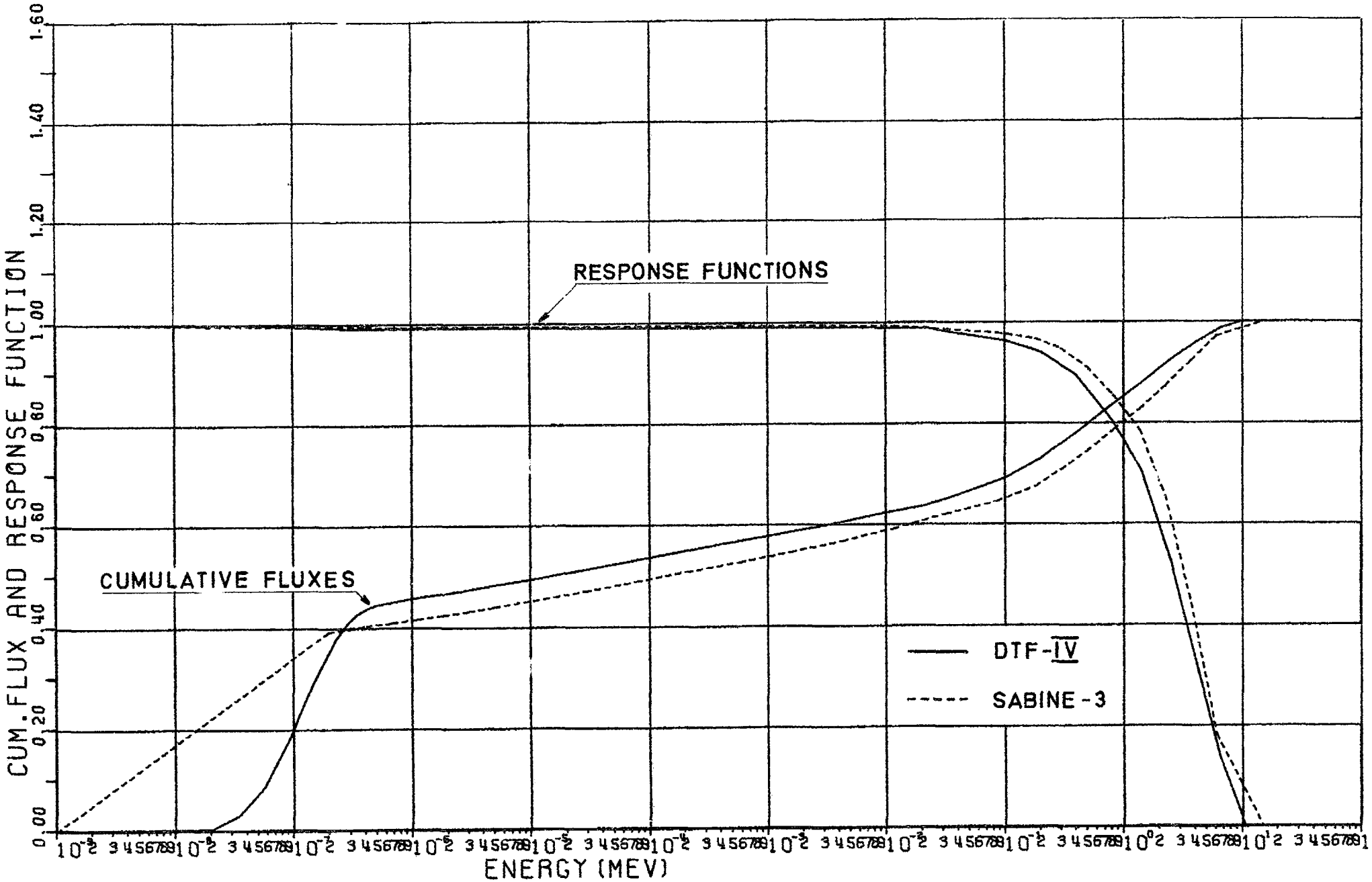

Fig. 4. Cumulative fluxes and response functions at inner mesh of pressure vessel

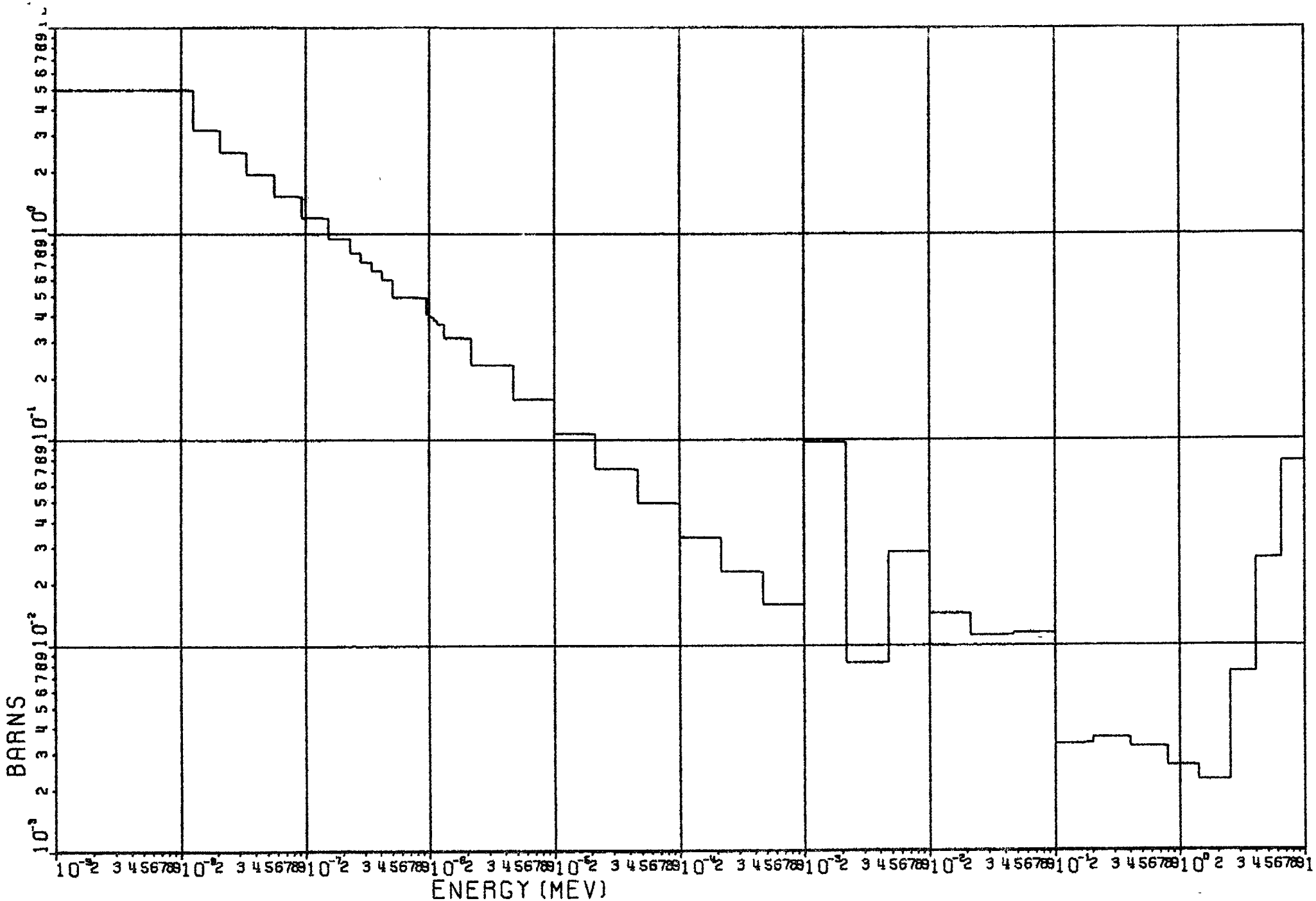

Fig. 5. Effective microscopic Fe cross sections (40-group structure)

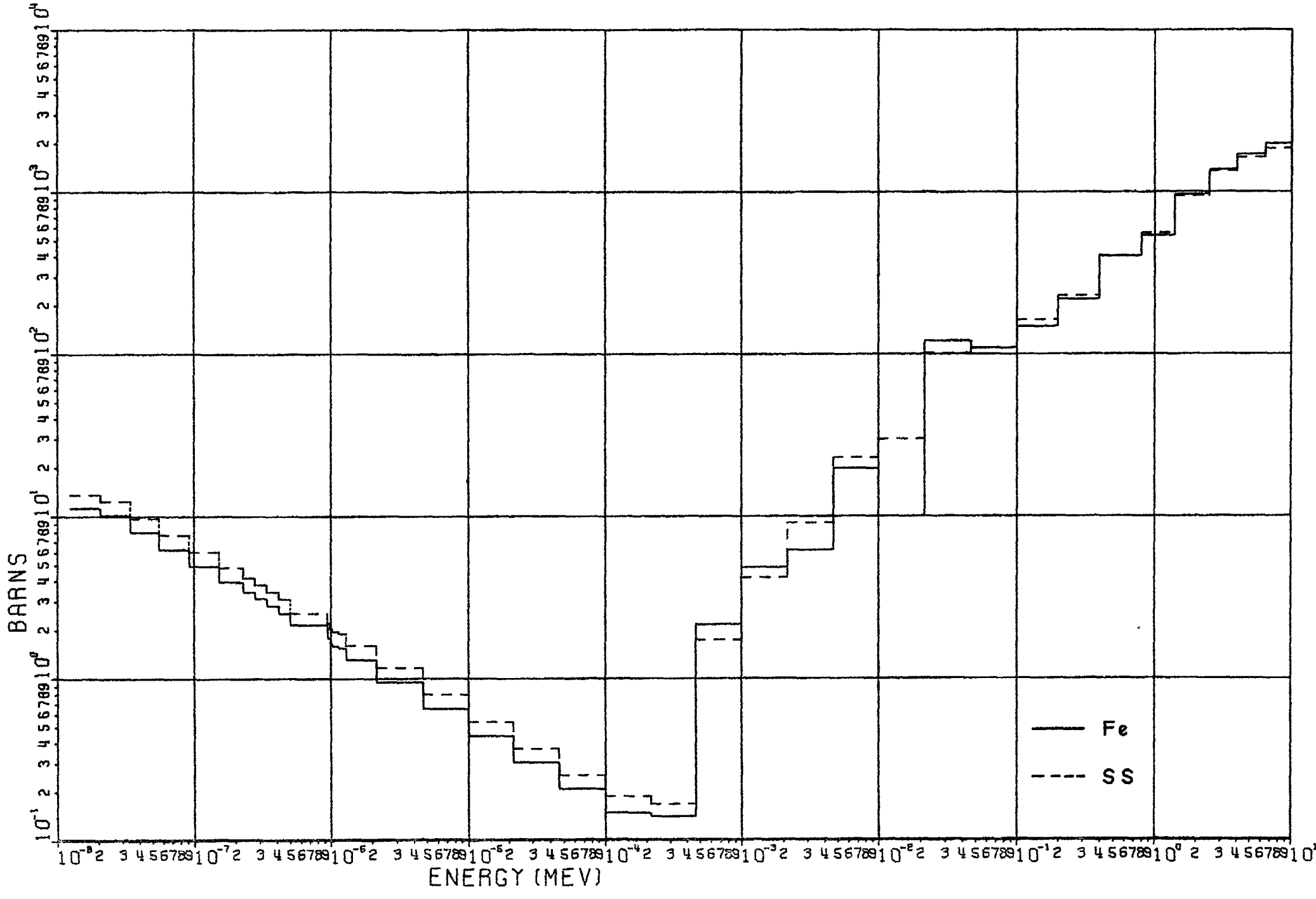

Fig. 6. Averaged DPA cross sections (40-group structure).

CONTRIBUTION TO THE EXERCISE ON SENSITIVITIES FOR THE NEA THEORETICAL PWR BENCHMARK

by

S D Lympany*
A K McCracken
A Packwood

Radiation Physics and Shielding Group
Reactor Physics Division
UKAEA, AEE Winfrith
Dorchester
Dorset

Abstract

Sensitivity studies on a benchmark PWR shield configuration using UKNDL data have been performed and led to the identification of the cross-sections whose accuracy must influence the calculation of design parameters of interest for PWRs.

Calculations for both neutrons and gamma rays were carried out using ANISN in one-dimensional cylindrical geometry in the P_3S_8 approximation and SWANLAKE was used for the calculation of cross-section sensitivities.

1 INTRODUCTION

Participants at the NEA meeting on Sensitivity Studies and Shielding Benchmarks at Paris in October 1975 agreed to submit calculations for reference designs of PWR and Fast Reactor shields. The object of this exercise is the assessment of the influence of different data sets on the accuracy of shielding calculations and the identification by means of sensitivity studies of the cross-sections whose accuracy most influence the calculation of design parameters of interest. A description and full specification of the Fast Reactor shield problem is given by Hehn (1) and is not repeated here. For both Fast Reactor and PWR problems a 42-group subset of the 100-group EURLIB energy scheme given in (1) was used for neutron calculations. For gamma-ray calculations a 16-group scheme, based on that of Sidebotham (2), was used. Calculations for both neutrons and gamma-rays were carried out using ANISN in one-dimensional cylindrical geometry in the P_3 S_8 approximation using the mesh structure proposed in (1), and SWANLAKE (3) was used for the calculation of cross-section sensitivities.

*Work performed during the author's attachment from Imperial College, London

2 DETAILS OF THE FORWARD CALCULATIONS

All basic nuclear data was taken from the UK Nuclear Data Library (4) and the appropriate Data File Number (DFN) for each element is given in the text.

2.1 Detector Cross-Sections

The Fe displacement cross-sections were calculated by applying the IAEA recommended displacement cross-section model of Norgett (5), Robinson and Torrens to Fe data (DFN 906). Displacement cross-sections were calculated in 2000 groups and collapsed into the 42-group scheme with and $[E\,x_t(E)]^{-1}$ weighting, where $x_t(E)$ is the energy-dependent total cross-section of Fe. (DFN 908 which was used in the penetration calculations for Fe is a minor revision of DFN 906 in the energy range 100 keV-300 keV. Above 330 keV both DFN 906 and DFN 908 are based on the ENDFB-3 file for Fe.) The neutron energy-group scheme and the components of the Fe displacement cross-section are given in Table 1.

Basic nuclear data for gamma-ray heating cross-sections was based on a revision of the photon interaction data in the UK Nuclear Data Library by Knipe (6). Gamma-ray flux-to-dose conversion factors, based on ICRP recommended values, were taken from (7). The gamma-ray energy group structure and the above group conversion factors are given in Table 2, together with the spectrum of gamma-rays produced by fission in U-235.

2.2 Cross-Sections for Penetration Calculations

Basic nuclear data was drawn from the UKNDL - (DFN's 923, 933, 908, 159 and 160 respectively for H, O, Fe, U-235 and U-238). This basic data for neutrons was processed into group form by GALAXY (8) using an $[E\,x_t(E)]^{-1}$ weighting where $x_t(E)$ is the energy-dependent total cross-section of the appropriate mixture in which the element occurs. Gamma-ray production cross-sections from neutron capture were taken from the compilation for thermal c pture of Sideboth) (2), and it was assumed that the source spectrum of gamma-rays produced was independent of the energy of the captured neutron; the capture source spectrum employed is given in Table 3. The group interaction cross-sections for the gamma-ray transmission calculations were processed by an adapted version of MUG (9) from Knipe's (6) revision of gamma-ray interaction data in the UKNDL.

3 CALCULATION OF THE REQUESTED QUANTITIES

3.1 Calculation of Integral Quantities

Results of calculations of the requested quantities are given below, the number in brackets referring to the appropriate section of (1).

(i) Displacement-rate per atom in the pressure vessel at interval number 120 (1.1) = 1.39×10^{-12} d.p.a. sec^{-1}.

(ii) Gamma-ray heating rate in the concrete shield at interval number 147 (1.2) = 9.71×10^{-6} Watt cm^{-3}.

(iii) Biological dose-rate at the outer-side of the concrete shield at interval number 202 (1.3):-

Due to gamma-rays = $1.04 \times 10^{1}_{0}$ mr hr^{-1}
Due to neutrons = 4.42×10^{0} mrem hr^{-1}

3.2 Calculation of Cross-Section Sensitivities for Damage, Heating and Biological Dose

3.2.1 Total sensitivities to neutron and gamma-ray cross-sections summed over energy groups of gamma-ray dose-rate (item 2.1) are given in Table 4 below.

3.2.2 The percentage change in predicted reaction-rates caused by changing the scattering approximation from P_3 to P_2, P_1 and P_0 (item 2.2) are given in Tables 5, 6 and 7 below.

Figures 1 to 4 inclusive show the total cross-section sensitivity profiles of those elements which most influence the calculation of the gamma-ray heating-rate, the gamma-ray dose-rate and the Fe displacement-rate at the specified positions. On each graph the total cross-section sensitivity summed over all contributing elements is also shown. As we did not use a coupled neutron-gamma data the calculation of neutron cross-section sensitivities for gamma-ray reaction-rates involved the running of both gamma-ray and neutron adjoint calculations before using SWANLAKE for neutrons. The form of the adjoint neutron source is given in the Appendix.

Figures 5 and 6 compare respectively the Fe displacement-rates and the neutron dose-rate predictions of ANISN and REDIFFUSION (10), a removal-diffusion design code in regular use in the UK; the agreement is seen to be generally very satisfactory.

It will be noticed that the sensitivities of both gamma-ray dose-rate and gamma-ray heating-rate to neutrons is identical, as is the effect of altering the neutron angular scattering approximation. It would appear that the same adjoint gamma-ray calculation might have been used in the expression of the Appendix for constructing the adjoint neutron source for both gamma-ray heating-rate and dose-rate. Checks suggest that this is not in fact the case; this apparent agreement in neutron sensitivities is receiving further scrutiny, although it seems physically reasonable to expect broad agreement.

4 IMPLICATIONS FOR DATA

In a companion paper (11) is described the calculation of $\sigma(R)/R$ which takes account of the negative correlations between measured partial cross-sections and of varying degrees of energy-dependent positive correlations. This exercise has been carried out for the prediction of displacement-rate in the pressure vessel. The fractional standard deviations attributed to the measured cross-sections of Fe and O are shown in Table 1; it is assumed that errors in the H cross-sections are negligible. The fractional standard deviation on the iron displacement-rate, caused by the measurement uncertainties of Table 1, is shown in Table 8 for three types of energy-dependent correlation, viz:- zero correlation ($r = 0$), a correlation which decreases linearly with energy separation $r = 1 - |i - j|/41$ and perfect correlation over all energies ($r = 1$). The first and last of these clearly represent the bounds for the measurement errors assumed.

No special significance attaches to the intermediate case which is included for interest. It is clear that if significant long range energy correlations exist they have an important effect on the confidence of prediction of design parameters. In Table 8 the column headed Total takes account of the small contribution made by elements other than Fe and O.

It is of interest now to consider sensitivity functions W_x (where x represents any measured cross-section) which represent the fractional improvement in $\sigma(R)/R$ per unit fractional improvement in the standard deviation of the measurement x. This is discussed in (11) and we merely note here that

$$W_{xi} = \frac{\delta\left(\frac{\sigma(R)}{R}\right)}{\frac{\sigma(R)}{R}} \Bigg/ \frac{\delta_{\sigma(x)}}{\sigma(x)}$$

which may be considered a "measurement profile" since it makes assumptions about the quality of a basic measurement. The measurement profiles of the measured cross-sections of Fe and Oxygen for Fe displacement-rate in the pressure vessel are shown in Figures 7 and 8. These profiles show more clearly than the normal total cross-section profiles which cross-section uncertainties may be most profitably investigated. Thus for iron displacements the Oxygen inelastic cross-sections between 7 MeV and 12.5 MeV and the total cross-sections between 4.5 MeV and 7 MeV are the only ones of importance; for iron only the non-elastic cross-section between 4.5 MeV and 10 MeV need be considered for the problem studied.

ACKNOWLEDGEMENT

We are very obliged to Mr A F Avery for useful discussions and advice.

REFERENCES

1 Hehn, G and Koban, J
Reactor Shield Benchmark No 2
Special Issue No 4, ESIS Newsletter

2 Sidebotham, E W
Spectra of Energy Released by Thermal Neutron Capture
TRG Report 2189(R)

3 Bartine, D E et al
SWANLAKE, A Computer Code Utilising ANISN Radiation Transport Calculations for Cross-Section Sensitivity Analysis
ORNL-TM-3809

4 Pope, A L
The Current Edition of the Main Tape NDL-1 of the UK Nuclear Data Library
AEEW-M 1208

5 Norgett, M J et al
IAEA Specialist Meeting on Radiation Damage Units for Ferritic and Stainless Steels, Seattle, Washington, 1972

6 Knipe, A D
A Revision of the Photon Interaction Data in the UKAEA Nuclear Data Library
AEEW-M 1368

7 Engineering Compendium on Radiation Shielding, Springer-Verlag, New York, 1968

8 Price, J A
A Guide to GALAXY 6
AWRE O/13/75

9 Knight, J R; Mynatt, F R
MUG, A Program for Generating Multigroup Photon Cross-Sections
ORNL, CTC-17 (1970)

10 Unpublished

11 Lympany, S D et al
Contribution to the Exercise on Sensitivities for the NEA Theoretical Fast Reactor Benchmark

APPENDIX

The Adjoint Source for Coupled Gamma-Ray Neutron Sensitivity Calculations

Let $S_j^+(r)$ be the source importance of gamma-rays in gamma group j and position r given by an adjoint calculation for which the source is the gamma-ray flux-to-dose conversion factor at the dose point.

$\phi_i(r)$ be the neutron flux in neutron group i

$\alpha_{i,\ell}(r)$ be the capture cross-section in neutron group i

$N_j(r)$ be the number of gamma-rays produced in gamma group j per capture.

Then the dose-rate at the dose point caused by captures in neutron group i is

$$R_i(r) = \phi_i(r)\,\alpha_{i,\ell}(r) \sum_j N_j(r)\, S_j^+(r)$$

The space and group dependent adjoint source for determining the sensitivity of the gamma-ray dose-rate to neutron cross-sections is therefore:-

$$H_i^+(r) = \alpha_{i,\ell}(r) \sum_j N_j(r)\, S_j^+(r)$$

This form of adjoint neutron source was used for determining the sensitivity of both gamma-ray heating-rate and dose-rate to neutron cross-sections.

TABLE 1

Detector Cross-Sections and Fractional Errors on Fe and O Cross-Sections

Group	Upper Energy	Cross-Section - Barns					Fe			O		
		$Na^{23}(n,\gamma)$	Fe dpa	Fe (cap)	Fe (el)	Fe (in)	J_T	J_{NE}	J_A	J_T	J_{IN}	J_A
1	1.492+1	2.05-4	2.666+3	1.335+0	5.689+2	2.096+3						
2	1.221+1	1.800-4	2.082+3	1.027+0	5.131+2	1.567+3						
3	1.000+1	1.730-4	2.011+3	7.168-1	5.298+2	1.480+3						
4	8.187+0	1.690-4	1.941+3	4.745-1	5.560+2	1.385+3				0.05		
5	6.703	1.650-4	1.772+3	2.972-1	6.431+2	1.129+3						
6	5.488	1.620-4	1.656+3	1.779-1	6.829+2	9.726+2	0.05					
7	4.493	1.610-4	1.514+3	1.196-1	7.112+2	8.031+2						
8	3.679	1.680-4	1.315+3	6.044-2	7.228+2	5.925+2		0.10				
9	3.011	1.768-4	1.193+3	2.933-2	7.675+2	4.253+2					0.30	0.20
10	2.466	1.828-4	1.084+2	1.985-2	7.202+2	3.641+2						
11	2.346	1.904-4	9.509+2	1.604-2	6.678+2	2.830+2						
12	1.827	2.017-4	7.574+2	1.575-2	5.886+2	1.687+2						
13	1.496	2.214-4	7.157+2	1.616-2	5.878+2	1.279+2						
14	1.225	2.237-4	4.880+2	1.785-2	3.911+2	9.697+1				0.04		
15	1.003	2.401-4	3.805+2	2.820-2	3.567+2	2.381+1	0.04					
16	8.209-1	3.257-4	4.212+2	3.451-2	4.212+2	0						
17	6.081-1	3.190-4	3.153+2	3.448-2	3.153+2	0			0.15			
18	4.979-1	2.533-4	3.618+2	3.304-2	3.618+2	0						
19	4.076-1	3.607-4	2.323+2	3.333-2	2.322+2	0						
20	3.337-1	7.325-4	1.479+2	3.867-2	1.478+2	0						
21	1.111-1	2.968-4	8.877+1	7.020-2	8.870+1	0						
22	6.738-2	6.536-4	5.489+1	4.707-2	5.484+1	0						
23	4.087-2	2.848-3	6.723+1	1.082-1	6.712+1	0						
24	3.183-2	4.795-4	1.869+2	1.431-1	1.867+2	0	0.05	0.15				
25	2.650-2	5.611-4	6.062+0	7.009-2	5.992+0	0						
26	2.187-2	8.953-4	1.131+1	2.407-2	1.129+1	0				0.15		
27	1.171-2	1.717-3	2.374+1	1.053-1	2.364+1	0						
28	7.102-3	3.317-3	1.229+1	6.726-2	1.222+1	0						
29	4.307-3	3.609-2	6.016+0	4.429-2	5.971+0	0						
30	2.035-3	9.404-3	3.995+0	1.0540	2.941+0	0						
31	9.611-4	5.677-3	8.399-1	7.533-2	7.645-1	0						
32	4.540-4	6.808-3	1.550-1	1.550-1	0	0						
33	1.670-4	9.449-3	2.169-1	2.169-1	0	0						
34	1.013-4	1.181-2	2.796-1	2.796-1	0	0						
35	6.144-5	1.565-2	3.745-1	3.745-1	0	0						
36	2.902-5	2.063-2	5.374-1	5.374-1	0	0	0.03			0.03		
37	1.760-5	2.733-2	7.063-1	7.063-1	0	0						
38	8.315-6	3.604-2	1.027+0	1.027+0	0	0		0.04	0.04			
39	5.044-6	5.065-2	1.588+0	1.588+0	0	0						
40	1.855-6	9.265-2	2.214+0	2.214+0	0	0						
41	4.140.7	1.685-1	5.410+0	5.410+0	0	0						
42	7.600-8	3.511-1	1.360+1	1.360+1	0	0						

TABLE 2

Gamma-Ray Group Structure and Cross-Sections and Gamma-Ray Spectrum from Fission

Group	Lower Energy MeV	Flux Conversion Factors		Photons Per Fission
		Heating in Concrete[1]	Dose in Concrete[2]	
1	0.01	0.0831	0.322,-3	0.958
2	0.08	0.0104	0.162,-3	1.47
3	0.15	0.0182	0.447,-3	4.74
4	0.39	0.0346	0.868,-3	3.68
5	0.635	0.0500	0.125,-2	2.18
6	0.88	0.0674	0.169,-2	2.32
7	1.275	0.0902	0.228,-2	1.75
8	1.875	0.112	0.286,-2	0.775
9	2.35	0.128	0.323,-2	0.369
10	2.7	0.142	0.359,-2	0.305
11	3.2	0.165	0.404,-2	0.279
12	4.0	0.195	0.478,-2	0.109
13	4.95	0.227	0.546,-2	0.0247
14	5.8	0.256	0.609,-2	0.0169
15	6.6	0.284	0.668,-2	0.00246
16	7.4-9.0	0.328	0.753,-2	0.00223

1 MeV cm^{-1}

2 mr hr^{-1}/unit flux

TABLE 3

Gamma-Ray Source Spectrum - MeV per Capture

Kernel Energy MeV	0.045	0.115	0.23	0.51	0.76	1.0	1.55	2.2	2.5	2.9	3.5	4.5	5.4	6.2	7.0	8.2
Group / Element	1	2	3	4	5	6	7	8	9	10	11	12	13	14	15	16
H								2.25								
O			0.440		0.579	0.492		0.986			0.679					
Al			1.290	0.015	0.047	0.121	3.724	0.482	0.370	0.834	0.862	1.134	0.239	0.268	1.367	
Si			0.038	0.009	0.012	0.121	0.093	0.544	0.098	0.124	2.805	3.130	0.162	0.808	0.794	
Ca			0.325	0.067	0.063	0.174	0.453	2.688	0.159	0.173	0.469	0.802	0.362	2.466	0.179	
Cr			0.176	0.016	0.281	0.040	0.246	0.591	0.251	0.248	0.387	0.300	0.375	0.439	5.891	
Mn			0.886	0.012	0.975	0.020	1.320	0.559	0.297	0.168	0.513	0.723	1.389	0.260	2.756	
Fe			0.007	0.020	0.114	0.109	0.356	0.173	0.145	0.268	0.417	0.507	0.095	1.052	4.524	
Ni			0.030	0.061	0.034	0.021	0.057	0.065	0.047	0.084	0.091	0.142	0.226	0.471	7.207	
Zr			0.088	0.156	0.172	0.731	0.645	0.640	0.540	0.644	0.943	0.913	0.570	1.562	0.203	
U-235			0.786	0.871	0.664	0.844	1.395	1.029	0.262	0.154	0.289	0.114	0.080			
U-238			0.573	0.634	0.483	0.615	1.016	0.750	0.190	0.122	0.210	0.083				

Table 4

Total Sensitivities to Neutron and Gamma-Ray Cross-Sections

Element	Displacement Mesh 120	Gamma Heating		Gamma Dose-Rate	
	Neutrons	Neutrons	Gammas	Neutrons	Gammas
H	-5.02,0	-2.71,0	-1.83,-1	-2.71,0	-1.33,-1
O	-1.66,0	-3.91,-1	-8.93,-1	-3.91,-1	-4.66,0
Fe	-1.50,0	-3.78,-2	-5.51,0	-3.78,-2	-2.90,0
Zr	-1.23,-1	-6.63,-2	-2.42,-2	-6.63,-2	-3.82,-3
U-235	-9.48,-3	-1.72,-2	)	-1.72,-2	)
U-238	-3.04,-1	-2.29,-1	)-1.23,-1	-2.29, 1	)-2.05,-2
Cr	-3.64,-1	-6.42,-2	-2.95,-1	-6.42,-2	-1.52,-1
Ni	-2.06,-1	-4.41,-2	-1.82,-1	-4.41,-2	-9.48,-2
Mn	-2.72,-1	-7.00,-3	-2.06,-2	-7.00,-3	-1.06,-2
Al	)		-5.44,-3	)	-3.81,-1
Si	) ~10^{-4}	~10^{-4}	-2.30,-2	) ~10^{-4}	-1.60,0
Ca	)		-2.79,-2	)	-1.73,0
TOTAL	-9.46	-3.57,0	-7.29,0	-3.57,0	-1.17,1

Table 5

Percentage Change in Prediction of Gamma-Ray Heating in Mesh 147 by Dif erent Scattering M ments

Element	Neutrons			Gamma-Rays		
	P_0	P_1	P_2	P_0	P_1	P_2
H	-9.14,1	-2.45,0	-2.13,-2	-2.47,0	-8.33,-1	-1.01,-1
O	-1.66,1	-4.97,-1	-4.36,-5	-4.18,0	-3.38,0	-1.46,0
Fe	-1.15,0	-2.66,-2	+4.44,-3	-9.09,+1	-2.89,+1	-3.80,0
Zr	-1.50,0	+7.54,-2	+6.34,-3	-1.53,-2	-1.17,-2	-7.30,-3
U-235	-1.24,-1	+8.21,-3	+8.02,-4	)		
U-238	-3.74,0	+2.43,-1	+2.35,-2	)-5.31,-2	-4.06,-2	-2.53,-2
Cr	-2.49,0	-1.26,-1	+8.19,-3	-2.88,0	-1.23,0	-3.02,-1
Ni	-1.06,0	-4.83,-2	+2.92,-3	-1.70,0	-7.34,-1	-1.78,-1
Mn	-1.45,-1	-7.15,-3	+4.55,-4	-1.98,-1	-8.47,-2	-2.08,-2
Al	-2.27,-4	+8.89,-7	+2.99,-8	+5.00,-1	-3.53,-3	-9.18,-2
Si	-9.57,-4	+3.85,-6	+1.26,-7	+2.07,0	-1.46,-2	-3.80,-1
Ca	-5.21,-4	+4.49,-6	+1.77,-7	+2.07,0	-1.46,-2	-3.80,-1
TOTAL	-1.18,2	-2.83,0	+2.53,-2	-9.78+1	-3.52,+1	-6.75,0

Table 6

Percentage Change in Prediction of Gamma-Ray Dose-Rate in Mesh 202 by Different Scattering Moments

Element	Neutrons			Gamma-Rays		
	P_0	P_1	P_2	P_0	P_1	P_2
H	-9.14,1	-2.45,0	-2.13,-2	-1.23,0	-3.27,-1	-2.14,-2
O	-1.66,1	-4.97,-1	-4.36,-5	-6.13,1	-1.42,1	-1.43,0
Fe	-1.15,0	-2.66,-2	+4.44,-3	-1.34,1	-7.91,0	-2.94,0
Zr	-1.50,0	+7.54,-2	+6.34,-3	+9.94,-3	-8.55,-3	-4.60,-3
U-235	-1.24,-1	+8.21,-3	+8.02,-4	)		
U-238	-3.74,0	+2.43,-1	+2.35,-2	)+3.45,-2	-2.96,-2	-1.59,-2
Cr	-2.49,0	-1.26,-1	+8.19,-3	-6.06,-1	-2.86,-1	-8.81,-2
Ni	-1.06,0	-4.83,-2	+2.92,-3	-3.57,-1	-1.68,-1	-5.19,-2
Mn	-1.45,-1	-7.15,-3	+4.55,-4	-4.18,-2	-1.97,-2	-6.07,-3
Al	-2.27,-4	+8.89,-7	+2.99,-8	-4.94,0	-1.13,0	-1.17,-1
Si	-9.57,-4	+3.85,-6	+1.26,-7	-2.04,1	-4.68,0	-4.85,-1
Ca	-5.21,-4	+4.49,-6	+1.77,-7	-2.05,1	-4.68,0	-4.85,-1
TOTAL	-1.18,2	-2.83,0	+2.53,-2	-1.22,2	-3.34,1	-5.79,0

Table 7

Percentage Change in Prediction of Displacement-Rate in Mesh 120 by Different Scattering Moments

Element	Neutrons		
	P_0	P_1	P_2
H	-9.90,1	-2.16,1	-1.32,0
O	-5.52,1	-8.80,0	-5.32,-1
Fe	-5.72,1	-1.24,1	-2.56,0
Zr	-2.42,0	+3.98,-1	+1.10,-1
U-235	-2.20,-1	+3.82,-2	+1.09,-2
U-238	-6.16,0	+1.08,0	+3.08,-1
Cr	-2.08,1	-4.42,0	-3.08,-1
Ni	-9.06,0	-1.88,0	-1.25,-2
Mn	-1.16,0	-2.50,-1	-1.69,-3
Al	)		
Si	)	NEGLIGIBLE	
Ca	)		
TOTAL	-2.50,2	-4.78,1	-4.44,0

Table 8

Percentage Uncertainties in Displacement-Rate Prediction

Element / Correlation	Percentage Standard Deviation on Displacement Rate Caused by Errors in:-			Total
	Fe	O	Fe + O	
r = 0	3.30	3.65	4.93	6.56
$r = 1 - \lvert i - j \rvert / 41$	7.67	8.24	11.30	14.9
r = 1	7.85	8.45	11.50	15.3

	Sensitivity to Iron Cross-Section			Sensitivity to Oxygen Cross-Section		
GROUP	$W_{(\alpha i)}$	$W_{(\sigma i)}$	$W_{(\tau i)}$	$W_{(\alpha i)}$	$W_{(n'i)}$	$W_{(\tau i)}$
1	0.3420E-04	0.2897E-02	0.5530E-04	0.3457E-02	0.2093E-01	0.1118E-02
2	0.1427E-03	0.2556E-01	0.3578E-03	0.1073E-01	0.1083E+00	0.9790E-02
3	0.2844E-03	0.1392E+00	0.2632E-02	0.9927E-02	0.2297E+00	0.5464E-01
4	0.2350E-03	0.2861E+00	0.7307E-02	0.9275E-02	0.1109E+00	0.1032E+00
5	0.1611E-03	0.3342E+00	0.1592E-01	0.5988E-02	0.9763E-04	0.1732E+00
6	0.4406E-04	0.1215E+00	0.4605E-02	0.3256E-02	0.9498E-03	0.1044E+00
7	0.8566E-05	0.9295E-02	0.4432E-03	0.7026E-03	0.1151E-04	0.2358E-01
8	0.1890E-05	0.1803E-02	0.2072E-02	0.1671E-08	0.6057E-13	0.7405E-02
9	0.6160E-06	0.2780E-02	0.2926E-02	0.0	0.0	0.5130E-02
10	0.2078E-07	0.6183E-04	0.2111E-03	0.0	0.0	0.6704E-04
11	0.1739E-06	0.2057E-03	0.1160E-01	0.0	0.0	0.2379E-02
12	0.7233E-07	0.7539E-04	0.7804E-02	0.0	0.0	0.5257E-03
13	0.3856E-07	0.1402E-03	0.4386E-02	0.0	0.0	0.2131E-03
14	0.2186E-07	0.1335E-03	0.1920E-02	0.0	0.0	0.4786E-04
15	0.2306E-07	0.2615E-04	0.1230E-02	0.0	0.0	0.1450E-04
16	0.7777E-08	0.3334E-06	0.4592E-02	0.0	0.0	0.2073E-04
17	0.1590E-08	0.7508E-07	0.1050E-02	0.0	0.0	0.2754E-05
18	0.3660E-09	0.2426E-07	0.8002E-03	0.0	0.0	0.3130E-05
19	0.5905E-09	0.5466E-07	0.1026E-02	0.0	0.0	0.9430E-06
20	0.4503E-08	0.1613E-06	0.4142E-02	0.0	0.0	0.7433E-06

TABLE 9: Group Contribution to the Measurement Sensitivities of Iron Displacement Rate by Iron and Oxygen Cross-Sections

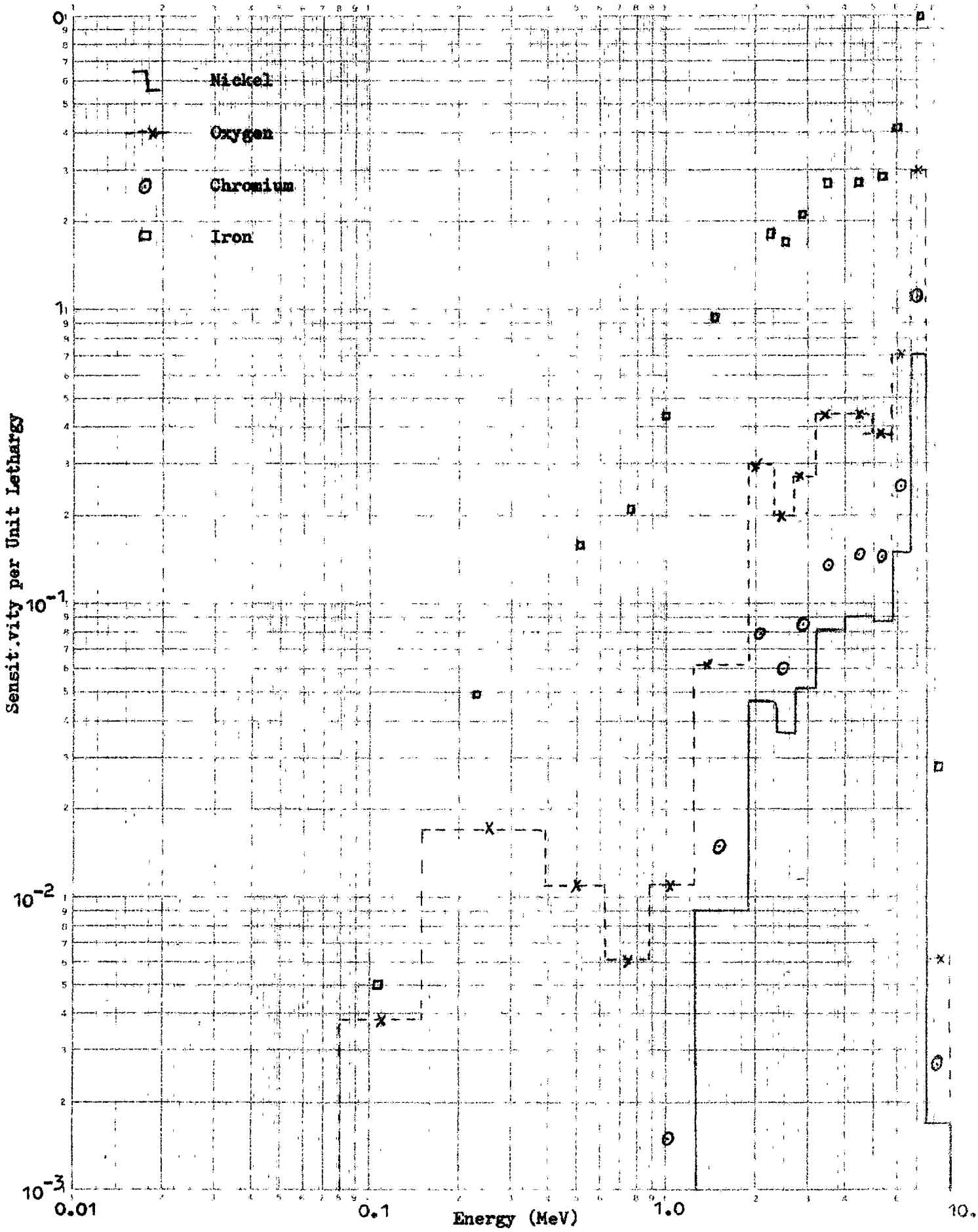

FIGURE 1: Sensitivity of Gamma-Ray Heating Rate to Nickel, Oxygen, Chromium and Iron Gamma-Ray Cross-Sections

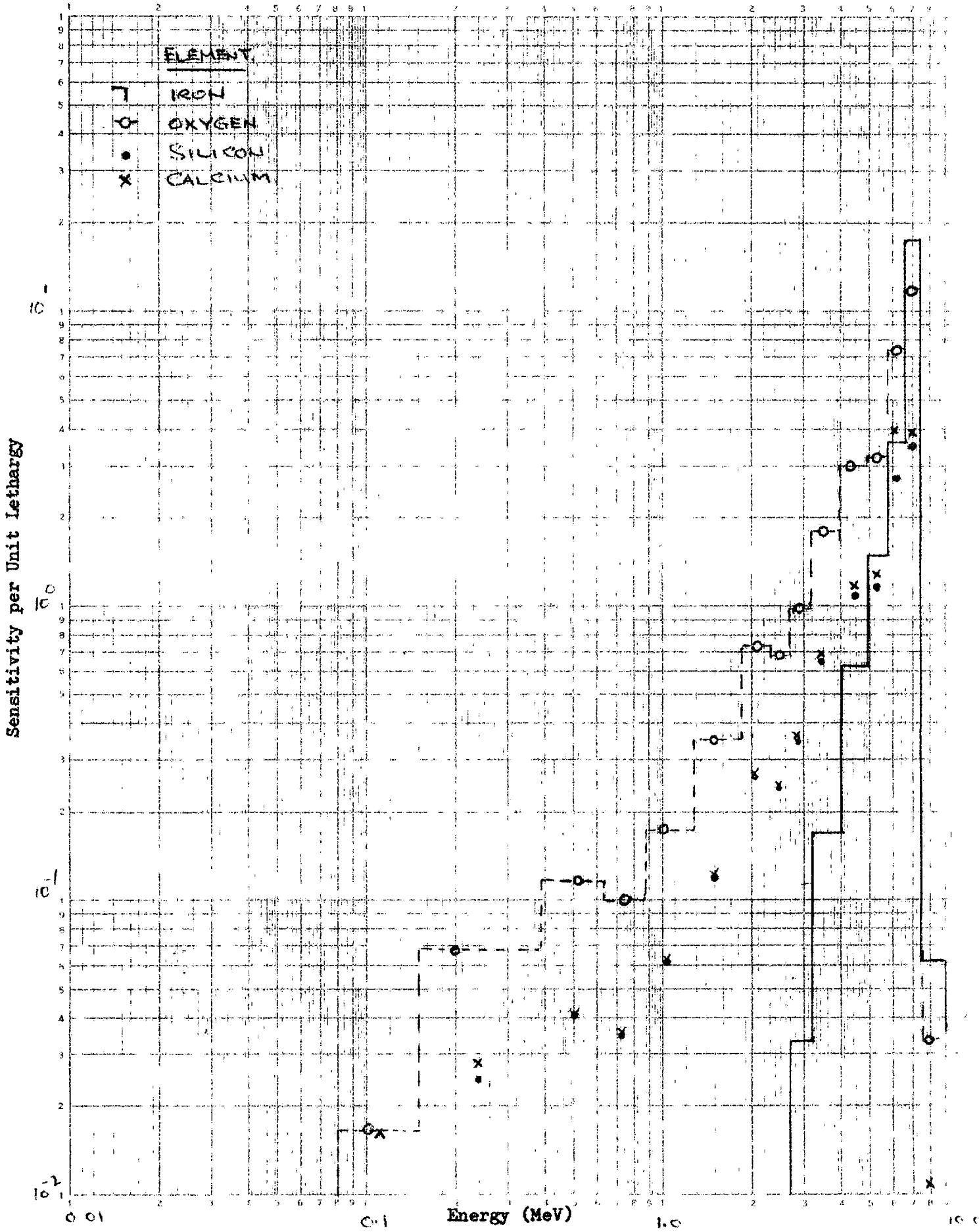

FIGURE 2 : Sensitivity of the Gamma-Ray Dose-Rate to Iron, Oxygen Silicon and Calcium Gamma-Ray Cross-Sections

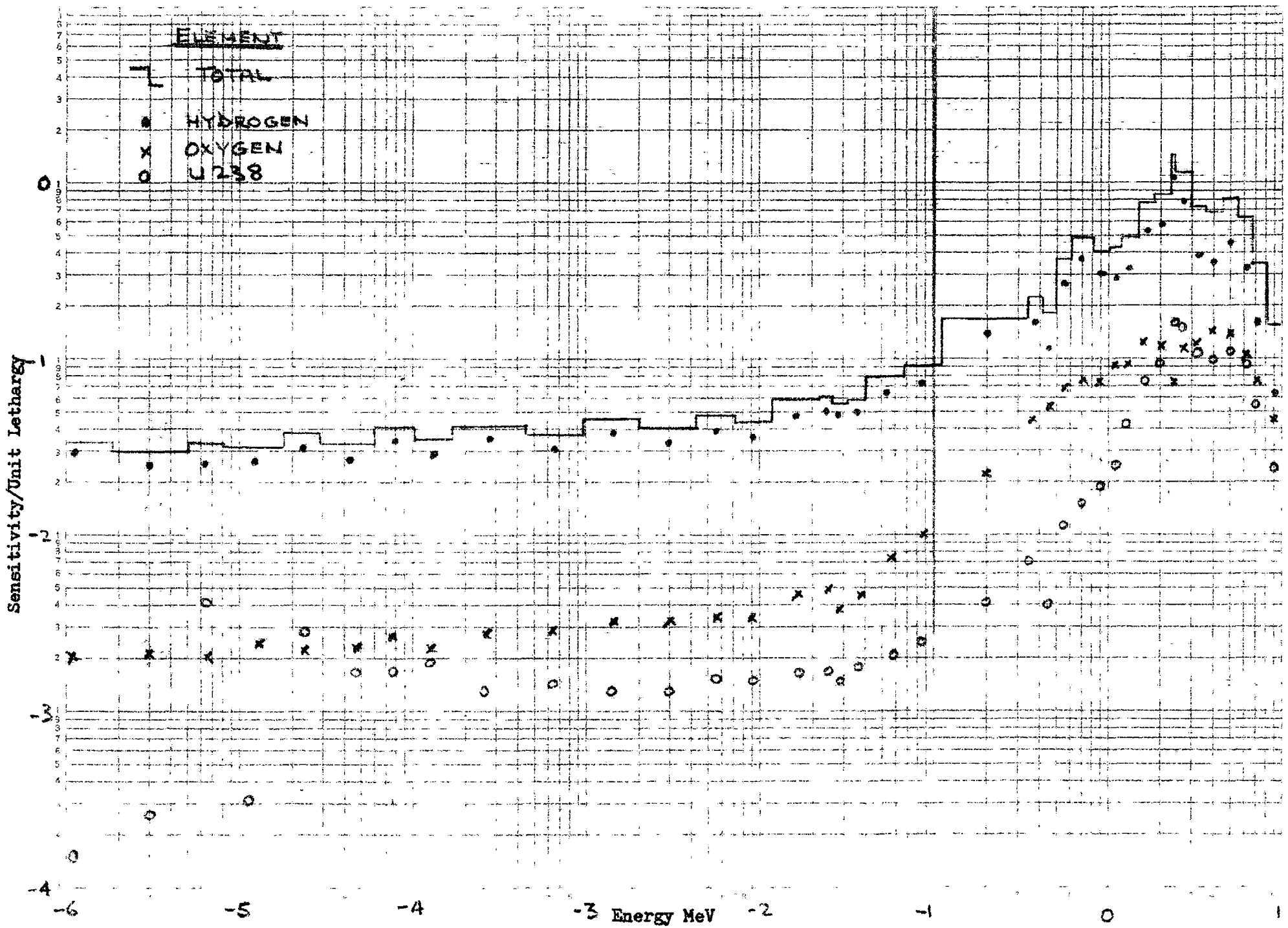

FIGURE 3: Sensitivity of the gamma heating Rate to the Hydrogen, Oxygen and U-238 Neutron Cross-Sections

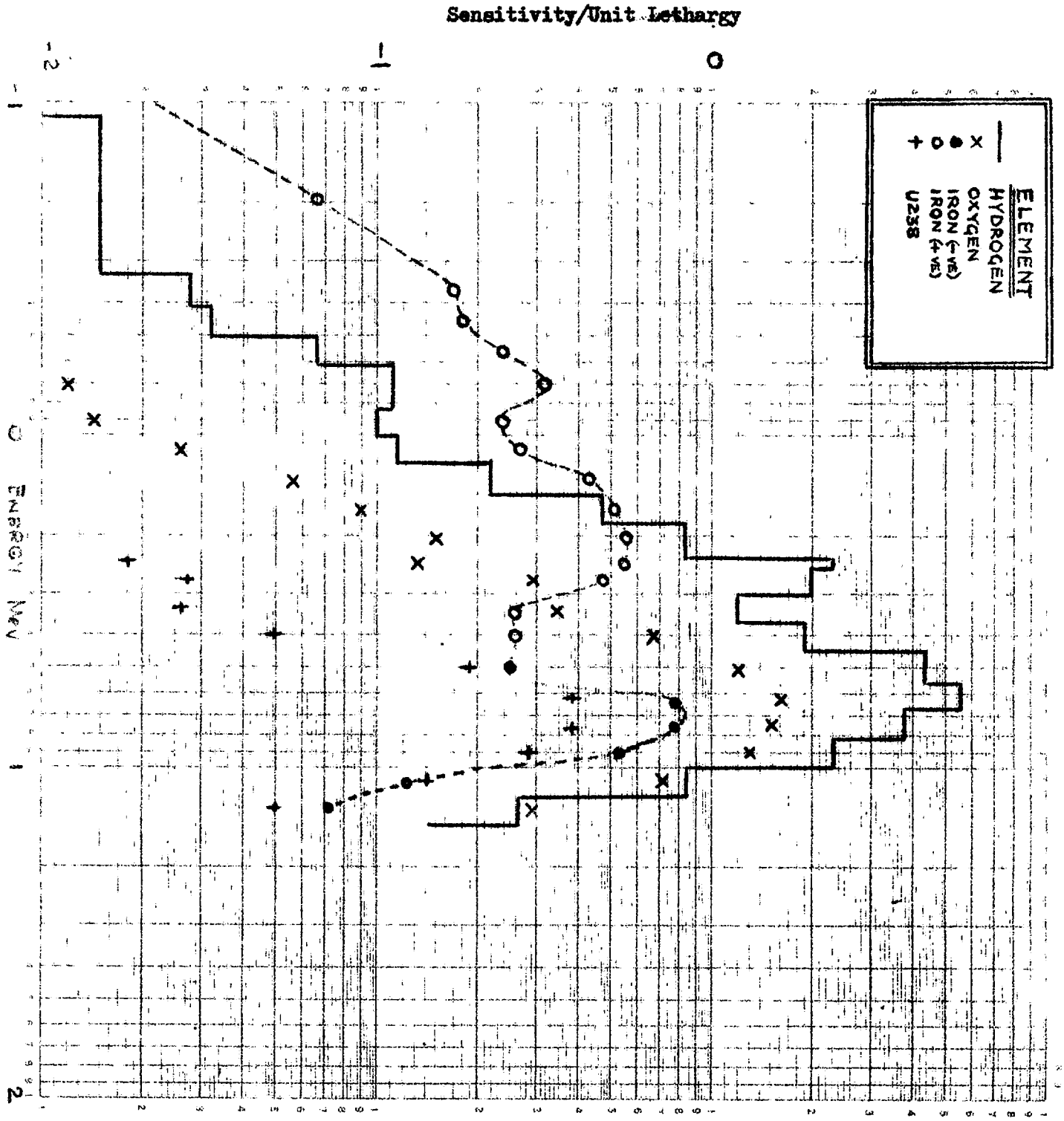

FIGURE 4 : Sensitivity of the Iron Displacement Rate to Hydrogen, Oxygen and Iron Cross-Sections

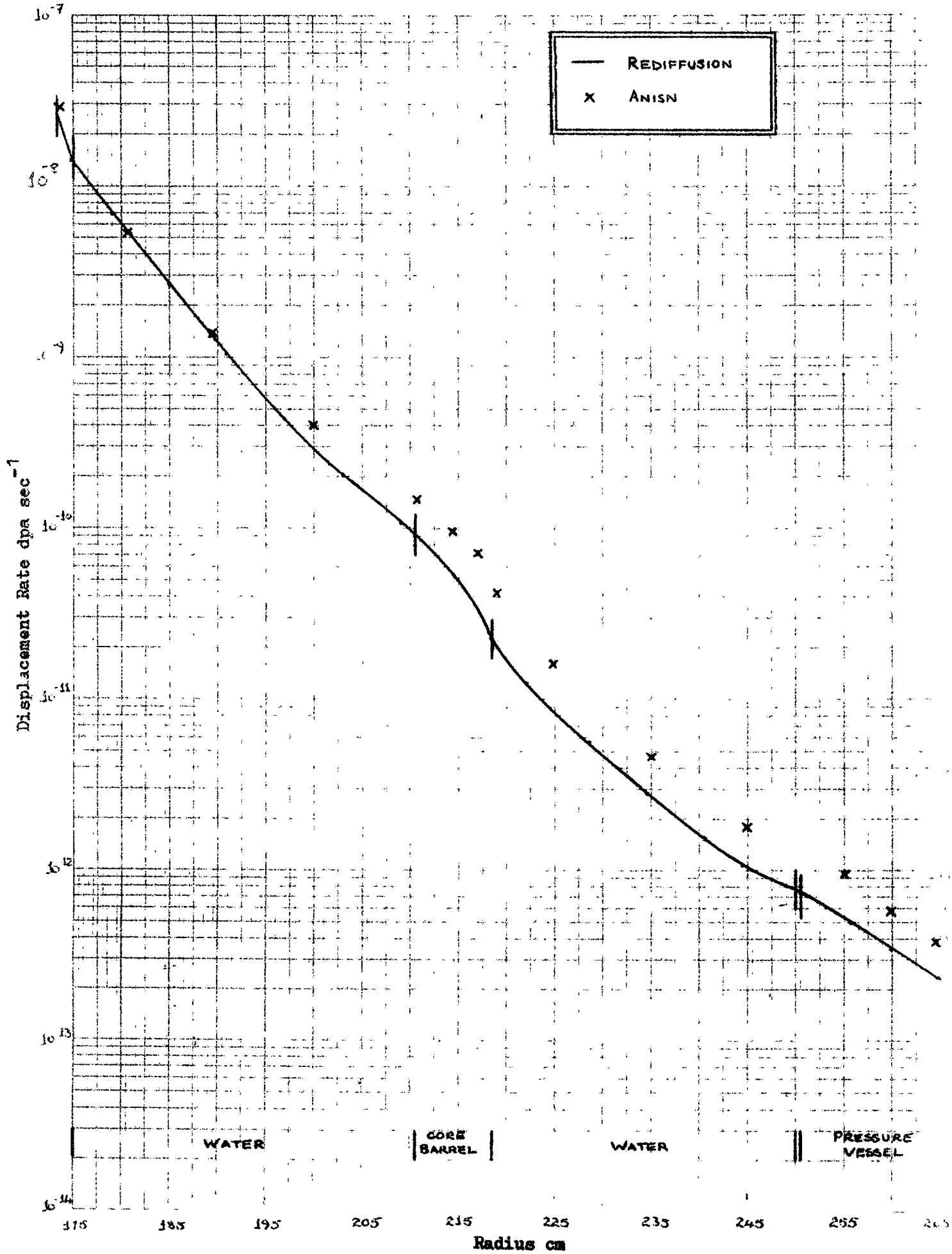

FIGURE 5: ANISN and REDIFFUSION Predictions of Iron Displacement Rate

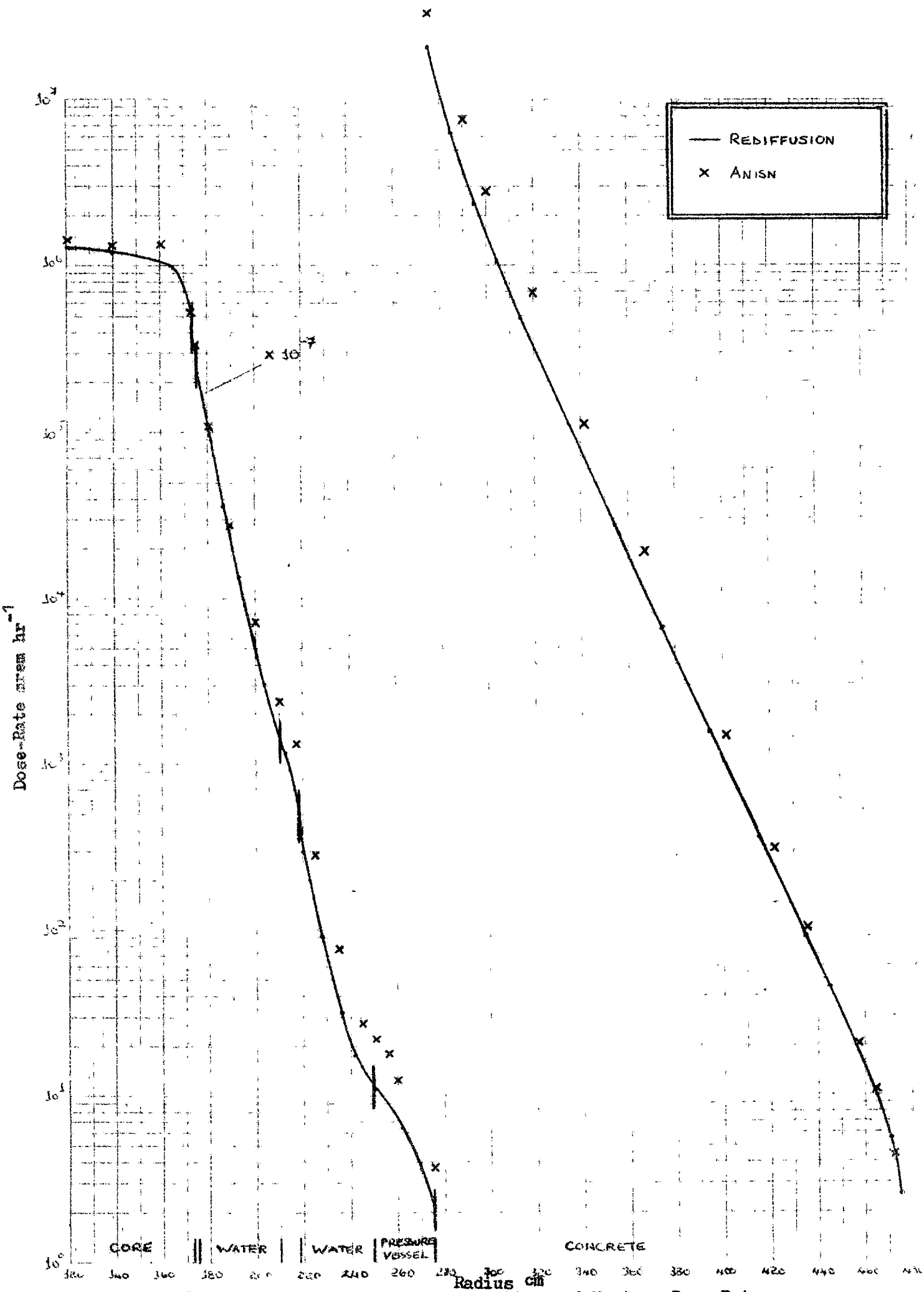

FIGURE 6: ANISN and REDIFFUSION Predictions of Neutron Dose-Rate

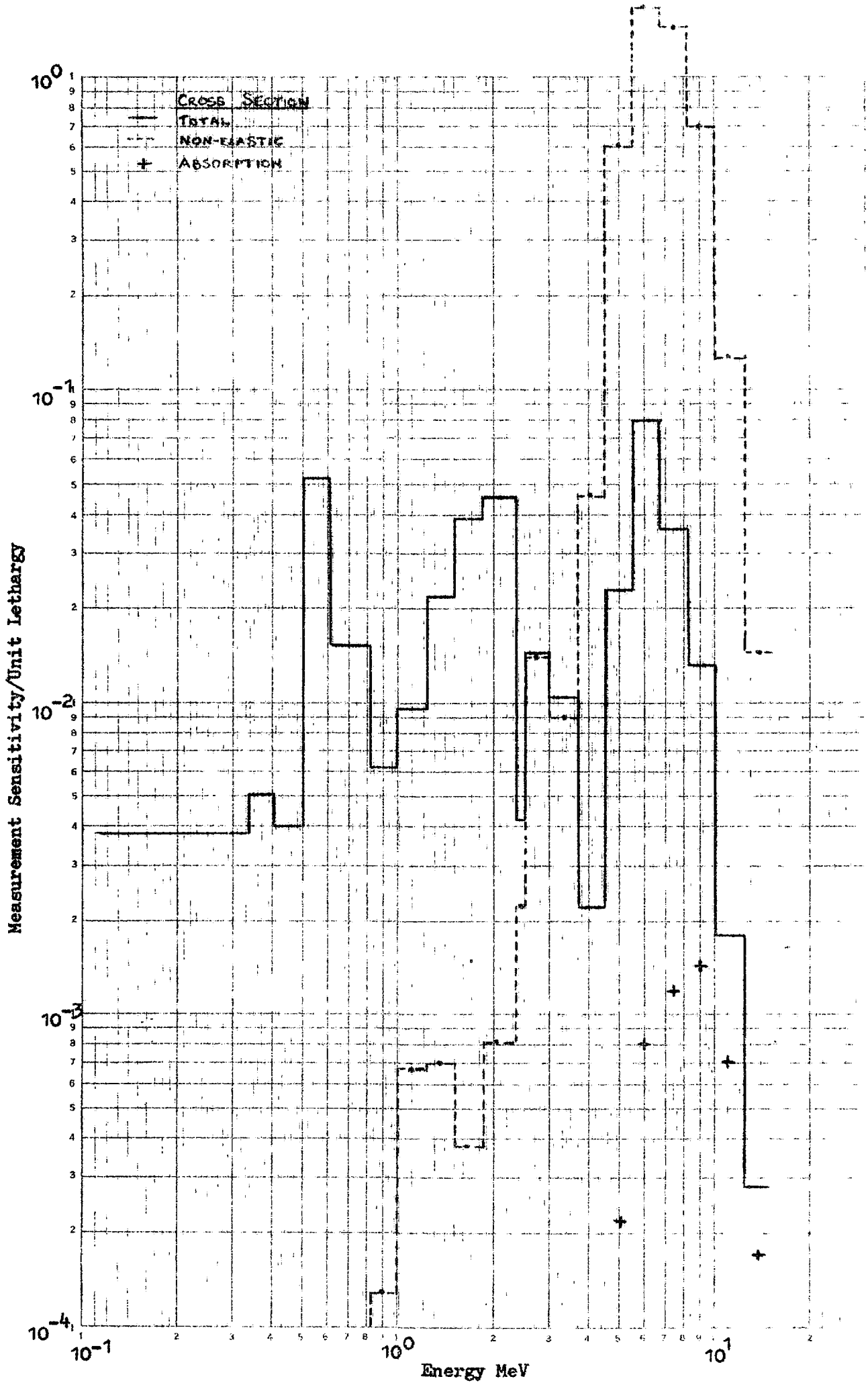

FIGURE 7: Measurement Sensitivity of the Iron Displacement Rate to Iron Cross-Sections

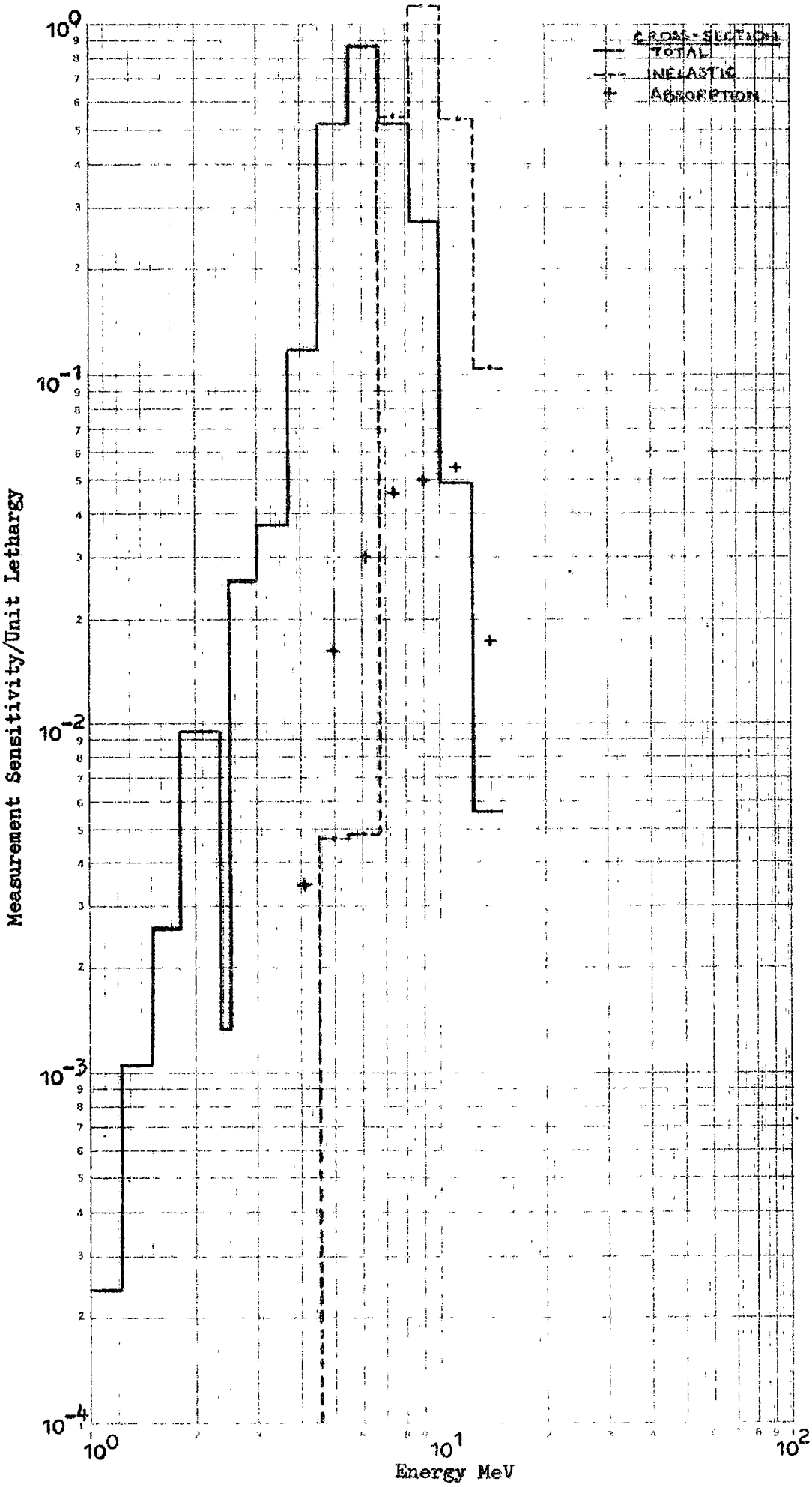

FIGURE 8: Measurement Sensitivity of the Iron Displacement Rate to Oxygen Cross-Sections

```
DIBWG  19/10/76  09:57:11
1200 DISTRIBUTION
1100 DIBWG MEMBERS
1300 DR J P ASHEW                 165/A32, AEEW
1400 MR J AUSTIN                  CEGB BARNWOOD, GLOUCESTER
1500 DR A R BAKER                 E454, RISLEY
1800 DR R F BURSTALL              E410, RISLEY
1900 DR A T D BUTLAND (5)         221/B21, AEEW (SECRETARY)
1950 DR C G CAMPBELL              225/B21, AEEW (CHAIRMAN)
2000 MR E A C CROUCH              220, AERE
2050 DR J EMMETT                  CEGB BERKELEY NUCLEAR LABS.
2100 MR E W ETHERINGTON           DN023, DERE
2200 DR A T G FERGUSON            DF.8, AERE
2400 MR M F JAMES                 102/B21, AEEW
2500 DR J E LYNN                  NF.418, AERE
2600 MR M H MCTAGGART             A70.2, AWRE
2700 MR J G MOORE                 SRD, CULCHETH
2800 MR J L ROWLANDS              220/B21, AEEW
2900 DR J E SANDERS               108/D53, AEEW
3000 DR R D SMITH                 E458, RISLEY
3100 DR M G SOWERBY               NF.418, AERE
3200 MR J S STORY                 108/B21, AEEW
3300 MR A WHITTAKER               BNFL, WINDSCALE
3400 ADDITIONAL
3600 DR R C BANNERMAN             171/A32, AEEW
3650 MR K W BRINDLEY              NPC, RISLEY
3700 MR R J BRISSENDEN            220/B21, AEEW
3800 DR J BUTLER                  116/B21, AEEW
3830 MR M H BUTTERFIELD           309/B41, AEEW
3900 MR J G CUNINGHAME            540.1, AERE
4000 MR J CODD                    108/B21, AEEW
4050 MR R J COX                   312/B41, AEEW
4100 MR C DEAN                    215/B21, AEEW
4200 DR A C DOUGLAS               N56, AWRE
4300 DR F J FAYERS                164/A32, AEEW
4400 DR W N FOX                   158/A32, AEEW
4500 MR G INGRAM                  106/D53, AEEW
4600 DR I H GIBSON                282/A32, AEEW
4610 DR J E R HOLMES              372/A32, AEEW
4620 MR C P GRATTON               236/A32, AEEW
4650 MR W B KEMMISH               CEGB BARNWOOD, GLOUCESTER
4700 MR G H KINCHIN               SRD, CULCHETH
4800 MR R LESLIE                  CTS, RISLEY
4900 MR J E MANN                  CTS, RISLEY
5000 MR M C MCXON                 NF.418/T, AERE
5100 MR A L POPE                  202/B21, AEEW
5200 DR B ROSE                    NF.8, AERE
5300 MR D C G SMITH               DN023, DERE
5400 MR R W SMITH                 123/B21, AEEW
5500 MR J M STEVENSON             001/D57, AEEW
5600 DR D E J THORNTON            CTS, RISLEY
5700 MR D WARDLEWORTH             262/A32, AEEW
5800 MR R C WHEELER               DN023, DERE
5900 MR M J GRIMSTONE             128/B21, AEEW
6200 MR P H W WOLFF               NPC, CAMBRIDGE RD, WHETSTONE,
6300                                        LEICESTER LE8 3LH
6400 MR R M NUNN                  CEGB BERKELEY NUCLEAR LABS.
6500 MR R I VAUGHAN               CEGB BARNWOOD, GLOUCESTER
6600 MR M WHITMARSH-EVERISS       CEGB BARNWOOD, GLOUCESTER
6700 DR D L LINNING               E484, RISLEY
6800 MR H J TEAGUE                CL 132, CULCHETH
7200 DR J W WEALE                 A70.2, AWRE
7300 MR J A SCOTT                 NPC WHETSTONE
7400 DR N DICKINSON               NPC RISLEY
```

Neutron Induced Gamma-Ray Sources in Shielding Benchmark Calculations

Shun-ichi MIYASAKA, Kinji KOYOMA, Kazuyoshi MINAMI*
and Satoshi TSUZUKI**

Japan Atomic Energy Research Institute,
* Fujitsu Limited,
** Power Reactor and Nuclear Fuel Development Corporation
Tokai, Ibaraki, Japan

Shielding benchmark calculations proposed by the NEA have been carried out laying emphasis on comparison between the results of the gamma-ray dose obtained with different neutron induced gamma-ray yield data of iron, nickel, chromium and sodium.

The region-wise, coupled neutron-gamma multigroup cross-sections (100n + 20γ) were generated from the ENDF/B-IV libraries for neutrons and the POPOP4 library for gamma-ray production cross-sections by using the code system RADHEAT-V3. The effective microscopic neutron cross-sections were obtained from the infinite dilution values applying the ABBN type self-shielding factors. Using these sets, the secondary gamma-ray doses in the shield of the benchmark problem No. 1 were calculated and compared with each other.

A change in the secondary gamma-ray dose resulted from a change in the neutron cross-section can be estimated by giving the perturbation to the external source term of the Boltzmann equation for gamma rays.

1. Introduction

Secondary gamma-rays due to neutron capture and inelastic scattering in reactors and shields give often a large contribution to the radiation dose and heat generation in the shield. These gamma-ray sources are calculated by using the spacial distribution of neutron-flux density and the secondary gamma-ray production cross sections. Therefore, the accuracy of the source estimation depends directly on that of flux density calculations and of secondary gamma-ray production cross sections.

In this study, at first, the characteristics of the secondary gamma-ray production cross sections of iron, nickel, chromium and sodium were investigated by using the benchmark problem No. 1[1] proposed by NEA. The calculations have been carried out laying emphasis on comparison between the results of the gamma-ray dose obtained with different gamma-ray yield data.

The region-wise, coupled neutron-gamma multi-group cross sections were produced by using the code system RADHEAT-V3.[2] As basic neutron cross sections, the ENDF/B-IV libraries were used, and the concept of the resonance self-shielding effect of ABBN type[3] is introduced for generating the effective neutron group cross sections of homogenized mixture. The neutron induced gamma-ray yield data were taken from the POPOP4 library which contains several data sets for a particular reaction of a nuclide.

In addition, the sensitivity calculations for the benchmark problem No. 1 and No. 2 [4] have been carried out. In this calculations, a change in the gamma-ray dose resulted from a change in the neutron cross section was estimated by giving the perturbation to the external source term of the Boltzmann transport equation for gamma rays.

2. Group Cross Sections

The region-wise, coupled neutron-gamma multi-group cross sections were produced by using the code system RADHEAT-V3. The basic cross sections for neutrons were taken from ENDF/B-IV libraries. The MAT numbers of the nuclides are shown in Table 1. For producing reasonable and accurate effective region-wise, macroscopic cross sections in resonance energy regions, we have introduced the self-shielding factors given in the f-table of JAERI-Fast set[5] into making the cross sections of mixture.

The identification numbers of the neutron induced gamma-ray yield data taken from the POPOP4 libraly are shown also in Table 1. For investigations of the characteristics of the neutron-capture gamma-ray yield data of iron, nickel, chromium and sodium, two or three data with different Q values, which

were calculated from the library data, were chosen for each nuclide. The gamma-ray production cross sections were generated from those yield data and the effective region-wise, microscopic neutron cross sections.

The DLC-2[6] and EURLIB neutron energy group structures were used for the benchmark problem No. 1 and No. 2 respectively, and the EURLB gamma-ray energy structure was used for both the problems.

3. The Investigations of the Capture Gamma-Ray Yield Data

Parametric calculations using the different capture gamma-ray yield data for iron, nickel, chromium and sodium have been performed for the investigations of the characteristics of those yield data. As shown in Fig. 1, the calculational geometry was chosen with reference to that of the problem No. 1. The first shield is a multi-layer of iron (nickel or chromium) and sodium slabs with total thickness of 180 cm, having the same volume ratio of stainless steel to sodium as for the neutron shield given in Table 2 of Ref. 1). The second shield is a pure sodium layer with thickness of 500 cm. We assumed that the iron shield was the pure iron, nickel or chromium with the same atomic number density. The capture gamma-ray production yield data were given for each nuclide as shown in Table 2.

The neutron source spectrum and its angular distribution was taken from Table 5 of Ref. 1). The calculations were carried out with P_5-S_4 approximation by using the ANISN code.

The calculated gamma-ray dose distributions for each case given in Table 2 are shown in Figs. 2 to 4. Figure 2 presents the results for the pure iron and sodium configurations. Table 3 shows the dose rate ratios or the result using the capture gamma-ray yield data of ID No. 260101 to that of 260106, that of 260104 to 260106 for iron, and that of 110103 to 110101 for sodium. The gamma-ray dose using the yield data of ID number 260101 is smaller by about 3 % than that using 260106, and that using 260104 is larger by about 10 % than that using 260106. Therefore, there is a difference of about 13 % between those using 260101 and 260104. The difference between doses using 110103 and 110101 for sodium reaches about 70 to 90 %.

The dose rate ratios for nickel and chromium are shown in Tables 4 and 5, respectively. As for nickel, there is a maximum difference of about 80 % between doses using 280105 and 280106. As for chromium, there is also a maximum difference of about 50 % between doses using 240101 and 240104.

For the geometry given by benchmark problem No. 1, gamma-ray dose distributions have been calculated by using different neutron capture gamma-ray yield data of each nuclide. Table 6 presents the calculational cases, where the case 1 using the data of ID numbers 260106, 280104, 240104 and 110101 was taken as a standard for iron, nickel, chromium and sodium, respecti-

vely. Figure 5 shows the dose rate ratios of other cases to the standard value. The difference between iron data is at largest about ± 50 %, and is not so large. However, effects of nickel and chromium data are relatively large in spite of their less contents in the stainless steel. The maximum differences are about 10 % for nickel and about 13 % for chromium. These differences of dose rate distributions become smaller in the sodium region. On the other hand, the effect of the sodium data is very remarkable as shown in Fig. 5. The difference is about 50 to 90 % in the sodium region and about 5 % in the multi-layer region.

4. Results for the Benchmark Problem No. 1

The calculations have been performed with the calculational conditions given by the benchmark problem No. 1. The distributions of total scalar flux, scalar flux in the energy range above 111 keV, thermal equivalent flux, fission rate of ^{235}U and displacement rate for iron (used NEA displacement cross section) are shown in Fig. 6(a) and Table 7. The distributions of heat generation, reaction rates for ^{59}Co and sodium, neutron dose and displacement rate for iron (used JAERI displacement cross section) are shown in Fig. 6(b) and Table 7. Figure 7 shows the comparison between total scalar fluxes calculated by using the region-wise, macroscopic cross sections and the infinite dilution cross sections respectively. The flux using the infinite dilution cross sections is smaller by about a factor of 2 than that using the region-wise, macroscopic cross sections.

The average cross sections of ^{235}U, ^{59}Co and ^{23}Na present in Fig. 8(a) and Table 8. The average heating factor of iron and the average displacement factor of iron using NEA and JAERI displacement cross sections present in Fig. 8(b) and Table 8.

5. Results for the Benchmark Problem No. 2

The sensitivity calculations by using ROSETTA[7] have been performed with the calculational conditions given by the benchmark problem No. 2. Table 9 is the values of neutron damage at interval number 120, gamma heating rate at interval number 147, and neutron and gamma-ray biological dose rates at interval number 202.

The calculated results of the cross section sensitivities for neutron damage at interval number 120 summed over energy groups and spacial zones are shown in Table 10. The sensitivities for neutron damage become smaller in the order H, O, Fe, Cr, ^{238}U, Ni, Zr, Mn and ^{235}U. The important zones for neutron damage at interval number 120 are the zones 3 and 5 containing H and O and zone 4 containing Fe and Cr. Figure 9 presents the cross section sensitivities of neutron damage per unit lethargy summed over spacial zones for H, O, Fe and Cr.

From this figure, it is seen that the important energy regions for neutron damage are in the range above about 1 MeV for each nuclide, and the maximum sensitivity is in the 6.37 MeV to 6.70 MeV range. In the energy range below 0.1 MeV, the sensitivities for neutron damage are less significant.

The cross section sensitivities for neutron dose at interval number 202 summed over energy groups and spacial zones are given in Table 11. The importance of sensitivities for neutron dose become smaller in the order H, Fe, Si, Ca, O, Al, Cr, ^{238}U, Ni, Zr, Mn and ^{235}U. The important zones for neutron dose at interval number 202 are the zone 7 containing Fe and zone 8 containing H, O, Si and Ca. The zones 3 and 5 containing H and O have also big contributions to the total sensitivities. Figure 10 shows the cross section sensitivities for neutron dose per unit lethargy summed over spacial zones for H, Fe and O. The important energy regions for neutron dose are in the range above about 0.1 MeV for H and O and 2 MeV for Fe, respectively. For H and O, the sensitivities in the energy region below 0.1 MeV are nearly constant. The sensitivity for iron decreases rapidly below 2 MeV. The sensitivity profile for each nuclide has two large peaks at about 6.5 MeV and at 2.4 MeV, and a deep valley at about 3.5 MeV.

Table 12(a) and 12(b) present, respectively, the secondary gamma-ray production cross section sensitivities and the gamma-ray cross section sensitivities for gamma-ray heating at interval number 147 summed over energy groups and spacial zones. The secondary gamma-ray production cross section sensitivities for heat generation of all nuclides are positive for all energy regions, which indicate that an increase in the secondary gamma-ray production cross section causes an increase in the gamma-ray heating. The sensitivity becomes smaller in the order Fe, Cr, Ni, ^{235}U, ^{238}U, H, Mn, Zr, and O. The important zones for heating due to the secondary gamma rays are the zone 7 containing Fe, the zone 2 containing Fe, Cr and Ni, and the zone 1 containing ^{235}U and ^{238}U. The gamma-ray cross section sensitivities become smaller in the order Fe, O, Cr, Ni, H, ^{238}U, Zr, Mn and ^{235}U. The important zones for the sensitivities of heating are the zones 2, 4 and 7 containing Fe and the zones 3 and 5 containing H and O. As shown in Fig. 11, the energy profiles of the secondary gamma-ray production cross section sensitivities of Fe and Cr for the gamma-ray heating summed over energy groups are similar to the shape of the capture cross sections of Fe and Cr, respectively. The energy regions of importance for the Fe secondary gamma-ray production cross sections are in the thermal (below 0.4 eV), the 0.96 keV to 1.23 keV, 220 keV to 300 keV and the 3 MeV to 10 MeV ranges. At about 1.7 MeV, the profile of Fe has a deep valley. As for Cr, the energy regions of importance for the secondary gamma-ray production cross sections are in the thermal (below 0.4 eV), the 1.6 keV to 2.0 keV and the 5 MeV to 10 MeV range. The sensitivity in the energy range from about 30 keV to 4 MeV is less significant for Cr.

Tables 13(a) and 13(b) present, respectively, the secondary gamma-ray production cross section sensitivities and the gamma-ray cross section sensitivities for gamma-ray dose at interval number 147 summed over energy groups and spacial zones. The secondary gamma-ray production cross section sensitivity for gamma-ray dose becomes smaller in the order Fe, Cr, Ca, Ni, Si, Al, Mn, ^{235}U, H, ^{238}U and O. The important zones for gamma-ray dose due to the secondary gamma rays are the zone 7 containing Fe, the zone 2 containing Fe, Cr and Ni, and the zone 8 containing Ca, Si and Al. The gamma-ray cross section sensitivities for gamma-ray dose are significant in the order O, Fe, Ca, Si, Al, Cr, H, Ni, ^{235}U, Mn, Zr and ^{235}U. The important zones for the sensitivities are the zone 8 containing O, Ca, Si and Al, and the zone 7 containing Fe. The energy profiles of the secondary gamma-ray production cross section sensitivities summed over energy groups are shown in Fig. 12. Also these profiles are similar to the shape of the capture cross sections of Fe and Cr respectively. For both nuclides, the contributions in the energy region above about 100 keV are not so significant except the peak values at about 1 keV for Fe and 2 keV for Cr.

In order to investigate how estimations of the secondary gamma-ray sources are susceptible to change of neutron flux density, the percent change in gamma-ray dose resulting from 1 % increase in the neutron cross section of specific reaction at any energy group for iron in the pressure vessel was calculated at interval number 202. This sensitivity calculations were required so huge computing times that they were only performed for the changes of elastic, inelastic and (n,γ) cross sections of 5th, 10th, 36th, 60th, 64th, 75th, 85th and 100th energy group. The results are present in Table 14. Though the calculated energy groups are few, the followings may be generally concluded. Inelastic scattering cross sections are relatively important for secondary gamma-ray sources at neigh energy region as is expected. Elastic scattering cross sections have almost same importance in all energy region. The importance of (n,γ) cross sections are less by about a factor of 10 than that of elastic scattering cross section.

6. Conclusions

From the investigation of the different capture gamma-ray yield data for iron, nickel, chromium and sodium, it was seen that the gamma-ray doses differ fairly by data using the calculations. Especially the difference of the data for sodium was large. Though the differences between iron data were not so large, effects of nickel and chromium data were relatively large in spite of their less contents in the materials.

Nuclides including the shield material such as hydrogen, oxygen, iron, chromium and nickel have large sensitivities for neutron damage, gamma-ray heating, neutron and gamma-ray dose. From the analysis for the benchmark problem No. 2, it

was seen that the importance of water layer far from the considering point is considerably large. From this fact, it should be noted that the calculational accuracies depend directly on both the accuracies of the cross sections and that of atomic number densities contained in the material.

The important energy regions for neutron damage and neutron dose are in the energy range above about 1 MeV and 0.1 MeV respectively. The sensitivity profiles to secondary gamma-ray cross sections for gamma-ray heating and dose are very similar to the shapes of capture cross section, and has importance in the lower energy region.

For accuracies of the estimations for secondary gamma-ray source, the inelastic scattering cross sections at high energy region and the elastic scattering cross sections in all energy region have larger importance than the (n,γ) cross sections.

Reference

1) Barre, J.Y.; "Reactor Shielding Benchmark No. 1 for a Sodium-Cooled Fast Reactor", NEACRP-L-152 (1976)
2) Koyama, K. et al.; to be published (JAERI-report)
3) Abagjan, L.P. et al.; "Group Constants for Nuclear Reactor Calculations", Consultant Bureau, N.Y. (1964)
4) Hehn, G. and Koban, J.; "Reactor Shielding Benchmark No. 2 for a Pressurised Water Reactor", NEACRP-L-151 (1976)
5) Katsuragi, S. et al.; "JAERI Fast Reactor Group Constants Systems Part II-1", JAERI 1199 (1970)
6) RSIC Data Library Collection, "99-Group Neutron Cross-Section Data Bassed on ENDF/B", ORNL-TM-3049.

Table 1 MAT numbers and identification numbers of nuclides

	MAT No. (ENDF/B-IV)	ID No. (POPOP4)				
		(n,γ)	(n,α)	(n,n')	(n,p)	other
H	1269	10101				
O	1276		80201	86301	86601	
Na	1156	110101 110103			115301	
Al	1193	130101			130302	
Si	1194	140104		140302	140601	
Ca	1195	200102		200301		200701
Cr	1191	240104 240101 240102		240301		
Mn	1197	250101				
Fe	1192	260106 260101 260104		260301		
Ni	1190	280104 280105 280106		280301		
Zr	1284	400102		400301		
U^{235}	1261	925101		925301		925801
U^{238}	1262	928112		928301		

Table 2 Case identifications of the characteristic calculations for neutron capture gamma-ray yield data of iron, nickel, chromium and sodium

Case	FE	NI	CR	NA
1	260106			110101
2	260101			110101
3	260104			110101
4	260106			110103
5		280104		110101
6		280105		110101
7		280106		110101
8			240104	110101
9			240101	110101
10			240102	110101

Table 3 REACTOR SHIELDING BENCHMARK (PURE FE,NA)
PARAMETER STUDY FOR CAPTURE-GAMMA YIELD DATA IN POPOP-4

I	R(I)	260106 / 110101	260101 / 260106	260104 / 260106	110103 / 110101
2	2.375E+02	4.231E+06	9.789E-01	1.107E+00	1.002E+00
5	2.435E+02	5.040E+06	9.804E-01	1.118E+00	1.016E+00
8	2.495E+02	4.860E+06	9.755E-01	1.097E+00	1.098E+00
11	2.555E+02	4.389E+06	9.778E-01	1.115E+00	1.031E+00
14	2.615E+02	3.745E+06	9.722E-01	1.095E+00	1.102E+00
17	2.675E+02	3.197E+06	9.760E-01	1.113E+00	1.033E+00
20	2.735E+02	2.606E+06	9.709E-01	1.093E+00	1.103E+00
23	2.795E+02	2.156E+06	9.750E-01	1.111E+00	1.034E+00
26	2.855E+02	1.708E+06	9.701E-01	1.092E+00	1.103E+00
29	2.915E+02	1.381E+06	9.743E-01	1.109E+00	1.034E+00
32	2.975E+02	1.070E+06	9.695E-01	1.091E+00	1.103E+00
35	3.035E+02	8.515E+05	9.738E-01	1.108E+00	1.034E+00
38	3.095E+02	6.501E+05	9.687E-01	1.090E+00	1.102E+00
41	3.155E+02	5.103E+05	9.734E-01	1.107E+00	1.034E+00
44	3.215E+02	3.848E+05	9.684E-01	1.088E+00	1.102E+00
47	3.275E+02	2.987E+05	9.731E-01	1.107E+00	1.035E+00
50	3.335E+02	2.229E+05	9.680E-01	1.088E+00	1.102E+00
53	3.395E+02	1.713E+05	9.728E-01	1.106E+00	1.035E+00
56	3.455E+02	1.265E+05	9.678E-01	1.087E+00	1.101E+00
59	3.515E+02	9.635E+04	9.745E-01	1.105E+00	1.035E+00
62	3.575E+02	7.058E+04	9.675E-01	1.087E+00	1.101E+00
65	3.635E+02	5.329E+04	9.722E-01	1.104E+00	1.035E+00
68	3.695E+02	3.873E+04	9.672E-01	1.086E+00	1.101E+00
71	3.755E+02	2.902E+04	9.719E-01	1.104E+00	1.035E+00
74	3.815E+02	2.094E+04	9.670E-01	1.085E+00	1.100E+00
77	3.875E+02	1.558E+04	9.717E-01	1.103E+00	1.035E+00
80	3.935E+02	1.118E+04	9.668E-01	1.085E+00	1.100E+00
83	3.995E+02	8.279E+03	9.716E-01	1.103E+00	1.036E+00
86	4.055E+02	5.918E+03	9.673E-01	1.085E+00	1.103E+00
89	4.115E+02	4.381E+03	9.725E-01	1.103E+00	1.044E+00
92	4.175E+02	2.660E+03	9.805E-01	1.066E+00	1.343E+00
95	4.235E+02	2.448E+03	9.763E-01	1.042E+00	1.465E+00
98	4.325E+02	2.186E+03	9.765E-01	1.019E+00	1.605E+00
101	4.445E+02	1.896E+03	9.793E-01	1.005E+00	1.722E+00
102	4.515E+02	1.750E+03	9.809E-01	1.000E+00	1.764E+00
107	5.015E+02	9.368E+02	9.896E-01	9.916E-01	1.899E+00
112	5.515E+02	4.380E+02	9.940E-01	9.935E-01	1.926E+00
117	6.015E+02	1.765E+02	9.961E-01	9.954E-01	1.923E+00
122	6.515E+02	6.178E+01	9.971E-01	9.966E-01	1.905E+00
127	7.015E+02	1.906E+01	9.976E-01	9.973E-01	1.877E+00
132	7.515E+02	5.273E+00	9.977E-01	9.976E-01	1.840E+00
137	8.015E+02	1.335E+00	9.976E-01	9.977E-01	1.795E+00
142	8.515E+02	3.148E-01	9.973E-01	9.978E-01	1.742E+00
147	9.015E+02	6.699E-02	9.966E-01	9.976E-01	1.671E+00

Table 4 REACTOR SHIELDING BENCHMARK (PURE NI+NA)
PARAMETER STUDY FOR CAPTURE-GAMMA YIELD DATA IN POPOP-4

I	R(I)	280104	280105 / 280104	280106 / 280104
2	2,375E+02	5,616E+06	1,339E+00	5,094E-01
5	2,435E+02	6,105E+06	1,360E+00	4,916E-01
8	2,495E+02	4,965E+06	1,320E+00	5,205E-01
11	2,555E+02	3,805E+06	1,355E+00	4,860E-01
14	2,615E+02	2,579E+06	1,319E+00	5,099E-01
17	2,675E+02	1,785E+06	1,350E+00	4,823E-01
20	2,735E+02	1,124E+06	1,316E+00	5,051E-01
23	2,795E+02	7,519E+05	1,346E+00	4,804E-01
26	2,855E+02	4,644E+05	1,314E+00	5,024E-01
29	2,915E+02	3,081E+05	1,344E+00	4,792E-01
32	2,975E+02	1,891E+05	1,314E+00	5,008E-01
35	3,035E+02	1,248E+05	1,343E+00	4,786E-01
38	3,095E+02	7,604E+04	1,313E+00	4,998E-01
41	3,155E+02	4,982E+04	1,343E+00	4,782E-01
44	3,215E+02	3,004E+04	1,313E+00	4,990E-01
47	3,275E+02	1,949E+04	1,342E+00	4,779E-01
50	3,335E+02	1,162E+04	1,313E+00	4,982E-01
53	3,395E+02	7,452E+03	1,341E+00	4,777E-01
56	3,455E+02	4,385E+03	1,312E+00	4,975E-01
59	3,515E+02	2,781E+03	1,339E+00	4,774E-01
62	3,575E+02	1,616E+03	1,311E+00	4,969E-01
65	3,635E+02	1,013E+03	1,338E+00	4,772E-01
68	3,695E+02	5,819E+02	1,310E+00	4,963E-01
71	3,755E+02	3,609E+02	1,337E+00	4,769E-01
74	3,815E+02	2,052E+02	1,309E+00	4,955E-01
77	3,875E+02	1,259E+02	1,336E+00	4,766E-01
80	3,935E+02	7,083E+01	1,308E+00	4,951E-01
83	3,995E+02	4,306E+01	1,334E+00	4,765E-01
86	4,055E+02	2,395E+01	1,307E+00	4,950E-01
89	4,115E+02	1,437E+01	1,333E+00	4,780E-01
92	4,175E+02	5,543E+00	1,254E+00	5,877E-01
95	4,235E+02	4,905E+00	1,205E+00	6,302E-01
98	4,325E+02	4,167E+00	1,150E+00	6,890E-01
101	4,445E+02	3,436E+00	1,102E+00	7,506E-01
102	4,515E+02	3,107E+00	1,083E+00	7,771E-01
107	5,015E+02	1,538E+00	1,018E+00	8,900E-01
112	5,515E+02	7,051E-01	1,002E+00	9,341E-01
117	6,015E+02	2,871E-01	9,977E-01	9,550E-01
122	6,515E+02	1,038E-01	9,962E-01	9,653E-01
127	7,015E+02	3,356E-02	9,953E-01	9,701E-01
132	7,515E+02	9,814E-03	9,945E-01	9,715E-01
137	8,015E+02	2,633E-03	9,934E-01	9,704E-01
142	8,515E+02	6,560E-04	9,918E-01	9,668E-01
147	9,015E+02	1,443E-04	9,888E-01	9,581E-01

Table 5 REACTOR SHIELDING BENCHMARK (PURE CR+NA)
PARAMETER STUDY FOR CAPTURE-GAMMA YIELD DATA IN POPOP-4

I	R(I)	240104	240101 / 240104	240102 / 240104
2	2,375E+02	6,796E+06	4,825E-01	7,057E-01
5	2,435E+02	7,119E+06	4,779E-01	7,047E-01
8	2,495E+02	6,016E+06	5,031E-01	7,122E-01
11	2,555E+02	5,335E+06	4,801E-01	7,025E-01
14	2,615E+02	4,403E+06	4,994E-01	7,082E-01
17	2,675E+02	3,887E+06	4,793E-01	7,010E-01
20	2,735E+02	3,153E+06	4,977E-01	7,065E-01
23	2,795E+02	2,739E+06	4,790E-01	7,002E-01
26	2,855E+02	2,178E+06	4,970E-01	7,056E-01
29	2,915E+02	1,859E+06	4,791E-01	6,998E-01
32	2,975E+02	1,451E+06	4,967E-01	7,050E-01
35	3,035E+02	1,217E+06	4,790E-01	6,994E-01
38	3,095E+02	9,341E+05	4,965E-01	7,045E-01
41	3,155E+02	7,708E+05	4,791E-01	6,990E-01
44	3,215E+02	5,825E+05	4,964E-01	7,041E-01
47	3,275E+02	4,735E+05	4,792E-01	6,987E-01
50	3,335E+02	3,529E+05	4,963E-01	7,036E-01
53	3,395E+02	2,830E+05	4,793E-01	6,983E-01
56	3,455E+02	2,083E+05	4,962E-01	7,032E-01
59	3,515E+02	1,650E+05	4,794E-01	6,979E-01
62	3,575E+02	1,201E+05	4,962E-01	7,028E-01
65	3,635E+02	9,403E+04	4,795E-01	6,975E-01
68	3,695E+02	6,773E+04	4,961E-01	7,024E-01
71	3,755E+02	5,250E+04	4,796E-01	6,972E-01
74	3,815E+02	3,746E+04	4,961E-01	7,020E-01
77	3,875E+02	2,876E+04	4,797E-01	6,968E-01
80	3,935E+02	2,036E+04	4,963E-01	7,017E-01
83	3,995E+02	1,553E+04	4,805E-01	6,970E-01
86	4,055E+02	1,099E+04	4,984E-01	7,029E-01
89	4,115E+02	8,486E+03	4,862E-01	7,010E-01
92	4,175E+02	4,874E+03	5,990E-01	7,635E-01
95	4,235E+02	4,276E+03	6,529E-01	7,887E-01
98	4,325E+02	3,626E+03	7,226E-01	8,237E-01
101	4,445E+02	2,997E+03	7,913E-01	8,605E-01
102	4,515E+02	2,708E+03	8,184E-01	8,758E-01
107	5,015E+02	1,248E+03	9,174E-01	9,346E-01
112	5,515E+02	4,874E+02	9,471E-01	9,532E-01
117	6,015E+02	1,637E+02	9,591E-01	9,606E-01
122	6,515E+02	4,901E+01	9,639E-01	9,627E-01
127	7,015E+02	1,340E+01	9,648E-01	9,615E-01
132	7,515E+02	3,409E+00	9,630E-01	9,575E-01
137	8,015E+02	8,209E-01	9,586E-01	9,504E-01
142	8,515E+02	1,897E-01	9,515E-01	9,398E-01
147	9,015E+02	4,106E-02	9,397E-01	9,227E-01

Table 6 Parameter studies for neutron capture gamma-ray yield data in the geometry of the benchmark problem No. 1

Case	FE	NI	CR	NA
1	260106	280104	240104	110101
2	260101	280104	240104	110101
3	260104	280104	240104	110101
4	260106	280105	240104	110101
5	260106	280106	240104	110101
6	260106	280104	240101	110101
7	260106	280104	240102	110101
8	260106	280104	240104	110103

Table 7 REACTOR SHIELDING BENCHMARK NO.1 (STANDARD)
PARAMETER STUDY OF NEUTRON REACTION RATE DISTRIBUTIONS

N	I	R(I)	IZ(I)	TOTAL FLUX	III keV FLUX	I/V DETECTOR	U-235 (N,F)	FE DAMAGE	FE HEAT(MEV)	CO-59(N,G)	NA-23(N,G)	NEUT DOSE (mrem/h)
1	2	2.380E+02	2	5.810E+13	1.333E+13	1.482E+11	2.680E+14	1.359E+16	9.041E+11	6.481E+13	3.779E+11	1.680E+09
2	3	2.410E+02	2	5.215E+13	1.099E+13	1.839E+11	3.105E+14	1.117E+16	7.324E+11	9.819E+13	3.806E+11	1.397E+09
3	4	2.440E+02	2	4.613E+13	9.056E+12	2.058E+11	3.322E+14	9.164E+15	5.931E+11	1.185E+14	3.545E+11	1.160E+09
4	5	2.470E+02	2	4.057E+13	7.451E+12	2.176E+11	3.396E+14	7.531E+15	4.817E+11	1.286E+14	3.297E+11	9.643E+08
5	6	2.500E+02	2	3.546E+13	6.125E+12	2.204E+11	3.348E+14	6.192E+15	3.916E+11	1.300E+14	3.036E+11	8.008E+08
6	7	2.530E+02	2	3.082E+13	5.030E+12	2.160E+11	3.210E+14	5.095E+15	3.187E+11	1.252E+14	2.784E+11	6.647E+08
7	8	2.560E+02	2	2.665E+13	4.127E+12	2.061E+11	3.007E+14	4.193E+15	2.597E+11	1.165E+14	2.530E+11	5.512E+08
8	9	2.590E+02	2	2.294E+13	3.382E+12	1.925E+11	2.764E+14	3.451E+15	2.118E+11	1.057E+14	2.284E+11	4.565E+08
9	10	2.620E+02	2	1.965E+13	2.768E+12	1.765E+11	2.501E+14	2.840E+15	1.729E+11	9.409E+13	2.042E+11	3.776E+08
10	11	2.650E+02	2	1.677E+13	2.262E+12	1.594E+11	2.233E+14	2.337E+15	1.412E+11	8.253E+13	1.812E+11	3.120E+08
11	12	2.680E+02	2	1.426E+13	1.845E+12	1.421E+11	1.972E+14	1.921E+15	1.153E+11	7.160E+13	1.596E+11	2.574E+08
12	13	2.710E+02	2	1.208E+13	1.503E+12	1.252E+11	1.725E+14	1.579E+15	9.414E+10	6.161E+13	1.396E+11	2.120E+08
13	14	2.740E+02	2	1.021E+13	1.222E+12	1.094E+11	1.497E+14	1.297E+15	7.686E+10	5.268E+13	1.212E+11	1.744E+08
14	15	2.770E+02	2	8.599E+12	9.941E+11	9.482E+10	1.291E+14	1.064E+15	6.272E+10	4.484E+13	1.047E+11	1.433E+08
15	16	2.800E+02	2	7.226E+12	8.037E+11	8.163E+10	1.107E+14	8.723E+14	5.115E+10	3.802E+13	8.998E+10	1.175E+08
16	17	2.830E+02	2	6.058E+12	6.499E+11	6.989E+10	9.444E+13	7.145E+14	4.168E+10	3.215E+13	7.696E+10	9.628E+07
17	18	2.860E+02	2	5.069E+12	5.245E+11	5.955E+10	8.026E+13	5.847E+14	3.394E+10	2.712E+13	6.555E+10	7.877E+07
18	19	2.890E+02	2	4.233E+12	4.224E+11	5.055E+10	6.797E+13	4.780E+14	2.761E+10	2.282E+13	5.563E+10	6.437E+07
19	20	2.920E+02	2	3.528E+12	3.395E+11	4.276E+10	5.740E+13	3.903E+14	2.244E+10	1.918E+13	4.706E+10	5.253E+07
20	21	2.950E+02	2	2.936E+12	2.724E+11	3.606E+10	4.835E+13	3.184E+14	1.822E+10	1.609E+13	3.970E+10	4.281E+07
21	22	2.980E+02	2	2.440E+12	2.181E+11	3.034E+10	4.063E+13	2.595E+14	1.477E+10	1.348E+13	3.340E+10	3.485E+07
22	23	3.010E+02	2	2.024E+12	1.743E+11	2.547E+10	3.408E+13	2.112E+14	1.197E+10	1.127E+13	2.804E+10	2.834E+07
23	24	3.040E+02	2	1.677E+12	1.390E+11	2.134E+10	2.853E+13	1.717E+14	9.682E+09	9.416E+12	2.349E+10	2.302E+07
24	25	3.070E+02	2	1.387E+12	1.106E+11	1.785E+10	2.384E+13	1.394E+14	7.825E+09	7.854E+12	1.964E+10	1.867E+07
25	26	3.100E+02	2	1.146E+12	8.791E+10	1.491E+10	1.989E+13	1.131E+14	6.316E+09	6.543E+12	1.639E+10	1.513E+07
26	27	3.130E+02	2	9.458E+11	6.972E+10	1.243E+10	1.658E+13	9.157E+13	5.091E+09	5.443E+12	1.366E+10	1.224E+07
27	28	3.160E+02	2	7.794E+11	5.519E+10	1.035E+10	1.379E+13	7.408E+13	4.099E+09	4.522E+12	1.136E+10	9.900E+06
28	29	3.190E+02	2	6.414E+11	4.362E+10	8.608E+09	1.146E+13	5.986E+13	3.296E+09	3.752E+12	9.439E+09	7.994E+06
29	30	3.220E+02	2	5.271E+11	3.441E+10	7.148E+09	9.506E+12	4.831E+13	2.647E+09	3.109E+12	7.830E+09	6.449E+06
30	31	3.250E+02	2	4.326E+11	2.710E+10	5.927E+09	7.876E+12	3.893E+13	2.123E+09	2.572E+12	6.486E+09	5.196E+06
31	32	3.280E+02	2	3.546E+11	2.131E+10	4.909E+09	6.517E+12	3.134E+13	1.700E+09	2.126E+12	5.366E+09	4.182E+06
32	33	3.310E+02	2	2.903E+11	1.673E+10	4.060E+09	5.385E+12	2.519E+13	1.360E+09	1.754E+12	4.433E+09	3.362E+06
33	34	3.340E+02	2	2.373E+11	1.312E+10	3.353E+09	4.444E+12	2.022E+13	1.086E+09	1.446E+12	3.657E+09	2.700E+06
34	35	3.370E+02	2	1.937E+11	1.027E+10	2.766E+09	3.662E+12	1.622E+13	8.664E+08	1.190E+12	3.013E+09	2.166E+06
35	36	3.400E+02	2	1.580E+11	8.024E+09	2.278E+09	3.014E+12	1.299E+13	6.903E+08	9.776E+11	2.478E+09	1.736E+06
36	37	3.430E+02	2	1.286E+11	6.263E+09	1.874E+09	2.477E+12	1.039E+13	5.492E+08	8.022E+11	2.036E+09	1.390E+06
37	38	3.460E+02	2	1.046E+11	4.881E+09	1.540E+09	2.033E+12	8.296E+12	4.364E+08	6.574E+11	1.671E+09	1.111E+06
38	39	3.490E+02	2	8.494E+10	3.800E+09	1.263E+09	1.666E+12	6.618E+12	3.463E+08	5.379E+11	1.369E+09	8.876E+05
39	40	3.520E+02	2	6.889E+10	2.954E+09	1.035E+09	1.364E+12	5.272E+12	2.744E+08	4.395E+11	1.120E+09	7.082E+05
40	41	3.550E+02	2	5.579E+10	2.293E+09	8.464E+08	1.114E+12	4.195E+12	2.172E+08	3.586E+11	9.152E+08	5.645E+05
41	42	3.580E+02	2	4.513E+10	1.778E+09	6.914E+08	9.095E+11	3.334E+12	1.717E+08	2.921E+11	7.467E+08	4.495E+05
42	43	3.610E+02	2	3.645E+10	1.378E+09	5.640E+08	7.413E+11	2.646E+12	1.356E+08	2.376E+11	6.085E+08	3.575E+05
43	44	3.640E+02	2	2.941E+10	1.066E+09	4.595E+08	6.033E+11	2.098E+12	1.069E+08	1.930E+11	4.951E+08	2.840E+05

Table 7 (continued)

N	I	R(I)	IZ(I)	TOTAL FLUX	III keV FLUX	I/V DETECTOR	U-235 (N,F)	FE DAMAGE	FE HEAT(MEV)	CO-59 (N,G)	NA-23(N,G)	NEUT DOSE (mrem/h)
44	45	3,670E+02	2	2,369E+10	8,236E+08	3,737E+08	4,903E+11	1,661E+12	8,417E+07	1,566E+11	4,023E+08	2,255E+05
45	46	3,700E+02	2	1,906E+10	6,397E+08	3,036E+08	3,979E+11	1,314E+12	6,621E+07	1,268E+11	3,264E+08	1,788E+05
46	47	3,730E+02	2	1,531E+10	4,902E+08	2,462E+08	3,225E+11	1,038E+12	5,201E+07	1,025E+11	2,645E+08	1,416E+05
47	48	3,760E+02	2	1,229E+10	3,776E+08	1,995E+08	2,610E+11	8,186E+11	4,081E+07	8,281E+10	2,140E+08	1,120E+05
48	49	3,790E+02	2	9,847E+09	2,906E+08	1,613E+08	2,109E+11	6,450E+11	3,198E+07	6,677E+10	1,730E+08	8,856E+04
49	50	3,820E+02	2	7,881E+09	2,234E+08	1,303E+08	1,702E+11	5,076E+11	2,504E+07	5,376E+10	1,395E+08	6,993E+04
50	51	3,850E+02	2	6,298E+09	1,715E+08	1,051E+08	1,371E+11	3,990E+11	1,957E+07	4,321E+10	1,124E+08	5,516E+04
51	52	3,880E+02	2	5,026E+09	1,316E+08	8,460E+07	1,103E+11	3,132E+11	1,528E+07	3,469E+10	9,046E+07	4,345E+04
52	53	3,910E+02	2	4,005E+09	1,008E+08	6,802E+07	8,862E+10	2,455E+11	1,191E+07	2,780E+10	7,267E+07	3,419E+04
53	54	3,940E+02	2	3,186E+09	7,711E+07	5,460E+07	7,109E+10	1,921E+11	9,271E+06	2,225E+10	5,828E+07	2,686E+04
54	55	3,970E+02	2	2,531E+09	5,890E+07	4,375E+07	5,693E+10	1,500E+11	7,200E+06	1,778E+10	4,668E+07	2,107E+04
55	56	4,000E+02	2	2,006E+09	4,490E+07	3,499E+07	4,552E+10	1,168E+11	5,576E+06	1,419E+10	3,732E+07	1,649E+04
56	57	4,030E+02	2	1,587E+09	3,411E+07	2,792E+07	3,634E+10	9,069E+10	4,302E+06	1,131E+10	2,980E+07	1,287E+04
57	58	4,060E+02	2	1,251E+09	2,580E+07	2,222E+07	2,896E+10	7,005E+10	3,297E+06	9,004E+09	2,378E+07	1,001E+04
58	59	4,090E+02	2	9,839E+08	1,936E+07	1,763E+07	2,311E+10	5,367E+10	2,497E+06	7,151E+09	1,904E+07	7,734E+03
59	60	4,120E+02	2	7,704E+08	1,432E+07	1,395E+07	1,845E+10	4,056E+10	1,849E+06	5,655E+09	1,531E+07	5,923E+03
60	61	4,150E+02	2	6,022E+08	1,028E+07	1,105E+07	1,558E+10	2,977E+10	1,285E+06	4,478E+09	1,315E+07	4,467E+03
61	62	4,185E+02	3	5,096E+08	7,625E+06	9,574E+06	1,482E+10	2,304E+10	9,327E+05	3,901E+09	1,257E+07	3,600E+03
62	76	4,745E+02	3	1,828E+08	4,456E+05	4,548E+06	9,025E+09	2,749E+09	9,331E+04	1,857E+09	7,981E+06	8,788E+02
63	92	5,385E+02	3	5,203E+07	1,742E+04	1,526E+06	3,508E+09	2,549E+08	6,090E+03	5,426E+08	3,286E+06	2,241E+02
64	108	6,025E+02	3	1,322E+07	6,584E+02	4,105E+05	1,111E+09	3,403E+07	4,065E+02	1,269E+08	1,098E+06	5,637E+01
65	124	6,665E+02	3	2,959E+06	2,471E+01	9,042E+04	2,996E+08	6,632E+06	3,089E+01	2,754E+07	3,071E+05	1,268E+01
66	140	7,305E+02	3	5,831E+05	9,438E-01	1,670E+04	6,986E+07	1,421E+06	2,744E+00	5,705E+06	7,289E+04	2,509E+00
67	156	7,945E+02	3	1,017E+05	3,830E-02	2,650E+03	1,420E+07	2,829E+05	2,699E-01	1,094E+06	1,488E+04	4,385E-01
68	172	8,585E+02	3	1,589E+04	1,797E-03	3,701E+02	2,540E+06	5,018E+04	2,752E-02	1,898E+05	2,652E+03	6,847E-02
69	186	9,145E+02	3	2,961E+03	1,628E-04	6,458E+01	4,553E+05	9,263E+03	4,068E-03	3,440E+04	4,846E+02	1,279E-02
70	187	9,175E+02	4	2,557E+03	1,438E-04	5,633E+01	3,629E+05	7,562E+03	3,554E-03	2,791E+04	3,926E+02	1,107E-02
71	188	9,200E+02	4	2,075E+03	1,263E-04	4,625E+01	2,663E+05	5,731E+03	2,919E-03	2,098E+04	2,946E+02	9,010E-03
72	189	9,230E+02	4	1,618E+03	1,078E-04	3,635E+01	1,912E+05	4,232E+03	2,283E-03	1,536E+04	2,156E+02	7,038E-03
73	190	9,260E+02	4	1,267E+03	9,179E-05	2,857E+01	1,422E+05	3,206E+03	1,780E-03	1,160E+04	1,626E+02	5,517E-03
74	191	9,290E+02	4	9,939E+02	7,817E-05	2,246E+01	1,078E+05	2,462E+03	1,387E-03	8,875E+03	1,245E+02	4,333E-03
75	192	9,320E+02	4	7,810E+02	6,660E-05	1,765E+01	8,274E+04	1,908E+03	1,079E-03	6,859E+03	9,620E+01	3,407E-03
76	193	9,350E+02	4	6,142E+02	5,678E-05	1,387E+01	6,407E+04	1,487E+03	8,400E-04	5,337E+03	7,487E+01	2,681E-03
77	194	9,380E+02	4	4,833E+02	4,844E-05	1,089E+01	4,992E+04	1,164E+03	6,533E-04	4,171E+03	5,854E+01	2,110E-03
78	195	9,410E+02	4	3,803E+02	4,134E-05	8,547E+00	3,904E+04	9,134E+02	5,078E-04	3,269E+03	4,590E+01	1,661E-03
79	196	9,440E+02	4	2,991E+02	3,531E-05	6,700E+00	3,061E+04	7,180E+02	3,944E-04	2,567E+03	3,606E+01	1,306E-03
80	197	9,470E+02	4	2,352E+02	3,015E-05	5,246E+00	2,404E+04	5,648E+02	3,061E-04	2,017E+03	2,835E+01	1,027E-03
81	198	9,500E+02	4	1,847E+02	2,575E-05	4,099E+00	1,890E+04	4,445E+02	2,371E-04	1,586E+03	2,230E+01	8,067E-04
82	199	9,530E+02	4	1,448E+02	2,198E-05	3,196E+00	1,486E+04	3,498E+02	1,833E-04	1,247E+03	1,755E+01	6,325E-04
83	200	9,560E+02	4	1,132E+02	1,874E-05	2,482E+00	1,171E+04	2,753E+02	1,412E-04	9,809E+02	1,381E+01	4,947E-04
84	201	9,590E+02	4	8,828E+01	1,594E-05	1,918E+00	9,263E+03	2,171E+02	1,082E-04	7,732E+02	1,090E+01	3,856E-04
85	202	9,620E+02	4	6,851E+01	1,351E-05	1,469E+00	7,425E+03	1,724E+02	8,214E-05	6,147E+02	8,671E+00	2,991E-04
86	203	9,650E+02	4	5,300E+01	1,138E-05	1,111E+00	6,295E+03	1,418E+02	6,119E-05	5,088E+02	7,191E+00	2,310E-04

Table 8 REACTOR SHIELDING BENCHMARK NO.1
PARAMETOR STUDY OF EFFECTIVE CROSS SECTION DISTRIBUTIONS

N	I	R(I)	IZ(I)	Total Flux	Ave.Xsec U235	Ave.disp.(eV) Xsec(NRA)	Ave.disp(MeV) Xsec(JAERI)	Ave.Heating Factor	Ave.Xsec Co59	Ave.Xsec Na23
1	2	2.380E+02	2	5.810E+13	4.612E+00	2.340E+02	1.686E-04	1.556E-02	1.115E+00	6.504E-03
2	3	2.410E+02	2	5.215E+13	5.955E+00	2.141E+02	1.546E-04	1.405E-02	1.883E+00	7.294E-03
3	4	2.440E+02	2	4.613E+13	7.200E+00	1.986E+02	1.427E-04	1.286E-02	2.569E+00	7.664E-03
4	5	2.470E+02	2	4.057E+13	8.370E+00	1.856E+02	1.326E-04	1.187E-02	3.168E+00	8.127E-03
5	6	2.500E+02	2	3.546E+13	9.443E+00	1.746E+02	1.239E-04	1.104E-02	3.665E+00	8.562E-03
6	7	2.530E+02	2	3.082E+13	1.041E+01	1.653E+02	1.166E-04	1.034E-02	4.063E+00	9.034E-03
7	8	2.560E+02	2	2.665E+13	1.128E+01	1.573E+02	1.102E-04	9.745E-03	4.373E+00	9.495E-03
8	9	2.590E+02	2	2.294E+13	1.205E+01	1.505E+02	1.046E-04	9.235E-03	4.609E+00	9.956E-03
9	10	2.620E+02	2	1.965E+13	1.273E+01	1.445E+02	1.001E-04	8.796E-03	4.787E+00	1.039E-02
10	11	2.650E+02	2	1.677E+13	1.331E+01	1.393E+02	9.609E-05	8.416E-03	4.920E+00	1.081E-02
11	12	2.680E+02	2	1.426E+13	1.383E+01	1.347E+02	9.254E-05	8.084E-03	5.021E+00	1.119E-02
12	13	2.710E+02	2	1.208E+13	1.428E+01	1.307E+02	8.939E-05	7.791E-03	5.096E+00	1.155E-02
13	14	2.740E+02	2	1.021E+13	1.467E+01	1.270E+02	8.658E-05	7.529E-03	5.161E+00	1.188E-02
14	15	2.770E+02	2	8.599E+12	1.501E+01	1.237E+02	8.403E-05	7.293E-03	5.214E+00	1.218E-02
15	16	2.800E+02	2	7.226E+12	1.532E+01	1.207E+02	8.171E-05	7.078E-03	5.262E+00	1.245E-02
16	17	2.830E+02	2	6.058E+12	1.559E+01	1.179E+02	7.956E-05	6.880E-03	5.306E+00	1.270E-02
17	18	2.860E+02	2	5.069E+12	1.583E+01	1.154E+02	7.755E-05	6.696E-03	5.350E+00	1.293E-02
18	19	2.890E+02	2	4.233E+12	1.606E+01	1.129E+02	7.567E-05	6.523E-03	5.393E+00	1.314E-02
19	20	2.920E+02	2	3.528E+12	1.627E+01	1.106E+02	7.388E-05	6.359E-03	5.436E+00	1.334E-02
20	21	2.950E+02	2	2.936E+12	1.647E+01	1.084E+02	7.217E-05	6.204E-03	5.480E+00	1.352E-02
21	22	2.980E+02	2	2.440E+12	1.665E+01	1.063E+02	7.053E-05	6.055E-03	5.524E+00	1.369E-02
22	23	3.010E+02	2	2.024E+12	1.684E+01	1.043E+02	6.894E-05	5.912E-03	5.569E+00	1.385E-02
23	24	3.040E+02	2	1.677E+12	1.701E+01	1.024E+02	6.741E-05	5.774E-03	5.615E+00	1.400E-02
24	25	3.070E+02	2	1.387E+12	1.718E+01	1.005E+02	6.591E-05	5.640E-03	5.661E+00	1.415E-02
25	26	3.100E+02	2	1.146E+12	1.736E+01	9.862E+01	6.446E-05	5.509E-03	5.708E+00	1.430E-02
26	27	3.130E+02	2	9.458E+11	1.752E+01	9.682E+01	6.304E-05	5.383E-03	5.755E+00	1.444E-02
27	28	3.160E+02	2	7.794E+11	1.769E+01	9.506E+01	6.165E-05	5.259E-03	5.802E+00	1.458E-02
28	29	3.190E+02	2	6.414E+11	1.786E+01	9.333E+01	6.029E-05	5.139E-03	5.850E+00	1.472E-02
29	30	3.220E+02	2	5.271E+11	1.803E+01	9.165E+01	5.896E-05	5.021E-03	5.898E+00	1.486E-02
30	31	3.250E+02	2	4.326E+11	1.821E+01	8.999E+01	5.765E-05	4.906E-03	5.946E+00	1.499E-02
31	32	3.280E+02	2	3.546E+11	1.838E+01	8.837E+01	5.638E-05	4.794E-03	5.995E+00	1.513E-02
32	33	3.310E+02	2	2.903E+11	1.855E+01	8.678E+01	5.513E-05	4.684E-03	6.043E+00	1.527E-02
33	34	3.340E+02	2	2.373E+11	1.873E+01	8.523E+01	5.390E-05	4.577E-03	6.092E+00	1.541E-02
34	35	3.370E+02	2	1.937E+11	1.890E+01	8.370E+01	5.270E-05	4.472E-03	6.140E+00	1.555E-02
35	36	3.400E+02	2	1.580E+11	1.908E+01	8.221E+01	5.153E-05	4.370E-03	6.189E+00	1.569E-02
36	37	3.430E+02	2	1.286E+11	1.926E+01	8.075E+01	5.038E-05	4.270E-03	6.237E+00	1.583E-02
37	38	3.460E+02	2	1.046E+11	1.943E+01	7.931E+01	4.925E-05	4.172E-03	6.285E+00	1.597E-02
38	39	3.490E+02	2	8.494E+10	1.961E+01	7.791E+01	4.815E-05	4.077E-03	6.333E+00	1.612E-02
39	40	3.520E+02	2	6.889E+10	1.979E+01	7.654E+01	4.708E-05	3.984E-03	6.380E+00	1.626E-02
40	41	3.550E+02	2	5.579E+10	1.997E+01	7.519E+01	4.603E-05	3.893E-03	6.427E+00	1.640E-02
41	42	3.580E+02	2	4.513E+10	2.016E+01	7.388E+01	4.500E-05	3.805E-03	6.474E+00	1.655E-02
42	43	3.610E+02	2	3.645E+10	2.034E+01	7.260E+01	4.400E-05	3.719E-03	6.519E+00	1.669E-02
43	44	3.640E+02	2	2.941E+10	2.052E+01	7.134E+01	4.303E-05	3.635E-03	6.565E+00	1.684E-02
44	45	3.670E+02	2	2.369E+10	2.070E+01	7.012E+01	4.208E-05	3.553E-03	6.609E+00	1.698E-02
45	46	3.700E+02	2	1.906E+10	2.088E+01	6.892E+01	4.115E-05	3.474E-03	6.653E+00	1.713E-02
46	47	3.730E+02	2	1.531E+10	2.106E+01	6.775E+01	4.025E-05	3.396E-03	6.696E+00	1.727E-02
47	48	3.760E+02	2	1.229E+10	2.124E+01	6.661E+01	3.937E-05	3.321E-03	6.739E+00	1.742E-02
48	49	3.790E+02	2	9.847E+09	2.142E+01	6.550E+01	3.852E-05	3.248E-03	6.780E+00	1.756E-02
49	50	3.820E+02	2	7.881E+09	2.159E+01	6.442E+01	3.766E-05	3.177E-03	6.821E+00	1.771E-02
50	51	3.850E+02	2	6.294E+09	2.177E+01	6.335E+01	3.687E-05	3.108E-03	6.862E+00	1.785E-02
51	52	3.880E+02	2	5.026E+09	2.195E+01	6.232E+01	3.608E-05	3.040E-03	6.902E+00	1.800E-02
52	53	3.910E+02	2	4.005E+09	2.213E+01	6.129E+01	3.531E-05	2.974E-03	6.942E+00	1.814E-02
53	54	3.940E+02	2	3.186E+09	2.231E+01	6.028E+01	3.454E-05	2.909E-03	6.983E+00	1.829E-02
54	55	3.970E+02	2	2.531E+09	2.250E+01	5.927E+01	3.378E-05	2.845E-03	7.027E+00	1.844E-02
55	56	4.000E+02	2	2.006E+09	2.269E+01	5.824E+01	3.301E-05	2.780E-03	7.075E+00	1.860E-02
56	57	4.030E+02	2	1.587E+09	2.290E+01	5.716E+01	3.220E-05	2.711E-03	7.131E+00	1.876E-02
57	58	4.060E+02	2	1.251E+09	2.314E+01	5.597E+01	3.129E-05	2.634E-03	7.195E+00	1.900E-02
58	59	4.090E+02	2	9.839E+08	2.349E+01	5.455E+01	3.014E-05	2.538E-03	7.268E+00	1.935E-02
59	60	4.120E+02	2	7.704E+08	2.394E+01	5.265E+01	2.848E-05	2.400E-03	7.340E+00	1.987E-02
60	61	4.150E+02	2	6.022E+08	2.588E+01	4.944E+01	2.527E-05	2.134E-03	7.437E+00	2.183E-02
61	62	4.185E+02	3	5.098E+08	2.908E+01	4.520E+01	2.161E-05	1.830E-03	7.652E+00	2.466E-02
62	76	4.745E+02	3	1.828E+08	4.937E+01	1.504E+01	5.832E-06	5.105E-04	1.016E+01	4.366E-02
63	92	5.385E+02	3	5.203E+07	6.742E+01	4.900E+00	1.190E-06	1.171E-04	1.043E+01	6.316E-02
64	108	6.025E+02	3	1.322E+07	8.404E+01	2.574E+00	2.404E-07	3.074E-05	9.596E+00	8.305E-02
65	124	6.665E+02	3	2.959E+06	1.013E+02	2.241E+00	5.077E-08	1.044E-05	9.307E+00	1.036E-01
66	140	7.305E+02	3	5.831E+05	1.198E+02	2.437E+00	1.158E-08	4.706E-06	9.784E+00	1.250E-01
67	156	7.945E+02	3	1.017E+05	1.395E+02	2.780E+00	2.954E-09	2.653E-06	1.075E+01	1.462E-01
68	172	8.585E+02	3	1.589E+04	1.598E+02	3.157E+00	9.000E-10	1.731E-06	1.194E+01	1.669E-01
69	186	9.145E+02	3	2.961E+03	1.558E+02	3.128E+00	4.257E-10	1.374E-06	1.162E+01	1.636E-01
70	187	9.175E+02	4	2.557E+03	1.419E+02	2.957E+00	4.284E-10	1.390E-06	1.091E+01	1.535E-01
71	188	9.205E+02	4	2.075E+03	1.283E+02	2.762E+00	4.380E-10	1.407E-06	1.011E+01	1.420E-01
72	189	9.235E+02	4	1.616E+03	1.182E+02	2.616E+00	4.449E-10	1.411E-06	9.507E+00	1.334E-01
73	190	9.265E+02	4	1.267E+03	1.123E+02	2.532E+00	4.495E-10	1.405E-06	9.157E+00	1.284E-01
74	191	9.295E+02	4	9.939E+02	1.084E+02	2.477E+00	4.539E-10	1.395E-06	8.930E+00	1.252E-01
75	192	9.325E+02	4	7.810E+02	1.059E+02	2.443E+00	4.585E-10	1.382E-06	8.783E+00	1.232E-01
76	193	9.350E+02	4	6.142E+02	1.043E+02	2.421E+00	4.637E-10	1.366E-06	8.684E+00	1.219E-01
77	194	9.380E+02	4	4.833E+02	1.033E+02	2.408E+00	4.697E-10	1.352E-06	8.630E+00	1.211E-01
78	195	9.410E+02	4	3.803E+02	1.027E+02	2.402E+00	4.766E-10	1.335E-06	8.596E+00	1.207E-01
79	196	9.440E+02	4	2.991E+02	1.023E+02	2.400E+00	4.846E-10	1.319E-06	8.580E+00	1.205E-01
80	197	9.470E+02	4	2.352E+02	1.022E+02	2.402E+00	4.937E-10	1.302E-06	8.576E+00	1.206E-01
81	198	9.500E+02	4	1.847E+02	1.023E+02	2.407E+00	5.040E-10	1.284E-06	8.586E+00	1.208E-01
82	199	9.530E+02	4	1.448E+02	1.027E+02	2.416E+00	5.155E-10	1.266E-06	8.613E+00	1.212E-01
83	200	9.560E+02	4	1.132E+02	1.034E+02	2.431E+00	5.281E-10	1.247E-06	8.662E+00	1.220E-01
84	201	9.590E+02	4	8.826E+01	1.049E+02	2.459E+00	5.412E-10	1.226E-06	8.739E+00	1.234E-01
85	202	9.620E+02	4	6.851E+01	1.084E+02	2.516E+00	5.534E-10	1.199E-06	8.971E+00	1.268E-01
86	203	9.650E+02	4	5.300E+01	1.188E+02	2.676E+00	5.586E-10	1.154E-06	9.800E+00	1.397E-01

Table 9 Neutron damage, gamma heating rate, neutron and gamma-ray biological dose rates

Neutron damage at interval number 120	Gamma heating rate at interval number 147 (W/cm)	Neutron dose at interval number 202 (mrem/hr)	Gamma dose at interval number 202 (mR/hr)
1.684×10^{9}	8.290×10^{-8}	1.008×10^{-2}	8.114×10^{-2}

Table 10 Sensitivities for neutron damage summed over energy groups and spacial zones at interval number 120

Element	Zone 1	Zone 2	Zone 3	Zone 4	Zone 5	Zone 6	Total zone
H	-4.772E-1		-2.407E+0		-2.244E+0		-5.128E+0
O	-2.719E-1		-9.046E-1		-7.097E-1		-1.886E+0
Cr		-9.108E-2		-2.878E-1		-6.156E-3	-3.850E-1
Mn		-6.808E-3		-2.110E-2		-5.034E-4	-2.841E-2
Fe	-2.469E-2	-3.675E-1		-1.151E+0		-3.140E-2	-1.575E+0
Ni		-4.824E-2		-1.525E-1		-4.783E-3	-2.055E-1
Zr	-1.247E-1						-1.247E-1
U5	-4.112E-3						-4.112E-3
U8	-2.295E-1						-2.295E-1

Table 11 Sensitivities for neutron dose summed over energy groups and spacial zones at interval number 202

Element	Zone 1	Zone 2	Zone 3	Zone 4	Zone 5	Zone 6	Zone 7	Zone 8	Total zone
H	-4.923E-1		-2.903E+0		-2.567E+0			-2.922E+0	-8.979E+0
O	-4.021E-1		-1.236E+0		-1.029E+0			-8.445E+0	-2.667E+0
Al								-8.654E-1	-8.654E-1
Si								-3.289E+0	-3.289E+0
Ca								-3.089E+0	-3.089E+0
Cr		-1.173E-1		-3.011E-1		-2.646E-2			-4.449E-1
Mn		-8.887E-3		-2.947E-2		-1.960E-3			-4.032E-2
Fe	-3.384E-2	-4.571E-1		-1.544E+0		-1.074E-1	-5.667E+0		-7.805E+0
Ni		-6.230E-2		-1.979E-1		-1.415E-2			-2.744E-1
Zr	-1.691E-1								-1.691E-1
U5	-4.693E-3								-4.673E-3
U8	-2.945E-1								-2.945E-1

Table 12 Sensitivities for gamma-ray heat summed over energy groups and spacial zones at interval number 147

a) Secondary gamma-ray production cross sections

Element	Zone 1	Zone 2	Zone 3	Zone 4	Zone 5	Zone 6	Zone 7	Total zone
H	4.813E-4		3.065E-2		3.997E-3			3.513E-2
O	1.328E-3		1.266E-3		2.015E-4			2.796E-3
Cr		1.291E-1		1.185E-2		2.747E-4		1.412E-1
Mn		2.219E-2		2.169E-3		5.828E-5		2.442E-2
Fe	8.956E-3	3.054E-1		2.988E-2		7.322E-4	9.998E-1	1.345E+0
Ni		8.274E-2		7.373E-3		1.705E-4		9.028E-2
Zr	1.104E-2							1.104E-2
U5	7.747E-2							7.747E-2
U8	4.766E-2							4.766E-2

b) Gamma-ray cross sections

Element	Zone 1	Zone 2	Zone 3	Zone 4	Zone 5	Zone 6	Zone 7	Total zone
H	-2.898E-3		-9.844E-2		-9.470E-2			-1.960E-1
O	-2.383E-2		-5.542E-1		-4.285E-1			-9.065E-1
Cr		-3.896E-2		-2.763E-1		-2.057E-2		-3.358E-1
Mn		-2.718E-3		-1.929E-2		-1.435E-3		-2.344E-2
Fe	-3.266E-3	-1.651E-1		-1.172E+0		-8.711E-2	-5.075E+0	-6.503E+0
Ni		-2.411E-2		-1.716E-1		-1.273E-2		-2.084E-1
Zr	-2.469E-2							-2.469E-2
U5	-4.087E-3							-4.087E-3
U8	-1.225E-1							-1.225E-1

Table 13 Sensitivity for gamma-ray dose summed over energy groups and spacial zones at interval number 202

a) Secondary gamma-ray production cross sections

Element	Zone 1	Zone 2	Zone 3	Zone 4	Zone 5	Zone 6	Zone 7	Zone 8	Total zone
H	4.739E-7		2.996E-5		4.070E-6			4.115E-3	4.150E-3
O	7.150E-4		6.789E-4		1.107E-4			7.017E-4	2.206E-3
Al								4.909E-2	4.909E-2
Si								1.206E-1	1.206E-1
Ca								1.657E-1	1.657E-1
Cr		2.040E-1		1.826E-2		4.216E-4			2.227E-1
Mn		1.916E-2		1.677E-3		3.876E-5			2.089E-2
Fe	8.760E-3	3.060E-1		2.863E-2		6.949E-4	3.944E-1		7.385E-1
Ni		1.392E-1		1.238E-2		2.891E-4			1.519E-1
Zr	4.610E-3								4.610E-3
US	1.265E-2								1.265E-2
U8	3.052E-3								3.052E-3

b) Gamma-ray cross sections

Element	Zone 1	Zone 2	Zone 3	Zone 4	Zone 5	Zone 6	Zone 7	Zone 8	Total zone
H	-4.487E-4		-8.372E-2		-7.948E-2			-5.918E-2	-2.228E-1
O	-3.953E-3		-4.081E-1		-3.850E-1			-5.911E+0	-6.704E+0
Al								-5.414E-1	-5.414E-1
Si								-2.280E+0	-2.280E+0
Ca								-2.525E+0	-2.525E+0
Cr		-2.843E-2		-2.732E-1		-2.024E-2			-3.219E-1
Mn		-1.993E-3		-1.916E-2		-1.418E-3			-2.257E-2
Fe	-6.152E-4	-1.214E-1		-1.168E+0		-8.646E-2	-4.565E+0		-5.941E+0
Ni		-1.789E-2		-1.722E-1		-1.274E-2			-2.028E-1
Zr	-4.947E-3								-4.947E-3
US	-8.731E-4								-8.731E-4
U8	-2.618E-2								-2.618E-2

Table 14 Sensitivities of gamma-ray dose to neutron cross sections of iron in the pressure vessel at interval number 202

Group	Gamma-ray dose (ΔR/R)		
	Elastic	Inelastic	(n,γ)
5	-6.789E-3	-8.443E-3	
10	-8.663E-4	-9.513E-3	
36	-3.343E-3		-5.693E-4
60	-1.113E-3		-5.547E-4
64	-2.402E-4		-2.237E-5
75	+1.313E-3		-1.377E-3
85			-7.398E-5
100			3.924E-3

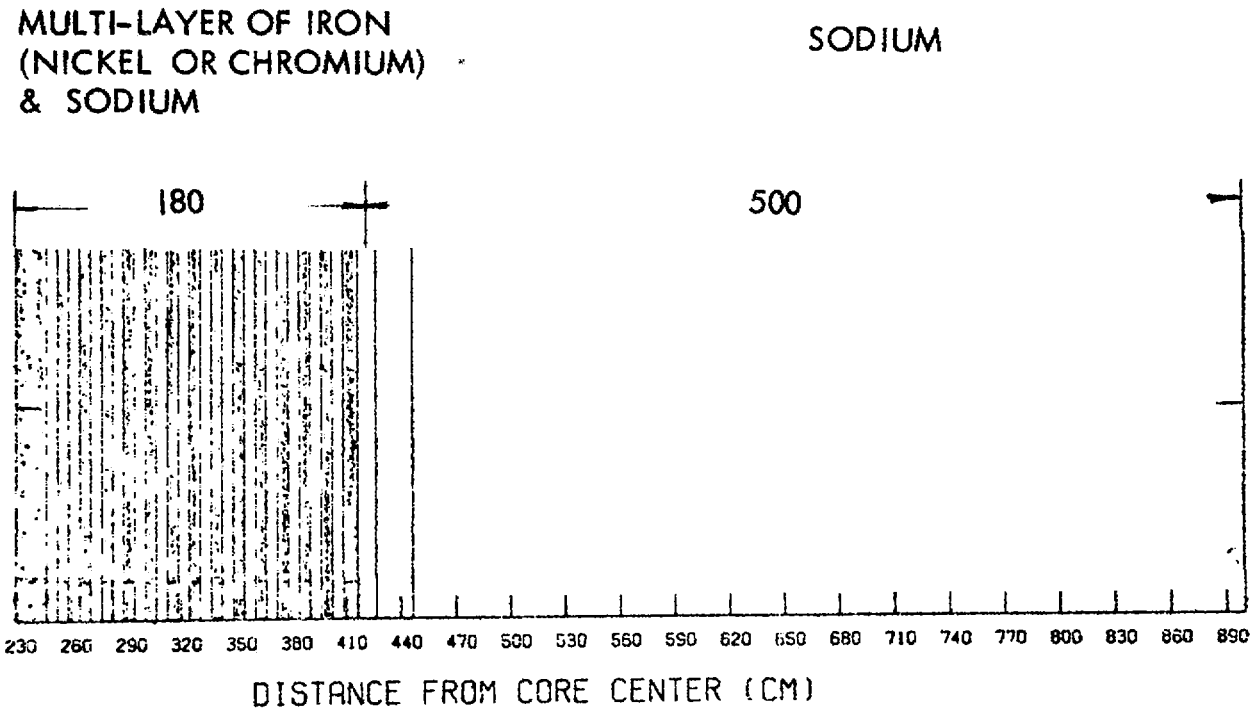

Fig.1 Calculational geometry used for parametric studies of neutron capture gamma-ray yield data

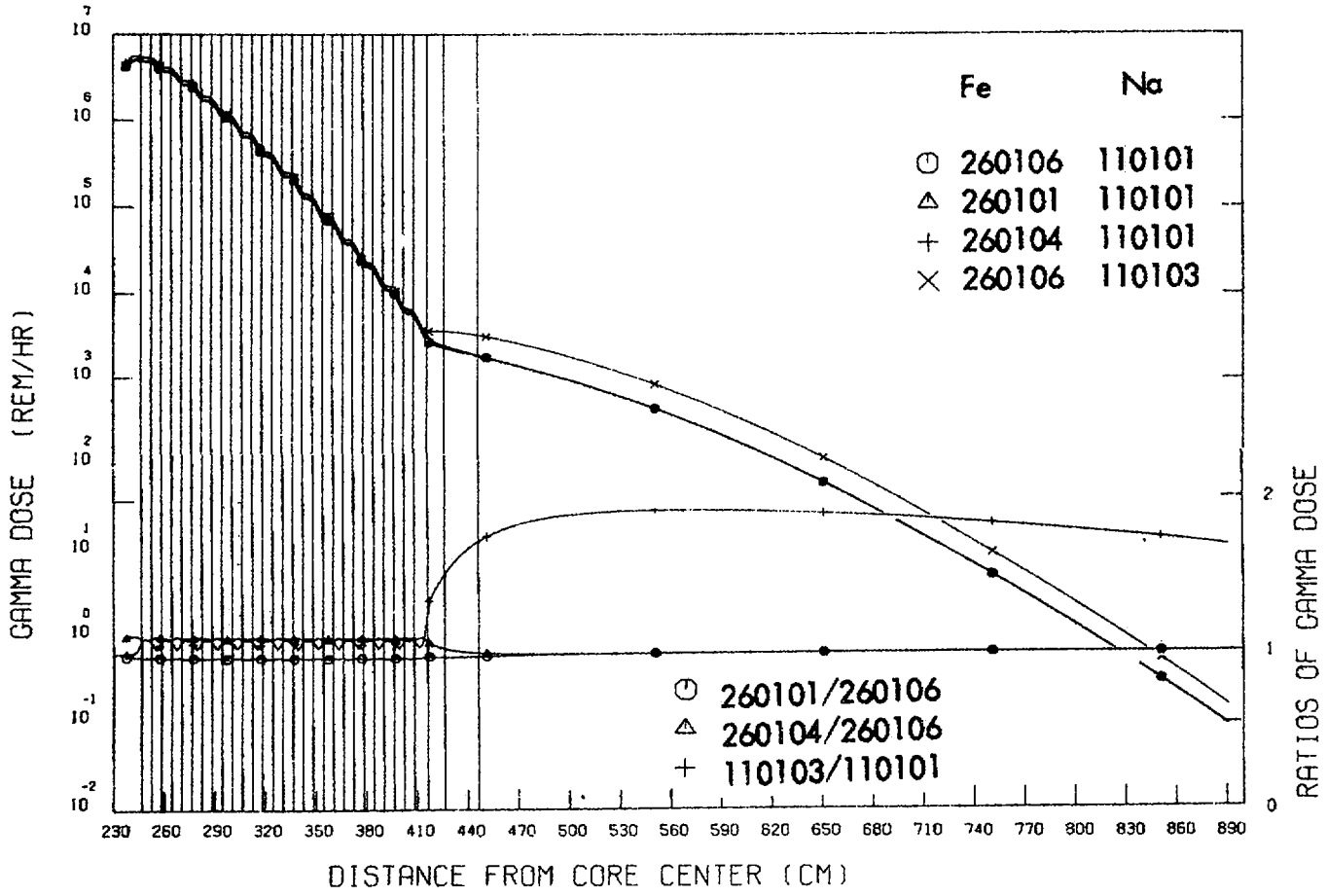

Fig.2 REACTOR SHIELDING BENCHMARK (PURE FE.NA) PARAMETER STUDY FOR CAPTURE-GAMMA YIELD DATA IN POPOP-4

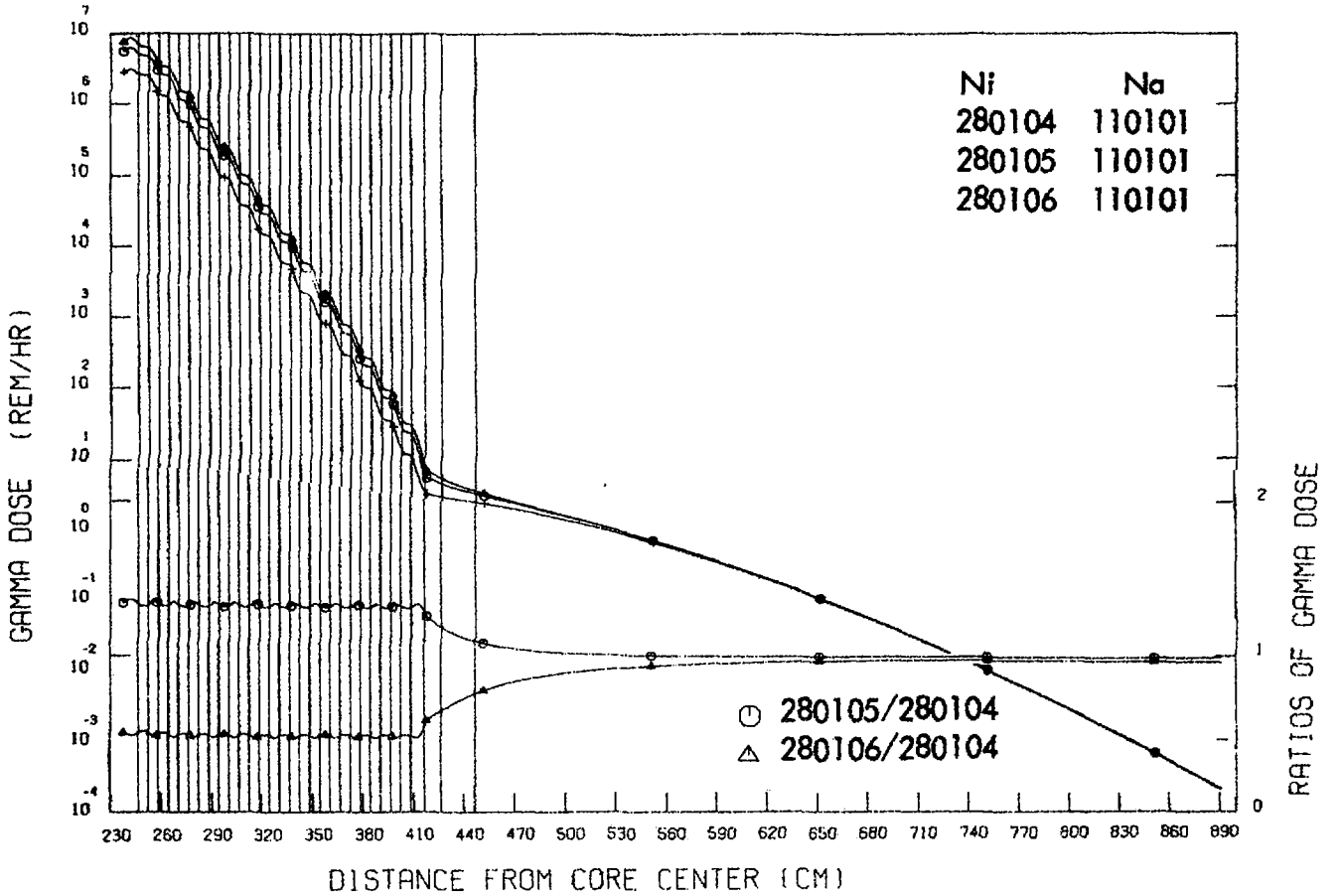

Fig.3 REACTOR SHIELDING BENCHMARK (PURE NI,NA)
PARAMETER STUDY FOR CAPTURE-GAMMA YIELD DATA IN POPOP-4

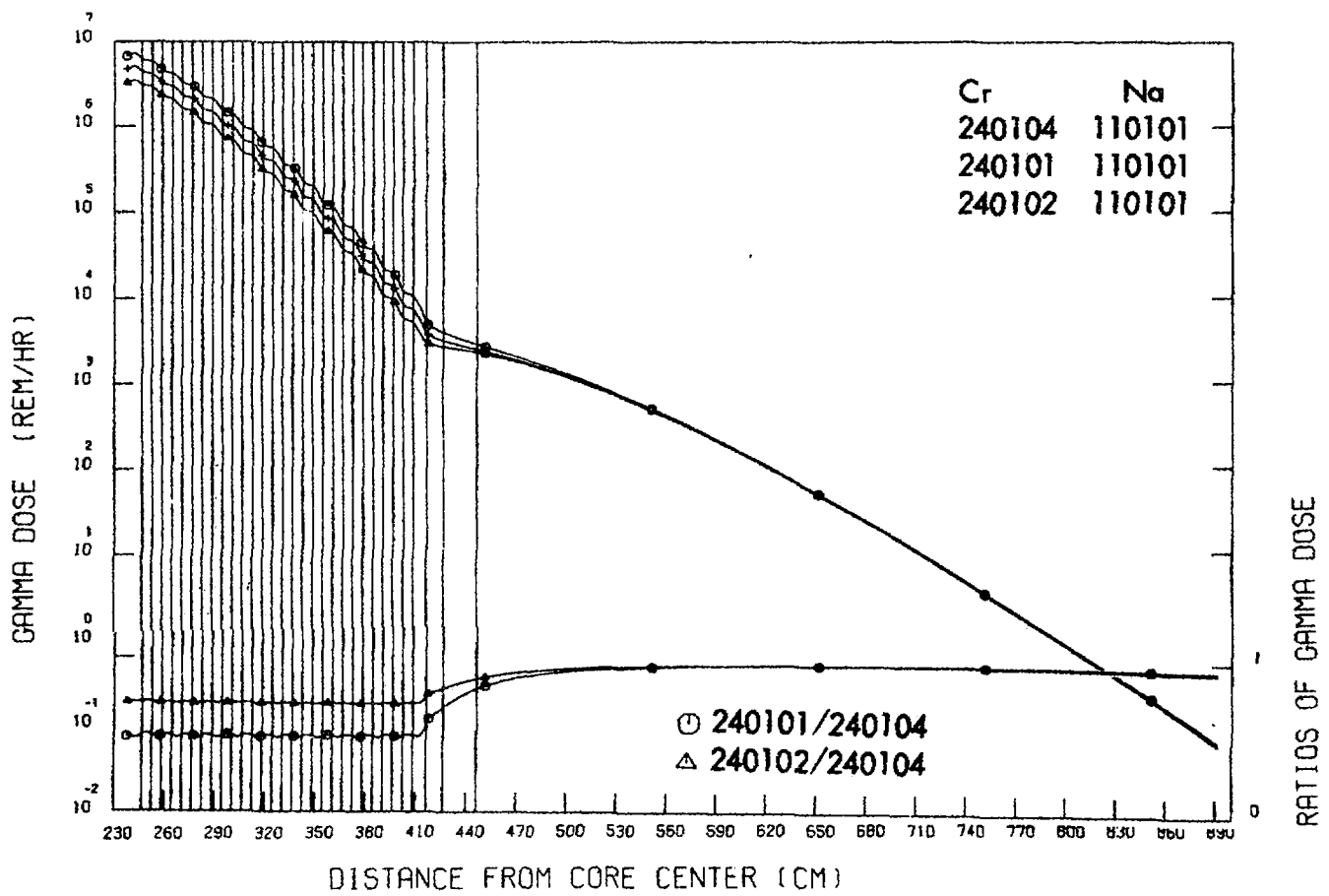

Fig.4 REACTOR SHIELDING BENCHMARK (PURE CR,NA)
PARAMETER STUDY FOR CAPTURE-GAMMA YIELD DATA IN POPOP-4

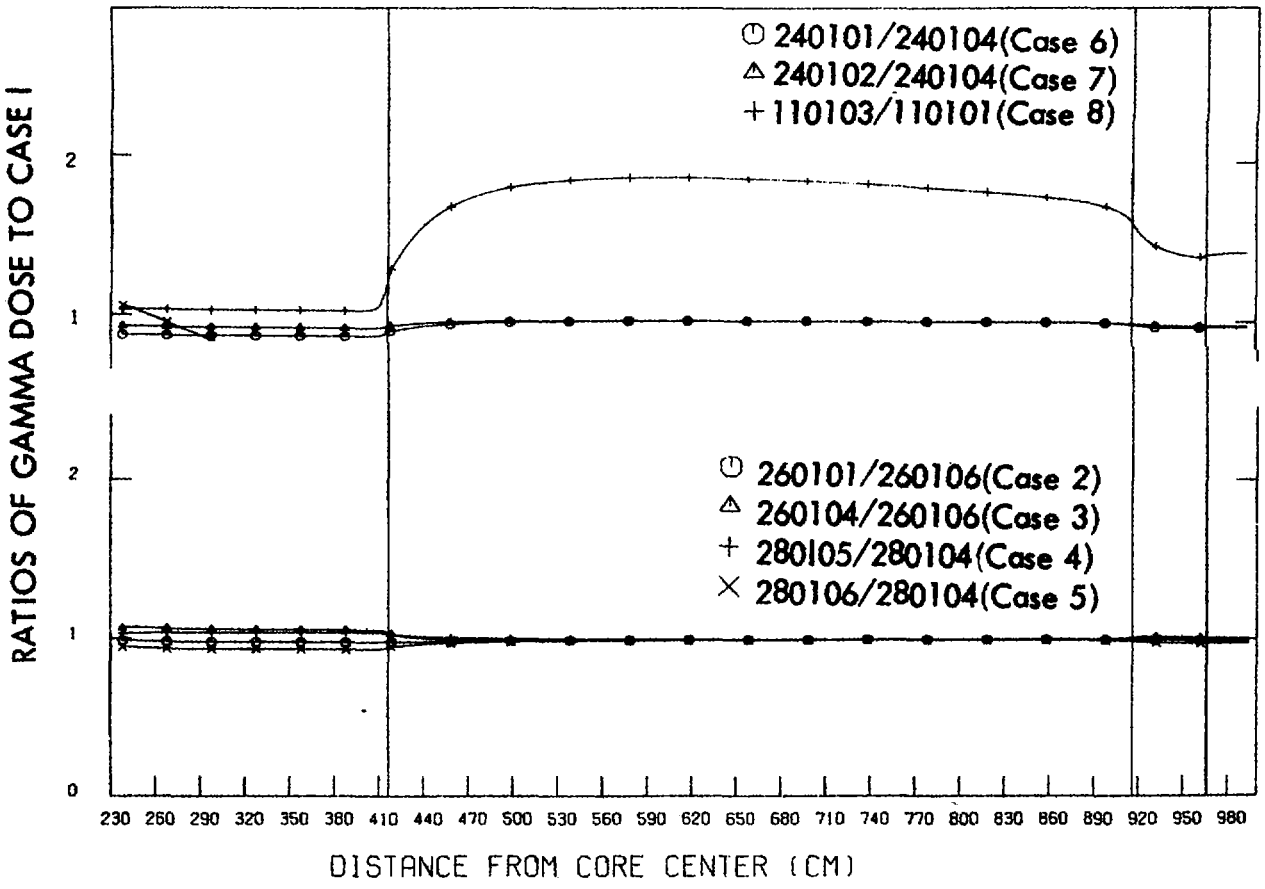

Fig. 5 Parameter study of capture gamma-ray yield data using the geometry given by the benchmark problem I

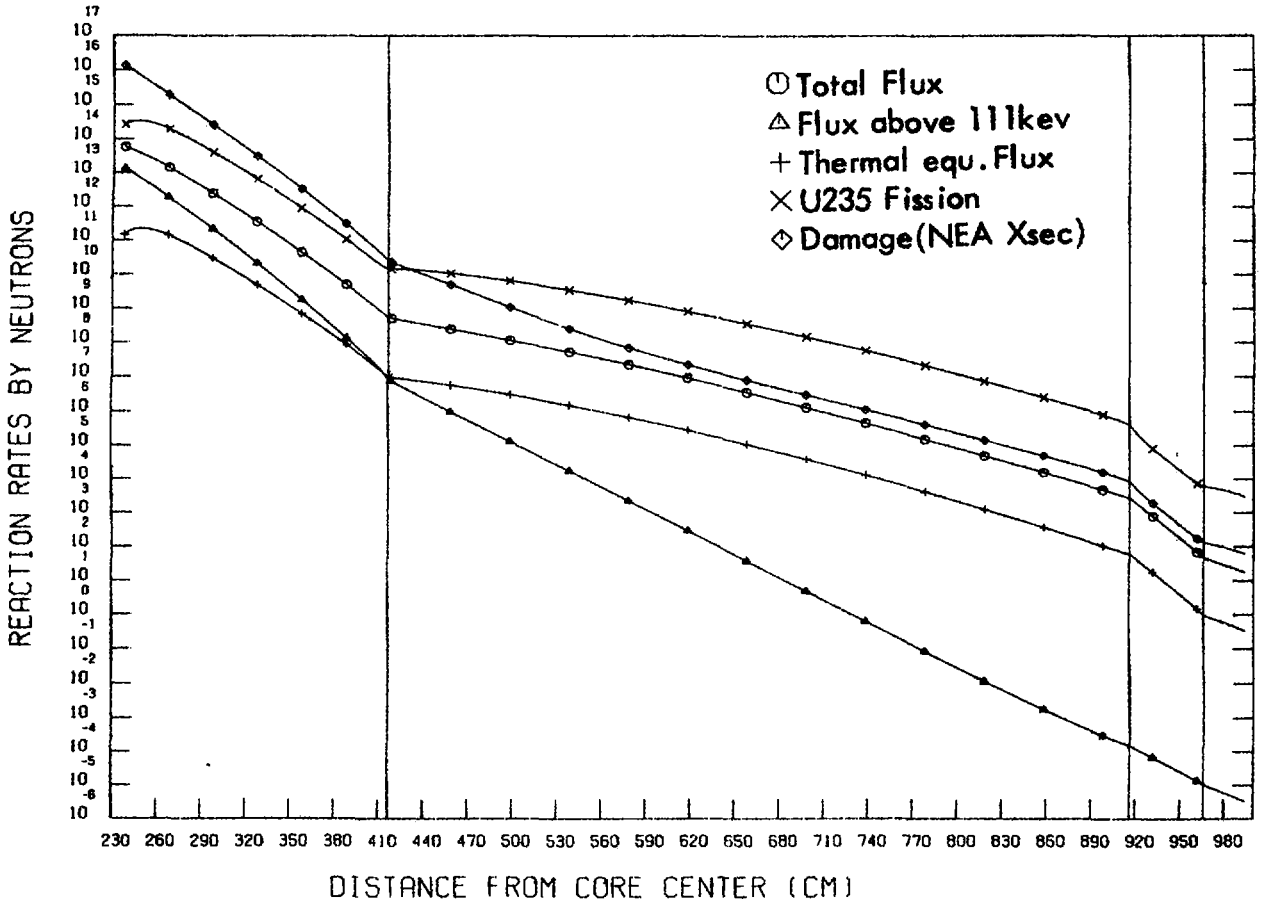

Fig.6(a) REACTOR SHIELDING BENCHMARK NO.1
PARAMETER STUDY OF REACTION RATE DISTRIBUTIONS BY NEUTRONS (1)

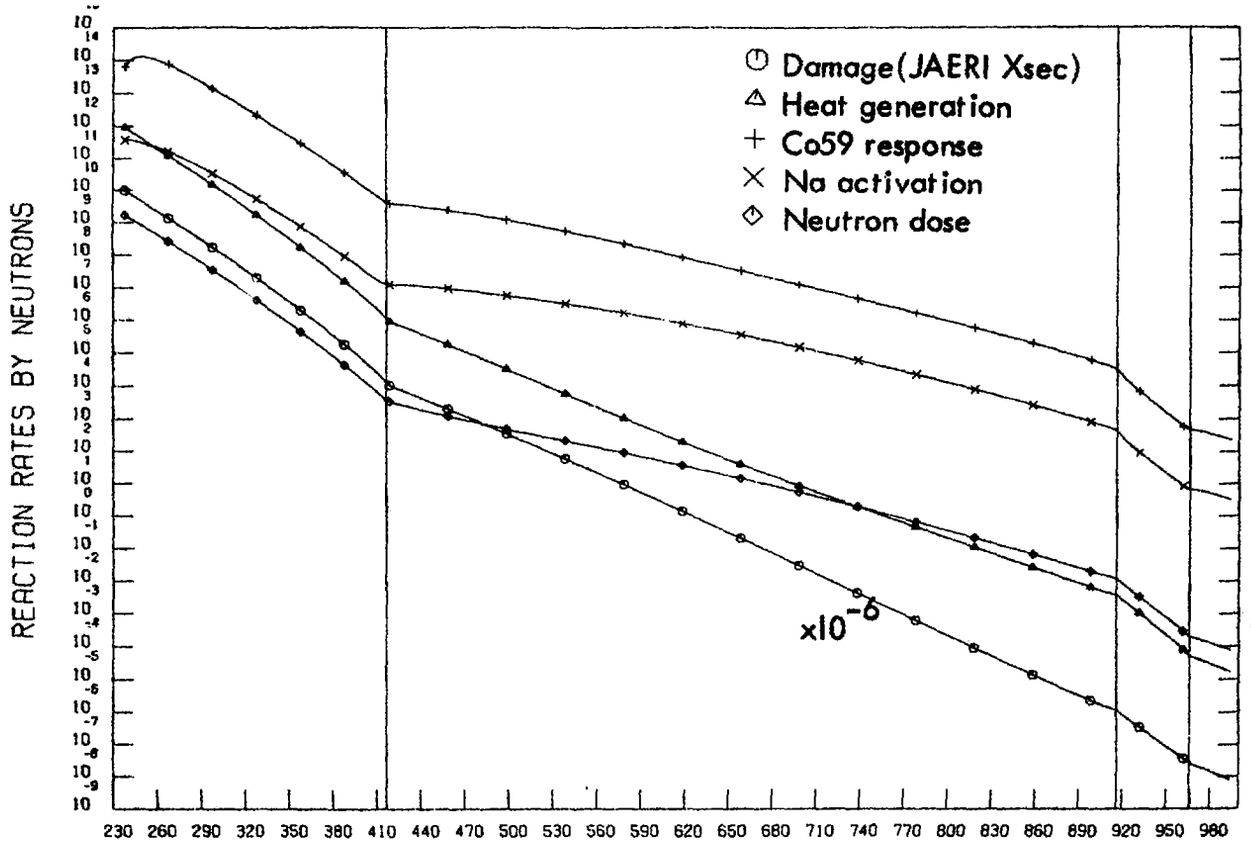

Fig.6(b) REACTOR SHIELDING BENCHMARK NO.1
PARAMETER STUDY OF REACTION RATE DISTRIBUTIONS BY NEUTRONS (2)

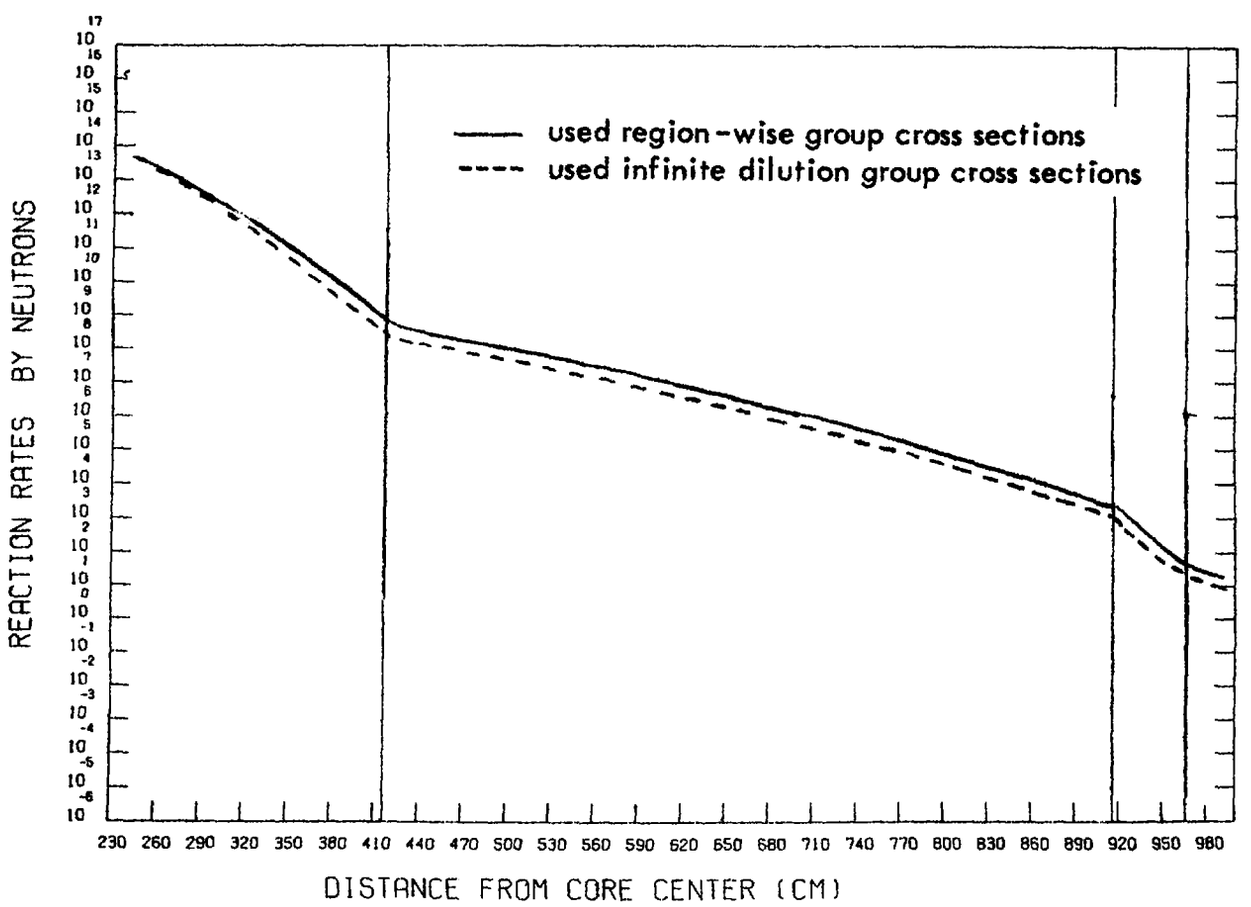

Fig. 7 Comarison of total scalar fluxes used region-wise group cross sections and infinite dilution group cross sections respectively

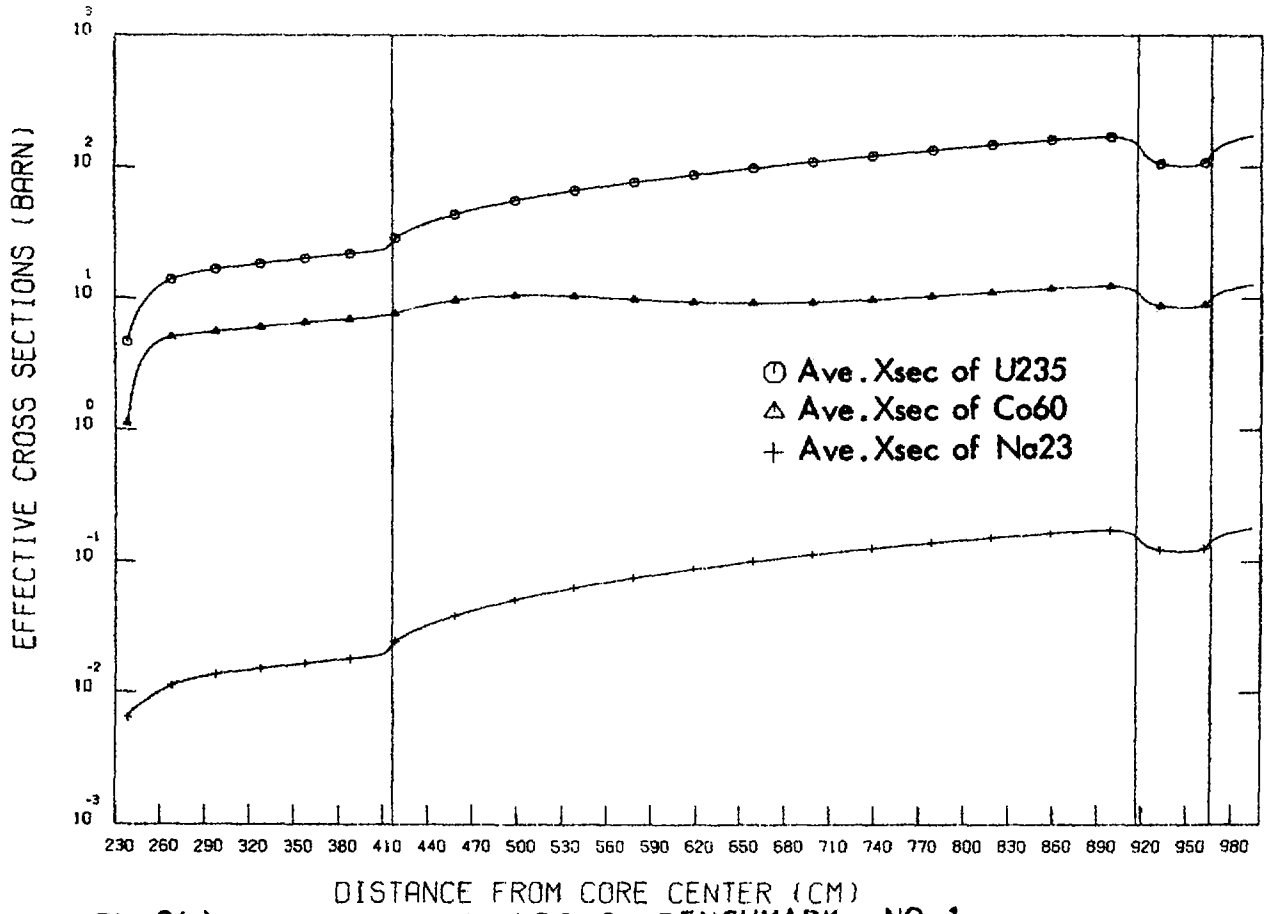

Fig.8(a) REACTOR SHIELDING BENCHMARK NO.1
PARAMETOR STUDY OF EFFECTIVE CROSS SECTION DISTRIBUTIONS

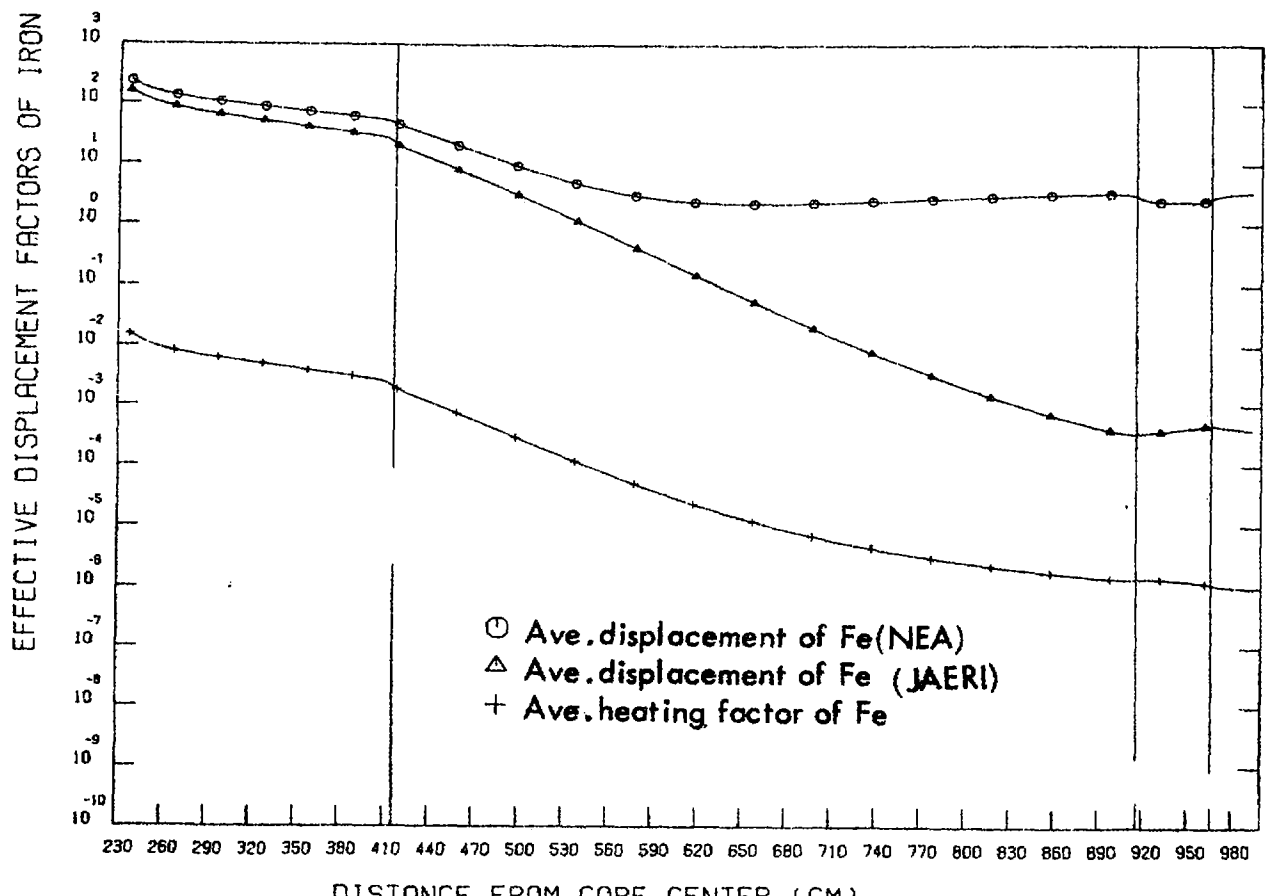

Fig.8(b) REACTOR SHIELDING BENCHMARK NO.1
PARAMETOR STUDY OF EFFECTIVE CROSS SECTION DISTRIBUTIONS

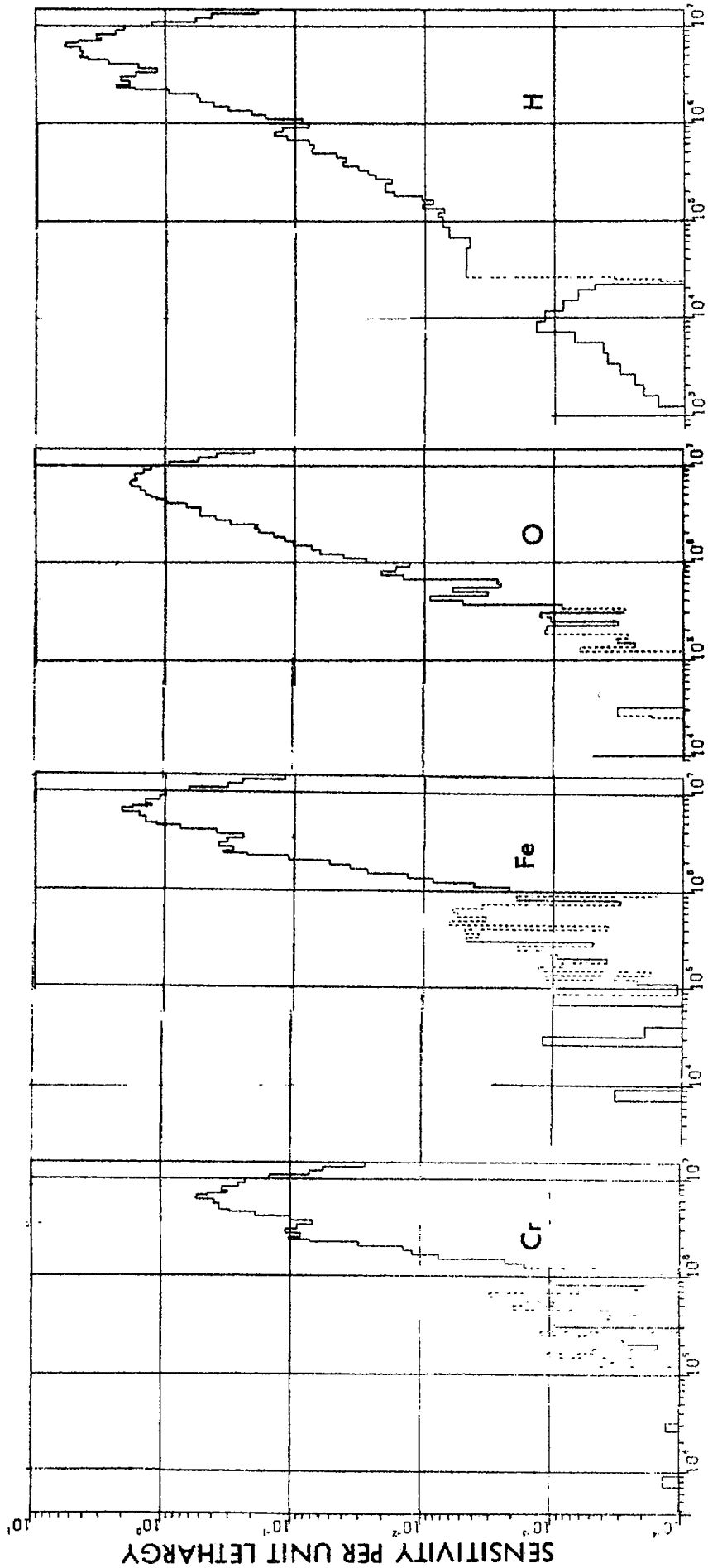

Fig. 9 Cross section sensitivities for neutron damage per unit lethargy summed over spacial zones at interval number 120

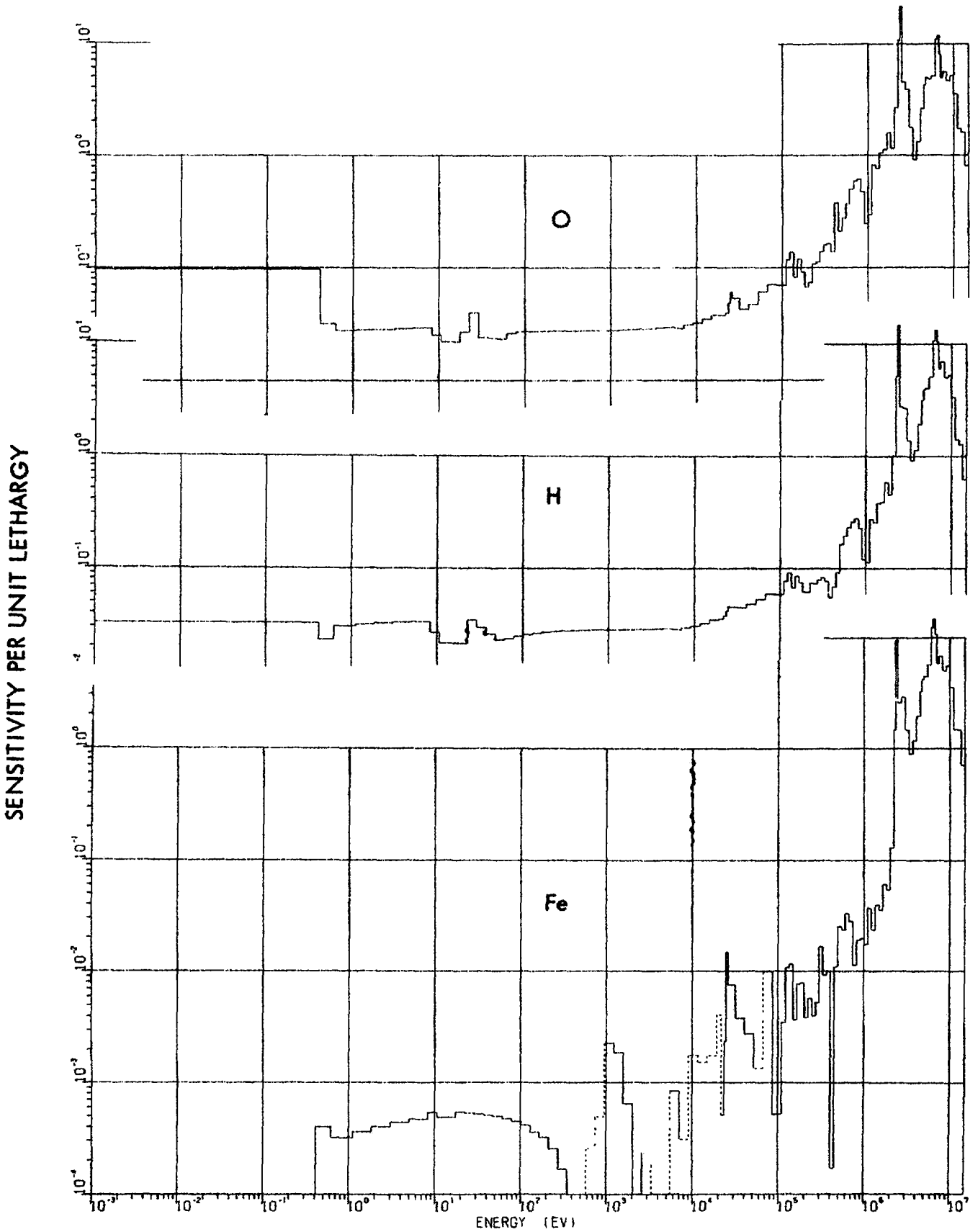

Fig. 10 Cross section sensitivities for neutron dose per unit lethargy summed over spacial zones at interval number 202

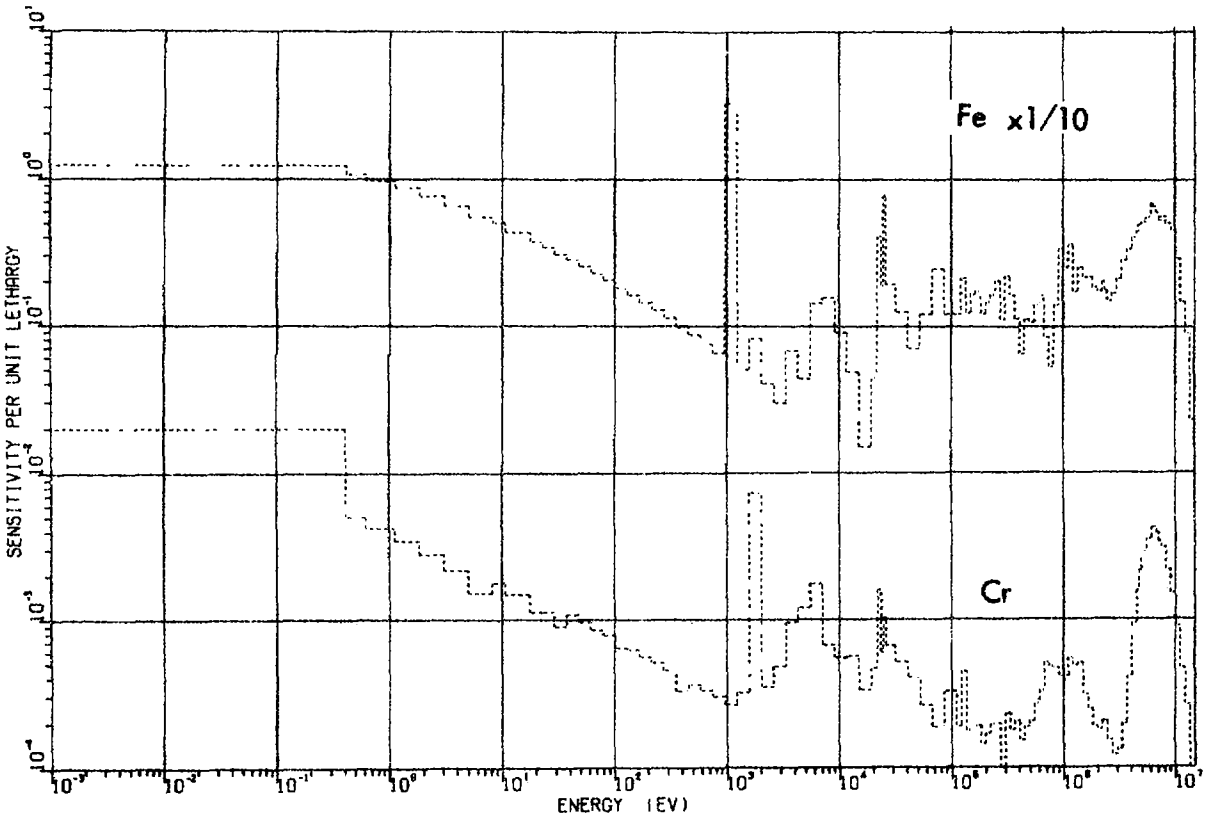

Fig. 11 Secondary gamma-ray production cross section sensitivities for gamma-ray heating per unit lethargy summed over spacial zones at interval number 147

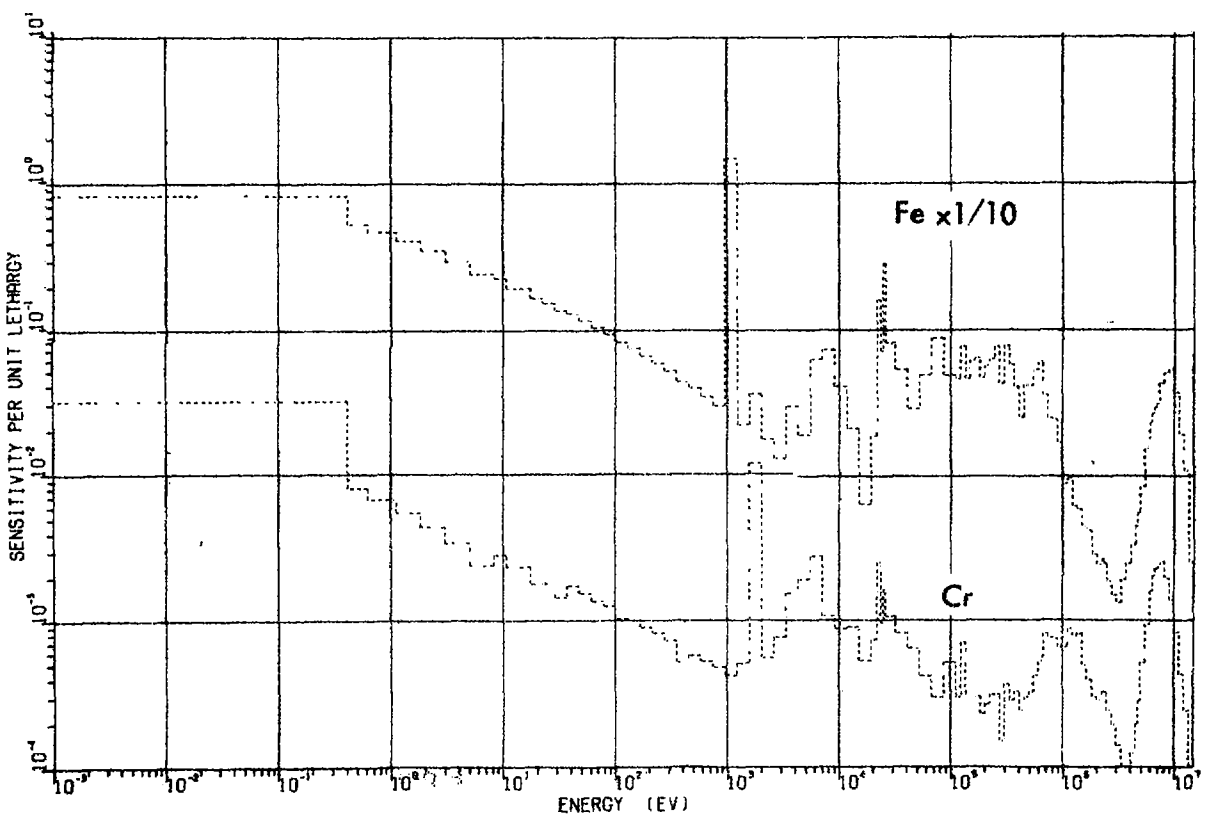

Fig. 12 Secondary gamma-ray production cross section sensitivities for gamma-ray dose summed over spacial zones at interval number 202

PROBLEME DE REFERENCE POUR LES PROTECTIONS D'UN REACTEUR A NEUTRONS RAPIDES

J.C.ESTIOT, J.P.TRAPP CEA/CEN CADARACHE

ABSTRACT

The BENCHMARK calculations are performed using the calculationnal scheme (formulaire) for fast reactor shielding PROPANE O, i.e :

- 26 groups, P_1, S_4
- the spatial meshes recommanded in the BENCHMARK specifications
- non adjusted cross sections, derived from the 100 g DLC2 cross sections set (ENDF/BII)
- the source is the surface anisotropic source given in the BENCHMARK specifications condensed to 26 groups
- the calculated integral responses are those of the BENCHMARK specifications, i.e :

Total flux, equivalent thermal flux, flux above 800 and 111 Kev, damage rate in steel, capture rate of sodium, Sulphur and Rhodium responses, Manganese and Sodium responses, U235 fission rate and Co_{59} capture rate.

RESUME

Les calculs de référence sont réalisés en utilisant le formulaire de calcul PROPANE O pour la protection des réacteurs rapides :

- 26 groupes, P1, S4
- maillage spatial recommandé dans les spécifications du problème de référence
- sections efficaces non ajustées tirées de la bibliothèque à 100 groupes DLC.2 (ENDF/BII)
- source de surface anisotrope donnée dans les spécifications condensées à 26 groupes.

Les réponses intégrales calculées sont : le flux total, le flux thermique équivalent, les flux supérieurs à 800 Kev et 111 Kev, les taux de dommage dans l'acier, le taux de capture du sodium, les réponses du Rhodium et du Soufre exprimées en flux de fission équivalent, les réponses du Manganèse et du Sodium exprimées en flux thermique équivalent, le taux de fission de l'U235 et le taux de capture du Cobalt 59.

I - INTRODUCTION

La configuration traitée est la configuration étalon proposée pour représenter les protections neutroniques de réacteur à neutrons rapides du niveau de puissance 3000 Mwth.

Les calculs sont réalisés à l'aide du formulaire de calcul PROPANE O, utilisé pour le calcul des protections des réacteurs rapides. Les options retenues sont les options de référence recommandées dans la définition de la configuration étalon. Il n'y a pas eu de tests de maillage ou d'anisotropie autour de ces options de référence.

II - GEOMETRIE ET CONDITIONS DE CALCUL

La géométrie du calcul est sphérique.

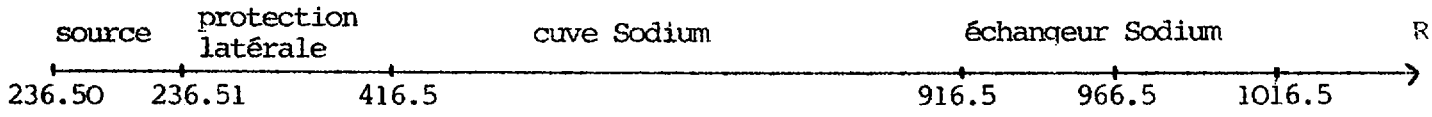

On rappelle en annexe I le découpage spatial et la composition (pour une T = 400°C)

Les conditions de calculs sont les suivantes :

- Code ANISN monodimensionnel sphérique
- Découpage angulaire : S_4
- Anisotropie du choc : P_1
- Conditions aux frontières : vide à droite et à gauche
- Bibliothèque de sections efficaces, de PROPANE O : sections efficaces, non ajustées, issues de la bibliothèque à 100 groupes DLC2 (ENDF/BII) et condensées à 26 groupes sur un flux neutronique dans le milieu acier-sodium (50-50%Vo) pour la PNL et l'échangeur et sur un flux dans un milieu de Na pur pour la cuve sodium.
- La source de surface, condensée dans les découpages à 26 groupes, est donnée en annexe II ; seules les directions $\emptyset_4$ et $\emptyset_5$ sont utilisées.

III - PARAMETRES ETUDIES

III-1. DISTRIBUTION SPATIALE DU FLUX SCALAIRE TOTAL Ø (r)

- Figure 1

Dans le PNL (L = 180 cm), atténuation de $4.62\ 10^4$

Dans le Na (L' : 500 cm), atténuation de $8.9\ 10^4$

III-2. DISTRIBUTION SPATIALE DU FLUX THERMIQUE EQUIVALENT

- Figure 2

$$\phi_{th}(r) = \int_0^{\infty} \sqrt{\frac{Eo}{E}} \; \phi\,(E,r)\, dE$$

Eo = 0.025 eV

E = énergie correspondant à la léthargie moyenne du groupe.

Dans le PNL, atténuation de : $1.4\ 10^4$

Dans le Na, atténuation de : $2.5\ 10^4$

III-3. DISTRIBUTION SPATIALE DU FLUX SCALAIRE SUPERIEUR à 0.8 Mev

- Figure 3

Dans le PNL, atténuation de : $5.5\ 10^7$

Dans le Na, atténuation de : $5.5\ 10^9$

III-4. DISTRIBUTION SPATIALE DE FLUX SCALAIRE SUPERIEUR à 111 Kev

- Figure 4

Dans le PNL, atténuation de : $8.5\ 10^5$

Dans le Na , atténuation de : $2.6\ 10^{11}$

III-5. DISTRIBUTION SPATIALE DU TAUX DE DEPLACEMENT PAR ATOME POUR LE FER

- Figure 5

$$\bar{T}_{dpa}(x) = \int_0^{\infty} f_{dpa}(E)\ \phi\,(E,r)\, dE$$

où f_{dpa} est la fonction dommages par atomes pour le Fer.

III-6. DISTRIBUTION SPATIALE DE LA VALEUR MOYENNE DE LA FONCTION DOMMAGE UTILISEE POUR LE FER

- Figure 6

$$\bar{f}_{dpa}(r) = \frac{\bar{T}_{dpa}(r)}{\bar{\phi}(r)}$$

III-7. DISTRIBUTION SPATIALE DU TAUX DE CAPTURE SODIUM POUR UN ATOME

- Figure 7

$$\bar{T}_{Na}(r) = \int_0^{\infty} \sigma^{Na}_{n,\gamma}(E)\ \phi(E,r)\ dE$$

III-8. DISTRIBUTION SPATIALE DE LA SECTION MOYENNE DE CAPTURE Na UTILISEE EN BARN

- Figure 8

$$\bar{\sigma}_{Na}\ [(n,\gamma), r] = \bar{T}_{Na}(r) / \bar{\phi}(r)$$

III-9. DISTRIBUTION SPATIALE DES DETECTEURS : Rh - S - Mn - Na

Les taux de réaction sont exprimés en termes de flux thermique équivalent pour le Mn et le Na, et en flux de fission équivalent pour le Rh et le S.

- Figures 9 à 12

III-10. DISTRIBUTION SPATIALE DE LA FISSION DE L'U_{235}

- Figure 13

III-11. DISTRIBUTION SPATIALE DE LA CAPTURE DE Co_{59}

- Figure 14.

ANNEXE-I

DECOUPAGE SPATIAL

ZONE	N°	NOMBRE D'INTERVALLES PAR ZONE	EPAISSEUR cm	RAYON ext (cm)	COMPOSITION N°	POURCENTAGE D'ACIER EN VOLUME
SOURCE	1	1	0.01	236.5	1	53 %
PNL	2	60	1x2.99 59x3.00	239.5 416.5	1	53 %
Na	3	125	125x4	916.5	2	0 %
ECHANGEUR	4	17	1x2.0 16x3.0	918.5 966.5	3	15 %
Na	5	13	1x2.0 12x4.0	968.5 1016.5	2	0 %

COMPOSITIONS ATOMIQUES EN 10^{24} ATOMES/cm^3

	Fer	Nickel	Chrome	Sodium
Composition 1	0.0320	0.00423	0.00860	0.01045
Composition 2				0.02223
Composition 3	0.00906	0.00120	0.00243	0.01890

ANNEXE II

N° DE GROUPE	ϕ_4	ϕ_5	N° DE GROUPE	ϕ_4	ϕ_5
1	2.1300+11	4.6300+11	14	6.0500+11	7.9800+11
2	6.7700+11	1.0070+12	15	1.0160+12	7.5000+11
3	1.2900+12	1.5500+12	16	1.6000+12	1.8600+12
4	1.9800+12	2.1700+12	17	1.2000+13	7.1100+12
5	3.9200+12	2.5300+12	18	1.3100+13	5.0900+12
6	1.9300+12	5.4200+11	19	2.7000+11	1.2600+11
7	8.6100+10	2.1700+09	20	3.5200+11	7.5300+11
8	9.0200+11	1.0700+12	21	9.4600+11	1.4000+12
9	6.2500+12	8.6600+11	22	1.6000+12	1.9500+12
10	1.9900+12	2.3000+12	23	2.4000+12	2.6300+12
11	1.4300+13	7.8200+12	24	4.4300+12	2.8500+12
12	1.4200+13	5.0300+12	25	1.8000+12	3.9300+11
13	2.1500+11	9.9500+10	26	7.4900+10	1.9700+09

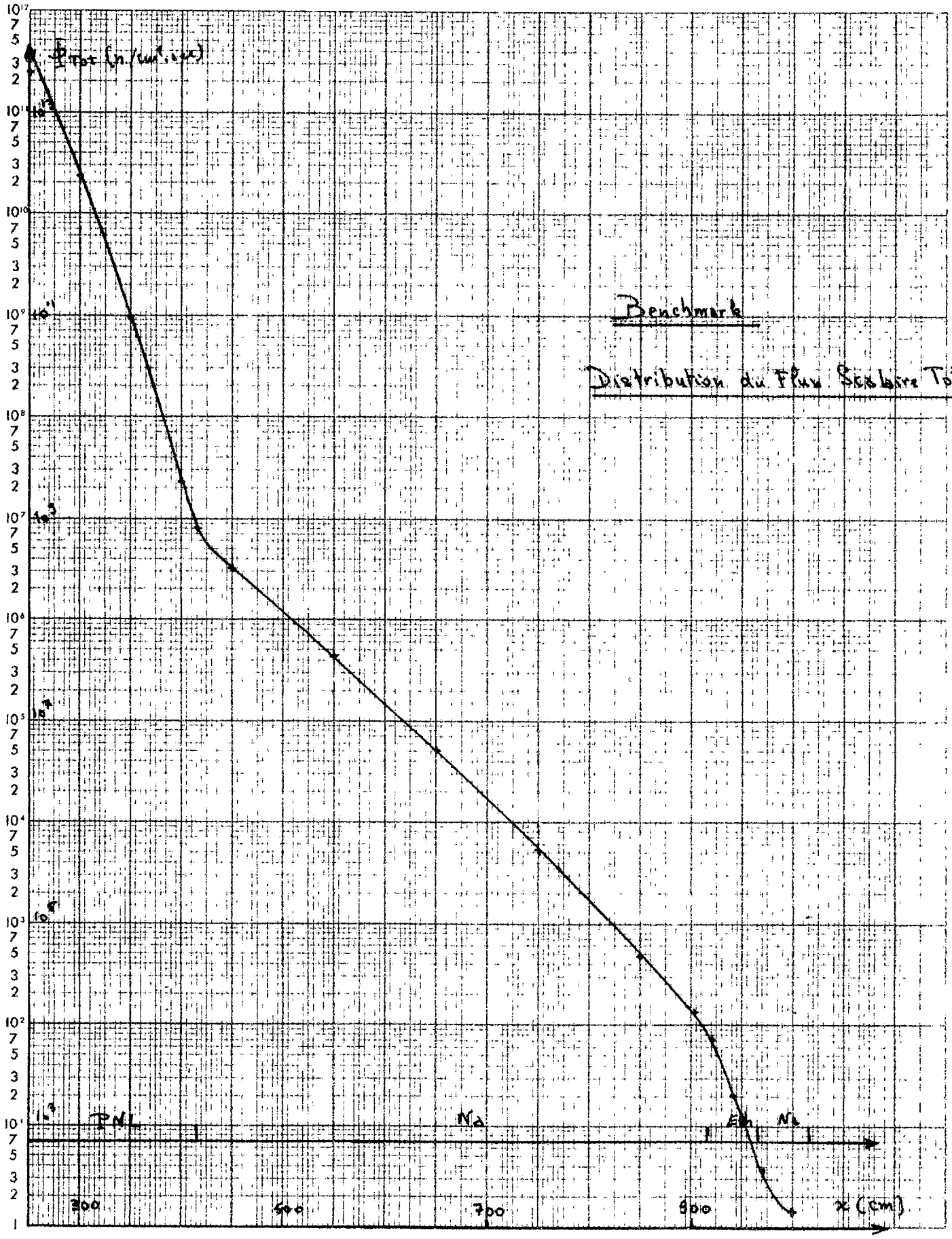
Benchmark
Distribution du Flux Scalaire Total
Φ_{Tot} (n./cm².sec)
PNL
N_a
E_{th} N_t
200
400
700
900
x (cm)

Fig. 1

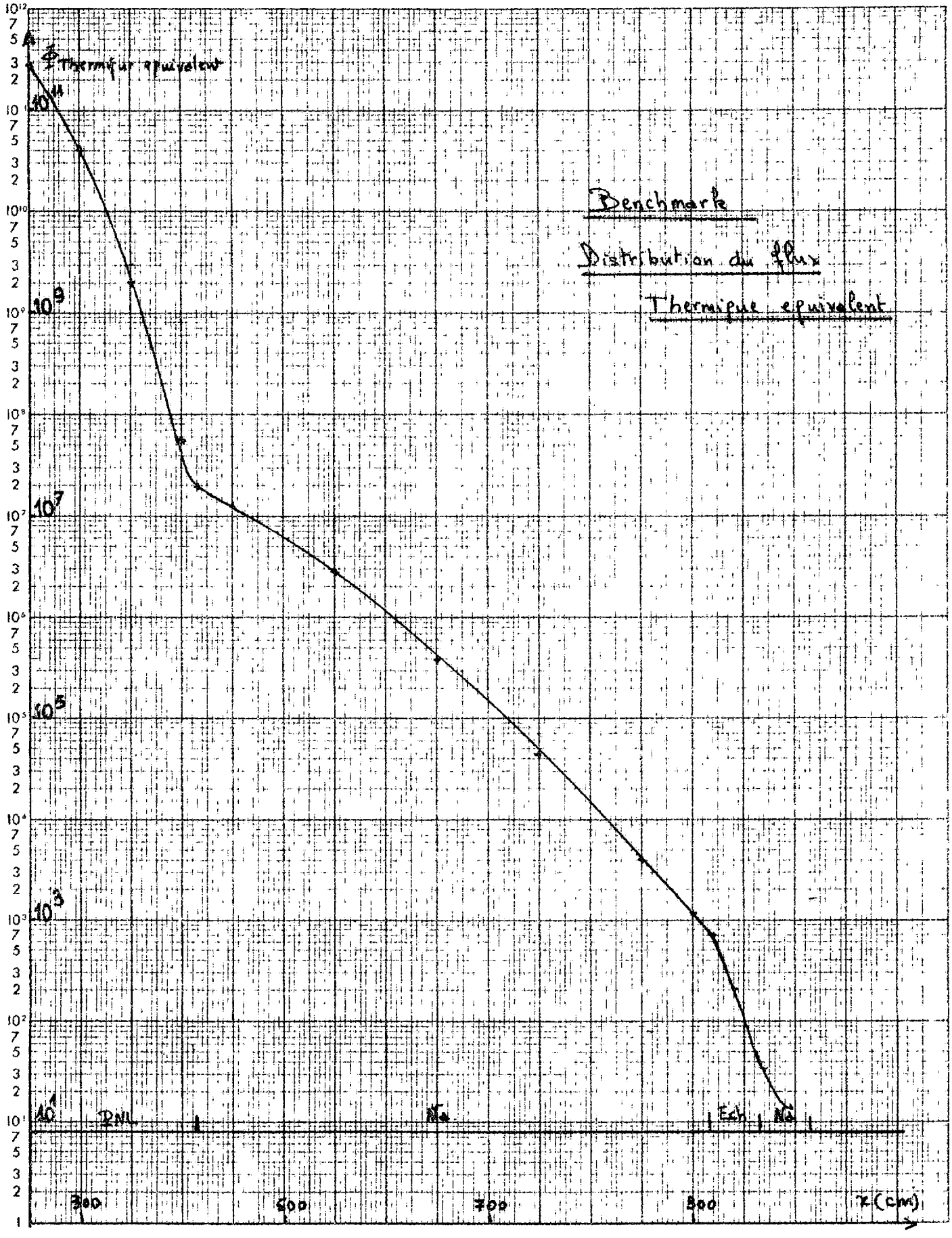
Benchmark
Distribution du flux
Thermique equivalent
Φ Thermique equivalent
10^11
10^9
10^7
10^5
10^3
10^1
RNL
Ech
300
500
700
900
x (cm)

Fig.2

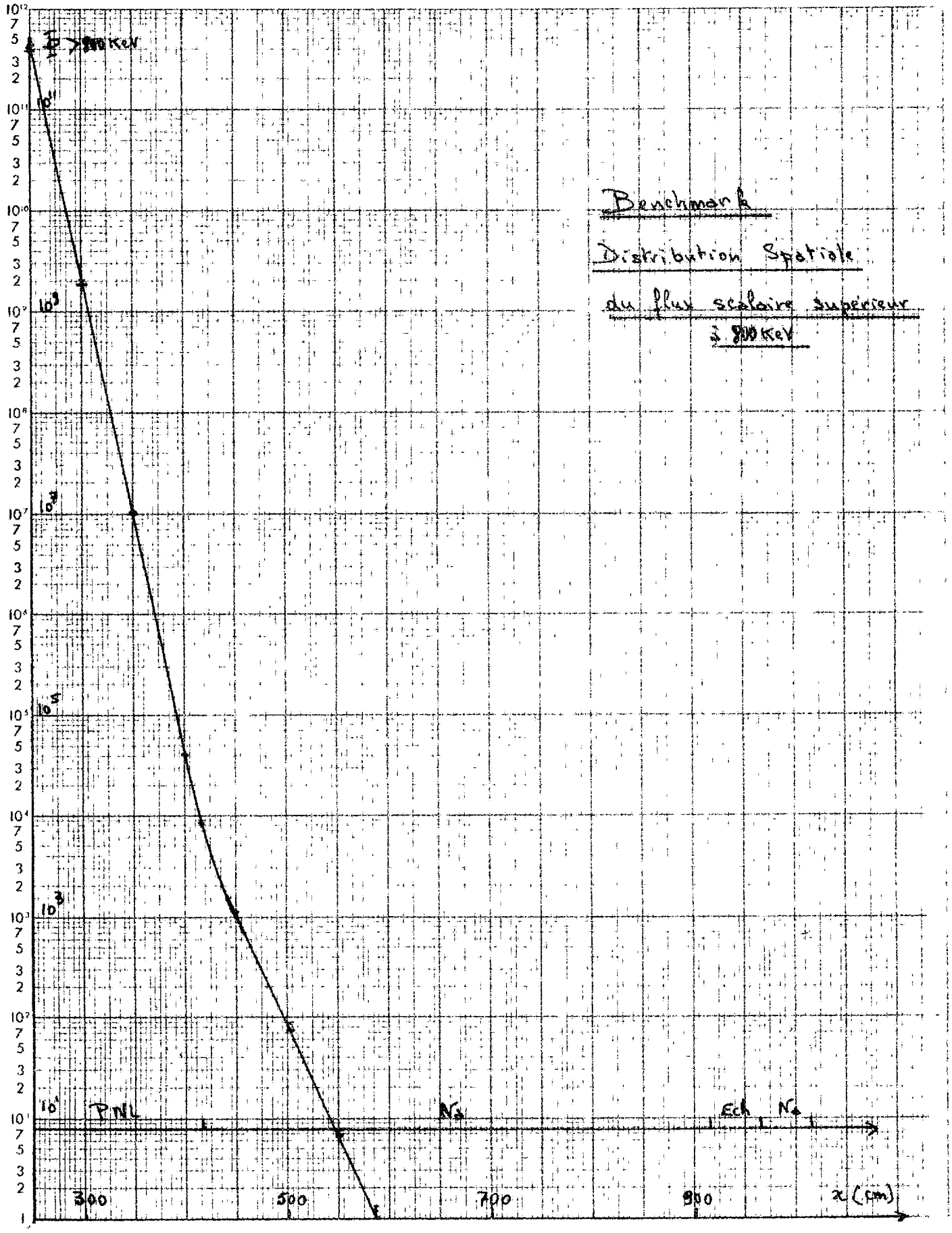
Benchmark
Distribution Spatiale
du flux scalaire supérieur
à 800 KeV
PNL
Ech
x (cm)
300
500
700
900

Fig. 3

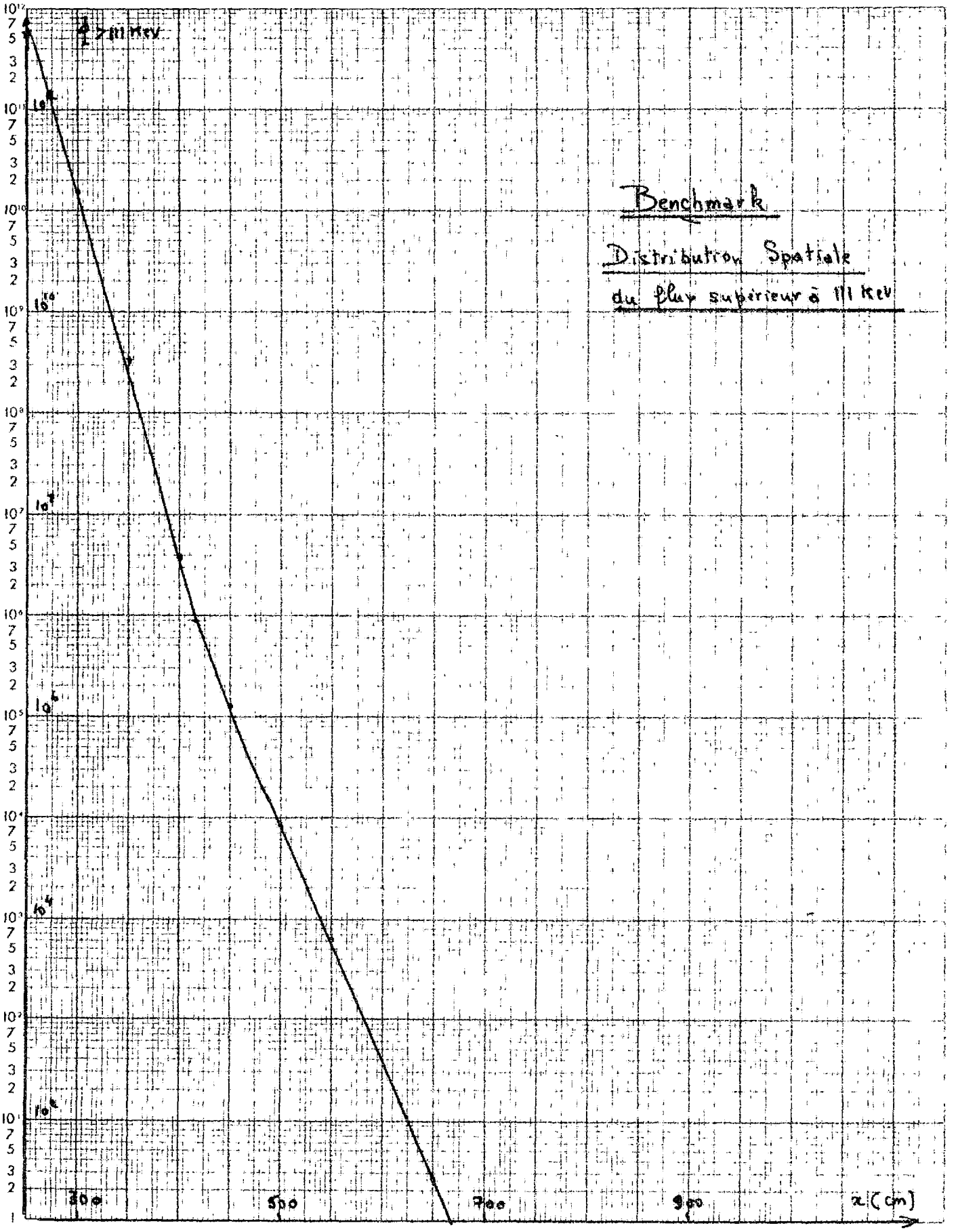
Benchmark
Distribution Spatiale
du flux supérieur à 111 Kev
Φ > 111 Kev
10¹⁰
10⁹
10⁸
10⁷
10⁶
10⁵
10⁴
10³
10²
10¹
300
500
700
900
z (cm)

Fig. 4

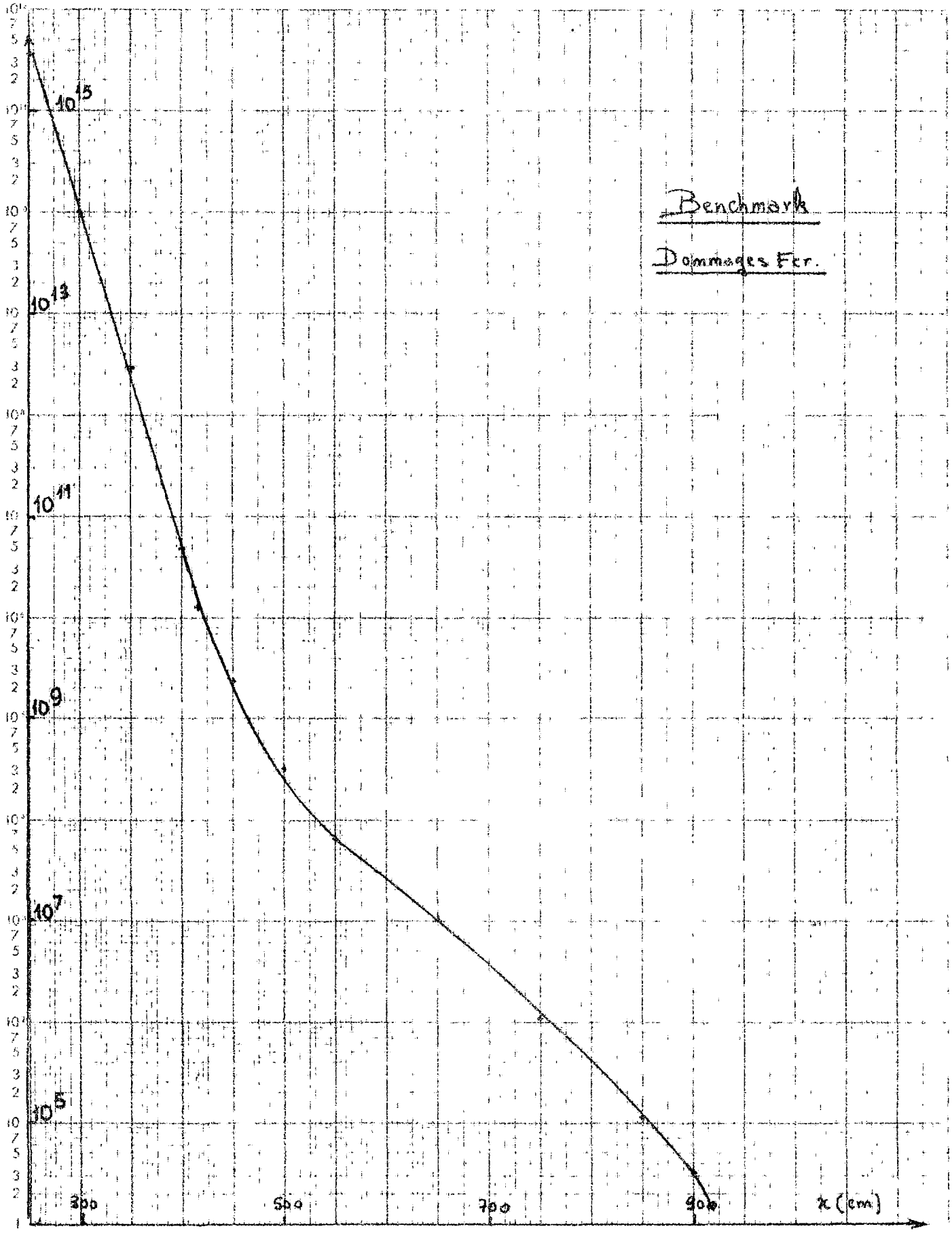
Benchmark
Dommages Fer.
10^{15}
10^{13}
10^{11}
10^{9}
10^{7}
10^{5}
300
500
700
900
x (cm)

Fig. 5

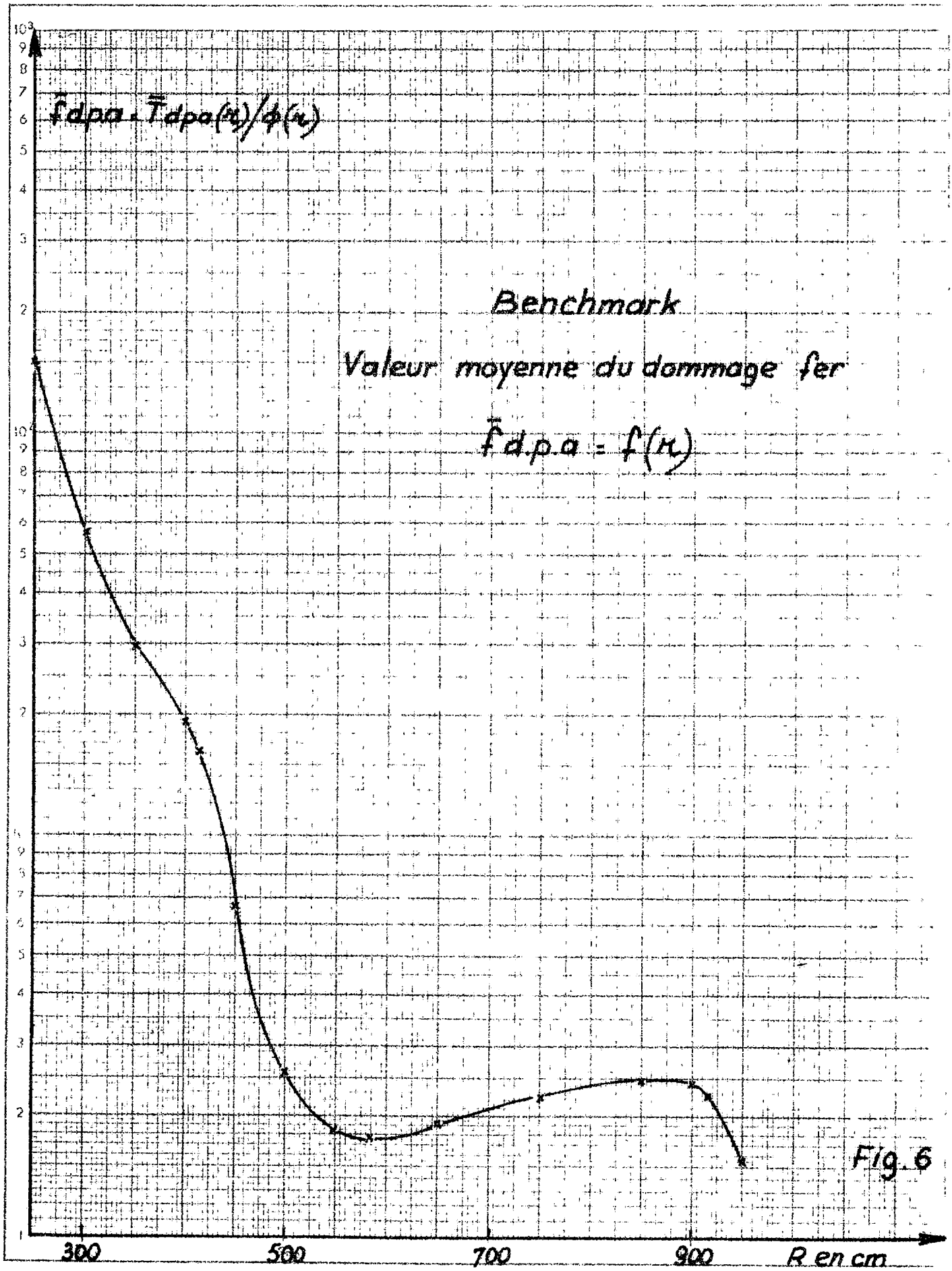
$\bar{f}dpa = \bar{T}dpa(r)/\phi(r)$
Benchmark
Valeur moyenne du dommage fer
$\bar{f}d.p.a = f(r)$
300
500
700
900
R en cm

Fig. 6

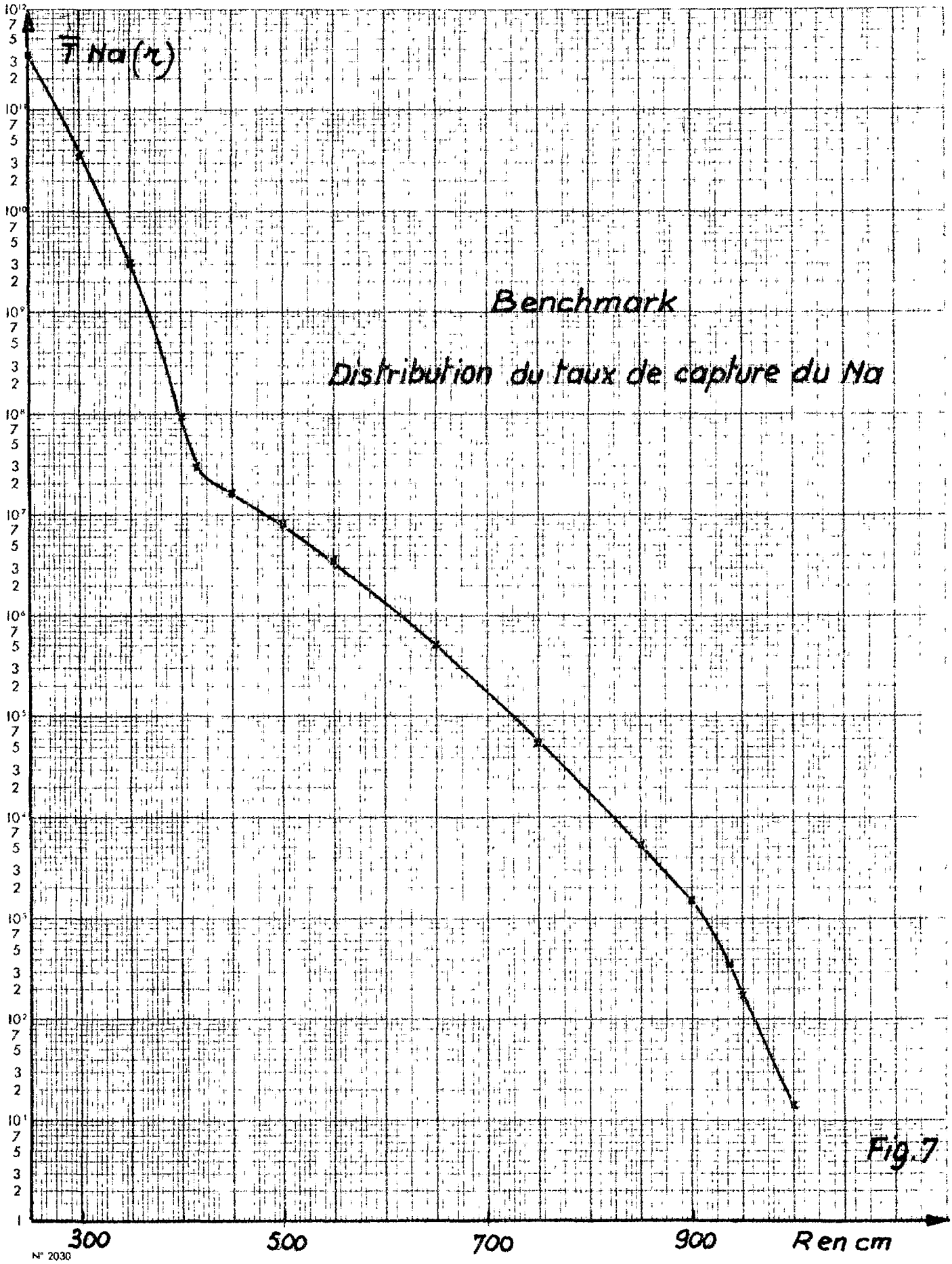
$\bar{T}_{Na}(r)$
Benchmark
Distribution du taux de capture du Na
300
500
700
900
R en cm
N° 2030

Fig. 7

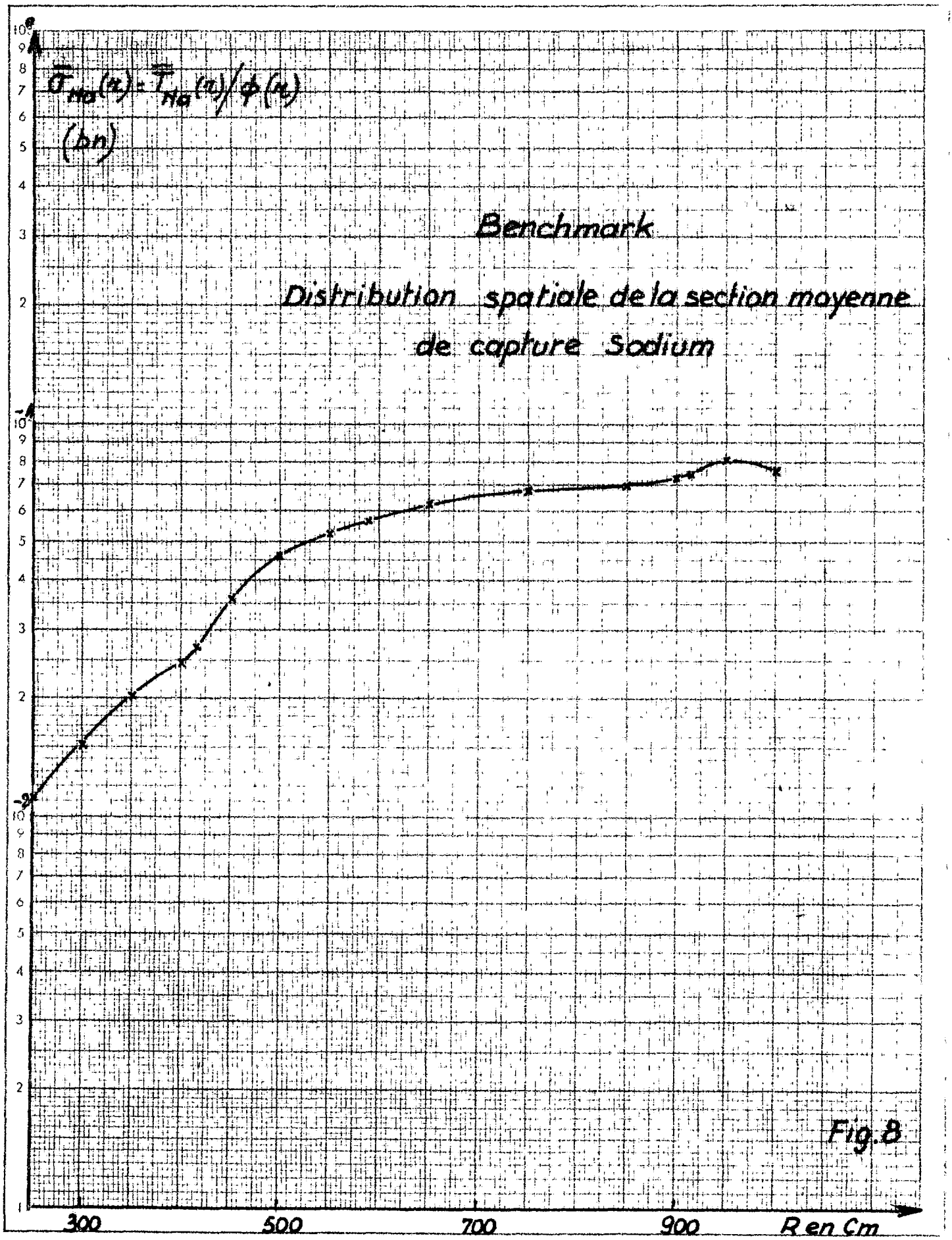
$\bar{\sigma}_{Na}(r) = \bar{T}_{Na}(r)/\phi(r)$
(bn)
Benchmark
Distribution spatiale de la section moyenne de capture Sodium
10^{-2}
300
500
700
900
R en Cm
Fig. 8

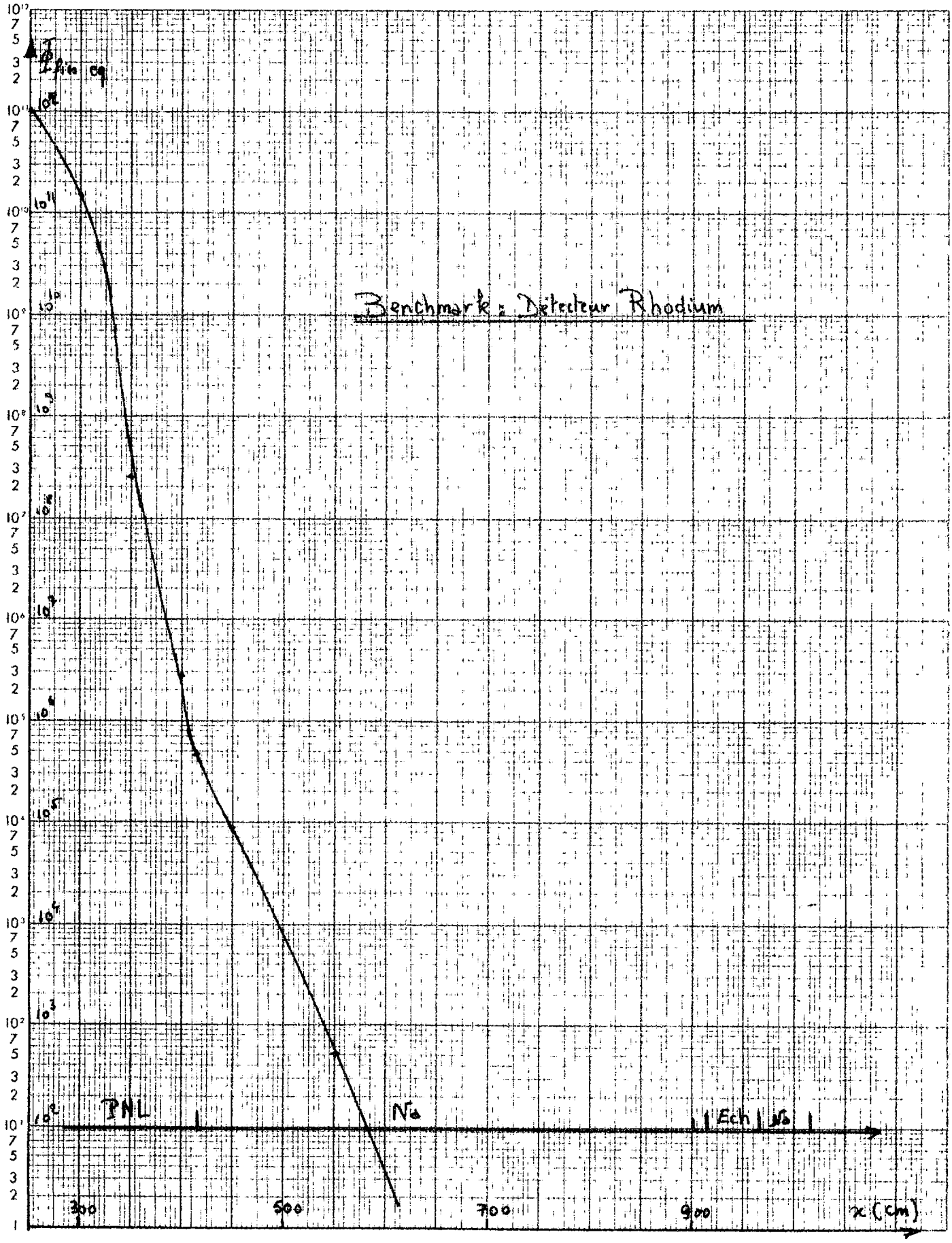
Benchmark : Détecteur Rhodium
PNL
Na
Ech Na
300
500
700
900
x (cm)

Fig. 9

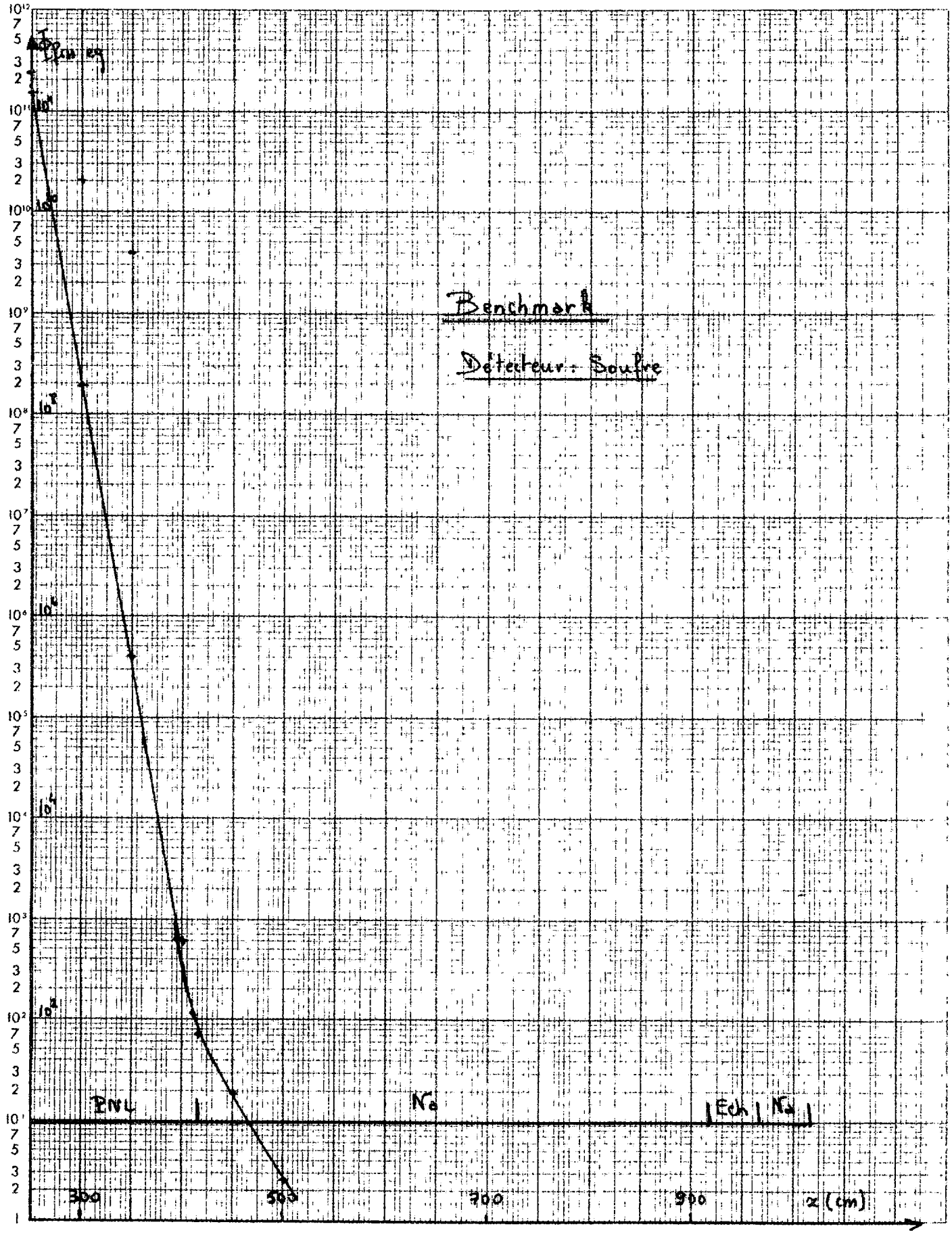

Fig. 10

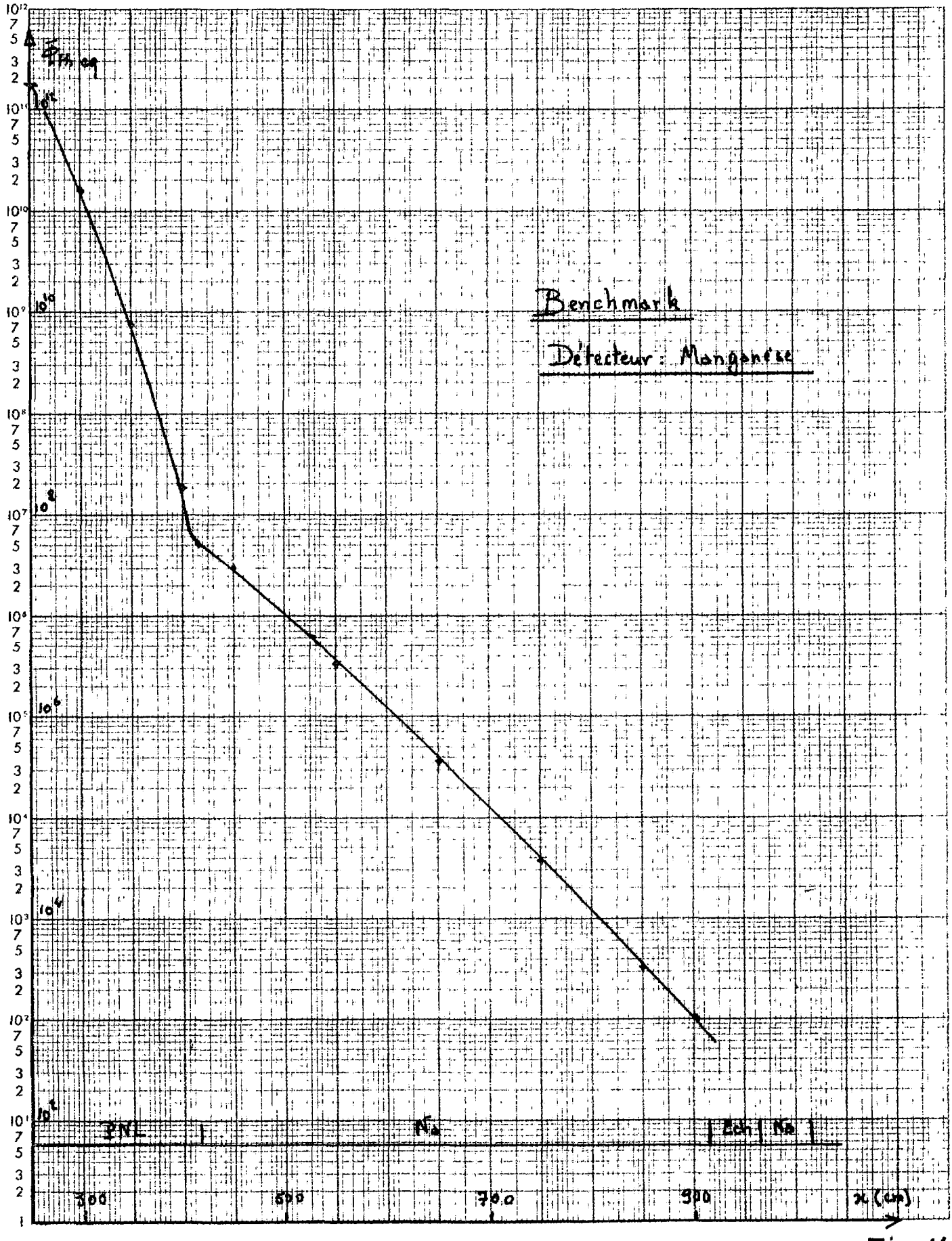

Fig. 11

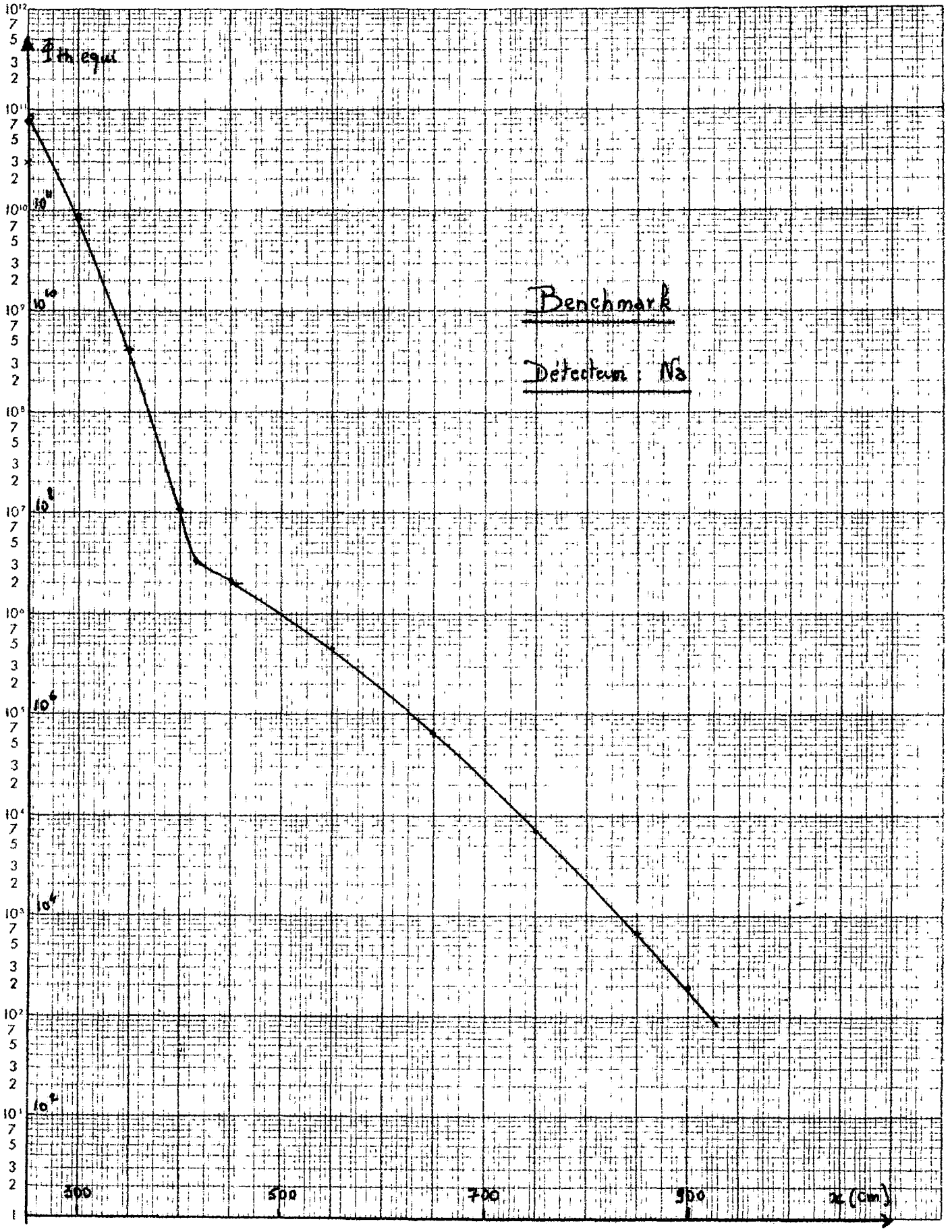

Fig. 12

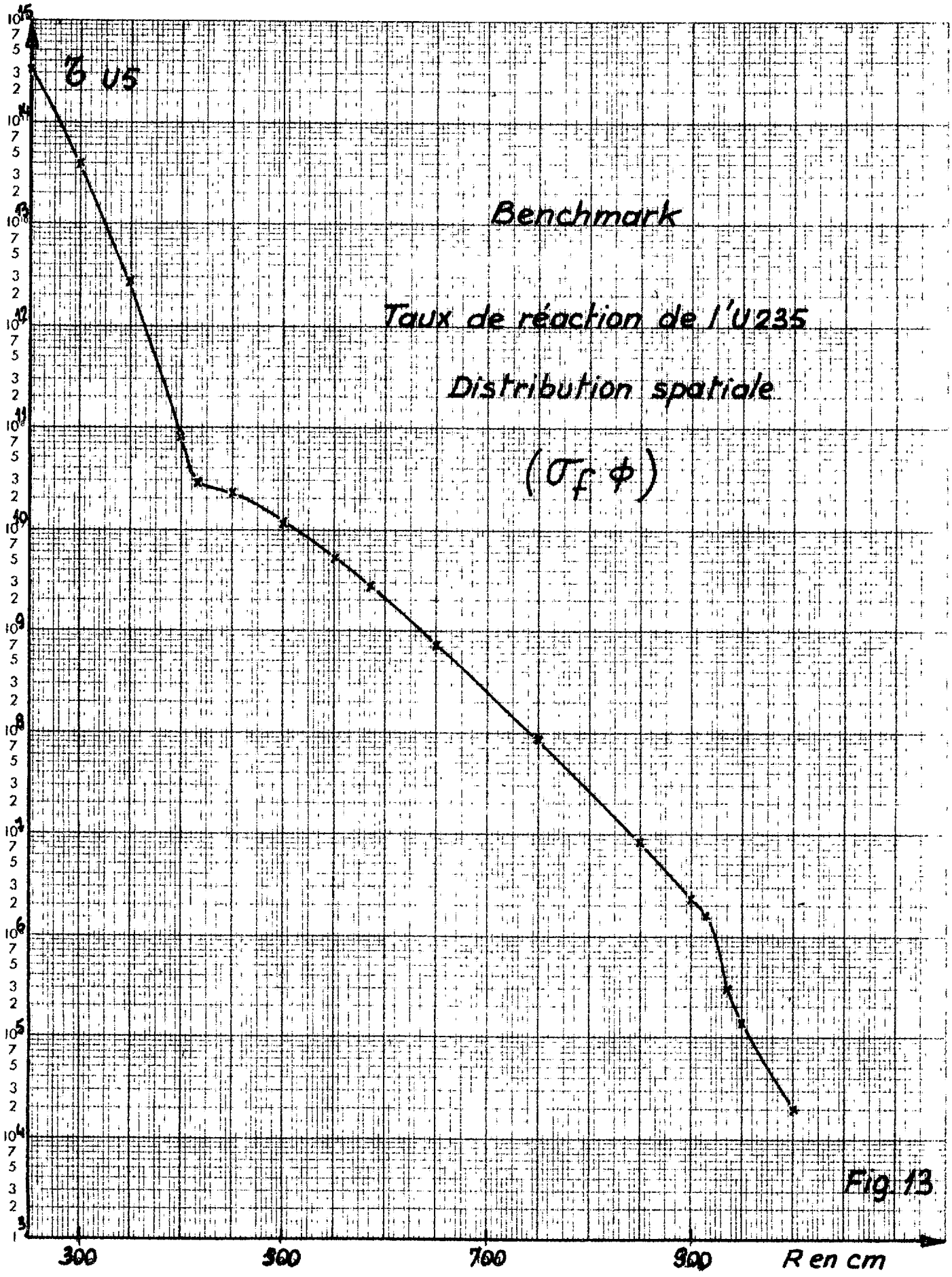
Benchmark
Taux de réaction de l'U235
Distribution spatiale
$(\sigma_f \phi)$
R en cm

Fig. 13

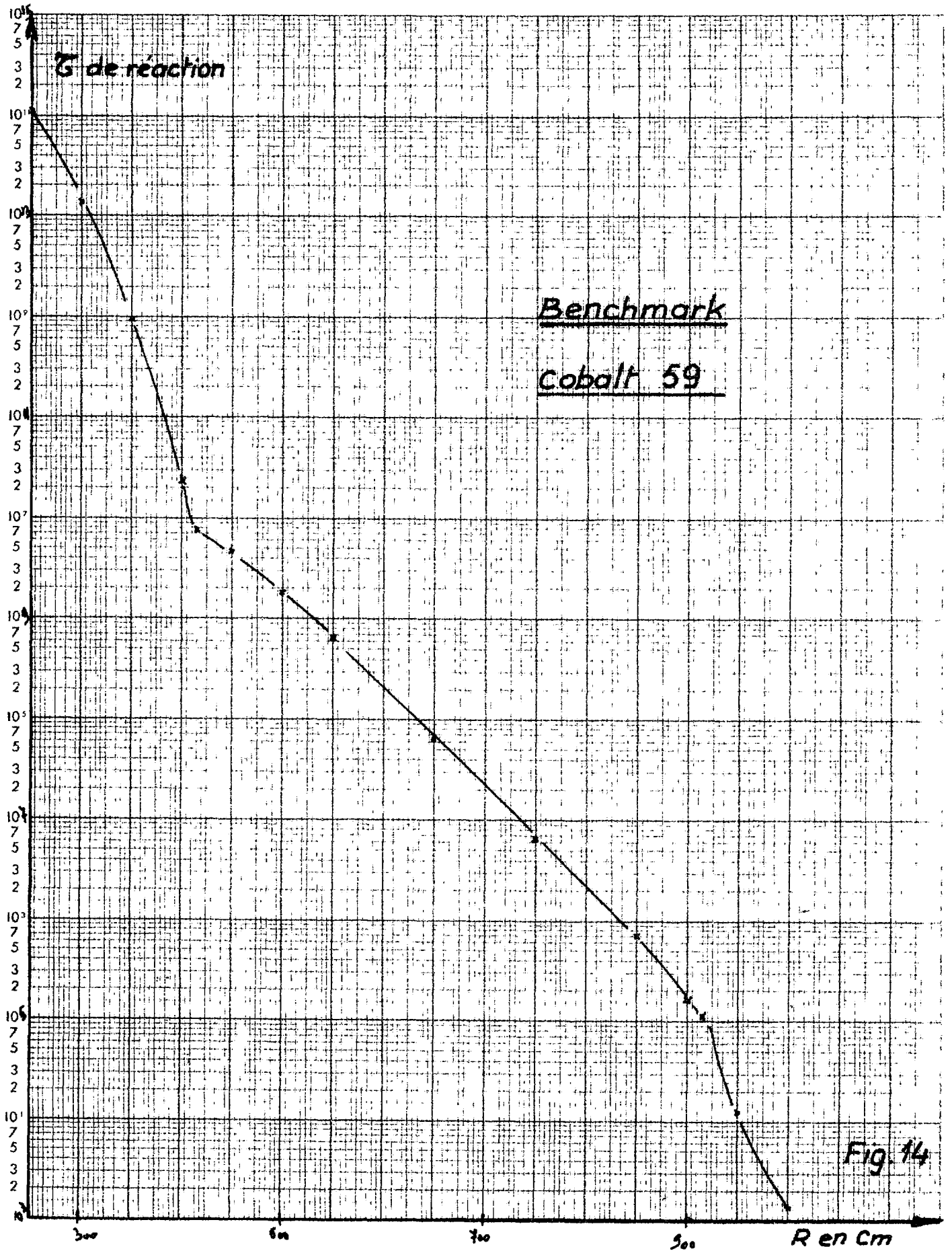

Fig. 14

SESSION C

APPLICATION OF SENSITIVITY AND UNCERTAINTY ANALYSIS TO DESIGN SITUATIONS: FISSION AND FUSION REACTOR SYSTEMS

ETUDE SPATIO ENERGETIQUE DE LA SENSIBILITE DU FLUX THERMIQUE EQUIVALENT SUR L'ECHANGEUR DANS UN CAS TYPE DE REACTEUR RAPIDE REFROIDI AU SODIUM (1ère PARTIE)

* A. BOIOLI - L. FIORINI* - J. MOREAU** - G. SUNTINGER**

* NIRA

** CEA Cadarache

Résumé :

Ce papier se rapporte à la rubrique 2-1 du Programme.

L'objet essentiel des protections intégrées d'un réacteur rapide refroidi au sodium étant de limiter la valeur du flux thermique équivalent sur l'échangeur, l'étude de la sensibilité du flux thermique équivalent à divers paramètres permet une approche méthodique de l'optimisation des protections.

La communication présentée porte sur la première partie d'une étude dont les traits essentiels sont les suivants :

1) Sensibilité du flux thermique équivalent sur l'échangeur au spectre des neutrons fuyant la couverture radiale, et à la distribution spatiale des sources dans la couverture.

2) Efficacité spatio-énergétique de l'acier inox, sensibilité du flux thermique équivalent aux sections efficaces des mélanges acier sodium - profils de sensibilités.

La première partie de l'étude présentée est relative au réacteur SUPER PHENIX dont la protection latérale est constituée par un mélange acier Na de composition (Inox 53 % Na 47 % en volume).

La méthode de calcul est constituée par la résolution monodimensionnelle de l'équation de transport sous ses formes directe et adjointe, à l'aide du code ANISN.

Les calculs sont faits avec les paramètres suivants :

Découpage en énergie 100 g - Bibliothèque DCC2 extraite de ENDFB, 16 directions angulaires (Gauss Legendre sphérique) développement à l'ordre 3 des sections efficaces.

L'étude présentée met en évidence, notamment, la grande sensibilité du flux thermique à la distribution spatio-énergétique des sources dans la couverture, en particulier à la périphérie.

I - INTRODUCTION

Le calcul de la pénétration profonde des neutrons est essentiellement basé sur la résolution de l'équation de transport sous sa forme directe ; cependant l'étude de la sensibilité d'une grandeur intégrale par des méthodes basées sur l'équation de transport adjointe permet de mettre en évidence avec une grande économie de moyens certains paramètres auxquels les résultats sont sensibles. Le calcul du flux thermique équivalent ($\int \frac{\sqrt{E_0}}{\sqrt{E}} \varphi(E)\, dE$) sur l'échangeur intermédiaire d'un réacteur rapide refroidi au sodium étant le problème essentiel du calcul de protection on a étudié la sensibilité de ce flux aux sources de fission dans la couverture.

II - GEOMETRIE DU PROBLEME ETUDIE

Les calculs effectués en géométrie sphérique sont relatifs à la pénétration profonde des neutrons suivant une traverse radiale du réacteur Super Phénix au niveau du plan médian du coeur.

On rencontre successivement le coeur 186.5 cm, la couverture 50 cm, la protection latérale 180 cm (53%/INOX 47% Na), le sodium 220cm et l'échangeur. La grandeur étudiée est le flux thermique équivalent à l'entrée de l'échangeur.

III - METHODE DE CALCUL

Les calculs effectués reposent essentiellement sur les propriétés des flux directs et adjoints qui apparaissent dans la relation générale de réciprocité explicitée ci-dessous.

La relation générale de réciprocité pour les fonctions de green peut s'écrire

(1)

$$\varphi(r_1, E_1, \Omega_1 ; r_0, E_0 \Omega_0) = \varphi^+(r_0, E_0, \Omega_0 ; r_1, E_1, \Omega_1)$$

avec

φ flux direct en $r_1, E_1 \Omega_1$ du à la source r_0, E_0, Ω_0 (fonction de green normale).

φ^+ flux adjoint en r_0, E_0, Ω_0 .du à la source $r_1, E_1 \Omega_1$ (fonction de green pour l'équation adjointe).

Si on considère un domaine $\mathcal{U}$, limité par une surface A la relation de réciprocité s'applique en tout point de $\mathcal{U}$ et de sa frontière si les conditions imposées sur la frontière dans le cas direct et adjoint sont cohérentes entre elles* (ce que l'on supposera toujours par la suite)

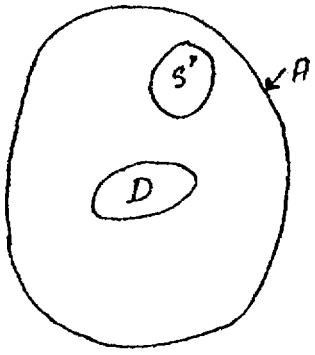

Soit à calculer la grandeur intégrale

$$I = \int R(E,\Omega,r)\, \varphi(r,E,\Omega ; r',E',\Omega')\, S(r',E',\Omega')\, dr'\, dE'\, d\Omega'\, dr\, dE\, d\Omega$$

avec les notations suivantes

$S(r',E',\Omega')$ source définie dans $S' \in \mathcal{U}$

$R(E,\Omega,r)$ réponse définie dans $\mathcal{D} \in \mathcal{U}$

On a la relation d'identité

$$I \equiv \int R(E,\Omega,r)\ \varphi^+(r',E',\Omega';\ E r,\Omega)\ S(r'E'\Omega')\ \underline{d}r'dE'd\Omega'\underline{d}r\,dE\,d\Omega$$

qui résulte de l'application de la relation de réciprocité (1)

Les équations 2 et 3 s'écrivent sous une forme explicite qui représente le mode habituel de résolution.

En effet dans le cas direct on a

$$I = \int \varphi(r,E\Omega)\ R(r,E\Omega)\ \underline{d}r\,dE\,d\Omega \qquad (4)$$

avec

$$\varphi(r,E,\Omega) = \int \varphi(r,E\Omega\,;\,E',r'\Omega')\ S(E',r',\Omega')\ \underline{d}r'\,dE'\,d\Omega' \qquad (5)$$

* exemple de conditions à la limite cohérentes :

$\varphi(r_A,E\Omega_A)=0$, $\vec{\Omega}_A.\vec{n}<0$ flux rentrant nul cas direct avec vide à l'extérieur

$\varphi^+(r_A,E,\Omega_A)=\ .\vec{\Omega}_A.\vec{n}>0$ cas adjoint équivalent

dans le cas adjoint on a

$$I = \int \varphi^+(r',E',\Omega')\ S(r',E',\Omega')\ \underline{d}r'\,dE'\,d\Omega' \qquad (6)$$

avec

$$\varphi^+(r',E',\Omega') = \int \varphi(r',E',\Omega';\ r,E,\Omega)\ R(E,R,\Omega)\ \underline{d}r\,dE\,d\Omega \qquad (7)$$

l'examen des équations 4-5-6-7 met en évidence les conclusions suivantes :

La résolution du problème direct comporte 2 étapes

a) intégration de la fonction de green sur le volume source $S(r',E',\Omega')$ et sur l'espace des phases (équation 5) c'est à dire la résolution de l'équation de transport direct dans laquelle $S(r',E',\Omega')$ est la source extérieure.

b) Calcul de la réponse pour une intégrale banale dont la valeur ne dépend que de la réponse. De même la résolution du problème adjoint comporte 2 étapes

a) intégration de la fonction de green adjointe dans le domaine $\mathcal{D}$ de la fonction de la réponse $R(E,r,\Omega)$ et dans l'espace des phases, c'est à dire la résolution de l'équation de transport adjointe dans laquelle $R(E,\Omega,r)$ définie dans $\mathcal{D}$ est la source extérieure.

b) le calcul de l'intégrale du flux adjoint sur le volume source $S'(r',E',\Omega')$ et sur l'espace des phases ; la valeur de cette intégrale ne dépend que de la valeur de $S(r',E',\Omega')$

Dans le cas de l'étude considérée les calculs se réduisent au formalisme suivant :

Calcul direct

$$\varphi^{th}_{(n_0)} = \int_{E_0}^{14\,MeV} \varphi^{\gamma}_{n_0}(E)\, \frac{\sqrt{E_0}}{\sqrt{E}}\, dE$$

$\varphi_{n_0}(E)$ flux à l'entrée de l'échangeur résultant d'un calcul direct avec sources extérieures de fission

$\varphi^{th}_{n}(n_0)$ flux thermique équivalent sur l'échangeur

Calcul adjoint

$$\varphi^{th}_{(n_0)} = \frac{1}{\Delta V} \iiint \varphi^{*}(E,r)\, S(r)\, \chi(E)\, dE\, dr$$

avec $\varphi^{*}(E,r)$ flux adjoint résultant d'un calcul adjoint ayant pour source $\frac{\sqrt{E_0}}{\sqrt{E}}$ à l'entrée de l'échangeur.

ΔV volume source

$S(r)$ distribution spatiale des sources

$\chi(E)$ spectre de fission associé à la zone source considérée

Tous les calculs ont été effectués avec ANISN. Les paramètres retenus sont les suivants :

- découpage en énergie 100 groupes bibliothèque DLC 2 extrait de ENDFB III

- découpage angulaire S16 Gauss Legendre developpement des sections efficaces à l'ordre 3 en polynomes de Legendre

IV - RESULTATS

IV a) - Calcul direct

La figure (2) comportant une traverse radiale de flux depuis le centre du coeur jusqu'à l'échangeur, avec contribution séparée des sources de fissions dans la couverture radiale, met en évidence la contribution très importante de la couverture.

IV b) - Calculs adjoints

L'examen de l'intégrale

$$\varphi^{H}_{n_0}(\epsilon) = \int_{\epsilon_0}^{14\,Mev} \int_{r_1}^{r_2} S(\epsilon) \cdot \chi(\epsilon) \cdot \varphi^{*}(E, r)\, dr\, d\epsilon$$

représentée sur les figures 3 et 4 met en évidence un certain nombre de résultats.

IV b-1 - Influence de l'energie des neutrons

Seuls les neutrons d'énergie supérieure à 1 Mev contribuent à la valeur du flux sur l'échangeur. la contribution des neutrons d'énergie supérieure à 4 Mev décroit très rapidement. Ces résultats sont confirmés par l'examen du spectre $J_E^{*} \varphi^{*}(\epsilon)$ de la sensibilité du flux thermique équivalent aux neutrons fuyant de la couverture (figure 5).

IV b-2 - Importance spatiale des sources

L'importance spatiale des sources diminue très rapidement à mesure que l'on s'éloigne (vers le centre du réacteur) de la surface externe des milieux sources. Ce résultat apparait sur les figures 3 et 4 ou les contributions des couvertures 1,2,3 sont rapidement croissantes. La variation spatiale, sensiblement exponentielle du flux adjoint figure (6), traduit à un effet de spectre près (dû à la variation du spectre du flux adjoint) la variation de l'importance spatiale des sources. On peut noter que cette importance diminue d'un facteur 200 environ à la traversée des 50 cm de couverture.

A l'intérieur d'une zone source la distribution spatiale des sources est un paramètre très sensible comme l'indique la pente du flux adjoint.

On a calculé (figure 7) la sensibilité du flux thermique équivalent sur l'échangeur à la distribution des sources dans une couverture avec les hypothèses suivantes : distribution exponentielle à pente variable, intégrale en volume constante.

Il résulte de ce fait que les calculs d'évolution qui ne respectent pas la distribution spatiale des sources dans la couverture peuvent conduire à surestimer la contribution de ces sources au flux thermique sur l'échangeur.

IV-b-3 - Influence de l'évolution des couvertures

L'évolution des couvertures avec le temps a une incidence considérable sur le flux thermique équivalent au niveau de l'échangeur (voir figures 3 et 4). Ce résultat est résumé dans le tableau ci-après :

Influence de l'évolution des couvertures sur le flux thermique équivalent au niveau de l'échangeur

		Source Coeur	Source Coeur + Couverture
début de vie	0.157	0.10	0.24
fin de vie	0.90	0.10	1*

Les valeurs relatives sont normées à 1 pour la valeur nominale de fin de vie qui conditionne les protections.

IV b-4 - Influence des spectres de fission

Les spectres de fission utilisés sont calculés suivant les formules de Watt CRAMBERG.

$$\chi(E) = \frac{\exp(-E_F/T)\,\exp(-E/T)\,\sinh\left(\frac{2}{T}\sqrt{E E_F}\right)}{\sqrt{\pi E_F T}}$$

avec

T = température de Watt

E_F = 0.533 d'où $\bar{E} = \frac{3}{2} T + EF$

on a adopté les valeurs suivantes extraites de CARNAVAL III

U238 et U235	T = 0.965 Mev	($\bar{E}$ = 1.98 Mev)
Pu239	T = 1.044 Mev	($\bar{E}$ = 2.1 Mev)

tous les calculs ont été effectués avec les spectres des mélanges U5 U8 - Pu9 de chaque zone.

L'utilisation du spectre de Pu 239 majore les résultats de 3 % l'utilisation du spectre de fission de l'U5 minore les résultats de 5 %.

CONCLUSION

La connaissance précise des taux de fissions dans les couvertures revet une grande importance du point de vue de la précision des calculs de protection. En particulier les incertitudes sur la distribution spatiale des sources (formation du Pu 239 dans les couvertures) peuvent introduire des erreurs importantes sur le flux au niveau de l'échangeur. D'autre part le fait que les neutrons d'énergie supérieurs à 1Mev ont une contribution dominante ($>$ 95 %) met en évidence l'importance des sections efficaces inélastiques de l'acier INOX et de l'anisotropie des chocs dans le calcul de la pénétration profonde des neutrons.

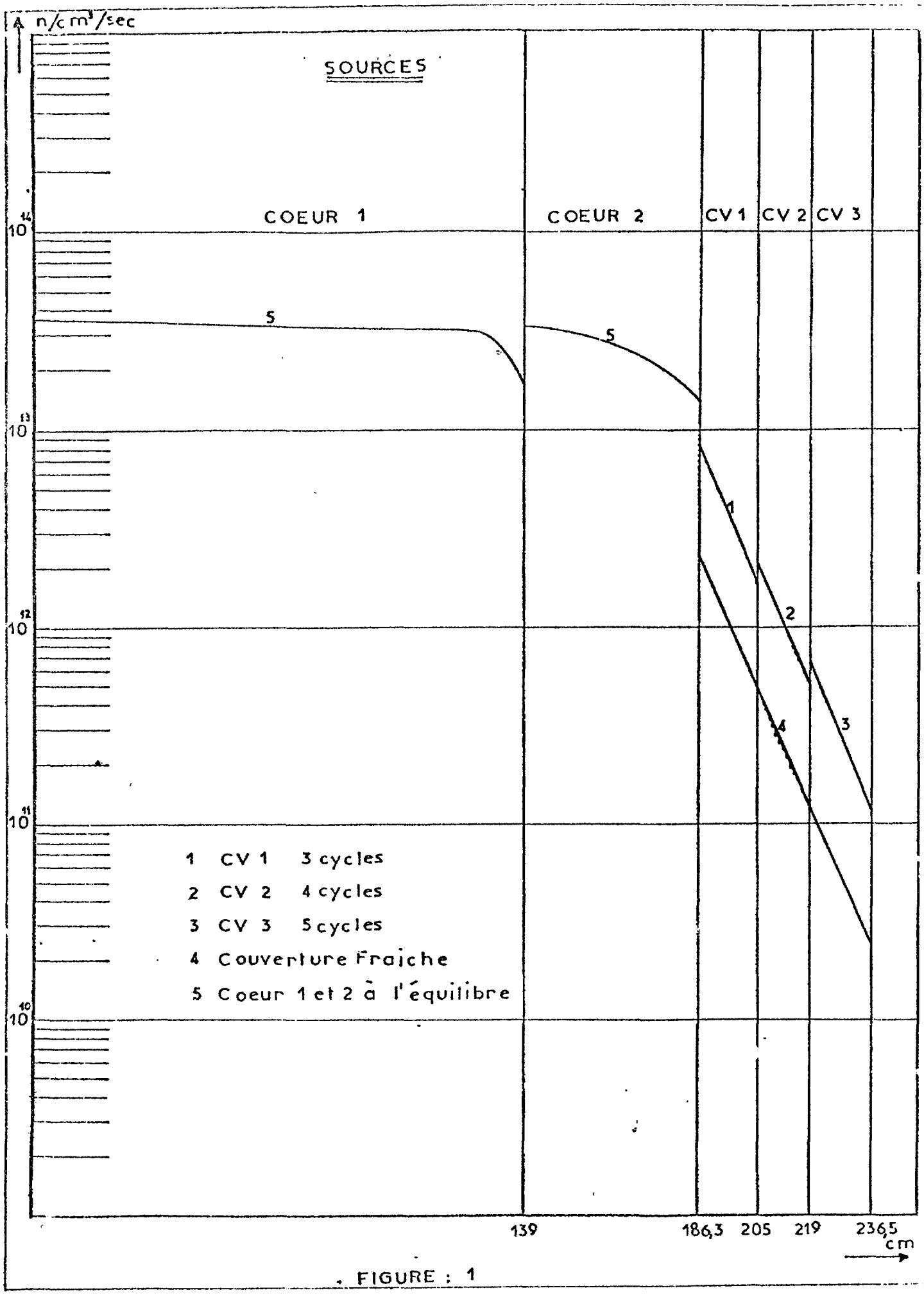
n/cm³/sec
SOURCES
COEUR 1
COEUR 2
CV 1
CV 2
CV 3
10¹⁴
10¹³
10¹²
10¹¹
10¹⁰
5
5
1
2
3
4
1 CV 1 3 cycles
2 CV 2 4 cycles
3 CV 3 5 cycles
4 Couverture Fraiche
5 Coeur 1 et 2 à l'équilibre
139
186,3
205
219
236,5
cm

FIGURE : 1

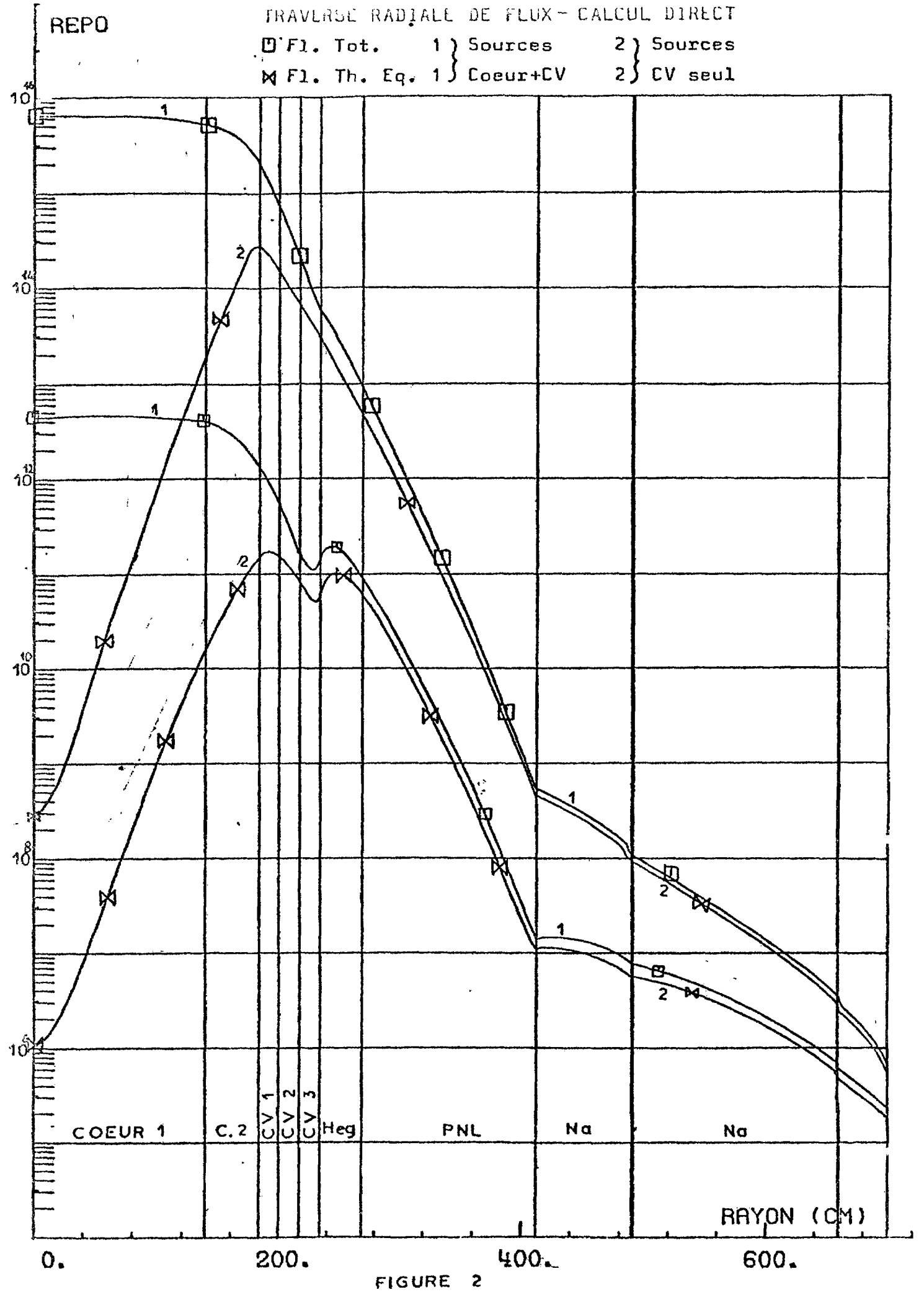
REPO
TRAVERSE RADIALE DE FLUX - CALCUL DIRECT
Fl. Tot. 1 } Sources 2 } Sources
Fl. Th. Eq. 1 } Coeur+CV 2 } CV seul
10^14
10^12
10^10
10^8
10^6
1
2
COEUR 1
C.2
CV 1
CV 2
CV 3
Heg
PNL
Na
Na
RAYON (CM)
0.
200.
400.
600.

FIGURE 2

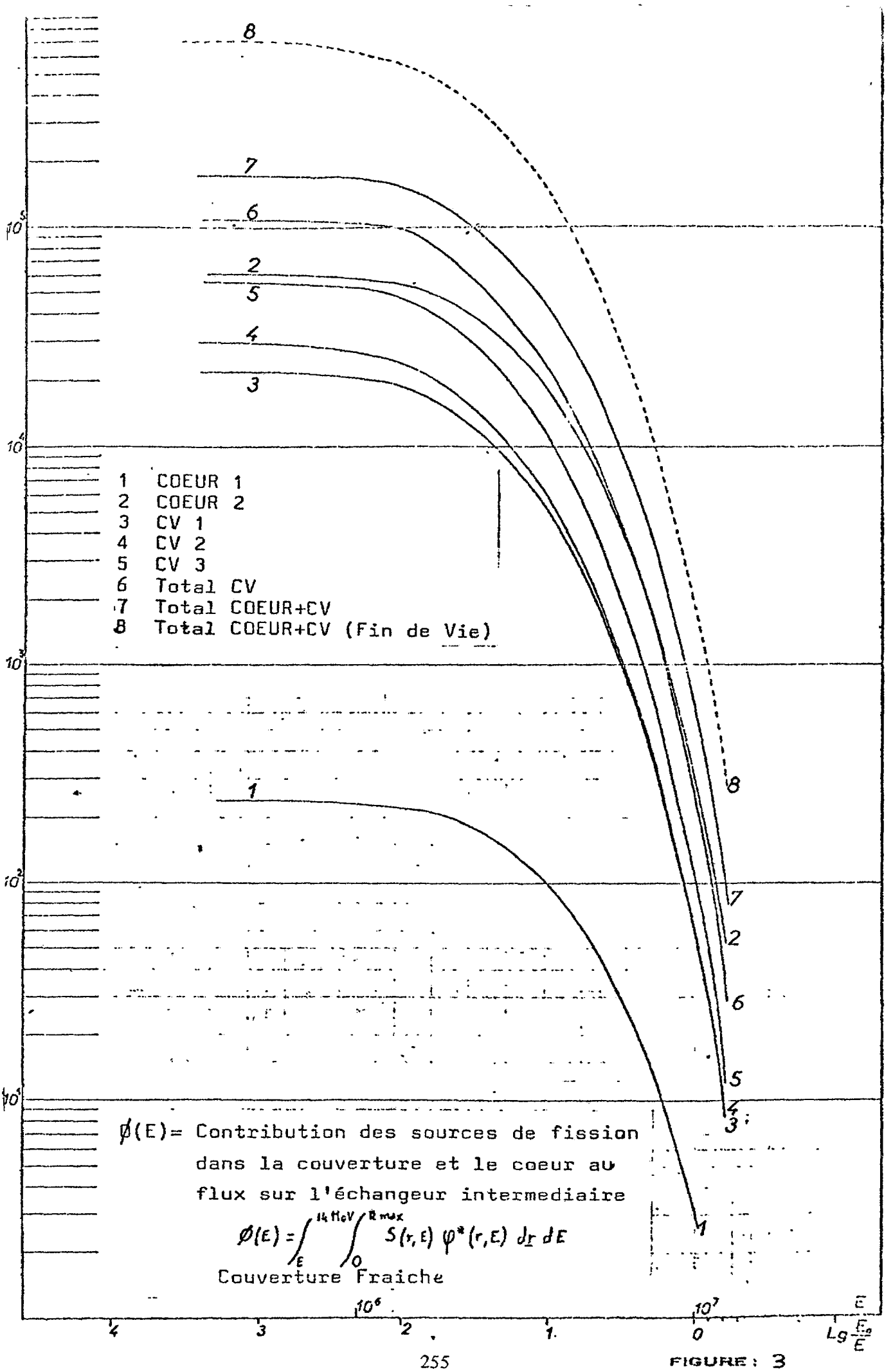
1 COEUR 1
2 COEUR 2
3 CV 1
4 CV 2
5 CV 3
6 Total CV
7 Total COEUR+CV
8 Total COEUR+CV (Fin de Vie)
$\phi(E)$= Contribution des sources de fission dans la couverture et le coeur au flux sur l'échangeur intermediaire
$\phi(E) = \int_E^{14\,MeV} \int_0^{R\,max} S(r,E)\,\varphi^*(r,E)\,dr\,dE$
Couverture Fraiche
10^6
10^7
E
$Lg \frac{E_o}{E}$

FIGURE : 3

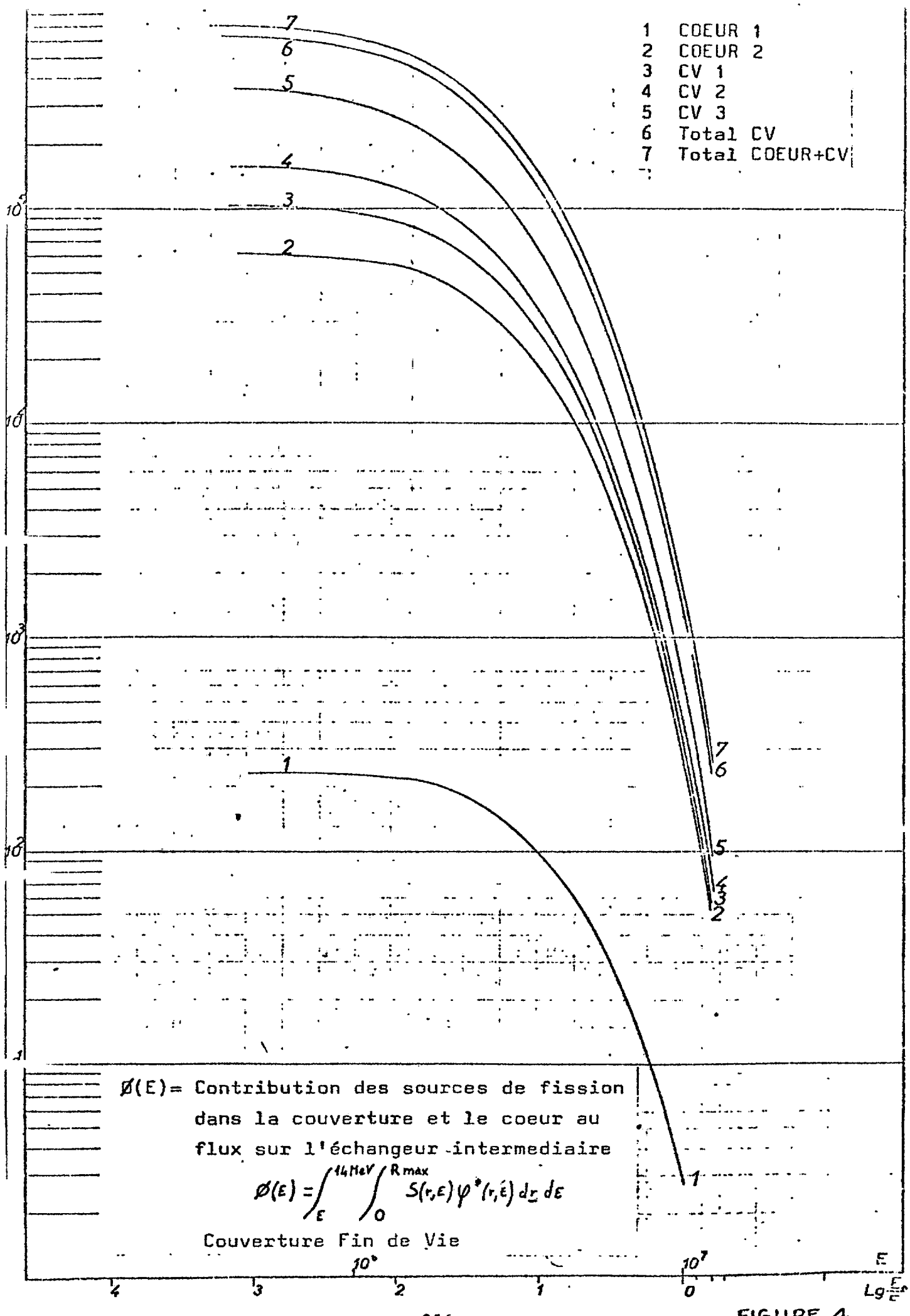

$\phi(E)$= Contribution des sources de fission dans la couverture et le coeur au flux sur l'échangeur intermediaire

$$\phi(E) = \int_{E}^{14\,MeV} \int_{0}^{R\,max} S(r,\varepsilon)\,\varphi^{*}(r,\varepsilon)\,dr\,d\varepsilon$$

Couverture Fin de Vie

FIGURE 4

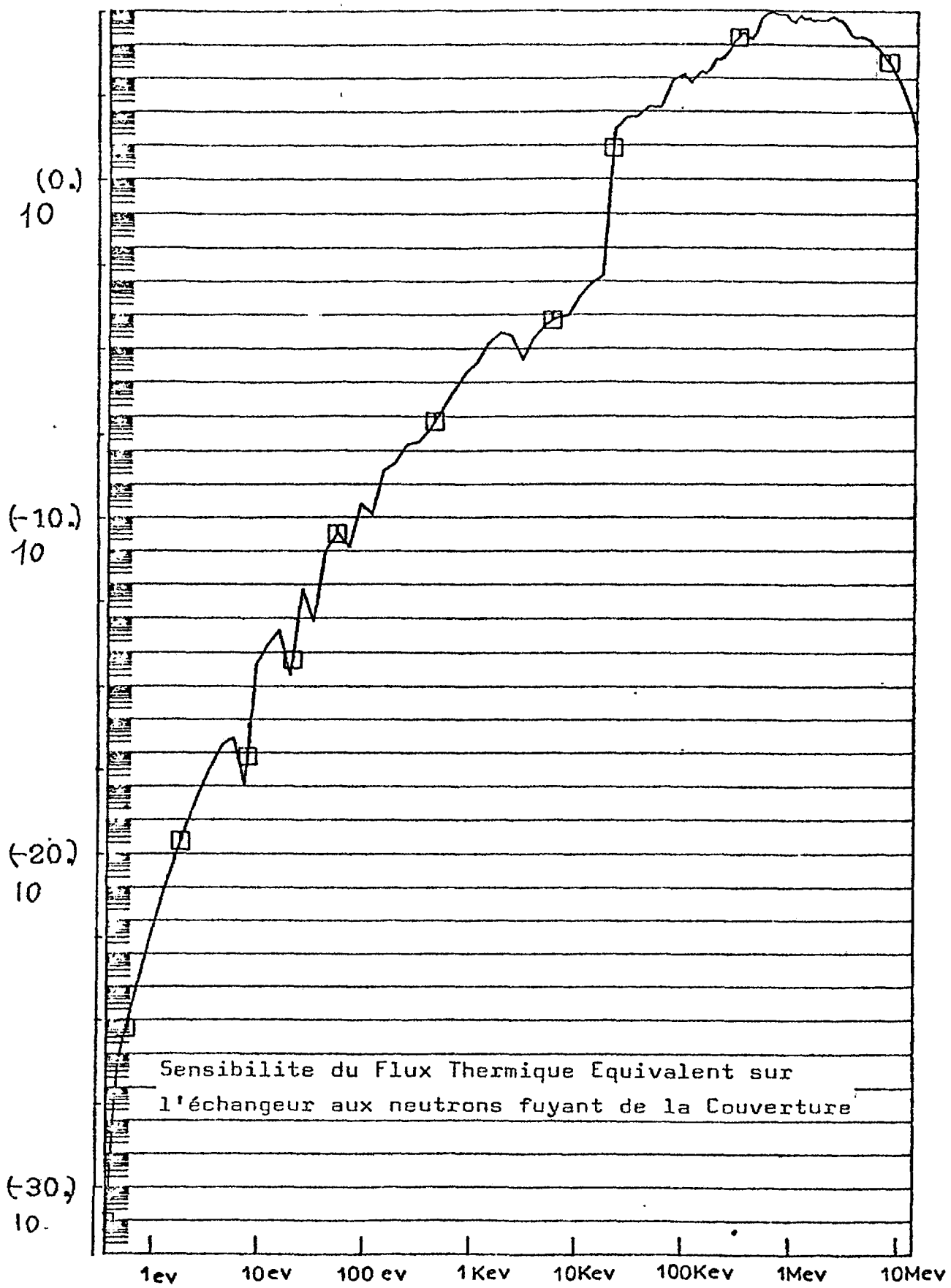
(0.)
10
(-10.)
10
(-20.)
10
(-30.)
10.
Sensibilite du Flux Thermique Equivalent sur
l'échangeur aux neutrons fuyant de la Couverture
1ev
10ev
100 ev
1Kev
10Kev
100Kev
1Mev
10Mev

FIGURE: 5

TRAVERSE RADIALE DU FLUX ADJOINT

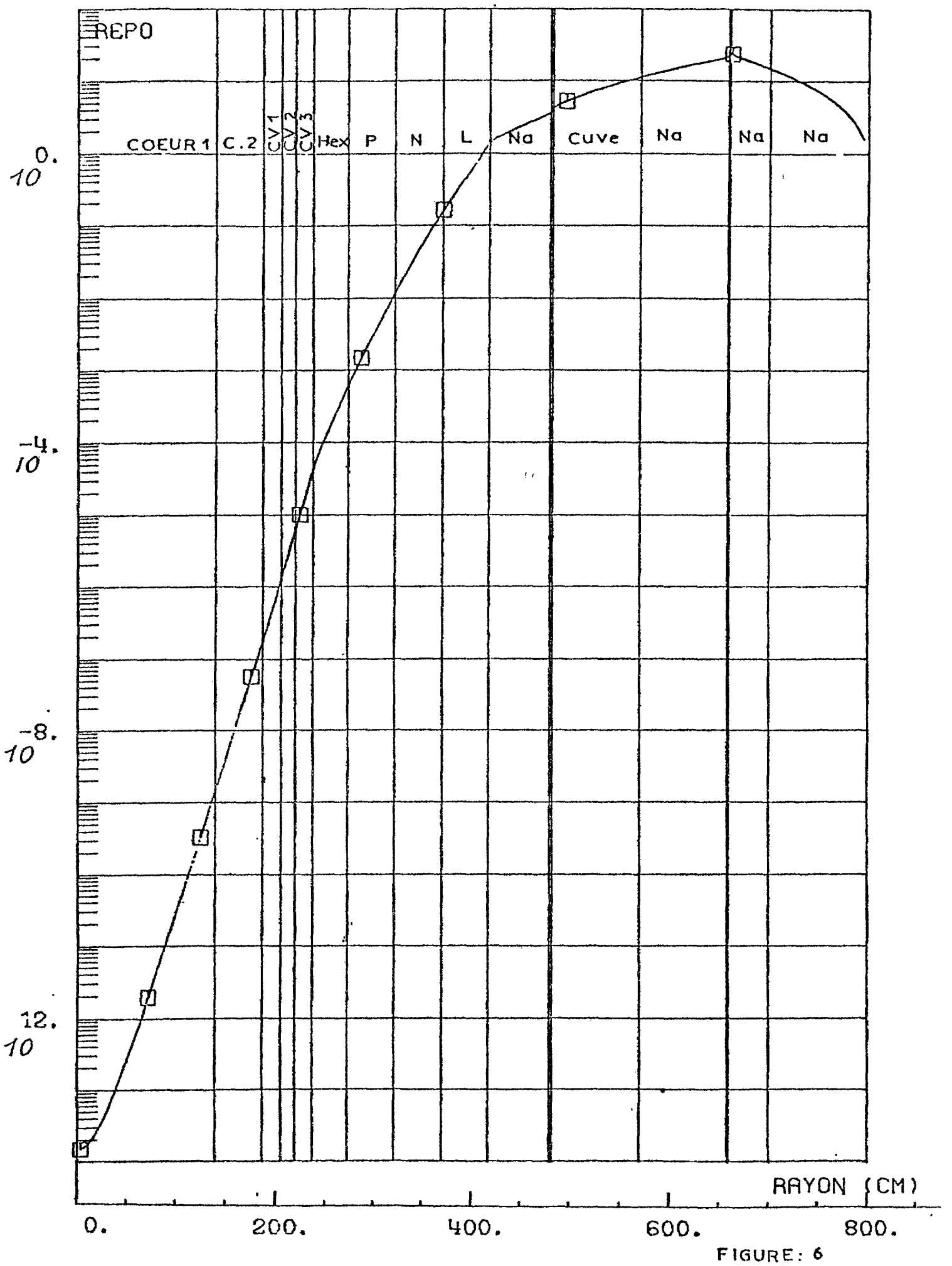

FIGURE: 6

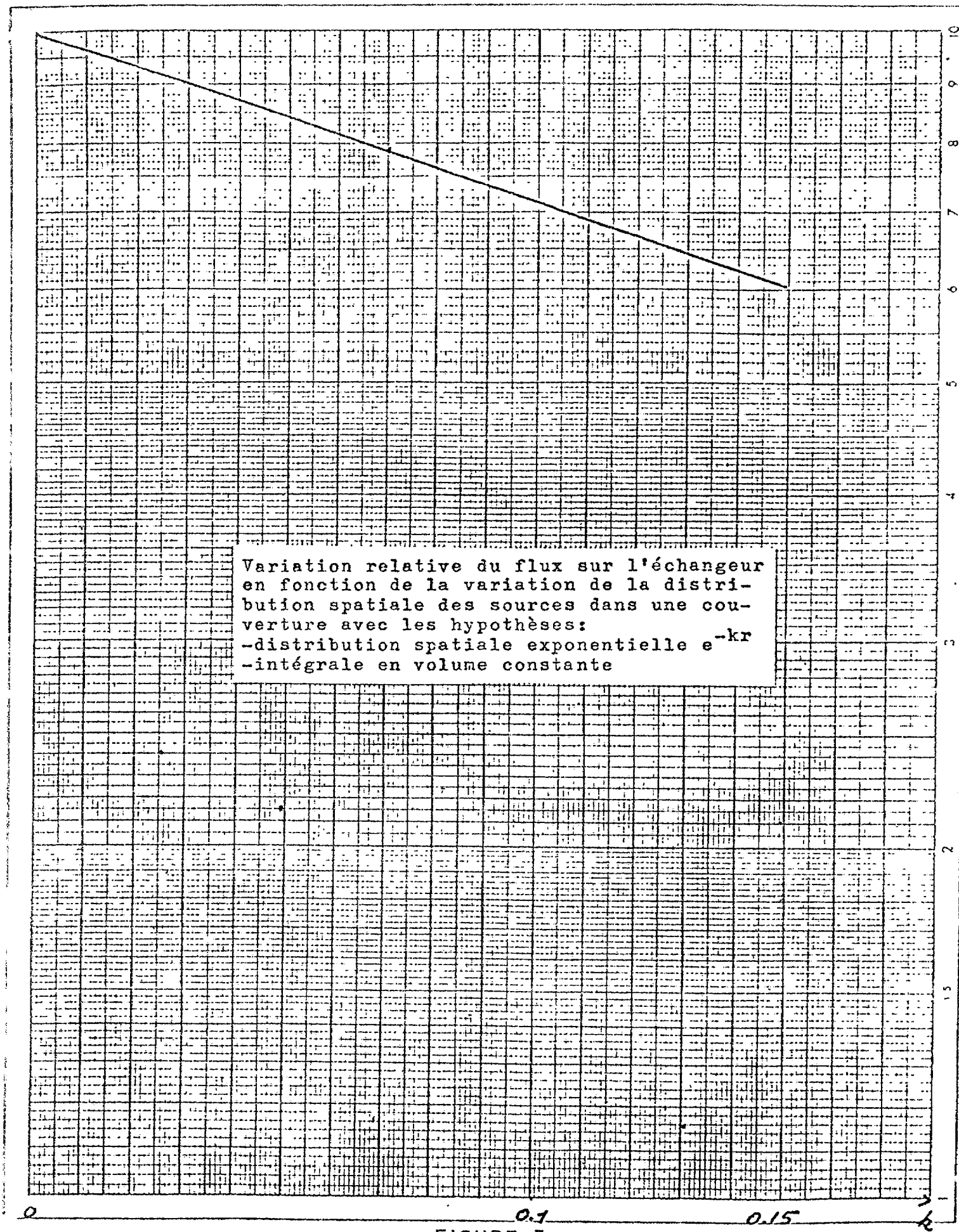
Variation relative du flux sur l'échangeur en fonction de la variation de la distribution spatiale des sources dans une couverture avec les hypothèses:
-distribution spatiale exponentielle e^{-kr}
-intégrale en volume constante
0
0.1
0.15
k

FIGURE: 7

RECENT PROGRESS AT ORNL IN DETERMINING NUCLEAR DATA REQUIREMENTS FOR FAST REACTOR SHIELD DESIGN USING ADVANCED SENSITIVITY TECHNIQUES*

E. M. Oblow and C. R. Weisbin

Oak Ridge National Laboratory
Oak Ridge, Tennessee 37830
USA

A study was made of the adequacy of current sodium and iron data files for fast reactor shield design work. Experimental data from seven fast reactor shield configurations containing large thicknesses of steel, sodium, and iron were analyzed with discrete ordinates calculations and sensitivity methods to determine the data needs. Included in the sensitivity effort were the results of the new developments in "channel theory" and the cross section adjustment algorithms added to the FORSS code system. Conclusions were drawn about the need for more accurate data for sodium and iron elastic and discrete inelastic cross sections from 1 to 5 MeV and the values of the total cross section in the vicinity of important minima.

*Research performed at Oak Ridge National Laboratory for Union Carbide Corp. under contract with U.S. Energy Research and Development Administration.

I. Introduction

For the past five years, a sizeable effort has been mounted at ORNL to develop the sensitivity methodology needed to address a wide range of cross section data problems in fast reactor core and shield design. Considerable progress was made early in the program in developing the methodology. More recently a large scale sensitivity code development effort has been pursued, as was reported in the Sensitivity Specialist's Meeting[1] in Paris last year. With most of the computational tools now available for more routine use at ORNL, a core physics and shielding benchmark integral experiment analysis program has begun. The philosophy guiding these studies is to try to incorporate the results of both integral and differential measurements of basic nuclear data into a data and methods testing program. Results from this effort will be used to quantitatively assess reactor design uncertainties and guide future methods development and data measurement programs.

For the purposes of this paper, a complete study was made of a series of integral experiments on a fast reactor shield mockup to determine the adequacy of the ENDF/B-IV nuclear data files for sodium and iron. Because of the short time intervening between the Paris and Vienna meetings, this course was felt to be a more productive use of the methods and data available at ORNL than the analysis of a hypothetical reactor shielding benchmark problem. In the past year, an extensive series of integral measurements on a steel-sodium-iron fast reactor shield were performed at the Tower Shielding Facility at ORNL and subsequently analyzed.[2] This information, together with the data from other recent experiments and preliminary ENDF/B error files, made it feasible to evaluate the adequacy of iron and sodium cross section data at this time.

In the course of analyzing the TSF experiments, several new additions to the FORSS[3] code system were implemented and tested. These developments are significant enough to also be reviewed briefly in this paper. Under the heading of new methodology, a procedure for combining integral and differential data (i.e., a cross section "adjustment" scheme) based on the methodology proposed by Gandini[4] has been implemented. A new analytical technique for better understanding transport processes, called "channel theory,"[5] has also been developed. In the area of data improvements, a preliminary attempt was made to evaluate ENDF/B-format uncertainty files for both sodium and iron. All these new developments were employed in analyzing the TSF experimental data and each contributed significantly to the results to be presented in the following sections.

II. Description of TSF Experiments and Sensitivity Results

A brief description of the TSF experiments, suitable for discussion purposes, is presented in Fig. 1 and Table I. More complete information will be published in a forthcoming ORNL report and will be presented at the International Shielding Meeting in 1977. The basic materials and geometry shown in Fig. 1 were used to create a dozen or more deep penetration experimental configurations for the measurements. Table I shows the seven particular arrangements used as the basis for the present study. In all the configurations a 4-in. Bonner ball neutron detector (similar in response to a total flux detector in the energy range from 1 eV to 1 MeV) was used to measure the penetration of neutrons from a fission-like source spectrum through thick layers of steel, sodium, and iron. The measurements were made in successive stages as the shield was built up to the full configuration shown in Fig. 1.

The experiments were analyzed by R. E. Maerker using a 51-group cross section library and the two-dimensional discrete ordinates code DOT. These results were corrected with one-dimensional ANISN calculations using a 171-group ENDF/B-IV cross section library to take into account important cross section effects not treated properly in the 51-group calculations. Results of the analysis are given in Table I as ratios of the calculated-to-measured Bonner ball responses. A full one-dimensional sensitivity analysis was also performed, using a 128-group cross section set specifically chosen for this study.

A representative sampling of the sensitivity results for sodium and iron cross sections in two of the seven configurations is shown in Figs. 2 and 3. These curves show clearly that the total sensitivity of the Bonner ball responses to these data is very high (ranging from 1 to 18) and covers a wide range of neutron energies from 1 eV to 10 MeV. Special note should be made of the regions of unusually high sensitivity in the vicinity of the 300 keV and 500 keV sodium total cross section minima (see Fig. 2b) and the 24 keV iron minima (see Fig. 2c). The data in these regions play a large role in determining the overall neutron transmission through these shield systems and are projected to be important for future design work. Obtaining high sensitivity to such a wide range of nuclear data is an essential goal of the data testing program, since high accuracy integral measurements are then certain to contribute a significant amount of information about the adequacy of the cross section data for design work.

III. Channel Theory Analysis

It is useful at this point to digress from the main discussion for a moment to briefly discuss the development of "channel theory." The concepts of "channels" and "contributons," basic to this theory, were created to better understand radiation penetration mechanisms and data sensitivity. They provide a means of representing the "channels" in space and energy, through which those particles that are eventually detected must pass, as they move from the source to the detector. These detected particles, called "contributons," are really what all measurements deal with and the paths which they take to ultimately penetrate a shield are most important in understanding any shield system. The theory of contributon transport (i.e., channel theory) makes use of the simple fact that forward and adjoint flux calculations can both be used to calculate a detector response. In one case, at the source position, the inner product $\langle \phi^* S \rangle$ gives the response and in the other case, at detector position, the product of $\langle \phi S^* \rangle$ yields the same total response. This fact leads naturally to development of equations for a function representing the detector response along any surface in particle phase space separating the source and the detector. This function, involving products of forward and adjoint fluxes, can then be broken up into two vectors which describe: a) the net spatial current of contributons, K_R, moving from source to detector (spatial streaming channels have high K_R currents) and b) the net slowing down current, K_E, for contributons slowing down in energy at any spatial position (high currents here would indicate slowing down channels). The net current out of any surface surrounding only the source or detector will always be equal to the response since contributons are conserved as they pass from source to detector (i.e., contributons cannot be lost in the transport process). The channel theory equations thus describe the flow of an incompressible fluid in phase space.

Figure 4 shows a representative series of curves of the contributon current, K_R, denoting the spatial channels from source to detector for the deepest penetration TSF experiment. For this case the spatial current as a function of energy E, at each space point x, is related to the response R as:

$$R = \int K_R(x,E)\, dE = \iint \mu\, \phi^*(x,E,\mu)\, \phi(x,E,\mu)\, d\mu\, dE \qquad (1)$$

where μ is the angle between the neutron direction and the x-axis and ϕ and ϕ^* are the forward and adjoint angular fluxes. Note that where the K_R values are large, a great deal of spatial streaming is occurring.

Close examination of these curves reveals that those neutrons that are eventually detected stream through three dominant channels in the steel and sodium parts of the shield (mesh numbers 1-26 and 27-135 respectively in Fig. 4). One channel is at high energies from 2-4 MeV (groups 21-25 in Fig. 4) and the other two are in the vicinity of 300 keV and 500 keV total cross section minima in sodium (corresponding to groups 34 and 40). Both of these latter channels eventually feed a strong channel around the 24 keV (group 65) total cross section minimum in the iron end of the shield. Similar curve for K_E (not shown) show that there are strong slowing down channels in the steel, feeding the 300 keV sodium minimum and in the sodium and iron feeding the 24 keV iron minimum. Such information makes it clear that this particular response at the back of the iron slab is made up of those particles which stream through sodium total cross section minima, into the 24 keV iron minimum, and then slow down in iron before detection. If less material were present between source and detector the picture becomes much different (see the K_R curves for the 6-in. Fe TSF experiment given in Fig. 5). The contributons in this case bypass the total cross section minima channels and primarily elastically slow down in the sodium before they are detected at very low energies. Both figures clearly show the dominant transport process in the system and allow a better understanding to be had of what was measured. Such information coupled with sensitivity profiles, illustrating how these channels are altered by perturbations, give a very clear picture of the transport and slowing down physics of any shield system.

IV. Results of Uncertainty Analysis

With the sensitivity information and an understanding of the channel theory results in hand, FORSS was used to perform an uncertainty analysis of the seven shield configurations described previously. Table II gives the results of this analysis in terms of predicted uncertainties (1σ) for the Bonner ball responses both with and without integral information. The predicted uncertainties using differential cross section data alone are fairly large for the intermediate and deep penetration configurations and indicate that calculating the deep penetration of neutrons in sodium, steel, and iron shields is at best done to within a factor of two when 90% confidence limits are to be achieved. Three important shield design problems which might fall under this heading would be estimations of dose, core barrel damage, and neutron sources for secondary sodium activation calculations. For such problems the results here would indicate that in the absence of better differential cross section data, good integral measurements are needed to achieve design objectives.

Including the integral measurements and reported disagreements between calculated and measured responses in the analysis sheds light on the adequacy of the basic cross section data and the calculational methods. The newly implemented cross section adjustment routines were used in this step primarily as a tool to identify the cross sections and methods most probably responsible for the disagreements found in analysis (i.e., the C/E ratios in Table I). Results of one of several trial "adjustments" are also given in Table II in terms of the most important cross section changes needed to improve the agreement between experiment and calculation. Since the integral results were far less uncertain than the calculated quantities (see Table I), adjustments were made primarily in the sodium and iron data and specifically where the cross sections were most uncertain (i.e., at high energies). It should be noted that the residual in the adjustments were all somewhat larger than expected from statistical considerations alone, indicating that some methods problems might also exist.

One particular feature of the adjustment results which might be attributed to a methods problem is the rather large change in the elastic cross sections for iron and sodium below 1 keV. The elastic cross section is almost constant below 1 keV in sodium and iron and the adjustment in this region most likely represents a need to carefully flux weight the group-to-group transfer cross sections so as to properly balance the within-group and outscatter transfers. These transfer cross sections are primarily responsible for the continuous slowing down channel which occurs in most of the configurations except those characterized by the deepest penetrations.

V. Conclusions

A. Iron Data Needs. From the direct evidence presented by the TSF experimental results only a slight indication is given that significant uncertainties might be present in the nonelastic iron cross section data. Other evidence, derived from pulsed sphere integral experiments,[6] however, support the conclusion that in this energy region it would be most beneficial to remeasure and reevaluate the total inelastic and the first few discrete level inelastic cross sections. The specific problem would appear to be discrepancies in the discrete level inelastic excitation cross sections just above threshold. Evidence from other iron benchmark experiments[7-9] also indicate that discrete inelastic cross sections and statistical fluctuations in the elastic cross section are probably responsible for important discrepancies in the 1 to 4 MeV range. Outstanding problems with gamma-ray production[10] and gamma-heating measurements[11] would also be alleviated by 5 to 10% measurements of the inelastic data from about 1 to 4 MeV.

B. Sodium Data Needs. From the results presented, by far the strongest evidence for remeasurement and reevaluation is indicated for sodium data above 1 MeV. Considerable calculational uncertainty is due to the unacceptably large uncertainties in the sodium elastic and total nonelastic cross sections from 1 to 10 MeV. Measurements in the 5 to 10% range on both of these quantities will be needed if transport in sodium is to be understood well enough for design purposes. Two other key cross sections, the 300 keV and 500 keV total cross section minima, also need improvement if deep penetration problems in steel-sodium shield systems are to be calculated accurately. These two chief space channels for deep penetrations must be known to a few percent. Recent remeasurements[12,13] indicate that ENDF/B-IV data in the vicinity of the 300 keV minimum is off by up to 5% and this fact goes a long way to explain the observed discrepancies in the analysis of the TSF 24-in. Fe experiment.

References

1. E. M. Oblow, "The Sensitivity Analysis Development and Applications Program at ORNL," Proceedings of the Specialist's Meeting on Sensitivity Studies and Shielding Benchmarks, Paris, France (1975).

2. R. E. Maerker and F. J. Muckenthaler, "Measurements and Calculations of Neutron Fluxes Through a Simulation of the CRBR Upper Axial Shielding," Trans. Am. Nuc. Soc., 23, 611 (1976).

3. C. R. Weisbin et al., "Application of FORSS Sensitivity and Uncertainty Methodology to Fast Reactor Benchmark Analysis," ORNL/TM-5563, Oak Ridge National Laboratory (1976).

4. A. Gandini, "Nuclear Data and Integral Measurements for Fast Reactors," RT/F1 Parts 1, 2, and 3, Report from Comitate Nazionali Energia Nucleare, Italy (1973).

5. M. L. Williams and W. W. Engle, Jr., "The Concept of Spatial Channel Theory Applied to Reactor Shielding Analysis," accepted for publication in Nucl. Sci. Eng. (1976); see also, J. H. Marable and E. M. Oblow, "Theory of Contributons," ORNL report to be published (1976).

6. S. N. Cramer and E. M. Oblow, "Analysis of a Neutron Scattering Integral Experiment on Iron for Neutron Energies from 1 to 15 MeV," ORNL/TM-5548, Oak Ridge National Laboratory, to be published (1976).

7. A. M. McCracken and M. J. Grimstone, "Preliminary Analysis of the Winfrith Iron Benchmark Experiment," Proceedings of the Specialist's Meeting on Sensitivity Studies and Shielding Benchmarks, Paris, France (1975).

8. G. Hehn et al., "Calculations for Iron Benchmark Experiments with Californium and 14 MeV Neutron Sources," Proceedings of the Specialist's Meeting on Sensitivity Studies and Shielding Benchmarks, Paris, France (1975).

9. S. Miyasaka et al., "Sensitivity and Uncertainty Analysis for Iron Cross Sections," Proceedings of the Specialist's Meeting on Sensitivity Studies and Shielding Benchmarks, Paris, France (1975).

10. R. E. Maerker and T. J. Burns, "Analysis of TSF Experiments on Radiation Heating in Iron and Stainless Steel CRBR Radial Shield Mockups Using a 15-1/4-in.-Diameter Collimated Beam Source," ORNL/TM-5420, Oak Ridge National Laboratory (1976).

11. R. E. Maerker, "SB3. Experiment on Secondary Gamma-Ray Production Cross Sections Averaged Over a Fast-Neutron Spectrum for Each of 13 Different Elements Plus a Stainless Steel," ORNL/TM-5240, Oak Ridge National Laboratory (1976); see also, J. E. White et al., "Data Testing of the 126/36 Neutron-Gamma ENDF/B-IV Coupled Library for LMFBR Core and Shield Analysis," Trans. Am. Nucl. Soc. 23, 507 (1976).

12. D. Larsen, "Total Cross Section Measurements at ORELA for Sodium," ORNL private communication (1976).

13. R. Block, "Total Cross Section Measurements at RPI Linac for Sodium," private comminication (1976).

Table I. Comparison of Measured and Calculated 4-in. Bonner Ball Counting Rates in counts/min/watt

No.	Configuration[a]	Measured	Estimated Uncertainty (%)	Calc. (5lg) / Meas.	Scaled Calc. (17lg) / Meas.
1	18 in. SS	1.64(4)[b]	10	0.96	1.01
2	18 in. SS + 5 ft Na	9.40(3)	10	0.93	1.12
3	10 in. SS + 10 ft Na	1.62(2)	15	0.85	0.94
4	18 in. SS + 15 ft Na	128(0)	15	0.92	0.75
5	18 in. SS + 15 ft Na + 6 in. Fe	8.00(-3)	20	1.44	0.84
6	18 in. SS + 15 ft Na + 16 in. Fe	2.19(-5)	20	0.61	0.47
7	18 in. SS + 15 ft Na + 24 in. Fe	6.73(-6)	25	0.33	0.52

[a]The measurement and calculation behind the SS configuration were at a centerline point 5.5 ft beyond the SS slabs. All remaining configurations were measured and calculated at a centerline point 2.5 in. beyond the configuration, with lithium hydride backing the detector.

[b]Read as: 1.64×10^{4}.

Table II. Results of Uncertainty Analysis

No.	Configuration	Standard Deviation in Response Due to Nuclear Data Alone (%)	Standard Deviation in Response Including Integral Data (%)
1	Source + 18 in. SS	1.5	1.4
2	Source + 18 in. SS + 5 ft Na	10	3.2
3	Source + 18 in. SS + 10 ft Na	27	5.9
4	Source + 18 in. SS + 15 ft Na	48	11
5	Source + 18 in. SS + 15 ft Na + 6 in. Fe	60	11
6	Source + 18 in. SS + 15 ft Na + 16 in. Fe	64	17
7	Source + 18 in. SS + 15 ft Na + 24 in. Fe	48	21

Major Cross Section Changes (%)

Cross Section	< 1 keV	300 keV	> 1 MeV
Sodium elastic	-3	-5	+13
Sodium nonelastic	-	-	-14
Iron elastic	-6	-	+3
Iron nonelastic	-	-	-4

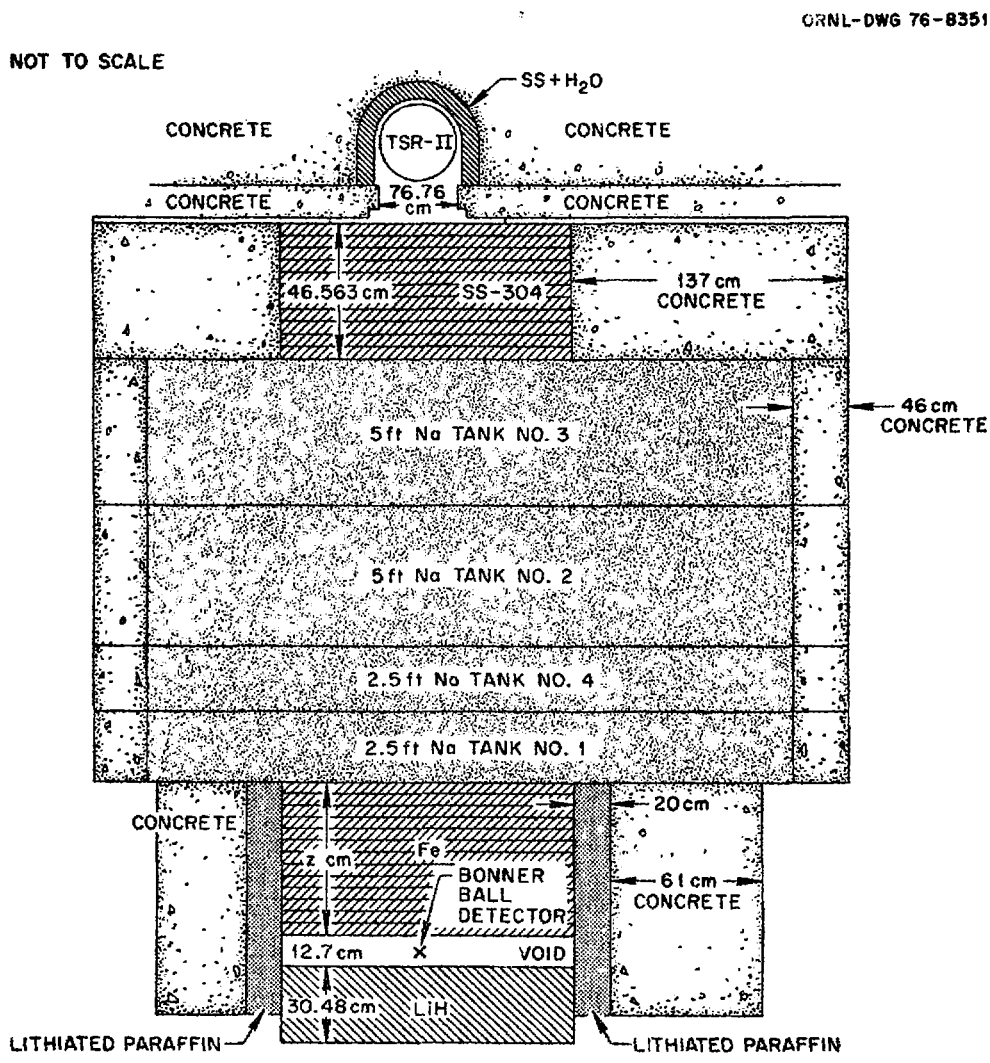

Fig. 1. Experimental Geometry for Measurements Behind 18-in. SS + 15-ft Na + z cm Fe, where $0 \leq Z \leq 32$ inches.

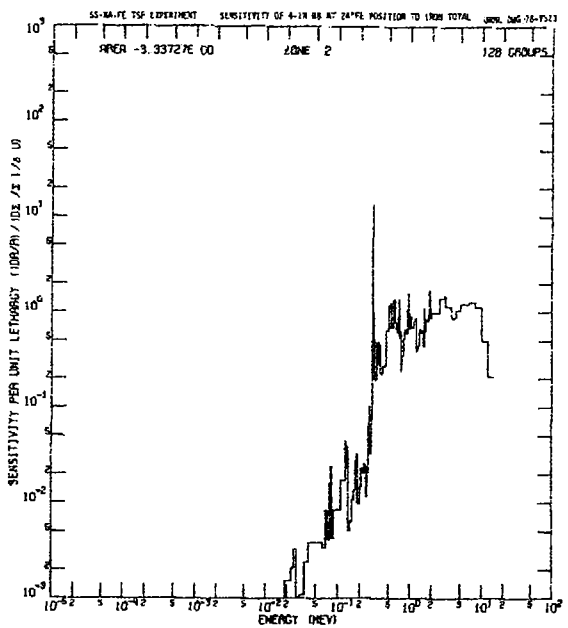

Fig. 2a. Total Iron Cross Section Sensitivity Profile for 18-in. Steel Region of TSF Experimental Configuration #7.

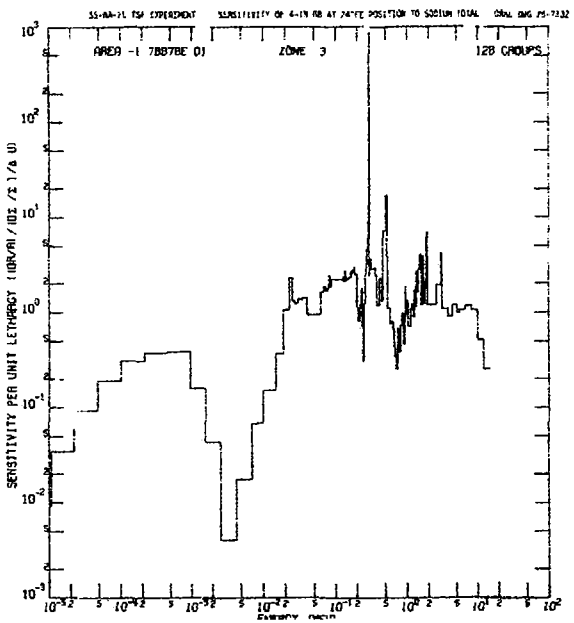

Fig. 2b. Total Sodium Cross Section Sensitivity Profile for 15-ft Sodium Region of TSF Experimental Configuration #7.

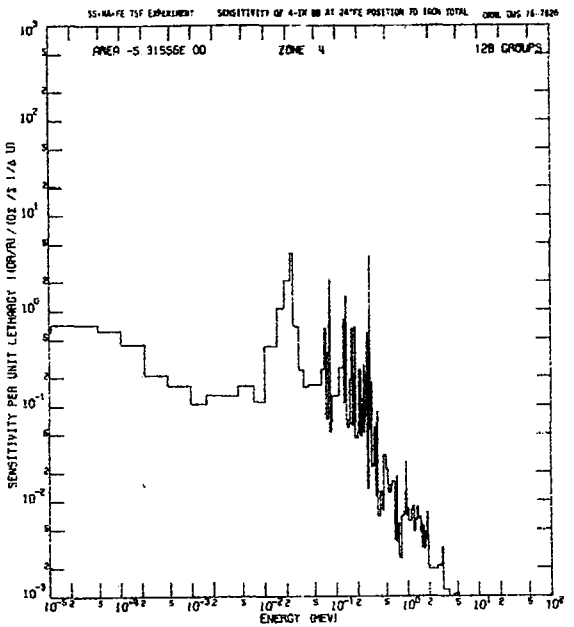

Fig. 2c. Total Iron Cross Section Sensitivity Profile for 24-in. Iron Region of TSF Experimental Configuration #7.

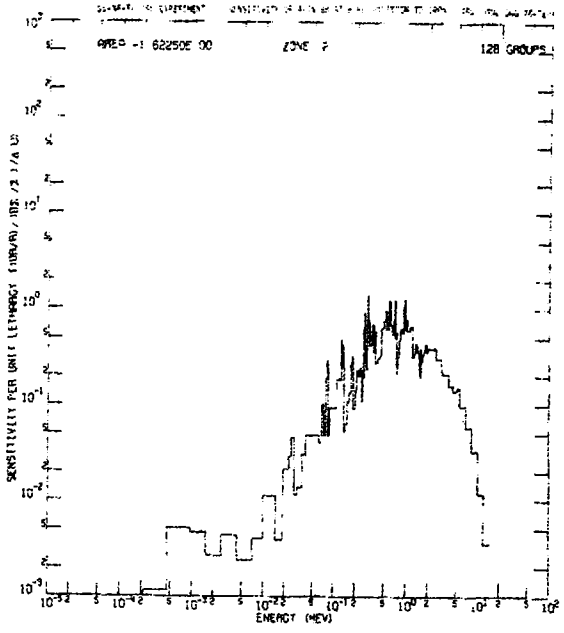

Fig. 3a. Total Iron Cross Section Sensitivity Profile for 18-in. Steel Region of TSF Experimental Configuration #5.

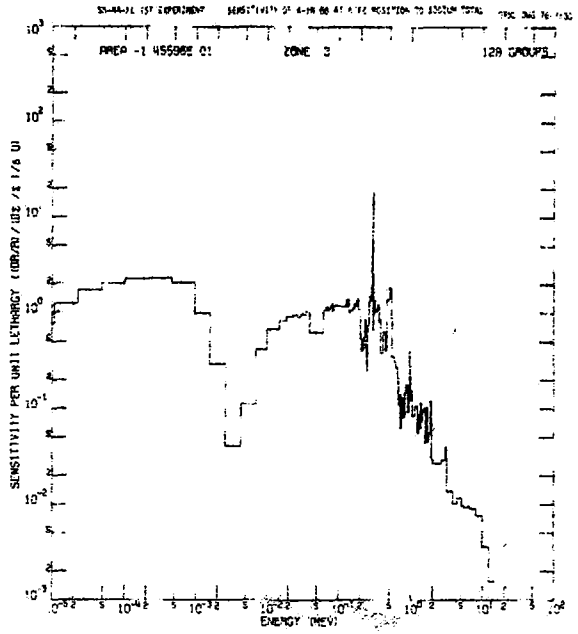

Fig. 3b. Total Sodium Cross Section Sensitivity Profile for 15-ft Sodium Region of TSF Experimental Configuration #5.

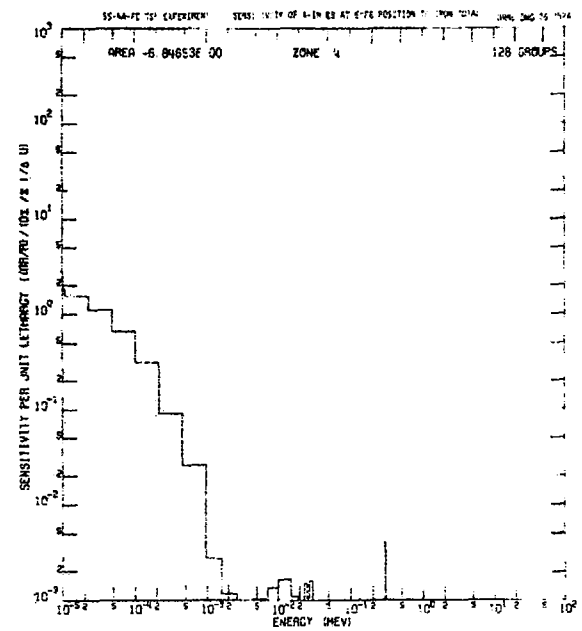

Fig. 3c. Total Iron Cross Section Sensitivity Profile for 6-in. Iron Region of TSF Experimental Configuration #5.

ORNL DWG 76-15162

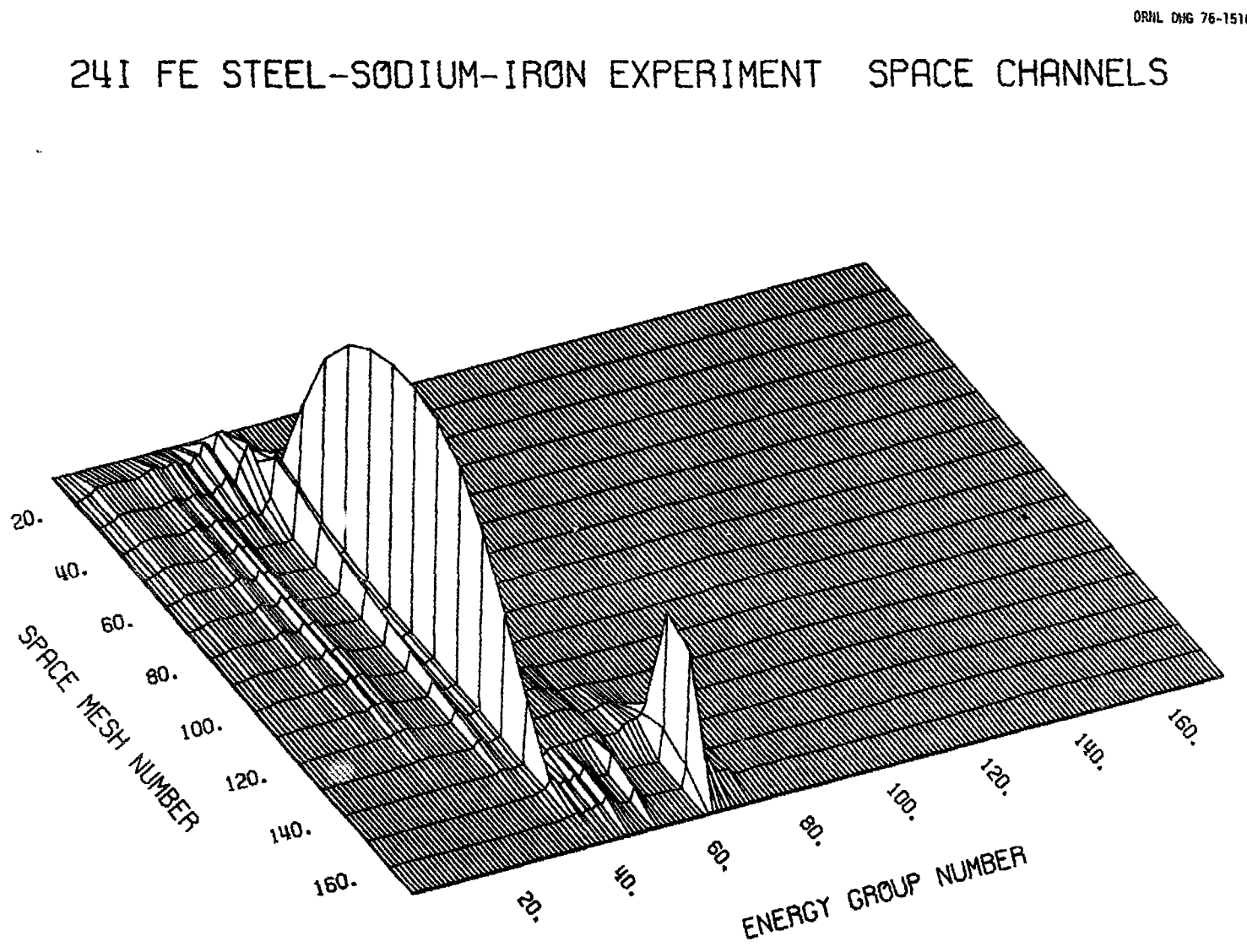

Fig. 4. Contributon Spatial Current, K_R, as a Function of Space and Energy for TSF Experiment #7.

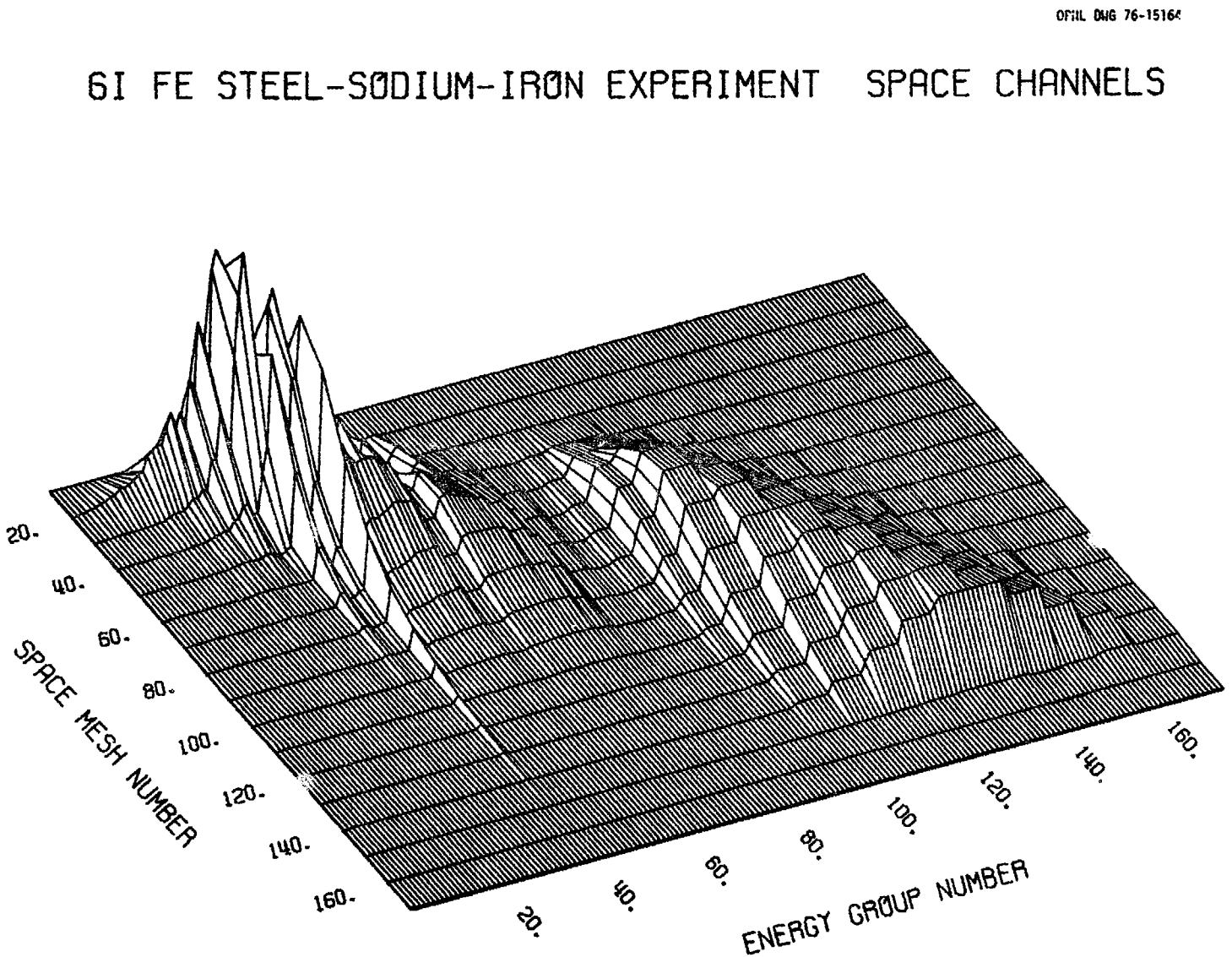

Fig. 5. Contributon Spatial Current, K_R, as a Function of Space and Energy for TSF Experiment #5.

INVESTIGATION OF CROSS SECTION REQUIREMENTS FOR SHIELDING OF POWER REACTORS

by Hehn, G., Rataj, J.
IKE, University of Stuttgart, Germany

Abstract

In sensitivity studies for reactor shielding one starts from integral target quantities of interest like biological dose outside the shield, gamma heating in the pressure vessel and concrete shield or radiation damage in essential structural components outside the core. For these target quantities we determined the importance and contribution:

1. of different neutron and gamma sources in the reactor (source data),
2. of the total radiation interactions with single isotopes or natural elements (total cross section),
3. of partial interactions of primary interest (partial cross sections),
4. of the most effective energy groups and
5. of the angular moments needed.

Such studies had been done to show the requirements of cross section data for shielding of a PWR and fast reactor.

1. Introduction

Systematic studies of cross section requirements for shielding calculations have been done in last years on power reactors of medium size like the PWR at Stade and the fast reactor SNR at Kalkar. Some rather incomplete experience on cross section requirements has been gained on the gas cooled reactor THTR at Uentrop. Recently the sensitivity benchmark has been completed treating a large PWR like that of Biblis. Sensitivity calculations were performed using the ANISN-SWAWLAKE

procedure /1/ in simplified one-dimensional geometry. Two-dimensional source configurations like that of PWR or neutron streaming effects along narrow slits of the gas cooled reactor can be estimated without large calculational effort of two-dimensional treatment. The target quantities of interest had been radiation damage in the form of displacement rates in important structural components outside the core, gamma heating in the shield or biological dose outside the shield. Of course the requirements of nuclear data are strongly dependent on the integral response function of interest, on the reactor type and the special design configurations fixed by a given geometry and material composition. On the other side reactor materials and specially materials for reactor shielding are often used for the same purpose, so that a survey of data requirements promises inspite of the differences given also some similarities for all reactor types. The following discussion of the results will be divided into special requirements of the neutron and gamma source data, the importance of the total radiation interaction with single isotopes or natural elements, the determination of the most important energy region including the partial interactions of primary interest and the angular information needed.

2. Requirements of source data for neutron and gamma radiation

For reactor shielding one normally starts from the distribution of fission sources in the important outer core regions with a time average value of the source for damage calculations and a maximum value for heat and dose calculations. Since the high energy part between 5 and 10 MeV of the neutron source is directly proportional to the damage production in the pressure vessel of a PWR, this is the most stringend requirement to the average number of neutrons per fission V as well as to the fission spectrum X of a single fissionable isotop e.g. U-35 or Pu-39. If mixtures of both are present or Pu-fuel is used in special positions in the core, the shift to harder fission neutrons can be appreciably high with large effects to damage and smaller to heat and biological dose.

Tab. 1 shows the importance of the prompt and delayed fission gammas of a PWR. They contribute with 20% to the maximum heat density in the pressure vessel, with 7% to the maximum heat density in the concrete shield and with only 1% to the gamma dose rate behind the primary shield. The secondary gammas from the steel components like thermal shield and pressure vessel are by far more important as well as those from the concrete shield. The same study for the fast reactor SNR shows even smaller importance of the fission gammas.

3. Importance of different nuclides

Fig. 1 gives the sensitivity of radiation damage in the pressure tank of a fast reactor (SNR) to the total cross section of different nuclides. According to their importance the nuclides can be devided into three categories.

Very important are the cross sections of sodium only, since a variation of the total cross section ($\Delta\Sigma/\Sigma$) by 1% results in a change of the response function ($\Delta R/R$) by 6.5%. The nuclides U-38, Fe, O, Cr, and Ni belong to the category of second importance. All the rest like Pu-39, Si, Zr, U-35 etc. have small effects on the damage response, so that their cross section errors can be neglected totaly.

In the diagram shown, there is additional information of the energy region of importance. The dashed lines represent the sensitivity to the cross section above 1 MeV and the doted lines below 1 MeV. Sodium has the dominant part of the reactions (71%) below 1 MeV, whereas in the case of U-38 the MeV energy region is most important (81%).

As can be seen from the sensitivity calculations for the PWR benchmark /2/ the most important cross sections for radiation damage are those of H, O, and Fe. The nuclides of Cr, Ni, and Zr belong to the category of second importance, whereas the rest like Mn, U-38 and U-35 are unimportant. For all nuclides the energy region of interest lies above 1 MeV.

Of course, one has to be cautious, to take the sensitivity of the total cross section summed over energy groups as the only

measure for classification of nuclides. Linear superpositions of group values with opposit signs have to be avoided, which means that for the sensitivity of heat and biological dose comparisons have to be done with the energy profiles.

4. Determination of important energy regions, partial cross sections and angular moments

Having a classification of the important nuclides, we can further determine the important energy regions of the total cross section. For radiation damage of a fast reactor details of the energy profile are shown in fig. 2 for sodium and iron. For sodium the sensitivity per lethargy has two maxima in the upper keV region at 300 keV and 500 keV and a third peak in the lower MeV region around 2 MeV. For iron we get a shift of the important cross section into the MeV region, whereas the keV region is less important. Sensitivity profiles are given in fig. 3 for damage in the pressure vessel of a PWR (Stade).

The cross sections are specified for different material zones like core, core baffle (Fe 1), 1. coolant zone (H_2O 1), core barrel (Fe 2), and 2. coolant zone (H_2O 2). There is a strong confinement of the sensitivity to the MeV region with two peaks at 3 MeV and 6 MeV.

If partial cross sections are available in a group library the final step can be done in the sensitivity analyses, to show the contributions of partial interactions within the important energy regions. And last not least the importance of the scatter matrix can be studied as shown in tab. 2 for a fast reactor configuration. For this problem P_1-approximation is good enough. The high values for P_0-approximation should be taken with the limitations of linear pertubation theory in mind.

References:

/1/ Bartine, D.E., Mynatt, F.R., Oblow, E.M.
SWANLAKE, a computer code utilizing ANISN radiation transport calculations for cross section sensitivity analysis
ORNL - TM - 3809, 1973

/2/ Hehn, G., Koban, J.
Reactor Shield Benchmark No. 2
ESIS, Special Issue No. 4, 1976

Tab. 1

	CORE		SHIELD		
			steel (pr.v.)	H_2O coolant	concrete shield
	(f,γ)	(n,γ)	(n,γ)	(n,γ)	(n,γ)
max. heat density in pressure vessel	19.89%	13.10%	42.25% (2.26%)	24.65%	0.11%
max. heat density in concrete shield	7.25%	4.35%	41.78% (14.20%)	3.60%	43.02%
γ-dose rate behind primary shield	1.58%	1.04%	69.88% (12.19%)	0.04%	27.46%

I K E Stuttgart	Contribution of γ-sources to heat production and biological dose of a P W R (Stade)	

Tab. 2

Nuclide	$\frac{\Delta R/R}{\Delta\Sigma/\Sigma}$	$\frac{\Delta R/R}{\Delta\Sigma/\Sigma}$	$\frac{\Delta R/R}{\Delta\Sigma/\Sigma}$	P0/P3	P1/P3	P2/P3
	E>1MeV	E<1MeV	total	%	%	%
Na	-1.86	-4.68	-6.54	-67.1	-1.51	-0.03
U-38	-0.98	-0.23	-1.21	-23.9	-0.39	-0.20
Fe	-0.62	-0.38	-1.00	-16.9	-0.98	-0.11
O	-0.31	-0.35	-0.66	- 8.06	-0.04	-0.03
Cr	-0.18	-0.12	-0.30	- 5.17	-0.24	-0.03
Ni	-0.12	-0.10	-0.22	- 2.20	-0.11	-0.01
Pu-39	-0.03	-0.01	-0.04	- 0.39	0	0
other	-0.01	-0.02	-0.03	- 0.31	0.01	0
total	-4.11	-5.89	-10.00	- 124	-3.26	-0.41

I K E	Sensitivity of rad. damage in pressure vessel - SNR - to total cross section	

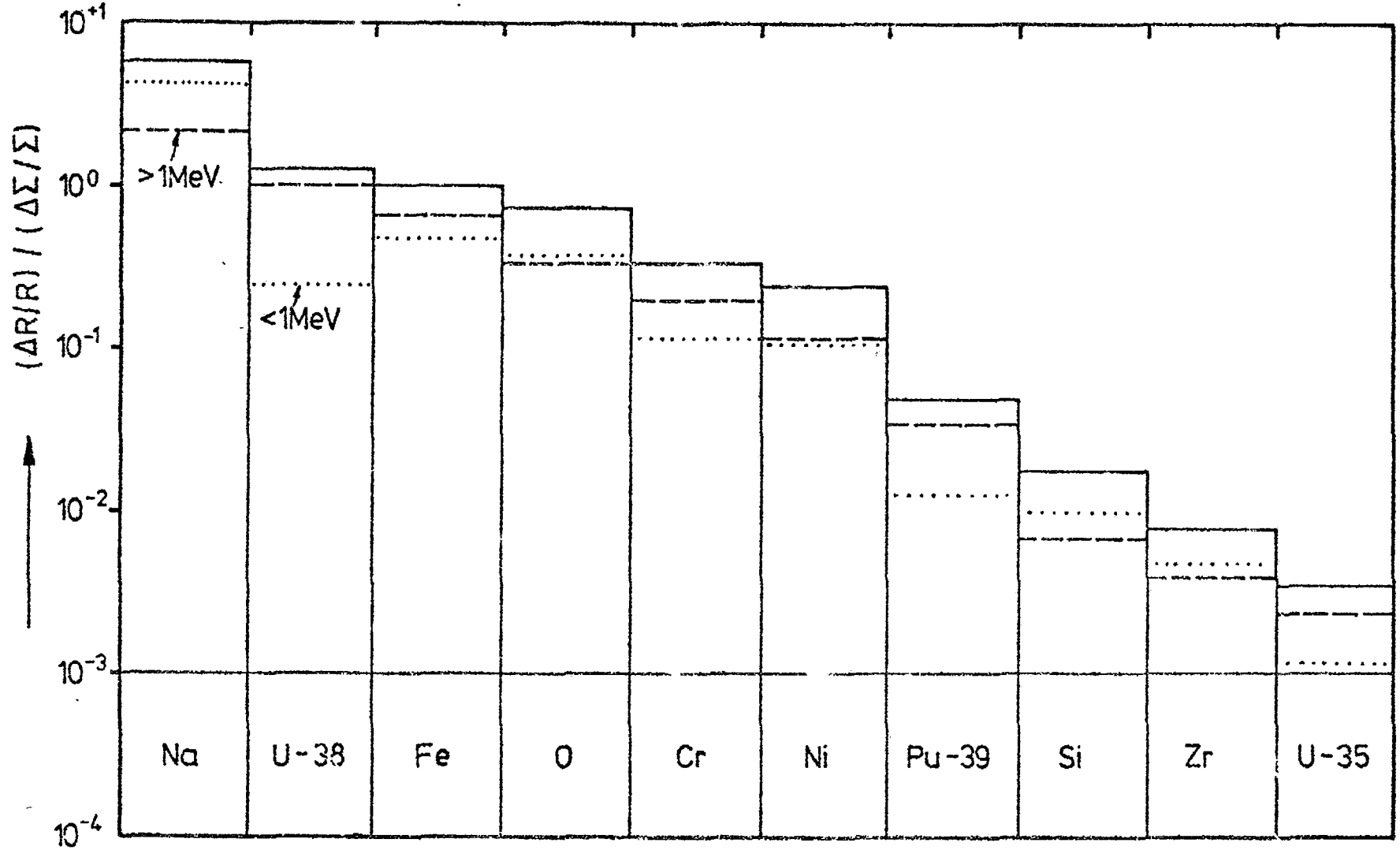

Fig.:1

IKE Stuttgart	Sensitivity of rad. damage in pressure tank (SNR) to total cross section of nuclides	160.05.003.4 1974

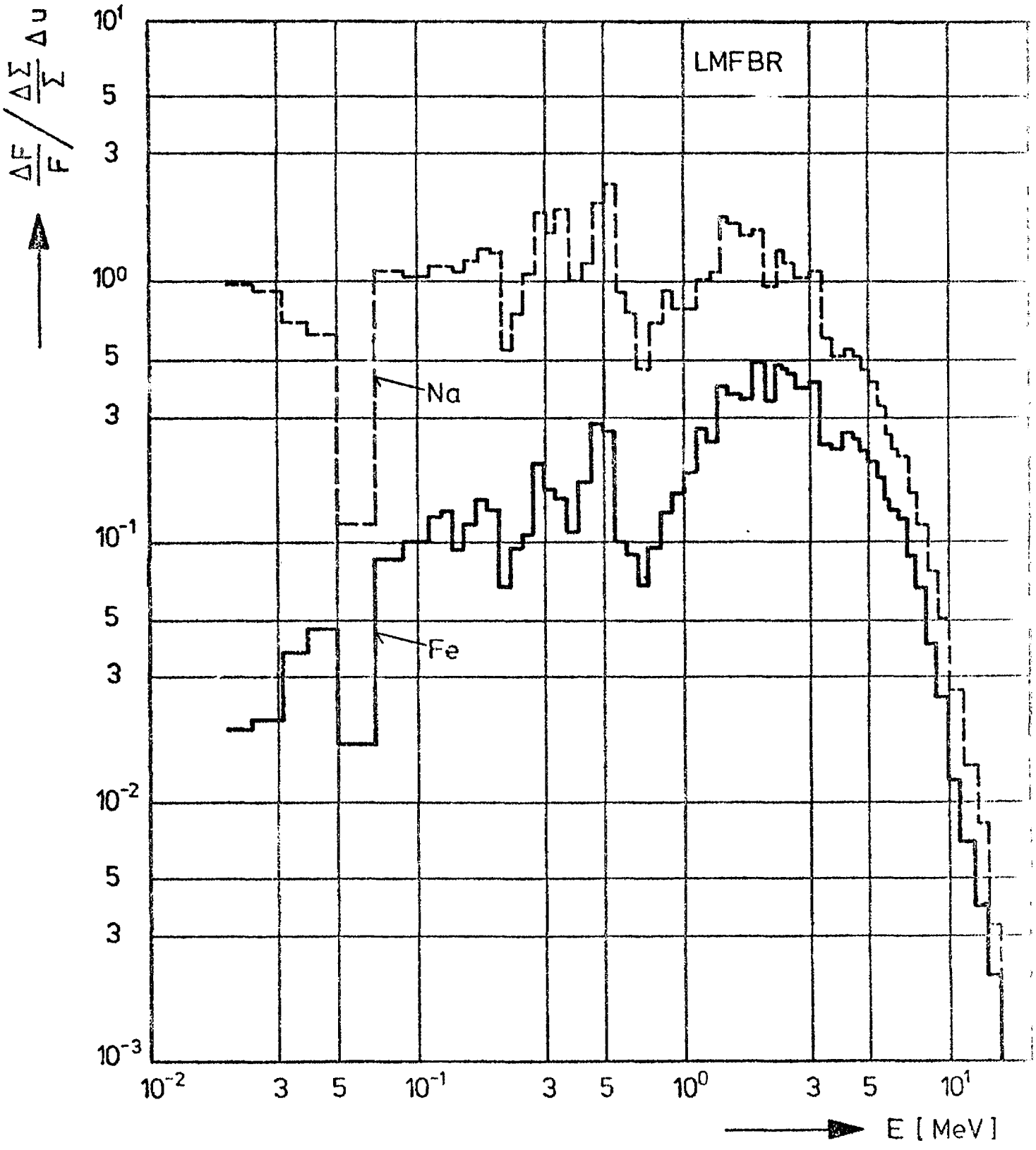

Fig. 2: Sensitivity of rad. damage in the tank (SNR) · to the total cross section of Fe and Na

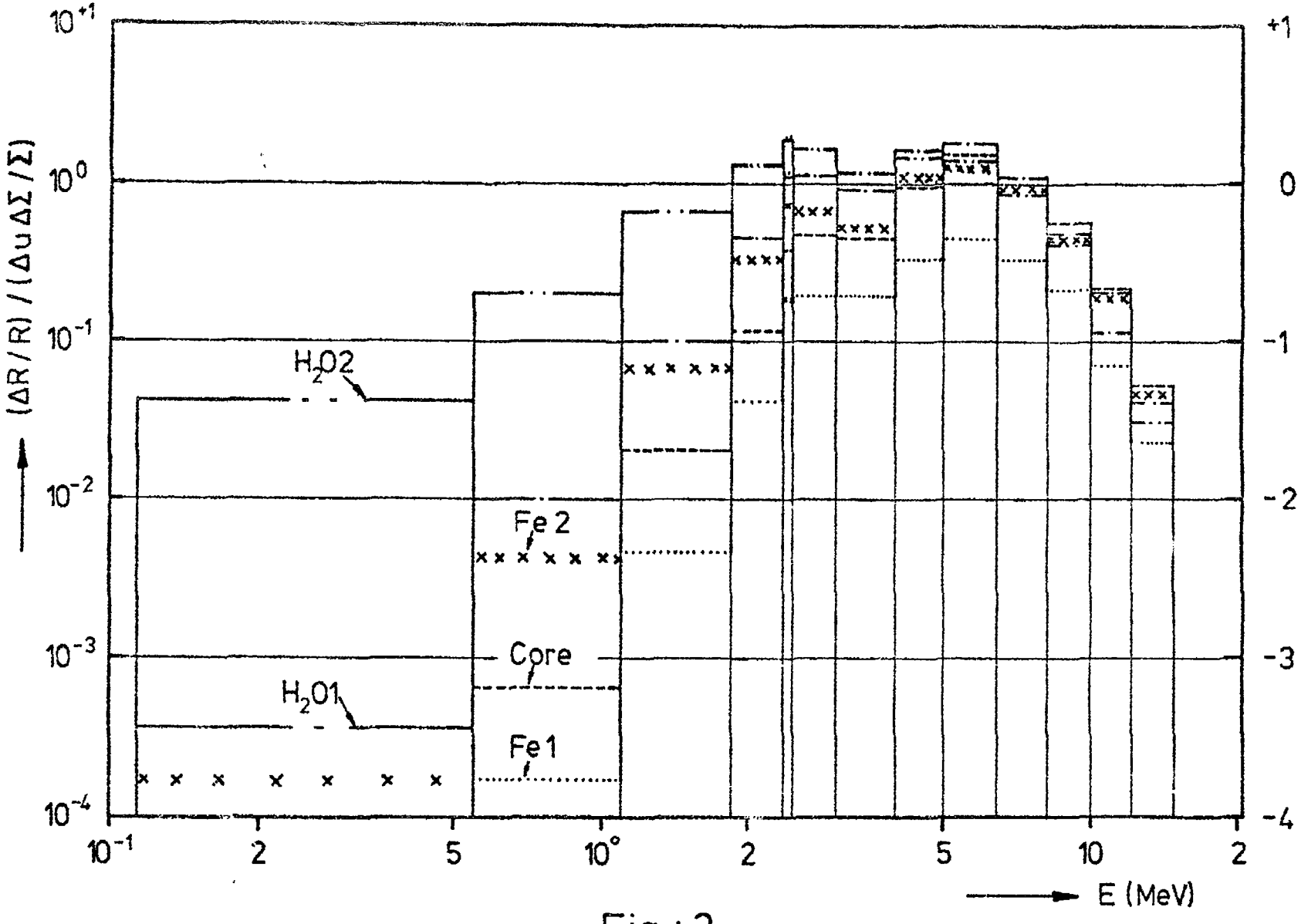

Fig.: 3

IKE Stuttgart	Sensitivity of rad. damage in pressure vessel (PWR) to total cross section of material zones	160.05.002.4 1974

CONTRIBUTION TO THE EXERCISE ON SENSITIVITY STUDIES FOR THE NEA THEORETICAL FAST REACTOR BENCHMARK

by

S D Lympany*
A K McCracken
A Packwood

Radiation Physics and Shielding Group
Reactor Physics Division
UKAEA, AEE Winfrith
Dorchester
Dorset

Abstract

Sensitivity studies on a benchmark fast reactor radial shield design using UKNDL data in the codes ANISN and SWANLAKE are described. Target accuracies for various reaction rates are given. The variance on the calculation of these reaction rates caused by uncertainties in data are calculated using the accuracy assessments of Schmidt in EANDC-E-35U. Consideration is given to the influence of cross-section averaging and of energy-dependent correlations of data.

1 Introduction

Participants at the NEA meeting on Sensitivity Studies and Shielding Benchmarks at Paris in October 1975 agreed to submit calculations for reference designs of PWR and Fast Reactor shields. The object of this exercise is the assessment of the influence of different data sets on the accuracy of shielding calculations and the identification by means of sensitivity studies of the cross-sections whose accuracy most influence the calculation of design parameters of interest. A description and full specification of the Fast Reactor shield problem is given by Barré (1) and is not repeated here but Tables 1, 2 and 3, reproduced from the above document, give all essential details and are included for convenience. The 100-group structure offered for condensation by Barre is broadly similar to the EURLIB 100-group structure specified by Hehn (2) and Koban for the PWR reference calculations, but there are differences in some energy boundaries. In order to avoid unnecessary processing of data we have used for both problems a 42-group structure based on the EURLIB boundaries. The solution has been found for the problem exactly as specified by Barré using ANISN in the P_1 S_4 approximation, with data from the UK Nuclear Data Library (3); in addition a P_3 S_4 ANISN calculation has been carried out.

*Work performed during the author's attachment from Imperial College, London

The sensitivity to some important cross-sections of the activation-rate of sodium in the heat exchanger and of the iron displacement-rate in the Fe/Na shield region have been investigated using ANISN and SWANLAKE (4).

2 Details of the Forward Calculations

The group structure used in both the P_1 S_4 and P_3 S_4 calculations and the group-averaged detector cross-sections are given in Table 4. The basic nuclear data for Na, Fe, Ni and Cr was provided respectively by the UK Nuclear Data Library Data File Numbers (DFN's) 93, 908, 907 and 45. This basic data was transformed into group cross-sections, averaged over a spectrum varying as $[E\,\sigma_T(E)]^{-1}$, by the program GALAXY (5), the output of which was processed into a form suitable for input to ANISN BY GALCON, (6).

The detector cross-sections for Na(n,γ) Co(n,γ) and U235 (n,f) were taken from DFN's 93, 1210 and 159 respectively. The latter two cross-sections, unlike that of Na, were averaged by GALAXY over an E^{-1} spectrum, a test with the U235 cross-section having shown that this produced results only marginally different from a $[E\,\sigma_T(E)]^{-1}$ weighting. The displacement cross-sections for Fe were calculated by applying the IAEA recommended displacement cross-section of Norgett (7), Robinson and Torrens to Fe data (DFN 906). Displacement cross-sections were calculated in 2000 groups and collapsed into the 42-group scheme with a $[E\,\sigma_T(E)]^{-1}$ weighting. (DFN 908 which was used in the penetration calculations is a minor revision of DFN 906 in the energy range 100 keV-300 keV. Above 330 keV both DFN 906 and DFN 908 are based on the ENDFB-3 file for Fe.)

3 Results and Discussion

Neutron group fluxes were calculated through the shield using ANISN in both the P_1 S_4 and P_3 S_4 approximations. The agreement between these two cases was generally better than 1%; in what follows the results of the P_3 calculation are quoted.

Figure 1 shows the attenuation of total flux equivalent thermal flux and Co59 (n,γ) Co60 reaction-rate through the shield, and Figure 2 compares the neutron flux above 0.111 MeV with the atomic displacement rate in iron calculated according to the NRT model. The strong spectral dependence of the effective displacement cross-section for use with flux above 0.11 MeV is clearly shown in the latter figure; a cross-section of approximately 300b is appropriate to the Fe/Na shield but in the softer spectrum at the start of the heat-exchanger this rises to approximately 10^5b. Figure 3 shows the distribution of the U235 (n,f) and Na23 (n,γ) Na24 reaction-rates in the shield and Figure 4 the effective cross-sections (ie total reaction-rate divided by total flux) for the iron displacement, U235 (n,f) Co59 (n,γ) Co60 and Na23 (n,γ) Na24 reaction-rates. The above results are collected in Table 13.

Utilising the output of both forward and adjoint ANISN calculations with the perturbation programme SWANLAKE profiles were obtained of the sensitivity of the iron displacement rate per atom at mesh 61 and the Na (n,γ) activation-rate in the heat-exchanger to both partial and total cross-sections of shield materials. All sensitivities have been corrected, where necessary, for the effect of detector cross-section changes; these corrections and the derivation of sensitivities are discussed in Appendix I. Figure 5 shows the sensitivity of iron atomic displacement rate to Fe, Na and Ni total cross-sections and Figure 6 that of the capture-rate of Na in

the heat-exchanger to Fe and Na total cross-sections. Figures 7 and 8 show the sensitivity of the Fe displacement rate to the total and inelastic cross-sections of Fe and Na respectively and in Figures 9 and 10 are displayed the sensitivities of sodium activation in the heat-exchanger to the total, inelastic and capture cross-sections of Fe and Na respectively. These results are also presented in Tables 5 to 10, the Table numbers corresponding with the Figure numbers; in the Tables group values of sensitivities are given as distinct from the values per unit lethargy given in the graphs. In the latter all sensitivities are negative unless specifically noted as positive.

Inspection of Figures 5, 7 and 8 shows that the energy range of interest of those cross-sections which contribute significantly to the Fe displacement rate at mesh 61 is confined between approximately 50 keV and 3 MeV. Above the thresholds for inelastic scattering the elastic cross-sections of both Na and Fe are of the same order of importance as the inelastic cross-sections; both are very much less important than the elastic cross-sections in the energy range 0.1 MeV - 1 MeV.

Figures 6, 9 and 10 show a much less peaked energy distribution of sensitivities of cross-sections which influence the capture-rate of Na in the heat-exchanger; with the exception of the dip caused by the 3 KeV Na resonance the elastic cross-section of Na is of importance at all energies from thermal to 1 MeV - the non-elastic cross-sections are of relatively minor importance. Below 1 MeV the elastic cross-section of Na is almost equal to the total cross-section whose accuracy in this energy range is given by Schmidt as approximately 10%. Fe cross-sections are considerably less important than those of Na below 0.1 MeV but above this energy this relativity is reversed; both cross-sections are of rapidly diminishing signifance above 1 MeV for causing heat exchanger activation.

The total sensitivities given by SWANLAKE for an increase of the Cr, Fe, Ni and Na total cross-sections (with all partial cross-sections being increased in the same proportion) is given in Table 11 below; also included is the effect of reducing the Legendre scattering expansion from P_3 to P_1:-

The above numbers can be rather misleading as the type of cross-section variation assumed takes no account of negative correlations which exist between the components of a total cross-section. Table 12 below shows the fractional standard deviations $\sigma\left(\delta R/R\right)$ calculated by the method of Appendix II in which correlations between partial cross-sections are considered.

In the above table only the effects of the Na and Fe, the most influential, isotopes have been considered in detail; the final column is the result of including contributions from Cr and Ni on the assumption that they contribute in the same proportion as in Table 11.

The effect of increasing the angular expansion of scattering from P_1 to P_3 is clearly negligible but SWANLAKE shows that attempting to calculate with P_0 would introduce errors of some tens of percent in the reaction-rates. It remains to consider the significance for each reaction-rate of the total sensitivity given in Table 11 and for the three estimates of total fractional errors given in Table 12. The total sensitivity of -10.69 in Table 11 for the Fe displacement rate is derived on the assumption that the fractional variation in all partial cross-sections

and thus in the total cross-section is the same. This takes no account of the essentially negative correlations which exist between the partial cross-sections and requires the blanket attribution of a given fractional error to all reactions at all energies; it will generally lead to a large overestimate of the variance on a reaction-rate.

Thus by inspecting the accuracy assignments of Na and Fe in Table 4 one could reasonably guess - (and it amounts to precisely this) - 10% as a representative standard deviation on the cross-sections. This combined with the total sensitivity of -10.69 suggests a fractional error of 107% in the Fe displacement reaction-rate. Table 12, however, gives for the same quantity bounds of 22% and 31% (r = 0 and r = 1 respectively) derived by the methods of Appendix II. The best estimate lying between these bounds can only be determined if a realistic estimate of the energy-dependent correlations r_{ij} is available. (The numbers corresponding to $r_{ij} = 1 - |i - j|/4$ are not offered as realistic; they were calculated for interest as one of a class of numbers obtained for an 'intermediate' correlation). It may well be that evaluators ascribe a rather short effective energy range to the energy-dependent correlations, in which case the best estimate may not be greatly larger than that for r = 0; what is clear is that long-range correlations can significantly increase the best estimate of error on a calculated quantity.

For Na activation in the heat-exchanger the total sensitivity given in Table 11 would predict an error of 236% in reaction-rate for an average 10% error in data. Table 12 shows the bounds for our estimate of this quantity as 25% - 71%. The very drastic effect of long-range energy correlations is caused by the relatively flat sensitivity profile of Na; as for the Fe displacement rate the best estimate for the error on the Na activation-rate in the heat-exchanger may lie near the lower bound but again it is clearly of some interest to establish the nature of energy-dependent correlations. At present a designer intent on guaranteeing a confidence of 99.5% (ie 3 s.d.) in Na reaction-rate would need to multiply the calculated reaction-rate by 3.1.

4 Implications for Data

In Section 3 qualitative comment was passed on the cross-sections of interest on the basis of conventional sensitivity curves; a more informative type of sensitivity can, however, be produced. Consider, for example, the influence of Na cross-sections on the sodium capture-rate in the heat-exchanger. The independent measurements are of X_t, $X_{n'}$, and X_a, and Appendix II shows that the variance on $\delta R/R$ can be written as:

$$\sigma^2\left(\frac{\delta R}{R}\right) = \left\langle \left\{ \sum_i \left(\alpha_{ai}\,\delta x_{ai} + \alpha_{n'i}\,\delta x_{n'i} + \alpha_{ti}\,\delta x_{ti} \right)^2 \right\} \right\rangle$$

where $\alpha_{ai} = \left(\frac{U_{ai}}{x_{ai}} - \frac{U_{ni}}{x_{ni}}\right)$ with similar expressions for $\alpha_{n'i}$ and α_{ti}. We can now ignore X_n (as it is not proposed to make independent measurements of this) and regard X_n and X_a as the only components of X_t, since all correlations between X_n and $X_{n'}$ and X_a are taken account of in the α. From this point of view we can now regard $x_{ai}\,\alpha_{ai}\left(= U_{ai} - \frac{x_{ai}}{x_{ni}} U_{ni}\right)$ $x_{n'i}\,\alpha_{n'i}$ and $x_{ti}\,\alpha_{ti}$ as the sensitivity quantities we should

be inspecting; they give a true profile of the relative importance of improving the accuracy of those cross-sections which have been measured.

Thus $$\sigma^2\left(\frac{\delta R}{R}\right) = \sum_i \left(\alpha_{ai}^2 \sigma_{ai}^2 + \alpha_{n'i}^2 \sigma_{n'i}^2 + \alpha_{ti}^2 \sigma_{ti}^2\right)$$

if energy-dependent correlations are neglected.

Then for example:-

$$\frac{\delta\sigma\left(\frac{\delta R}{R}\right)}{\sigma\left(\frac{\delta R}{R}\right)} \Bigg/ \frac{\delta\sigma_{ai}}{\sigma_{ai}} = \frac{\alpha_{ai}^2 \sigma_{ai}^2}{\sigma^2\left(\frac{\delta R}{R}\right)} = W_{ai},$$

with similar expressions for $W_{n'i}$ and W_{ti}

These numbers, which give directly the fractional improvement in the standard deviation of the calculated design parameters per unit fractional improvement in the standard deviations of the measured cross-sections, we may consider as components of "measurement profiles". Figures 12 to 14 inclusive show the measurement profiles per unit lethargy of Fe displacement rate and Na activation in the heat-exchanger to the measured cross-sections of Fe and Na; group values are detailed in Tables 14 and 15. Table 14 shows that, for iron displacements, for a uniform fractional reduction in the uncertainty of all Na cross-section standard deviations 96.8% of the effect is attributable to the standard deviation on the total cross-section in group 20 (0.11 MeV-0.33 MeV); the corresponding figure for Fe cross-sections is 96.4% - again for group 20 and the total cross-section. Both of the cross-sections in this group have a standard deviation of 5% according to Schmidt. Assuming that this were reduced to 3% we should find for iron displacements the standard deviations caused by data uncertainties due to Fe and Na were reduced from 12.3% and 9.7% to 7.7% and 6.1% respectively (for r = 0) and the total uncertainty from 21.7% to 15.9%. Assuming that the upper bound estimates (r = 1) behaved in roughly the same way would lead to a reduction from 31% to 21%. For the effect of Fe and Na cross-section errors on the Na capture rate in the heat exchanger Table 15 shows again the importance of the accuracy of the Fe total cross-section in group 20 (95.4% of the effect due to all Fe cross-sections). In this case, however, the Na sensitivity profile is flatter and group 20 contributes 48.7% of all Na cross-section effects with 46.3% coming from groups 31-40 (energies below 0.96 KeV) - again only the total cross-section is of any importance. Assuming again a reduction the standard deviation on the total cross-sections in these energy ranges to 0.6 of their quoted values leads to reductions in the heat exchanger activation-rate uncertainty from 24.9% to 16.9% (r = 0) and 71.3% to 48.3% (r = 1).

From the foregoing calculations the following conclusions can be drawn on the basis of the cross-section accuracies assigned by Schmidt:

(i) The Fe atomic displacement rate near the outside of the sodium shield can be calculated to 22%-31% (1σ), and the activation-rate of Na in the heat-exchanger to 25%-71%.

(ii) A more precise allocation of error depends on having available a reasonable estimate of the energy-dependent correlations on measured cross-sections.

(iii) For the problems investigated the only Fe cross-section of interest is the total cross-section between 0.11 MeV and 0.33 MeV - further investigation with a finer energy resolution is merited here; the total cross-section of Na in the same energy range is of interest for Fe displacement and for heat-exchanger activation the total cross-section below 500 eV is of importance. No refinement of cross-sections other than these would improve the accuracy of prediction by more than a few percent.

(iv) The method of averaging group cross-sections could easily produce errors greater than the 5% s.d. attributable to basic data - fine group calculations in regions of high measurement sensitivity are indicated.

Acknowledgements

We are obliged to Mr A F Avery for many useful discussions; we have also benefited from his earlier work on this subject.

References

1 Barré, J Y
Fast Reactors: Definition of a Standard Configuration for the Comparison of Shielding Calculations (Note circulated to participants)

2 Hehn, G and Koban, J
Reactor Shield Benchmark No 2
ESIS Newsletter, Special Issue No 4

3 Pope, A L
The Current Edition of the Main Tape NDL-1 of the UK Nuclear Data Library
AEEW-M 1208

4 Bartine, D E et al
SWANLAKE, A Computer Code Utilising ANISN Radiation Transport Calculations for Cross-Section Sensitivity Analysis
ORNL-TM-3809

5 Price, J A
A Guide to GALAXY6
AWRE O/13/75

6 Dean, C
Unpublished

7 Norgett, M J et al
IAEA Specialist Meeting on Radiation Damage Units for Ferritic and Stainless Steels, Seattle, Washington, 1972

8 Schmidt, J J
Neutron Cross-Sections for Fast Reactor Materials Part 1: Evaluation
KFK 120 (EANDC-E-35U)

APPENDIX I

DERIVATION OF SENSITIVITIES

1 The quantities available to SWANLAKE for any group are the components $X_{gg'}$ of the scattering matrix (wherein elastic and inelastic events are not distinguished), the total cross-section X_T and hence the absorption cross section

$$x_a = x_T - \sum_{g'} x_{gg'}$$

The sensitivity $V_g = \sum_{g'} V_{gg'}$ given by SWANLAKE is the fractional change in the reaction-rate of a detector per unit fractional change in x_g with the total cross-section held constant, ie a reduction in x_a is implied. Similarly V_T is the effect on a reaction-rate of increasing x_T without altering x_g, an implied increase in x_a. Thus we can choose to work in 'true' partial sensitivities U, in which any increase in a partial cross-section leads to the same increase in the total cross-section, by means of the following relations:-

$$U_a = V_T \frac{x_a}{x_T}$$

(This manipulation is performed by SWANLAKE and printed as Va).

$$U_{gg'} = V_{gg'} + \frac{x_{gg'}}{x_a} U_a$$

and hence

$$U_g = V_g + \frac{x_g}{x_a} U_a$$

(The quantity $V_g + V_T$ is also given by SWANLAKE; this equals $U_g + U_a$ and is the fractional increase in detector reaction-rate per unit fractional increase in the partial cross-sections and hence also in the total cross-section).

2 Analysis of Elastic and Inelastic Scattering Components

This is most readily achieved by carrying out two SWANLAKE calculations as follows:-

(i) Present SWANLAKE with only the elastic component x_n of the scattering matrix and put $x_T = x_n$. This provides the components $U_{ngg'}$ of the elastic scattering sensitivity.

(ii) Use the correct x_T and the total scattering matrix. This provides U_a and $U_T = U_a + U_n + U_{n'}$ and hence, with the results of (i) a complete separation of U_a, U_n and $U_{n'}$.

An alternative approach, adopted in this work, is to derive the inelastic sensitivity by inspection of the Legendre coefficients of both elastic and inelastic scattering cross-sections displayed by the data processing program GALAXY. Experience suggests that the former method involves less effort.

3 Compensation for Detector Sensitivities

The alteration of the cross-section of a shield component will sometimes affect the response of the detector; an example is the detection of the $Na(n,\gamma)$ rate in a heat exchanger in a fast reactor. In these cases we may write:-

$$U^* = U + U'$$

where U, the sensitivity given by SWANLAKE, takes account only of the change in flux at the detector position and U' takes account of the detector response. This term is simply shown to be:

$$U_{\gamma i} = \frac{\phi_i \sigma_{\gamma i}}{\sum_i \phi_i \sigma_{\gamma i}}$$

for capture reactions where ϕ_i is the group i flux at the detector position.

For neutron-displacement rate iniron using the N.R.T. model we can write the displacement cross-section as

$$\sigma_d = \sigma_{d\gamma} + \sigma_{dn} + \sigma_{dn'}$$

ie the sum of the cross-sections for displacement by capture, elastic and inelastic scattering.

The sensitivity of iron displacement rate to the iron inelastic cross-section in group i throughout a shield is then

$$U^*_{n'i} = U_{n'i} + \frac{\phi_i \sigma_{dn'i}}{\sum_i \phi_i \sigma_{di}}$$

with similar expressions for the elastic and absorption sensitivities.

APPENDIX II

ASSESSMENT OF ERRORS ON THE CALCULATION OF INTEGRAL QUANTITIES

In order to calculate the variance on an integral quantity one requires both the sensitivities of the quantity to nuclear data used in the calculation, and an estimate of correlation function of the errors on this nuclear data. The latter information is not generally available although a start has been made to provide a correlated error file for the ENDF/B4 library. A cross-section compilation by Schmidt (8) does, however, give an estimate of the accuracy of the cross-sections of interest for this work (without considering energy-dependent correlations); these accuracies have been assumed to apply to the data in the UK Nuclear Data Library and form the basis of the accuracy assessments made in this work. The fractional standard deviations used are shown in Table 4. The elastic scattering cross-section is always a dependent variable in evaluations. Most commonly the total, non-elastic and absorption cross-sections are measured independently in which case $\sigma_n = \sigma_t - \sigma_x$; this situation applies for Fe, Ni and Cr. Less often the independent measurements are of total, inelastic and absorption

cross-sections when $\chi_n = \chi_T - (\chi_{n'} + \chi_a)$; Na and O are in this category.

Consider the former case, for example the errors induced by Fe data uncertainties on the Na activation rate in the heat-exchanger. Then

$$\sigma^2\left(\frac{\delta R}{R}\right) = \left\langle \left\{ \sum_i \left(U_{ai} \frac{\delta \chi_{ai}}{\chi_{ai}} + U_{n'i} \frac{\delta \chi_{n'i}}{\chi_{n'i}} + \frac{U_{ni}}{\chi_{ni}} \delta \chi_{ni} \right) \right\}^2 \right\rangle$$

where R is the Na activation rate,

U_i is a sensitivity for data in group i

and $\langle\ \rangle$ denotes expected value.

Putting $\delta \chi_{\chi i} - \delta \chi_{ai} = \delta \chi_{n'i}$ and $\delta \chi_{Ti} - \delta \chi_{\chi i} = \delta \chi_{ni}$ and re-arranging gives:-

$$\sigma^2\left(\frac{\delta R}{R}\right) = \left\langle \left\{ \sum_i \left[\left(\frac{U_{ai}}{\chi_{ai}} - \frac{U_{n'i}}{\chi_{n'i}} \right) \delta \chi_{ai} + \left(\frac{U_{n'i}}{\chi_{n'i}} - \frac{U_{ni}}{\chi_{ni}} \right) \delta \chi_{\chi i} + \frac{U_{ni}}{\chi_{ni}} \delta \chi_{Ti} \right] \right\}^2 \right\rangle$$

$$= \sum_i \left[\left(\frac{U_{ai}}{\chi_{ai}} - \frac{U_{n'i}}{\chi_{n'i}} \right)^2 \sigma^2(\chi_{ai}) + \left(\frac{U_{n'i}}{\chi_{n'i}} - \frac{U_{ni}}{\chi_{ni}} \right)^2 \sigma^2(\chi_{\chi i}) + \left(\frac{U_{ni}}{\chi_{ni}} \right)^2 \sigma^2(\chi_{Ti}) \right]$$

$$+ 2 \sum_{j=i+1} \sum_i \left(\frac{U_{ai}}{\chi_{ai}} - \frac{U_{n'i}}{\chi_{n'i}} \right) \left(\frac{U_{aj}}{\chi_{aj}} - \frac{U_{n'j}}{\chi_{n'j}} \right) \rho_{ij}\, \sigma_{ai}\, \sigma_{aj}$$

$$+ 2 \sum_{j=i+1} \sum_i \left(\frac{U_{n'i}}{\chi_{n'i}} - \frac{U_{ni}}{\chi_{ni}} \right) \left(\frac{U_{n'j}}{\chi_{n'j}} - \frac{U_{nj}}{\chi_{nj}} \right) \rho_{ij}\, \sigma_{\chi i}\, \sigma_{\chi j}$$

$$+ 2 \sum_{j=i+1} \sum_i \frac{U_{ni}\, U_{nj}}{\chi_{ni}\, \chi_{nj}} \rho_{ij}\, \sigma_{Ti}\, \sigma_{Tj}$$

A similar expression is found when X_T, $X_{n'}$, X_a are the independent measurements, thus:-

$$\sigma^2\left(\frac{\delta R}{R}\right) = \sum_i \left[\left(\frac{U_{ai}}{x_{ai}} - \frac{U_{ni}}{x_{ni}} \right)^2 \sigma^2(x_{ai}) + \left(\frac{U_{n'i}}{x_{n'i}} - \frac{U_{ni}}{x_{ni}} \right)^2 \sigma^2(x_{n'i}) + \left(\frac{U_{ni}}{x_{ni}} \right)^2 \sigma^2(x_{Ti}) \right]$$

$$+ 2 \sum_{j=i+1} \sum_i \left(\frac{U_{ai}}{x_{ai}} - \frac{U_{ni}}{x_{ni}} \right) \left(\frac{U_{aj}}{x_{aj}} - \frac{U_{nj}}{x_{nj}} \right) r_{ij} \sigma_{ai} \sigma_{aj}$$

$$+ 2 \sum_{j=i+1} \sum_i \left(\frac{U_{n'i}}{x_{n'i}} - \frac{U_{ni}}{x_{ni}} \right) \left(\frac{U_{n'j}}{x_{n'j}} - \frac{U_{nj}}{x_{nj}} \right) r_{ij} \sigma_{n'i} \sigma_{n'j}$$

$$+ 2 \sum_{j=i+1} \sum_i \left(\frac{U_{ni} U_{nj}}{x_{ni} x_{nj}} \right) r_{ij} \sigma_{Ti} \sigma_{Tj}$$

In each of these equations the first sum gives the variance derived on the assumption that measurements of the same quantity at different energies are independent, and the final three sums give the contribution to the variance caused by correlations between measurements of a quantity at different energies. (It is assumed that all components of the total cross-section show the same energy-dependent correlation so that a single symbol r_{ij} can be used). Realistic values of r_{ij} for all reactions are, not yet available but it is of interest to make some reasonable assumptions to assess the importance of energy dependent correlations. Thus:

$$r_{ij} = 1 - |i-j|/4|$$

satisfies common sense in that it is always non-negative and that correlations are strong for neighbouring groups and decrease monotonically as the energy difference between groups increases. These values of r_{ij} have been used in the error analysis and separate calculations have been performed with $r_{ij} = 0$ and $r_{ij} = 1$. Thus the first set of values should give rise to a semi-realistic estimate of total variance and the last two calculations to upper and lower bounds of the variance.

TABLE 1

Spherical Shield Geometry

Zone	Number	Inner Radius (cm)	Outer Radius (cm)	Thickness (cm)	Mixture Number
Source	1	236.5	236.51	0.01	1
Lateral Shield	2	236.51	416.5	179.99	1
Sodium Tank	3	416.5	916.5	500	2
Heat Exchanger	4	916.5	966.5	50	3
Sodium	5	966.5	1016.5	50	2

TABLE 2

Composition of Shield

Medium	Source and Lateral Shield	Sodium	Heat Exchanger
Mixture Number	1	2	3
Volume Fractions			
Steel	0.53	0	0.15
Sodium	0.47	1.0	0.85
Atoms/cm^3 x 10^{24}			
Sodium	0.01045	0.02223	0.01890
Iron	0.03200	0	0.00906
Nickel	0.00423	0	0.00120
Chrome	0.00860	0	0.00243

TABLE 3

Reference Spatial Mesh

Zone	Number of Zone	Total Number of Intervals in Zone	Interval Range in Zone	Interval Sizes		Outer Radius (cm)
				Number	Thickness	
Source	1	1	1	1	0.01	236.5 236.51
Radial Shield	2	60	2-61	1 59	2.99 3.00	239.5 416.5
Sodium Tank	3	125	62-186	125	4.00	916.5
Heat Exchanger	4	17	187-203	1 16	2.00 3.00	918.5 966.5
Sodium	5	13	204-216	1 12	2.00 4.00	968.5 1016.5

TABLE 4

Detector Cross-Sections and Fractional Errors on Fe and Na Cross-Sections

Group	Upper Energy	Cross-Section - Barns					Fe			Na		
		$Na^{23}(n\gamma)$	Fe dpa	Fe (cap)	Fe (el)	Fe (in)	σ_T	σ_{NE}	σ_A	σ_T	σ_{IN}	σ_A
1	1.492+1	2.05-4	2.666+3	1.335+0	5.689+2	2.096+3						
2	1.221+1	1.800-4	2.082+3	1.027+0	5.131+2	1.567+3						
3	1.000+1	1.730-4	2.011+3	7.168-1	5.298+2	1.480+3						
4	8.187+0	1.690-4	1.941+3	4.745-1	5.560+2	1.385+3					0.10	
5	6.703	1.650-4	1.772+3	2.972-1	6.431+2	1.129+3						
6	5.488	1.620-4	1.656+3	1.779-1	6.829+2	9.726+2	0.05			0.05		
7	4.493	1.610-4	1.514+3	1.196-1	7.112+2	8.031+2						
8	3.679	1.680-4	1.315+3	6.044-2	7.228+2	5.925+2		0.10				
9	3.011	1.768-4	1.193+3	2.933-2	7.675+2	4.253+2					0.20	0.15
10	2.466	1.828-4	1.084+2	1.985-2	7.202+2	3.641+2						
11	2.346	1.904-4	9.509+2	1.604-2	6.678+2	2.830+2						
12	1.827	2.017-4	7.574+2	1.575-2	5.886+2	1.687+2						
13	1.496	2.214-4	7.157+2	1.616-2	5.878+2	1.279+2				0.075		
14	1.225	2.237-4	4.880+2	1.785-2	3.911+2	9.697+1						
15	1.003	2.401-4	3.805+2	2.820-2	3.567+2	2.381+1	0.04					
16	8.209-1	3.257-4	4.212+2	3.451-2	4.212+2	0						
17	6.081-1	3.190-4	3.153+2	3.448-2	3.153+2	0			0.15			
18	4.979-1	2.533-4	3.618+2	3.304-2	3.618+2	0						
19	4.076-1	3.607-4	2.323+2	3.333-2	2.322+2	0						
20	3.337-1	7.325-4	1.479+2	3.867-2	1.478+2	0				0.05		
21	1.111-1	2.968-4	8.877+1	7.020-2	8.870+1	0						
22	6.738-2	6.536-4	5.489+1	4.707-2	5.484+1	0						
23	4.087-2	2.848-3	6.723+1	1.082-1	6.712+1	0						
24	3.183-2	4.795-4	1.869+2	1.431-1	1.867+2	0	0.05	0.15				
25	2.650-2	5.611-4	6.062+0	7.009-2	5.992+0	0						0.075
26	2.187-2	8.953-4	1.131+1	2.407-2	1.129+1	0						
27	1.171-2	1.717-3	2.374+1	1.053-1	2.364+1	0					0.10	
28	7.102-3	3.317-3	1.229+1	6.726-2	1.222+1	0				0.10		
29	4.307-3	3.609-2	6.016+0	4.429-2	5.971+0	0						
30	2.035-3	9.404-3	3.995+0	1.0540	2.941+0	0				0.05		
31	9.611-4	5.677-3	8.399-1	7.533-2	7.645-1	0						
32	4.540-4	6.808-3	1.550-1	1.550-1	0	0						
33	1.670-4	9.449-3	2.169-1	2.169-1	0	0						
34	1.013-4	1.181-2	2.796-1	2.796-1	0	0						
35	6.144-5	1.565-2	3.745-1	3.745-1	0	0						
36	2.902-5	2.063-2	5.374-1	5.374-1	0	0	0.03			0.04		0.05
37	1.760-5	2.733-2	7.063-1	7.063-1	0	0						
38	8.315-6	3.604-2	1.027+0	1.027+0	0	0		0.04	0.04			
39	5.044-6	5.065-2	1.588+0	1.588+0	0	0						
40	1.855-6	9.265-2	2.214+0	2.214+0	0	0						
41	4.140.7	1.685-1	5.410+0	5.410+0	0	0						
42	7.600-8	3.511-1	1.360+1	1.360+1	0	0						

TABLE 5 SENSITIVITY OF THE IRON DISPLACEMENT RATE TO IRON, CHROMIUM, NICKEL AND SODIUM CROSS-SECTIONS

	GROUP SENSITIVITY			
GRP.	IRON	CHROMIUM	NICKEL	SODIUM
1	-8.46E-05	-2.18584E-05	-1.36806E-05	-2.20824E-05
2	-3.60E-04	-8.84172E-05	-6.00028E-05	-9.09550E-05
3	-1.24E-03	-3.07873E-04	-2.15212E-04	-2.92340E-04
4	-2.87E-03	-6.83309E-04	-4.81562E-04	-6.00879E-04
5	-6.20E-03	-1.61242E-03	-1.10867E-03	-1.38004E-03
6	-9.80E-03	-2.57384E-03	-1.67015E-03	-2.06870E-03
7	-1.16E-02	-2.88435E-03	-1.67469E-03	-2.16765E-03
8	-1.80E-02	-4.72431E-03	-2.71309E-03	-3.56880E-03
9	-3.11E-02	-9.34543E-03	-5.31228E-03	-7.16881E-03
10	-7.61E-03	-2.51331E-03	-1.11526E-03	-2.24748E-03
11	-4.79E-02	-1.60761E-02	-7.07468E-03	-1.26106E-02
12	-5.29E-02	-1.92505E-02	-1.01881E-02	-1.69982E-02
13	-5.78E-02	-1.14319E-02	-7.03088E-03	-1.09479E-02
14	-8.34E-02	-1.10066E-02	-6.18355E-03	-1.44354E-02
15	-1.30E-01	-3.13148E-02	-1.54080E-02	-5.75326E-02
16	-1.42E-01	-4.87981E-02	-2.76909E-02	-1.51726E-01
17	-2.63E-01	-7.14923E-02	-4.36637E-02	-1.64090E-01
18	-1.62E-01	-3.59676E-02	-2.07040E-02	-7.07961E-02
19	-2.06E-01	-8.90487E-02	-7.00087E-02	-1.78000E-01
20	-2.48E+00	-1.12483E+00	-9.11382E-01	-1.90366E+00
21	-5.30E-02	-7.15512E-02	-1.05909E-01	-1.36382E-01
22	-3.60E-02	-2.36862E-02	-3.14425E-01	-8.17417E-02
23	1.08E-02	-5.13059E-03	-7.89043E-03	-2.79062E-02
24	2.71E-03	-2.75C71E-04	-6.08175E-04	-2.16860E-03
25	-8.54E-03	-1.41715E-02	-3.15965E-02	-3.60146E-02
26	1.15E-02	-9.93670E-03	-4.09719E-02	-2.25682E-02
27	1.95E-02	-9.89101E-03	-3.60586E-03	-2.11387E-02
28	1.27E-02	-4.22505E-03	-2.55263E-03	-8.55231E-03
29	3.74E-03	-4.85323E-04	-4.97600E-04	-4.31038E-03
30	1.10E-03	-1.86340E-03	-2.19447E-03	-5.78172E-03
31	-1.89E-03	-7.89639E-04	-1.15969E-03	-1.09940E-03
32	-3.46E-03	-6.19392E-04	-8.66387E-04	2.05246E-04
33	-1.37E-03	-3.07400E-04	-4.06121E-04	1.00734E-04
34	-1.21E-03	-3.18444E-04	-4.01742E-04	8.73776E-05
35	-1.51E-03	-5.09643E-04	-5.98676E-04	9.91775E-05
36	-7.20E-04	-3.67739E-04	-4.06352E-04	1.93499E-05
37	-6.80E-04	-5.67228E-04	-5.81299E-04	-1.65864E-05
38	-9.00E-05	-3.98751E-04	-3.91363E-04	-1.16941E-04
39	7.20E-04	-7.13246E-04	-6.56833E-04	-5.30169E-04
40	1.49E-03	-6.50469E-04	-4.92959E-04	-7.52417E-04

TABLE 6 SENSITIVITY OF THE SODIUM CAPTURE RATE IN THE HEAT EXCHANGER TO IRON, CHROMIUM, NICKEL AND SODIUM CROSS-SECTIONS

	GROUP SENSITIVITY			
GRP.	IRON	CHROMIUM	NICKEL	SODIUM
1	-7.55522E-05	-1.95230E-05	-1.24479E-05	-2.01E-05
2	-3.27060E-04	-7.97440E-05	-5.51486E-05	-8.31E-05
3	-1.14752E-03	-2.82815E-04	-2.01013E-04	-2.71E-04
4	-2.69436E-03	-6.39947E-04	-4.57394E-04	-5.66E-04
5	-5.86045E-03	-1.51981E-03	-1.05759E-03	-1.31E-03
6	-9.32622E-03	-2.44687E-03	-1.60287E-03	-1.97E-03
7	-1.10799E-02	-2.76227E-03	-1.61553E-03	-2.08E-03
8	-1.71471E-02	-4.49055E-03	-2.58588E-03	-3.40E-03
9	-2.94611E-02	-8.86708E-03	-5.05934E-03	-6.78E-03
10	-7.24171E-03	-2.39467E-03	-1.06604E-03	-2.15E-03
11	-4.54147E-02	-1.51077E-02	-6.67515E-03	-1.20E-02
12	-4.90081E-02	-1.81624E-02	-9.63507E-03	-1.60E-02
13	-5.42490E-02	-1.09687E-02	-6.76790E-03	-1.04E-02
14	-7.80740E-02	-1.02979E-02	-5.79790E-03	-1.28E-02
15	-1.18245E-01	-2.79033E-02	-1.37541E-02	-5.06E-02
16	-1.35735E-01	-4.60520E-02	-2.60025E-02	-1.42E-01
17	-2.50049E-01	-6.77787E-02	-4.13577E-02	-1.55E-01
18	-1.58584E-01	-3.47930E-02	-2.00918E-02	-6.90E-02
19	-2.04981E-01	-8.64174E-02	-6.79725E-02	-1.74E-01
20	-2.73806E+00	-1.03363E+00	-8.38378E-01	-2.30E+00
21	-2.69997E-01	-8.96018E-02	-1.26787E-01	-3.66E-01
22	-2.06357E-01	-3.78683E-02	-4.83652E-02	-2.36E-01
23	-6.88797E-02	-7.54497E-03	-1.21030E-02	-1.00E-01
24	-7.06517E-03	-4.03578E-04	-1.04165E-03	-5.51E-02
25	-5.75763E-02	-4.98432E-02	-1.11243E-01	-2.00E-01
26	-8.42953E-02	-3.05617E-02	-1.27568E-01	-3.04E-01
27	-4.87740E-02	-1.66192E-02	-7.08039E-03	-1.36E-01
28	-1.33008E-02	-1.16128E-02	-6.32592E-03	-5.37E-02
29	-3.59239E-03	-1.98637E-03	-1.61507E-03	-8.60E-03
30	-8.86960E-02	-1.32253E-02	-1.52368E-02	-2.36E-01
31	-9.20417E-02	-1.24871E-02	-1.95155E-02	-8.92E-01
32	-7.56963E-02	-9.41839E-03	-1.51666E-02	-1.71E+00
33	-1.37754E-02	-1.76881E-03	-2.75178E-03	-6.43E-01
34	-9.06512E-03	-1.22139E-03	-1.74601E-03	-6.26E-01
35	-9.78084E-03	-1.55318E-03	-1.62985E-03	-9.92E-01
36	-4.76849E-03	-1.00062E-03	-5.17125E-04	-5.72E-01
37	-1.00639E-02	-2.55453E-03	-5.60591E-04	-8.72E-01
38	-9.35987E-03	-2.70022E-03	-3.01853E-04	-4.97E-01
39	-4.04220E-02	-1.14487E-02	-9.87577E-04	-9.80E-01
40	-1.21331E-01	-3.48691E-02	-2.76747E-03	-9.60E-01

GROUP SENSITIVITIES

GRP.	U(T).	U(AB).	U(IN).	U(EL).
1	-8.46E-05	-1.89E-05	-4.27E-05	-2.31E-05
2	-3.60E-04	-6.38E-05	-2.02E-04	-9.43E-05
3	-1.24E-03	-1.53E-04	-7.38E-04	-3.53E-04
4	-2.87E-03	-2.24E-04	-1.70E-03	-8.87E-04
5	-6.20E-03	-3.24E-04	-3.34E-03	-2.53E-03
6	-9.80E-03	-3.07E-04	-4.77E-03	-4.73E-03
7	-1.16E-02	-2.46E-04	-3.15E-03	-8.16E-03
8	-1.80E-02	-2.20E-04	-7.40E-03	-1.04E-02
9	-3.11E-02	-2.10E-04	-1.03E-02	-1.45E-02
10	-7.61E-03	-4.15E-05	-3.83E-03	-3.74E-03
11	-4.79E-02	-2.14E-04	-2.40E-02	-2.37E-02
12	-5.29E-02	-2.61E-04	-2.18E-02	-3.09E-02
13	-5.78E-02	-2.86E-04	-3.23E-02	-2.52E-02
14	-8.34E-02	-3.98E-04	-6.20E-02	-2.04E-02
15	-1.30E-01	-1.21E-03	-6.19E-02	-6.62E-02
16	-1.42E-01	-3.09E-03	0.0	-1.40E-01
17	-2.63E-01	-4.14E-03	0.0	-2.58E-01
18	-1.62E-01	-3.02E-03	0.0	-1.59E-01
19	-2.06E-01	-4.50E-03	0.0	-2.02E-01
20	-2.48E+00	-8.69E-02	0.0	-2.40E+00
21	-5.30E-02	-9.05E-03	0.0	-4.40E-02
22	-3.60E-02	-2.99E-03	0.0	-3.30E-02
23	1.08E-02	-1.24E-03	0.0	1.21E-02
24	2.71E-03	-5.66E-04	0.0	3.27E-03
25	-8.54E-03	-1.23E-03	0.0	-7.30E-03
26	1.15E-02	-6.61E-04	0.0	2.21E-02
27	1.95E-02	-1.02E-03	0.0	2.05E-02
28	1.27E-02	-2.56E-04	0.0	1.30E-02
29	3.74E-03	-8.28E-05	0.0	3.66E-03
30	1.10E-03	5.20E-04	0.0	5.80E-04
31	-1.89E-03	-2.00E-05	0.0	-1.87E-03
32	-3.46E-03	6.60E-05	0.0	-3.53E-03
33	-1.37E-03	1.45E-04	0.0	-1.51E-03
34	-1.21E-03	1.91E-04	0.0	-1.40E-03
35	-1.51E-03	3.67E-04	0.0	-1.88E-03
36	-7.20E-04	4.18E-04	0.0	-1.14E-03
37	-6.80E-04	7.10E-04	0.0	-1.39E-03
38	-9.00E-05	7.44E-04	0.0	-6.54E-04
39	7.20E-04	1.89E-04	0.0	5.31E-0
40	1.49E-03	1.70E-03	0.0	-2.10E-04

DETECTOR CONTRIBUTIONS

GRP.	U(DET).	U(AB)D.	U(IN)D.	U(EL)D.
1	4.40E-08	0.0	3.47E-08	9.37E-09
2	1.12E-07	0.0	8.43E-08	2.89E-08
3	1.59E-07	0.0	1.17E-07	4.18E-08
4	1.27E-07	0.0	9.07E-08	3.63E-08
5	1.87E-07	0.0	1.19E-07	6.79E-08
6	2.05E-07	0.0	1.21E-07	8.45E-08
7	2.33E-07	0.0	1.23E-07	1.10E-07
8	4.72E-07	0.0	2.13E-07	2.59E-07
9	9.99E-07	0.0	3.57E-07	6.42E-07
10	2.73E-07	0.0	9.17E-08	1.81E-07
11	3.70E-06	0.0	1.10E-06	2.60E-06
12	1.33E-05	0.0	2.97E-06	1.03E-05
13	2.38E-05	0.0	4.26E-06	1.95E-05
14	4.17E-05	0.0	8.30E-06	3.34E-05
15	1.90E-04	0.0	1.20E-05	1.78E-04
16	5.80E-04	0.0	0.0	5.80E-04
17	1.31E-03	0.0	0.0	1.31E-03
18	2.21E-03	0.0	0.0	2.21E-03
19	3.83E-03	0.0	0.0	3.83E-03
20	4.94E-01	0.0	0.0	4.94E-01
21	1.59E-01	0.0	0.0	1.59E-01
22	1.03E-01	0.0	0.0	1.03E-01
23	5.93E-02	0.0	0.0	5.93E-02
24	7.55E-03	0.0	0.0	7.55E-03
25	7.86E-03	0.0	0.0	7.78E-03
26	3.89E-02	0.0	0.0	3.89E-02
27	4.81E-02	0.0	0.0	4.80E-02
28	1.74E-02	0.0	0.0	1.74E-02
29	5.32E-03	0.0	0.0	5.27E-03
30	1.37E-02	3.62E-03	0.0	1.01E-02
31	3.49E-03	3.14E-04	0.0	3.18E-03
32	8.35E-04	8.35E-04	0.0	0.0
33	5.62E-04	5.62E-04	0.0	0.0
34	6.99E-04	6.99E-04	0.0	0.0
35	1.32E-03	1.32E-03	0.0	0.0
36	1.18E-03	1.18E-03	0.0	0.0
37	2.01E-03	2.01E-03	0.0	0.0
38	1.71E-03	1.71E-03	0.0	0.0
39	3.73E-03	3.73E-03	0.0	0.0
40	3.65E-03	3.65E-03	0.0	0.0

TABLE 7 SENSITIVITY OF [illegible] S AND THE DETECTOR CONTRIBUTIONS

TABLE 8 SENSITIVITY OF FE DISPLACEMENT IN MESH 61 TO NA CROSS-SECTIONS

GROUP SENSITIVITIES

GRP.	U(T).	U(AB).	U(IN).	U(EL).
1	-2.21E-05	-6.05E-06	-1.19E-05	-4.15E-06
2	-9.10E-05	-2.72E-05	-4.87E-05	-1.51E-05
3	-2.92E-04	-5.60E-05	-1.91E-04	-4.57E-05
4	-6.01E-04	-6.27E-05	-4.25E-04	-1.13E-04
5	-1.38E-03	-6.54E-05	-9.59E-04	-3.56E-04
6	-2.07E-03	-1.19E-05	-1.31E-03	-7.51E-04
7	-2.17E-03	-1.32E-06	-1.47E-03	-6.97E-04
8	-3.57E-03	-1.29E-06	-1.98E-03	-1.59E-03
9	-7.17E-03	-2.71E-06	-4.03E-03	-3.14E-03
10	-2.25E-03	-8.33E-07	-7.67E-04	-1.48E-03
11	-1.26E-02	-5.55E-06	-5.91E-03	-6.70E-03
12	-1.70E-02	-7.31E-06	-5.47E-03	-1.15E-02
13	-1.10E-02	-8.22E-06	-1.93E-03	-9.02E-03
14	-1.44E-02	-1.09E-05	-6.29E-03	-8.14E-03
15	-5.75E-02	-2.31E-05	-1.87E-02	-3.88E-02
16	-1.52E-01	-6.36E-05	-4.09E-02	-1.11E-01
17	-1.64E-01	-8.31E-05	-1.63E-02	-1.48E-01
18	-7.08E-02	-5.11E-05	-2.68E-03	-6.81E-02
19	-1.78E-01	-1.06E-04	0.0	-1.78E-01
20	-1.90E+00	-4.27E-03	0.0	-1.90E+00
21	-1.36E-01	-1.31E-04	0.0	-1.36E-01
22	-8.17E-02	-1.42E-04	0.0	-8.16E-02
23	-2.79E-02	-1.68E-04	0.0	-2.77E-02
24	-2.17E-03	-1.07E-05	0.0	-2.16E-03
25	-3.60E-02	-3.24E-05	0.0	-3.60E-02
26	-2.26E-02	-1.15E-04	0.0	-2.25E-02
27	-2.11E-02	-9.09E-05	0.0	-2.11E-02
28	-8.55E-03	-5.81E-05	0.0	-8.49E-03
29	-4.31E-03	-2.19E-04	0.0	-4.10E-03
30	-5.78E-03	-2.42E-04	0.0	-5.54E-03
31	-1.10E-03	-1.34E-04	0.0	-9.66E-04
32	2.05E-04	-1.87E-04	0.0	-1.80E-05
33	1.01E-04	-1.28E-04	0.0	2.29E-04
34	8.74E-05	-1.58E-04	0.0	2.45E-04
35	9.92E-05	-3.03E-04	0.0	4.02E-04
36	1.93E-05	-2.61E-04	0.0	2.80E-04
37	-1.65E-05	-4.75E-04	0.0	3.09E-04
38	-1.17E-04	-3.93E-04	0.0	2.76E-04
39	-5.30E-04	-8.62E-04	0.0	3.32E-04
40	-7.52E-04	-1.30E-03	0.0	5.50E-04

TABLE 9 SENSITIVITY OF SODIUM CAPTURE RATE IN H.E. TO FE CROSS-SECTIONS

GROUP SENSITIVITIES

GRP.	U(T).	U(AB).	U(IN).	U(EL).
1	-7.56E-05	-1.76E-05	-3.70E-05	-2.10E-05
2	-3.27E-04	-5.99E-05	-1.80E-04	-8.70E-05
3	-1.15E-03	-1.46E-04	-6.68E-04	-3.35E-04
4	-2.69E-03	-2.16E-04	-1.63E-03	-8.45E-04
5	-5.86E-03	-3.14E-04	-3.12E-03	-2.43E-03
6	-9.33E-03	-3.00E-04	-4.47E-03	-4.56E-03
7	-1.11E-02	-2.42E-04	-4.98E-03	-5.86E-03
8	-1.72E-02	-2.15E-04	-6.89E-03	-1.00E-02
9	-2.95E-02	-2.05E-04	-1.54E-02	-1.39E-02
10	-7.24E-03	-4.07E-05	-3.63E-03	-3.58E-03
11	-4.54E-02	-2.09E-04	-2.24E-02	-2.25E-02
12	-4.90E-02	-2.54E-04	-1.98E-02	-2.89E-02
13	-5.43E-02	-2.81E-04	-2.97E-02	-2.42E-02
14	-7.81E-02	-3.87E-04	-5.86E-02	-1.91E-02
15	-1.18E-01	-1.15E-03	-5.81E-02	-5.89E-02
16	-1.36E-01	-3.04E-03	0.0	-1.33E-01
17	-2.50E-01	-4.11E-03	0.0	-2.46E-01
18	-1.59E-01	-3.06E-03	0.0	-1.56E-01
19	-2.05E-01	-4.56E-03	0.0	-2.00E-01
20	-2.74E+00	-8.39E-02	0.0	-2.65E+00
21	-2.70E-01	-1.39E-02	0.0	-2.56E-01
22	-2.06E-01	-6.01E-03	0.0	-2.00E-01
23	-6.89E-02	-3.27E-03	0.0	-6.56E-02
24	-7.07E-03	-1.85E-03	0.0	-5.21E-03
25	-5.76E-02	-4.15E-03	0.0	-5.34E-02
26	-8.43E-02	-2.15E-03	0.0	-8.22E-02
27	-4.88E-02	-3.52E-03	0.0	-4.52E-02
28	-1.33E-02	-1.35E-03	0.0	-1.20E-02
29	-3.59E-03	-5.59E-04	0.0	-3.03E-03
30	-8.87E-02	-2.40E-02	0.0	-6.47E-02
31	-9.20E-02	-3.08E-03	0.0	-8.90E-02
32	-7.57E-02	-4.88E-03	0.0	-7.08E-02
33	-1.38E-02	-1.09E-03	0.0	-1.27E-02
34	-9.07E-03	-1.08E-03	0.0	-7.98E-03
35	-9.78E-03	-2.33E-03	0.0	-7.45E-03
36	-4.77E-03	-2.28E-03	0.0	-2.49E-03
37	-1.01E-03	-6.86E-03	0.0	-3.20E-03
38	-9.36E-03	-7.92E-03	0.0	-1.71E-03
39	-4.04E-02	-3.34E-02	0.0	-7.05E-03
40	-1.21E-01	-1.02E-01	0.0	-1.90E-02

	GROUP SENSITIVITIES					DETECTOR CONTRIBUTIONS			
GRP.	U(T).	U(AB).	U(IN).	U(EL).	GRP.	U(DET).	U(AB)D.	U(IN)D.	U(EL)D.
1	-2.01E-05	-5.64E-06	-1.07E-05	-3.74E-06	1	0.0	0.0	0.0	0.0
2	-8.31E-05	-2.56E-05	-4.45E-05	-1.31E-05	2	0.0	0.0	0.0	0.0
3	-2.71E-04	-5.33E-05	-1.75E-04	-4.21E-05	3	0.0	0.0	0.0	0.0
4	-5.66E-04	-6.05E-05	-3.98E-04	-1.07E-04	4	0.0	0.0	0.0	0.0
5	-1.31E-03	-6.34E-05	-9.05E-04	-3.42E-04	5	0.0	0.0	0.0	0.0
6	-1.97E-03	-1.17E-05	-1.24E-03	-7.16E-04	6	0.0	0.0	0.0	0.0
7	-2.08E-03	-1.30E-06	-1.41E-03	-6.69E-04	7	0.0	0.0	0.0	0.0
8	-3.40E-03	-1.26E-06	-1.87E-03	-1.53E-03	8	0.0	0.0	0.0	0.0
9	-6.78E-03	-2.64E-06	-3.79E-03	-2.99E-03	9	0.0	0.0	0.0	0.0
10	-2.15E-03	-8.18E-07	-7.35E-04	-1.41E-03	10	0.0	0.0	0.0	0.0
11	-1.20E-02	-5.44E-06	-5.58E-03	-6.36E-03	11	0.0	0.0	0.0	0.0
12	-1.60E-02	-7.12E-06	-5.36E-03	-1.06E-02	12	0.0	0.0	0.0	0.0
13	-1.04E-02	-8.08E-06	-1.75E-03	-8.67E-03	13	0.0	0.0	0.0	0.0
14	-1.28E-02	-1.06E-05	-5.26E-03	-7.55E-03	14	0.0	0.0	0.0	0.0
15	-5.06E-02	-2.20E-05	-1.68E-02	-3.34E-02	15	0.0	0.0	0.0	0.0
16	-1.42E-01	-6.25E-05	-3.90E-02	-1.03E-01	16	0.0	0.0	0.0	0.0
17	-1.55E-01	-8.26E-05	-1.57E-02	-1.40E-01	17	0.0	0.0	0.0	0.0
18	-6.90E-02	-5.20E-05	-2.73E-03	-6.62E-02	18	0.0	0.0	0.0	0.0
19	-1.74E-01	-1.09E-04	0.0	-1.74E-01	19	0.0	0.0	0.0	0.0
20	-2.30E+00	-5.35E-03	0.0	-2.30E+00	20	4.28E-07	4.28E-07	0.0	0.0
21	-3.66E-01	-4.22E-04	0.0	-3.65E-01	21	1.22E-07	1.22E-07	0.0	0.0
22	-2.36E-01	-6.57E-04	0.0	-2.35E-01	22	2.86E-07	2.86E-07	0.0	0.0
23	-1.00E-01	-1.42E-03	0.0	-9.90E-02	23	7.39E-07	7.39E-07	0.0	0.0
24	-5.51E-02	-1.79E-04	0.0	-5.50E-02	24	6.96E-08	6.96E-08	0.0	0.0
25	-2.00E-01	-2.69E-04	0.0	-2.00E-01	25	1.45E-07	1.45E-07	0.0	0.0
26	-3.04E-01	-1.45E-03	0.0	-3.03E-01	26	9.65E-07	9.65E-07	0.0	0.0
27	-1.36E-01	-1.67E-03	0.0	-1.34E-01	27	9.45E-07	9.45E-07	0.0	0.0
28	-5.37E-02	-1.80E-03	0.0	-5.19E-02	28	1.60E-06	1.60E-06	0.0	0.0
29	-8.60E-03	-6.54E-03	0.0	-2.06E-03	29	7.53E-06	7.53E-06	0.0	0.0
30	-2.36E-01	-1.46E-02	0.0	-2.21E-01	30	1.50E-05	1.50E-05	0.0	0.0
31	-8.92E-01	-2.23E-02	0.0	-8.70E-01	31	5.03E-05	5.03E-05	0.0	0.0
32	-1.71E+00	-4.96E-02	0.0	-1.66E+00	32	8.51E-04	8.51E-04	0.0	0.0
33	-6.43E-01	-2.43E-02	0.0	-6.19E-01	33	9.82E-04	9.82E-04	0.0	0.0
34	-6.26E-01	-2.90E-02	0.0	-5.97E-01	34	1.97E-03	1.97E-03	0.0	0.0
35	-9.92E-01	-5.86E-02	0.0	-9.36E-01	35	7.65E-03	7.65E-03	0.0	0.0
36	-5.72E-01	-4.07E-02	0.0	-5.31E-01	36	9.40E-03	9.40E-03	0.0	0.0
37	-8.72E-01	-7.36E-02	0.0	-7.98E-01	37	2.91E-02	2.91E-02	0.0	0.0
38	-4.97E-01	-4.81E-02	0.0	-4.48E-01	38	2.94E-02	2.94E-02	0.0	0.0
39	-9.80E-01	-1.01E-01	0.0	-8.74E-01	39	1.20E-01	1.20E-01	0.0	0.0
40	-9.60E-01	-1.10E-01	0.0	-8.44E-01	40	3.13E-01	3.13E-01	0.0	0.0

TABLE 10 SENSITIVITY OF SODIUM CAPTURE RATE IN H.E TO NA CROSS SECTIONS. AND THE DETECTOR CONTRIBUTIONS.

Table 11 - Total Problem Sensitivities

	Cr	Fe	Ni	Na	Total	Reaction-Rate
Sensitivity	-1.63	-4.74	-1.37	- 2.95	-10.69	Fe d.p.a. Mesh 61
$P_3 \rightarrow P_1$ %	-0.34	-0.92	-0.15	- 0.25	- 1.66	
Sensitivity	-1.79	-5.40	-1.56	-14.89	-23.64	Na (n,γ) H.X.
$P_3 \rightarrow P_1$ %	-0.31	-0.83	-0.14	- 0.30	- 1.58	

Table 12 - Standard Deviations on Calculated Reaction-Rates

Energy Dependent Correlation	Fractional Error %				Reaction-Rate
	Fe	Na	Na + Fe	Total	
r = 0 r = 1-|i-j|/41 r = 1	12.3 16.4 16.8	9.66 14.3 14.6	15.6 21.8 22.2	21.7 30.3 30.9	Fe displacements Mesh 61
r = 0 r = 1-|i-j|/41 r = 1	13.6 21.5 22.5	16.5 50.7 56.9	21.4 55.1 61.2	24.9 64.2 71.3	Na (n,γ) H.X.

Radius CM	Mesh	Total Flux $\bar{\Phi}(\tau)$ cm^{-2} sec^{-1}	Equivalent Thermal Flux cm^{-2} sec^{-1}	Total Flux E>0.111 MeV cm^{-2} sec^{-1}	Atom Displacement Rate Fe d.p.a. $atom^{-1}$ sec^{-1}	$\frac{\text{Fe d.p.a.}}{\bar{\Phi}(\tau)}$ b	Sodium Activation Rate $atom^{-1}$ sec^{-1}	$\frac{\text{Sodium Activation}}{\bar{\Phi}(\tau)}$ b	$\frac{U235(n,f)}{\text{Reaction Rate}}$ $atom^{-1}$ sec^{-1}	$\frac{U235(n,f)}{\bar{\Phi}(\tau)}$ b	$Co^{59}(n,\gamma)$ Reaction Rate $atom^{-1}$ sec^{-1}	$\frac{Co^{59}(n,\gamma)}{\bar{\Phi}(\tau)}$ b
262	10	2.26,13	2.79,11	3.55,12	1.02,15	4.53,1	2.13,11	9.42,-3	2.99,14	1.32,1	1.22,14	5.39,0
292	20	4.71,12	8.24,10	5.80,11	1.57,14	3.34,1	5.73,10	1.22,-2	7.78,13	1.65,1	2.88,13	6.11,0
322	30	8.51,11	1.64,10	8.76,10	2.39,13	2.81,1	1.12,10	1.32,-2	1.50,13	1.76,1	5.43,12	6.38,0
352	40	1.43,11	2.94,9	1.27,10	3.53,12	2.46,1	1.99,9	1.39,-2	2.65,12	1.85,1	9.53,11	6.64,0
382	50	2.28,10	4.90,8	1.79,9	5.09,11	2.24,1	3.29,8	1.45,-2	4.37,11	1.92,1	1.56,11	6.86,0
415	61	2.68,9	7.13,7	1.79,8	5.32,10	1.99,1	4.57,7	1.71,-2	5.79,10	2.16,1	1.95,10	7.30,0
418.5	62	2.32,9	6.99,7	1.44,8	4.46,10	1.92,1	4.28,7	1.84,-2	5.40,10	2.33,1	1.73,10	7.48,0
498.5	82	5.55,8	3.83,7	6.97,6	3.3 ,9	5.95,0	2.171,7	3.91,-2	2.41,10	4.34,1	5.95,9	1.07,1
578.5	102	1.19,8	1.25,7	3.51,5	3.46,8	2.91,0	6.92,6	5.82,-2	7.06,9	5.93,1	1.25,9	1.05,1
666.5	124	1.90,7	2.69,6	1.34,4	4.90,7	2.59,0	1.47,6	7.76,-2	1.41,9	7.43,1	1.80,8	9.48,0
738.5	142	3.77,6	6.39,5	9.37,2	1.07,7	2.84,0	3.48,5	9.23,-2	3.23,8	8.57,1	3.44,7	9.12,0
818.5	162	5.65,5	1.11,5	4.95,1	1.83,6	3.24,0	6.04,4	1.07,-1	5.51,7	9.75,1	5.19,6	9.19,0
914.5	186	5.15,4	1.06,4	1.55,0	1.73,5	3.35,0	5.76,3	1.05,-1	5.17,6	9.37,1	4.62,5	8.96,0
917.5	187	4.55,4	9.15,3	1.39,0	1.48,5	3.26,0	4.96,3	1.09,-1	4.43,6	9.73,1	4.00,5	8.72,0
932	192	1.63,4	2.83,3	7.07,-1	4.53,4	2.78,0	1.54,3	9.44,-2	1.34,6	8.20,1	1.28,5	7.82,0
947	197	5.83,3	9.40,2	3.46,-1	1.50,4	2.82,0	5.13,2	8.80,-2	4.39,5	7.52,1	4.29,4	7.36,0
965	203	1.67,3	2.77,2	1.40,-1	4.44,3	2.91,0	1.51,2	9.06,-2	1.29,5	7.73,1	1.24,4	7.43,0

TABLE 13 - REACTION-RATES AND EFFECTIVE CROSS-SECTIONS IN SHIELD

GRP	Sensitivity to Iron Cross-Section			Sensitivity to Sodium Cross-Section		
	+W(ai)	W(xi)	W(Ti)	W(ai)	W(n'i)	W(Ti)
1	0.1844E-09	0.4220E-09	0.3905E-09	0.6116E-10	0.7566E-10	0.2015E-10
2	0.2092E-08	0.1377E-07	0.5329E-08	0.1227E-08	0.1088E-08	0.3592E-09
3	0.1255E-07	0.1770E-06	0.6752E-07	0.5255E-08	0.1723E-07	0.3818E-08
4	0.2810E-07	0.8757E-06	0.4194E-06	0.6567E-08	0.7822E-07	0.2080E-07
5	0.6819E-07	0.2222E-05	0.2872E-05	0.7025E-08	0.3741E-06	0.1452E-06
6	0.6918E-07	0.2465E-05	0.9788E-05	0.2311E-09	0.5821E-06	0.4718E-06
7	0.6268E-07	0.2338E-05	0.2912E-04	0.2314E-11	0.1234E-05	0.3214E-06
8	0.3834E-07	0.2703E-05	0.4179E-04	0.3034E-11	0.7332E-05	0.1373E-05
9	0.2688E-07	0.7584E-04	0.6795E-04	0.1399E-10	0.3097E-04	0.5391E-05
10	0.1215E-08	0.4033E-05	0.4367E-05	0.1271E-11	0.7044E-06	0.9098E-06
11	0.6396E-07	0.2135E-04	0.1680E-03	0.5885E-10	0.6003E-04	0.2110E-04
12	0.4712E-07	0.1134E-03	0.2628E-03	0.9462E-10	0.8598E-05	0.1206E-03
13	0.3533E-07	0.4320E-03	0.1102E-03	0.1352E-09	0.3881E-06	0.6463E-04
14	0.1912E-07	0.2070E-02	0.8075E-04	0.2572E-09	0.2458E-04	0.5611E-04
15	0.9356E-08	0.2042E-02	0.5810E-03	0.1007E-08	0.2415E-03	0.1090E-02
16	0.1430E-04		0.2098E-02	0.7751E-08	0.1275E-02	0.3698E-02
17	0.2568E-04		0.7123E-02	0.1103E-07	0.1779E-03	0.6150E-02
18	0.1366E-04		0.2691E-02	0.5039E-08	0.6111E-05	0.1255E-02
19	0.3034E-04		0.6825E-02	0.1879E-07		0.8501E-02
20	0.1131E-01		0.9628E+00	0.9077E-05		0.9692E+00
21	0.1227E-03		0.3240E-03	0.8738E-08		0.4960E-02
22	0.1339E-04		0.1821E-03	0.1046E-07		0.1786E-02
23	0.2304E-05		0.2444E-04	0.1668E-07		0.2060E-03
24	0.4799E-06		0.1780E-05	0.6601E-10		0.1251E-05
25	0.2267E-05		0.9072E-05	0.4671E-09		0.3477E-03
26	0.6546E-06		0.8130E-04	0.7386E-08		0.1358E-03
27	0.1559E-05		0.7011E-04	0.4307E-08		0.4779E-03
28	0.9818E-07		0.2821E-04	0.1839E-08		0.7737E-04
29	0.1027E-07		0.2436E-05	0.2810E-07		0.4514E-05
30	0.1175E-04		0.2868E-06	0.1457E-07		0.8258E-05
31	0.5993E-09		0.2100E-06	0.4693E-08		0.1608E-05
32	0.6526E-08		0.7425E-06	0.9373E-08		0.5587E-10
33	0.3150E-07		0.1366E-06	0.4444E-08		0.9055E-08
34	0.3887E-08		0.1175E-06	0.6777E-08		0.1038E-07
35	0.1435E-05		0.2156E-06	0.2496E-07		0.2803E-07
36	0.1861E-07		0.7926E-07	0.1853E-07		0.1364E-07
37	0.5370E-07		0.1178E-06	0.6121E-07		0.1668E-07
38	0.6218E-07		0.4276E-07	0.4210E-07		0.1338E-07
39	0.1343E-07		0.8494E-07	0.2018E-06		0.1954E-07
40	0.2365E-08		0.2831E-08	0.4644E-06		0.5496E-07

TABLE 14: Group Contribution to the Measurement Sensitivities of Sodium Capture Rate by Iron and Sodium Cross-Sections

+ See Page 5 for definition of

	Sensitivity to Iron Cross-Section			Sensitivity to Sodium Cross-Section		
Grp	+W(ai)	W(xi)	W(Ti)	W(ai)	W(n'i)	W(Ti)
1	0.1428E-09	0.2823E-09	0.2619E-09	0.1845E-10	0.2091E-10	0.5606E-11
2	0.1606E-08	0.8509E-08	0.3632E-08	0.3844E-09	0.3282E-09	0.9261E-10
3	0.9924E-08	0.1115E-06	0.4935E-07	0.1652E-08	0.4926E-08	0.1110E-08
4	0.2229E-07	0.5885E-06	0.3089E-06	0.2110E-08	0.2320E-07	0.6389E-08
5	0.5394E-07	0.1496E-05	0.2151E-05	0.2270E-08	0.1116E-06	0.4591E-07
6	0.5552E-07	0.1606E-05	0.7383E-05	0.7752E-10	0.1767E-06	0.1469E-06
7	0.3786E-07	0.1071E-05	0.1219E-04	0.1108E-11	0.3856E-06	0.1014E-06
8	0.3078E-07	0.1580E-05	0.3136E-04	0.9959E-12	0.2197E-05	0.4356E-06
9	0.2156E-07	0.5409E-04	0.5668E-04	0.4575E-11	0.9267E-05	0.1674E-05
10	0.9778E-09	0.2907E-05	0.1700E-04	0.4237E-12	0.2239E-06	0.2829E-06
11	0.2389E-07	0.1185E-03	0.1229E-03	0.1952E-10	0.1022E-04	0.6513E-05
12	0.3853E-07	0.7288E-04	0.1866E-03	0.3131E-10	0.3150E-05	0.3511E-04
13	0.3082E-07	0.2893E-03	0.8248E-04	0.4493E-10	0.8223E-07	0.2045E-04
14	0.1757E-07	0.1472E-02	0.5745E-04	0.8375E-10	0.5493E-05	0.1654E-04
15	0.9514E-08	0.1481E-02	0.3733E-03	0.9208E-09	0.6816E-04	0.2766E-03
16	0.1124E-04		0.1536E-02	0.2599E-08	0.4012E-03	0.1091E-02
17	0.2054E-04		0.5256E-02	0.3817E-08	0.5709E-04	0.1885E-02
18	0.1139E-04		0.2110E-02	0.1806E-08	0.2197E-05	0.4061E-03
19	0.2528E-04		0.5431E-02	0.7012E-08		0.2783E-02
20	0.6559E-02		0.9527E+00	0.4915E-05		0.4865E+00
21	0.2349E-03		0.8902E-02	0.3190E-07		0.1224E-01
22	0.4392E-04		0.5429E-02	0.8132E-07		0.5075E-02
23	0.1300E-04		0.5830E-03	0.4131E-06		0.9012E-03
24	0.4162E-05		0.3667E-05	0.6177E-08		0.2779E-03
25	0.2094E-04		0.3940E-03	0.1226E-07		0.3676E-02
26	0.5621E-05		0.9129E-03	0.4001E-06		0.8437E-02
27	0.1507E-04		0.2766E-03	0.5487E-06		0.6603E-02
28	0.2216E-05		0.1951E-04	0.6566E-06		0.9904E-03
29	0.3800E-06		0.1244E-05	0.8836E-05		0.3904E-06
30	0.7004E-03		0.5767E-03	0.1864E-04		0.4501E-02
31	0.1153E-04		0.3861E-03	0.3958E-04		0.4467E-01
32	0.2896E-04		0.2438E-03	0.1924E-03		0.1628E+00
33	0.1445E-05		0.7845E-05	0.4583E-04		0.2266E-01
34	0.1009E-06		0.3097E-05	0.6524E-04		0.2112E-01
35	0.4694E-06		0.2748E-05	0.2655E-03		0.5205E-01
36	0.4495E-06		0.3069E-06	0.1265E-03		0.1681E-01
37	0.4069E-05		0.5069E-06	0.4063E-03		0.3810E-01
38	0.5424E-05		0.1473E-06	0.1689E-03		0.1208E-01
39	0.9646E-04		0.2503E-05	0.6919E-03		0.4639E-01
40	0.8996E-03		0.1881E-04	0.6717E-03		0.4433E-01

TABLE 15: Group Contributions to the Measurement Sensitivities of Iron Displacement Rate by Iron and Sodium Cross-Sections

+ See Page 5 for definition of W

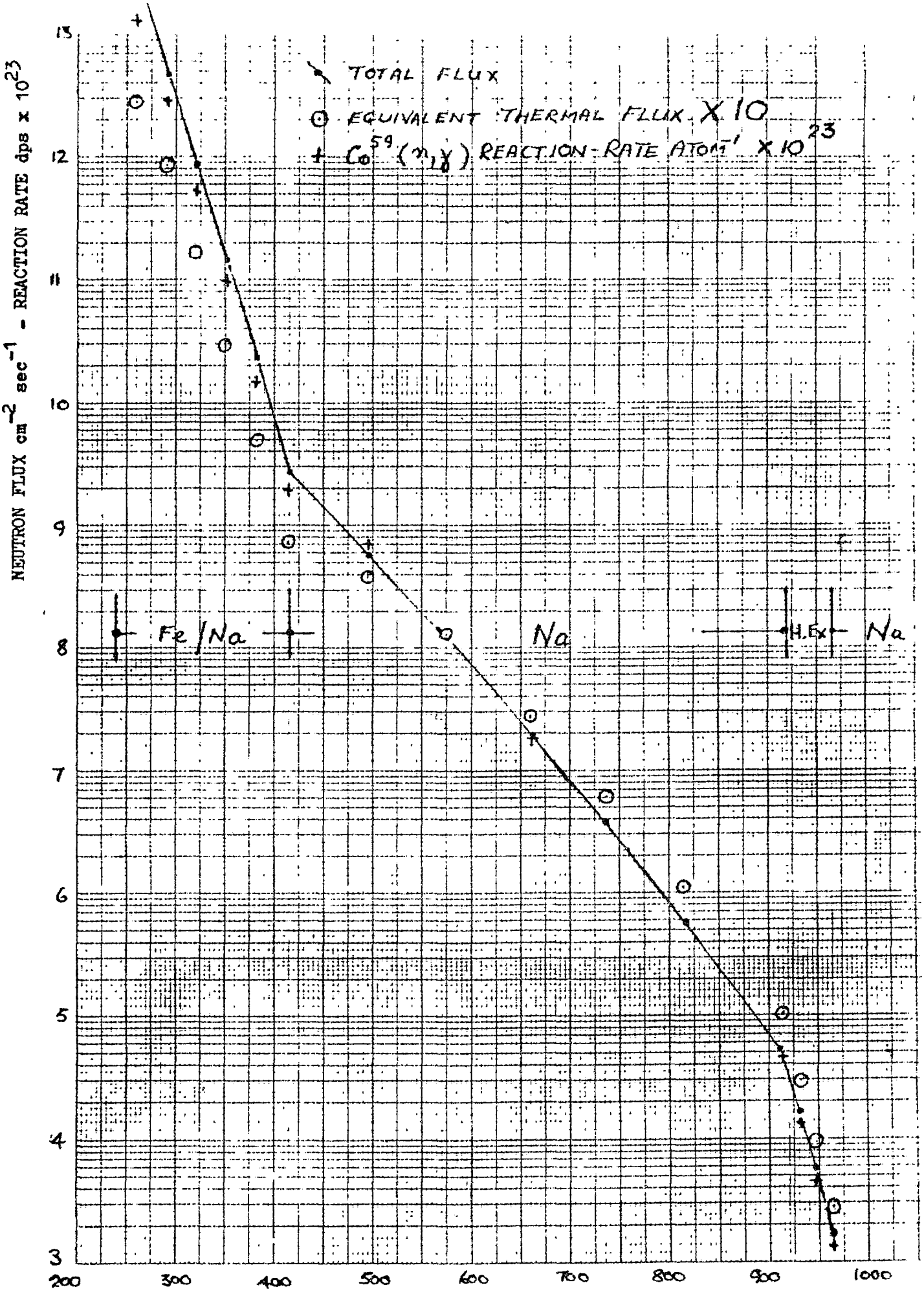

FIG. 1 TOTAL FLUX EQUIVALENT THERMAL FLUX AND CO^{59} (n,γ) REACTION RATE ATTENUATIONS

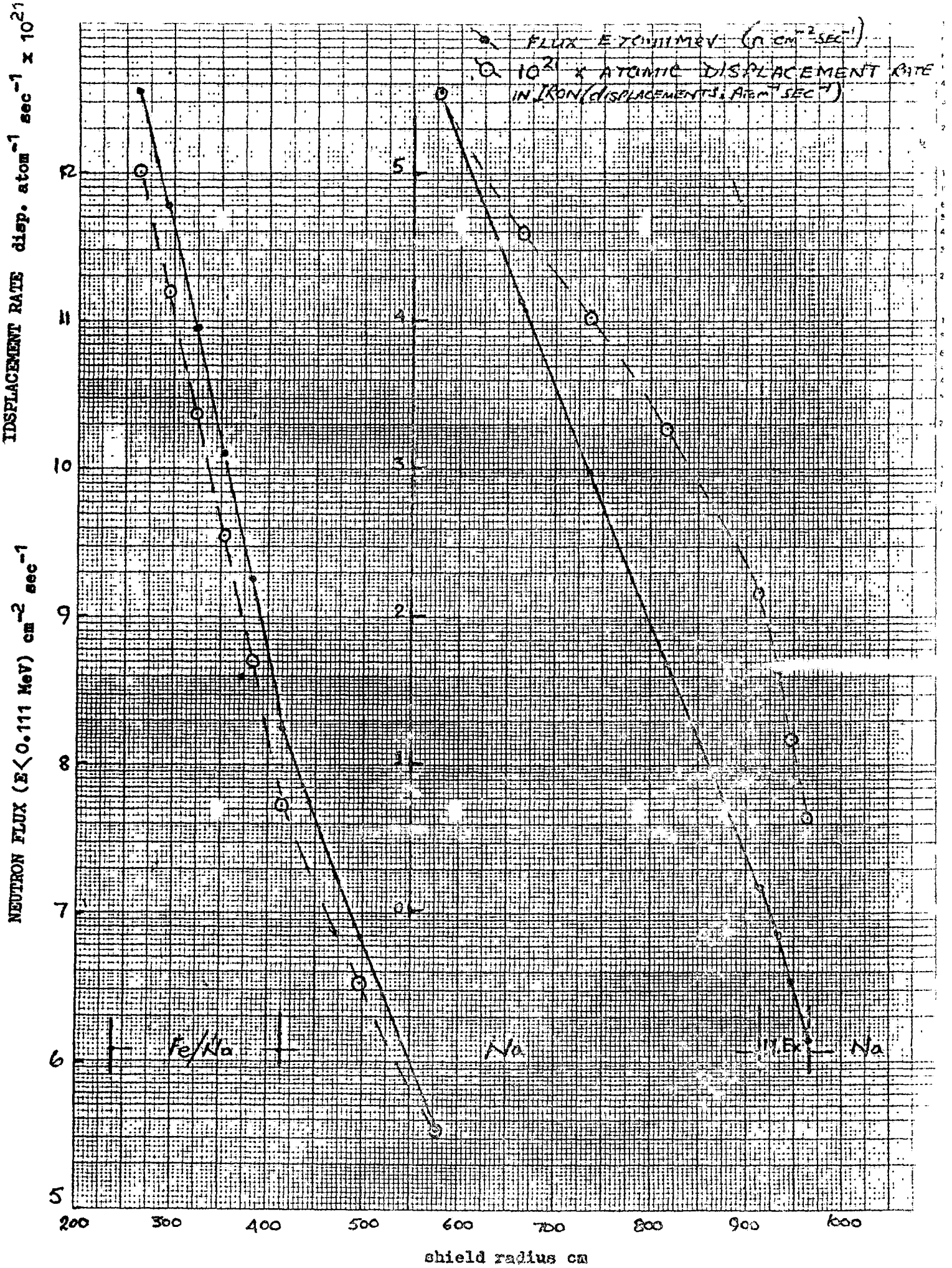

FIG. 2 FLUX ABOVE 0.111 MoV AND ATOMIC DISPLACEMENT RATE FOR IRON

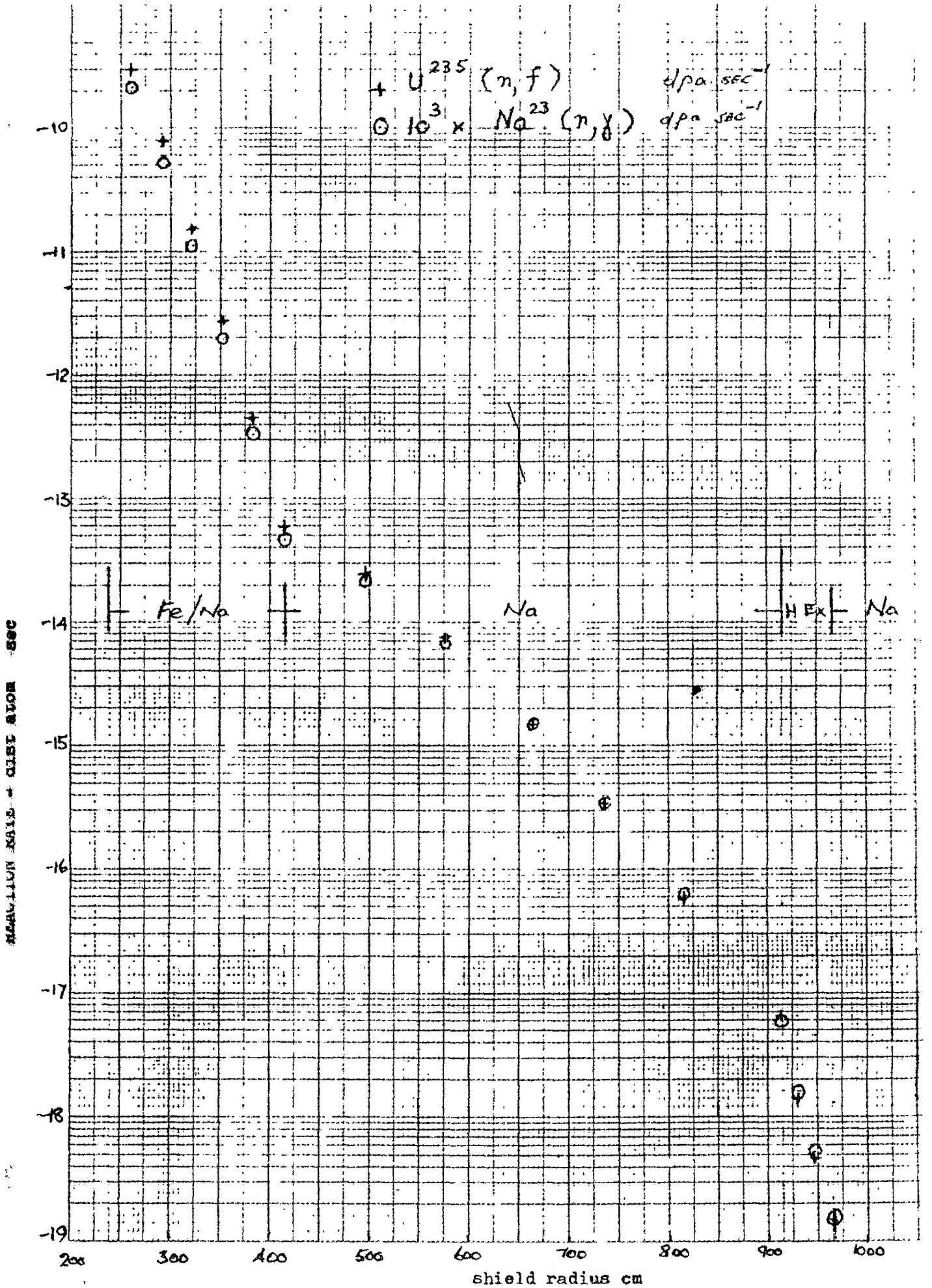

FIG. 3 U235 FISSION AND Na23 (n, γ) REACTION RATES

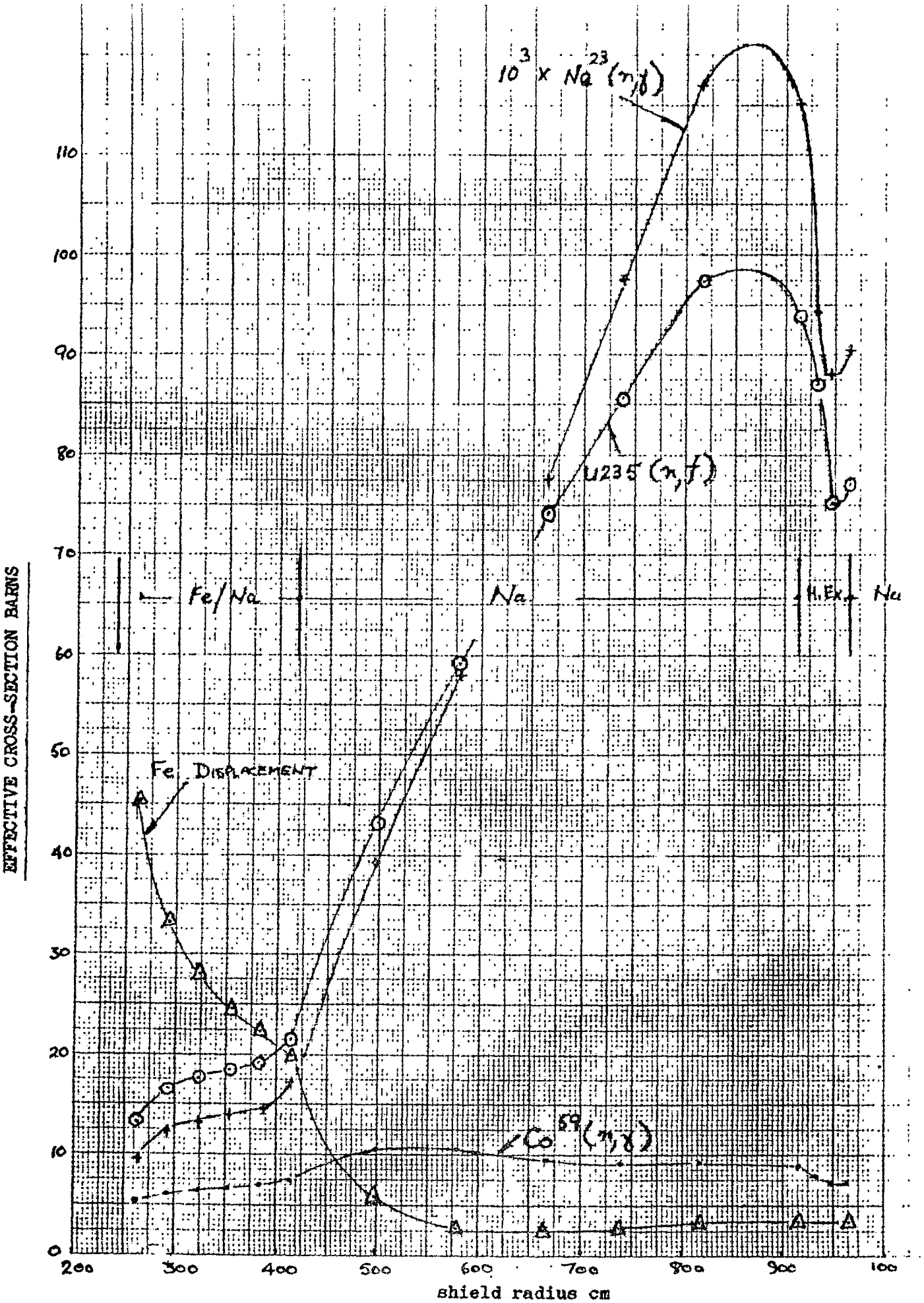

FIG. 4 EFFECTIVE CROSS-SECTIONS FOR U235 (n,f) Co^{59} (n,γ) Na^{23}(n,γ) AND Fe DISPLACEMENT RATE

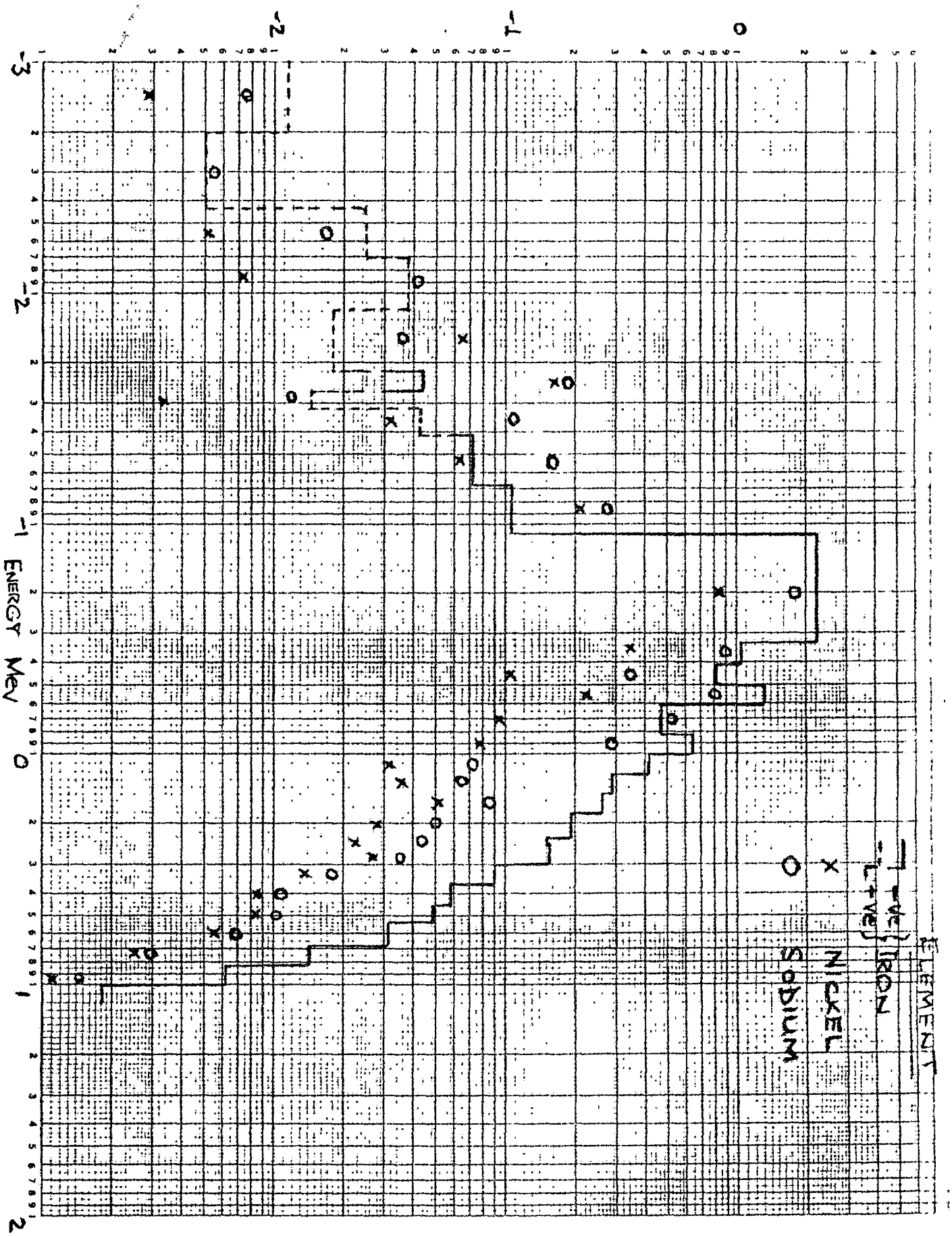

FIG. 5 SENSITIVITY OF THE IRON DISPLACEMENT RATE TO THE IRON, NICKEL, AND SODIUM CROSS-SECTIONS

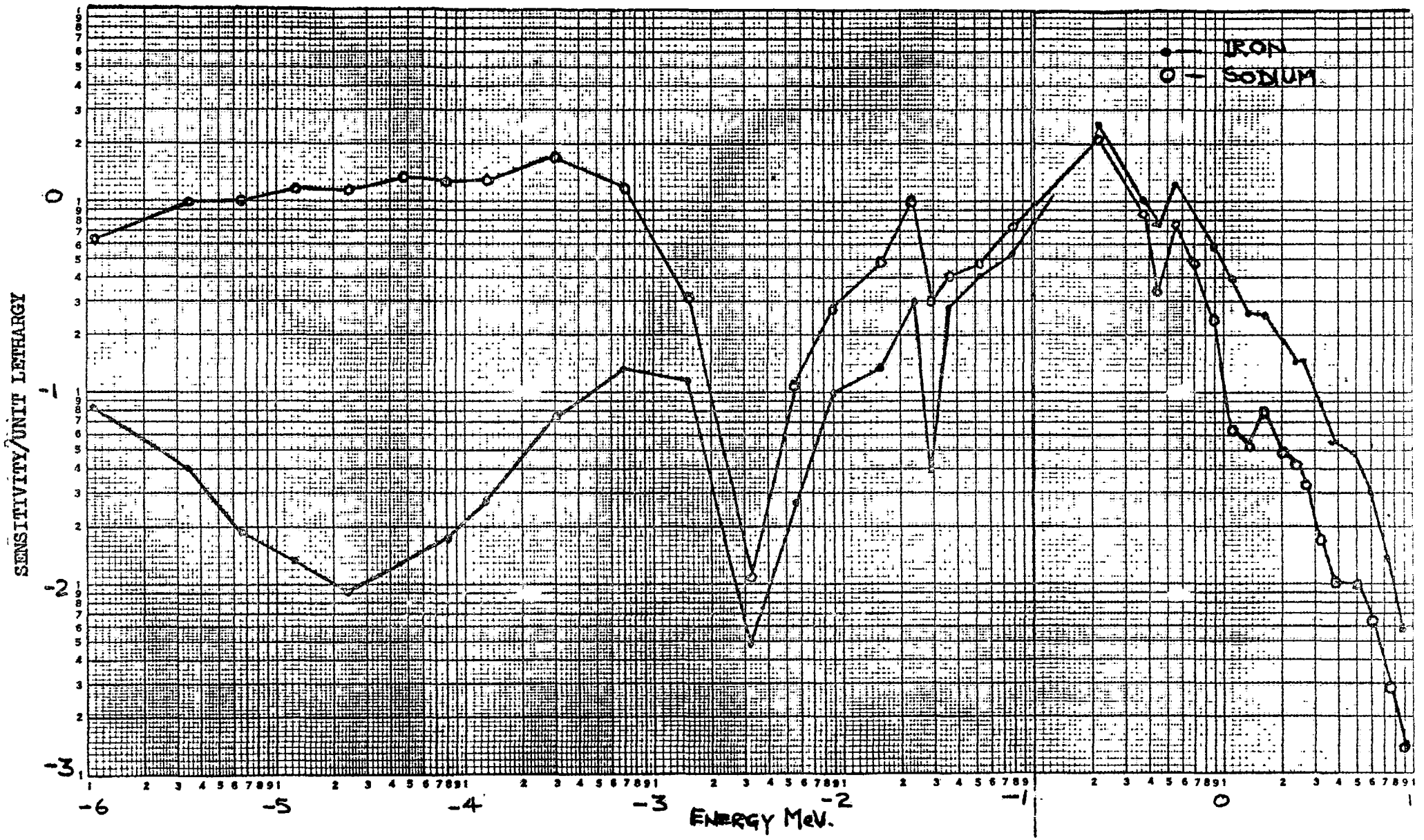

FIG. 6 SENSITIVITY OF THE SODIUM CAPTURE REATE IN THE HEAT EXCHANGER TO IRON AND SODIUM CROSS-SECTIONS

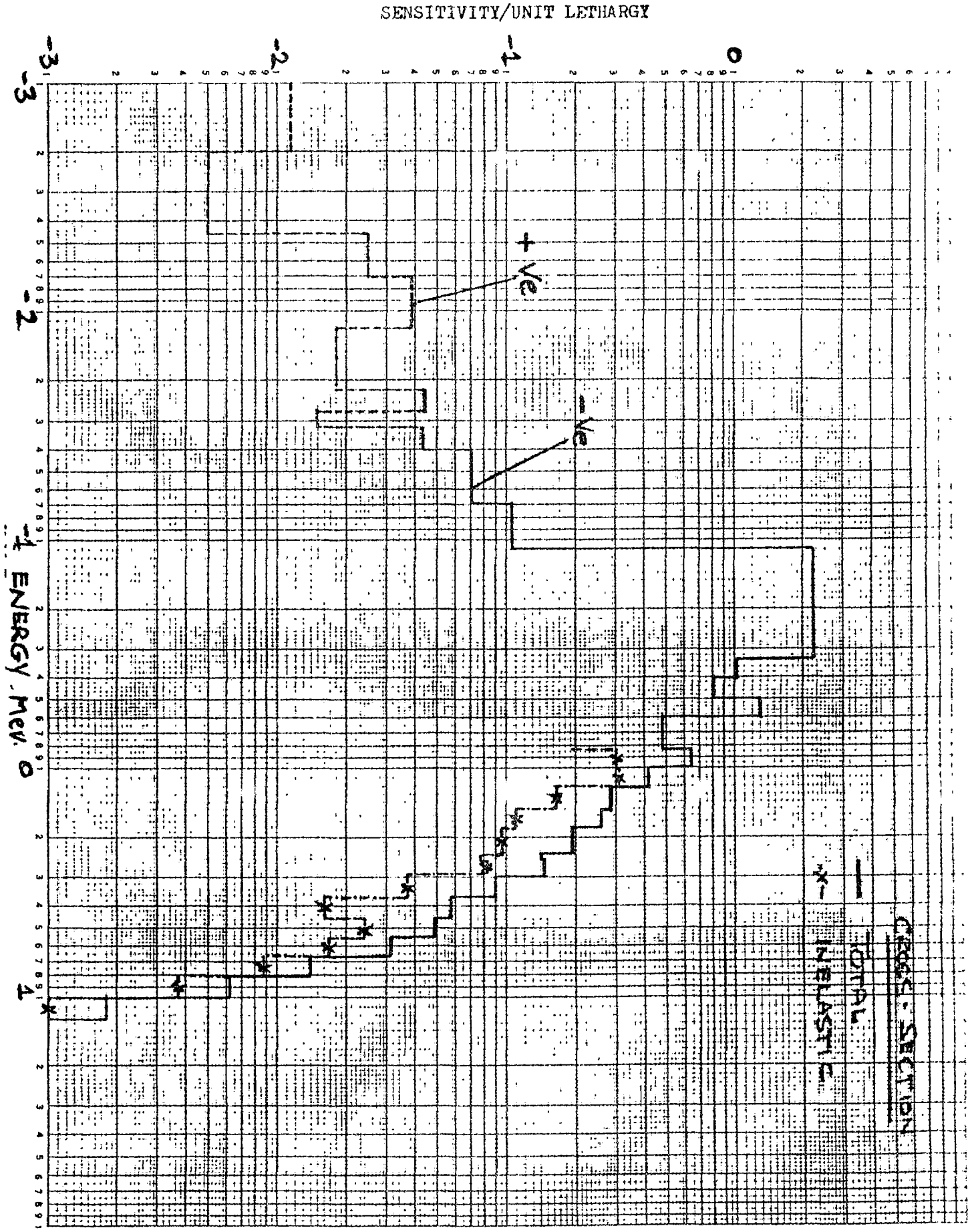

FIG. 7 SENSITIVITY OF IRON DISPLACEMENT RATE IN MESH 61 TO IRON CROSS-SECTION

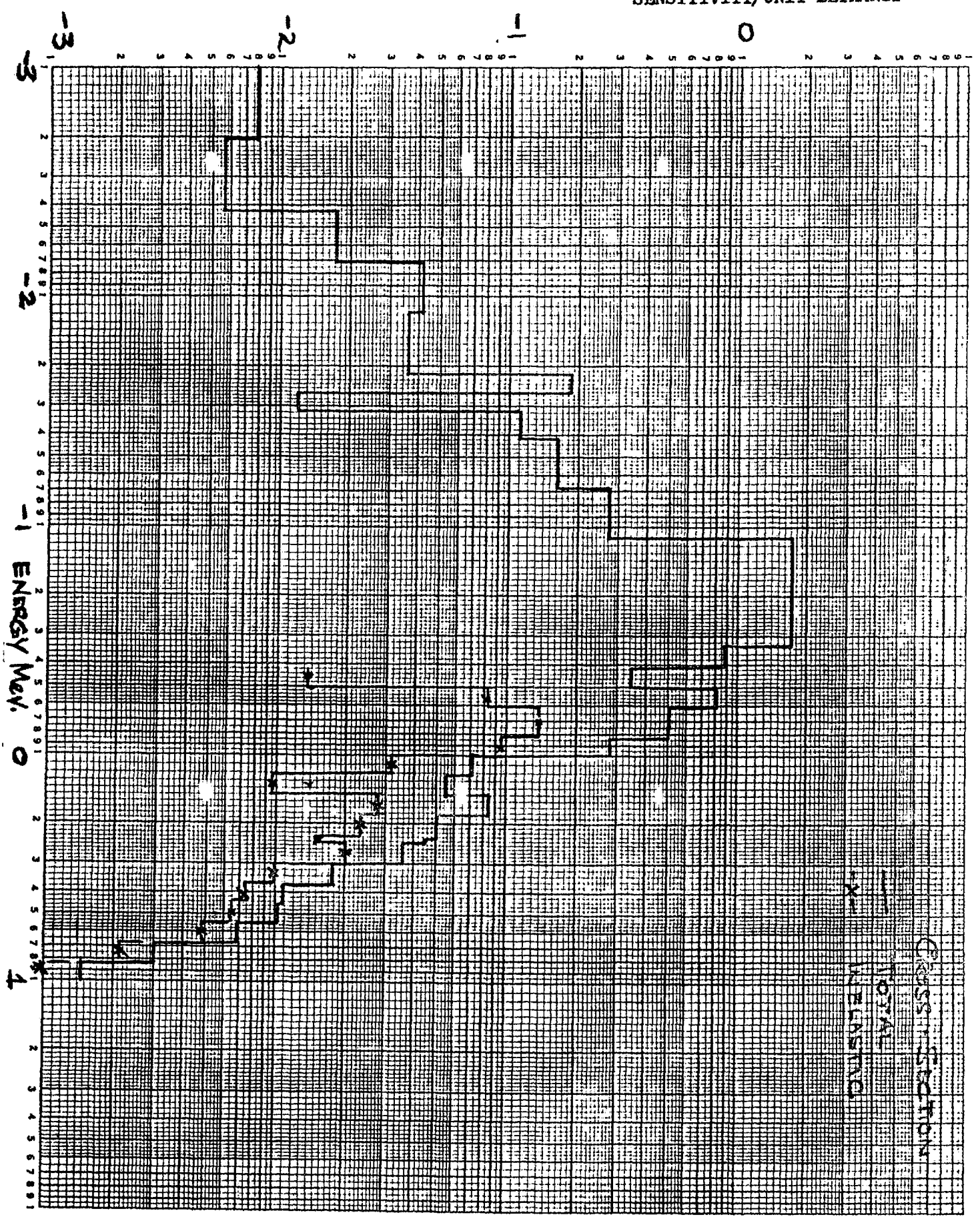

FIG. 8 SENSITIVITY OF IRON DISPLACEMENT RATE IN MESH 61 TO SODIUM CROSS-SECTIO

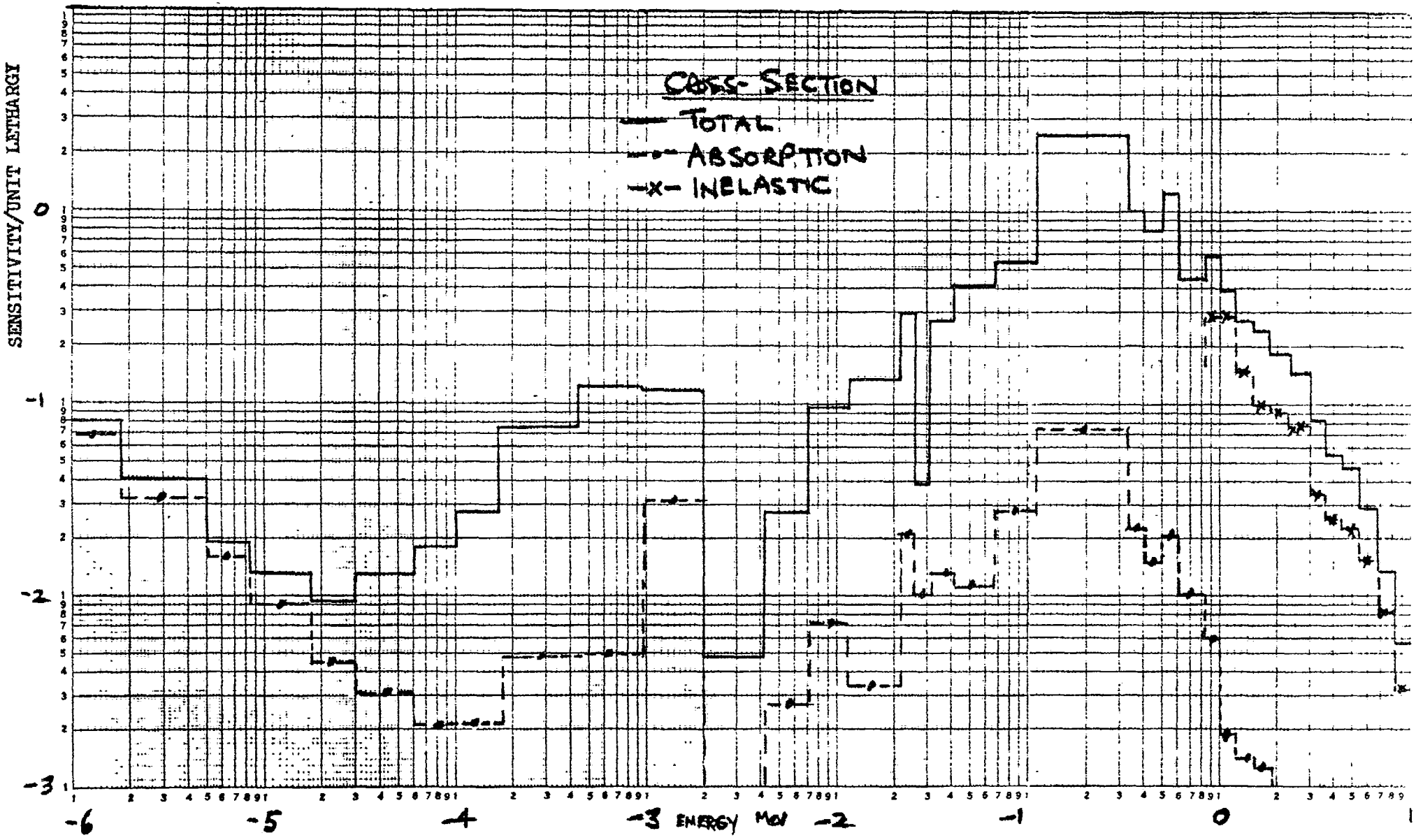

FIG. 9 SENSITIVITY OF THE SODIUM CAPTURE RATE IN THE HEAT EXCHANGER TO IRON CROSS-SECTIONS

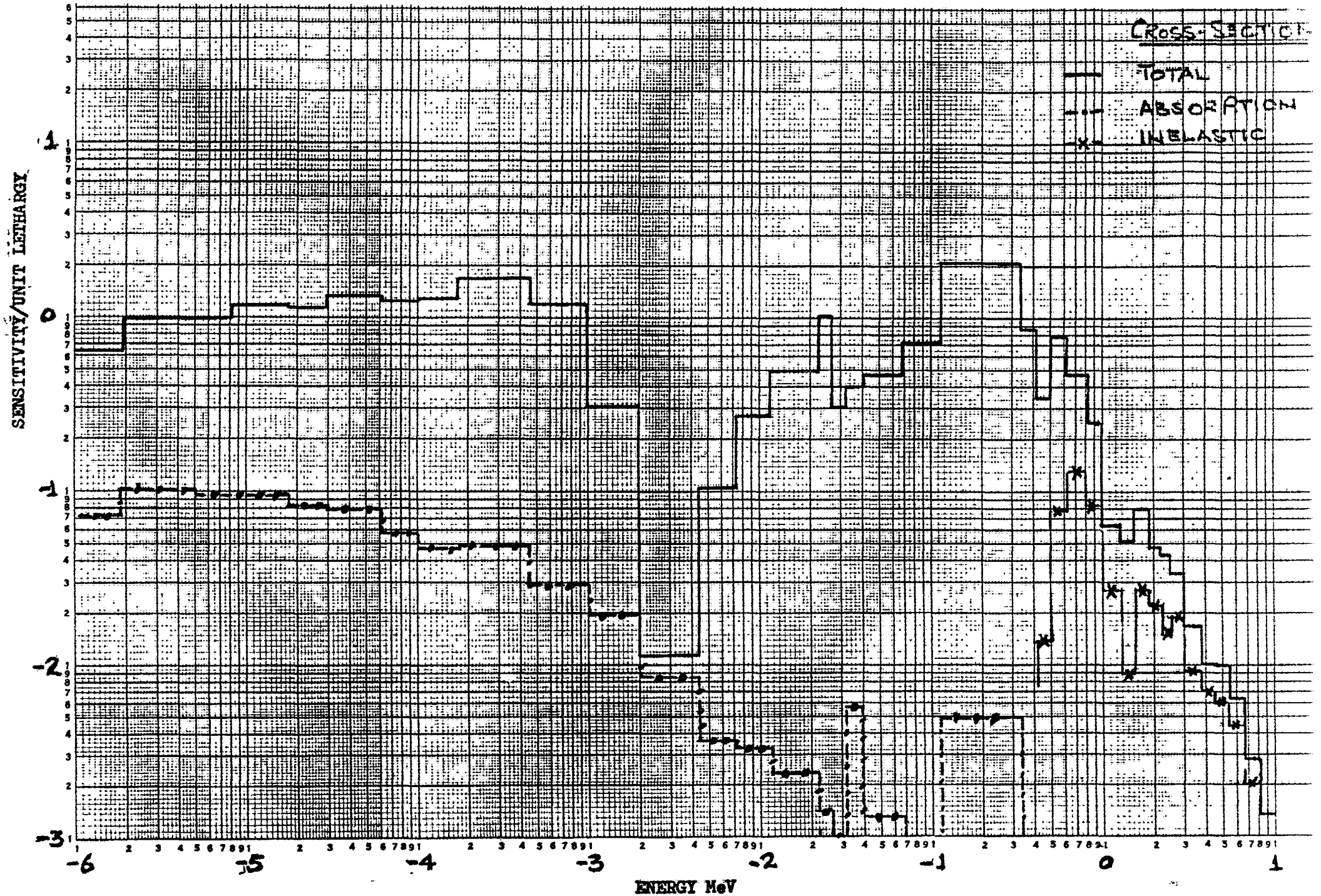

FIG. 10 SENSITIVITY OF THE SODIUM CAPTURE RATE IN THE HEAT EXCHANGER TO SODIUM CROSS-SECTIONS

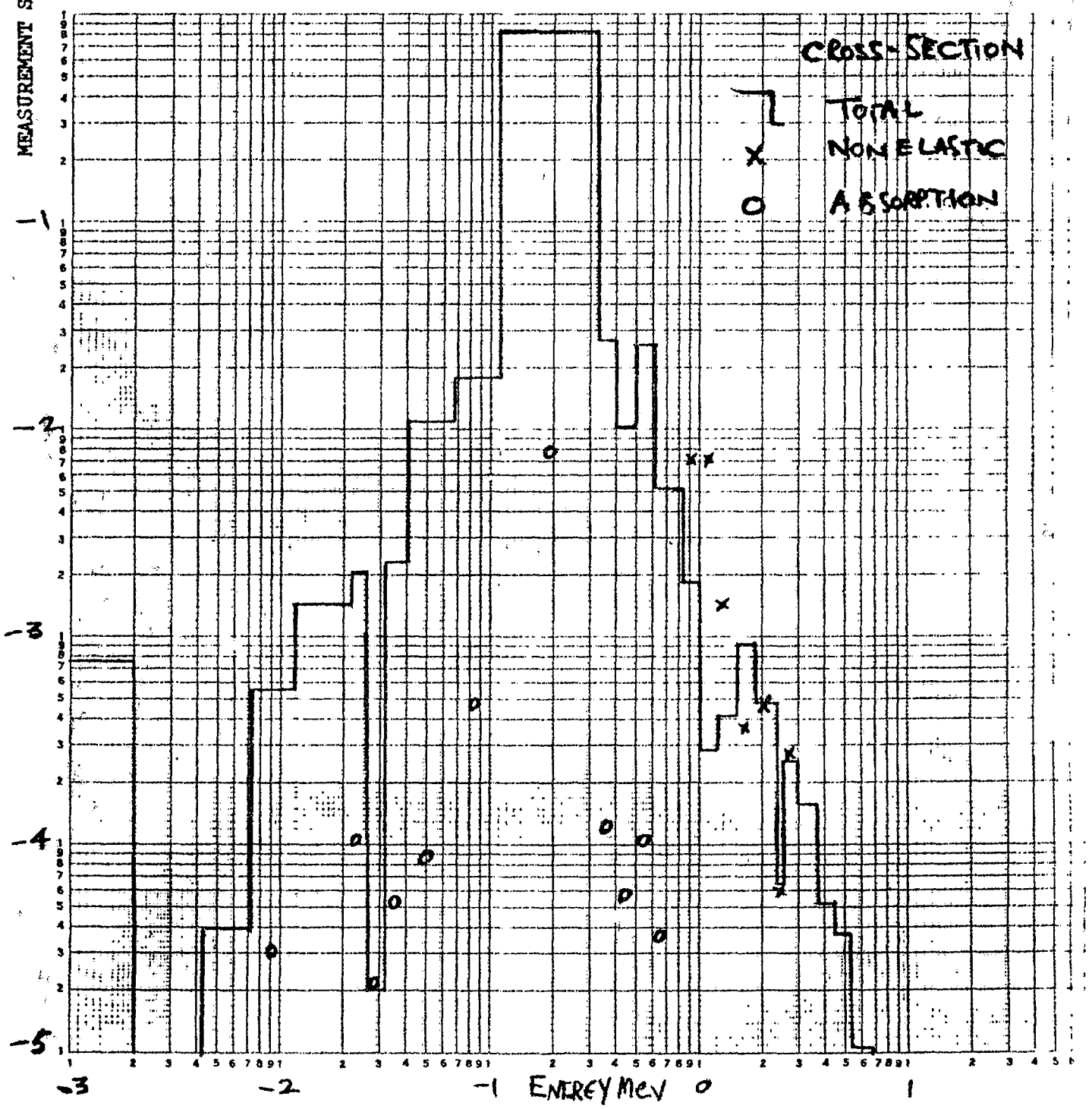

FIG. 11 MEASUREMENT SENSITIVITY OF THE SODIUM CAPTURE RATE IN THE HEAT EXCHANGER TO IRON CROSS-SECTIONS

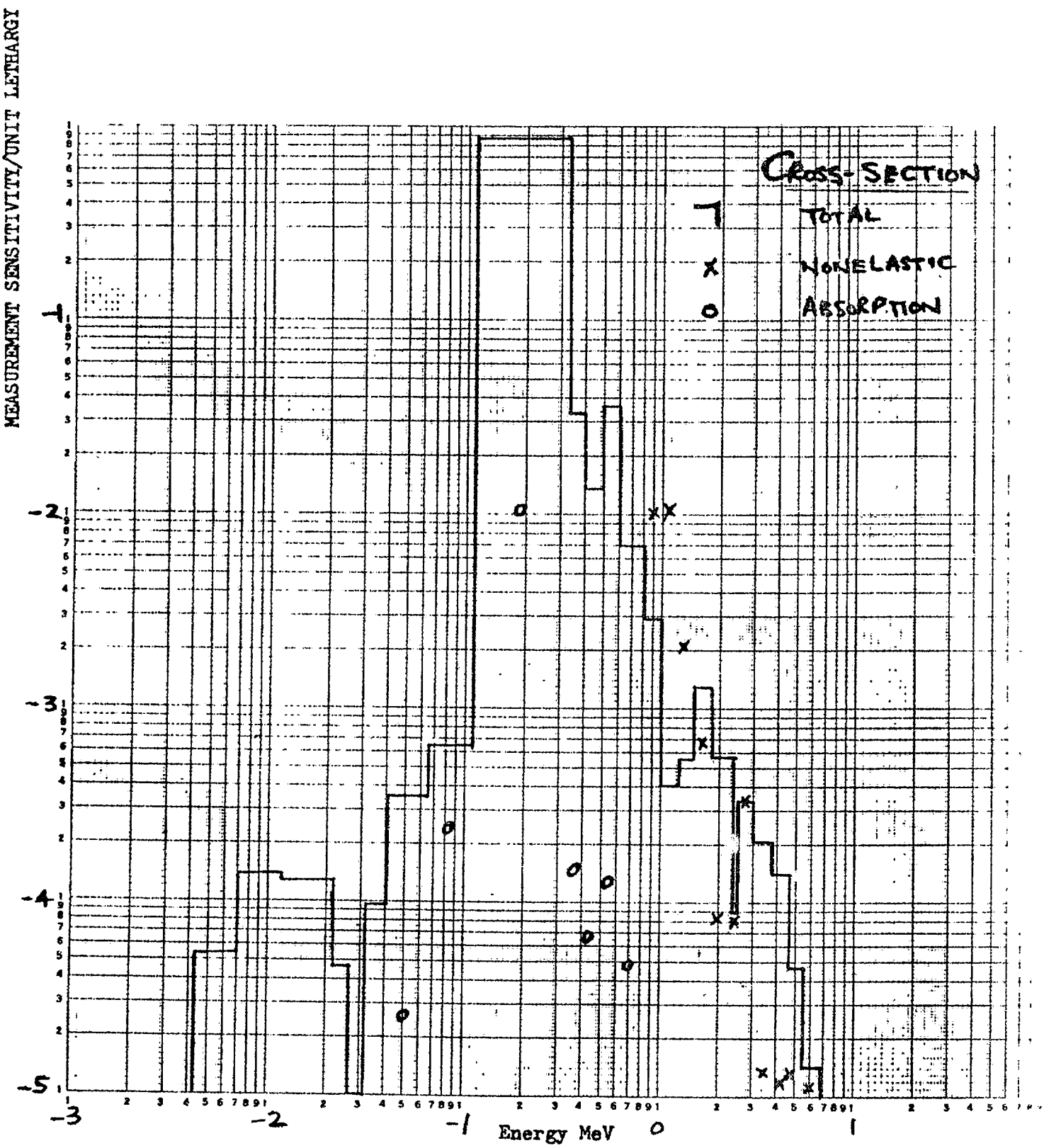

FIG. 12 MEASUREMENT SENSITIVITY OF THE IRON DISPLACEMENT RATE TO IRON CROSS-SECT

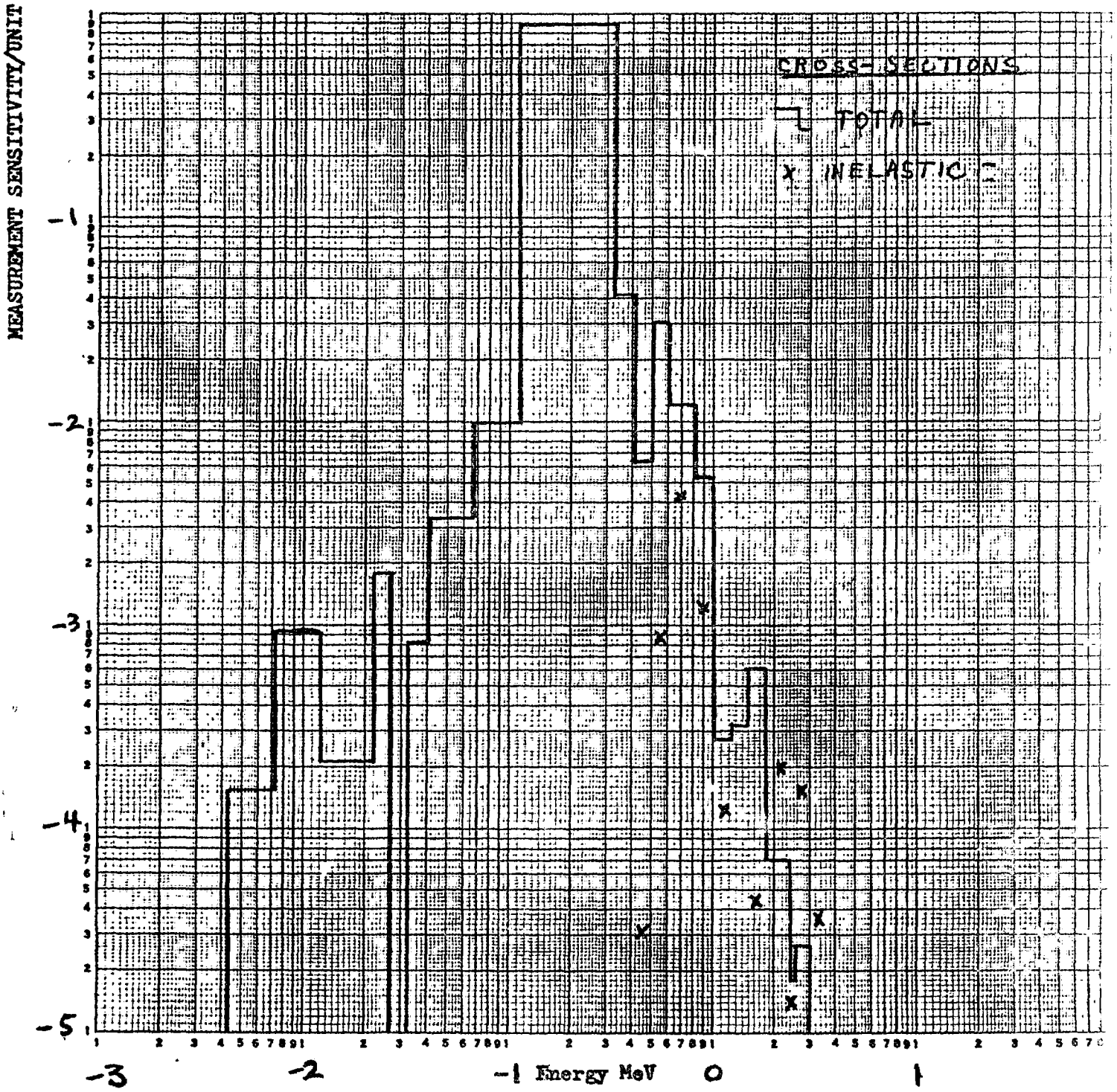

FIG. 13 MEASUREMENT SENSITIVITY OF THE IRON DISPLACEMENT RATE TO SODIUM CROSS-SECTIONS

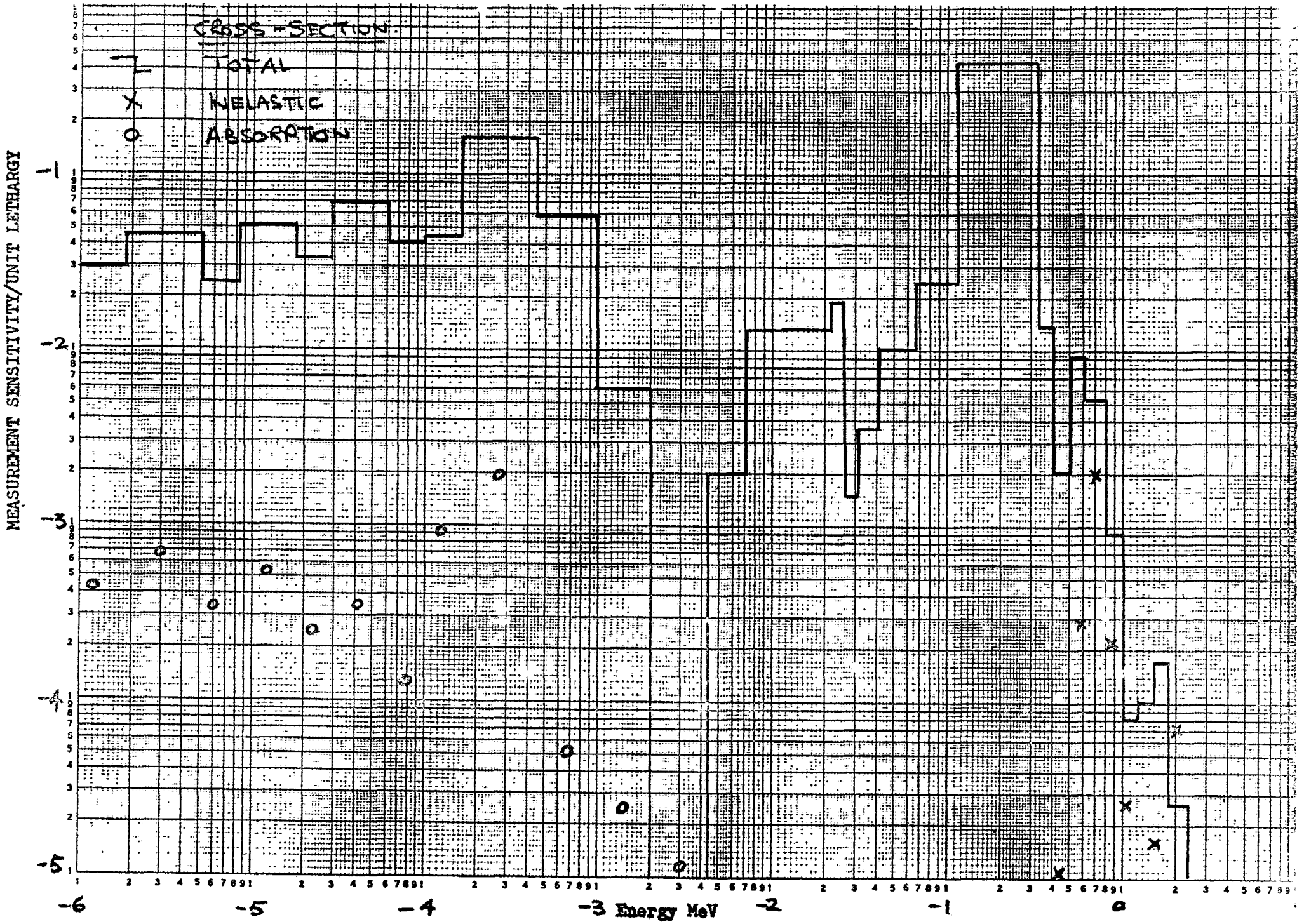

FIG.14 MEASUREMENT SENSITIVITY OF THE SODIUM CAPTURE RATE IN THE HEAT EXCHANGER TO SODIUM CROSS-SECTIONS

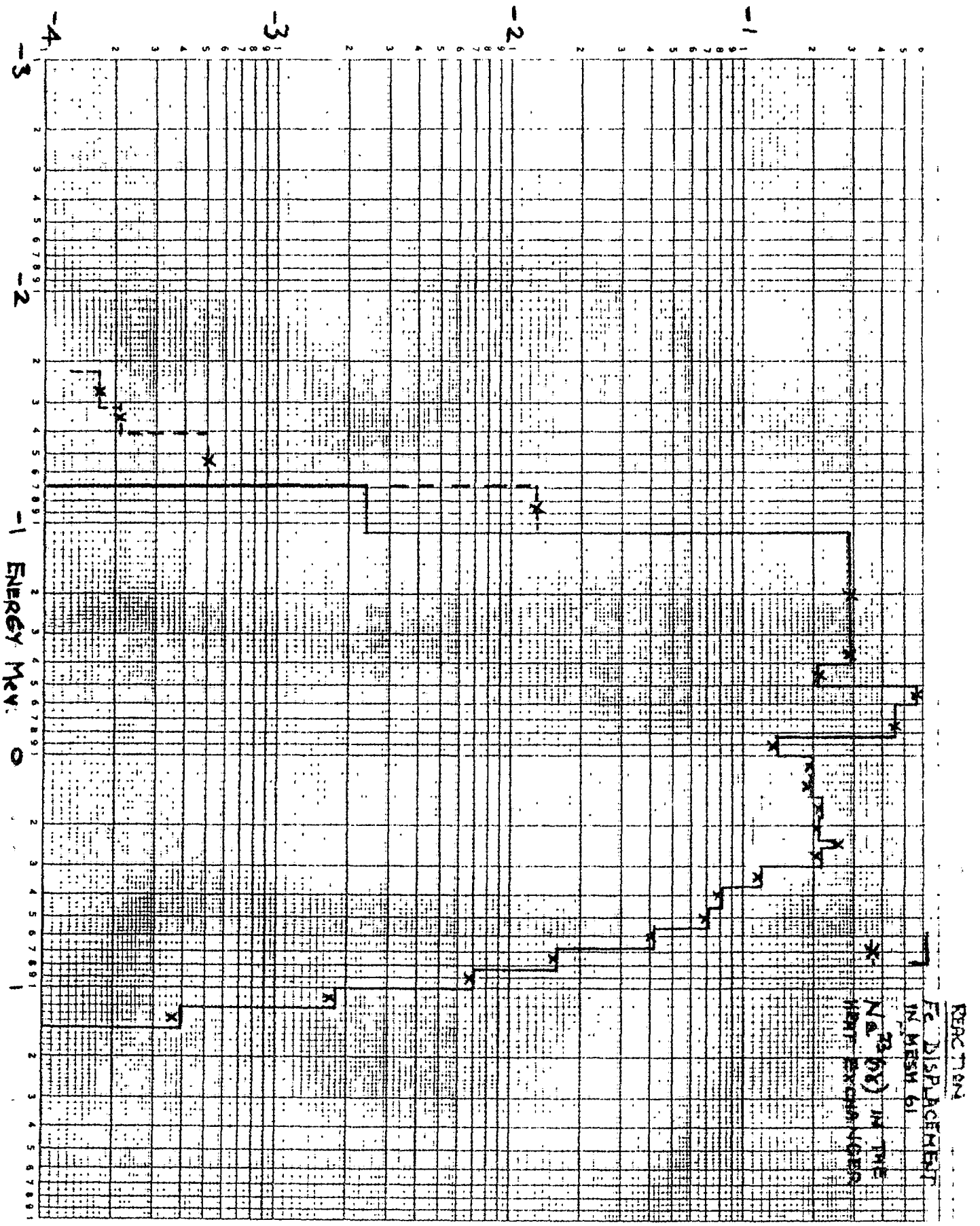

FIG.15 SENSITIVITY OF THE IRON DISPLACEMENT AND SODIUM CAPTURE RATES TO THE START... SPECTRA

APPLICATION OF THE SENSITIVITY AND UNCERTAINTY ANALYSIS SYSTEM LASS TO FUSION REACTOR NUCLEONICS*

by

Donald J. Dudziak
S. A. W. Gerstl
D. W. Muir

Theoretical Division
University of California
Los Alamos Scientific Laboratory
Los Alamos, New Mexico 87545

ABSTRACT

Sensitivity analysis, as applied to both nuclear design and data uncertainty, has developed into a valuable tool for fusion reactor nuclear analysis. Several such studies have been undertaken with the LASL sensitivity system LASS, which includes at its principal modules SENSIT-1D, ONETRAN, and ALVIN. These modules function in a multigroup environment using standard flux and data interface files for communication. The input multigroup cross-section data and uncertainties are obtained primarily from ENDF/B using the NJOY processing system. In particular cases, the input library can be modified by the ALVIN module to improve consistency with available integral experiments. The primary output from LASS is the uncertainty (or change) in important reactor parameters, as calculated in the SENSIT-1D module. Applications of LASS and its component parts have been made to the Tokamak Fusion Test Reactor (TFTR), the Reference Theta-Pinch Reactor (RTPR), and to an Experimental Power Reactor (EPR). This paper emphasizes the initial assessment of cross-section sensitivity for an EPR design. Nucleonic responses examined include neutron and gamma-ray kerma in the toroidal field coils and Mylar superinsulation, displacement damage and transmutation in the copper of the toroidal field coils, and activation of the outboard dewar. These sensitivities are now being used to narrow the range of uncertainty analyses required to quantitatively assess cross-section adequacy for EPR design calculations. Acceptable target uncertainties in nucleonic design parameters are simultaneously being formulated. Experience at LASL with sensitivity and uncertainty analysis techniques incorporated in LASS has provided convincing evidence of their value for fusion reactor studies. Many of these studies are of a shielding nature; e.g., deep penetrations of high-energy neutrons through steel, lead, boron carbide, and graphite, with responses such as activation and kerma.

*Work performed under the auspices of the U. S. Energy Research and Development Administration.

1 INTRODUCTION

There exists an extensive commonality of fusion reactor nucleonics, including of course fusion reactor shielding, with fission reactor shielding. For example, both generally involve moderate-to-deep penetration transport calculations for neutrons and gamma-rays, along with kerma responses. Those kermas may be manifested as heating in concrete or a superconducting magnet, or simply as absorbed biological dose. Similar commonality exists in neutron activation, although fusion nucleonics introduces a new class of often dominant reactions; e.g., (n,xp), (n,xα), (n,2n), and other threshold reactions producing radioactive nuclides. Interest also arises in the transmutation products, stable and unstable, of such reactions insofar as they affect material mechanical properties, electrical conductivity, etc.

Conversely, there are areas of less commonality, where fusion reactors (and even 2.25-pJ neutron irradiation facilities such as the INS[1]) present relatively new if not unique problems. Most such nucleonic interests are in blanket responses, or merely involve new response functions such as radiation damage in superconductors. However, both classes of problems, regardless of commonality, do in general require target accuracies which differ from those required for fission reactor shields. As a case in point, consider the superconducting (S/C) coil, where both radiation damage and heating are required to be known within approximately 10-20%, as a realistic goal. Such accuracies are perhaps consistent with the target goals for fission reactor nuclear heating analysis, but involve an essential difference. In the fusion reactor case, the accuracies are required after an attenuation of approximately 10^6 in the total neutron plus gamma-ray kerma. The pertinent point here is that fusion reactor data requirements may differ from those for fission reactors in two ways: (1) different reactions can be involved in both transport and response cross sections of interest; and (2) the accuracy requirements will in some cases, as for S/C magnet damage, be more stringent.

It is perhaps useful here to review some fusion reactor nucleonic problems in order to demonstrate the foundations for their data requirements. First in order are the intense 2.25-pJ neutron source facilities, where biological dose from primary neutron and secondary prompt gamma rays is of most concern, with activation gamma-ray doses also being important. Here, as with fission reactor biological shields, we are currently content with "factor of 2 or so" target accuracies, but we have hopes for better accuracy in the next generation of fusion devices (after approximately 1985). Shield design is presently underway[1] for the INS and the High Energy Gas Laser Facility (HEGLF), so cross-section requirements are somewhat academic; we make do with the best presently available data. It is worth pointing out that both the INS and HEGLF shield designs involve void penetrations with diameters of the order of one metre, so that streaming and reflection are the principal computational difficulties. Bulk concrete shields are approximately 3-m thick.

Conceptual design efforts in the USA which impact near-term data needs are mainly those evolving about the Experimental Power Reactor (EPR) projected for construction in the mid 1980's. The EPR is a next-generation Tokamak reactor after the Tokamak Fusion Test Reactor (TFTR), for which a thorough data assessment has been performed.[2] Whereas the only nucleonic parameter of crucial interest in the TFTR blanket/shield was activation dose levels after shutdown (biological shielding for primary radiation during operation is roughly comparable in extent and importance to that in HEGLF and INS), the EPR will have numerous important responses to consider. Most important

of these are the radiation effects in S/C toroidal field (TF) coils -- the principal substance of this paper. Details are given in Sec. 4 below.

From our experience in fusion reactor analysis we can make some general observations which may interest the shielding community. First, sensitivity analysis is of little use in improving data for the near-term devices INS, HEGLF, and TFTR. Even so, almost all detailed design calculations for these devices must be performed in complex geometries by Monte Carlo methods; hence, one-dimensional sensitivity calculations are of limited value. An important point to emphasize in this discussion is the requirement in many cases for two-dimensional discrete-ordinates calculations and associated sensitivity analysis, as well as the need for long-range development of Monte Carlo sensitivity methods. Streaming problems presently dominate the shield design for the EPR, especially for the TF coils. By dominating a design, we mean that the shield may well determine the TF coil magnet diameter, and hence have a major impact on the device cost. Thus, an essential difference immediately occurs from fission reactor shielding; the TF coil shield is ab initio a major plant cost determinant.

A second general observation of interest is that fusion reactor nucleonic analysis provides a fortuitous convergence of two technologies. That is, the sensitivity and uncertainty methods are maturing just as a vital requirement for them is emerging in the form of an embryonic fusion reactor nucleonics technology.

2 NUCLEAR DATA IMPLICATIONS OF FUSION TECHNOLOGY

Fusion reactor technology has introduced new materials and reactions of importance for nuclear analysis. Also, for materials and reactions of common interest in fusion and fission reactor programs, new energy ranges are now of primary interest for fusion. It rapidly becomes clear that fusion technology cannot depend completely on the nuclear data evaluation and assessment programs performed for the fission technologies. Not only are new materials (e.g., W, Cu, Pb mortars), reactions, and energy ranges of interest, but data assessment by sensitivity methods must direct added attention to new high-energy responses and to secondary energy/angular distributions. Consequences of changes in such secondary distributions are already known to be important in fusion systems,[3] and a methodology for their systematic analysis is the subject of a forthcoming paper by Gerstl.[4]

Although fusion technology presents many new demands in the nuclear data area, we are fortunate that it may not be too late to plan and execute an orderly, rational and coordinated program of data

- assessment of requirements
- measurements (differential and integral)
- evaluations.

Having at our disposal not only existing ENDF[5] data, but also fairly well-developed sensitivity and uncertainty analysis methods, we have the opportunity to avoid the pitfalls experienced by the fission reactor data programs, where the cost-effectiveness of the integral experiments was limited by the lack of modern sensitivity-based planning methods. We also feel that failure

to develop a coordinated (international) program for fusion technology nuclear data would be inexcusable. Initial efforts at defining high priority nuclear data needs within the U. S. A. fusion program have been published,[6] and are being used as the basis for the U. S. A. nuclear data measurement request lists. A review of nuclear data needs can be found in Ref. 7.

3 LASS SYSTEM AND APPLICATIONS

Sensitivity and uncertainty analysis is done within the Los Alamos Scientific Laboratory LASS system, as shown in Fig. 1. Partial cross sections and uncertainties, σ and $\Delta\sigma$, are processed from ENDF into multigroup form by the NJOY system.[8] Because covariance data in ENDF are presently very scarce, most multigroup covariance matrices $[\Delta\sigma]$ are produced by the COVMAT code described in Appendix A of Ref. 2. Forward and adjoint multigroup neutron/gamma-ray fluxes are computed by the ONETRAN code,[9] using standard cross-section and flux files. The actual calculation of sensitivities and uncertainties is performed by the SENSIT-1D code,[10] using the inputs shown in Fig. 1. Again, standard CCCC (Committee on Computer Code Coordination) interface files are used for cross-section and flux inputs. The ALVIN module for differential and integral data consistency analysis is discussed in detail by Reupke and Muir,[11] so it will not be considered in this paper.

Applications of LASS components have been made to several fusion facilities, including the Tokamak Fusion Test Reactor (TFTR),[2] the Reference Theta-Pinch Reactor (RTPR),[12,13] and the Intense Neutron Source (INS).[1] These applications have included design sensitivity as well as cross-section sensitivity, both of which use the same basic perturbation theory methodology incorporated in SENSIT-1D. That is, in both cases one is simply performing integrations over phase space of an integrand involving perturbations of the transport operator, ΔL; either cross-section changes or design changes are simply manifested as the difference operator of the perturbed and unperturbed transport operator. The sensitivity is given in the notation of Ref. 2 as

$$P_{\Sigma_i} = \frac{\langle \phi^*, L_{\Sigma} \phi \rangle_i}{R} .$$

All present day sensitivity studies based upon transport theory derive from the work of Prezbindowski.[14] Extension and computer coding of his methods have been discussed in detail by Gerstl, Bartine, and others.[2,4,15,16] In the discussions below we follow the terminology and notation of Ref. 2.

In all the applications discussed above, as well as the fusion EPR application which is the principal subject of this paper, we have consistently observed the limitations of one-dimensional analysis. Fusion reactor nucleonic design problems are frequently multidimensional, and the concommitant sensitivities are often most important for these problems. Thus sensitivity methods and code development at LASL is concentrated on multidimensional analysis, along with the secondary energy/angular distribution sensitivities mentioned above.

4 DATA ASSESSMENT FOR A FUSION EXPERIMENTAL POWER REACTOR (EPR)

Assessment of nuclear data needs for a fusion EPR is, of course, design dependent. However, the EPR designs currently extant, as well as later conceptual studies of Ignition Test Reactors (ITR), are generically similar. For example, several conceptual reactor designs use laminated stainless

steel/B_4C shields. For our assessment task we have chosen the EPR design of the Argonne National Laboratory, as described in Ref. 17 and in private communications. The design has two shield assemblies, denoted "inner" and "outer". The inner shield refers to a segment of shielding toward the toroidal axis of the torus; i.e., if one considers a major radius through the center of the plasma chamber, the inner shield is toward the origin. Figures 2 and 3 show one-dimensional models based upon radial traverses from the poloidal axis (plasma centerline) through the inner and outer shields, respectively. Observe that the thinner inner shield is of effective but costly stainless steel/B_4C, while the thicker outer shield is composed largely of less costly lead mortar. The technical basis for alternative shields is clear if the magnetic field profile is considered: With the D-shaped toroidal field (TF) coils, there exists a relatively large space for the outer shield, whereas the inner shield must be as thin as possible. The latter requirement arises from a desire to maximize the magnetic field in the plasma, and thus maximize power density.[17]

At this point we digress to discuss the general approach used in the EPR data assessment, as well as in the previous assessments.[2] First, a broad ranging sensitivity study is performed simply using the total, scattering (matrix) and absorption cross sections from the transport code cross-section sets. These included neutron interaction, gamma-ray production, and gamma-ray scattering matrices. From the large mass of these survey calculations, which are automated in SENSIT-1D, we then isolate materials, partial cross sections and energy regions of potential interest. This latter step is greatly assisted by computing integral sensitivities. After a semi-quantitative review of the germane cross-section errors, we chose a manageable number of potentially important materials and partial cross sections for more detailed error evaluation. For these we process available covariance data into multigroup form. However, as noted above, error data in ENDF are sparse, so most covariance data need to be evaluated on an ad hoc basis. Using such covariance matrices, an uncertainty analysis is performed for the suspect partial cross sections. This paper discusses the results for an EPR through the stage of evaluating and processing covariance data.

In the case of our EPR analysis, error data for C and O were taken from ENDF/B-IV and for Al from a LASL evaluation in ENDF/B format. Data for Fe were a combination of an ORNL evaluation at lower energies, and a LASL evaluation for (n,2n) and (n,n' continuum) cross section errors. Also, the LASL evaluation for Fe combines (n,n'p), (n,n'α), and (n,n'γ) reactions into a "macropartial", which makes possible a more reasonable estimate of the uncertainty in the elastic scattering cross section. These data were then all processed by the NJOY code into the 30-neutron-group structure[18] used for the 30 x 12-group coupled neutron/gamma-ray transport calculations.

4.1 Responses of Interest

Because of the thinner inner shield, radiation effects in the inner TF coils are more critical[17] than in the outer TF coils. However, for access during maintenance the outer structure and TF coil activation are important, as opposed to the inner. Thus, for our analysis we have chosen four radiation effects in the inner TFC, and activation of the stainless steel outer dewar. Specifically, we consider

INNER SHIELD

1) neutron and gamma-ray heating in the TF coil superconductor,
2) neutron and gamma-ray dose to the MYLAR insulation in the TF coils,

3) displacements per atom (dpa) in the Cu matrix of the TF coils, and
4) transmutation of the Cu matrix.

OUTER SHIELD

1) activation of the stainless steel (SS) dewar [e.g., $^{58}Ni(n,p)^{58}Co$ or $^{56}Fe(n,p)^{56}Mn$].

A typical response function is shown in Fig. 4, where we give the neutron and gamma-ray flux-to-dose response for MYLAR. Details of all the response functions, as well as sensitivities, etc., are presented in a forthcoming report.[19] In this paper we present only selected sample results.

4.2 Procedure and Results

All forward and adjoint flux calculations were performed in S_8-P_3, using the models shown in Figs. 2 and 3, and all cross sections were processed from ENDF/B-IV. As a check on proper convergence it was verified that

$$\langle \phi^*, Q \rangle \simeq \langle \phi, R \rangle \ .$$

Sensitivity profiles, P_{Σ_i}, were then computed for neutron and gamma-ray interactions, as well as for gamma-ray production.

As a sample case, let us consider the total neutron and gamma-ray heating in the inner TF coil. Table I shows the integral sensitivities,

$$S_\Sigma = \sum_i P_{\Sigma_i} ,$$

for this response, to SS total cross sections. From this table we find the region(s) in Fig. 2 which contribute most to the sensitivity. It is worth noting that these data also give insight into the sensitivity of the response to design alterations in these regions. From Table I it is clear that the blanket SS regions 6-8 are most important. Also, it can be seen that Fe is the largest contributor to the integral sensitivities, regardless of which region is considered.

Narrowing our example further we show in Table II the component sensitivities for Fe in regions 6-8. Here the sensitivity has been divided into the gain term and loss terms (cf., Ref. 2, App. B for details)

$$P_{\Sigma_i} = - P_{\Sigma_{i,\mathrm{loss}}^{\mathrm{tot}}} + P_{\Sigma_{i,\mathrm{gain}}^{\mathrm{scat}}} \ .$$

Most of the net integral sensitivity is clearly due to scattering. An anomolous appearing result in Table II warrants some discussions; viz, the negative loss term for Σ_a. Because of the idiosyncracies of the transport codes, the (n,2n) and (n,3n) reactions appear as a negative component in the absorption and total cross sections, and as a positive component in the scattering matrix. Thus, by using the transport code cross-section sets for scoping sensitivity analyses, one introduces an artifice in the results. This artifice is also seen in the fact that the scattering loss term, computed by summing diagonals of the scattering matrix, is larger than the total loss

term. In fusion reactor sensitivity analysis we often observe this effect, in particular when the sensitivity in the top (approximately 2.25 pJ, or 14 MeV) group is manifestly dominant.

A representative sensitivity profile is shown in Fig. 5, where the sensitivity of the TF coil heating to the Fe scattering cross section was selected. Notice the high sensitivity in the top two groups, with a subsidary peak below 160 fJ (1 MeV). This general shape is characteristic of all the sensitivity profiles, for all responses and all materials pertaining to this EPR design.

Referring again to Table II, the low sensitivity to the gamma-ray production cross section, $\Sigma_{(n\rightarrow\gamma)}$, is caused by the relatively short mean free path of the gamma-rays in SS. However, for regions closer to the TF coil the sensitivity increases monotonically.

Turning now to the B_4C component of the shield, Table III presents integral sensitivity results comparable to those of Table I for SS. Here we see that the sensitivity is highest for the outboard regions, where the neutron spectrum is softened somewhat. However, the spatial variation is not nearly as strong as for Fe (cf. Table I). Also, the ^{10}B component of the B_4C does not overwhelmingly dominate the sensitivity as does, for example, Fe in SS. As would be expected, the net integral sensitivity is in all cases negative, because almost any interaction decreases the probability of a neutron's transmission to the TF coil.

The spectrum of neutrons at the inner edge of the TF coil is of some interest, and is shown in Fig. 6. Sensitivity profiles for the B and C cross sections show the same general shape as those for Fe (Fig. 5), with a peak in the top group and another peak in the 16-160 fJ (100 keV-1 MeV) region. For ^{10}B, however, the sensitivity to the total cross section is of comparable magnitude in the two peaks, and the lower peak is much broader. This high sensitivity at the lower energy peak is due in part to the neutron spectrum, which shows this same peak at all positions in the shield regions 8-10. One can conclude that even though these lower energy neutrons have lower transmission probabilities to the TF coil, they are so prevalent in the spectrum as to be a major contributor to the flux reaching the TF coil. A more quantitative explanation of this phenomenon can be gleened from the χ and ψ functionals in Ref. 20.

Table IV shows the individual cross section integral loss and gain terms for the ^{10}B in region 17, the region with highest sensitivity. Here the integral loss term is positive because the $^{10}B(n,2n)$ cross section is very small.

As a final example from our detailed sensitivity analysis[19] of the EPR, consider the sensitivity of heating in the TF coils to the cross sections in the TF coil region itself. The response here is in the inboard edge (first mesh interval) of the TF coil, while the sensitivity is to cross sections in the entire region 24. Table V shows a very low sensitivity to all neutron cross sections except for Cu. This is to be expected because interactions in the TF coil itself do not significantly alter the probability of a neutron contributing to heating at the inboard edge of the coil. Although it is of somewhat academic interest (because of the precision with which gamma-ray interaction cross sections are known), the relatively high negative sensitivity to Cu gamma-ray interaction cross sections is as expected. Similarly, the integral sensitivity to the gamma-ray kerma response function has been observed to be a large positive value for Cu.

5 CONCLUSIONS

Several major conclusions have been reached thus far in our sensitivity and uncertainty analyses of fusion reactors. First, the wide ranging survey calculations, using transport-code cross sections, have provided a rapid and thorough coverage of all materials and regions of potential interest. This has proven to be an effective way of eliminating the need for further analyses of many partial cross-section sensitivities. From a pragmatic viewpoint, these partials are of interest only if they provide significant contributions to the total sensitivity, and have significant errors associated with them. In the case of the EPR study, we have now processed the partials of interest into multigroup form, and are currently performing uncertainty analyses.

A major effort in sensitivity and uncertainty analyses stems from the need for detailed covariance matrices. The lack of these data in either ENDF or individual laboratory files has been a serious deterrent to complete uncertainty determinations for the EPR. On a hopeful note, however, we expect that the error file data produced for our EPR study will provide the major expected uncertainty information. Especially valuable are the data for Fe and C, materials which figure prominently in present shield design concepts. In addition, error files for ^{7}Li, ^{9}Be and possibly ^{11}B will be forthcoming shortly.

REFERENCES

1. M. E. Battat and D. J. Dudziak, "Shield Analyses for Intense 14-MeV Neutron Sources," Proc. 5th International Conf. on Reactor Shielding, Knoxville, TN, USA, 18-23 April 1977 (to be published).

2. S. A. W. Gerstl, Donald J. Dudziak, and D. W. Muir, "Cross-Section Sensitivity and Uncertainty Analysis with Application to a Fusion Reactor," Nucl. Sci. Eng. 62(1), 137 (1977).

3. Patrick D. Soran, Donald J. Dudziak, and Douglas W. Muir, "Effect of Be(n,2n) Multigroup Treatment on Theta-Pinch Blanket Nucleonics," Proc. First Topical Meeting on Technology of Controlled Nuclear Fusion, San Diego, CA, 16-18 April 1974, CONF-740402.

4. S. A. W. Gerstl, "Sensitivity Profiles for Secondary Energy and Angular Distributions," Proc. 5th International Conf. on Reactor Shielding, Knoxville, TN, USA, 18-23 April 1977 (to be published).

5. M. K. Drake and Donald J. Dudziak (eds.), "ENDF Formats and Procedures," USAEC report ENDF-102, Vol. I (BNL 50274, 197) and Vol. II (LA-4549, 1971).

6. J. R. Powell, J. A. Fillo, B. G. Twining, and J. J. Dorning (eds.), Proc. of the Magnetic Fusion Energy Blanket & Shield Workshop - A Technical Assessment, Upton, NY, 29 March-2 April 1976, ERDA-76/117/1, CONF-760343.

7. Donald J. Dudziak, "An Assessment of Nucleonic Methods and Data for Fusion Reactors," Proc. Sec. Topical Meeting Technol. of Controlled Nucl. Fusion, Richland, WA, 21-23 Sept. 1976.

8. Robert E. MacFarlane and R. M. Boicourt, "NJOY: A Neutron and Photon Cross-Section Processing System," Trans. Am. Nucl. Soc. 22, 720 (1975).

9. T. R. Hill, "ONETRAN: A Discrete Ordinates Finite Element Code for the Solution of the One-Dimensional Multigroup Transport Equation," Los Alamos Scientific Laboratory report LA-5990-MS (1975).

10. S. A. W. Gerstl, "SENSIT-1D, A FORTRAN Code to Perform Cross-Section and Design Sensitivity Analyses in One-Dimensional Geometries," Los Alamos Scientific Laboratory report (to be published).

11. W. A. Reupke and D. W. Muir, "Neutronic Data Consistency Analysis for Lithium Blanket and Shield Design," Proc. Sec. Topical Meeting Technol. of Controlled Nucl. Fusion, Richland, WA, 21-23 Sept. 1976.

12. E. L. Simmons, Donald J. Dudziak, and S. A. W. Gerstl, "Nucleonic Design Sensitivity Analysis of the Reference Theta-Pinch Reactor (RTPR)," Trans. Am. Nucl. Soc., Vol. 22, 43 (1975).

13. E. L. Simmons, Donald J. Dudziak, and S. A. W. Gerstl, "Nuclear Design Sensitivity Analysis for a Fusion Reactor," Nucl. Technol., (to be published).

14. David Leon Prezbindowski, "An Analysis of the Effects of Cross Section Uncertainties on the Multitable S_n Solution of Neutron Transport through Air," Doctoral Dissertation, Purdue University (January 1968).

15. S. A. W. Gerstl, "Second-Order Perturbation Theory and its Application to Sensitivity Studies in Shield Design Calculations," Trans. Am. Nucl. Soc. 16, 342 (1973).

16. D. E. Bartine, E. M. Oblow, and F. R. Mynatt, "Radiation-Transport Cross-Section Sensitivity Analysis -- A General Approach Illustrated for a Thermonuclear Source in Air," Nucl. Sci. Eng. 55, 147 (1974).

17. M. A. Abdou, "Nuclear Design of the Blanket/Shield System for a Tokamak Experimental Power Reactor," Nucl. Technol. 29, 7 (1976).

18. H. A. Sandmeier, G. E. Hansen, R. E. Seamon, T. J. Hirons, and A. H. Marshall, "Coupled Neutron-Gamma Multigroup-multitable Cross Sections for 29 Materials Pertinent to Nuclear Weapons Effect Calculations Generated by LASL/TD Division," Los Alamos Scientific Laboratory report LA-5137 (1974).

19. E. L. Simmons, S. A. W. Gerstl, and Donald J. Dudziak, "Cross-Section Sensitivities of Nucleonic Characteristics in a Fusion Experimental Power Reactor (EPR)," Los Alamos Scientific Laboratory report (to be published).

20. S. A. W. Gerstl, "The Application of Perturbation Methods to Shield and Blanket Design Sensitivity Analyses," Argonne National Laboratory report AP/CTR/TM-28 (1974).

TABLE I

NEUTRON INTEGRAL SENSITIVITY, S_{Σ_T}, OF THE INNER TFC NUCLEAR HEATING RESPONSE TO THE TOTAL CROSS SECTIONS OF STAINLESS STEEL COMPONENTS

Component	Region					Total
	6-8	12	14	16	23	
Cr	-0.601	-0.212	-0.188	-0.150	-0.014	-1.168
Mn	-0.103	-0.034	-0.031	-0.026	-0.005	-0.202
Fe	-2.480	-0.868	-0.767	-0.602	-0.058	-4.775
Ni	-0.526	-0.182	-0.164	-0.140	-0.010	-1.032
Mo	-0.091	-0.033	-0.030	-0.024	-0.008	-0.187
TOTAL	-3.801	-1.330	-1.180	-0.944	-0.097	-7.375

TABLE II

PARTIAL AND NET NEUTRON INTEGRAL SENSITIVITIES OF THE INNER TFC NUCLEAR HEATING RESPONSE TO THE Fe COMPONENT IN STAINLESS STEEL REGION 6-8

Neutron Cross Section, Σ_x	Integral Loss Term	Integral Gain Term	Integral Net, S_{Σ_x}
Σ_a	- 0.17	----	0.17
Σ_s	12.98	10.33	- 2.65
Σ_T	12.81	10.33	- 2.48
$\Sigma_{(n\to\gamma)}$	----	0.014	0.014

TABLE III

NEUTRON INTEGRAL SENSITIVITY, S_{Σ_T}, OF THE INNER TFC NUCLEAR HEATING RESPONSE TO THE TOTAL CROSS SECTIONS OF B_4C COMPONENTS

Component	Region				Total
	11	13	15	17	
10_B	-0.221	-0.268	-0.375	-0.543	-1.409
C	-0.166	-0.190	-0.243	-0.196	-0.796
TOTAL	-0.387	-0.459	-0.618	-0.739	-2.206

TABLE IV

PARTIAL AND NET NEUTRON INTEGRAL SENSITIVITIES OF THE INNER TFC NUCLEAR HEATING RESPONSE TO CROSS SECTIONS OF THE ^{10}B COMPONENT IN B_4C REGION 17

Cross Section, Σ_x	Integral Loss Term	Integral Gain Term	Integral Net, S_{Σ_x}
Σ_a	0.41	----	-0.41
Σ_s	0.81	0.68	-0.13
Σ_T	1.22	0.68	-0.54
$\Sigma_{(n\rightarrow\gamma)}$	----	0.0009	0.0009

TABLE V

NEUTRON AND GAMMA-RAY SENSITIVITIES, S_{Σ_T}, OF THE FIRST INTERVAL OF TFC NUCLEAR HEATING RESPONSE TO TFC MATERIAL CROSS SECTIONS

Component	Neutron S_{Σ_T}	Gamma S_{Σ_T}
Cr	-0.000	-0.020
Mn	-0.001	-0.003
Fe	-0.003	-0.086
Ni	0.001	-0.019
Mo	-0.003	-0.004
Cu	-0.065	-0.150
Nb	-0.011	-0.015
Ti	0.001	-0.004
He	0.008	-0.002
TOTAL	-0.075	-0.306

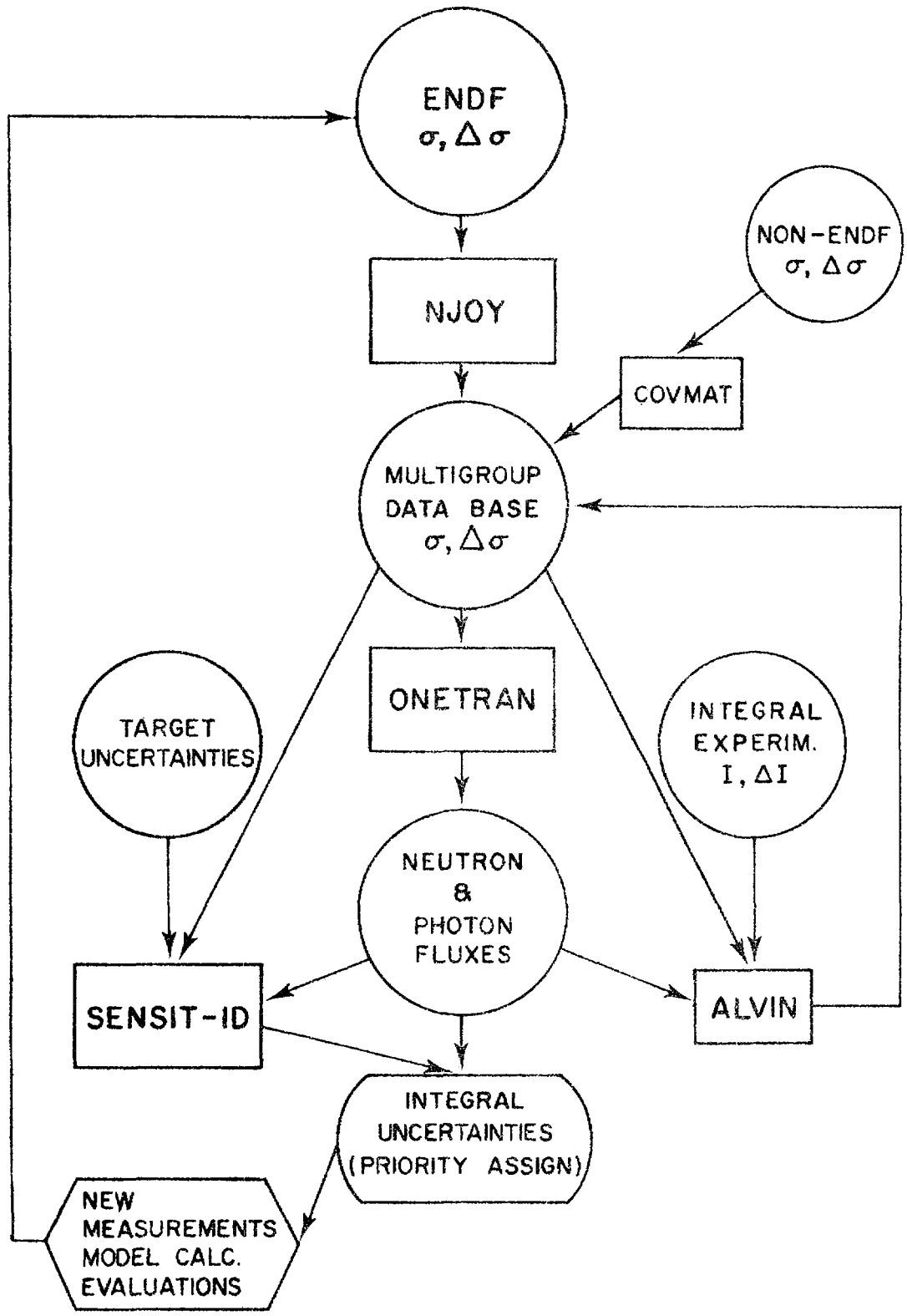

Fig. 1. The LASS system used for sensitivity, uncertainty, and differential/integral data consistency analysis.

Region No.	Region Material	Radius (cm)
		0.0
1	PLASMA	
		210.0
2	VACUUM	
		240.0
3	1st WALL S. S.	
		241.0
4	1st WALL S. S.	
		242.0
5	1st WALL S. S.	
		244.0
6	BLANKET S. S.	
		254.0
7	BLANKET S. S.	
		264.0
8	BLANKET S. S.	
		272.0
9	VACUUM	
		273.0
10	S. S.	
		276.0
11	B_4C	
		281.0
12	S. S.	
		291.0
13	B_4C	
		297.0
14	S. S.	
		307.0
15	B_4C	
		315.0
16	S. S.	
		325.0
17	B_4C	
		333.0
18	S. S.	
		335.0
19	TFC DEWAR S. S.	
		337.0
20	VACUUM, TUBING, ETC.	
		339.8
21	THERMAL SHIELD	
		340.7
22	VACUUM	
		343.2
23	TFC BOBBIN (S. S.)	
		345.7
24	TFC	
		350.7
25	TFC	
		355.7
26	TFC	
		360.7
27	TFC	
		416.2
28	SUPPORT CYLINDER	
		440.0
29	OHC	
		465.0

Fig. 2. One-dimensional model of the EPR inner blanket/shield.

REGION NO.	REGION MATERIAL	RADIUS (cm)
		0.0
1	PLASMA	210.0
2	VACUUM	240.0
3	1st WALL S. S.	241.0
4	1st WALL S. S.	242.0
5	1st WALL S. S.	244.0
6	BLANKET S. S.	254.0
7	BLANKET S. S.	264.0
8	BLANKET S. S.	272.0
9	VACUUM	273.0
10	S. S.	276.0
11	GRAPHITE	281.0
12	GRAPHITE	286.0
13	GRAPHITE	291.0
14	S. S.	296.0
15	LEAD MORTAR	301.0
16	LEAD MORTAR	311.0
17	LEAD MORTAR	321.0
18	LEAD MORTAR	331.0
19	LEAD MORTAR	341.0
20	LEAD MORTAR	351.0
21	LEAD MORTAR	356.0
22	LEAD MORTAR	361.0
23	S. S.	366.0
24	S. S.	370.0
25	VACUUM	440.6
26	TFC DEWAR	442.6
27	VACUUM	445.1
28	THERMAL SHIELD	446.0
29	VACUUM	448.5
30	TFC BOBBIN	451.0
31	TFC	456.0
32	TFC	461.0
33	TFC	466.0
34	TFC	521.5
35	HELIUM BATH	529.8
36	TFC BOBBIN	532.3
37	VACUUM	534.8
38	THERMAL SHIELD	535.7
39	VACUUM	538.2
40	TFC DEWAR	540.2

Fig. 3. One-dimensional model of the EPR outer blanket/shield.

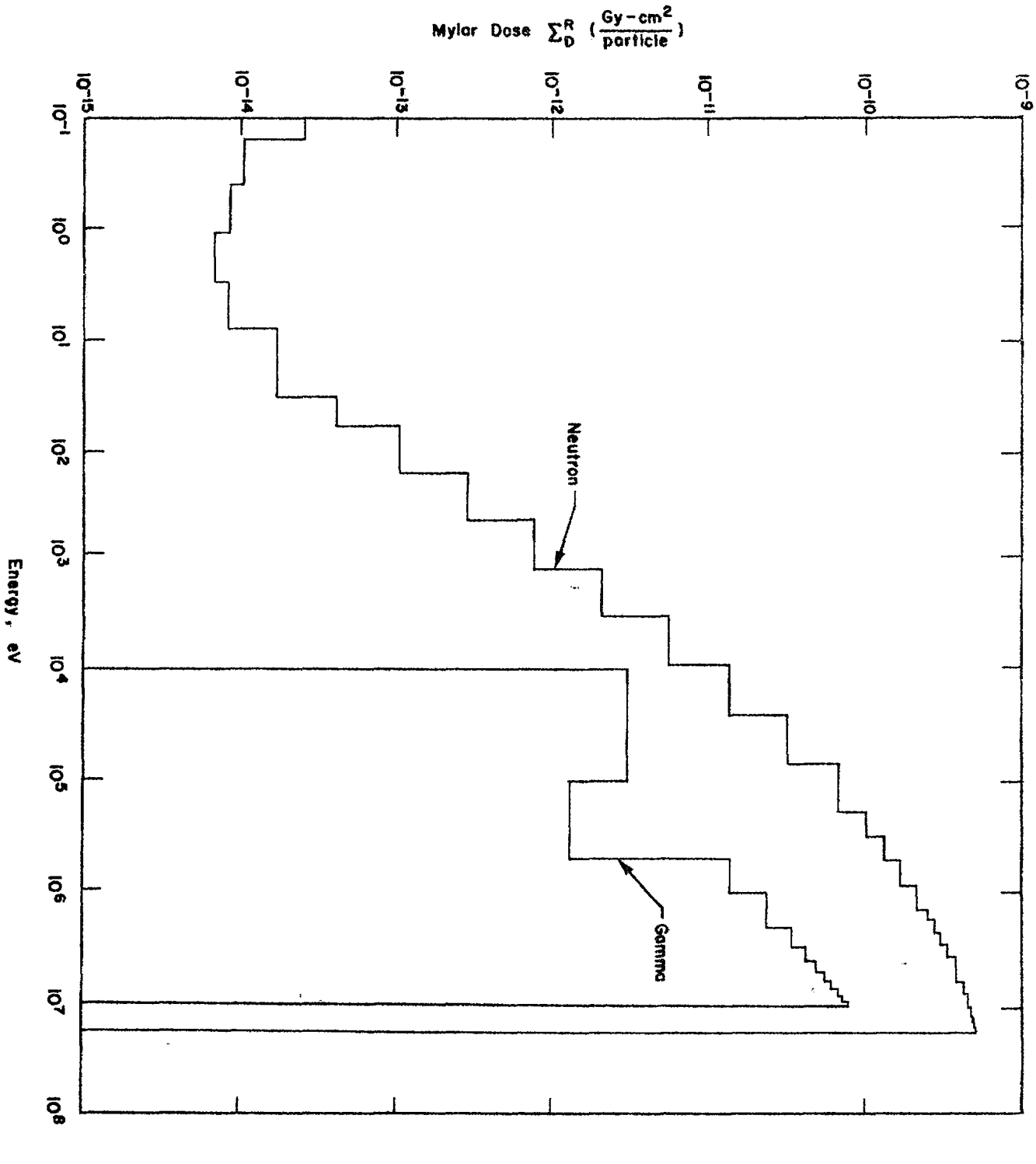

Fig. 4. Response function for absorbed dose in MYLAR insulation in the TF coils.

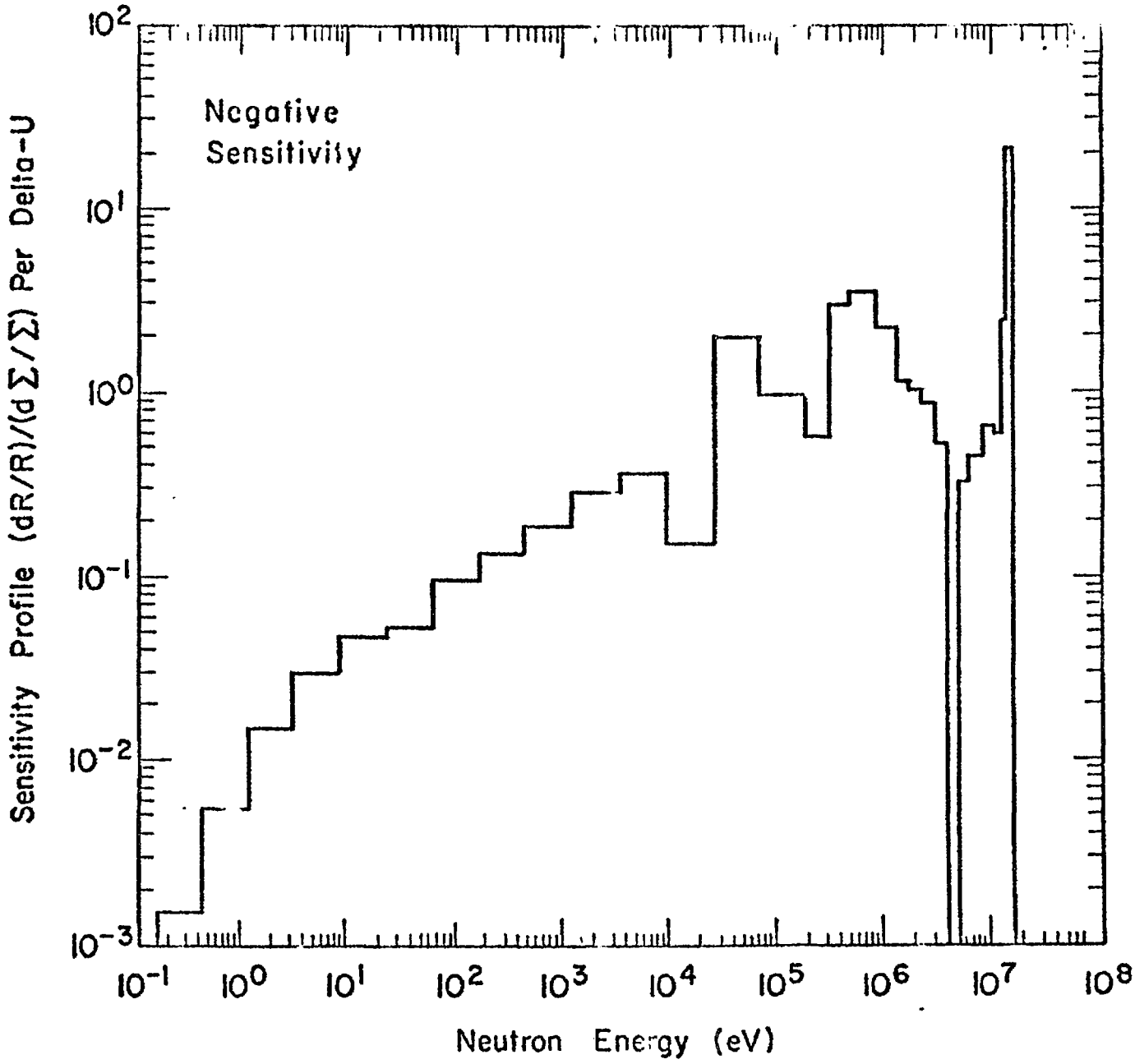

Fig. 5. Sensitivity of the maximum neutron plus gamma-ray heating in the TF coils to all scattering cross sections of Fe.

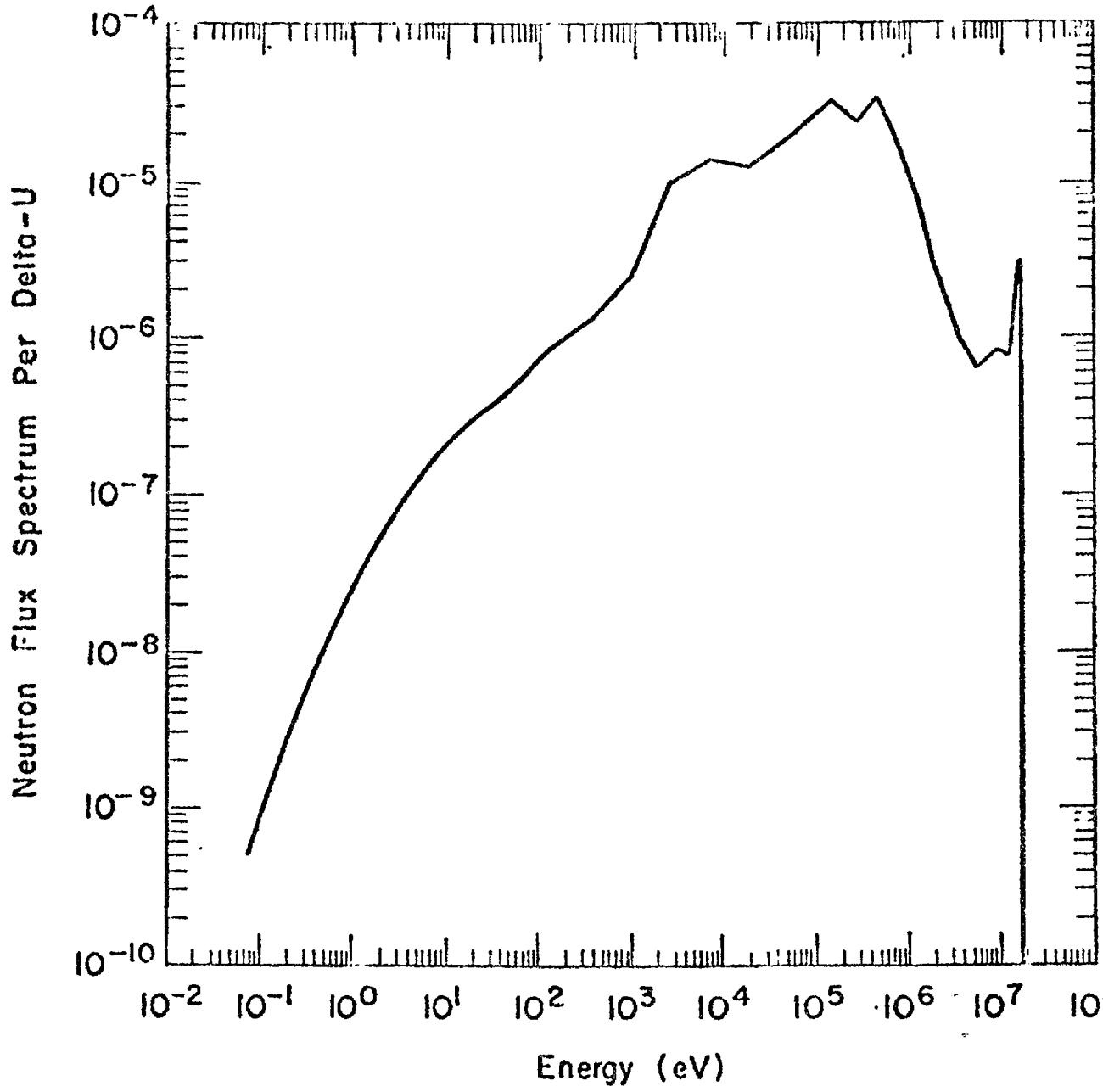

Fig. 6. Neutron flux spectrum at the inner edge of the TF coil (radius = 3.47 m).

SESSION D

STATUS OF THEORETICAL METHODS AND DATA

SENSITIVITY STUDIES IN 3D SHIELDING CONFIGURATIONS

(H. Rief)

Commission of the European Communities
C.C.R.-Euratom
Ispra

Abstract

As already reported previously[1], a program for sensitivity calculations in three dimensions is under development. Especially in shielding calculations where ducts and other heterogeneities are of primary importance, two and three dimensional sensitivity calculations are increansingly requested. Since shielding calculations for these problems are almost exclusively done by Monte Carlo techniques, the associated sensitivity studies also require the same methods.

The mathematical formulation of this problem was described earlier. Meanwhile the method has been incorporated into the TIMOC-program. So far mainly one and multigroup calculations in spherical geometries were performed and compared with equivalent ANISN-SWANLAKE runs.

The comparison of the two methods gave satisfactory results for both the sensitivities of the integral dose rates as well as for the sensitivity profile of the spectra.

As a first application to shielding benchmark experiments, the measurements of neutron spectra transmitted through iron slabs at the fast source reactor "YAYOI[3] have been investigated.

Introduction

Neutron transport calculations in 3-D geometries are almost exclusively done by Monte Carlo techniques. For this reason the associated sensitivity studies require the application of the same methods.

In the approach described here, one solves the "forward equation" and estimates the perturbation effects by correlated sampling in which the same tracks are used in the unperturbed and the perturbed cases. The effect of the perturbation (or the sensitivity) is calculated at each collision by weight

factors that correct for sampling from the unperturbed collision density functions. In addition to flux and sensitivity calculations by the"path length" estimator, the "next event" estimator and if necessary also the "once more collided" estimator (to remedy the infinite variance problem) are used to allow for the scoring at points. To meet the requirements of deep penetration problems this concept has been combined with a region dependent "expected leakage estimator" and an associated splitting procedure.

A rather detailed description of this approach has been presented at the Meeting on Sensitivity Studies and Shielding Benchmarks (Paris, Oct. 1975) and is available in the proceedings of that Conference (1).
Since then the proposed methods have been programmed, tested, and incorporated into the Monte Carlo program TIMOC-(2).

At present the program allows for the calculation of energy integrated sensitivity factors in multigroup, 3-D multimedia geometries and of energy dependent sensitivity profiles in 3-D single media geometries.

It is now the scope of this paper to present the test results which so far have been obtained.

1. One Dimensional Test Examples

In order to establish the necessary confidence in the methods proposed, a series of calculations were performed which could be compared with equivalent ANISN-SWANLAKE runs.
The first example was a monoenergetic calculation of a 10 m.f.p. radius sphere with a point source at the center:

Table I

Radius in MFP	ANISN-SWANLAKE FLUENCE	ANISN-SWANLAKE SENSITIVITY	Monte Carlo FLUENCE	Monte Carlo SENSITIVITY
10	3.02E-5	-4.34	3.4E-5±0.4E-5	-4.3±0.3

Sensitivity= $\frac{\partial J_1}{J_1} \Big/ \frac{\partial \Sigma_r}{\Sigma_r}$

This sphere of 10.f.p. radius represents a typical deep penetration problem and is, therefore, significant for shielding applications. The comparison of the results shows a very favorable agreement between the two methods.

The second test case deals with a multigroup problem in spherical geometry. In this example a californium source was assumed to be at the center of an iron sphere. The net current at the surface and its sensitivity profile was calculated. In both calculations (ANISN-SWANLAKE and Monte Carlo) the same 55 group cross-section set generated from ENDFB-4 in the energy range from 67.4 keV up to 14.9 Mev was used (EURLIB-III). So as to make easier comparison possible and improve statistics in the M.C. results the sampling of the neutron current and the calculation of the sensitivity profiles were performed for four macro groups only. The results of this exercise are listed in Table II.

Table II

Iron sphere with central Cf-source, R= 20 cm

Energy group (MeV)	ANISN-SWANLAKE		MONTE CARLO	
	Total Current	Sensitivity	Total Current	Sensitivity
0.0674-0.334	0.282	-5.9 E-2	0.286	-5.0 E-2 (1)
0.334-1.353	0.533	-4.7 E-2	0.533	-4.3 E-2 (1)
1.353-4.724	0.094	-2.0 E-2	0.095	-3.3 E-2 (1)
4.724.14.9	0.0050	-0.26E-2	0.0046	-0.20E-2 (1)
TOTAL	0.924	-0.13	0.918	-0.13 (2)

$$\text{Sensitivity (1)} = \frac{\partial J_{Total}}{J_{Total}} \Big/ \left(\quad \right)_{\text{group } i}$$

$$\text{Sensitivity (2)} = \frac{\partial J_{Total}}{J_{Total}} \Big/ \left(\quad \right)_{\text{all groups}}$$

The comparison shows a good agreement for the leakage current and the sensitivity profile in all four groups.

2. Transmission of Neutron Beams Through Iron Slabs Using the Fast Source Reactor "YAYOI"

As a typical example of interpreting a three-dimensional benchmark experiment, the neutron transmission measurements at the fast source reactor "YAYOI" were chosen. In one of these experiments a narrow collimated neutron beam is penetrating a 9.6 cm thick iron slab.
The spectra are measured at two positions, both at a distance of 100 cm from the surface of the iron slab.
One detector is located on the beam axis (0^o position) and the other at 30^o off the beam axis.
The calculations were performed again by the use of the previously mentioned 55 group cross-section set.

In Fig. 1 the measured and calculated spectra are plotted for both detector positions. In the calculations the source was represented by a monodirectional beam of 20 cm diameter.
The energy spectrum of the emitted neutrons was measured at the 0^o position in the absence of the iron slab, and it was this spectrum which was used in the calculations.
As can be seen, there is an excellent agreement in the 0^o position up to 10 MeV. Above this energy the Monte Carlo results had, for reasons of statistics, to be collapsed to a single energy group which again compared well with the integrated measurements.
The calculated and measured values in the 30^o position compare much less favorably. In this detector position one observes only scattered neutrons and it was obviously the scope of this experiment to obtain additional information on the scattering cross-sections. A study of the reasons for this deviation is being undertaken at the present time and will be facilitated by the help of the sensitivity profiles, shown in Fig. 2.

The sensitivity profiles show in the "0^o experiment" an approximate proportionality with the flux which means that scattering is of minor importance.
This proportionality holds much less for the 30^o experiment.

3. Space Dependency of Sensitivity Factors in the Case of a Monodirectional Source

In an attempt to improve the basic understanding of YAYOI-type experiments as discussed above, a more systematic analysis of the space dependency of sensitivity factors has been carried out.
For simplicity this analysis was limited to one-group calculations of spheres with a monodirectional source at the center.
The sensitivity of the net leakage current as a function of total cross-section change was calculated for different positions on the surface of the sphere (characterized by the angle of deviation from the source direction).

The space dependency of these sensitivity factors is shown in Fig. 3 for spheres of different radii. For each sphere the calculations were performed once for an isotropic scattering kernel and a second time for a P1 approximation with $\bar{\mu} = 0.3$. In all problems we assumed $\Sigma a / \Sigma t = 0.9$.

The graphs show that in the 0° position the sensitivity increases rapidly as R exceeds 2 m.f.p. On the other hand in smaller spheres the largest sensitivity is observed for the multiple scattered neutrons (position of $\vartheta > 30^{\circ}$).

Conclusions: In the near future the here presented studies will be completed. From the results obtained so far there is sufficient evidence, that some new criteria for the layout of shielding benchmark experiments should be established.

As a next projet typical shield configurations containing ducts will be analyzed.
It is also our intention to elaborate the necessary sampling procedures which allow the calculation of quantities needed in the nuclear data adjustment procedures based on the linear regression technique developed by W. Matthes (4).

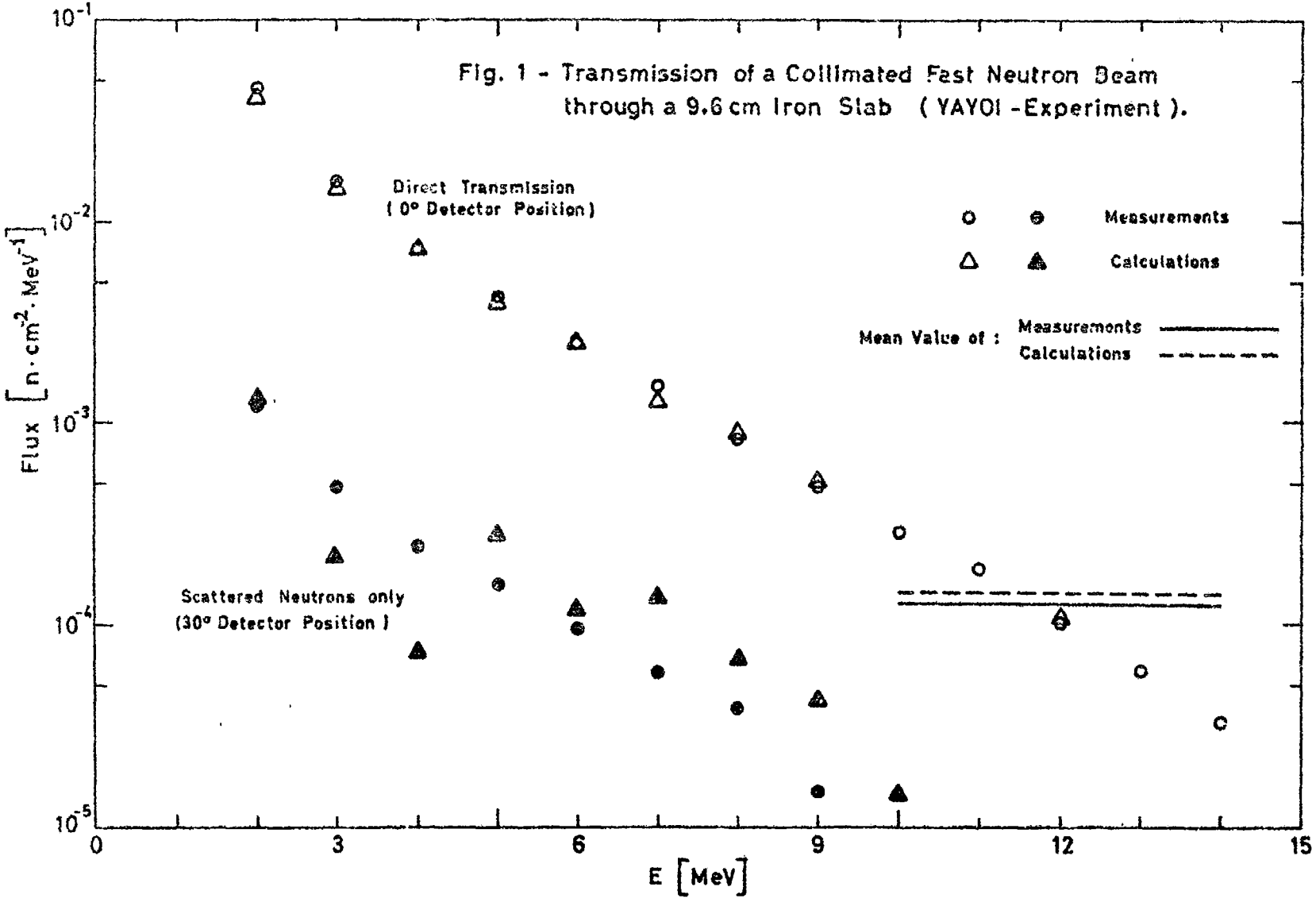

Fig. 1 - Transmission of a Collimated Fast Neutron Beam through a 9.6 cm Iron Slab (YAYOI -Experiment).

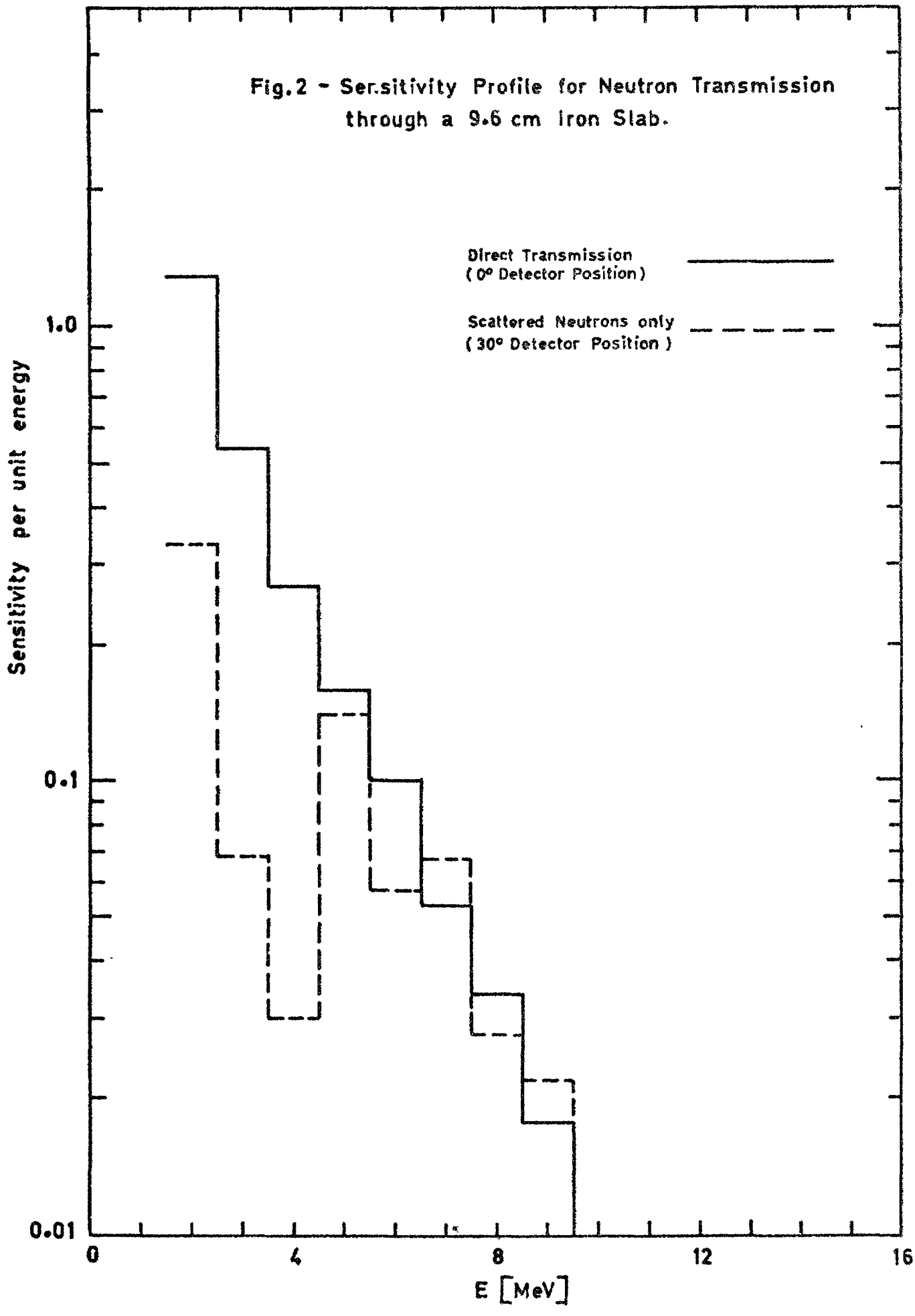

Fig. 2 - Sensitivity Profile for Neutron Transmission through a 9.6 cm Iron Slab.

SOME REQUIREMENTS AS REGARDS THE ACCURACY OF CONSTANTS FOR FAST POWER REACTOR SHIELDING CALCULATIONS

O.D. Bakumenko, M.Ya. Kulakovsky, V.I. Savitsky
USSR

Abstract

The intrinsic activity of sodium coolant, determined by the sodium activation components resulting from the reactions $^{23}Na(n,\gamma)^{24}Na$ and $^{23}Na(n,2n)^{22}Na$, was determined when the BN-350 reactor started up.

Another series of experiments in the BN-350 reactor was carried out for the purpose of determining the activity of the steel components resulting from reactions $^{50}Cr(n,\gamma)^{51}Cr$, $^{58}Fe(n,\gamma)^{59}Fe$, $^{58}Ni(n,p)^{58}Co$, $^{54}Fe(n,p)^{54}Mn$ and $^{59}Co(n,\gamma)^{60}Co$.

Comparison of calculated and experimental values are made. Some discrepancies are pointed out.

The use of thick layers of non-hydrogenous materials and the specific neutron leakage spectrum mean that the main process of neutron transport in the shielding of fast power reactors is the slowing-down of neutrons through elastic collisions. The maximum fraction of fast neutrons (at entry into shielding) does not exceed 5% (>1 MeV); the fraction of intermediate neutrons in the sodium layer is ~99.98%. The principal contribution to the value of the basic shielding functionals (density of sources of capture gamma radiation, dose rate) is made by neutrons of intermediate energies. More precise determination of the fluxes of neutrons with energies over 1 MeV has no effect on the precision of the determination of the practical characteristics of the shielding of this reactor type.

The main problem in shielding calculations is connected with the correct description of the slowing-down of neutrons at great distances from their source.

The main causes of errors in the calculated distribution of a neutron flux in the non-hydrogenous shielding of fast reactors are associated with the following factors:

(a) Limited allowance for the anisotropy of the flux;

(b) Limited allowance for the anisotropy of scattering;

(c) Errors in the initial information and in the averaging of constants;

(d) Use of an age approximation;

(e) Use of a group approximation.

The first three factors are traditional. Let us consider errors connected with the use of an age and a group approximation. We know that, at great distances from the source, the age approximation leads to excessively low neutron flux values. For example, at a distance of 40 free-path lengths, the density of slowing-down (from 100 keV to 1 eV) calculated on the basis of age theory is ~30 times too low in graphite.

On the other hand, the use of a limited number of groups - instead of the continuous slowing-down model - leads to excessively high values of the neutron fluxes at great distances from the source. When 15 groups in the energy range 100 keV-1 eV are used, the neutron fluxes at the same distance in graphite are ~10 times too high. These errors may cancel out. Also in principle, it is possible to select a group width such that one obtains the best correspondence to the results of neutron transmission experiments. However, this approach does not preclude possible errors when one switches to another shielding composition.

The use of higher approximations (than the age approximation) and of continuous spatial slowing-down models is a difficult business, and at the same time it is necessary to work out better methods of calculating the slowing-down of neutrons in fast reactor shielding. The job can be done only through the joint efforts of specialists in compiling constants and working out fast reactor shielding calculation methods. It should be noted that in shielding calculations, as a rule, use is made of reactor systems of constants (e.g. [1]) which naturally do not take into account the strong deformation of the neutron spectrum in shielding. In our opinion, the use of a simplified slowing-down model in the compilation of group constants is at present the main source of errors when calculating neutron penetration in the shielding of fast power reactors. As for requirements regarding the accuracy of the constants, the decisive factor in the shielding of fast reactors is the accuracy of the total interaction cross-section. To ensure $\pm$ 50% accuracy in calculating the flux of neutrons leaving the shielding, the total interaction cross-section must be known for the main shielding components (steel, sodium, carbon) with an accuracy of $\pm$1%

(in the energy range 1 MeV-1 eV)[4] the radiative capture cross-section influences the accuracy of calculations of heat generation and capture gamma radiation fluxes. The energy region below 10 keV is decisive in respect of the contribution to the capture gamma radiation in the shielding. In this region, one needs to know the radiative capture cross-sections to within ± 10%.

For calculations of gamma fluxes and of the heat generation caused by the absorption of gamma radiation one needs to know the gamma yield by energy interval in the radiative capture of neutrons. In the shielding of fast reactors, the capture gamma yield is due mainly to the absorption of epithermal neutrons. In the calculation of gamma fields, use is at present made of the yields of the gamma radiation resulting from thermal neutron capture, although the literature indicates that there exists a dependence of spectral composition on incident neutron energy. The published data on the gamma yield in thermal neutron capture do not correspond to the general binding energy released in the capture of a neutron by a nucleus. The difference is 30-40% for important elements such as Fe, Ni, Cr and Na. In investigations of the shielding of the BN-600 reactor on the BFS-2 test rig, a discrepancy of up to 30% was found between the experimental and computed data on integral characteristics (heat generation, dose rate, etc.); the discrepancy was ~100% as regards spectral characteristics at energies below 1 MeV.

The discrepancy between calculation and experiment is due mainly to the inaccuracy of the data on the gamma yield in neutron capture. When one is calculating heat generation in structural members of the core and the breeding zone, the accuracy of data on the yield of gamma radiation due to fission and inelastic scattering is important. The requirements regarding the accuracy of the calculation of heat generation in structural members are constantly increasing and must at least be better than 10%.

The intrinsic activity of sodium coolant is determined by the sodium activation components resulting from the reactions $^{23}Na(n,\gamma)^{24}Na$ and $^{23}Na(n,2n)^{22}Na$. When the BN-350 reactor started up, a series of experimental investigations was carried out for the purpose of determining the intrinsic activity of the coolant. The experimental results were compared with values obtained by calculations in which constants were used [1, 2, 3]. The measured activity attributable to ^{24}Na was 7.6 Ci/kg of Na and the computed value 8 Ci/kg of Na; the corresponding results for ^{22}Na were 9×10^{-5} Ci/kg and 1.2×10^{-4} Ci/kg [4].

It is worth noting the satisfactory agreement between experiment and calculation, although the results include - besides errors in the nuclear data - both experimental and computational errors. Another series of experiments in the BN-350 reactor was carried out for the purpose of determining the activity of the steel components resulting from the reactions $^{50}Cr(n,\gamma)^{51}Cr$, $^{58}Fe(n,\gamma)^{59}Fe$, $^{58}Ni(n,p)^{58}Co$, $^{54}Fe(n,p)^{54}Mn$ and $^{59}Co(n,\gamma)^{60}Co$.

In Table 1 we present calculated and experimental values for the specific activities of indicator nuclides irradiated at the centre of the BN-350 core.

Table 1

Comparison of calculated and experimental values for the specific activity of indicator nuclides

Nuclide	Ci/kg of indicator nuclide		Ratio of calculated to experimental values
	Calculation	Experiment	
^{60}Co	164	46	3.55
^{58}Co	14.7	12	1.22
^{51}Cr	2.83	2.38	1.19
^{54}Mn	0.95	0.58	1.64
^{59}Fe	0.044	0.039	1.13

In the calculations, use was made of activation cross-sections from Ref.[2]. The neutron fluxes were calculated on the basis of constants from Ref. [1].

The discrepancy between the calculated and experimental values for ^{58}Co, ^{51}Cr and ^{59}Fe is within the limits of the experimental error. The calculated activities of ^{54}Mn are 60% higher than the experimental value, which indicates a need for a review of cross-sections for the reaction $^{54}Fe(n,p)Mn^{54}$. The greatest discrepancy is found in the case of ^{60}Co, where a substantial contribution to activation is made by the resonance energy region, which is not described correctly enough within the framework of a 26-group energy breakdown; more detailed neutron spectra for this region are needed.

REFERENCES

[1] ABAGYAN, L.P. et al., "Group constants for nuclear reactor calculations" (in Russian), Atomizdat, Moscow (1964).

[2] ENDF/B "File for dosimetry applications", USA (1974).

[3] SLUCHEVSKAYA, V.M., "Effective cross-sections for (n,2n) reactions" (in Russian), Bulletin of the Nuclear Data Information Centre, issue 1 (1964).

[4] ORLOV, V.V. et al., "Investigation of physical characteristics at the start-up of the BN-350 reactor", At. Ehnerg. 36, issue 2, Feb. 1974.

The Track Rotation Estimator and It's Application To Shielding Benchmark Experiments

A. Dubi and Y. S. Horowitz
Physics Department, Ben Gurion University of the Negev
Beersheva, Israel

Abstract

A radically new approach is presented for the estimation of flux at a point by Monte Carlo methods. A mathematical review of the method is given followed by examples of isotropic and non-isotropic sources in spherical media which could be related to the interpretation of shielding benchmark experiments.

The Track Rotation Estimator

Monte Carlo estimators allowing the calculation of flux at a point are of primary importance in the interpretation of Shielding Benchmark and Sensitivity studies[1-3]. In a previous publication[4] we have shown that the flux at a phase space point $\bar{P}_0 = (\bar{r}_0, \bar{\Omega})$, ($\bar{r}$ - position vector, $\bar{\Omega}$ - unit direction vector) could be identified with the probability $\mu(\Lambda_{\bar{r}_0})$ where $\Lambda_{\bar{r}_0}$ is the group of all histories passing through $\bar{P}_0$ and $\mu(\Lambda_{\bar{r}_0})$ is the probability in the sense described by references 5 and 6. We first discuss the situation of a point source surronded by a spherical medium. Let

$$\tau_n(\bar{\Omega}_0, \bar{r}_0) = \left[\bar{\Omega}_1, (\bar{r}_1, \bar{\Omega}_2), (\bar{r}_2, \bar{\Omega}_3) \ldots (\bar{r}_n, \bar{\Omega}_{n+1}) | \bar{r}_0 \right] \quad (1)$$

denote a random walk of n collision points, $\vec{r}_i, \vec{\Omega}_{i+1}$ where $\vec{r}_i$ is the i'th collision point and $\bar{\Omega}_{i+1}$ is the direction of emerging from the i'th collision point. $\bar{\Omega}_1$ is the emission direction from the source and the history crosses the sphere at $(\bar{r}_0, \bar{\Omega}_0) = \bar{P}_0$. Let the group $R_L[\tau_n(\bar{\Omega}_0, \bar{r}_0)]$ denote the group of all histories obtained from $\tau_n(\bar{\Omega}_0, \bar{r}_0)$ by rotation around $\bar{r}_0$. That is we put

$$\vec{r}_1 = l_1 \bar{\Omega}_1 , \quad \vec{r}_2 = \vec{r}_1 + l_2 \bar{\Omega}_2 \ldots \vec{r}_n = \vec{r}_{n-1} + l_n \bar{\Omega}_n \quad (2)$$

where $\vec{\Omega}_i$ is defined in a spherical coordinate system centered at $\vec{r}_{i-1}$. Then rotate $\vec{\Omega}_1$ around $\vec{r}_0$ keeping everything else constant. Let $R[\tau_n(\vec{\Omega}_0, \vec{r}_0)]$ denote the group of random walks obtained from R_L by rotating $\vec{r}_0$ around the origin. It is then clear that if U is the group of all histories that crossed the sphere, then

$$\mu(U) = \sum_{n=0}^{\infty} \int \cdots \int \mu\{R[\tau_n(\vec{r}_0, \vec{\Omega}_0)]\} \sin\theta_1 \, d\theta_1 \, r_1^2 \, dr_1 \, d\vec{r}_2 \, d\vec{\Omega}_2 \cdots d\vec{r}_n \qquad (3)$$

where the integration is taken over the whole phase space with $\vec{\Omega}_0$ and $\vec{r}_0$ fixed. Thus the group R integrated over all the histories passing through $\vec{r}_0$ with $\vec{\Omega}_1$ fixed in a given plane presents the group of all histories crossing the sphere.

The flux at $\vec{P}_0$ can be written as

$$F(\vec{P}_0) \, ds = \mu(\Lambda_{\vec{P}_0}) \, ds = \sum_{K=0}^{\infty} \mu(\Lambda^K_{\vec{P}_0}) \, ds \qquad (4)$$

where $\Lambda^K_{\vec{P}_0}$ is a subgroup of $\Lambda_{\vec{P}_0}$ of those histories making K collisions before passing through $\vec{P}_0$. From the above discussion it is clear that

$$\mu(\Lambda^K_{\vec{P}_0}) \, ds = \frac{d\vec{\Omega}_S}{|\vec{\Omega}_S \cdot \vec{\Omega}_0|} \int \cdots \int \mu\left[R_L(\tau_n(\vec{r}_0, \vec{\Omega}_0)\right] \sin\theta_1 \, d\theta_1 \, r_1^2 \, dr_1 \, d\vec{r}_2 \, d\vec{\Omega}_2 \cdots d\vec{r}_n \qquad (5)$$

where $d\vec{\Omega}_S$ means $d\left(\frac{\vec{r}_0}{|r_0|}\right)$ such that $\vec{r}_0$ describes an area ds on the surface of the sphere.

Now let $\mu(R_L|R)$ be the conditional probability of the group R_L when it is known that a history from group R occured. Then

$$\mu(R_L) = \mu(R_L|R)\,\mu(R) \qquad (6)$$

so that upon substitution of (5) and (6) into (4) we obtain

$$F(\vec{P}_0) \, ds = \frac{d\vec{\Omega}_S}{|\vec{\Omega}_S \cdot \vec{\Omega}_0|} \sum_{K=0}^{\infty} \int \cdots \int \mu(R_L|R)\,\mu\left[R(\tau_n(\vec{\Omega}_0, \vec{r}_0))\right] \sin\theta_1 \, d\theta_1 \, r_1^2 \, dr_1 \, d\vec{r}_2 \, d\vec{\Omega}_2 \cdots d\vec{r}_K \qquad (7)$$

or by dividing both sides by ds, since $d\vec{\Omega} = d\vec{s}/\underline{R}^2$ ($\underline{R}$ is the radius of the sphere),

$$F(\vec{P}_0) = \frac{1}{|\vec{\Omega}_S \cdot \vec{\Omega}_0| R^2} \sum_{K=0}^{\infty} \int \cdots \int \mu(R_L|R)\,\mu\left[R(\tau_n(\vec{\Omega}_0, \vec{r}_0))\right] \sin\theta_1 \, d\theta_1 \, r_1^2 \, dr_1 \, d\vec{r}_2 \, d\vec{\Omega}_2 \cdots d\vec{r}_K \qquad (8)$$

Combining equations (3) and (8) it is easy to see that the estimator defined by

$$\{ = \begin{cases} 0 & \text{if the history is terminated inside the sphere} \\ \dfrac{\mu(R_L|R)}{R^2|\bar{\Omega}_s\cdot\bar{\Omega}_0|} & \text{when the history crosses the sphere at a direction } \bar{\Omega}_0. \end{cases} \tag{9}$$

is an unbiased estimator of the integrated flux at $\vec{r}_0$,

$$F(\bar{r}_0) = \int F(\bar{r}_0)\, d\bar{\Omega}_0 \tag{10}$$

Thus when we have a history crossing the sphere at any point $\bar{r}$, we adopt the following procedure. Let the history be denoted by $(\bar{\Omega}'_1, \bar{r}_1, \bar{\Omega}'_2, \ldots \bar{r}_n \bar{\Omega}'_0 | \bar{r})$ Then we rotate $\bar{\Omega}'_1$ untill $\bar{r}$ coincides with $\bar{r}_0$. Taking $\bar{r}_0$ as the z axis for $\bar{\Omega}'_1 = \bar{\Omega}_1$ we see that

$$\mu(R_L) = \int_0^{2\pi} q(\bar{\Omega}_1) T(\bar{\Omega}_1, \bar{o} \to \bar{r}_1) K(\bar{r}_1, \bar{r}_2) \ldots K(\bar{r}_{n-1}, \bar{r}_n) \frac{T(\Omega_0, \bar{r}_n \to \bar{r}_0)}{\Sigma_t(\bar{r}_0)} d\phi \tag{11}$$

where ϕ is the azimuthal angle of $\bar{\Omega}_1$ around $\bar{r}_0$, $q(\Omega)$ is the source angular density, T is the free flight kernel and K the transport kernel. Also

$$\mu(R) = \int_{4\pi} d\left(\frac{\bar{r}_0}{|\bar{r}_0|}\right) \mu(R_L) = \int_0^{2\pi} \int_{4\pi} q(\bar{\Omega}_1) \ldots d\bar{\Omega}_1 d\phi' \tag{12}$$

where $d\phi'$ is the azimuthal angle of $\bar{\Omega}_2$ around $\bar{\Omega}_1$. Then finally upon substituting equations (11) and (12) into (9) we obtain

$$\{ = \frac{\left[\int_0^{2\pi} q(\bar{\Omega}_1) T(\bar{\Omega}_1, \bar{o} - \bar{r}_1) \ldots T(\bar{\Omega}_0, \bar{r}_n \to \bar{r}_0) \frac{d\phi}{\Sigma_t(\bar{r}_0)}\right] \frac{1}{|\bar{\Omega}_s \cdot \bar{\Omega}_0|} \frac{1}{R^2}}{\left[\int_{4\pi} \int_0^{2\pi} q(\bar{\Omega}_1) T(\bar{\Omega}_1, \bar{o} - \bar{r}_1) \ldots T(\bar{\Omega}_n, \bar{r}_n \to \bar{r}_0) d\bar{\Omega}_1 d\phi'\right]} \tag{13}$$

Intuitively this is equivalent to taking the contribution to the flux from the history concerned as if it passed through the point multiplied by the conditional probability that such a history will occur given that any rotation of that history has occurred. The extension of the estimator to the general case is not difficult since we surrond the source by a fictitous sphere and use exactly the same arguments for those histories crossing the sphere from the outside. In spherically symmetric situations (13) reduces to a trivial form since the probability distribution function of the history is invarient

under rotation around the source and $q = 1/4\pi$ since the source intensity is normalized so that we obtain

$$\xi = \frac{1}{4\pi R^2 |\vec{\Omega}_0 \cdot \vec{\Omega}_s|} \tag{14}$$

For the case of an anisotropic source in a spherically symmetric medium we get

$$\xi = \frac{1}{2\pi} \int_0^{2\pi} g(\vec{\Omega}_1) d\phi \frac{1}{|\vec{\Omega}_s \cdot \vec{\Omega}_0|} \frac{1}{R^2} \tag{15}$$

In those cases where an exact analytic expression for the integral is difficult to evaluate, one can choose ϕ at random between 0 and 2π and use

$$\xi = g(\vec{\Omega}_1(\phi)) \frac{1}{|\vec{\Omega}_s \cdot \vec{\Omega}_0|} \frac{1}{R^2} \tag{16}$$

For non-spherically symmetric media the denominator of equation (13) must be evaluated. This could be achieved by a separate Monte Carlo estimation of the integral for each track by rotating the track randomly and evaluating the average of the integral.

In principle it is to be noted that the track rotation estimator presents an average over histories which were actually made to pass through the point of interest, whereas former estimators[7-9] are averages over the uncollided flux or the once collided flux contribution from collision points and thus depend on the accuracy with which the collision density is defined throughout the whole space. Moreover, because of the $1/|\vec{\Omega}_s \cdot \vec{\Omega}_0|$ factor the track rotation estimator may have an unbounded variance (although we have found that in practice the track rotation estimator converges very rapidly due to the angular dependence of the flux). Truncating the angular range of the flux integration in order to establish a bound for the variance will merely result in a loss of information and will not cause any bias whereas analog truncation for the other estimators will definitely bias the final results. It is thus expected that for a variety of problems, especially those with symmetrical or closely symmetrical media, and non-isotropic sources the track rotation estimator presents a new attractive option for obtaining fluxes at given points.

Applications

For comparitive purposes, the problem of an isotropic point source at the center of an absorbing and scattering sphere was solved by both the track rotation estimator and the un-collided flux estimator. In Figure 1 results are presented for the leakage flux as a function of the number of histories. The dramatic difference between the two methods is self evident. In terms of the quality factor[7] , Q = sample variance multiplied by the average time per history, the result is $Q(UCF)/Q(TRE) \cong 50$. An exact analytic solution to the above problem was not available in the literature and was therefore obtained by developing a modified Neuman series approach[10] in which the infinite medium solution[11] is compared to the point source finite medium problem resulting in a simple iterative procedure.

The two methods were also applied to a sensitivity study of the leakage flux from a non-isotropic source in a spherically symmetrical medium (a source emitting isotropically in the upper half-sphere) to a change in the density of the medium. The results obtained were that with the track rotation estimator it was possible to reliably detect changes of 0.6% of the integrated flux whereas with the uncollided flux estimator one could reliably detect only 10% changes (our criterion for reliability comes from the condition $\Delta F/F \Big/ \sigma\left(\frac{\Delta F}{F}\right) > 1$. Further results and comparisons with the once collided flux estimator are underway as well as further applications of the track rotation estimator to non-spherically symmetric media, e.g., point source and slab shield geometrical configuration.

Conclusions

A new Monte Carlo method for the estimation of flux at a point has been developed which enables the taking of full advantage of the symmetry properties of the source-medium configuration. The applicability and advantages of the method to isotropic and non-isotropic sources in spherical media has been established. The introduction of energy dependence in a multi-group calculation is both technical and straightforward and hence the applicability of the track rotation estimator to the interpretation of shielding benchmark and sensitivity studies should be realizable in the near future.

References

1) H. Rief, Proceedings of the Specialists' Meeting on Sensitivity Studies and Shielding Benchmarks, pp. 68-74, OECD-OCDE, Paris, 1975.
2) H. Werle et. al., Proceedings of the Specialists' Meeting on Sensitivity Studies and Shielding Benchmarks, pp. 98-103, OECD-OCDE, Paris, 1975.
3) Y. Furuta et. al., Proceedings of the Specialists' Meeting on Sensitivity Studies and Shielding Benchmarks, pp. 120-126, OECD-OCDE, Paris, 1975.
4) Y.S. Horowitz, A. Dubi and S. Mordechai, Nucl. Sci. Eng. 59, 427-429 (1976).
5) J. Spanier and E. Gelbard, Monte Carlo Principles and Neutron Transport Problems, Addison-Wesley, Reading, Mass. (1969).
6) R.R. Coveyou et. al., Nucl. Sci. Eng. 27, 219 (1967).
7) M.H. Kalos, Nucl. Sci. Eng. 16, 111 (1963)
8) T.M. Jordan, Nucl. Eng. Design, 13, 415 (1970).
9) H.A. Steinberg, and M.H. Kalos, Nucl. Sci. Eng., 44, 406 (1970)
10) A. Dubi, H. Rief and Y.S. Horowitz, Applications of the Track Rotation Estimator to Neutron Transport Problems, to be published
11) K.M. Case et. al., Introduction to the Theory of Neutron Diffusion, Vol. 1 LASL (1953)

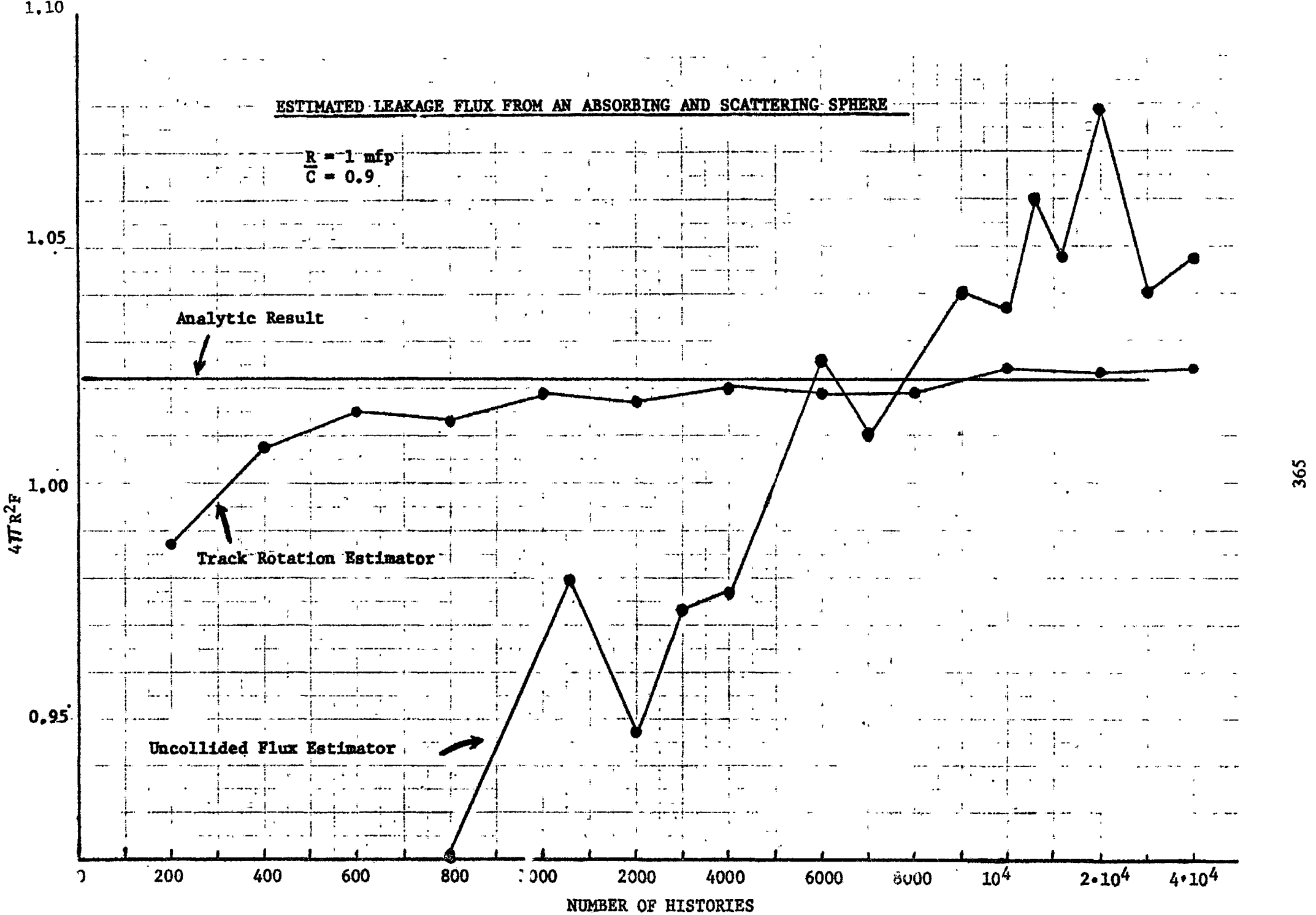
ESTIMATED LEAKAGE FLUX FROM AN ABSORBING AND SCATTERING SPHERE
R = 1 mfp
C = 0.9
Analytic Result
Track Rotation Estimator
Uncollided Flux Estimator
1.10
1.05
1.00
0.95
$4\pi R^2 F$
200
400
600
800
2000
4000
6000
10^4
$2 \cdot 10^4$
$4 \cdot 10^4$
NUMBER OF HISTORIES

INTEGRAL TESTS OF COUPLED MULTIGROUP NEUTRON AND GAMMA CROSS SECTIONS WITH FISSION AND FUSION SOURCES

by J. Schriewer, G. Hehn, M. Mattes, G. Pfister, and J. Keinert
IKE, University of Stuttgart, Germany

Abstract

Calculations were made for different benchmark experiments in order to test the coupled multigroup neutron and gamma library EURLIB-3 with 100 neutron groups and 20 gamma groups. In cooperation with EURATOM, Ispra, we produced this shielding library recently from ENDF/B-IV data for application in fission and fusion technology. Integral checks were performed for natural lithium, carbon, oxygen, and iron. Since iron is the most important structural material in nuclear technology, we started with calculations of iron benchmark experiments. Most of them are integral experiments of INR, Karlsruhe, but comparisons were also done with benchmark experiments from USA and Japan.

For the experiments with fission sources we got satisfying results. All details of the resonances cannot be checked with flux measurements and multigroup cross sections used. But some averaged resonance behaviour of the measured and calculated fluxes can be compared and checked within the error limits given. We get greater differences in the calculations of benchmark experiments with 14 MeV neutron sources. For iron the group cross sections of EURLIB-3 produce an underestimation of the neutron flux in a broad energy region below the source energy. The conclusion is that the energy degradation by inelastic scattering is too strong. For fusion application the anisotropy of the inelastic scatter process must be taken into account, which isn't done by the processing codes at present. If this effect isn't enough, additional corrections have to be applied to the inelastic cross sections of iron in ENDF/B-IV.

1. Introduction

One could expect, that the generation of multigroup libraries from evaluated point cross sections produces condensation of information, resulting in an effective reduction of the total number of cross section data to be stored in a library. But this isn't the case. The real effective reduction occurs in the group collapsing from multigroup libraries to the problem dependent few group data, which are finally used for design calculations.

In the ENDF/B-IV library approximately one million of data is of interest to reactor shielding. A multigroup library with 100 neutron groups and 20 gamma groups like EURLIB-3 has nearly the same amount of elements in the cross section matrices, which doesn't improve the survey. By transformation into the energy group model proper flux weighting is introduced, reducing the direct physical insight of the group data. Of course, consistency can be checked and the numerical effects of the generation programs can be studied. But the real and practical tests of a group library are calculations of benchmark experiments. A progress report of our data tests is given. Most of the integral experiments were performed at INR, Karlsruhe, but comparisons were also done with benchmark experiments from USA and Japan.

2. Results of calculations for fission sources

To check especially inelastic cross sections of iron below 5 MeV the neutron leakage spectra from iron spheres surrounding a Cf-source were calculated and compared with measurements of INR, Karlsruhe /1,2/. The calculated and measured leakage spectra of a sphere with 40 cm diameter are shown in fig. 1. The results of the calculation with ENDF/B-IV data are in good agreement with the experiment below 5 MeV.

More sophisticated measurements had been performed for the spectrum of the angular flux in forward direction, for which calculations with EURLIB data showed some difficulties in the upper keV-region /3/. We repeated the calculation with the finer CSEWG group structure within the energy region of interest. Fig. 2 shows the comparison between the different group structures and the experimental results. Likewise absolute values could be compared with the measurements of Johnson /4/ for a larger iron sphere as given in fig. 3. With the exception of a constant shift between measurement and calculation the agreement is good.

Further test calculations with the EURLIB library had been done for neutron and gamma fluxes of a Cf-source in homogeneous tissue aquivalent solution and for a (D,D)-source in water. Special tests are in progress concerning the gamma production data of iron. Measurements of the gamma spectrum in single material experiments with Cf-sources can be used for integral tests of the gamma production data. After 30 cm of iron the contribution of

gamma-rays from the fission source can be neglected totally in comparison to gamma radiation from inelastic neutron scattering and neutron capture at higher energies.

3. Results of calculations for fusion sources

The test calculation for fusion sources aren't so satisfying as those for fission sources. Fig. 4 shows a comparison of calculation and measurement of the neutron leakage spectrum from an iron cylinder (20 cm long and 30 cm diameter) placed axially adjacent to a generator target producing 14 MeV neutrons /1/. Both calculations, representing onedimensional and twodimensional geometries, give the same underestimation of the neutron flux below source energy in the upper MeV-region. It can be concluded, that the energy degradation by inelastic scattering is too strong. For fusion application the anisotropy of the inelastic scatter process must be taken into account, which isn't done by the processing codes at present. If this effect isn't enough, additional corrections have to be applied to the inelastic cross section of iron in ENDF/B-IV.

In studying the neutronics of fusion reactor blankets, the validity of EURLIB-3 was tested by calculating the ratio of $^{238}U/^{235}U$-fission rates in S_{40}/P_5-approximation for a spherical lithium metal assembly surrounding a 14 MeV target with (fig. 5) and without (fig. 6) a graphite reflector. The comparison with measurements of Maekawa et al. /5/ shows good agreement for the pure lithium assembly but gives larger discrepancies for the reflected assembly, which indicates some deficiencies in the group data of carbon at higher energies.

4. References

/1/ Bluhm, H., Fieg, G., Kappler, F., Kuhn, D., Lalovic, M., Rusch, D., Werle, H., Wiese, H.W.:
Einmaterial-Experimente in Kugelgeometrie zum Vergleich gemessener und gerechneter Neutronenspektren
Proc. Reaktortagung, Nürnberg, 285 - 288 (1975)

/2/ Werle, H.
private communication

/3/ Hehn, G., Schriewer, J., Mattes, M., Canali, U., Nicks, R.:
Calculations for iron benchmark experiments with californium and 14 MeV neutron sources
Proc. Specialists' Meeting on Sensitivity Studies and Shielding Benchmarks, Paris, 130 - 145 (1975)

/4/ Johnson, R.H., Dorning, J.J., Weh ng, B.W.:
Integral tests of neutron cross sections for iron above 1 MeV
Trans. ANS, 22, 799 - 800 (1975)

/5/ Maekawa, H., Seki, Y., Hiraoka, T., Moriyama, M.:
Uranium-238 to Uranium-235 Fission-Ratio Distribution in Spherical Lithium-Metal Assemblies With and Without a Graphite Reflector
Nucl. Sci. Eng., 57, 335 - 340 (1975)

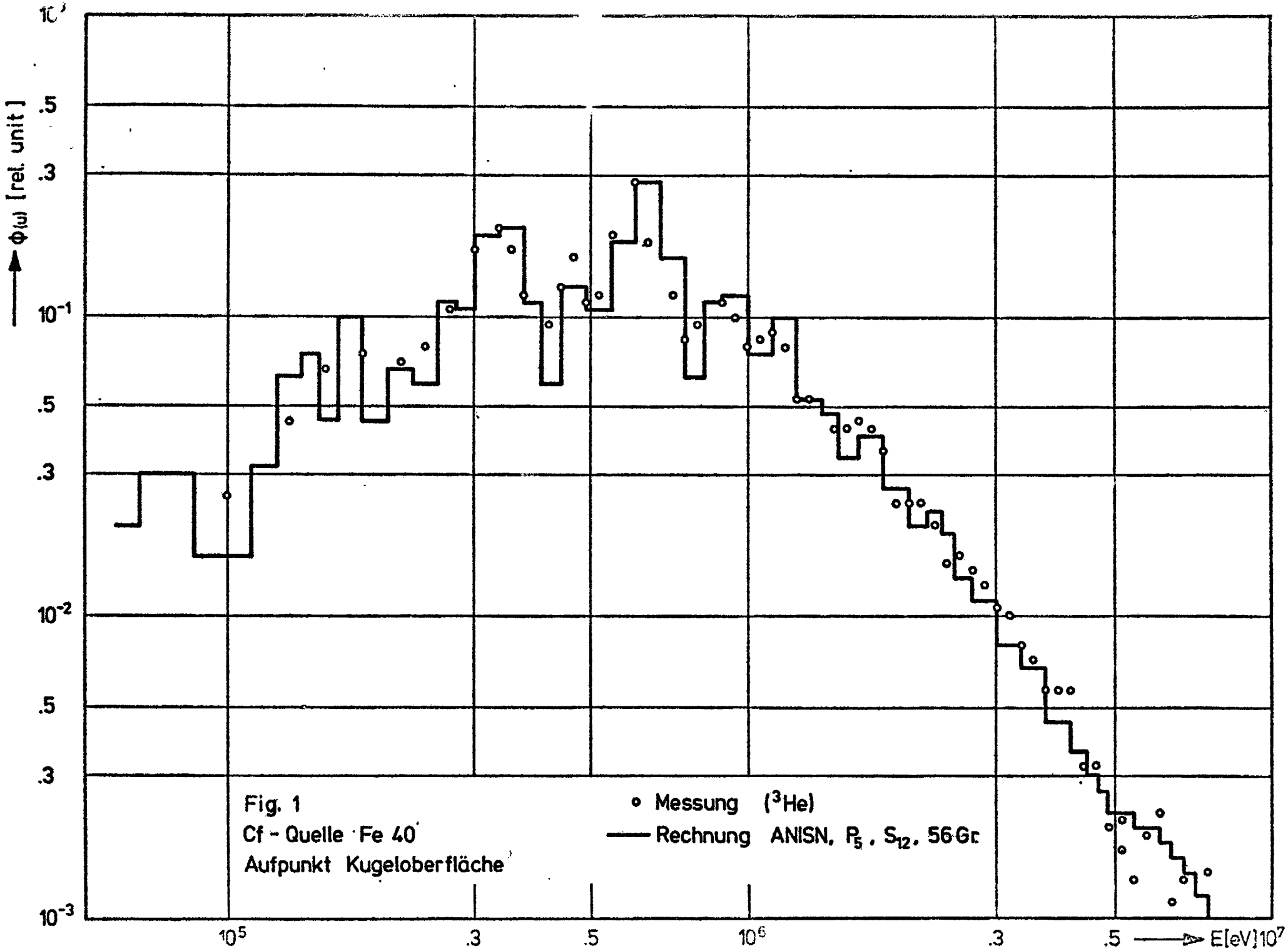
Φ(u) [rel. unit]
10⁰
.5
.3
10⁻¹
.5
.3
10⁻²
.5
.3
10⁻³
10⁵
.3
.5
10⁶
.3
.5
E[eV]10⁷
Fig. 1
Cf - Quelle Fe 40
Aufpunkt Kugeloberfläche
Messung (³He)
Rechnung ANISN, P₅, S₁₂, 56 Gr

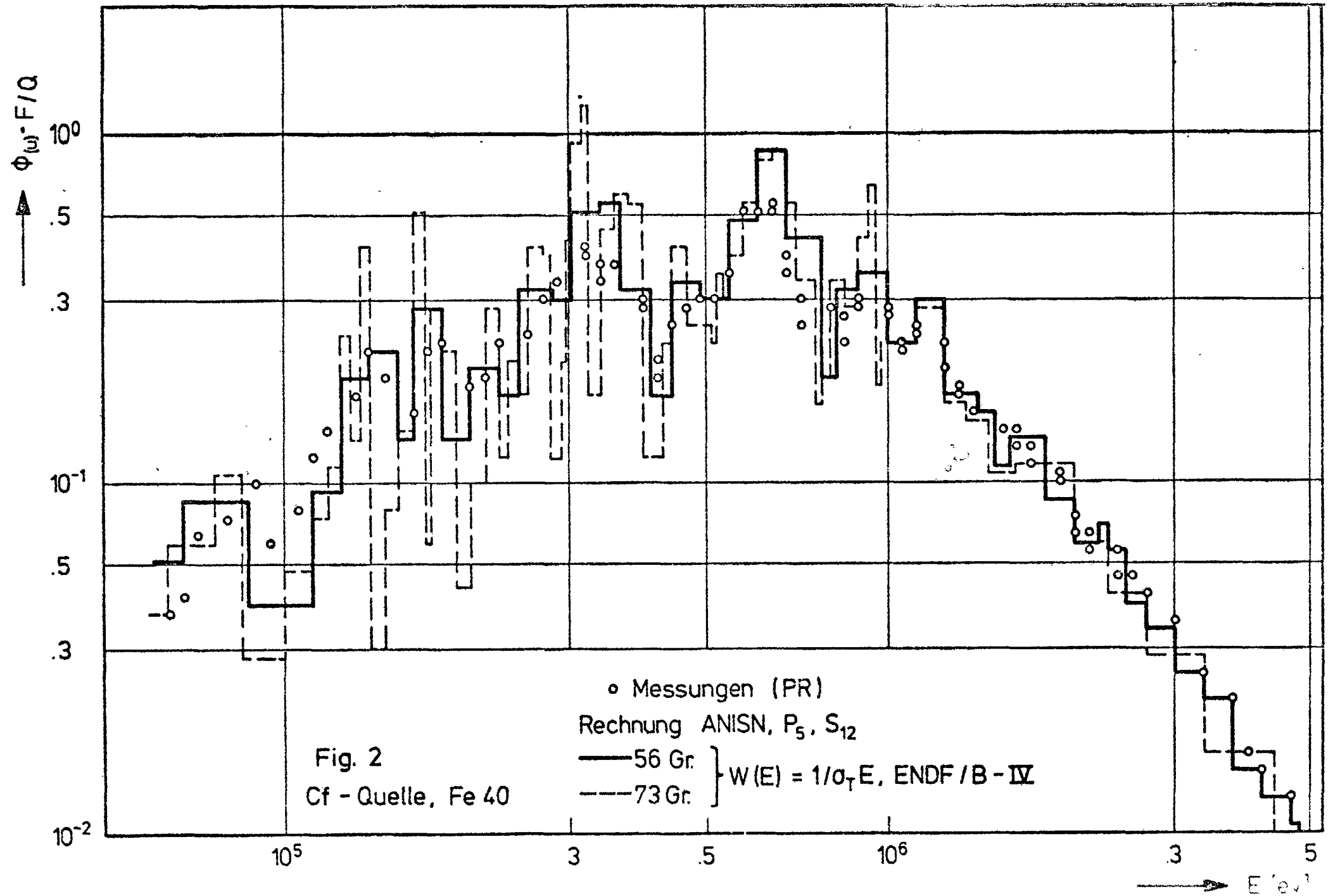

Fig. 2
Cf - Quelle, Fe 40

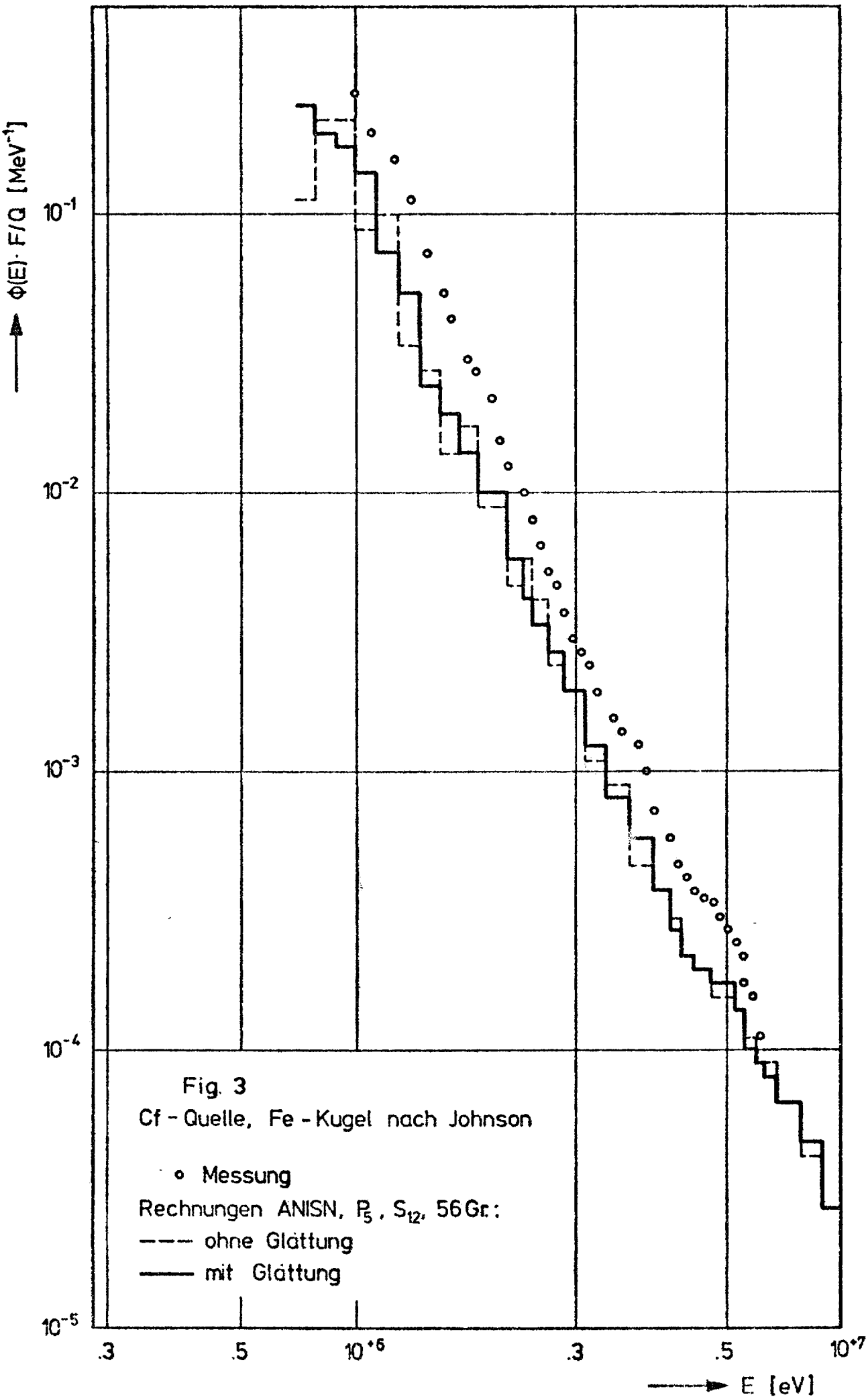

Fig. 3
Cf - Quelle, Fe - Kugel nach Johnson

o Messung
Rechnungen ANISN, P_5, S_{12}, 56 Gr.:
—— ohne Glättung
—— mit Glättung

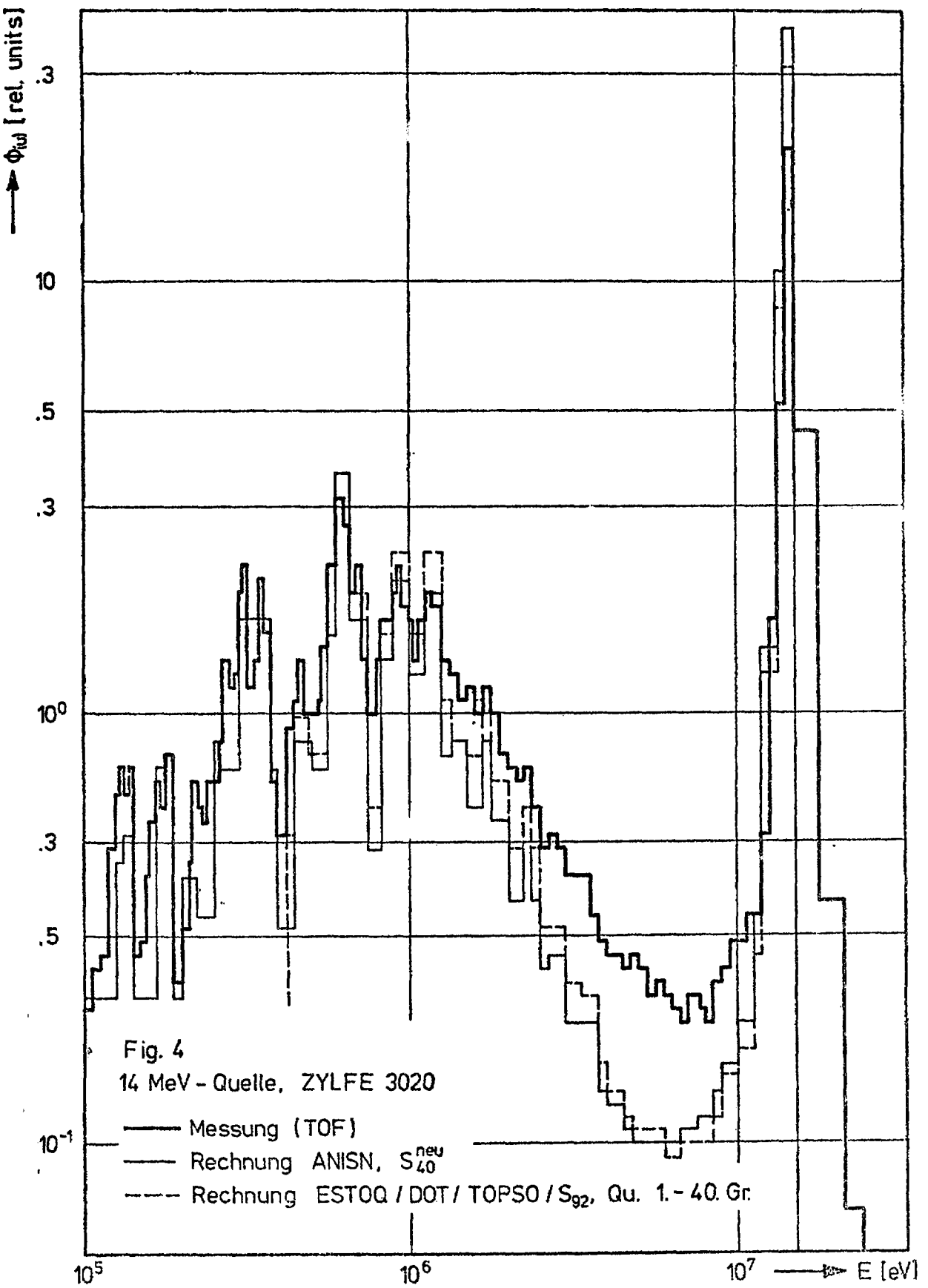
Φ_{lu} [rel. units]
.3
10
.5
.3
10^0
.3
.5
10^{-1}
10^5
10^6
10^7
E [eV]
Fig. 4
14 MeV - Quelle, ZYLFE 3020
Messung (TOF)
Rechnung ANISN, S_{40}^{neu}
Rechnung ESTOQ / DOT / TOPSO / S_{92}, Qu. 1. - 40. Gr.

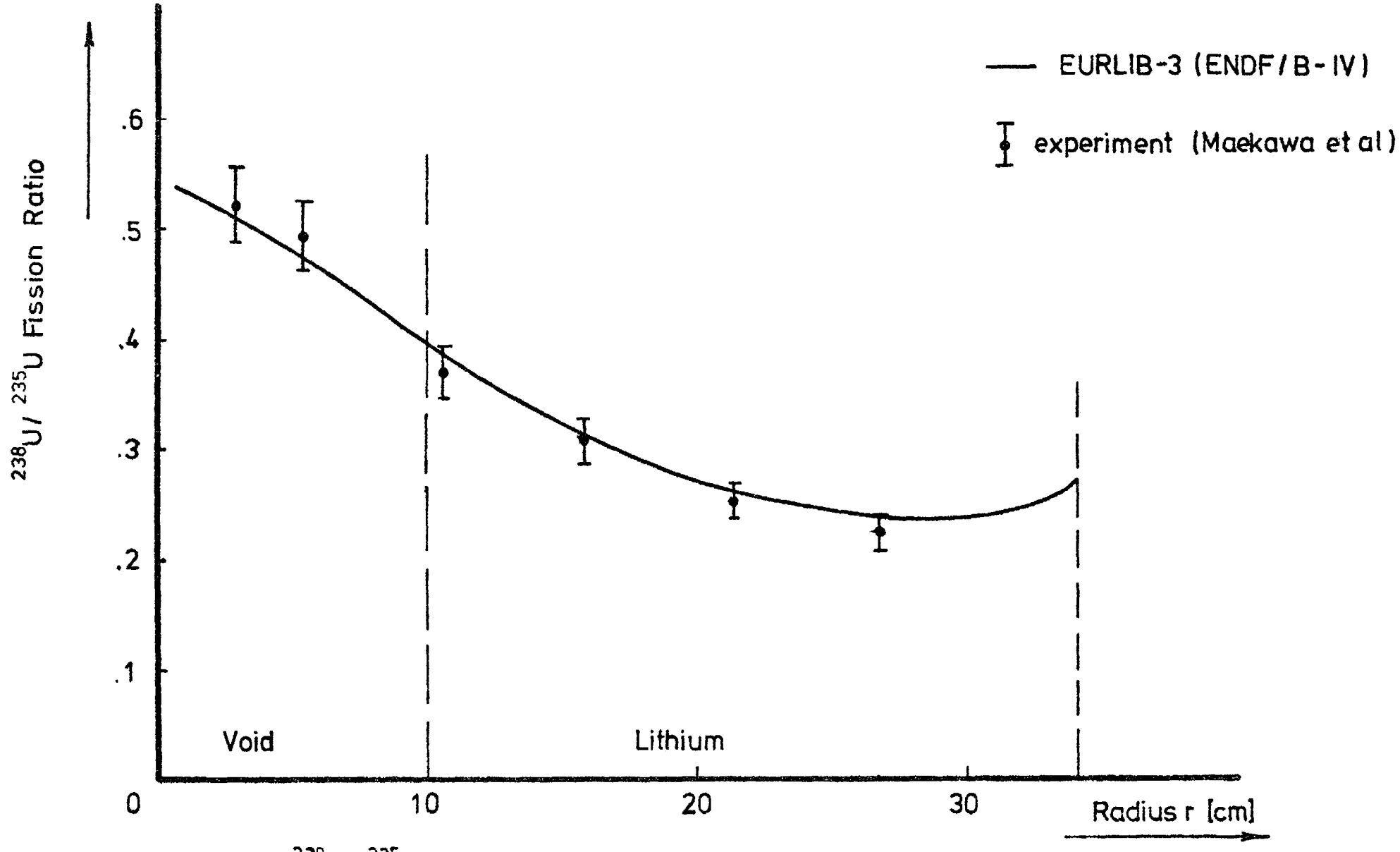

Fig. 5 $^{238}U/^{235}U$ Fission in a CTR-Blanket

Fig 6 $^{238}U/^{235}U$ Fission Ratio in a CTR-Blanket

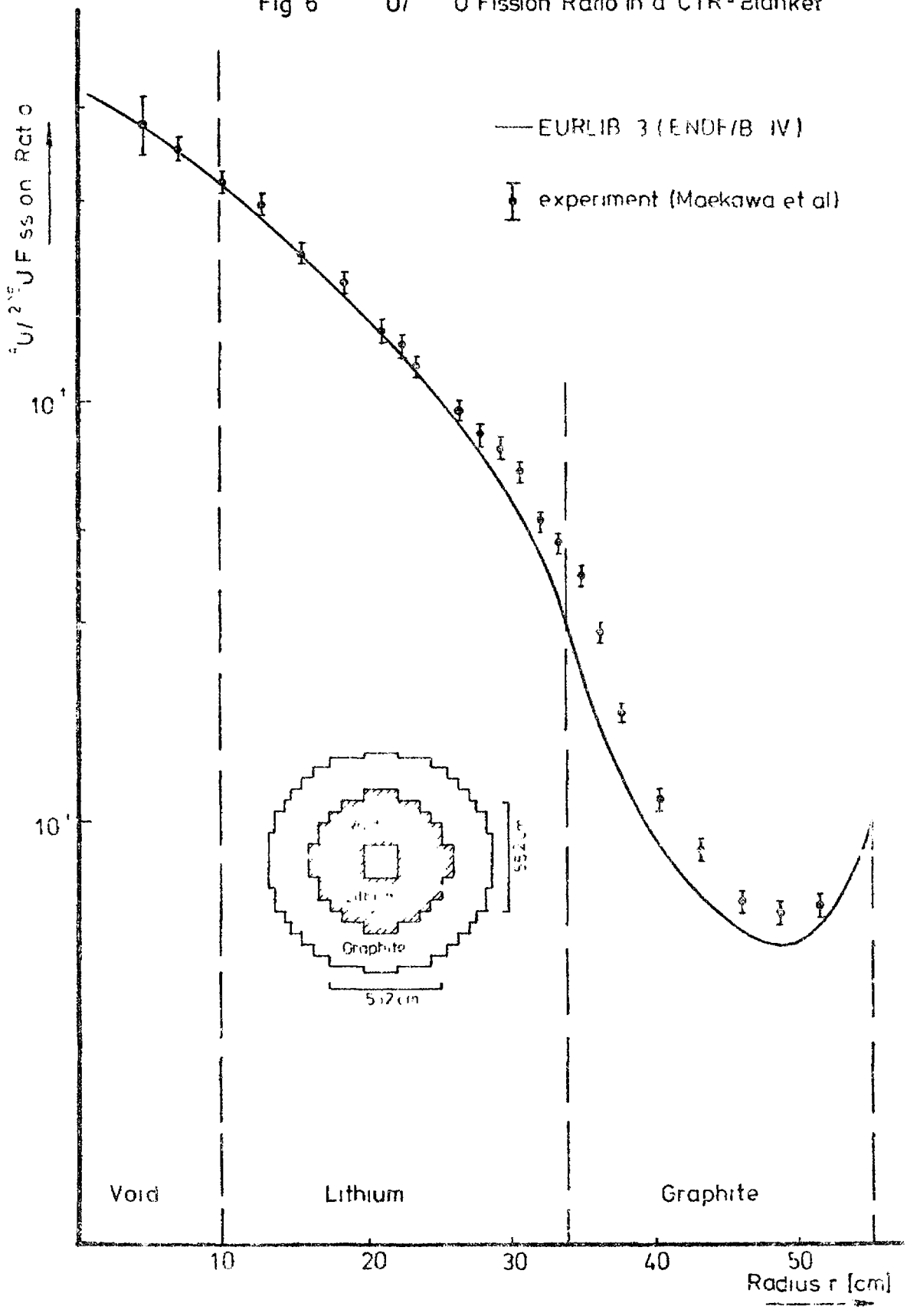

A GRAPHICAL COMPARISON OF CROSS SECTION EVALUATIONS FOR SOME STRUCTURE MATERIALS

by

L. Edvardson
OECD/NEA Neutron Data Compilation Centre (CCDN)
Boîte Postale 9
(Bâtiment 45)
F 91190 GIF SUR YVETTE, FRANCE

Abstract

A comparison of the evaluated total, inelastic and capture cross sections between four widely used libraries has been made. Some discrepancies are pointed out, and in a few cases comparison to experimental data is made.

Introduction

Cross section data for the elements O, Na, Cr, Fe, Ni and Pb from four evaluated libraries have been plotted in pairs to allow a simple comparison. It is hoped that such a comparison can be useful in order to shed some light on the accuracy of the evaluations and reveal the needs for new experimental data.

The following libraries have been considered :

ENDF/B-IV,
ENDL 76,
KEDAK 3, and
UKNDL-1.

No detailed criticism is attempted, partly due to the meagre or non-existing documentation of some of the libraries. This lack of documentation makes it, in general, impossible to identify the experimental data sets which have been used by the evaluators,if model calculations were made a.s.o. .

At present, ENDF/B-IV has by far the best documentation, and, as an example, it is interesting to note the frequent use of model calculations for the nuclei considered in this library.

For the resonance-rich elements Cr, Fe and Ni a numerical integration over five different energy intervals was made in order to facilitate the interpretation of the graphs. (See Table I).

In Table II a list of dates of the evaluations and the evaluations themselves is given. It should be added, that the 1975 revisions of KEDAK are due to B. Goël.

Although it is felt that the plots display the differences between the evaluations quite well, a short summary of the main differences is perhaps of some value :

OXYGEN

Total, good agreement. For KEDAK the minima at about 1 and 2 MeV are shallower than for the evaluations. The contrary is true at the important 5 MeV region. UKNDL differs more, especially for E above 10 MeV.

Inelastic, KEDAK and ENDF/B-IV seem to be identical, UKNDL differs a lot and is much higher (up to 50%) between 8 and 14 MeV. ENDF/B-III is lower for E less than 12 MeV.

SODIUM

Total, the high energy tail of the 3 keV resonance, and the 1-2 MeV region are lower in ENDF/B-IV than in the other evaluations. The UKNDL evaluation differs a lot above 4 MeV. It is an old evaluation and is going to be replaced.

Capture, ENDF/B-IV is much higher than ENDL and KEDAK from 0.1 to 4 keV. UKNDL is very different from 0.1 keV and onwards.

Inelastic, above 5 MeV the agreement is good, below rather good.

For Chromium, Iron and Nickel ; see Table I and figures. There are important discrepancies for the capture cross-section in particular.

LEAD

Total, the agreement is not so good, one notes that the ENDF/B-IV evaluation has more structure than the others.

Capture, UKNDL differs much and has very little structure.

Inelastic, not very good agreement.

Finally, one notes that there is a lack of experimental data for many of these reactions, e.g. inelastic and capture data for Sodium and Lead. For the rest of these elements there are, in general, only a few important data sets available for the capture and inelastic cross-sections, whereas the total cross-section has been measured more frequently.

TABLE I

$1/_E$-WEIGHTED INTEGRALS FOR Cr, Fe AND Ni

Integration intervals :
1. 10^{-2} - 10^{+2} eV
2. 10^{+2} - 10^{+4}
3. 10^{+4} - $2 \cdot 10^{+5}$
4. $2 \cdot 10^{+5}$ - 10^{+6}
5. 10^{+6} - $1.5 \cdot 10^{+7}$

The ENDF/B-IV integrals are normalized to 1.

GROUP	ENDL	KEDAK	UKNDL	EXPERIMENTAL DATA	
			Cr total		
1.	0.96	0.98	0.96		
2.	0.76	0.77	0.75		
3.	0.90	0.98	0.92		
4.	0.88	0.90	0.91	0.91, 0.84	(a)
5.	0.98	0.98	0.99	0.97	(b)
			Cr capture		
1.	1.0	1.0	0.99		
2.	0.60	0.63	0.59		
3.	0.27	0.34	0.26		
4.	0.85	0.92	0.84		
5.	0.59	0.50	0.48		
			Fe total		
1.	0.97	1.0	0.99		
2.	0.98	1.03	0.92		
3.	0.95	1.0	0.94		
4.	1.03	0.91	0.93	0.89	(a)
5.	1.0	0.98	1.0	0.99	(b)

Experimental data for the following laboratories :

(a) ORL
(b) KFK
(c) RPI

TABLE I (Cont/d)

$1/_E$-WEIGHTED INTEGRALS FOR Cr, Fe AND Ni

GROUP	ENDL	KEDAK	UKNDL	EXPERIMENTAL DATA	
		Fe capture			
1.	0.98	1.0	1.0		
2.	0.71	0.85	0.81		
3.	2.23	2.00	0.94	1.17	(c)
4.	0.98	1.0	0.91		
5.	1.03	1.12	0.99		
		Ni total			
1.	0.97	0.96	0.97		
2.	0.99	0.94	0.88		
3.	1.12	0.98	0.92		
4.	0.99	0.96	1.06		
5.	1.02	1.0	1.04	1.02	(b)
		Ni capture			
1.	1.02	0.97	0.94		
2.	1.28	0.92	0.81		
3.	1.73	0.94	0.86		
4.	1.24	0.98	1.01	1.32	(c)
5.	1.20	0.90	1.83		

TABLE II

ENDF/B-IV	ENDL 76	KEDAK 3	UKNDL-1 (1973)
	^{16}O		
MAT 1276 Aug.'73 Young, Foster, Hale (LAS) capt : Jurney, Mott 1964	MAT 7114 Jan. '74	J.J. Schmidt 1966 Revised 1975	DFN 933A E<15 keV : Butland, Pope, Story (WIN) 1967, 1971 E>15 keV : ENDF/B-II (MAT 1013) (1965)
	^{23}Na		
MAT 1156 Paik, Pitterle (WARD) 1971 Capt : Pitterle 1968, revised 1971 for 0.1<E<200 keV	MAT 7116 capt : Dec.'71 inel : Aug.'72	J.J. Schmidt 1966 Capt. re-eval. E>1 MeV 1970 res. data re-eval. 1971 scatt. data revised E>4 MeV capt. revised 0.06<E<1 MeV 1975	DFN 182E Moorhead (WIN) 1963 (To be replaced by ENDF/B-transl.)
	Cr		
MAT 1191 Prince (BNL) 1974	MAT 7130 inel : Sept.'73 capt : Apr.'73	J.J. Schmidt 1966 capt. improved E>1 MeV 1970 capt. revised E>0.1 Mev inel. revised E>4 MeV 1975	DFN 45E Ravier, Vastel (CAD) 1965 (re-eval. in progress)

TABLE II (Cont/d)

ENDF/B-IV	ENDL 76	KEDAK 3	UKNDL-1 (1973)
		Fe	
MAT 1192 Fu, Perey (ORL) Tot. revised 0.06<E<2 MeV else ≡ ENDF/B-III. ENDF/B-III : res. par. 1-60 keV : Hockenbury 1969 Story (WIN)1970 Capt : Hockenbury 1969 Story 1970	MAT 7132 inel : Feb.'72 capt : Aug.'72	J.J. Schmidt 1966 capt. re-eval E>1 MeV 1970 gen. revision 1975	DFN 908B E<330 keV Pope, Story 1971 Cameron, Dean (ALD) 1972 E>330 keV ≡ ENDF/B-III
		Ni	
MAT 1190 Bhat (BNL) For E<690 keV ≡ ENDF/B-III (MAT 1123) ENDF/B-III : Azziz, Cornyn (WNES) 1969, minor changes 1971	MAT 7136 May 1975	J.J. Schmidt 1966 capt. re-eval. E>1 MeV 1970 capt. re-eval. E>0.2 MeV inel. re-eval. E>4 MeV 1975	DFN 907A E<240 keV Moxon (HAR) 1970 Cameron, Dean 1972 E>240 keV ≡ ENDF/B-II (MAT 1123)
		Pb	
MAT 1288 Fu, Perey (ORL) 1 keV-1 MeV re-eval., else ≡ ENDF/B-III (ENDF/B-III, MAT 1136 Fu, Perey 1971)	MAT 7162 inel : Mar;'73 capt : Dec.'71		DFN 26C Buckingham, Pendlebury (WIN) 1960 Barrington (ALD) 1964

FIGURE CAPTIONS

The continuous line always indicates the ENDF/B-IV evaluation

Figure	1	O total, points	:	KEDAK	0.1 - 15 MeV
	2	" " "	:	UKNDL	- " -
	3	" inel. "	:	UKNDL	
	4	" " "	:	ENDF/B-III	
	5	" " "	:	KEDAK	
	6	Na total "	:	ENDL	10 eV - 0.1 MeV
	7	" " "	:	KEDAK	- " -
	8	" " "	:	ENDL	0.1 - 15 MeV
	9	" " "	:	KEDAK	- " -
	10	" " "	:	UKNDL	- " -
	11	" capture, points	:	UKNDL	therm. - 15 MeV
	12	" " "	:	Exp. data	1 keV - 15 MeV
	13	" inel., points	:	ENDL	
	14	" " "	:	KEDAK	
	15	Cr total, "	:	ENDL	10 eV - 0.1 MeV
	16	" " "	:	KEDAK	- " -
	17	" " "	:	UKNDL	0.1 keV - 0.1 MeV
	18	" " "	:	Exp. data	10 eV - 0.1 MeV
	19	" " "	:	ENDL	0.1 - 1 MeV
	20	" " "	:	KEDAK	- " -
	21	" " "	:	UKNDL	- " -
	22	" " "	:	ENDL	1 - 15 MeV
	23	" " "	:	KEDAK	- " -
	24	" " "	:	UKNDL	- " -
	25	" capture "	:	ENDL	10 eV - 0.1 MeV
	26	" " "	:	KEDAK	- " -

./..

Figure	27	" " "	:	UKNDL	- " -
	28	" " "	:	Exp. data	- " -
	29	" inel. "	:	ENDL	
	30	" " "	:	KEDAK	
	31	" " "	:	ENDF/B-III	
	32	Fe total, "	:	ENDL	0.1 keV - 0.1 MeV
	33	" " "	:	KEDAK	- " -
	34	" " "	:	UKNDL	- " -
	35	" " "	:	Exp. data	- " -
	36	" " "	:	ENDL	0.1 - 1 MeV
	37	" " "	:	KEDAK	- " -
	38	" " "	:	ENDL	1 - 15 MeV
	39	" " "	:	KEDAK	- " -
	40	" " "	:	UKNDL	- " -
	41	" capture, "	:	ENDL	0.1 keV - 0.1 MeV
	42	" " "	:	KEDAK	- " -
	43	" " "	:	UKNDL	- " -
	44	" " "	:	Exp. data	- " -
	45	" inel., "	:	ENDL	
	46	" " "	:	KEDAK	
	47	" " "	:	ENDF/BIII	
	48	Ni total "	:	ENDL	10 eV - 0.1 MeV
	49	" " "	:	KEDAK	- " -
	50	" " "	:	UKNDL	1 keV - 0.1 MeV
	51	" " "	:	ENDL	0.1 - 1 MeV
	52	" " "	:	KEDAK	- " -
	53	" " "	:	UKNDL	- " -
	54	" " "	:	ENDL	1 - 15 MeV
	55	" " "	:	KEDAK	- -
	56	" " "	:	UKNDL	- " -

Figure	57	" capture "	:	KEDAK	10 eV - 0.1 MeV
	58	" " "	:	UKNDL	0.1 keV - 0.1 MeV
	59	" inel. "	:	ENDL	
	60	" " "	:	KEDAK	
	61	" " "	:	ENDF/B-III	
	62	Pb total "	:	ENDL	0.1 keV - 0.1 MeV
	63	" " "	:	"	0.1 - 15 MeV
	64	" " "	:	UKNDL	- " -
	65	" inel. "	:	ENDL	
	66	" " "	:	ENDF/B-III	
	67	" capture "	:	UKNDL	1 eV - 0.1 MeV

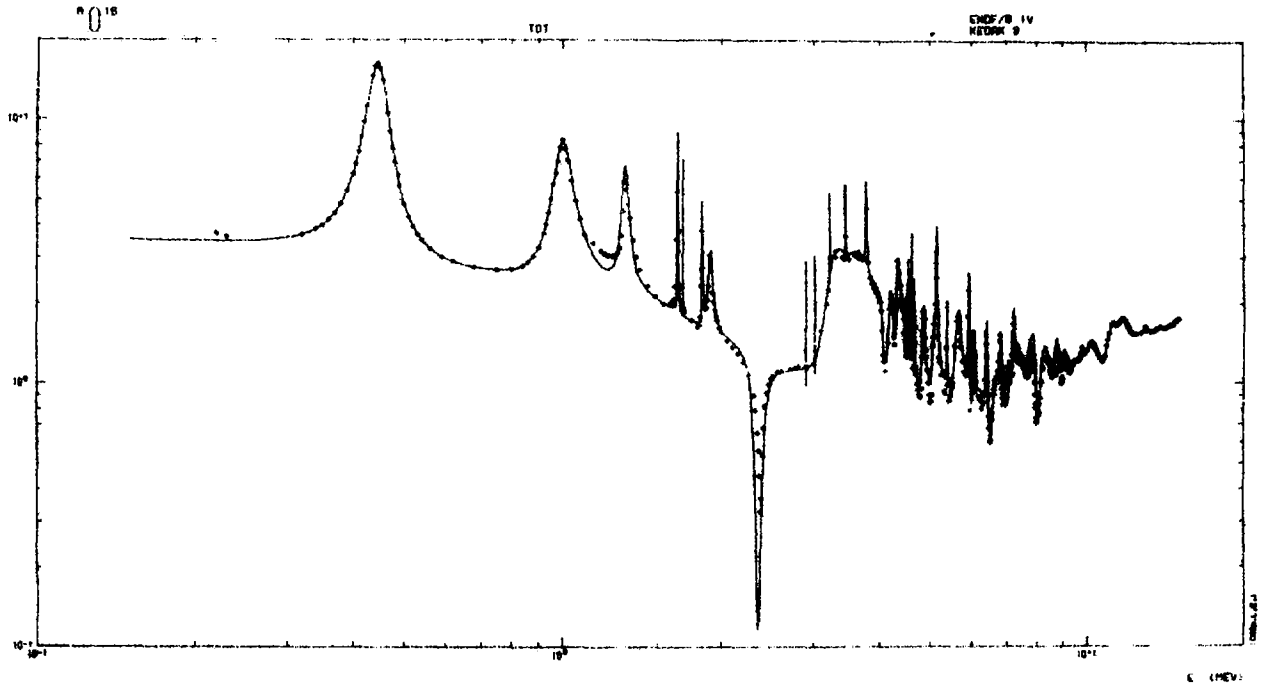

Figure 1.

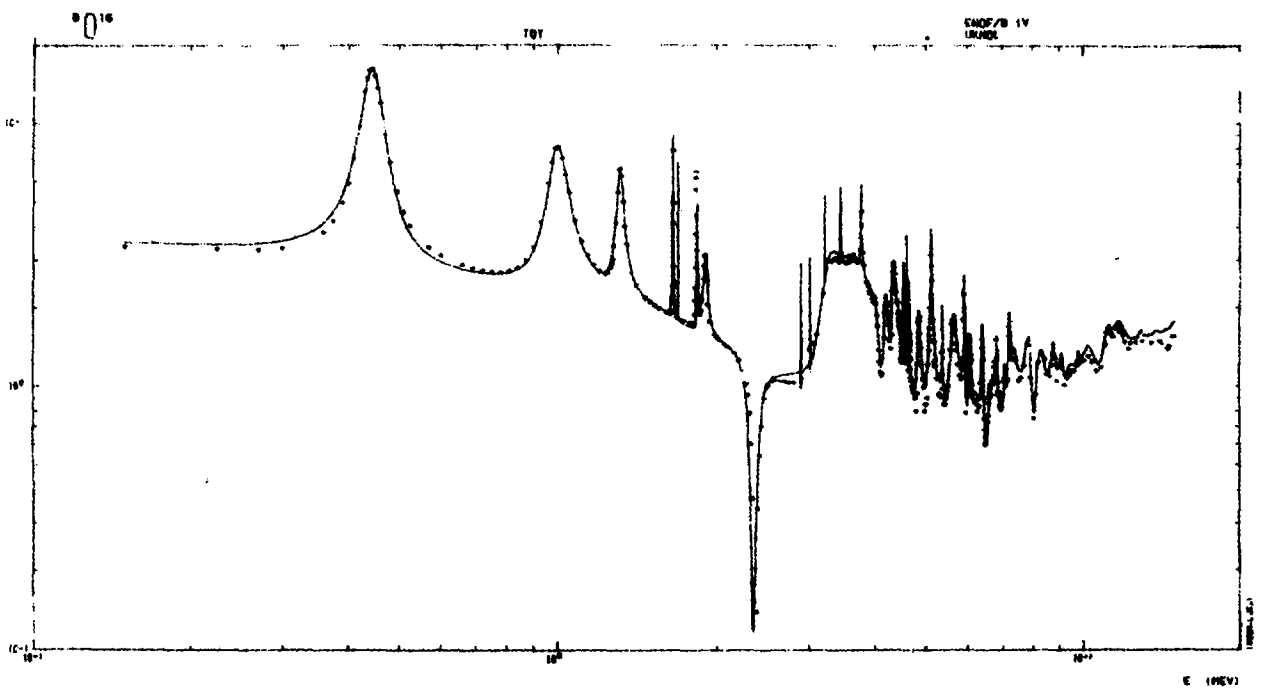

Figure 2.

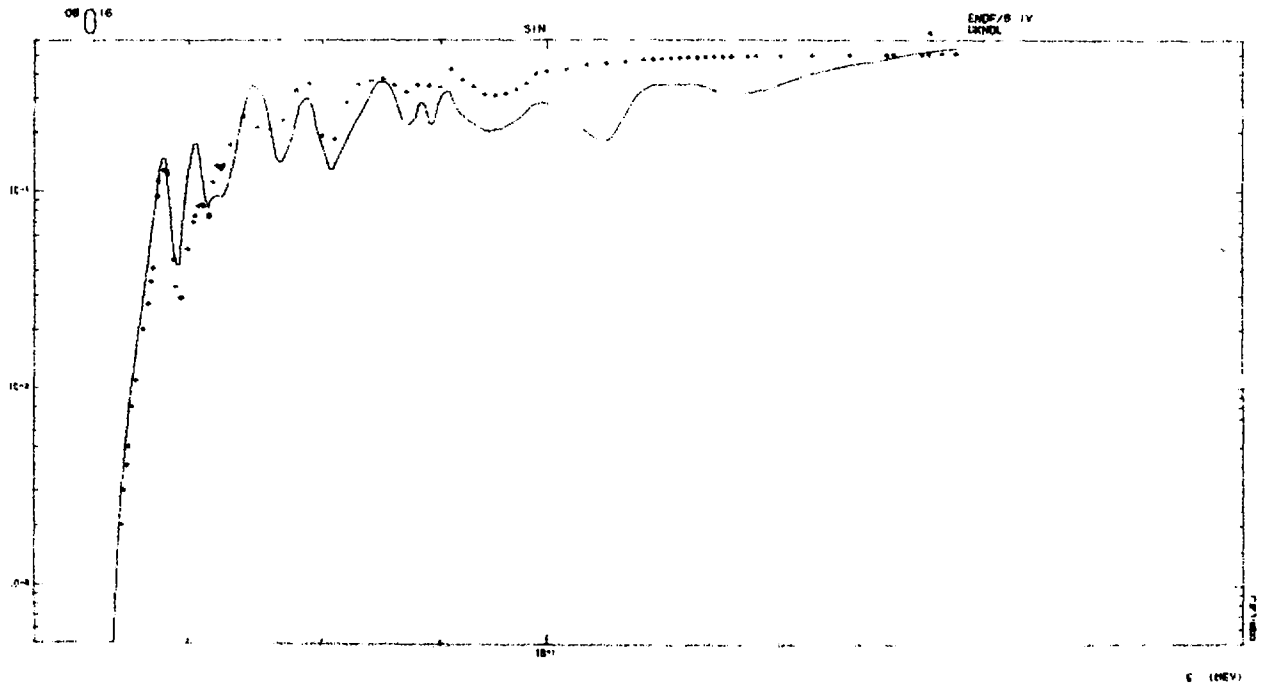

Figure 3.

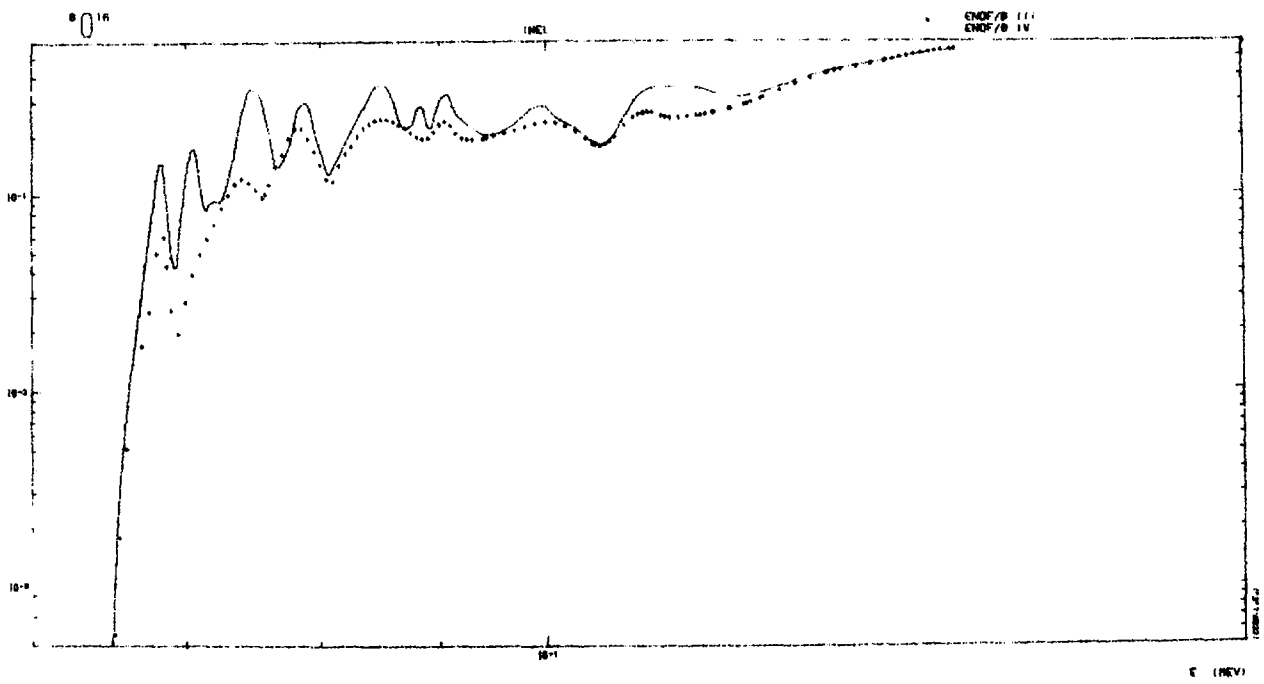

Figure 4.

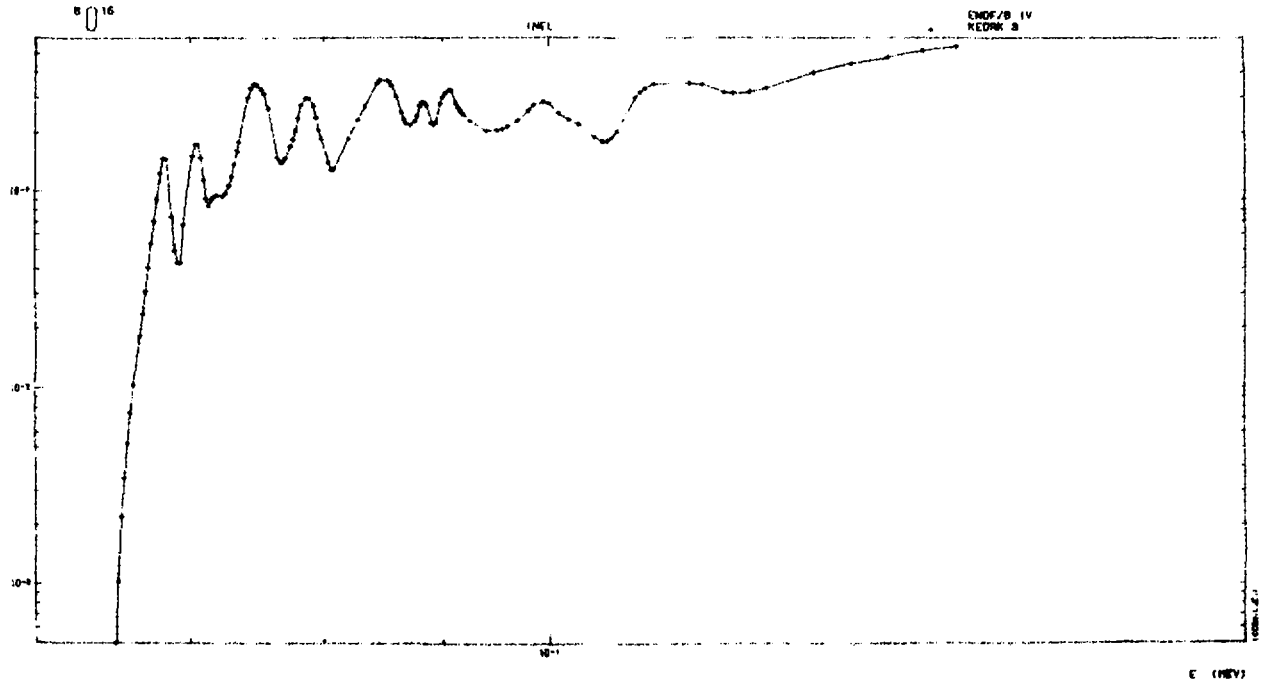

Figure 5.

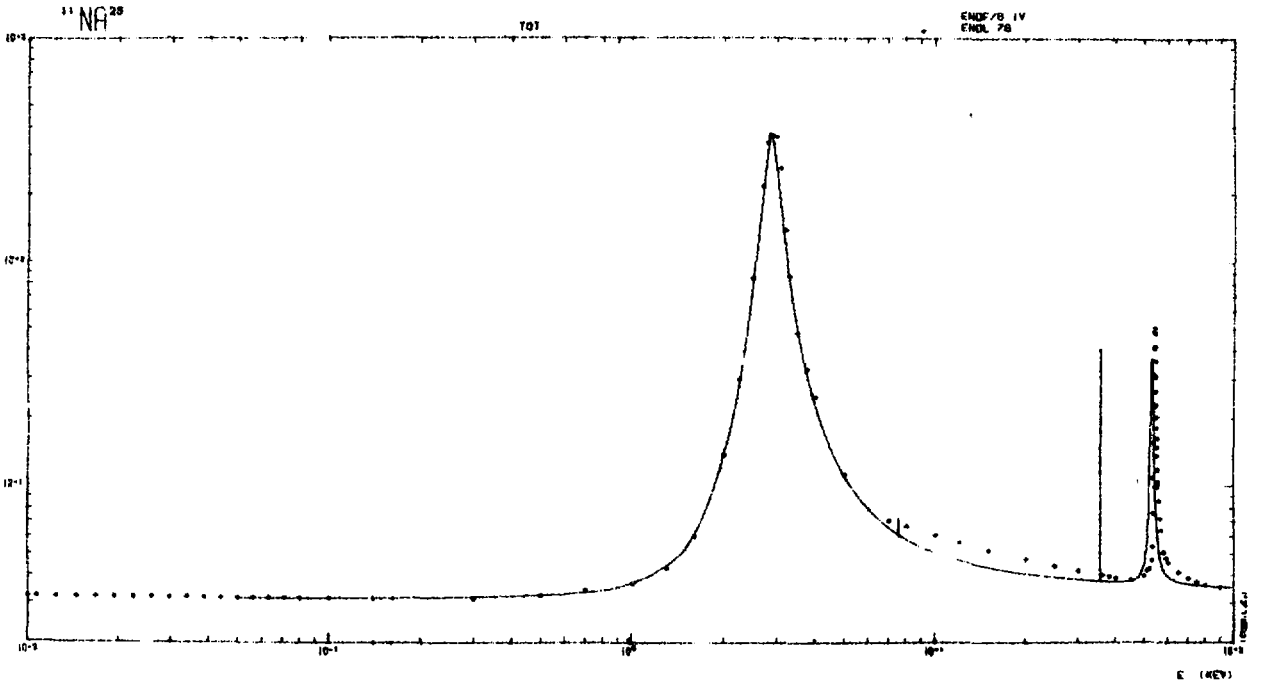

Figure 6.

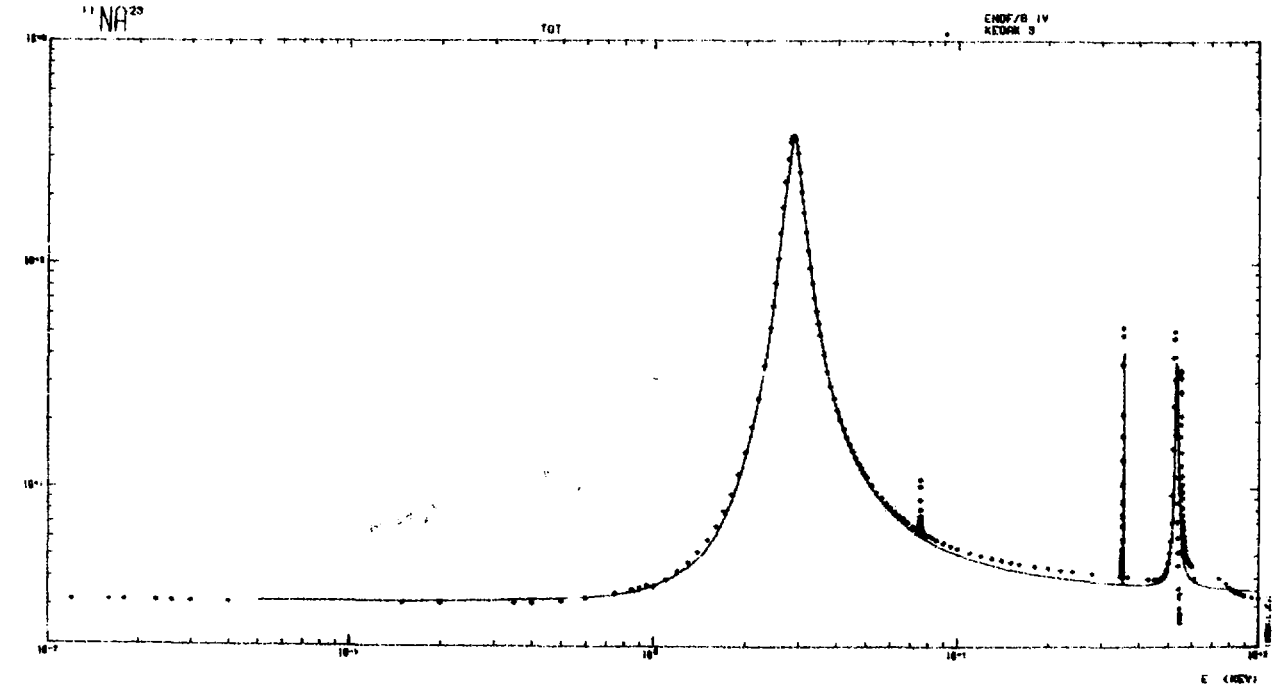

Figure 7.

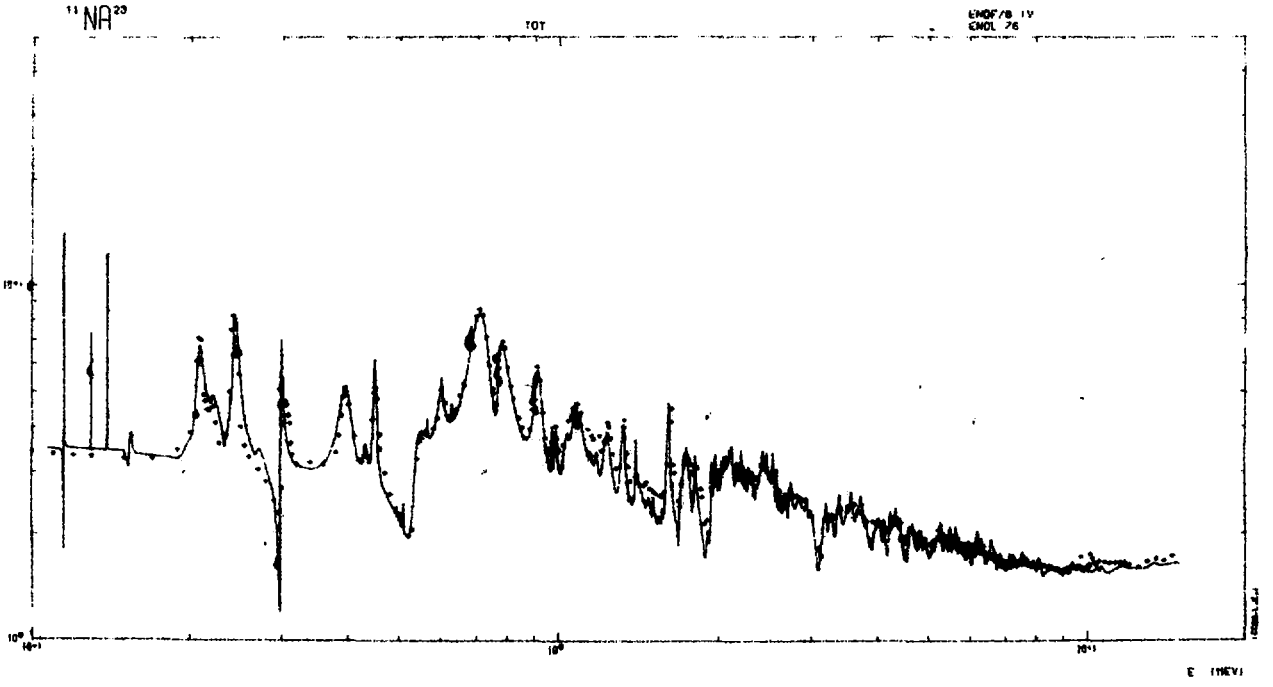

Figure 8.

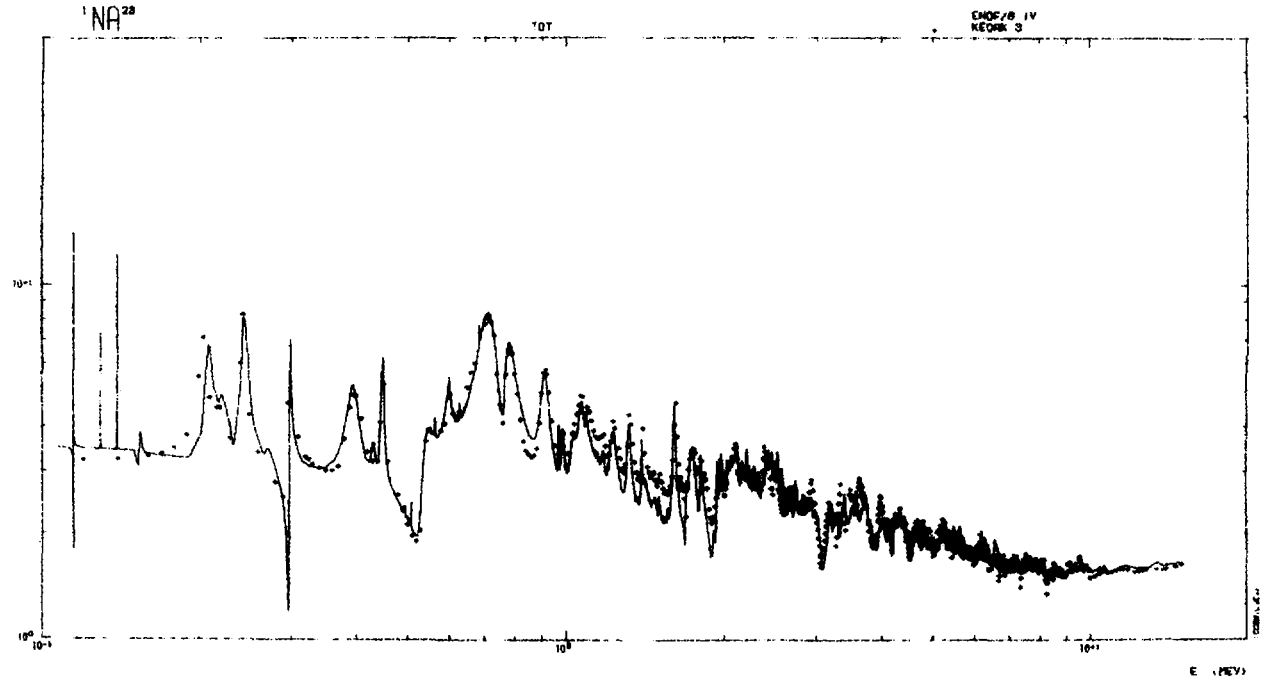

Figure 9.

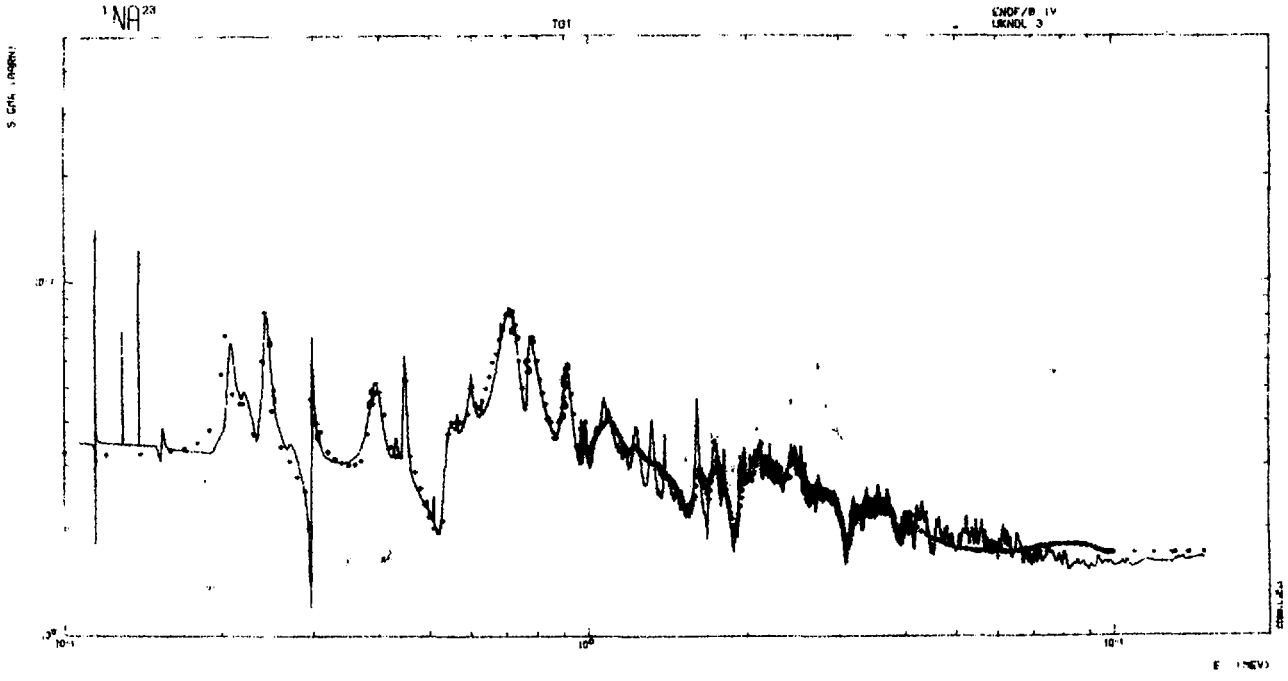

Figure 10.

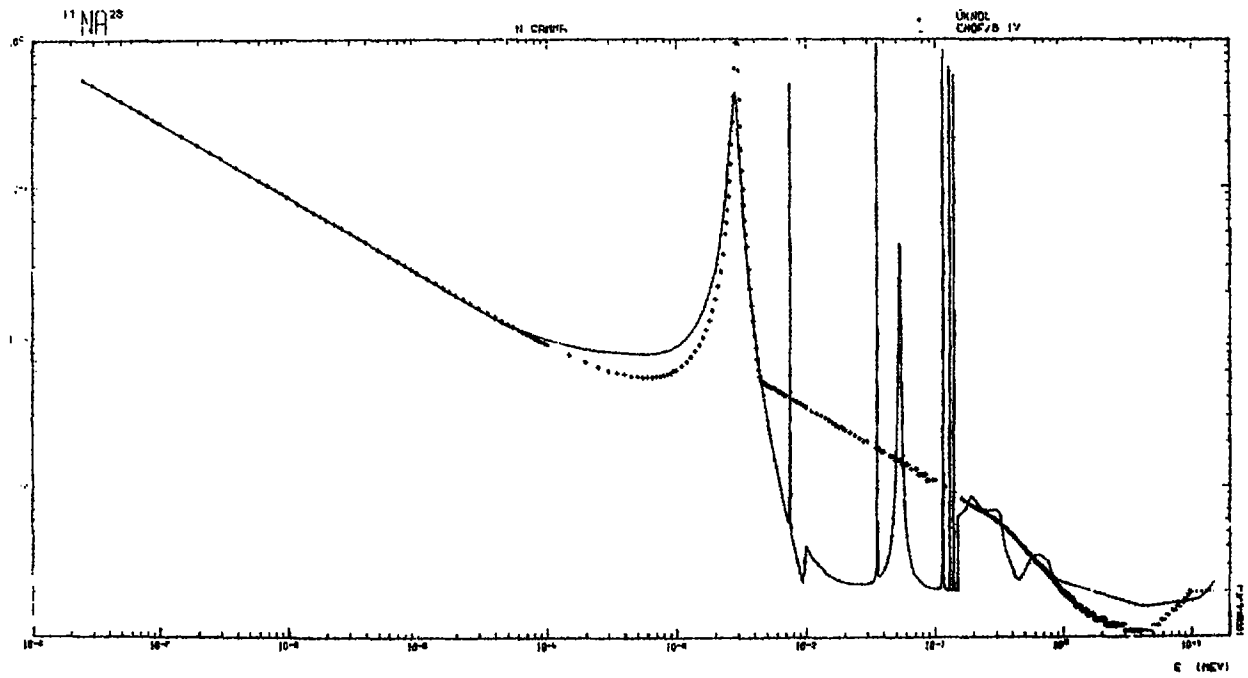

Figure 11.

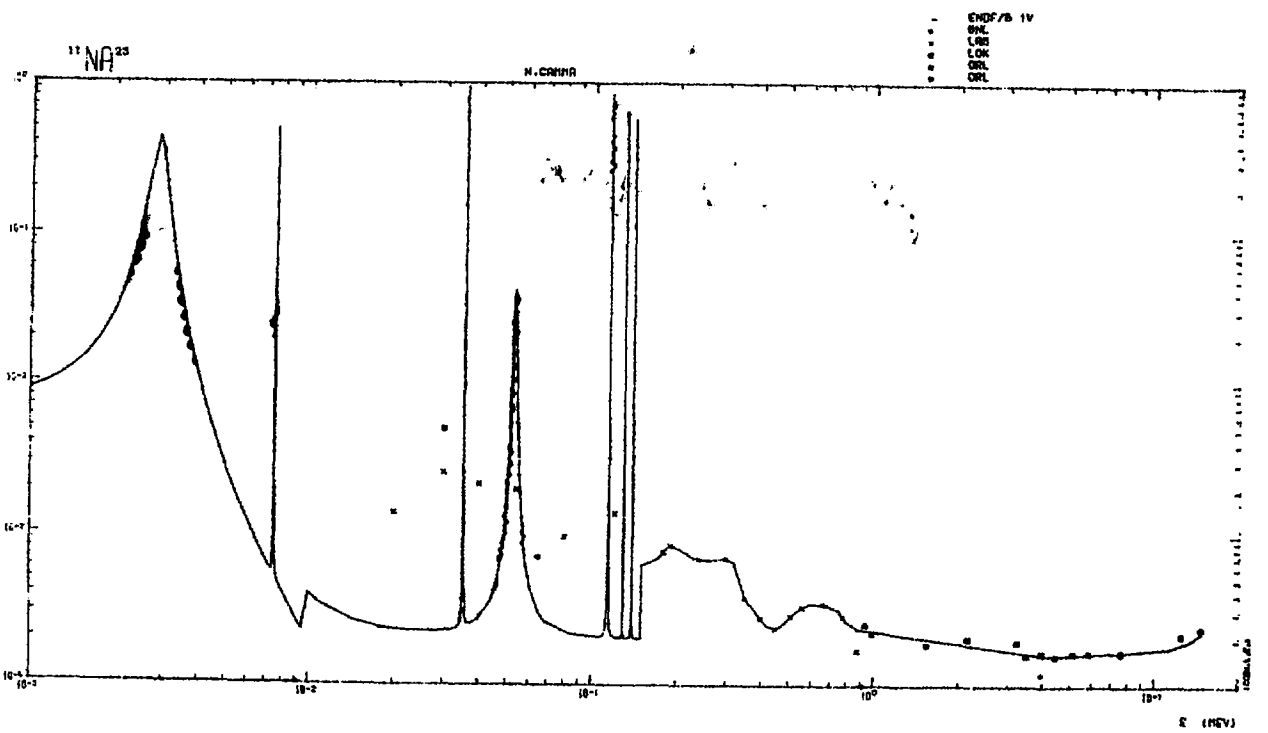

Figure 12.

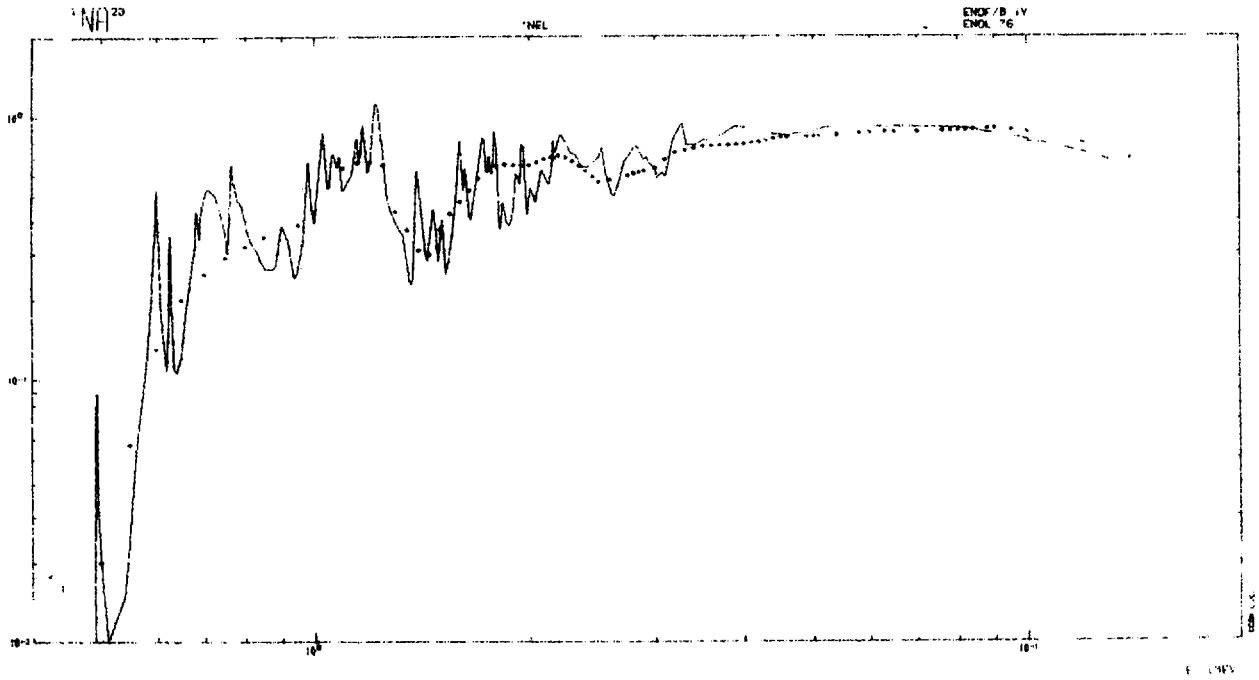

Figure 13.

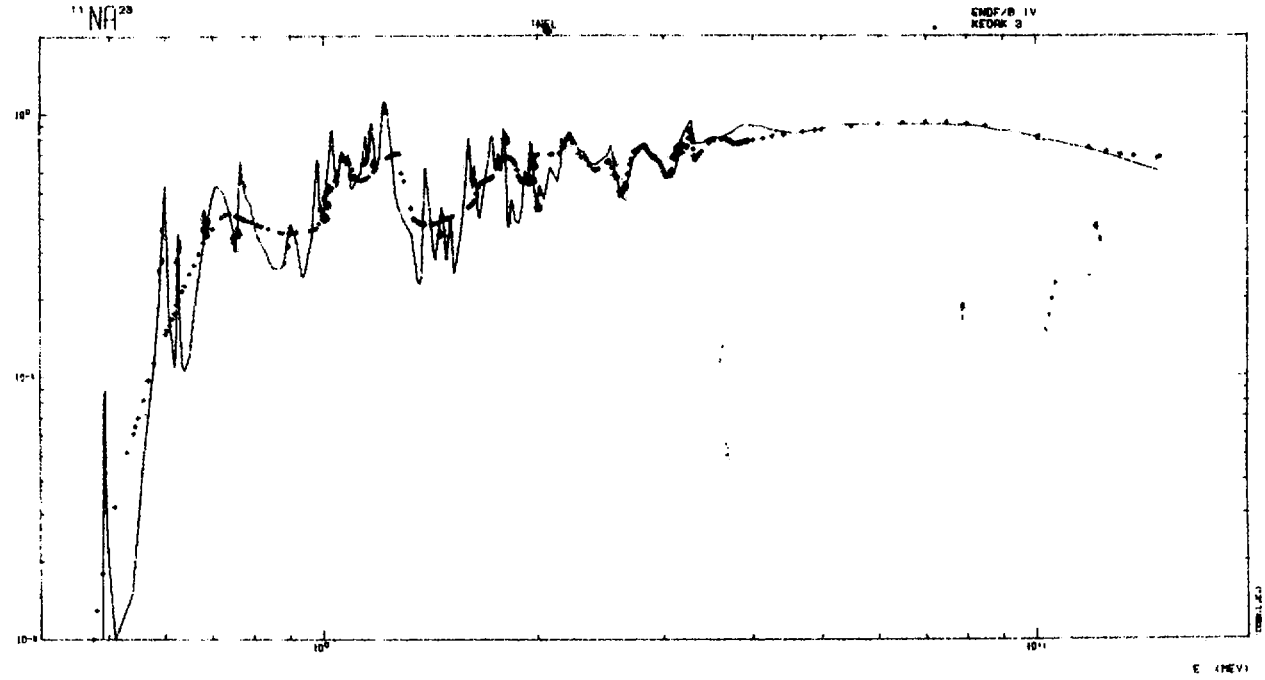

Figure 14.

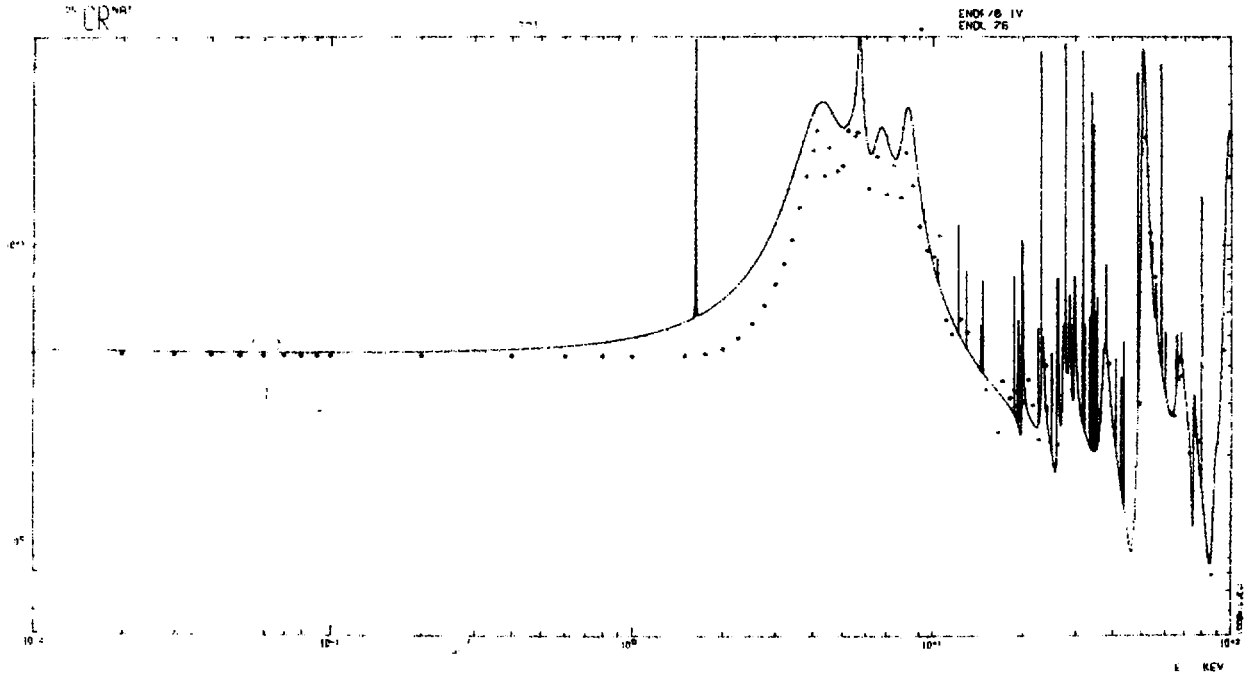

Figure 15.

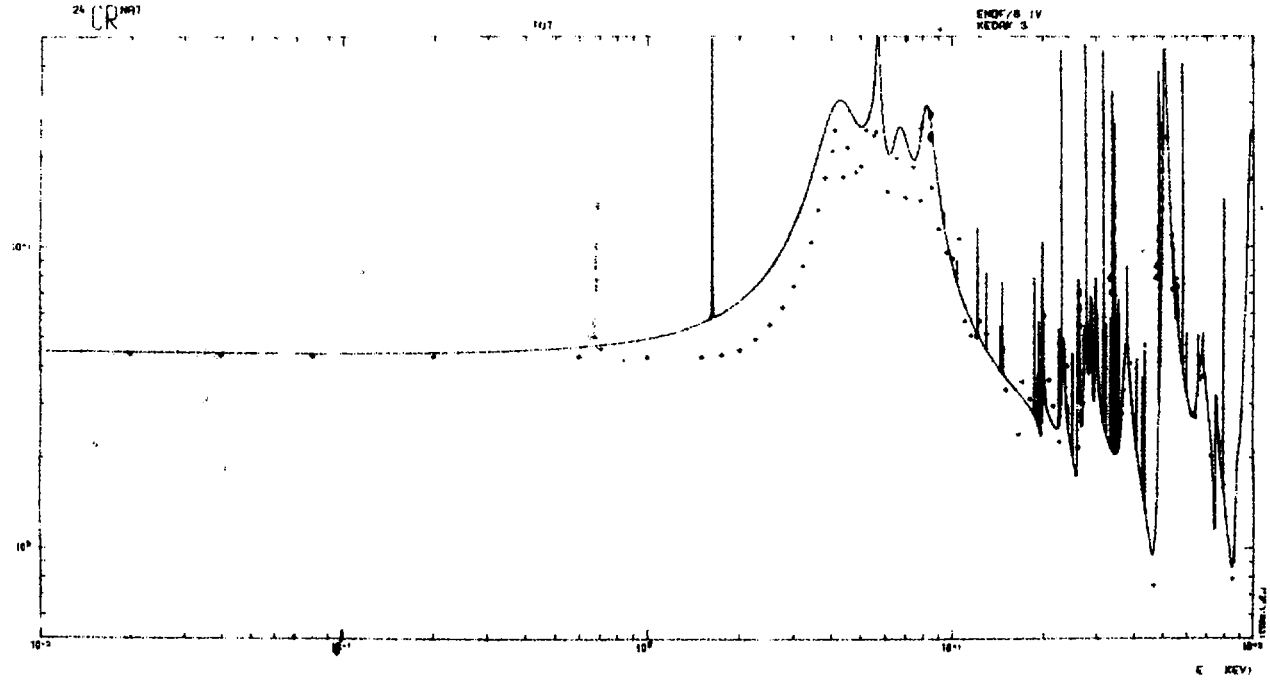

Figure 16.

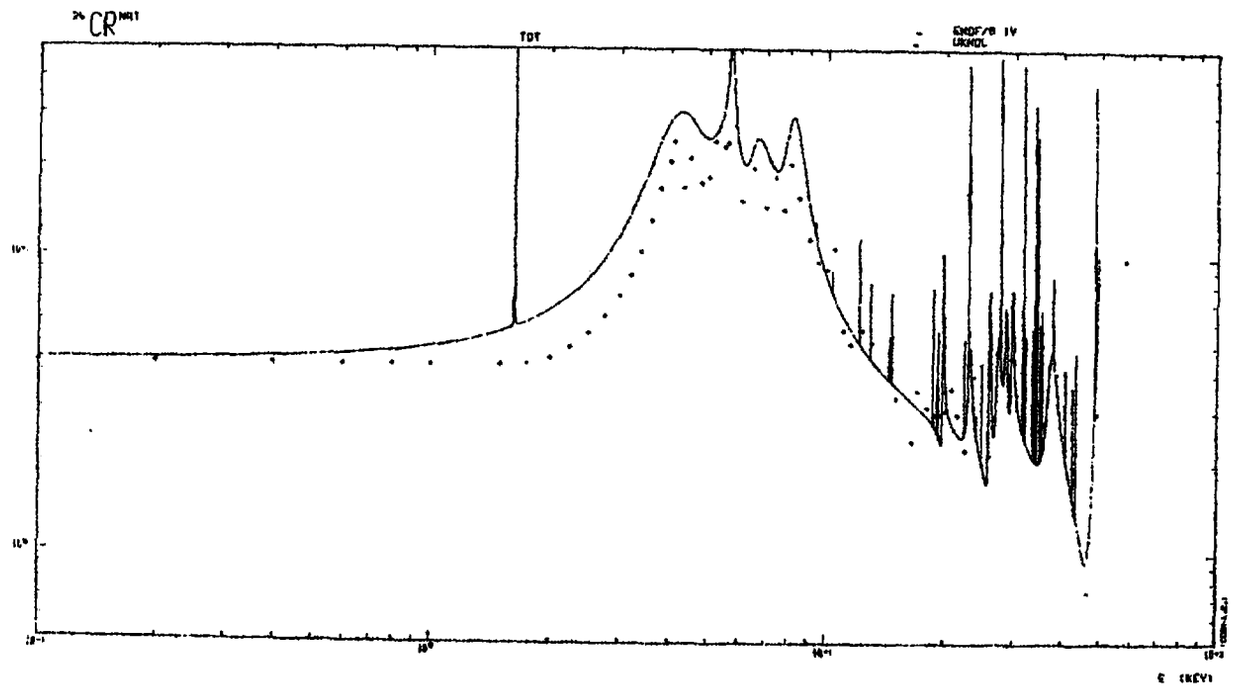

Figure 17.

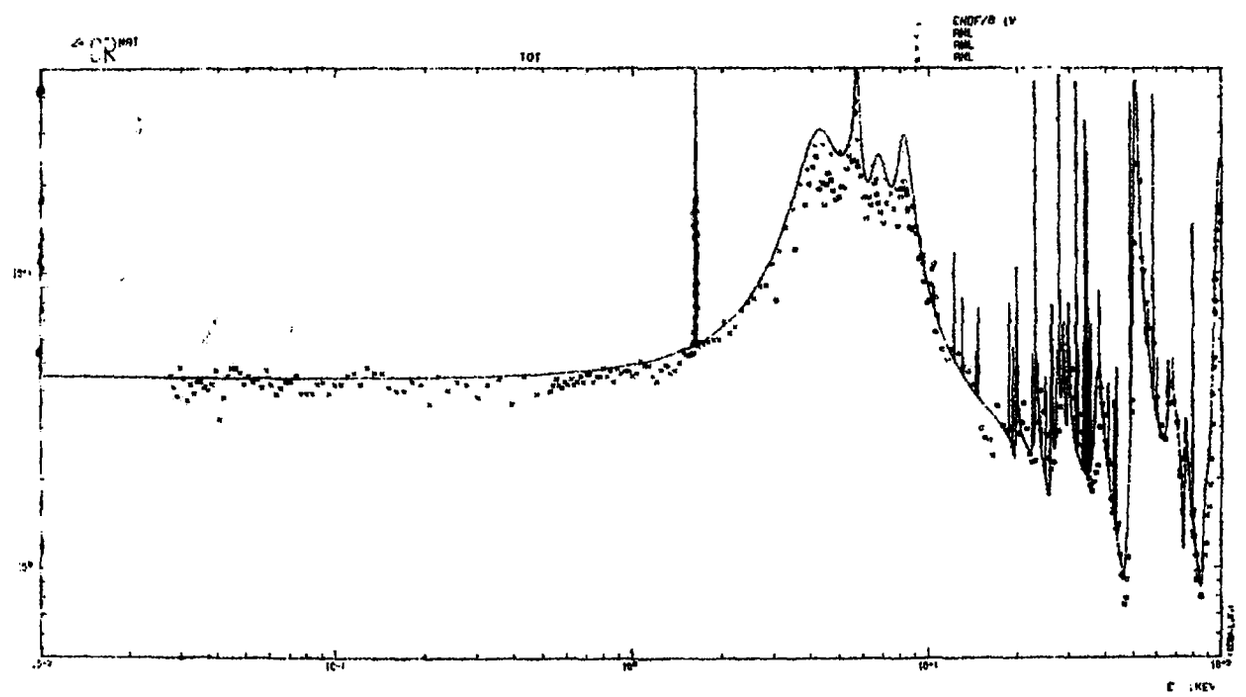

Figure 18.

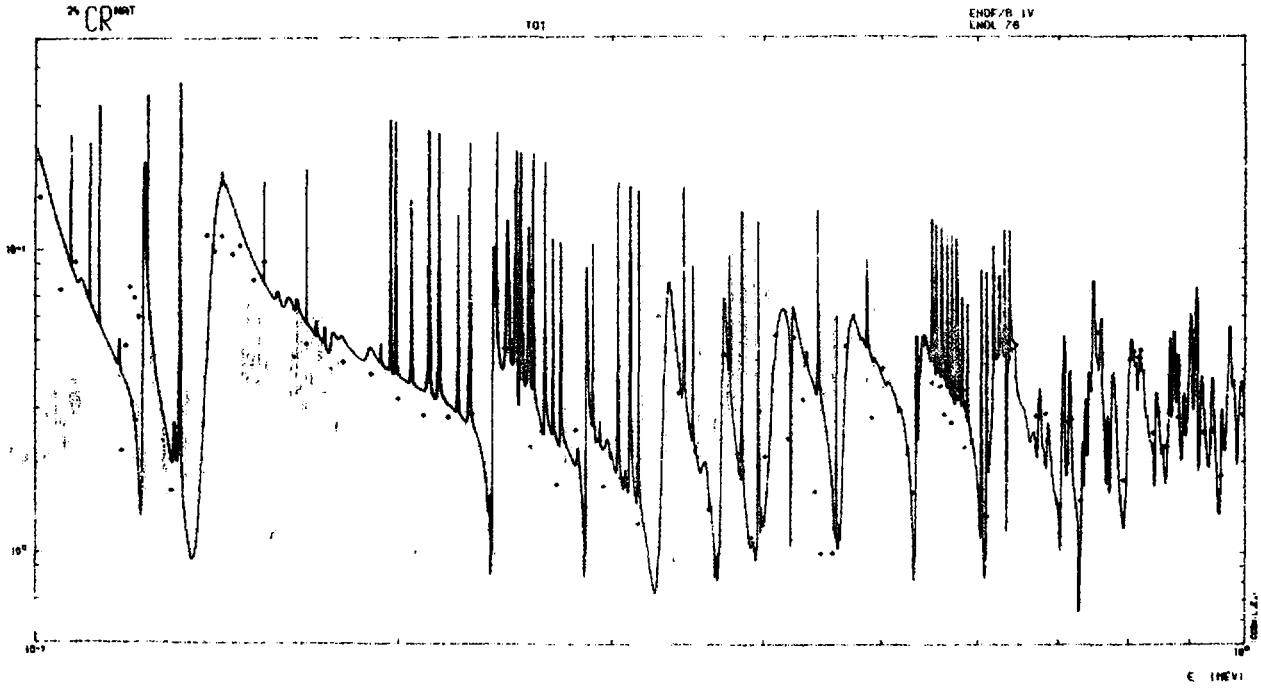

Figure 19.

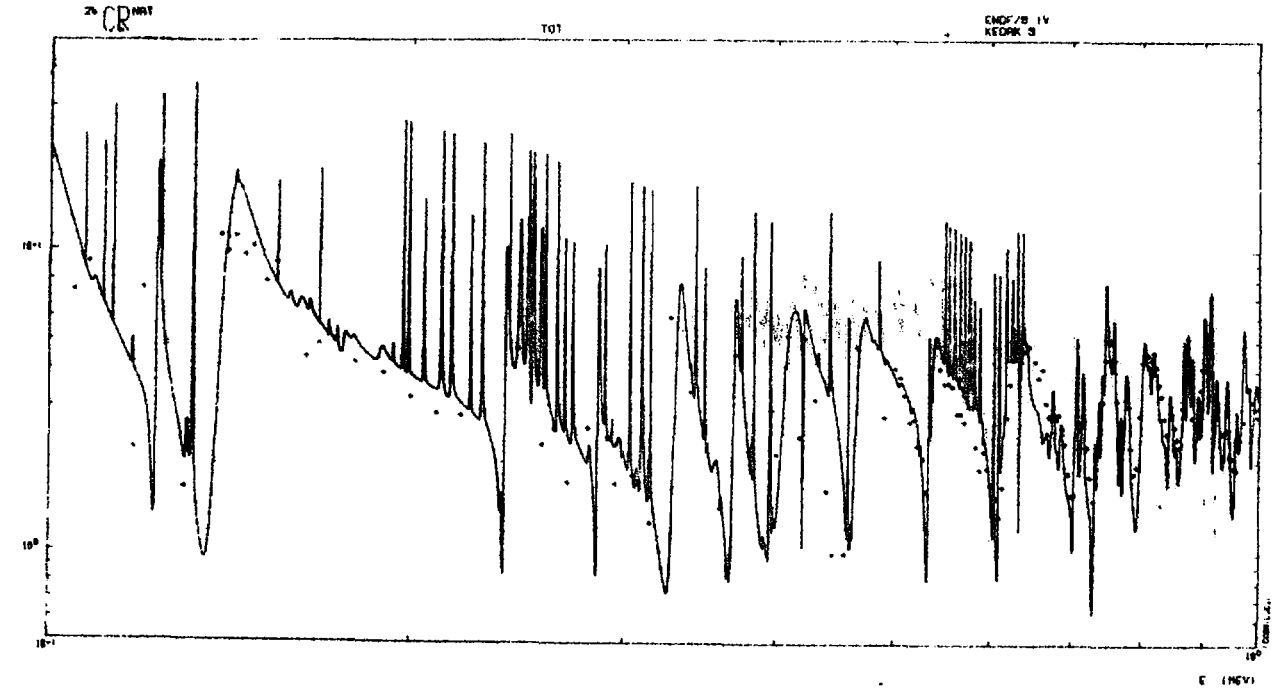

Figure 20.

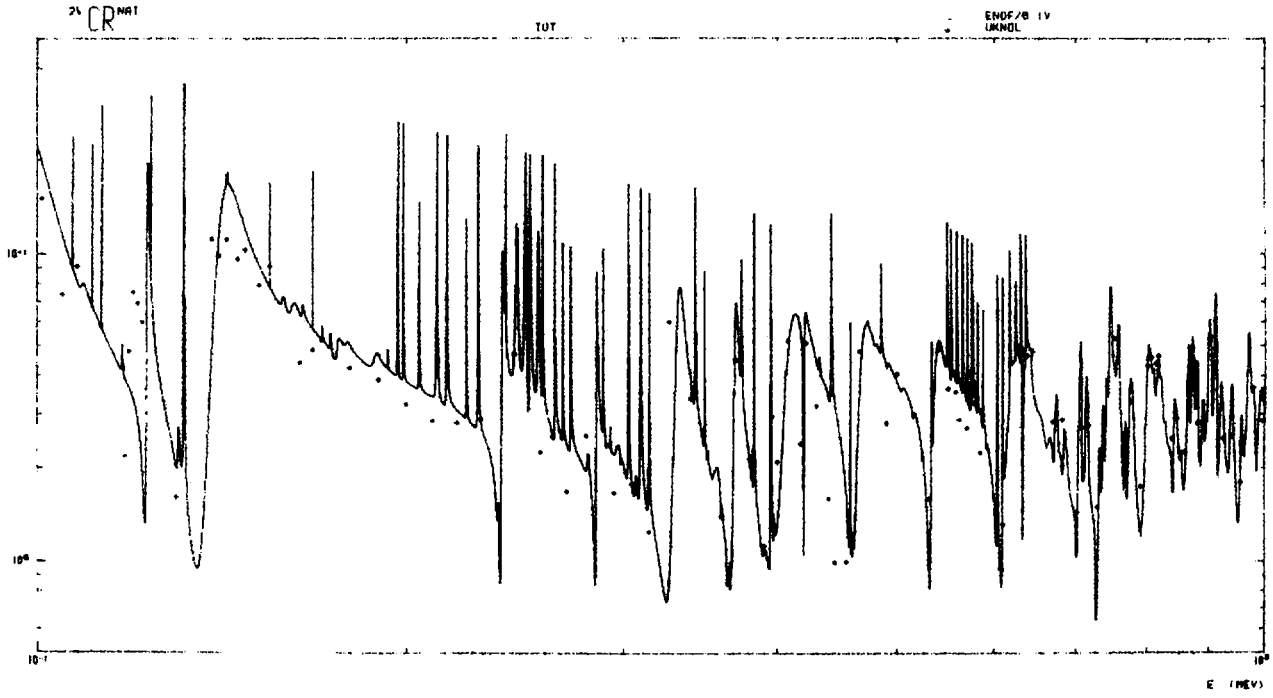

Figure 21.

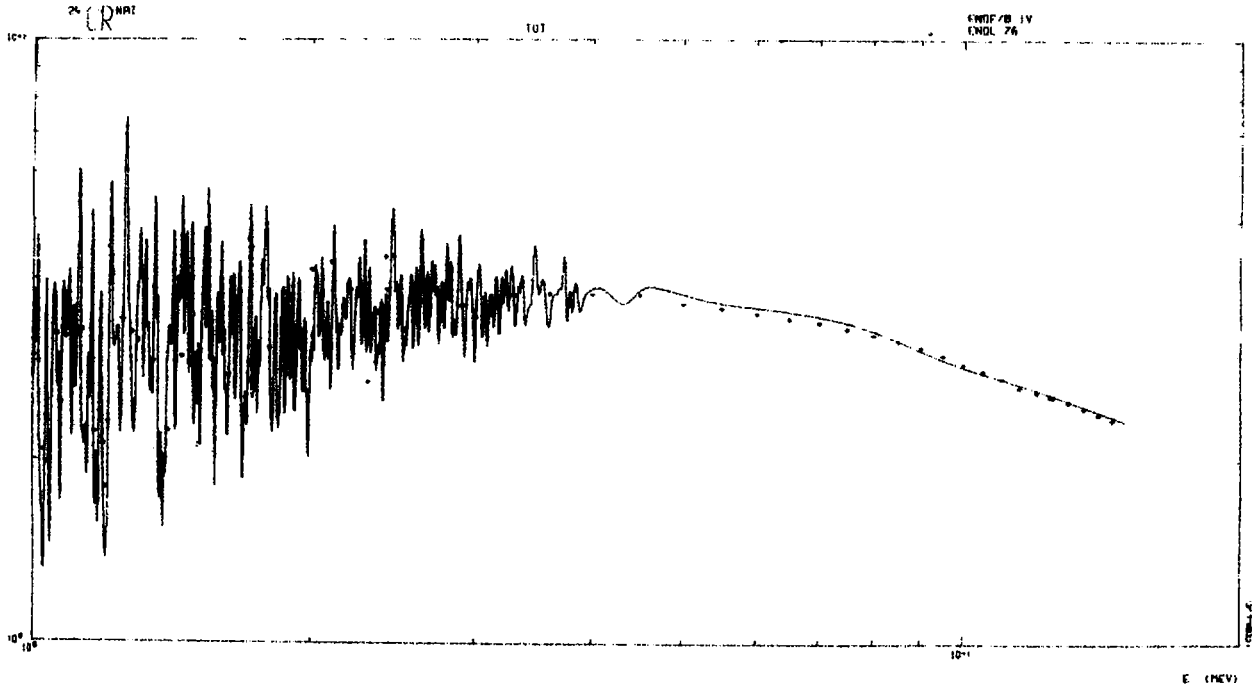

Figure 22.

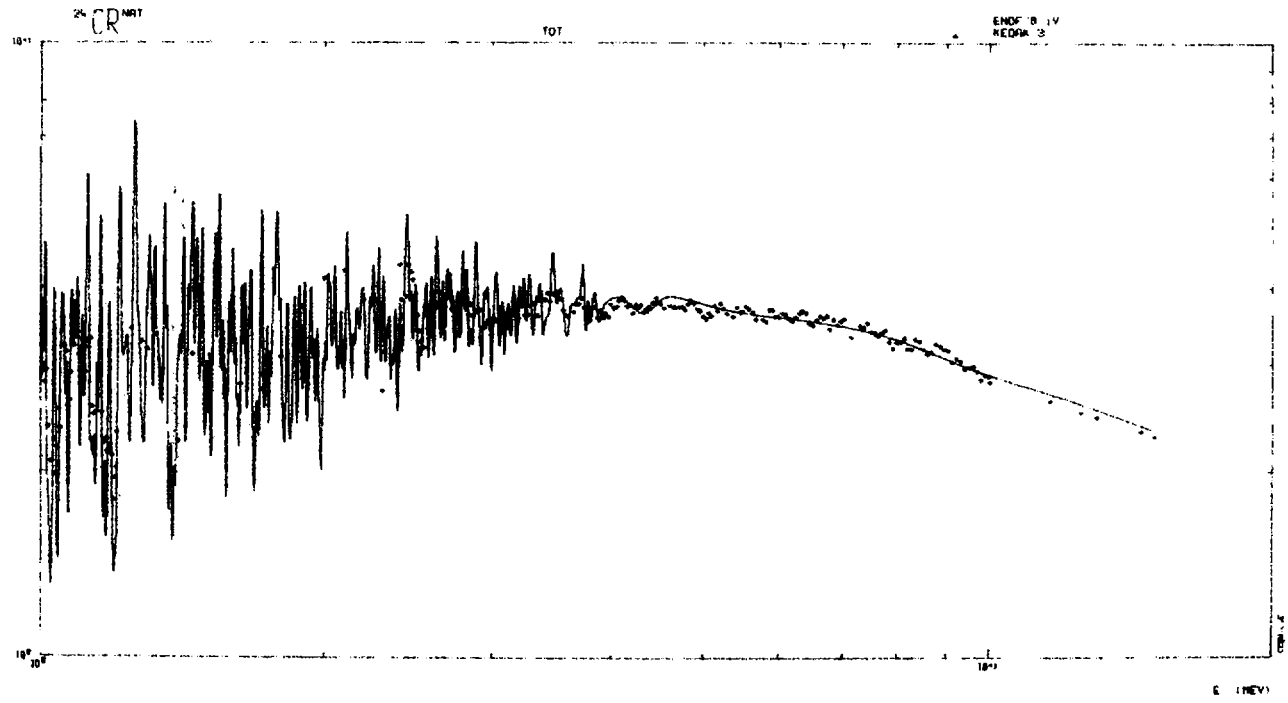

Figure 23.

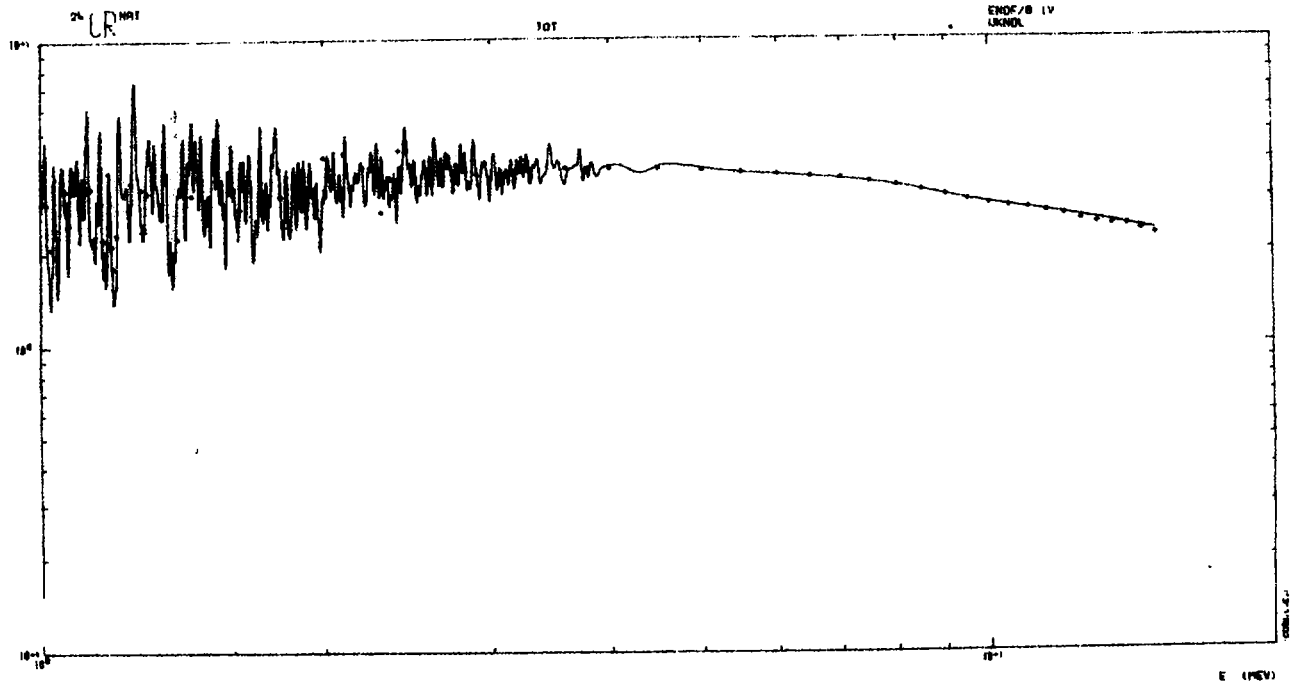

Figure 24.

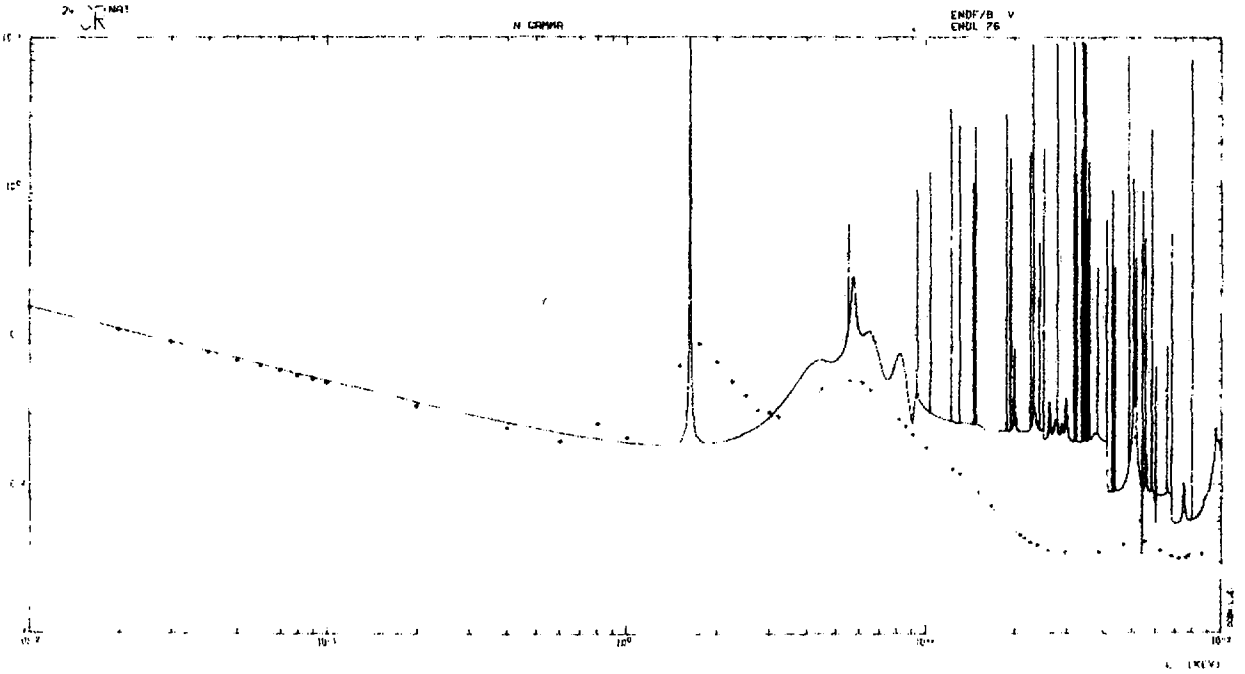

Figure 25.

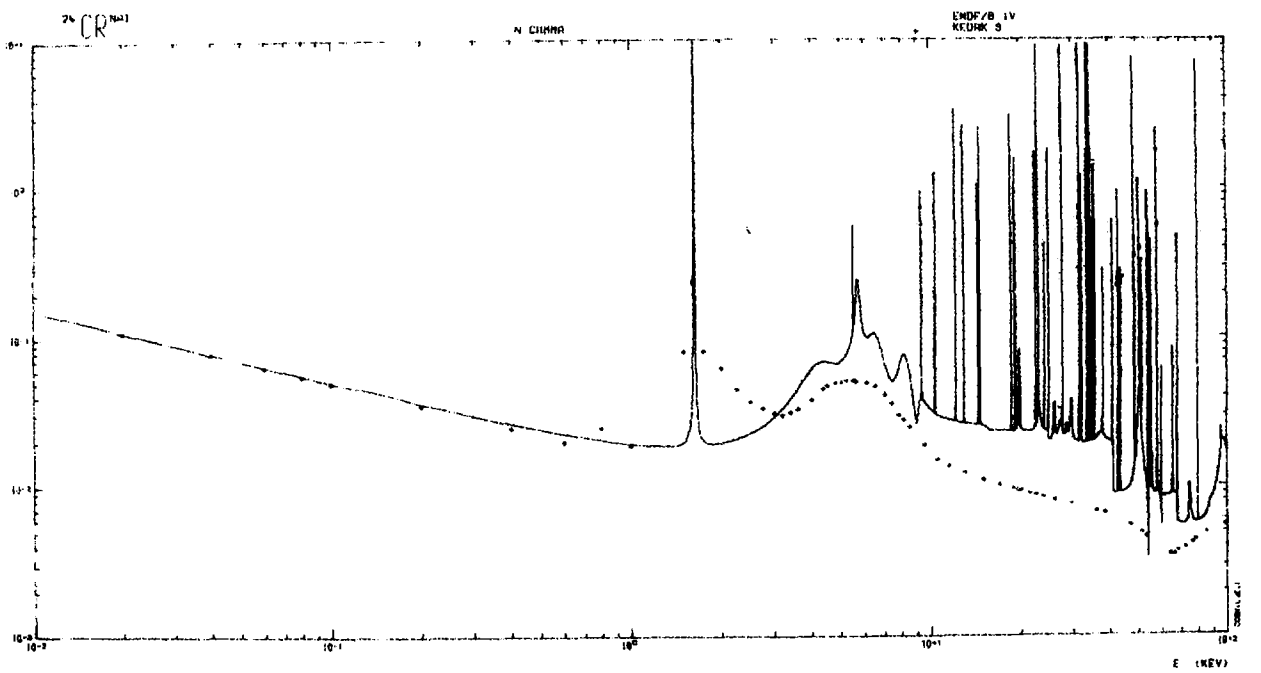

Figure 26.

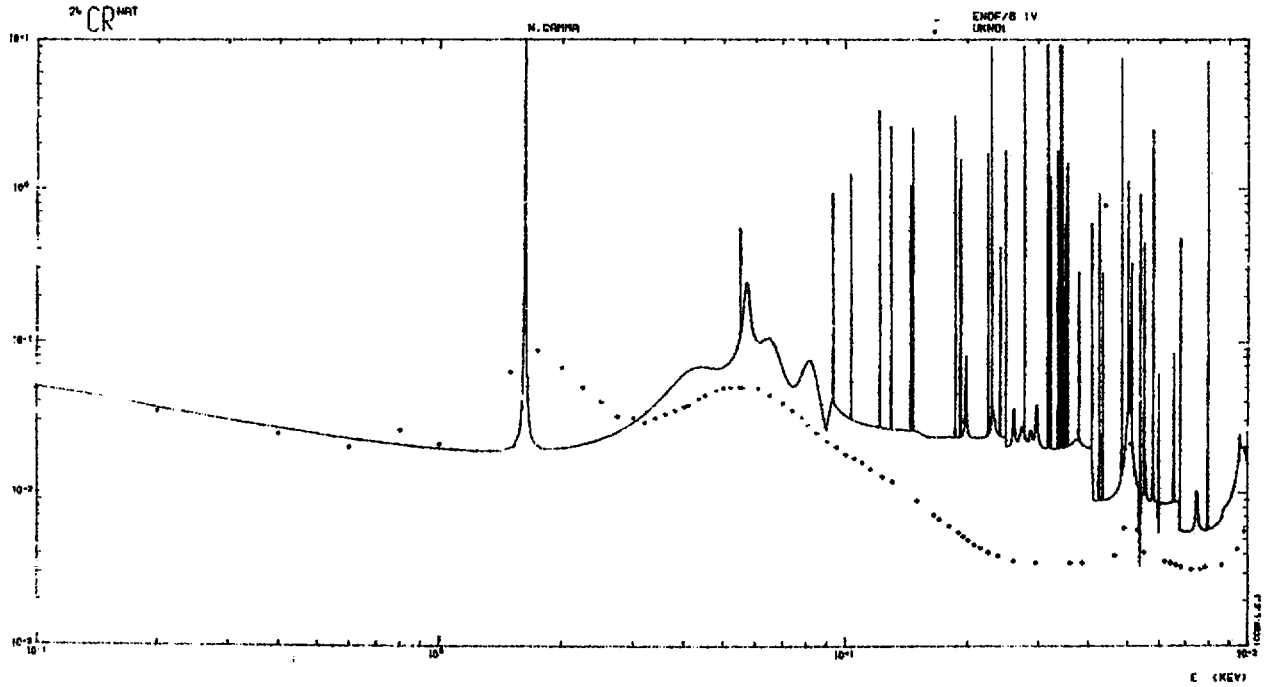

Figure 27.

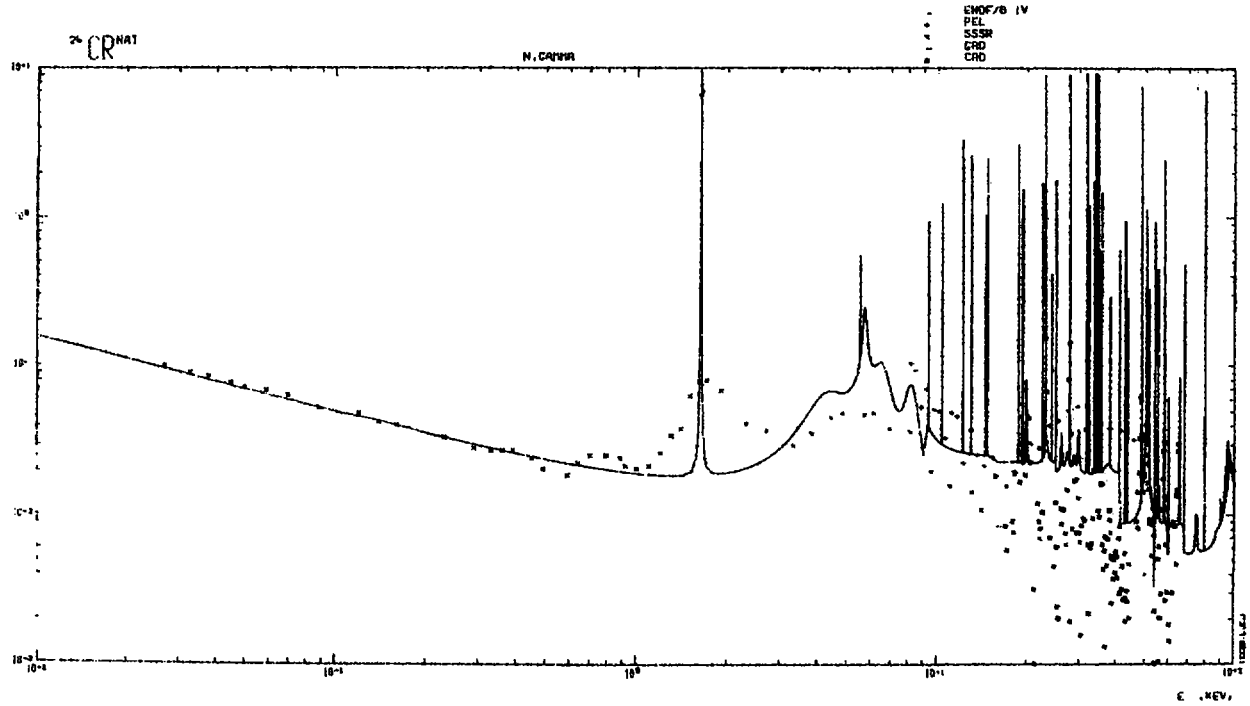

Figure 28.

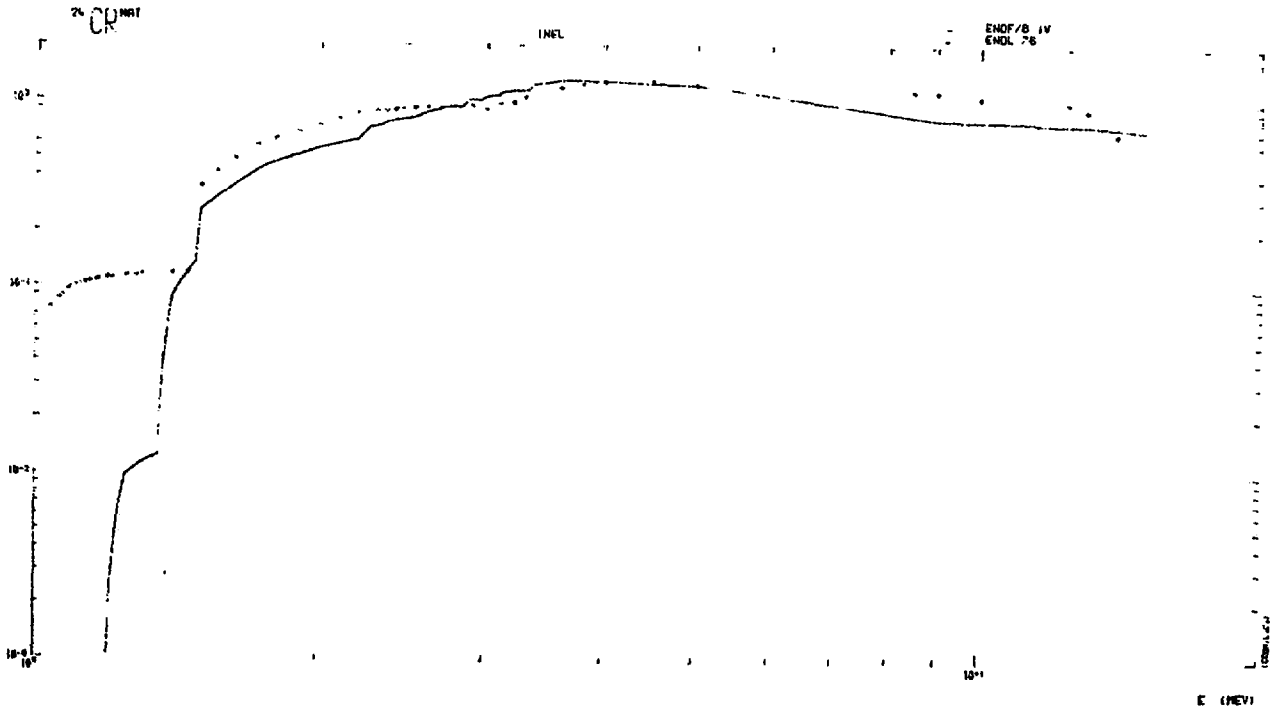

Figure 29.

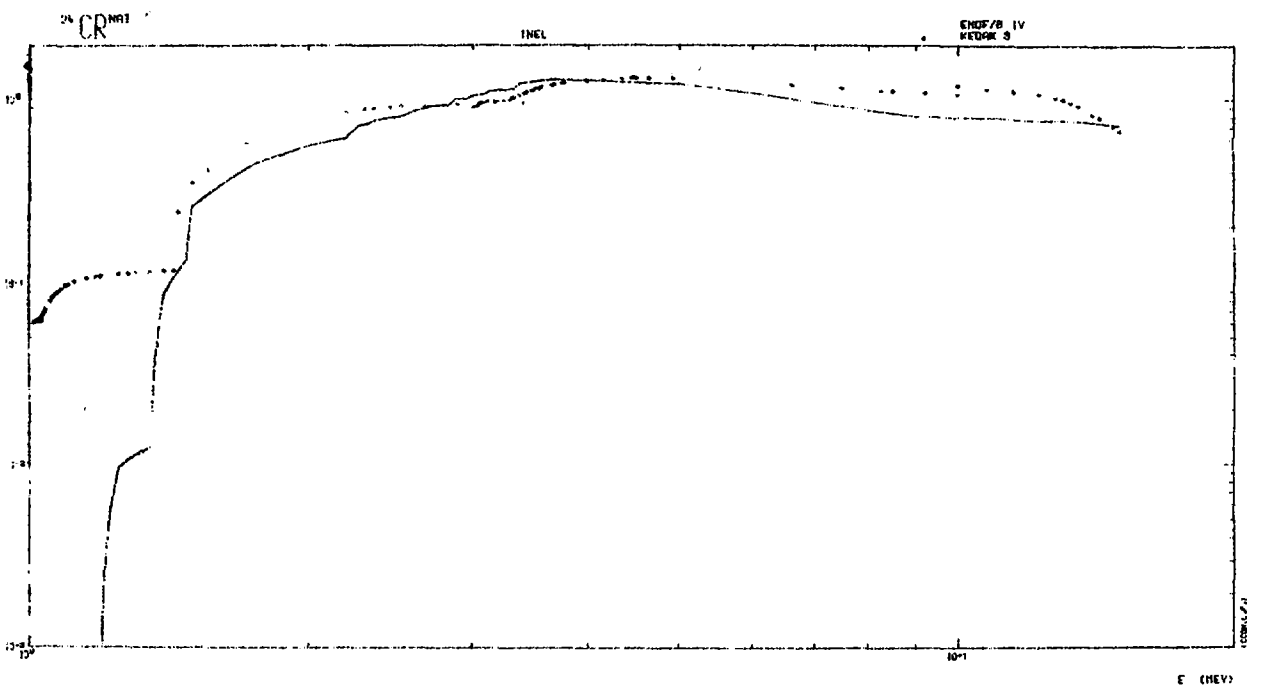

Figure 30.

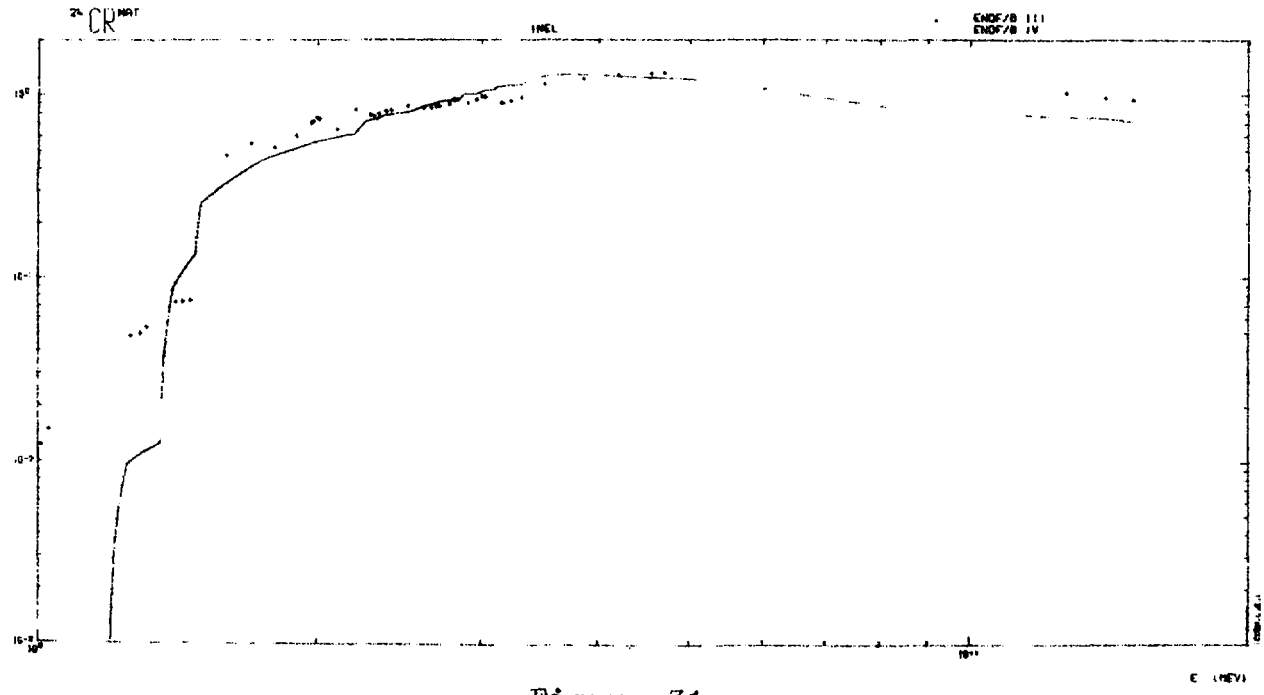

Figure 31.

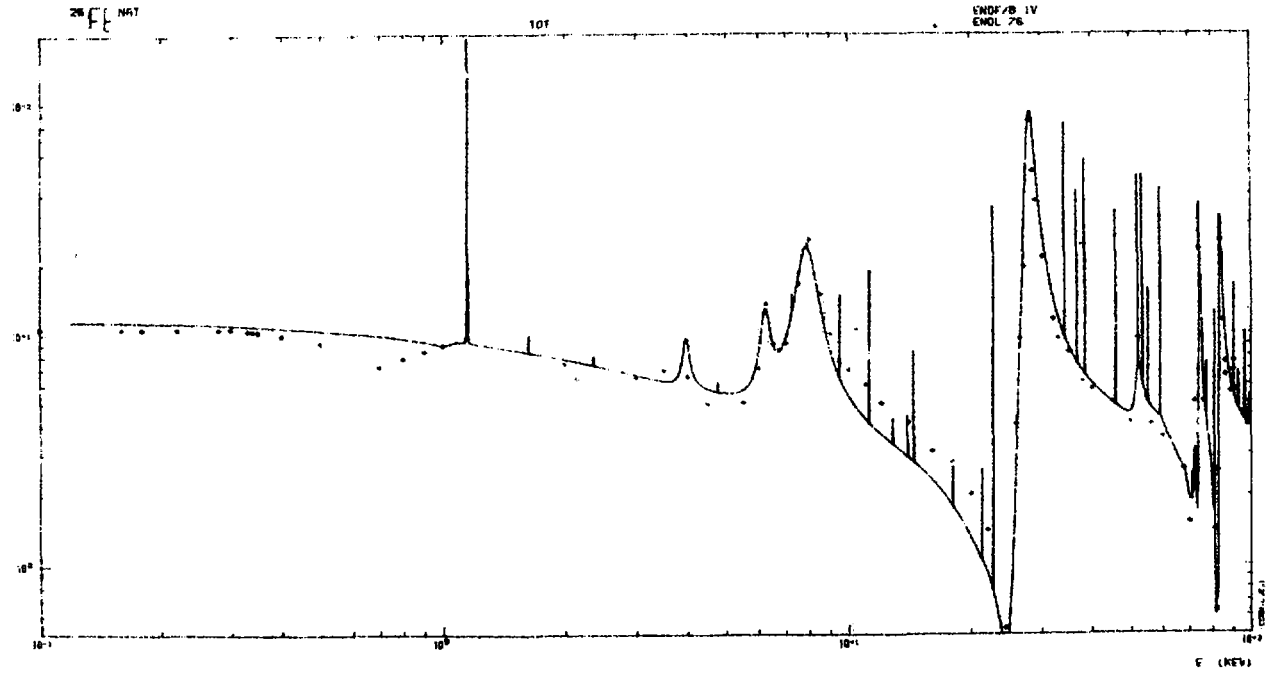

Figure 32.

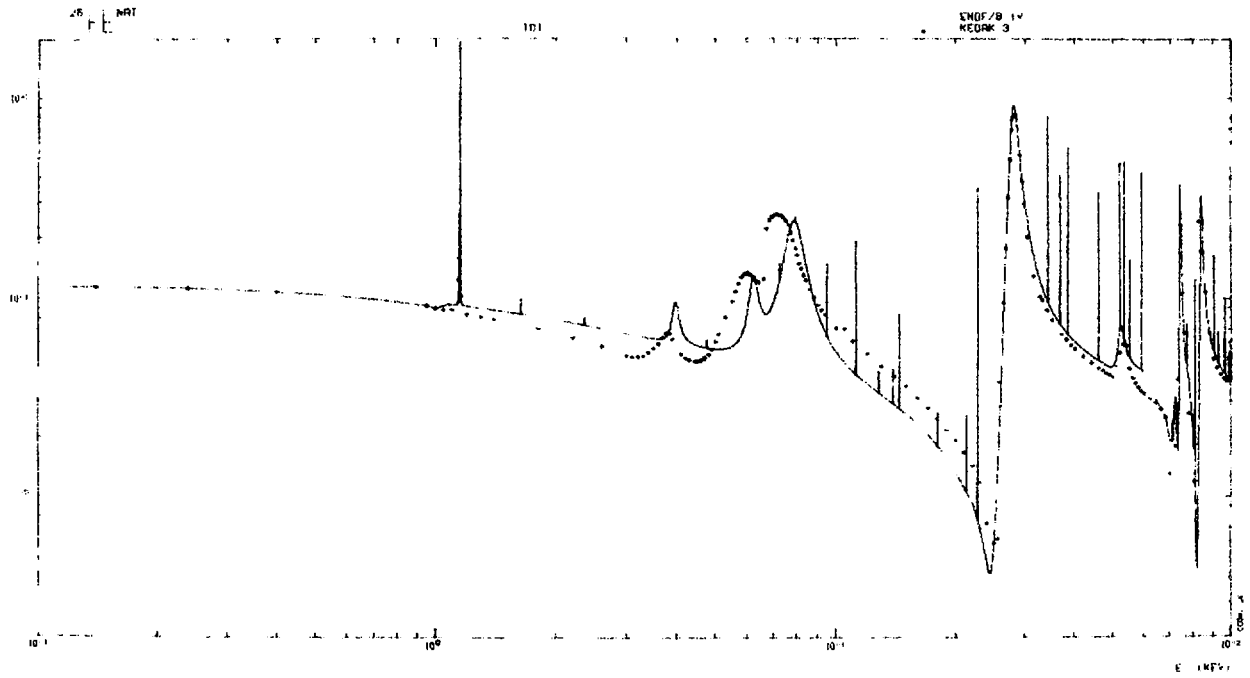

Figure 33.

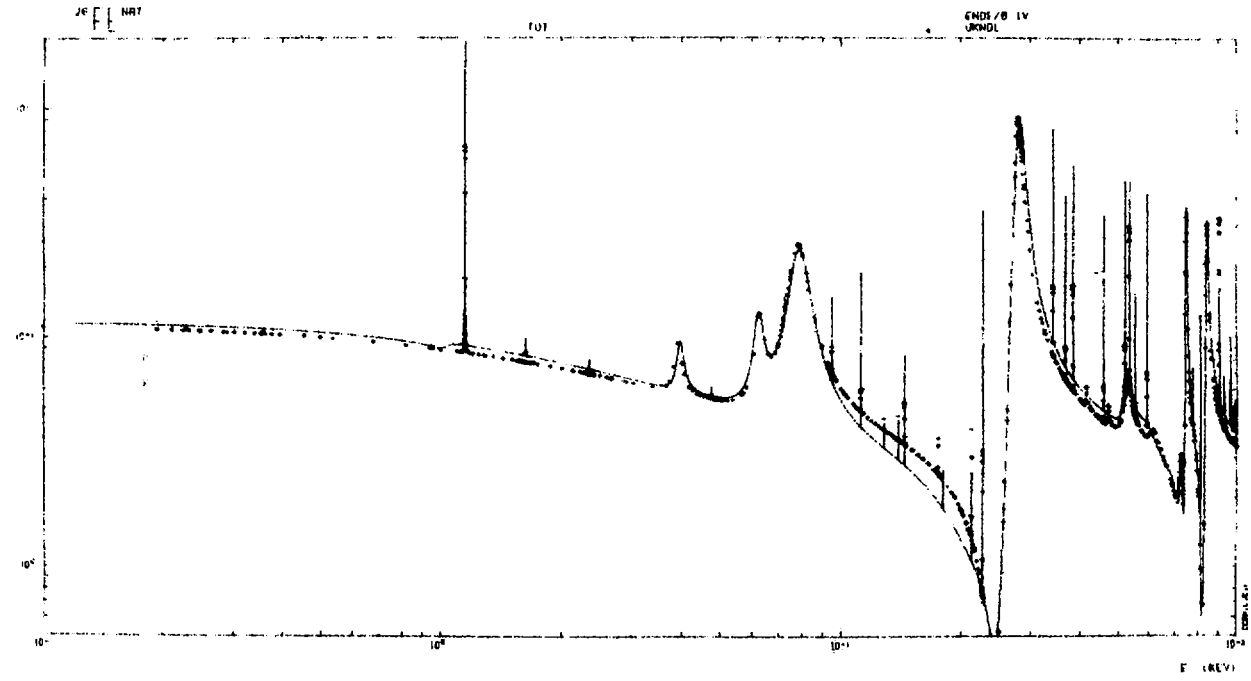

Figure 34.

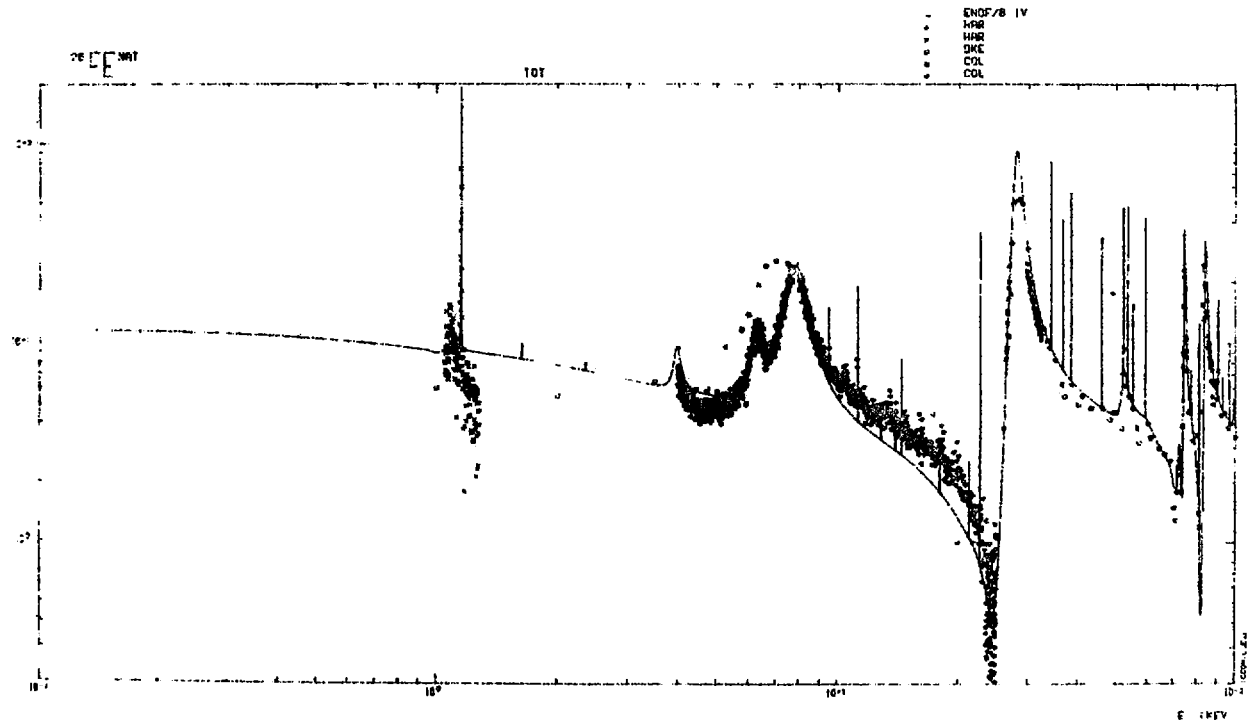

Figure 35.

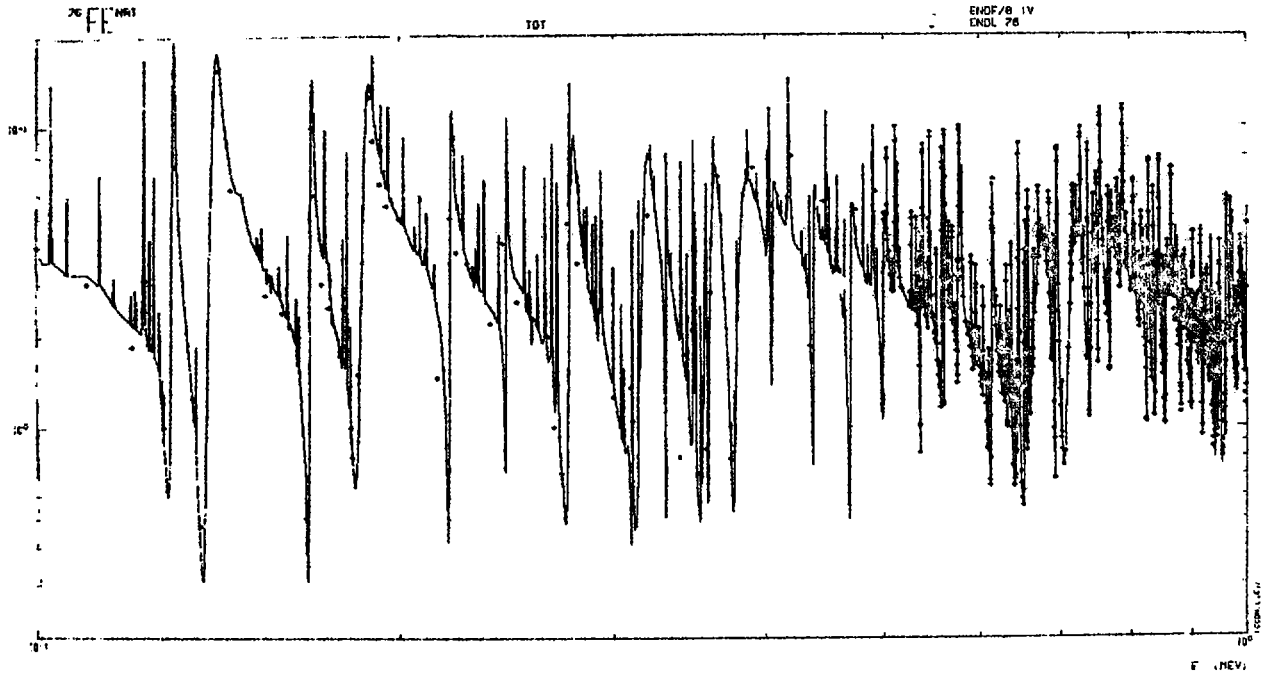

Figure 36.

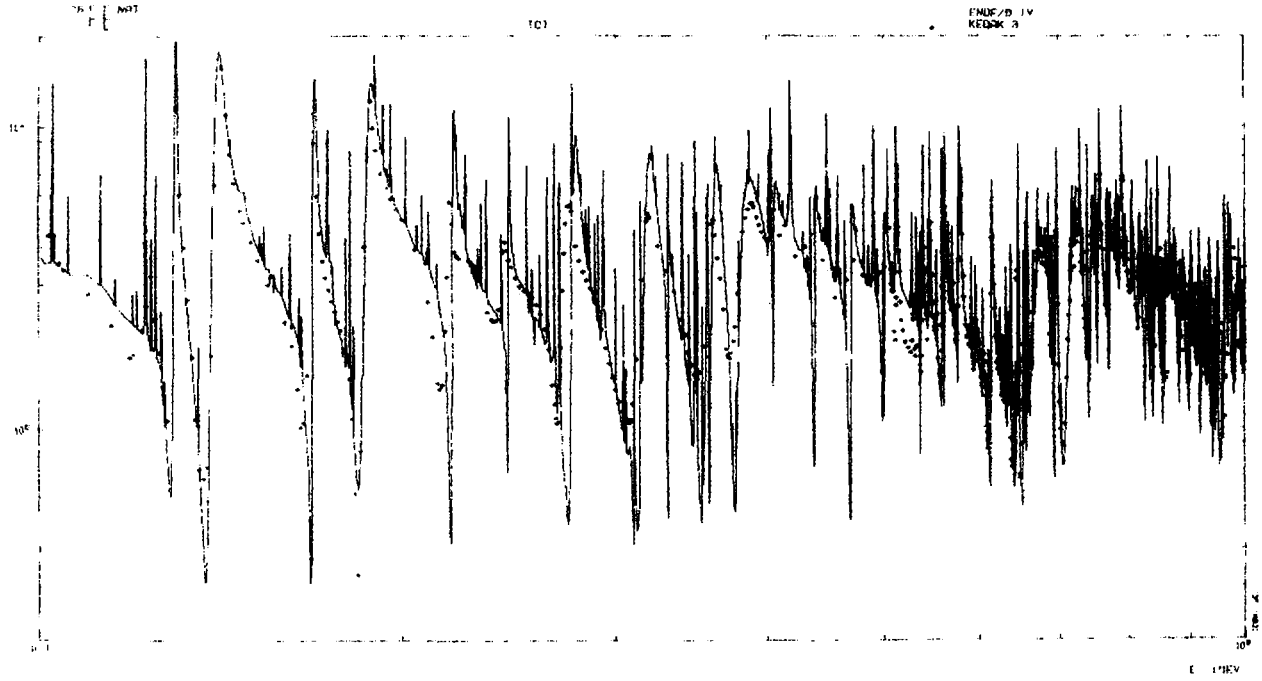

Figure 37.

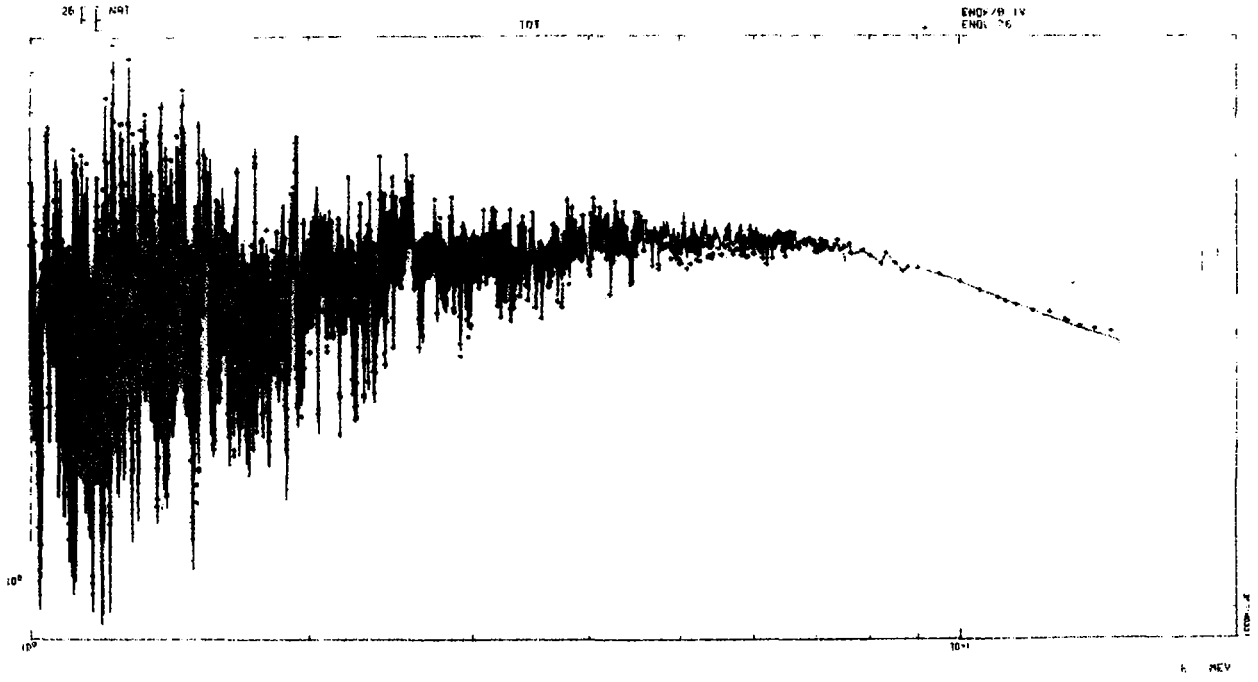

Figure 38.

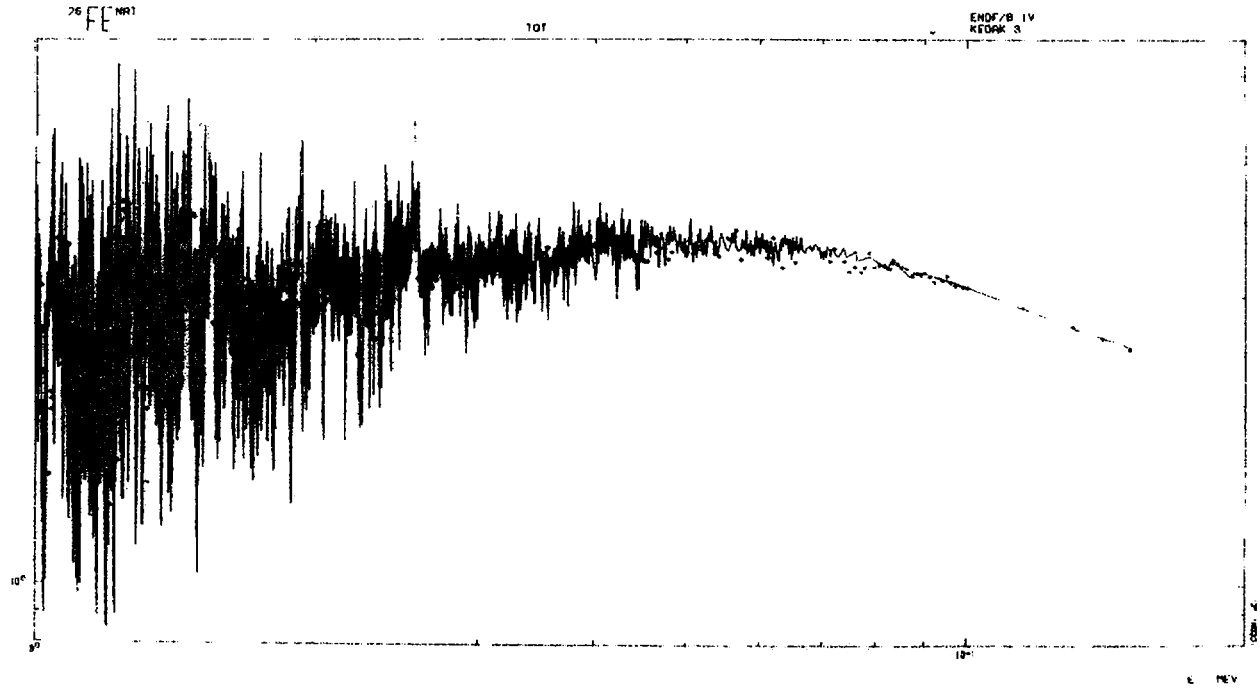

Figure 39.

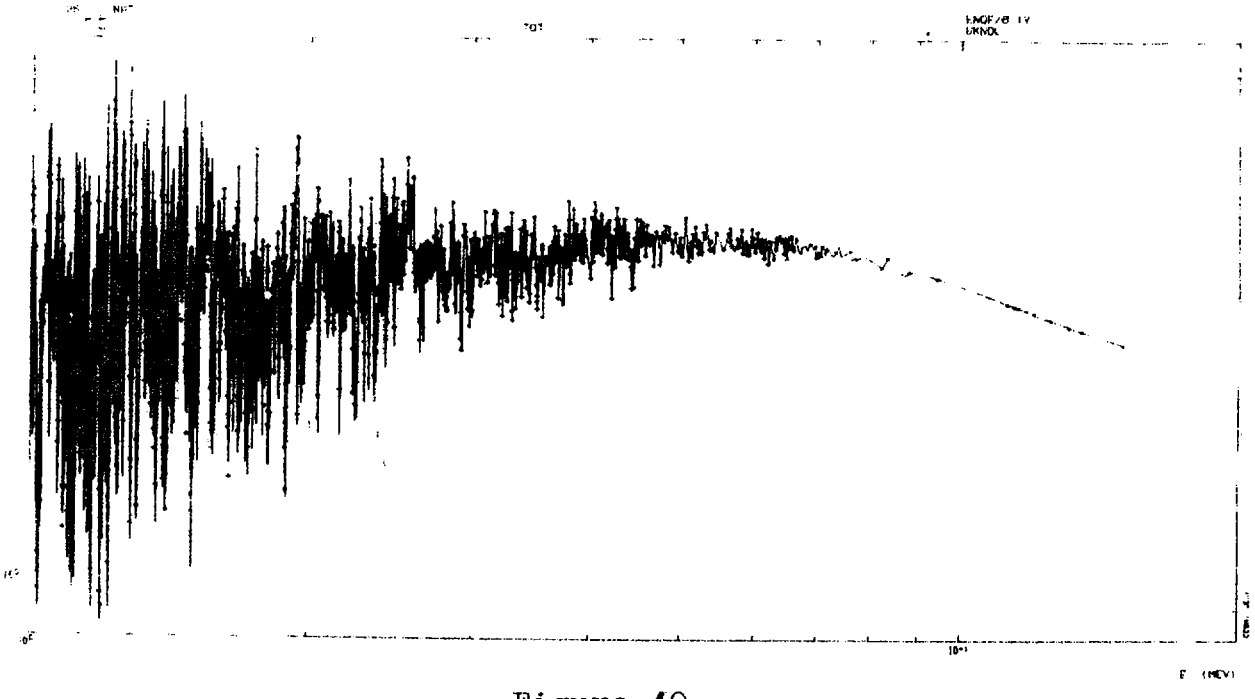

Figure 40

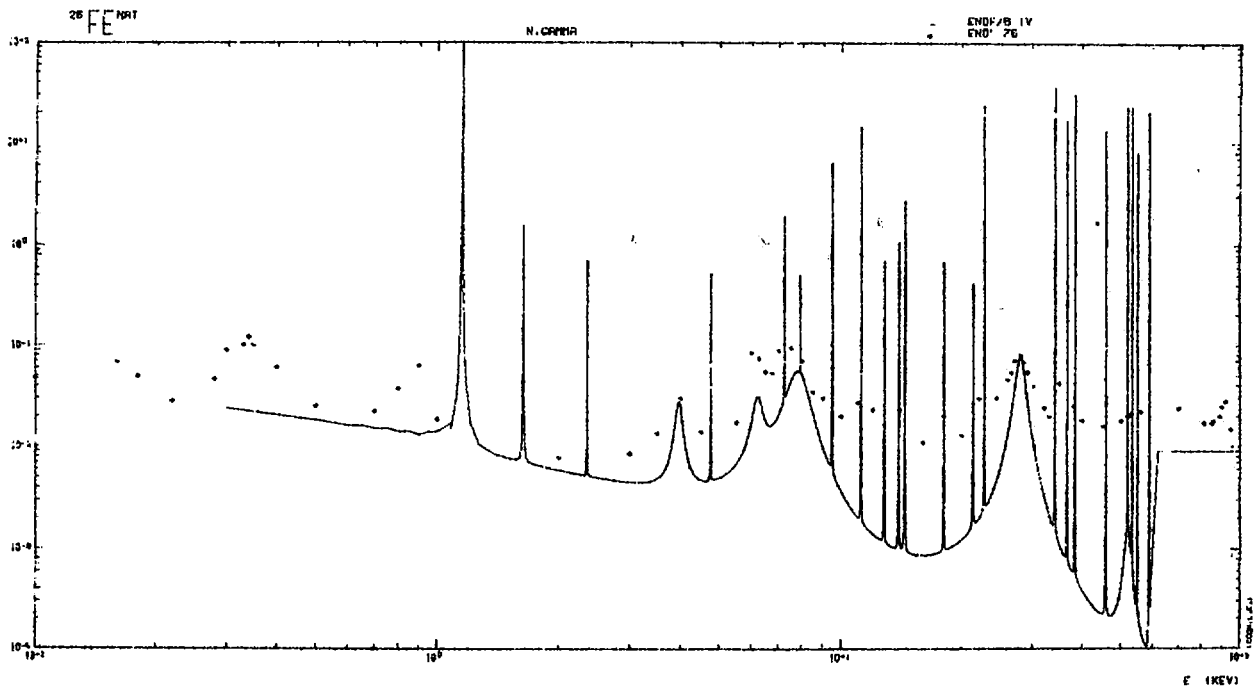

Figure 41.

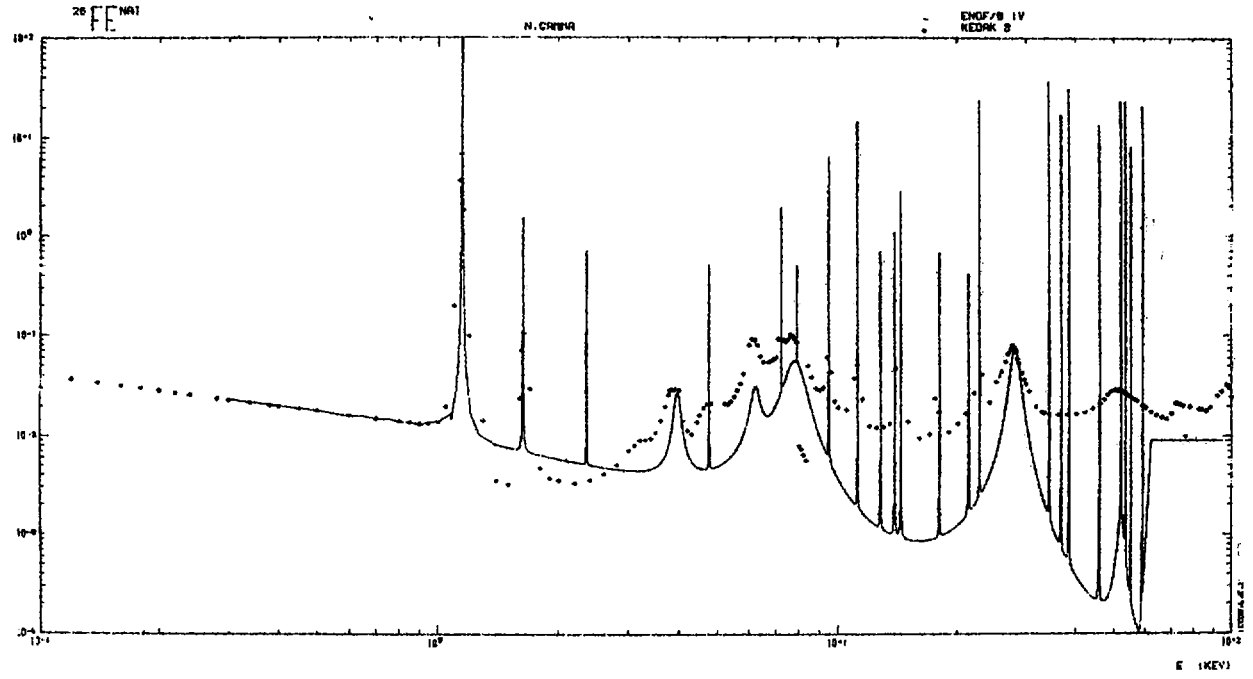

Figure 42.

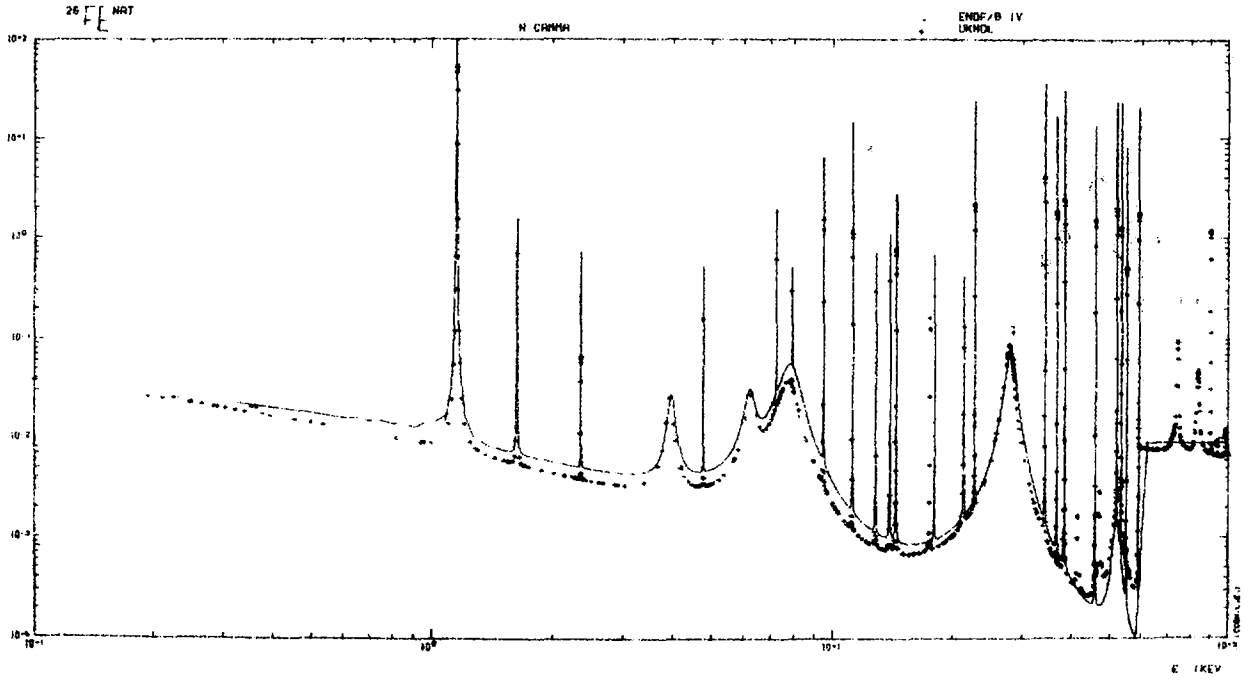

Figure 43.

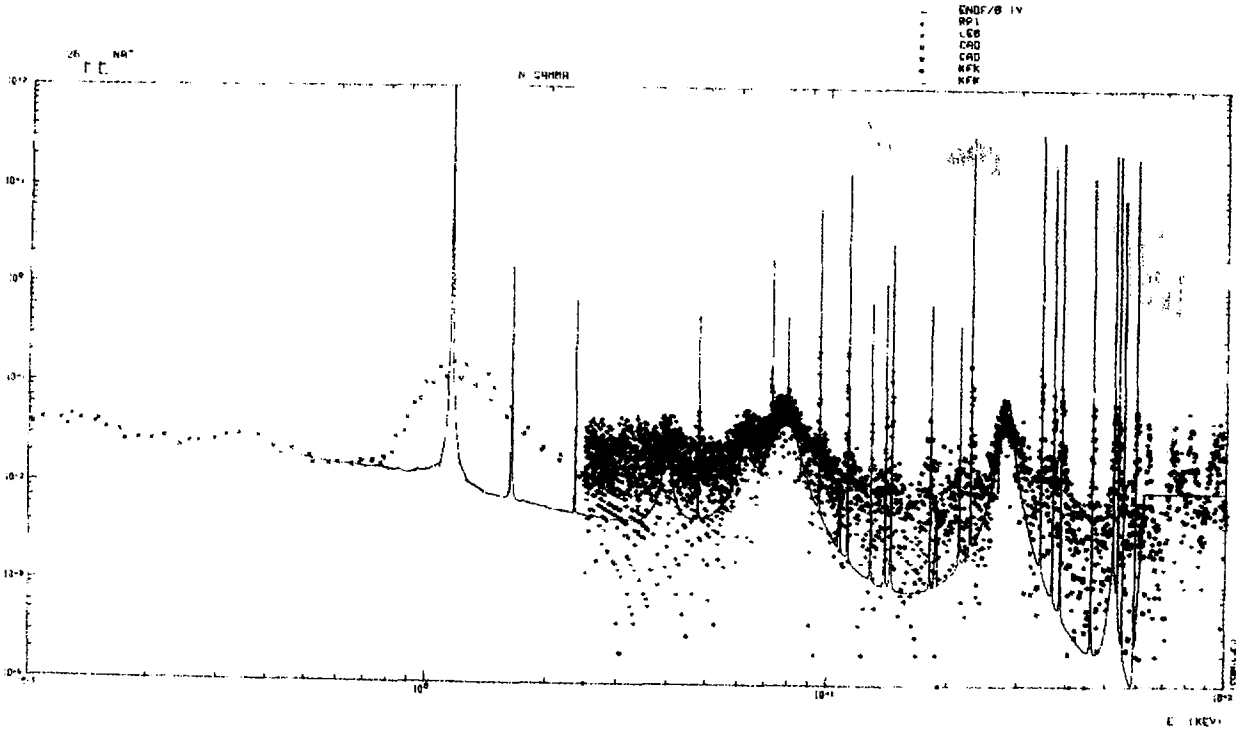

Figure 44.

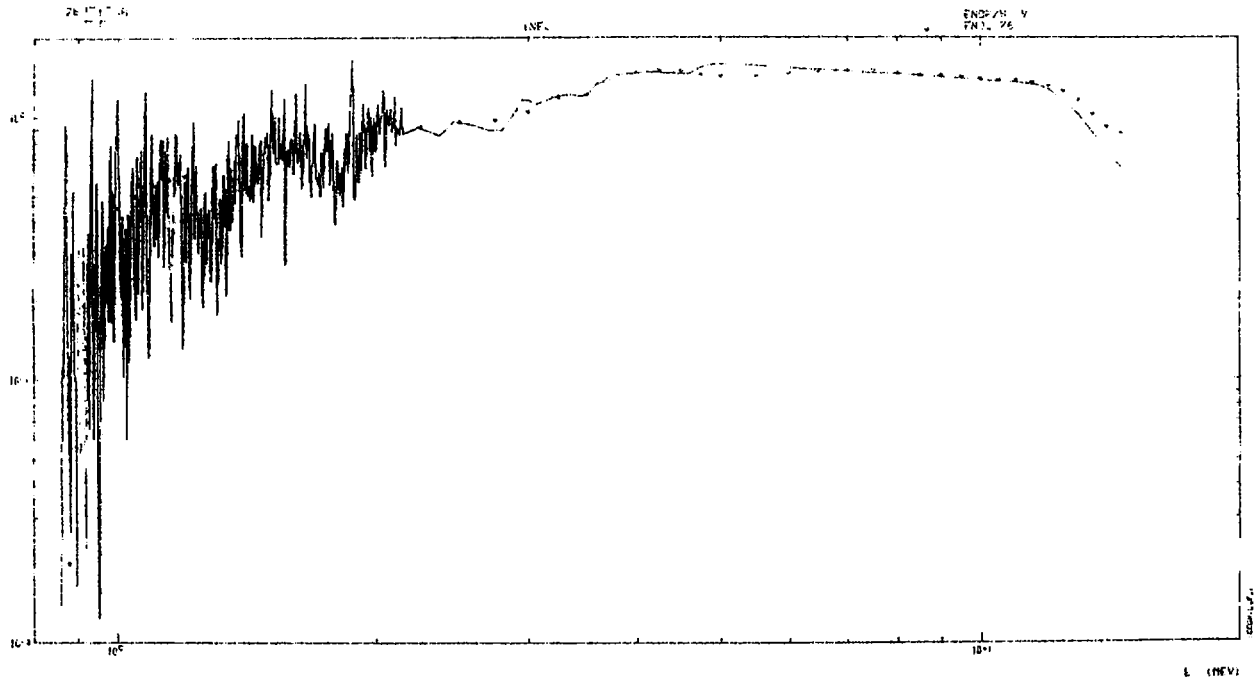

Figure 45.

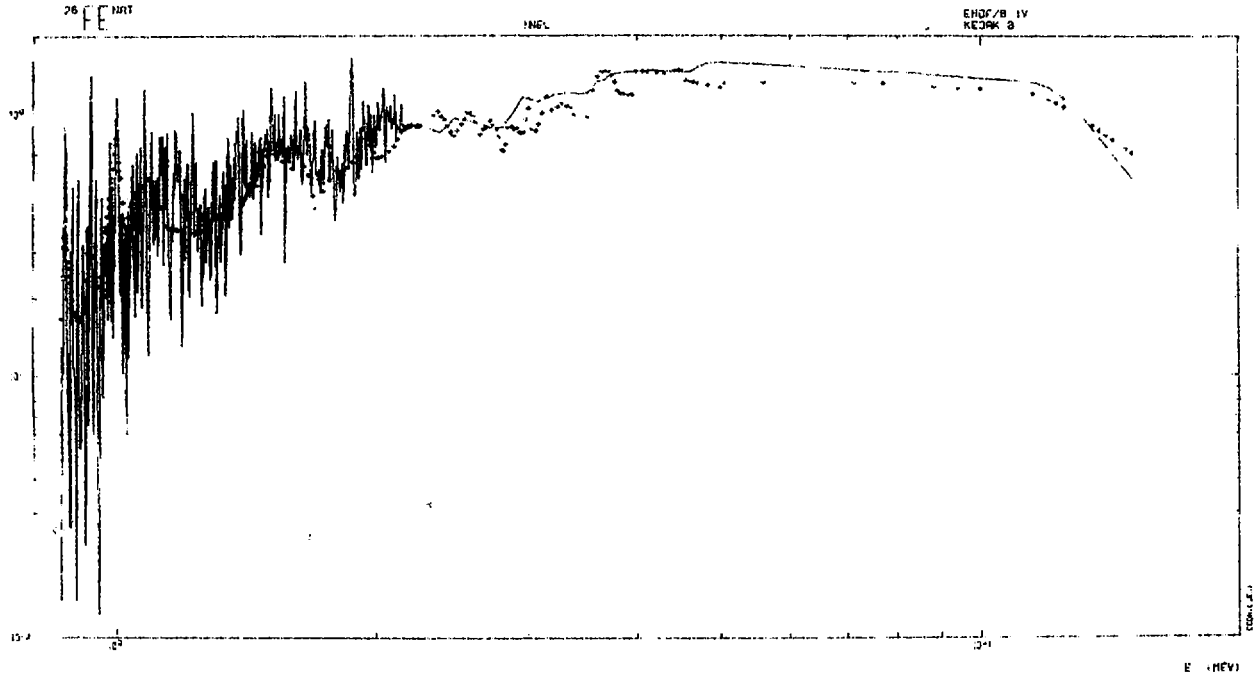

Figure 46.

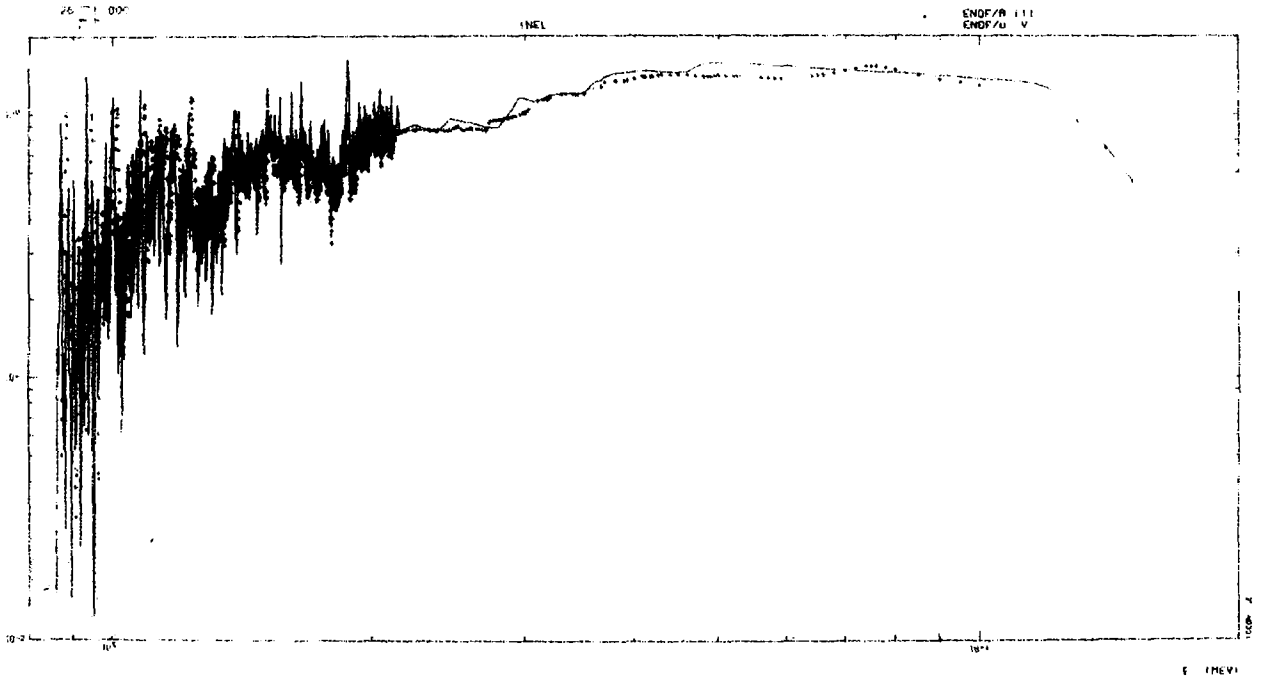

Figure 47.

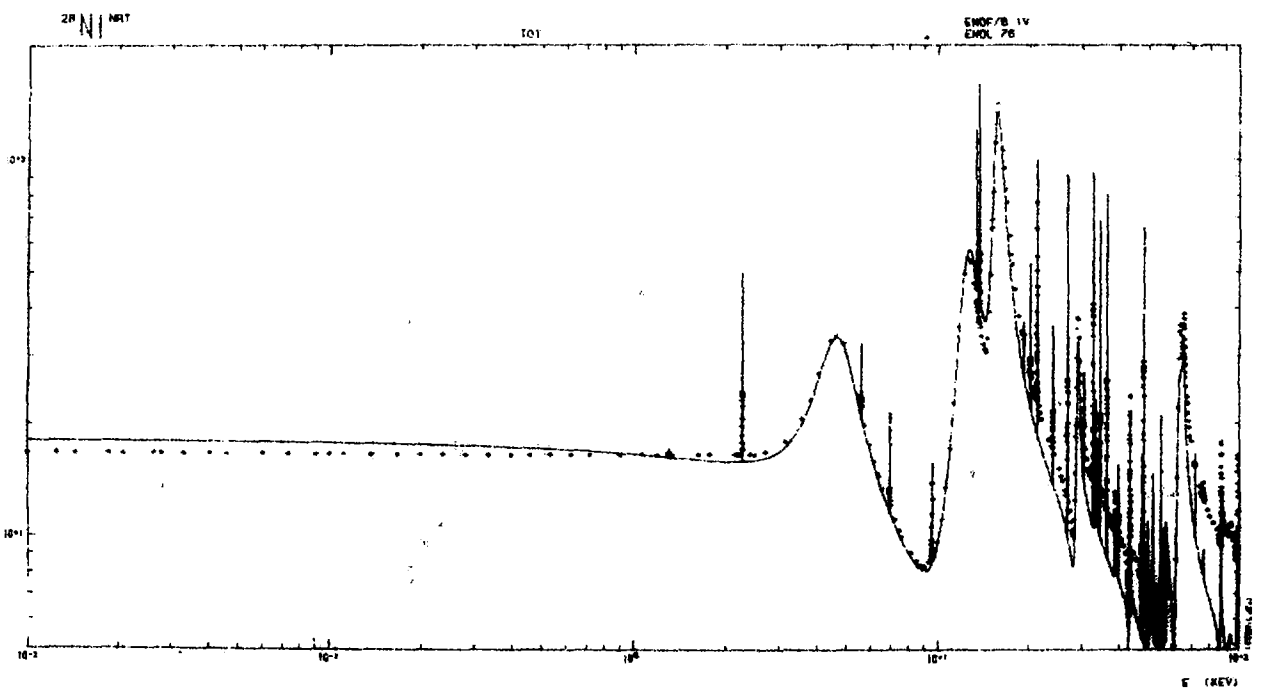

Figure 48.

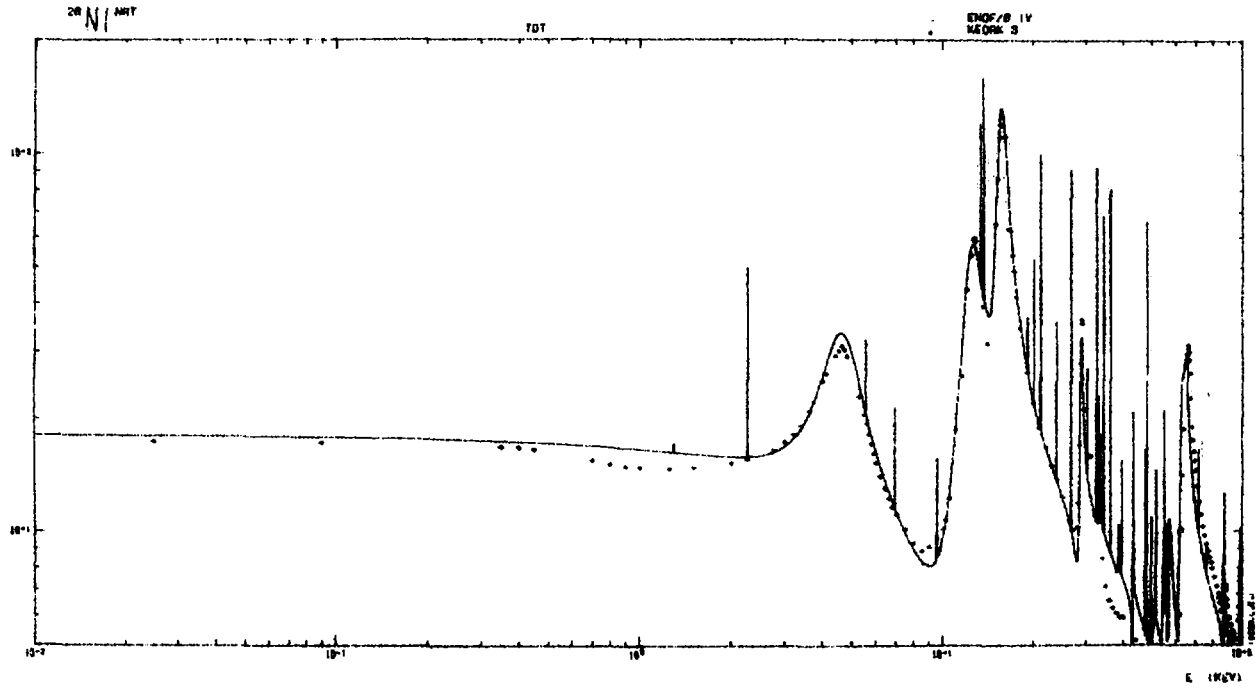

Figure 49.

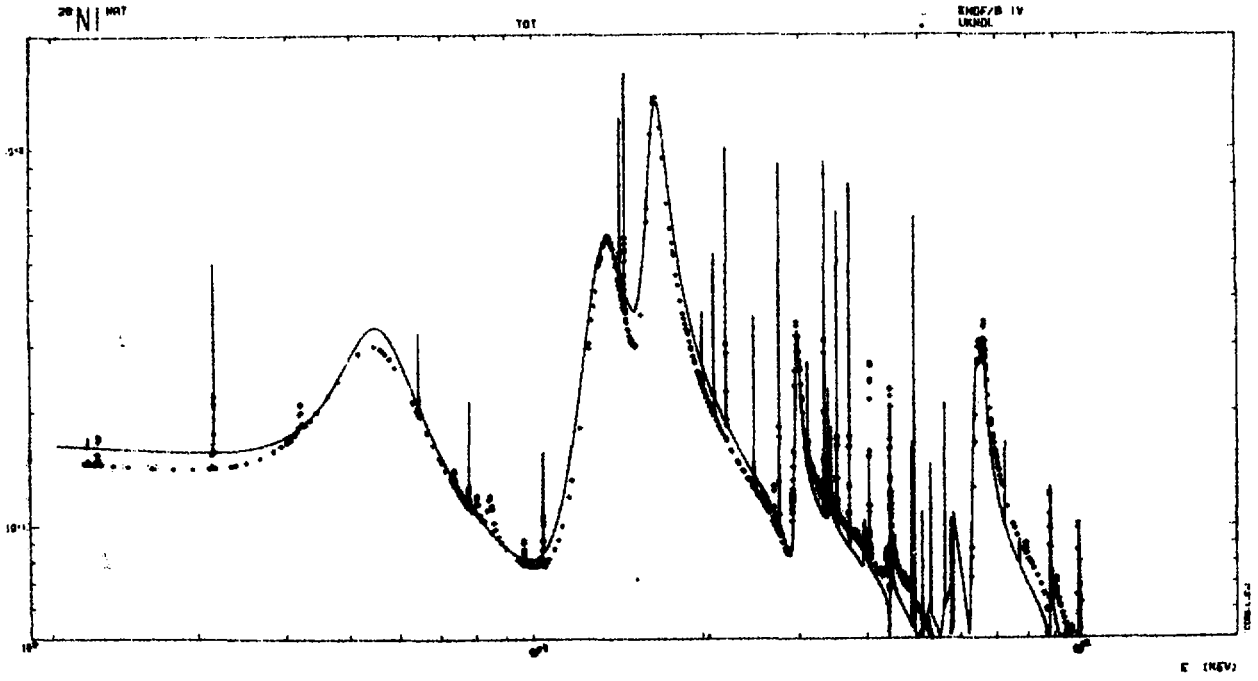

Figure 50.

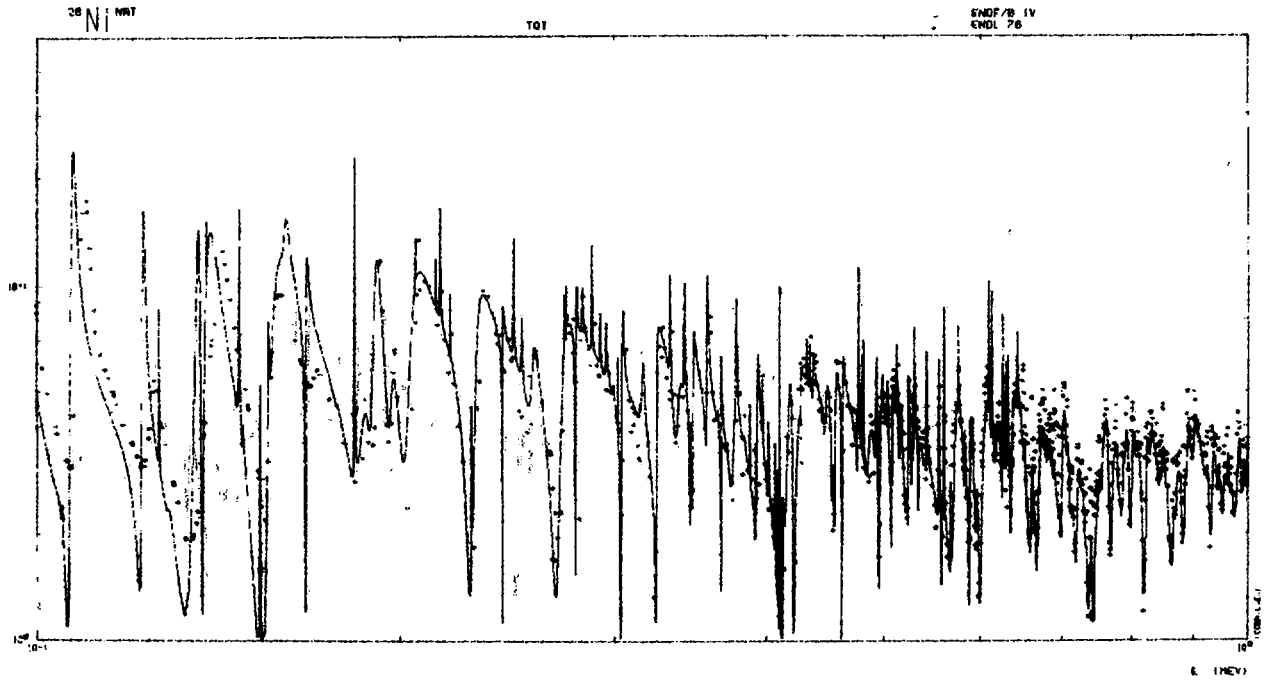

Figure 51.

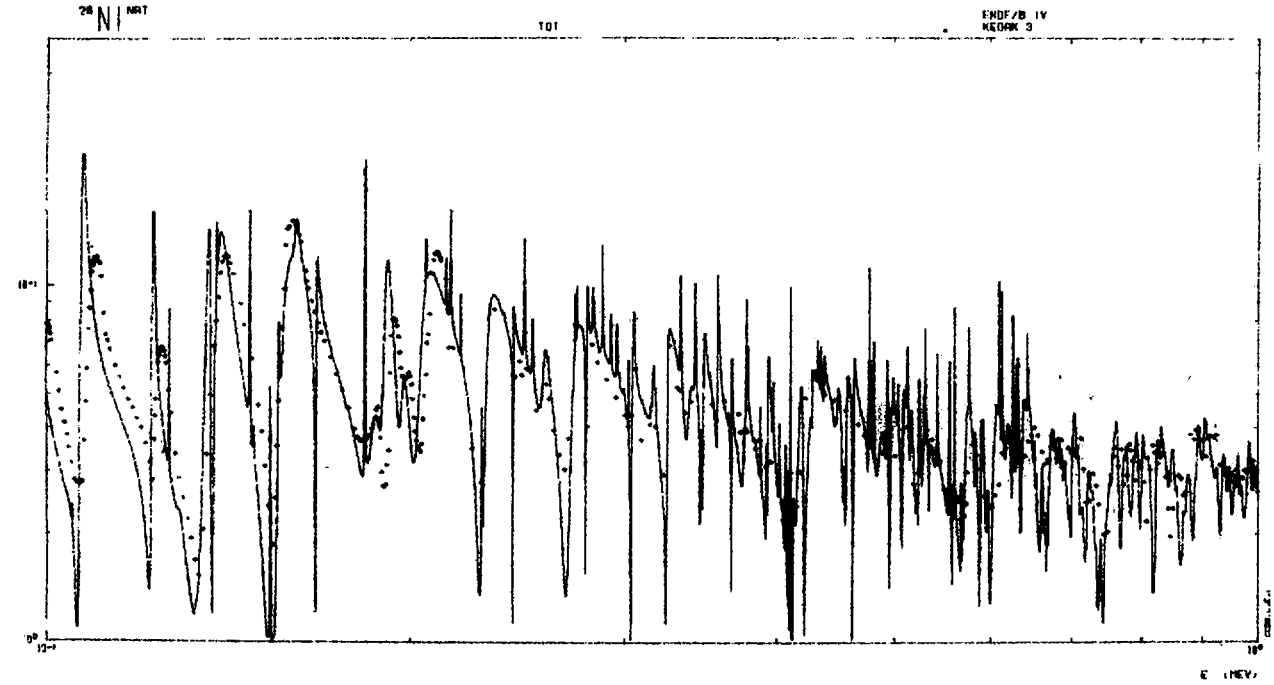

Figure 52.

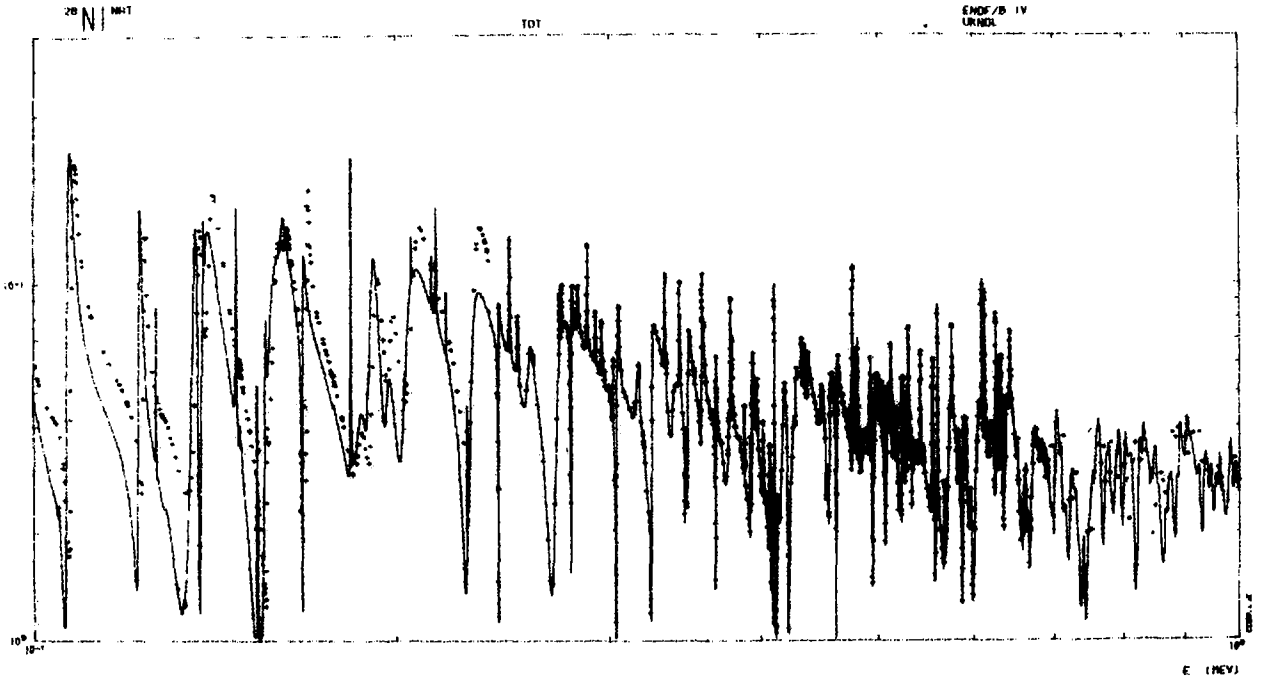

Figure 53.

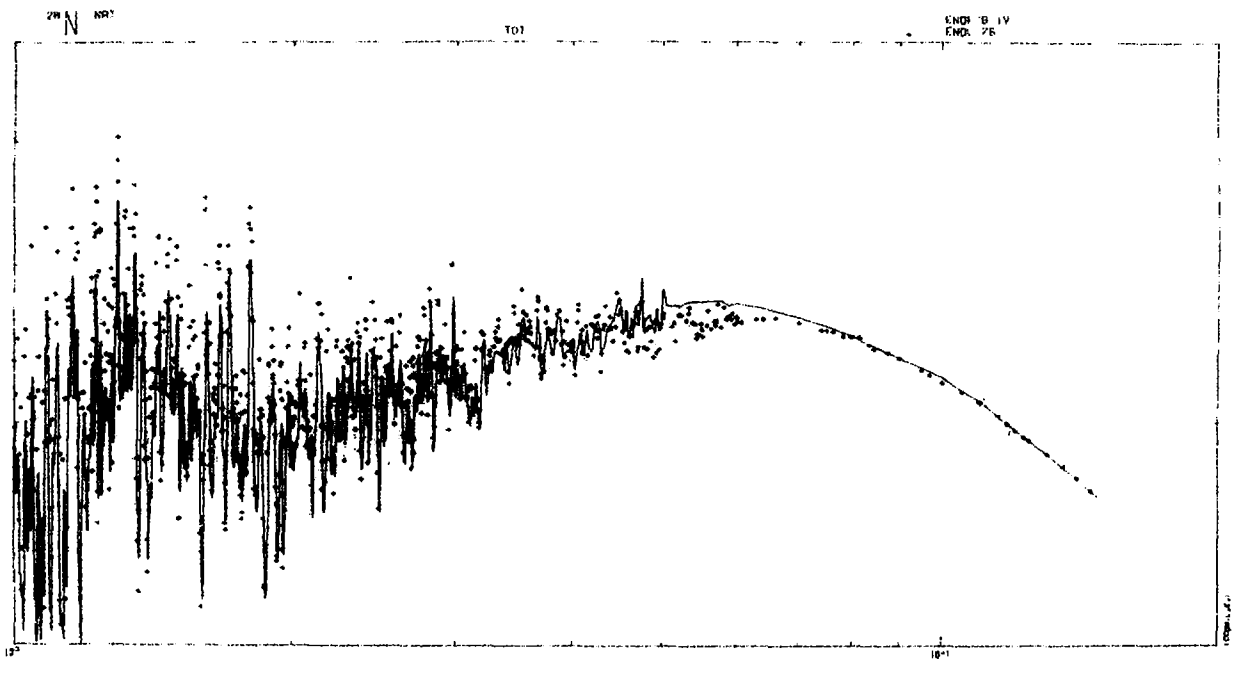

Figure 54.

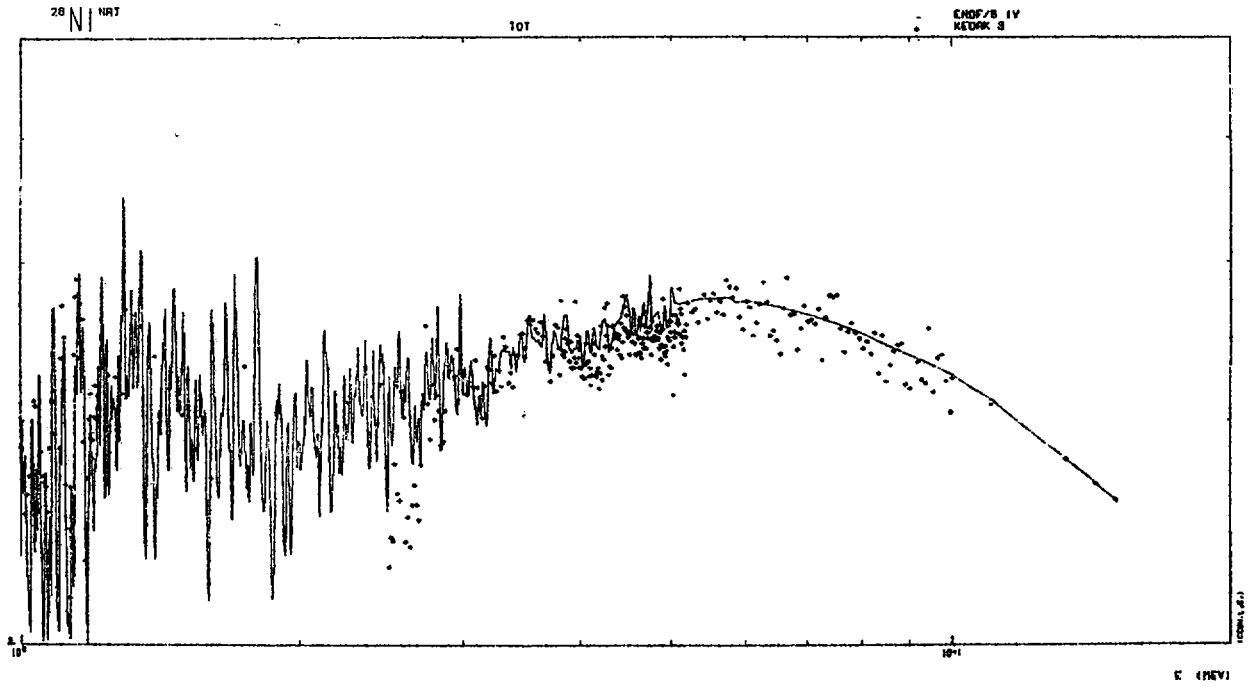

Figure 55.

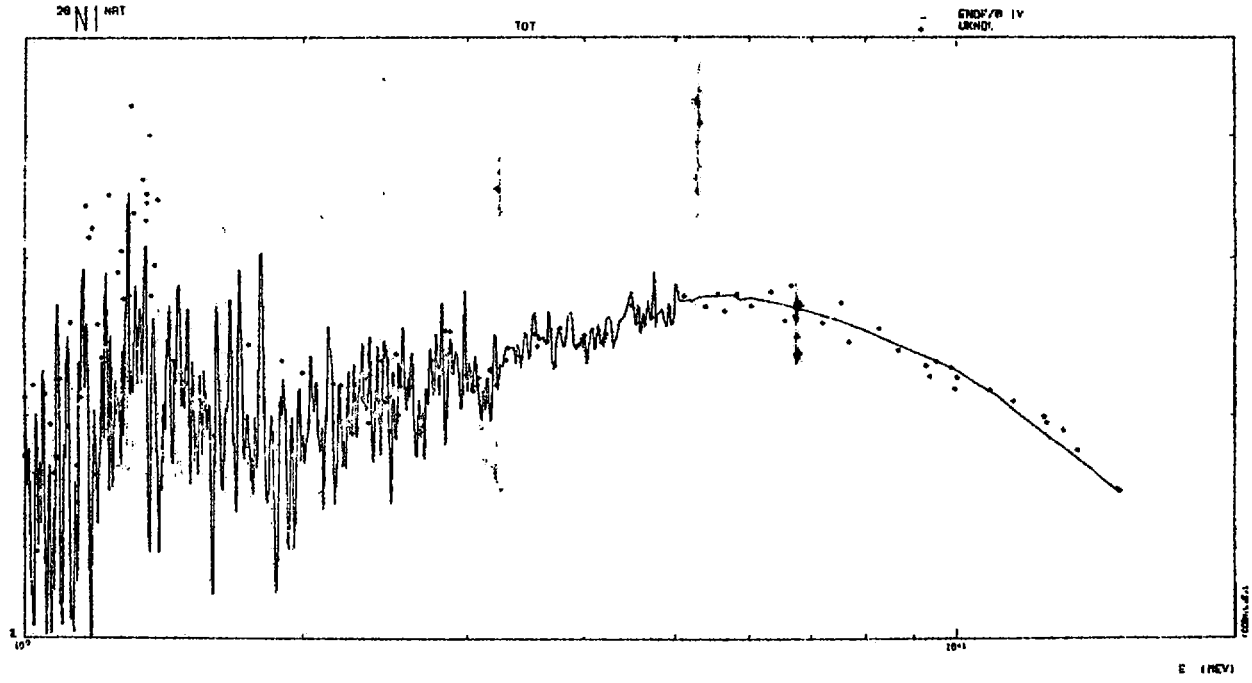

Figure 56.

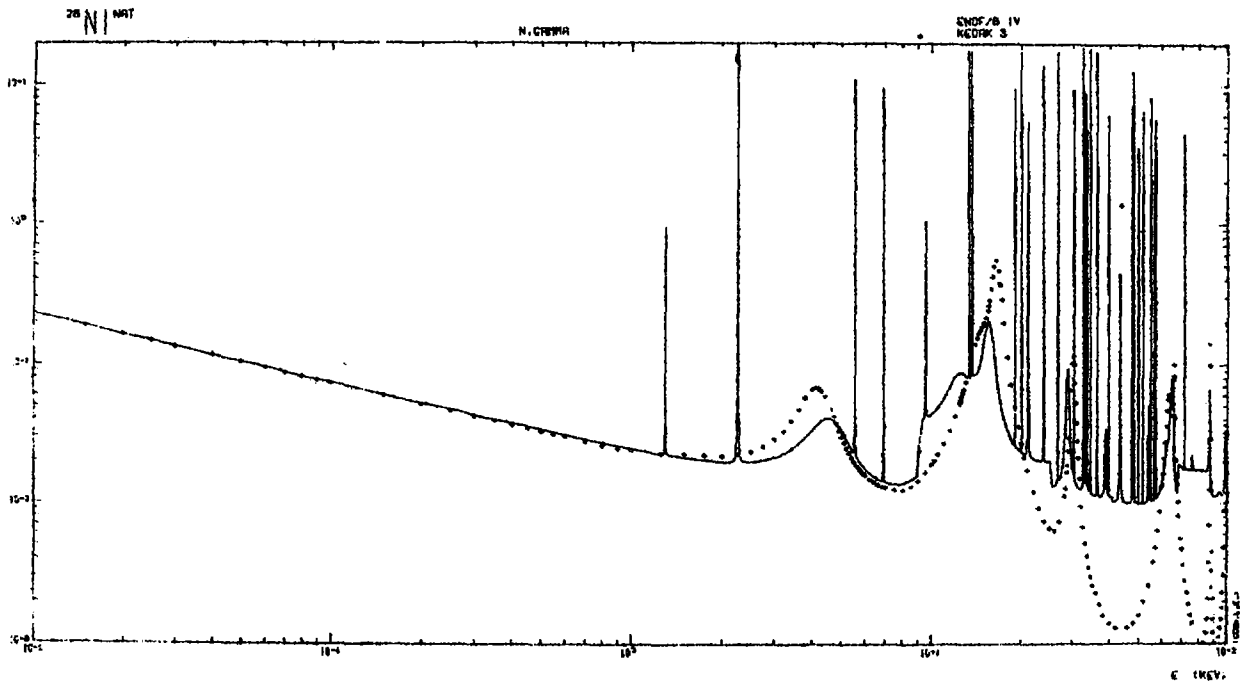

Figure 57.

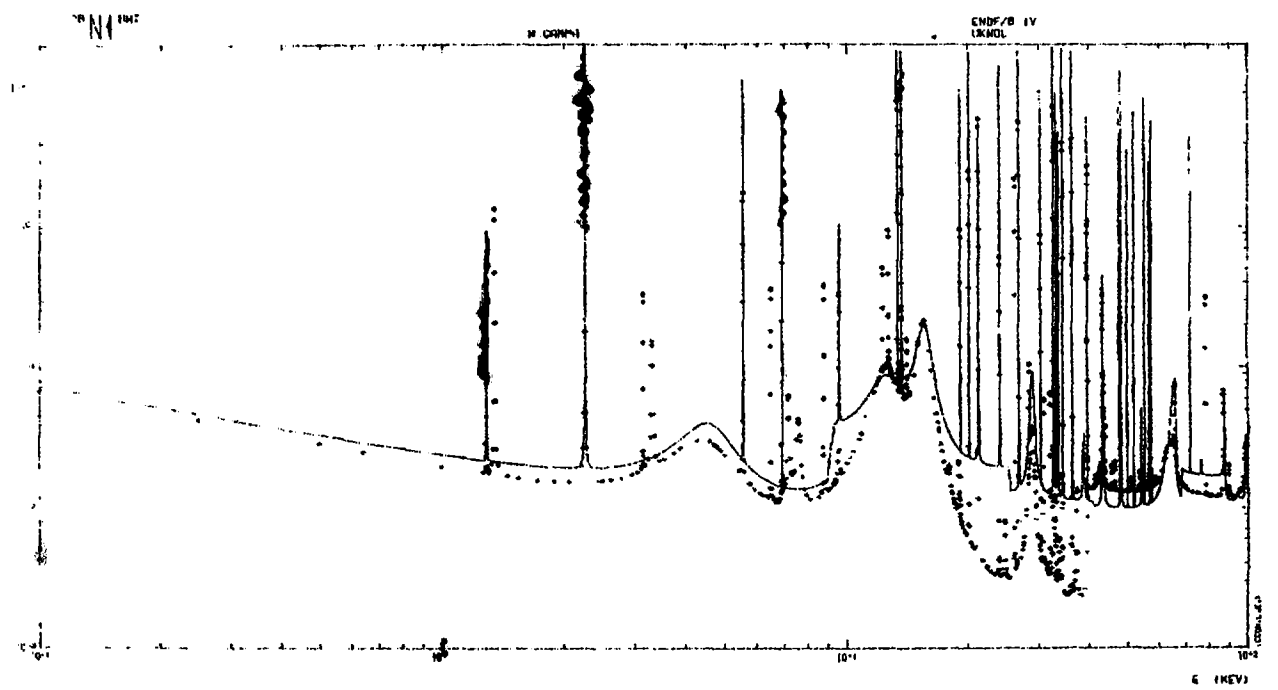

Figure 58.

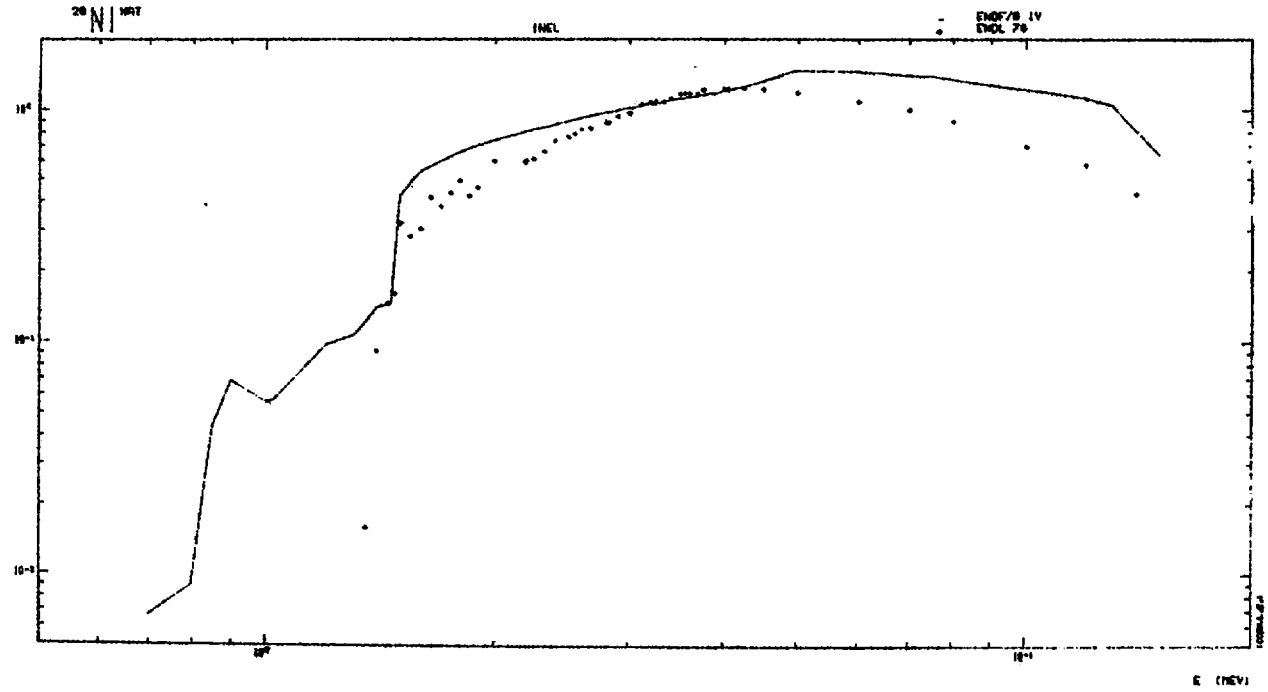

Figure 59.

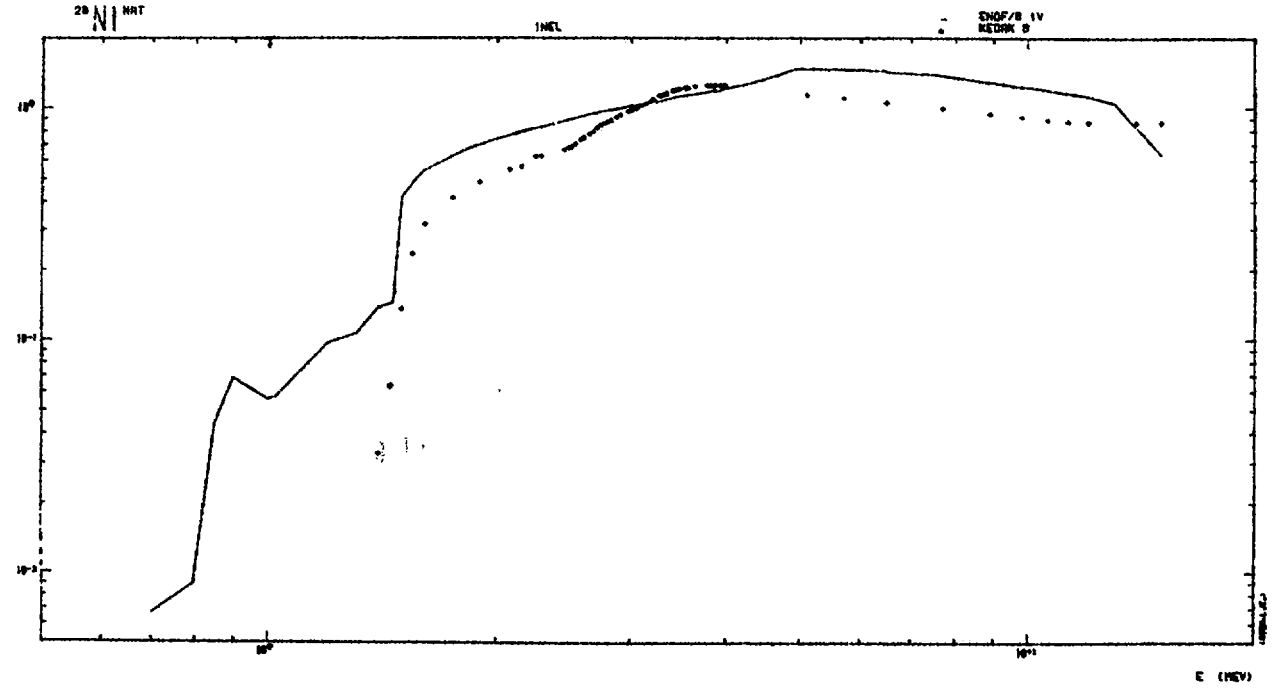

Figure 60.

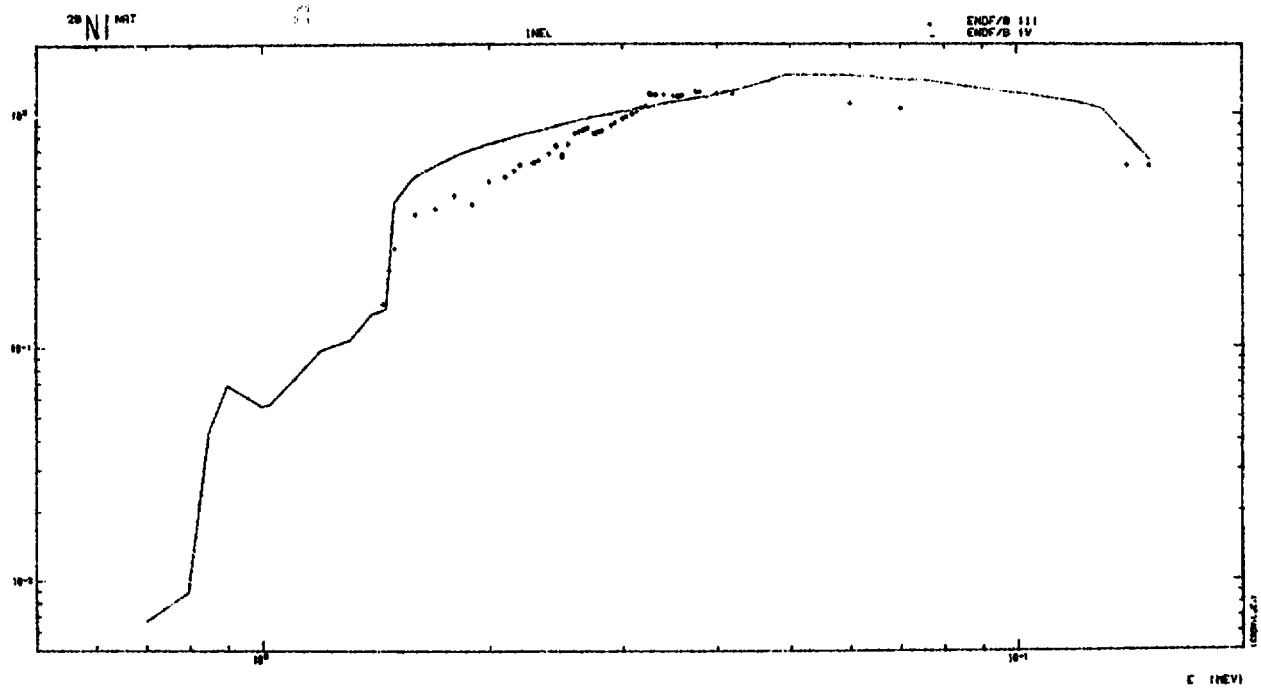

Figure 61.

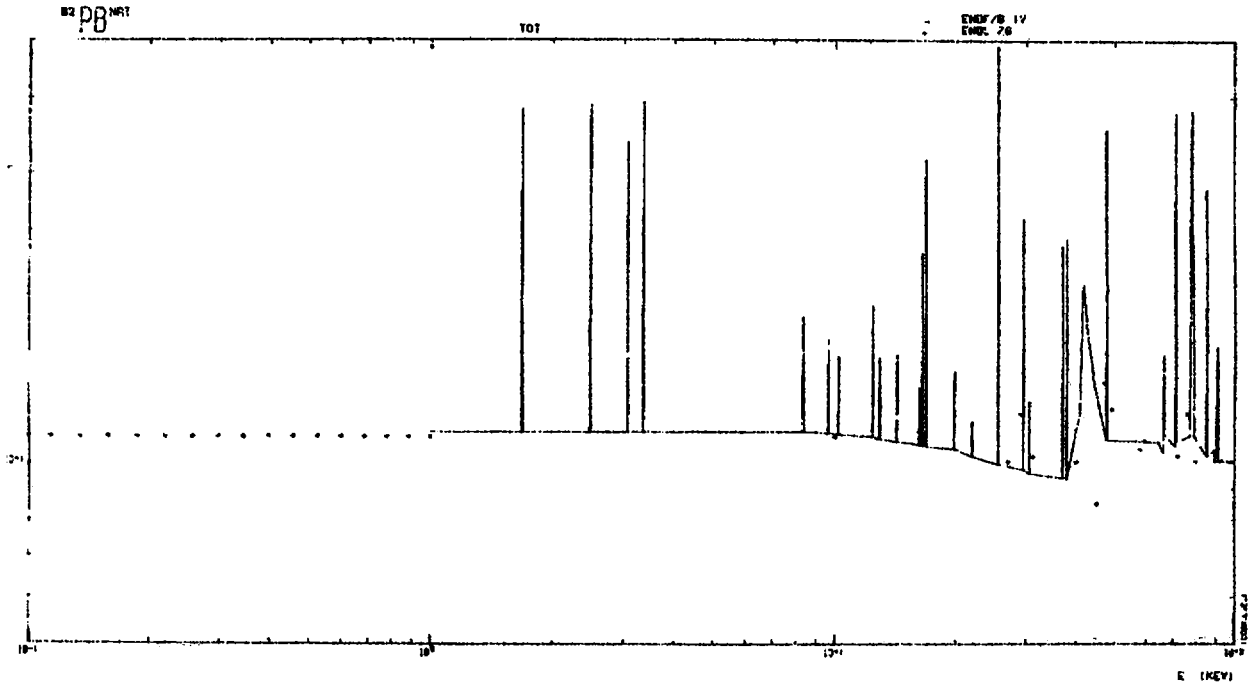

Figure 62.

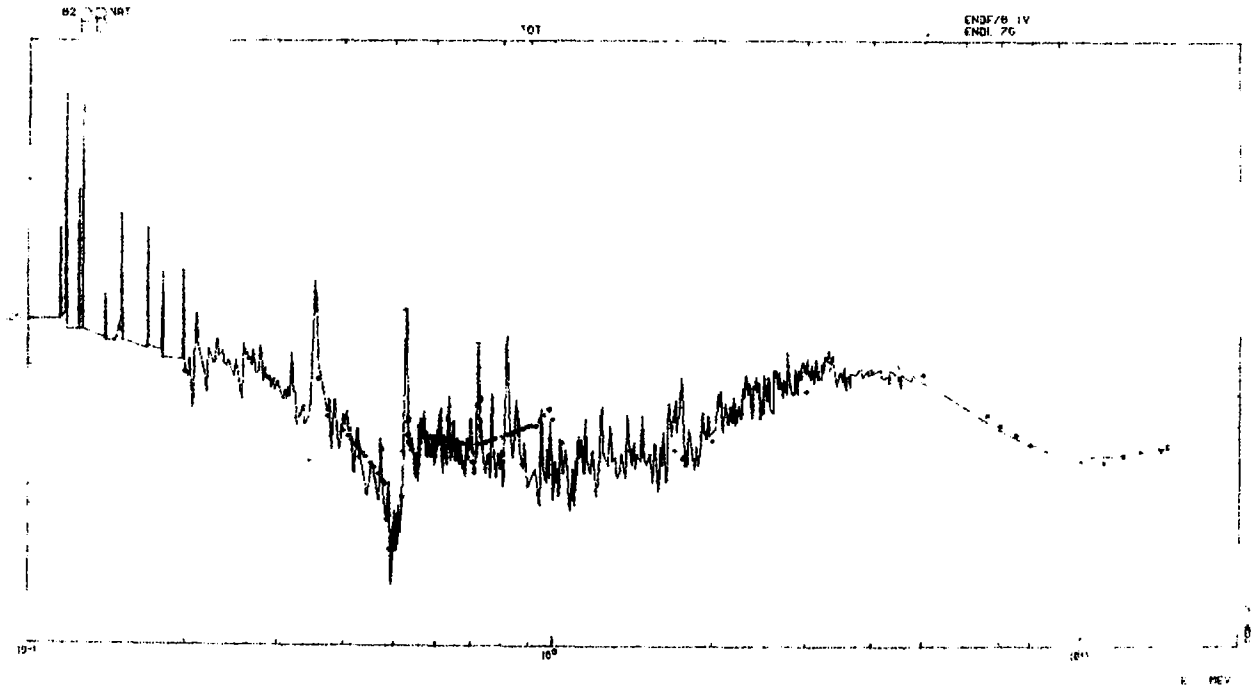

Figure 63.

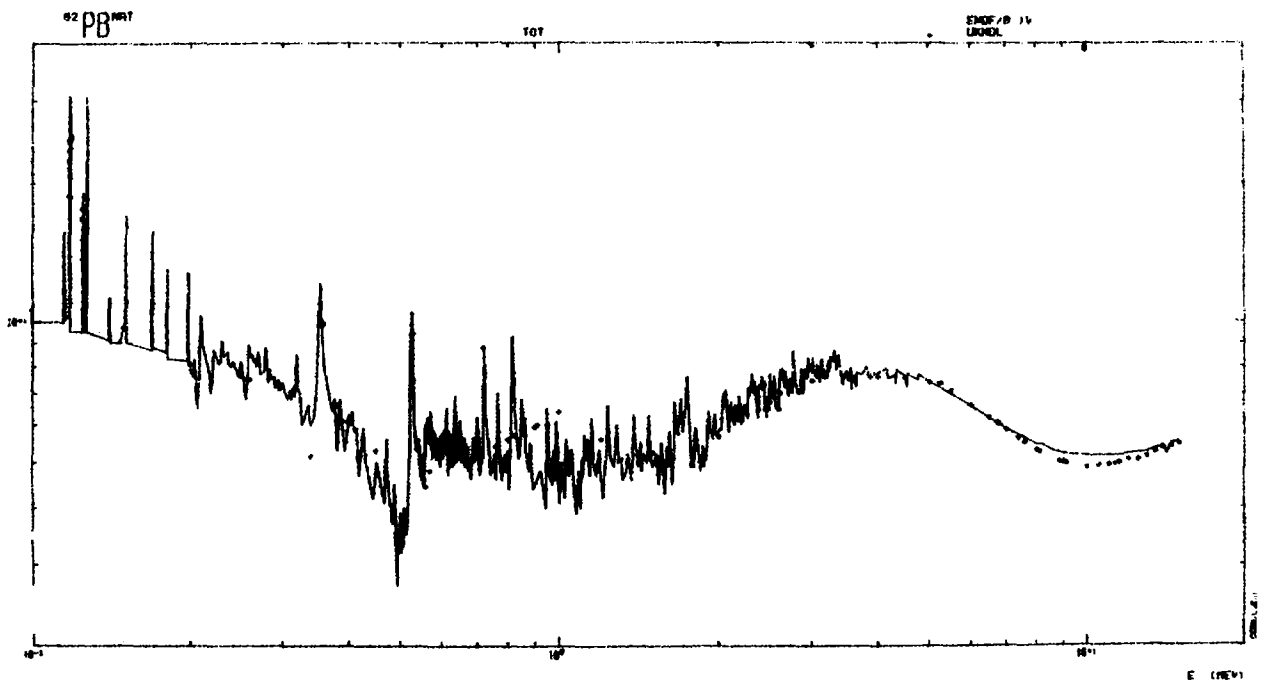

Figure 64.

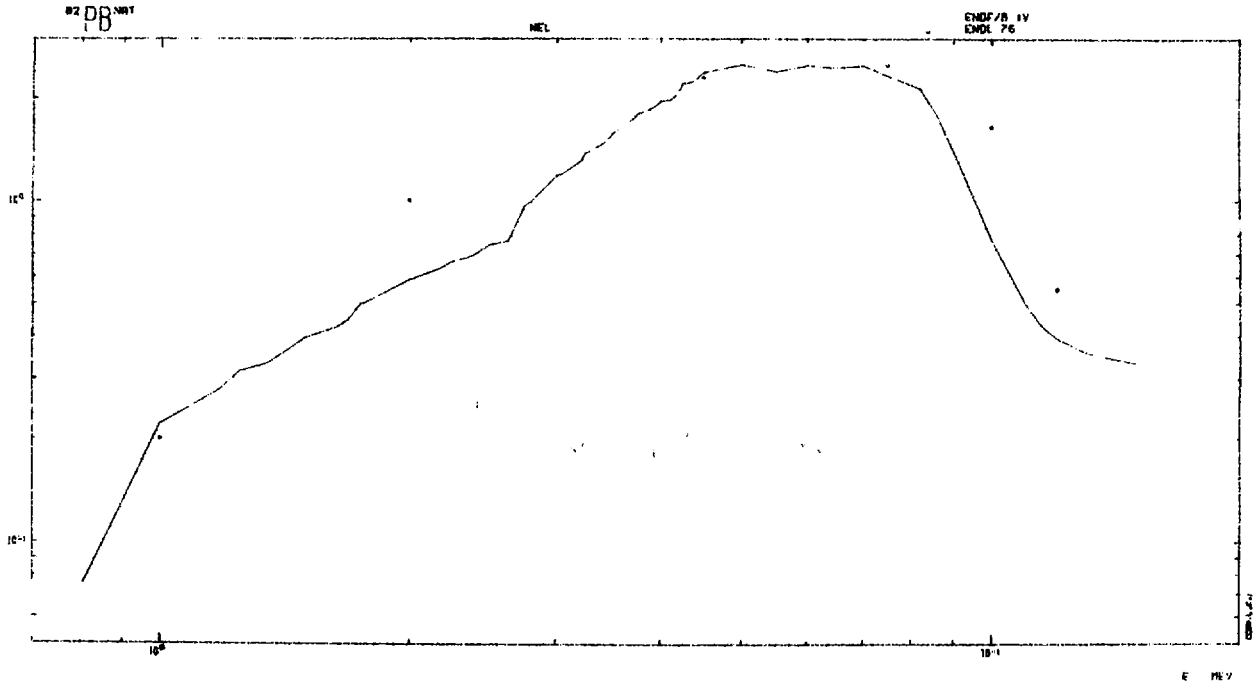

Figure 65.

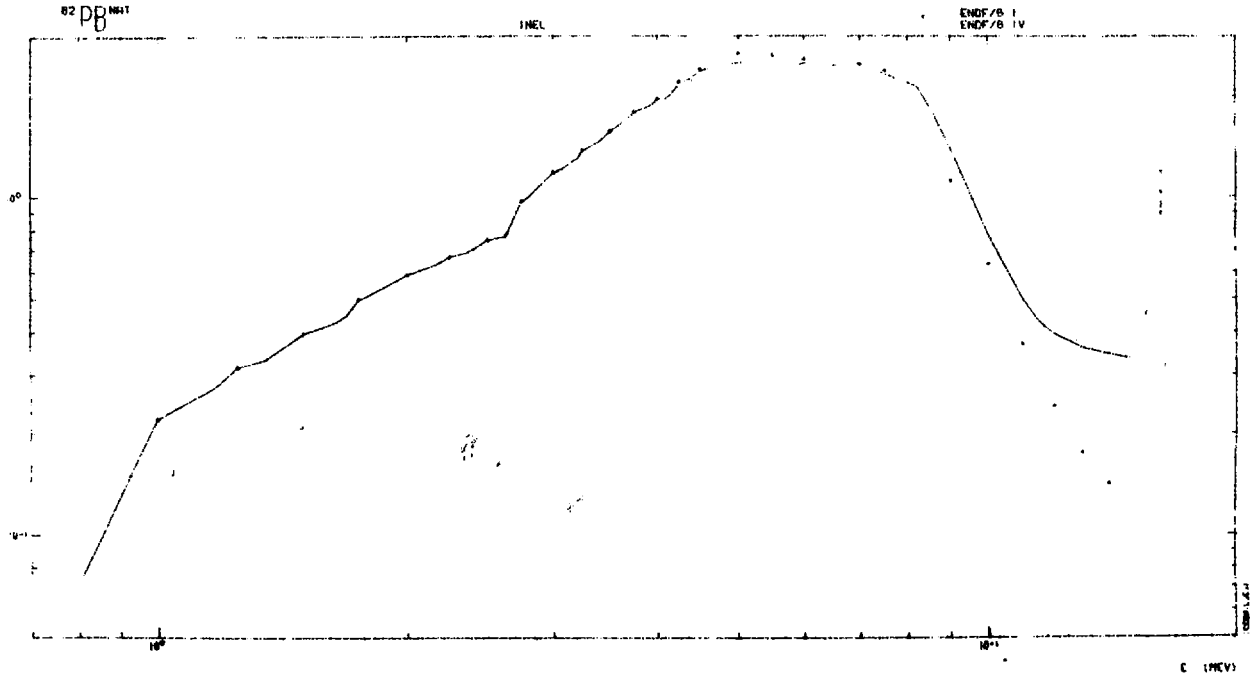

Figure 66.

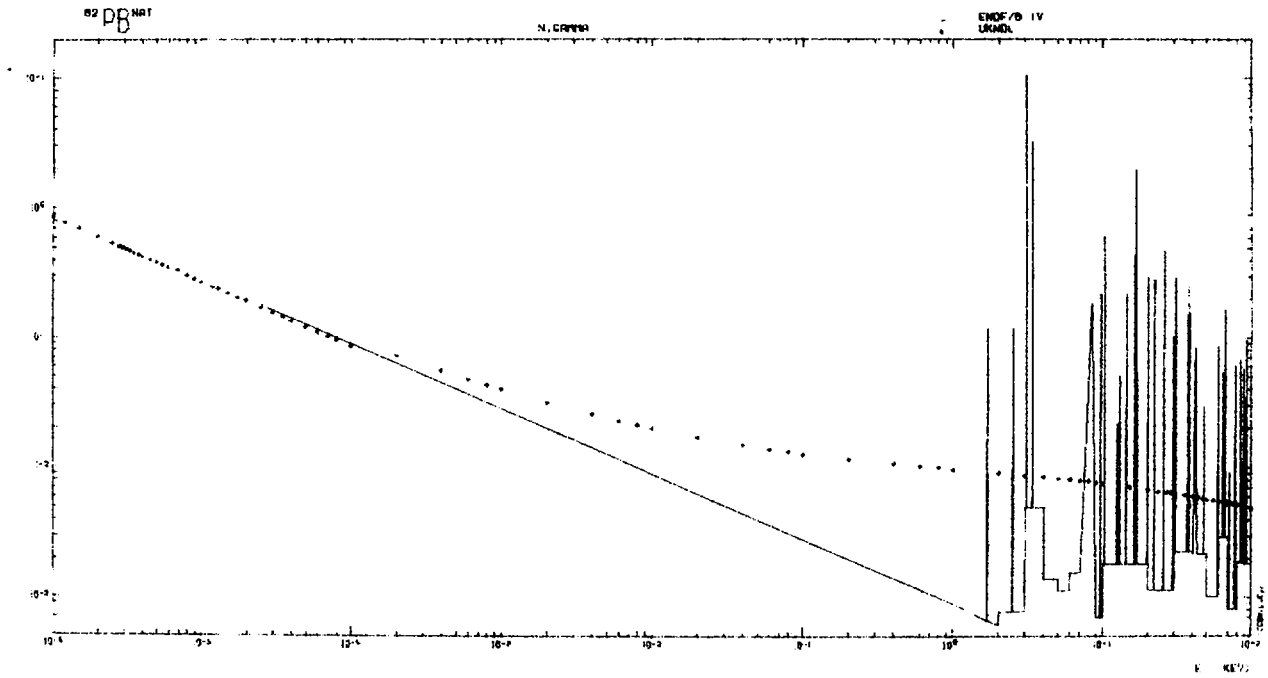

Figure 67.

International Nuclear Data Activities Related to Shielding Calculations

R. F. Lessler, NDS, IAEA

Abstract

The paper summarizes international nuclear data activities and provides information on the requested data needed for shielding calculations, for specific nuclides, the energy range of interest, the desired accuracy and priority which has been identified.

An international cooperative effort of national and regional nuclear data centers and laboratories exists as a result of the increasing demand for better and more accurate neutron nuclear data. This effort is being carried out by the following four neutron data centers:

- The National Neutron Cross Section Center (NNCSC) at Brookhaven National Laboratory in the United States which services the United States and Canada;
- The Neutron Data Compilation Center (CCDN) of NEA at Saclay, France, which essentially services Western Europe and Japan;
- The Nuclear Data Center (CJD) at Obninsk, USSR, which services the Soviet Union;
- The Nuclear Data Section (NDS) of the International Atomic Energy Agency which services the remaining countries of the world: Eastern Europe (except USSR), Asia (except Japan), Africa, Central and South America, Australia and New Zealand.

The data centers function is to bridge the information gap between the data users, such as those of you here at this meeting, and the data producers. This includes finding out who needs what data, collecting the data, evaluating the data, presenting the data in a form convenient to the users, obtaining feedback from the users, stimulating measurements where the data is insufficient for the users, reviewing data discrepancies, and other similar activities. To accomplish these functions, meetings are organized, data activities are coordinated computerized systems are operated and data files are maintained.

The following are some of the activities of the nuclear data community which are of interest to the shielding community:

CINDA (Computer Index to Neutron Data)

Bibliographic references to measurements, calculations, reviews and evaluations of neutron cross sections and other microscopic neutron data are

compiled by the four neutron data centers and stored in CINDA (Computer Index to Neutron Data). The content and format of CINDA is tailored to the needs of the nuclear science community and presents up-to-date information to all scientists interested in neutron physics. As of April 1976 the CINDA master file which is maintained at the CCDN center at Saclay contained about 115,000 entries.[1]

EXFOR (Computerized Exchange Format)

The four neutron data centers share the responsibility to collect, compile and disseminate experimental neutron data and exchange them in a common computer-compatible format. The data storage and retrieval system, EXFOR, developed for this purpose has about 1.7 million experimental data points, distributed among some 1600 entries in its file, where each entry corresponds to a single experiment or set of experiments performed in a laboratory by a research group.[2]

Evaluated Data

In the past, comprehensive computer files of evaluated neutron data have been developed and are continuously being updated in the United States (ENDF/B, Evaluated Nuclear Data File B), UK (UKNDL, the UK Nuclear Data Library), the Federal Republic of Germany (KEDAK, the Karlsruhe Evaluated Nuclear Data File), and the USSR (SOKRATOR library). In addition, a number of nuclear data libraries for special nuclides and purposes have been developed in several countries. Dr. Edvardson will present an interesting comparison between some of these files in his paper.

WRENDA (World Request List for Nuclear Data)

The IAEA has published annually a list of requirements for non-existent or improved nuclear data needed for nuclear energy programs from input provided on a world-wide basis by the four neutron data centers. The recently published 1976 edition of this list, WRENDA 76/77, consists of three parts: a fission reactor development list containing 1194 data requests; a fusion reactor development list containing 528 data requests, and a nuclear safeguards and accountability development list containing 150 data requests.[3]

The list of each individual request provides information on the requested data of the specific nuclide, the energy range of interest, the desired accuracy

and priority, the origin and justification of the request, and the status of work being performed on the requested data.

WRENDA provides useful information for the planning and coordination of research programs on nuclear data, particularly for smaller countries where the IAEA has a targets and samples program which provides targets to developing countries for measuring data requested in WRENDA. In the future WRENDA will be published biannually and the scope of the compilation is expected to be enlarged.

The following table contains the requests in WRENDA 76/77 which have been identified as needed for shielding calculations. The list contains 116 entries with iron having the most requests with 14 followed by nickel with 10 and vanadium with 8.

Isotope	Cross-Section	Energy	Accuracy	Priority
^{6}Li	Differential elastic	1–15 Mev	10 %	2
		1 Kev – 15 Mev	20 %	3
		4–15 Mev	10 %	2
	Total photon production	9–15 Mev	15 %	2
	Double differential n-emission	15 Mev	20 %	2
	N, ND	15 Mev	10 %	2
		15 Mev	10 %	1
^{7}Li	Differential elastic	1–15 Mev	10 %	1
	Inelastic	5–15 Mev	10 %	2
		15 Mev	15 %	1
	Total photon production	9–15 Mev	15 %	1
	N, NT	10–15 Mev	15 %	1
^{9}Be	Differential elastic	1–15 Mev	10 %	2
		2–15 Mev	10 %	2
	Inelastic	15 Mev	15 %	2
	Double differential inelastic	8–15 Mev	10 %	2
	Photon production in inelastic scattering	8–15 Mev	10 %	2
	Total photon production	3–15 Mev	15 %	2
	N, α	5 Kev – 10 Mev	2–3 %	1
^{14}N	Differential elastic	1–15 Mev	20 %	2
	Neutron emission	4–15 Mev	20 %	2
	N, P	1 Kev – 15 Mev	10 %	2
^{15}N	N, P	15 Mev	30 %	2
^{16}O	Differential elastic	8–14 Mev	10 %	2
	Total photon production	1 Kev – 15 Mev	10 %	2
	Total	5 Kev – 10 Mev	10 %	1
^{19}F	Inelastic	1–15 Mev	10 %	1
		1–15 Mev	15 %	2

Isotope	Cross-Section	Range	Accuracy	Priority
	Double differential inelastic	1–15 Mev	20 %	1
	Photon production in inelastic scattering	1–15 Mev	20 %	1
	Total photon production	0,5–15 Mev	15 %	2
^{23}Na	Energy differential inelastic	2–10 Mev	10 %	2
	Capture	5 Kev – 10 Mev	44–50 %	1
Al	Neutron emission	0,5–15 Mev	15 %	2
Si	Neutron emission	0,5–15 Mev	15 %	2
^{31}P	N, P	15 Mev	5–10 %	2
S	Total	10 Kev – 500 Kev	3 %	2
	Capture	10 Kev – 500 Kev	10 %	2
	Capture photon spectrum	10 Kev – 500 Kev	15 %	2
^{36}A	N, P	0,25 millielectron volts – 15 Mev	30 %	2
^{40}A	N, P	15 Mev	20 %	2
Ca	Elastic	1–15 Mev	15 %	3
	Total	1 Kev – 0,5 Mev	3–4 %	2
	Neutron emission	0,5–15 Mev	15 %	2
	Differential elastic	1–15 Mev	15 %	3
	Capture	1 Kev – 500 Kev	10 %	2
		25 millielectron volts – 15 Mev	15 %	3
Ti	Inelastic	3–14 Mev	10 %	3
	Total photon production	10 Kev – 16 Mev	20 %	1
	N, 2N	14 Mev	10 %	3
V	Elastic	2–15 Mev	10 %	1
	Inelastic	3–14 Mev	10 %	2

Isotope	Cross-Section	Range	Accuracy	Priority
	Energy differential inelastic	1,5–10 Mev	15 %	3
		2–15 Mev	15 %	1
	Capture	1 Kev – 2 Mev	15 %	1
		14 Mev	15 %	1
	Total photon production	0,3–15 Mev	15 %	1
	N, 2N	14 Mev	10 %	2
Cr	Differential elastic	2–16 Mev	20 %	2
	Inelastic	3–14 Mev	10 %	3
	Total production	1 Kev – 15 Mev	10 %	2
	Neutron emission	2–14 Mev	10 %	2
	Total photon production	15 Mev	10 %	2
Fe	Differential elastic	7–14 Mev	9 %	1
		0,5 – 3 Mev	5 %	1
		8–15 Mev	10 %	2
	Inelastic	3–14 Mev	10 %	2
	Energy differential inelastic	0,85–2 Mev	5 %	1
		2 – 5 Mev	10 %	2
		8–15 Mev	20 %	2
	Double differential inelastic	10 Mev	5–10 %	3
	Capture	1 millielectron volts – 1 Mev	10 %	2
	Total photon production	25 millielectron volts – 10 Mev	>15 %	1
		1 Kev – 15 Mev	10 %	2
		0,1 Kev – 15 Mev	15 %	2
	Neutron emission	50 Kev – 15 Mev	15 %	2
	Total	10 Kev – 1 Mev	5 %	2
Ni	Total	1 Kev – 20 Mev	3 %	2
	Differential elastic	1,5–14 Mev	9 %	1
		1,5 – 3 Mev	15 %	2
		8–15 Mev	20 %	2
		8–15 Mev	20 %	2
	Total photon production	25 millielectron volts – 0,3 Mev	20 %	1
		2–14 Mev	20 %	2
		1 Kev – 15 Mev	10 %	2
		25 millielectron volts – 10 Mev	20 %	2
	Neutron emission	2–15 Mev	10 %	2

Isotope	Cross-section	Energy	Accuracy	Figure
Cu	Elastic	8–15 Mev	10 %	2
	Photon production in inelastic scattering	15 Mev	15 %	2
	Total photon production	0,5–15 Mev	15 %	2
Zr	Elastic	5–15 Mev	10 %	2
	Energy differential inelastic	15 Mev	15 %	2
	Total photon production	15 Mev	15 %	2
^{93}Nb	Differential elastic	3–15 Mev	10 %	1
	Inelastic	15 Mev	10 %	2
	Energy differential inelastic	15 Mev	15 %	1
	Total photon production	15 Mev	15 %	1
Mo	Differential elastic	3–15 Mev	10 %	1
	Inelastic	3–14 Mev	10 %	3
	Energy differential inelastic	1,5–3 Mev 15 Mev	20 % 15 %	3 1
	Total photon production	25 millielectron volts – 15 Mev	15 %	1
^{135}Xe	Total photon production	25 millielectron volts	10–20 %	2
W	Inelastic	3–14 Mev	10 %	3
	Total photon production	1 Kev – 1 Mev	20 %	2
Pb	Total photon production	1 Kev – 16 Mev	10 %	2
		25 millielectron volts – 15 Mev	15 %	2
		25 millielectron volts – 15 Mev	15 %	2
	Neutron emission	2–16 Mev	5 %	2
		0,5–16 Mev	10 %	2
^{209}Bi	Total photon production	25 millielectron volts – 15 Mev	15 %	2
Fission products	Inelastic	0,8–5 Mev	13–30 %	1
	Capture	5 Kev – 10 Mev	7–48 %	1

Isotope	Cross-Section	Energy	Accuracy	Priority
Steel	Capture	5 Kev – 10 Mev	11–20 %	1
^{235}U	Total photon production	1 Kev – 15 Mev	10 %	1
^{238}U	Total photon production	1 millielectron volts – 15 Mev	10 %	2

REFERENCES

1. CINDA 76/77, An Index to the Literature on Microscopic Neutron Data, IAEA, Vienna (June 1976)

2. Lorenz, A., The IAEA Nuclear Data Centre, Its Role in the International Scientific Community, INDC (NDS)-76/LN, IAEA, Vienna (July 1976)

3. WRENDA 76/77, World Request List for Nuclear Data, R. M. Lessler, Editor, INDC (SEC)-55, IAEA, Vienna (August 1976).

SESSION E

REVIEW OF PROGRESS WITH BENCHMARK EXPERIMENTS: FISSION AND FUSION SOURCE SPECTRUM

RESULTATS EXPERIMENTAUX DANS HARMONIE ET TAPIRO

SUR LA PROPAGATION DES NEUTRONS DANS LES MELANGES Fe-Na.

F.BOUTEAU, D.CALAMAND, Y.OCERAIES, R.VIENOT*
D.ANTONINI, L.BOZZI, M.MARTINI, P.MOIOLI**

RESUME

Ce papier présente les résultats d'expériences de propagation de neutrons dans des mélanges fer-sodium utilisant les réacteurs source HARMONIE et TAPIRO.

Avec HARMONIE, cinq milieux ont été étudiés : sodium pur, fer pur, mélanges fer-sodium de concentrations volumiques respectives (30%-70%), (50%-50%), (70%-30%).

Deux types de résultats sont présentés :

- résultats bruts des mesures
- facteur de correction d'hétérogénéités et de fuite permettant de convertir les résultats bruts en des résultats correspondant à une expérience idéale en géométrie sphérique et milieux homogènes.

Enfin, une comparaison est faite entre les résultats obtenus à HARMONIE et TAPIRO dans le cas du sodium pur ; le but de cette comparaison est de vérifier si les différences de géométrie et de spectre de source sont correctement traitées dans les calculs.

* CEA/ CEN CADARACHE

** CNEN / CASACCIA

ABSTRACT

The results of neutron-propagation experiments performed in iron-sodium mixtures, using the source reactor HARMONIE and TAPIRO are presented :

- with HARMONIE : five media were studied : pure sodium and pure iron, and mixtures of iron and sodium (30 V/o, 50 V/o, 70 V/o) ;

- with TAPIRO the presently available results concern a pure sodium medium ;

Two types of results are given :

- first, the raw results;

- then, the correction factors for heterogeneity and leakage to convert the raw results into the ideal homogeneous and spherical model used in the calculations.

Finally, a comparison is made between results obtained with HARMONIE and TAPIRO for the pure sodium ; the aim of this comparison is to verify that the differences in geometry and source spectra are properly accounted for the calculations.

I - INTRODUCTION

Les mélanges acier-sodium constituent l'essentiel des protections neutroniques d'un réacteur rapide de puissance tel que SUPER-PHENIX. Un programme d'expériences intégrales de propagation dans de tels mélanges est conduit d'une part au CEA sur le réacteur source HARMONIE, d'autre part au CNEN sur le réacteur source TAPIRO, dans le but d'ajuster le formulaire de calcul des protections neutroniques.

Cette communication présente les résultats obtenus jusqu'ici sur les deux installations, concernant des mélanges fer-sodium ainsi que du fer pur et du sodium pur.

II - EXPERIENCES EFFECTUEES SUR LE REACTEUR SOURCE HARMONIE

II-1/1. ASSEMBLAGE SODIUM

Le sodium pur (20°C) est contenu dans un réservoir d'acier dont l'ensemble forme un cube de 3 mètres de côté. Les mesures sont effectuées dans la cuve centrale, dans 6 canaux horizontaux disposés en colimaçon (voir schéma 1).

L'ensemble est entouré d'une protection de bois de 30 cm d'épaisseur pour éviter le retour des neutrons qui ont quittés le système et constitueraient une source parasite.

II-1/2. ASSEMBLAGE FER-SODIUM

Chaque assemblage est constitué de deux cuves :

- 1 cuve inférieure qui contient le mélange fer-Na dont on fait varier les proportions : un réseau vertical de rondins de fer, de différents diamètres, sont disposés en un réseau au pas triangulaire de 165 mm et noyés dans le sodium. Cette cuve a 1 mètre de hauteur et 1 m de dimensions latérales.

1 cuve supérieure de 1,5 mètre de hauteur qui contient le sodium pur.

Les mélanges Fer-Na étudiés correspondent aux proportions ci-dessous (en volume)

Fer	27.1 %	47.7 %	70.4 %
Na	72.9 %	52.3 %	29.6 %

Les canaux de mesure sont de deux types :

- dans la cuve de sodium, des doigts de gant de faible diamètre dans lequels on introduit une chaussette de mesure

- dans la cuve fer-sodium, une chaussette centrale où l'on reconstitue exactement le pourcentage Fer-Na de l'assemblage étudié.

Les mesures axiales se font dans un trou central de 60 mm de diamètre au moyen d'un train de containers de sodium porte-détecteurs.

Dans la cuve supérieure de sodium, un canal vertical et deux canaux horizontaux permettent des mesures axiales et radiales.

L'ensemble des deux cuves est entouré de la protection de bois.

II-1/3. ASSEMBLAGE Fer

Il s'agit de la colonne intermédiaire du réacteur HARMONIE constituée d'un assemblage de blocs de fer de 1.77 m de long pour 1.20 x 1,50 mètre de section et entourée latéralement de protection bétons lourds.

Les mesures sont faites dans un canal longitudinal de section carrée (10 x 10 cm) et dans quatre canaux cylindriques (Ø 10 cm) disposés tous les 40 cm. Tous les canaux peuvent être obturés par des bouchons de fer.

II-1/4. PRECISIONS DES MESURES

Actuellement la précision des mesures avec les détecteurs par activation sont :

- Détecteurs Na et Mn/Cd : $\pm$ 5% sur toute la longueur de l'assemblage.

- Détecteurs Rhodium : $\pm$ 10% en début de massif, $\pm$ 25% en fin de massif lorsque les taux de comptage deviennent faibles.

- Détecteurs Soufre : $\pm$ 10% en début de massif, $\pm$ 25% en fin de massif .

Les détecteurs Na sont constitués par des disques de diamètre 18 mm et 2 à 5 mm d'épaisseur.

Les détecteurs Mn et Mn/Cd sont des disques de 1 à 3 cm de diamètre et de 0.1 à 0.5 mm d'épaisseur.

Les détecteurs Rhodium sont des disques de 1 à 3 cm de diamètre et 0.1 à 0.5 mm d'épaisseur.

Les détecteurs de Soufre sont compactés en bloc de quelques grammes à 300 g d'épaisseur : 3 à 6 cm.

II-2/ RESULTATS

Pour les détecteurs Na et Mn/Cd les résultats sont exprimés en flux thermique équivalent :

$$\phi_{th\ eq} = \frac{1}{\sigma_o} \int_0^\infty \sigma\ (E)\ \Psi\ (E)\ dE \qquad \sigma_0 = \text{section à 2200m/S}$$

Pour les détecteurs Rhodium et Soufre, ils sont exprimés en flux de fission équivalent.

$$\phi_{f\ eq} = \frac{1}{\sigma_f} \int_0^\infty \sigma(E)\ f\ (E)\ dE$$

avec $$\bar{\sigma}_f = \int_0^\infty \sigma\ (E)\ \chi\ (E)\ dE$$

On présente à la fois les résultats expérimentaux bruts, ainsi que les facteurs de correction d'hétérogénéité et de fuite définis au paragraphe II/2.2. Par ailleur, on ne retient pas les points de mesure trop proches des frontières entre milieux.

II-2/1. RESULTATS BRUTS

Les tableaux I et II présentent les résultats (en terme de flux) pour les différents assemblages et les divers détecteurs.

Les tableaux III et IV présentent les résultats en terme d'atténuation (rapport des flux relevés en diverses positions).

On constate une certaine saturation du pouvoir atténuateur lorsque le pourcentage de Fer dépasse 50% dans le mélange.
En effet pour le détecteur Na et pour une distance de propagation de 73,5 cm, l'atténuation croît d'un facteur 1.8 quand le pourcentage de Fer passe de 27 à 48 % puis seulement d'un facteur 1.16 lorsque ce pourcentage croît de 48 à 73%.

Il en est de même pour le détecteur Mn/Cd.

Pour le Soufre, l'atténuation croît exponentiellement avec le pourcentage de Fer ; l'efficacité du fer pour les neutrons rapides est donc la même quelque soit son pourcentage dans le mélange.

Pour le Rodhium, il en est de même.

II-2/2. RESULTAT CORRIGES

Les facteurs de correction d'hétérogénéité et de fuite permettent de convertir les résultats bruts en des résultats correspondant à une expérience idéale en géométrie sphérique et milieux homogènes. Ils sont définis par le rapport :

$$K = \frac{\text{Calcul monodimensionnel sphérique (homogène)}}{\text{Calcul bidimensionnel (R,Z) (hétérogène)}}$$

- Pour les massifs Fer-Na, ils ont été calculés au CEA.

- Pour la cuve de Na, ils ont été calculés au CNEN/CASACCIA /Réf 2 /.

- Pour l'assemblage Fer, le coût prohibitif d'un calcul DOT représentatif de la géométrie (26 groupes, 5400 mailles) nous a fait renoncer à poursuivre les calculs. Il semble toutefois

/Réf 3 / que, au moins pour les détecteurs Rh et S cette correction soit faible (de l'ordre ou inférieure à 10%) ; les calculs n' ayant pas été poursuivis pour les détecteurs thermiques.

Le tableau V présente ces facteurs correctifs ; indiquons que pour l'assemblage Na il s'agit seulement du facteur de fuite.

On notera l'importance de ces facteurs à partir de l'interface entre les 2 cuves Fer-Na et sodium, en particulier pour les détecteurs Na et Mn/Cd.

Les figures 1 à 8 présentent les résultats bruts ainsi que corrigés pour les massifs Fer-Na et la colonne Fer.

III - EXPERIENCE EFFECTUEE SUR LE REACTEUR TAPIRO : MASSIF DE SODIUM PUR

Le massif de sodium est constitué de deux cuves en aluminium, remplies de sodium pur. Les dimensions de chacune des cuves sont 1 x 1 x 1 m. Le fond de cuve s'adapte à la surface semi-cylindrique du réflecteur de cuivre du réacteur. L'ensemble est placé dans la cavité aménagée dans la protection du réacteur TAPIRO (schéma 2).

Les canaux de mesures sont remplis durant les irradiations de cylindres d'aluminium, de manière à assurer un positionnement exact des détecteurs et à réduire au minimum les perturbations de flux.

III-1/ PRECISION DES MESURES

Les comptages sont effectués en double sur 2 installations différentes. On admet que la précision, en relatif, pour chaque point de mesure est égale à la déviation standard σ enregistrée soit :

1% pour les détecteurs Au, Mn, Na, ^{235}U.

4% au début, 5% pour le point le plus éloigné, pour le Rh.

5% au début 10% pour le point le plus éloigné, pour le Soufre.

L'erreur de pesée est négligeable, de l'ordre de 10^{-4}.

III-2/ RESULTATS TAPIRO- facteurs correctifs - Comparasion TAPIRO/HARMONIE

Ils sont présentés en terme d'atténuation dans le tableau VI. Les positions 1 à 5 correspondent aux mêmes distances de pénétration que dans la cuve Na d'HARMONIE.

positions 1 : 18.5 cm
2 : 32
3 : 52
4 : 92
5 : 127

III-2/1. FACTEURS CORRECTIFS

Deux séries de facteurs correctifs de géométrie ont été calculés /tableaux 9, 10/ /12/ selon 2 modèles de calcul différents :

k 1 : calcul monodimensionnel sphérique ANISN
calcul bidimensionnel R Z DOT III

k 2 : calcul monodimensionnel plaque ANISN
calcul bidimensionnel RZ DOT III

Les résultats du tableau, dans la colonne "valeurs corrigées de fuite" ainsi que les valeurs représentées sur les courbes 9 à 13, sont corrigées du facteur k1.

On trouve une deuxième correction portée dans la colonne "valeurs corrigées de fuite et de spectre" c'est une correction de spectre destinée à tenir compte, pour les résultats de TAPIRO, de la différence de spectre de source à l'entrée du massif. Le tableau VII met en évidence cette différence de spectre.

Ces 2 corrections permettent de convertir les résultats d'HARMONIE et de TAPIRO au même modèle 1D sphérique avec source d'entrée HARMONIE.

III-2/2. COMPARAISON TAPIRO-HAMONIE

Elle a pour but de tester la validité du calcul des facteurs correctifs dus aux différences de géométrie et de spectre de source.

On peut remarquer que ces facteurs correctifs en particulier ceux de fuite sont assez importants et que de plus ceux de TAPIRO (en géométrie sphérique) sont supérieurs d'un facteur 2 à ceux d'HARMONIE * (tableaux 9 et 5).

Les atténautions corrigées de ces 2 assemblages sont comparées au tableau 6.

Les désaccords sont importants et largement en dehors des marges d'erreurs expérimentales en particulier pour les réponses de basse énergie : Na et Mn.

Ces désaccords montrent que les méthodes de calcul correctif ne sont probablement pas encore satisfaisantes.

*En fait pour TAPIRO le modèle 1 dimension le plus adapté est le modèle plan. En effet les facteurs correctifs pour ce modèle sont beaucoup plus faible (voir tableaux 8 et 9).

IV - CONCLUSION

Dans les milieux Fer-Na, on observe que l'atténuation présente une certaine saturation lorsque le pourcentage de Fer dépasse 50% (en volume) ; celà justifie les choix faits pour la PNL de SUPER-PHENIX.

Les résultats obtenus sur HARMONIE et TAPIRO doivent servir à effectuer un premier ajustement du formulaire de propagation PROPANE. Cependant, les résultats obtenus sur les deux installations dans le massifs de Na pur ne sont pas tout à fait cohérents, et cela est attribué au mauvais calcul des facteurs correctifs permettant de tenir compte des

différences de géométrie et de spectre de source. L'effort est consacré à la suppression de cette incohérence, avant de passer au stade de l'ajustement.

/ REFERENCES /

/1/ Y.OCERAIES,P.CAUMETTE,C.DEVILLERS - Utilisation des expériences intégrales pour améliorer les calculs de propagation de neutrons et d'échauffements gamma.
International Symposium on Physics of Fast Reactors, TOKYO 1973 - A.24

/ 2/ M.SALVATORES - Communication privée.

/ 3/ C.DEVILLERS - Communication privée.

/ 4 / L.BOZZI,M.MARTINI,M.MOIOLI - Confronto HARMONIE-TAPIRO. RIT/FIS-LNS(76)

/ 5 / J.C.ESTIOT,J.P.TRAPP,M.SALVATORES,G.PALMIOTTI - Interprétation des expériences de propagation dans des mélanges Fer-Na avec le formulaire PROPANE O. Communication à la réunion de VIENNE, oct. 76

TABLEAU I

RESULTATS HARMONIE — PUISSANCE HARMONIE : 2 Kw

RESULTATS BRUTS. DETECTEURS Na ET Mn/Cd — ϕ_{theq} en $(n/cm^2/sec)$

	Cotes	Na					Mn/Cd				
	(cm)	Na pur	Fer 27% Na 73%	Fer 48% Na 52%	Fer 70% Na 30%	Fer pur	Na pur	Fer 27% Na 73%	Fer 48% Na 52%	Fer 70% Na 30%	Fer pur
Position 1	71.5	$8.4\ 10^7$	$1.15\ 10^8$	$1.08\ 10^8$	$8.7\ 10^7$	$1\ 10^8$	$2.75\ 10^8$	$3.04\ 10^8$	$3\ 10^8$	$1.86\ 10^8$	$1.05\ 10^8$
2	85	6.8 -	$7.7\ 10^7$	$6.9\ 10^7$	5.5 -	$5.3\ 10^7$	2.3 -	2.4 -	1.87 -	1.18 -	$6\ 10^7$
3	105	4.85 -	4.8 -	3.5 -	2.4 -	2.2 -	1.6 -	1.3 -	$8.45\ 10^7$	4.99 -	2.5 -
4	145	2.35 -	1	$5.2\ 10^6$	$3.6\ 10^6$	$3.6\ 10^6$	$6.9\ 10^7$	$2.8\ 10^7$	1.26 -	$6.3\ 10^6$	$4.5\ 10^6$
5	180	1.2 -	$4\ 10^6$	1.3 -	1.4 -	$7.6\ 10^5$	$3\ 10^7$	$6.6\ 10^6$	$3.2\ 10^6$	2.05 -	$9.5\ 10^5$
6	220	$5.5\ 10^6$	1.34 -	$6.8\ 10^5$	$5.95\ 10^5$		1.1 -	2.4 -	1.3 -	1.25 -	
7	260	2.2 -	$5.4\ 10^5$	2.3 -	2.3 -		$3.55\ 10^6$	$6.9\ 10^5$	$3.9\ 10^5$	$3\ 10^5$	
8	300	$8.3\ 10^5$	1.64 -	$7.5\ 10^4$	$8.2\ 10^4$		1.3 -	1.7 -	$9.3\ 10^4$	$7.5\ 10^4$	

- Pour les méalnges Fer-Na, le trait horizontal indique la frontière entre le mélange Fer-Na et le Sodium pur.
- Les cotes sont comptées à partir du centre d'HARMONIE.

TABLEAU II

RESULTATS HARMONIE

Puissance HARMONIE : 2 Kw

ϕ_f équivalent $(n/cm^2/sec)$

RESULTATS BRUTS : RODHIUM ET SOUFRE

	Cotes (cm)	Détecteur : Rhodium					Détecteur : Soufre				
		Na pur	Fer 27% Na 73%	Fer 48% Na 52%	Fer 70% Na 30%	Fer pur	Na pur	Fer 27% Na 73%	Fer 48% Na 52%	Fer 70% Na 30%	Fer pur
Position 1	71.5	$1.45\ 10^8$	$1.7\ 10^8$	$1.7\ 10^8$	$1.7\ 10^8$	$2.1\ 10^8$	$2.05\ 10^6$	$1.82\ 10^6$	$1.76\ 10^6$	$8\ 10^5$	
2	85	$5.9\ 10^7$	$5.44\ 10^7$	$5.2\ 10^7$	$6.3\ 10^7$	$7.7\ 10^7$	$1.01\ -$	$4.7\ 10^5$	$3.03\ 10^5$	$7.2\ 10^4$	
3	105	$1.5\ -$	$1.18\ 10^7$	$1.27\ -$	$1.45\ -$	$1.9\ 10^7$	$4.7\ 10^5$	$6.8\ 10^4$	$5.10\ 10^4$	$7.8\ 10^3$	
4	145			$3.3\ 10^5$		$1.35\ 10^6$	$4.7\ 10^4$	$4.4\ 10^3$	$1.07\ 10^3$	$1.4\ 10^2$	

- Les cotes sont comptées à partir du centre d'HARMONIE
- L'expérience fer consignée ici est celle réalisée en 1975.

TABLEAU III

RESULTATS HARMONIE MESURES BRUTES ATTENUATIONS

	DETECTEURS Na					DETECTEURS Mn/Cd				
	Na pur	Fer 27% Na 73%	Fer 48% Na 52	Fer 70% Na 30%	Fer pur	Na pur	Fer 27% Na 73%	Fer 48% Na 52%	Fer 70% Na 30%	Fer pur
Position 1/3	1.73	2.40	3.09	3.63	4.55	1.72	2.34	3.55	3.72	4.2
Position 1/4	3.57	11.5	20.77	24.17	27.78	4	10.86	23.8	25.9	23.6
Position 5/8	14.46	24.39	17.33	17.07		23.1	38.9	34.4	27.3	

TABLEAU IV

	DETECTEUR RODHIUM					DETECTEUR SOUFRE				
	Na pur	Fer 27% Na 73%	Fer 48% Na 52%	Fer 70% Na 30%	Fer pur	Na pur	Fer 27% Na 73%	Fer 48% Na 52%	Fer 70% Na 30%	Fer pur
Position 1/2	2.46	3.1	3.3	2.7	2.8	2.03	3.87	5.80	11.1	
Position 1/3	9.67	14.4	13.4	11.7	11.1	4.36	26.76	34.5	102.6	
Position 1/4			515.		155	43.6	414	1644	5714.	

TABLEAU V

FACTEUR CORRECTIFS D'HETEROGENEITE ET DE FUITE POUR LES MAQUETTES

Na et Fer-Na d'HARMONIE

(le trait horizontal sépare les cuves Fer-Na de la cuve Na supérieure)

x (cm)	Distance de propagation	DETECTEUR SOUFRE				RHODIUM				Mn/Cd				Na			
		Na	Fer 27% Na 73%	Fer 50% Na 50%	Fer 70% Na 30%		Fer 27% Na 73%	Fer 50% Na 50%	Fer 70% Na 30%		Fer 27% Na 73%	Fer 50% Na 50%	Fer 70% Na 30%		Fer 27% Na 73%	Fer 50% Na 50%	Fer 70% Na 30%
71.5	18.5	0.75	0.77	0.85	0.80	0.99	1.1	1.10	1.12	1.2	1.71	1.54	1.38	1.32	1.7	1.52	1.36
85	32	0.64	0.71	0.79	0.62	0.96	1.1	1.08	1.07	1.7	1.65	1.47	1.20	1.42	1.7	1.49	1.27
105	52	0.5	0.64	0.56	0.365	0.93	1.1	1.05	1.	1.335	1.54	1.36	1.17	1.54	1.59	1.42	1.15
145	92	0.32	0.296	0.295	0.085		1.1	1.04	0.92	1.37	1.43	1.25	1.24	1.66	1.43	1.26	1.11
160	107	0.29	0.208	0.29	0.055		1.240	1.06	0.90	1.375	1.60	1.52	1.44	1.75	1.65	1.63	1.25
180	127	0.235	0.29	0.302	0.033		1.37	1.06	0.91	1.38	1.94	1.84	1.66	1.895	2.14	2.04	1.60
220	167			0.323	0.042		1.33		0.96	1.40	2.32	2.7	2.49	1.71	3.44	3.25	3.11
260	207			0.349	0.044		1.41		0.99	1.435	4.40	4.12	3.64	1.71	5.22	4.88	4.41
300	247			0.38	0.035		1.50			1.465	5.61	5.23	4.96	1.69	6.58	6.05	5.55

$$K = \frac{\text{ANISN sphérique homogène}}{\text{DOT cylindrique hétérogène}}$$

TABLEAU VI

REACTEUR TAPIRO — RESULTATS DES MESURES BRUTES ET CORRIGEES

COMPARAISON HARMONIE-TAPIRO

	Na					Mn				
	Valeurs brutes	Valeurs corrigées de fuites	Valeurs corrigées de fuites et de spectre	Valeurs HARMONIE corrigées	H/T	Valeurs brutes	Valeurs corrigées de fuites	Valeurs corrigées de fuites et de spectre	Valeurs HARMONIE corrigées	H/T
1/2	1.24	1.09	1.04	1.15	1.10	1.26	1.17	1.12	1.10	.98
1/3	1.780	1.28	1.17	1.49	1.27	1.95	1.52	1.34	1.54	1.15
1/4	3.87	1.87	1.48	2.84	1.92	4.57	3.04	2.50	3.59	1.43
1/5	0					11.3	5.86	4.21	7.97	1.89
	S					Rh				
	Valeurs brutes	Valeurs corrigées de fuites	Valeurs corrigées de fuites et de spectre	Valeurs HARMONIE corrigées	H/T	Valeurs brutes	Valeurs corrigées de fuites	Valeurs corrigées de fuites et de spectre	Valeurs HARMONIE corrigées	H/T
1/2	2.39	2.78	2.78	2.37	0.85	2.46	2.7	2.7	2.53	.94
1/3						5.88	10.38	11.30	10.29	.91

TABLEAU VII

COMPARAISON DES SPECTRES CALCULES A L'ENTREE DES CUVES Na.

E Min	3 Mev	800 Kev	100Kev	1 Kev	30 ev	thermique
HARMONIE	$1.29\ 10^{-5}$	$2.19\ 10^{-3}$	.292	.478	.165	.062
TAPIRO	$4.5\ \ 10^{-5}$	$5.7\ \ 10^{-3}$	.184	.536	.221	.054

TABLEAU VIII

FACTEUR CORRECTIF POUR TAPIRO, $\frac{\text{plaque}}{RZ}$

cm dans le Na	DETECTEUR		
	Na	S	Rh
2.5	1.	1.	1.
22.5	.824	.907	1.10
27.5	.972	.891	1.14
42.5	.997	.798	1.08
57.5	1.01	.729	1.04
62.5	1.04	.710	.994
87.5	1.10	.611	.872
102.5	1.11	.556	.823
117.5	1.17	.509	.761
147.5	1.23	.417	.623
162.5	1.26	.370	.559
182.5	1.31	.321	.485
207.5	1.28		
237.5	1.26		
267.5	1.18		

TABLEAU IX

FACTEURS CORRECTIFS POUR TAPIRO $(\frac{\text{SPHERE}}{\text{RZ}})$

CM DANS LE Na	DETECTEUR		
	Na	S	Rh
2.5	1.	1.	1.
22.5	1.21	.634	.855
27.5	1.25	.580	.852
42.5	1.44	.455	.737
57.5	1.66	.376	.665
62.5	1.78	.357	.636
87.5	2.30	.282	.541
102.5	2.63	.250	.498
117.5	4.02	.225	.460
147.5	4.19	.186	.389
162.5	4.88	.166	.358
182.5	5.93	.148	.322
207.5	7.14		
237.5	8.73		
267.5	9.77		

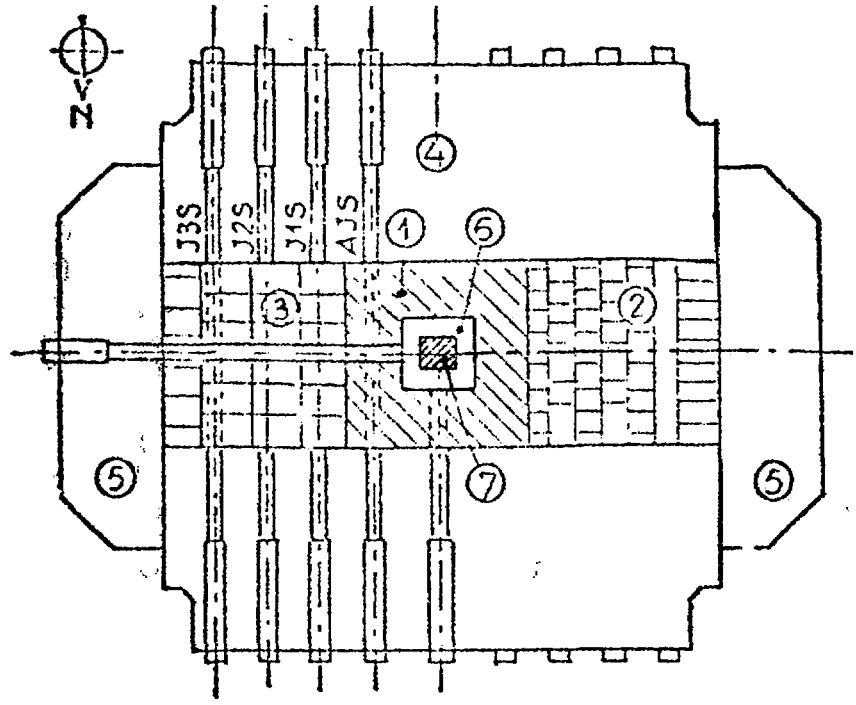

1-Bloc d'adaptation d'acier
2-Colonne Thermique
3-Colonne de Fer
4-5-Protection de béton lourd
6 -Couverture
7 -Coeur

SECTION HORIZONTALE D'HARMONIE MONTRANT LES CANAUX EXPERIMENTAUX DE LA COLONNE DE FER

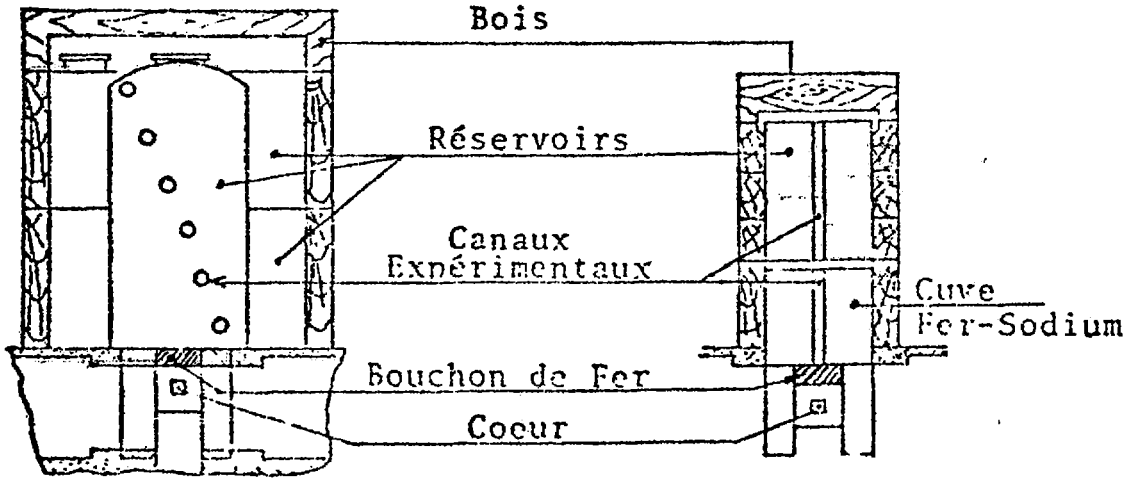

Assemblage Sodium

Assemblages Fer-Sodium

ASSEMBLAGES DISPOSÉS SUR LE REACTEUR HARMONIE

Schéma n° 1

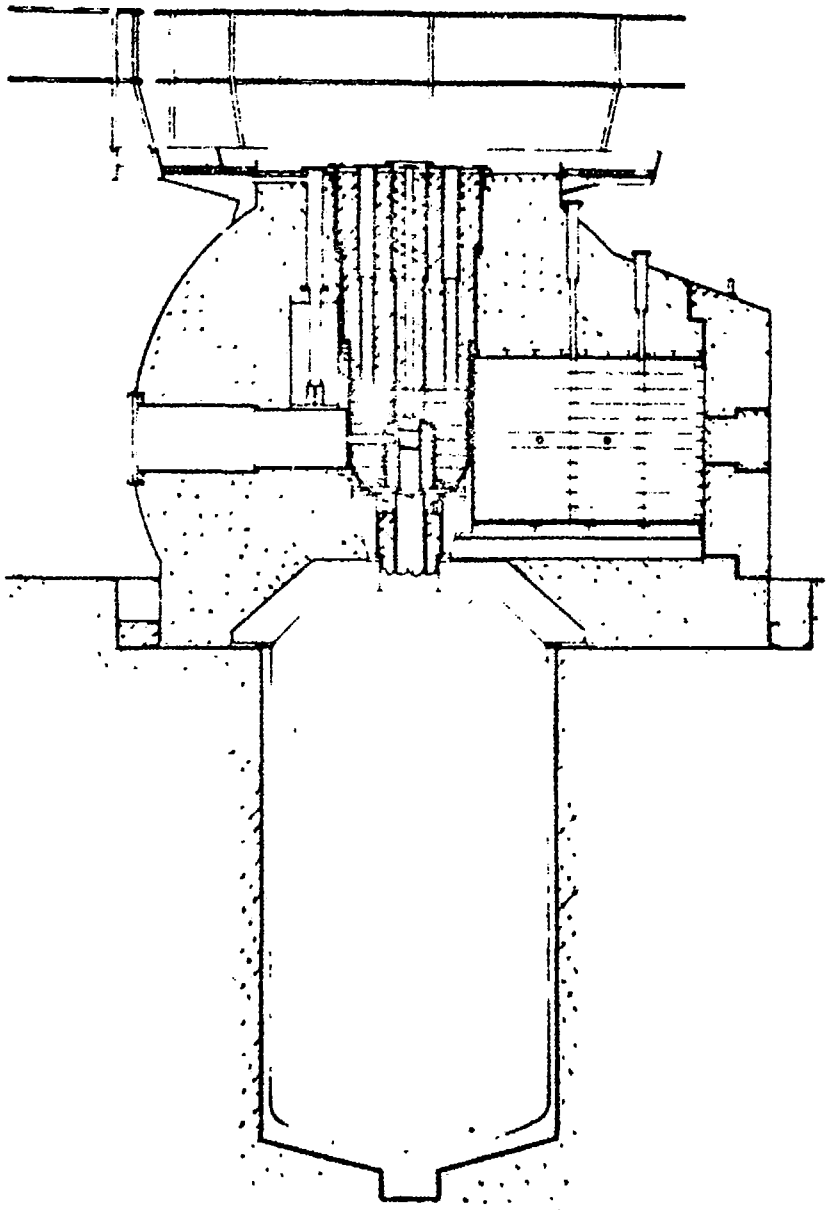

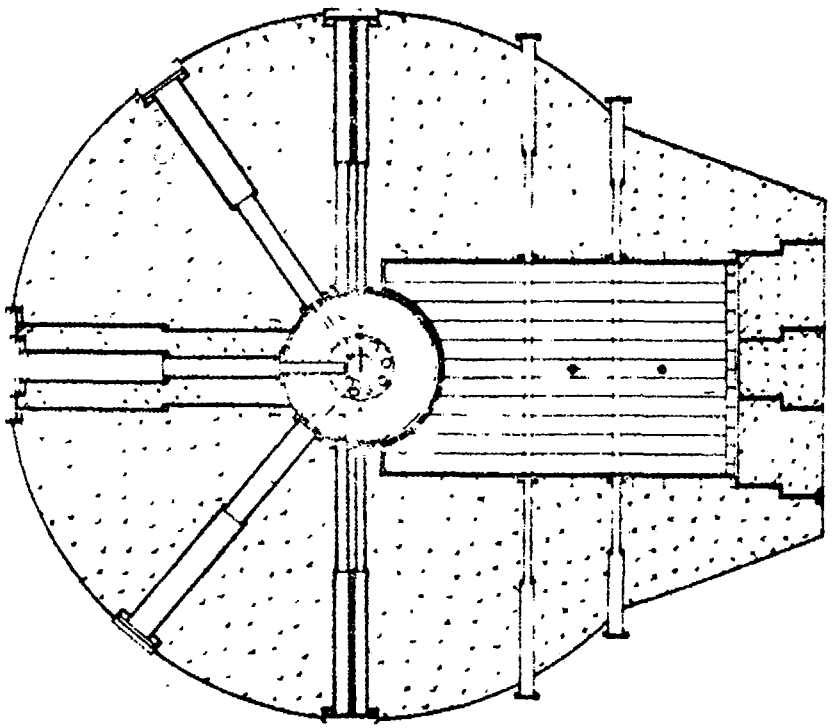

Schéma n° 2

Réacteur TAPIRO

Vue verticale et horizontale

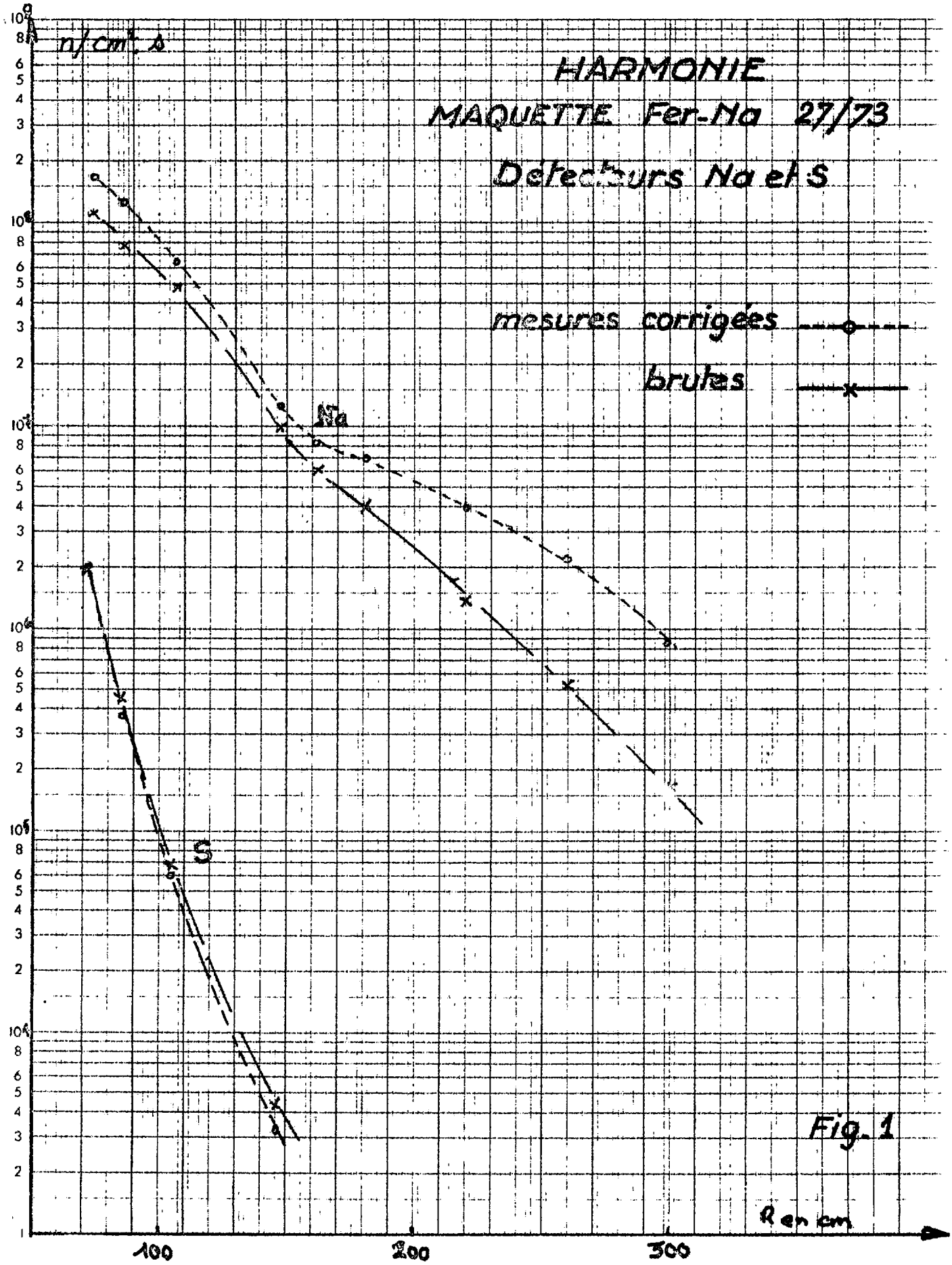
n/cm².s
HARMONIE
MAQUETTE Fer-Na 27/73
Détecteurs Na et S
mesures corrigées
brutes
Na
S
R en cm
100
200
300

Fig. 1

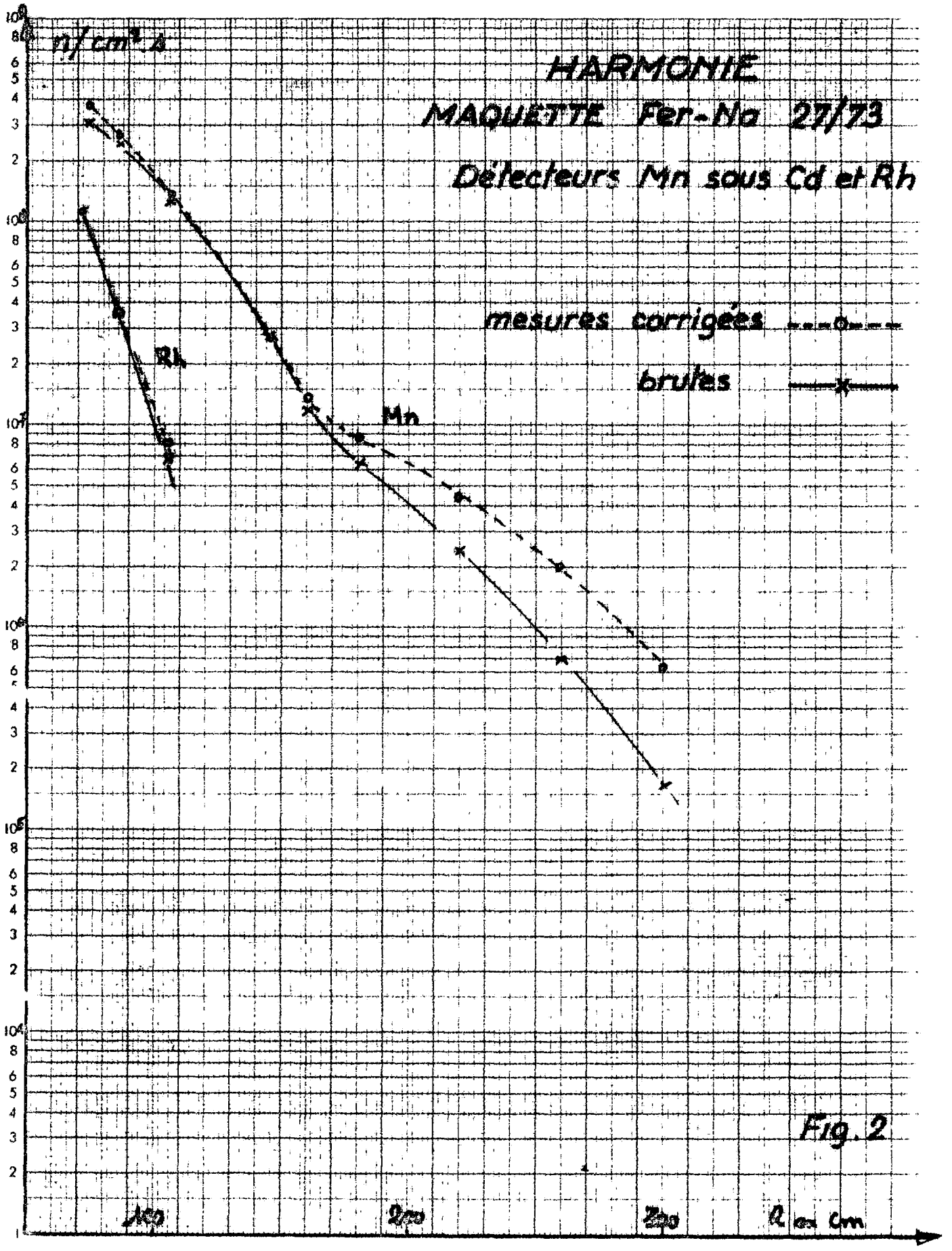
n/cm² s
HARMONIE
MAQUETTE Fer-No 27/73
Détecteurs Mn sous Cd et Rh
mesures corrigées
brutes
Rh
Mn
Fig. 2
Q en cm

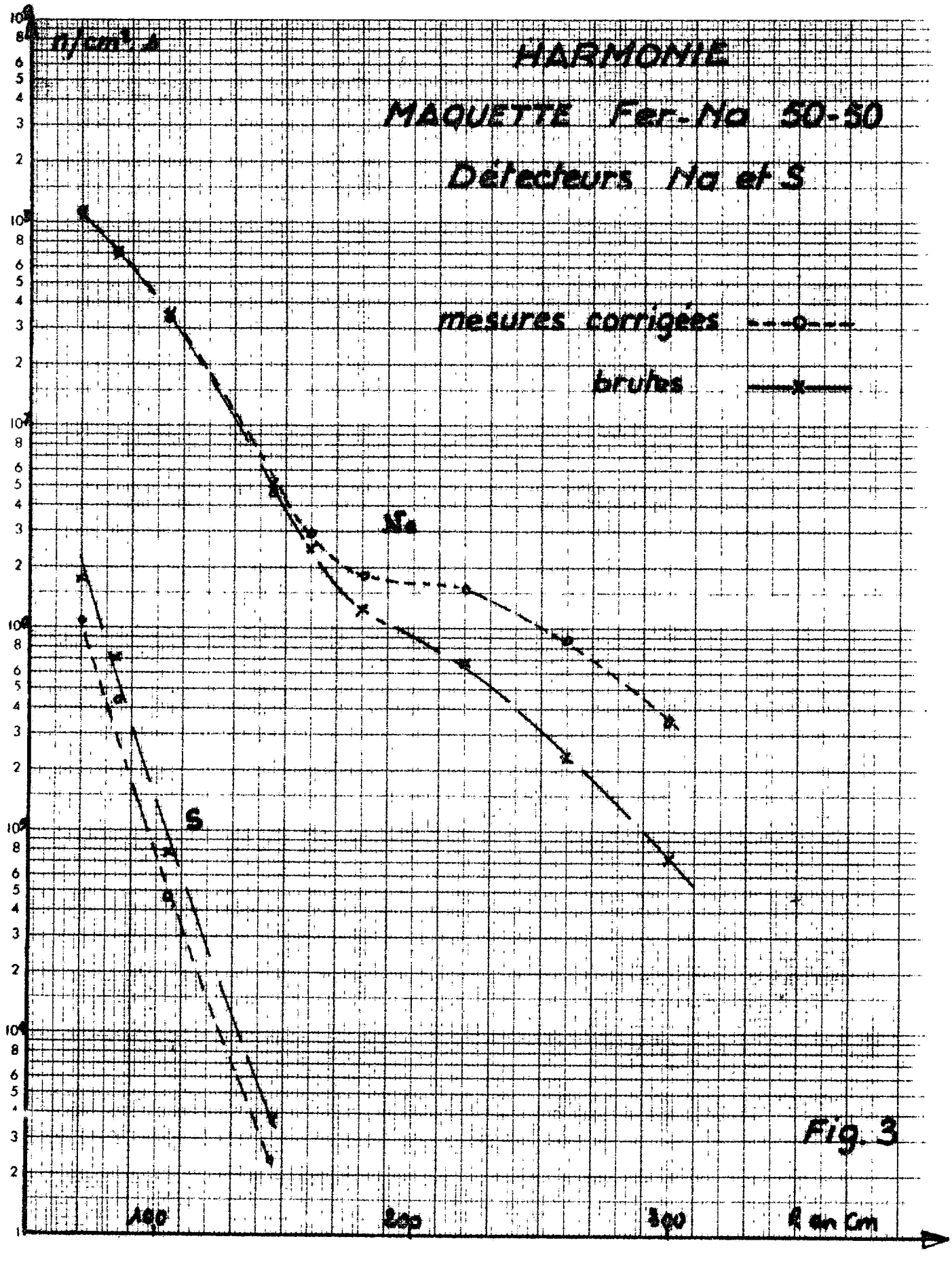
n/cm² s
HARMONIE
MAQUETTE Fer-Na 50-50
Détecteurs Na et S
mesures corrigées
brutes
Na
S
100
200
300
ℓ en cm

Fig. 3

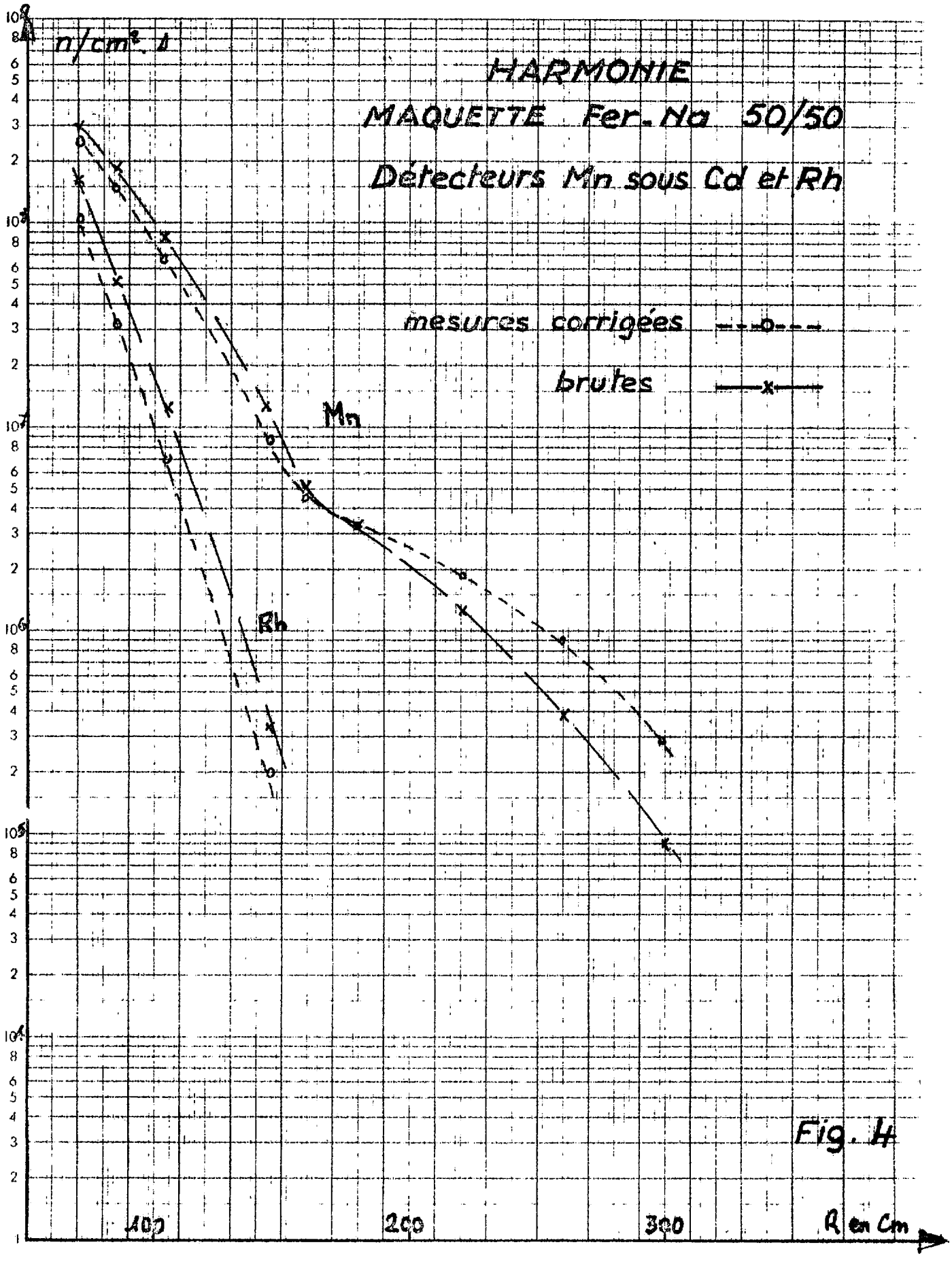
n/cm² s
HARMONIE
MAQUETTE Fer-Na 50/50
Détecteurs Mn sous Cd et Rh
mesures corrigées
brutes
Mn
Rh
100
200
300
R en Cm

Fig. 4

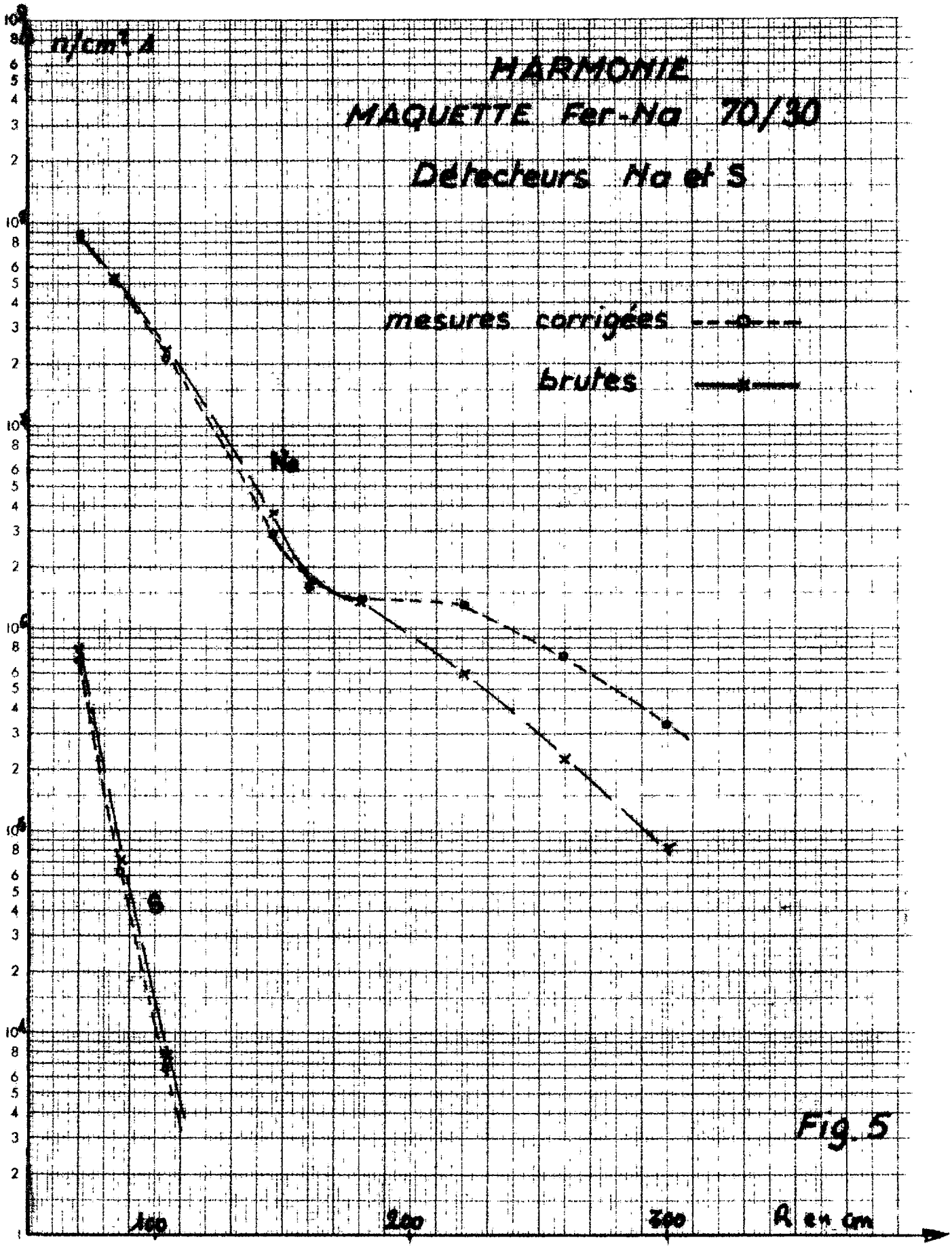
n/cm² A
HARMONIE
MAQUETTE Fer-Na 70/30
Détecteurs Na et S
mesures corrigées
brutes
Na
S
100
200
300
R en cm

Fig. 5

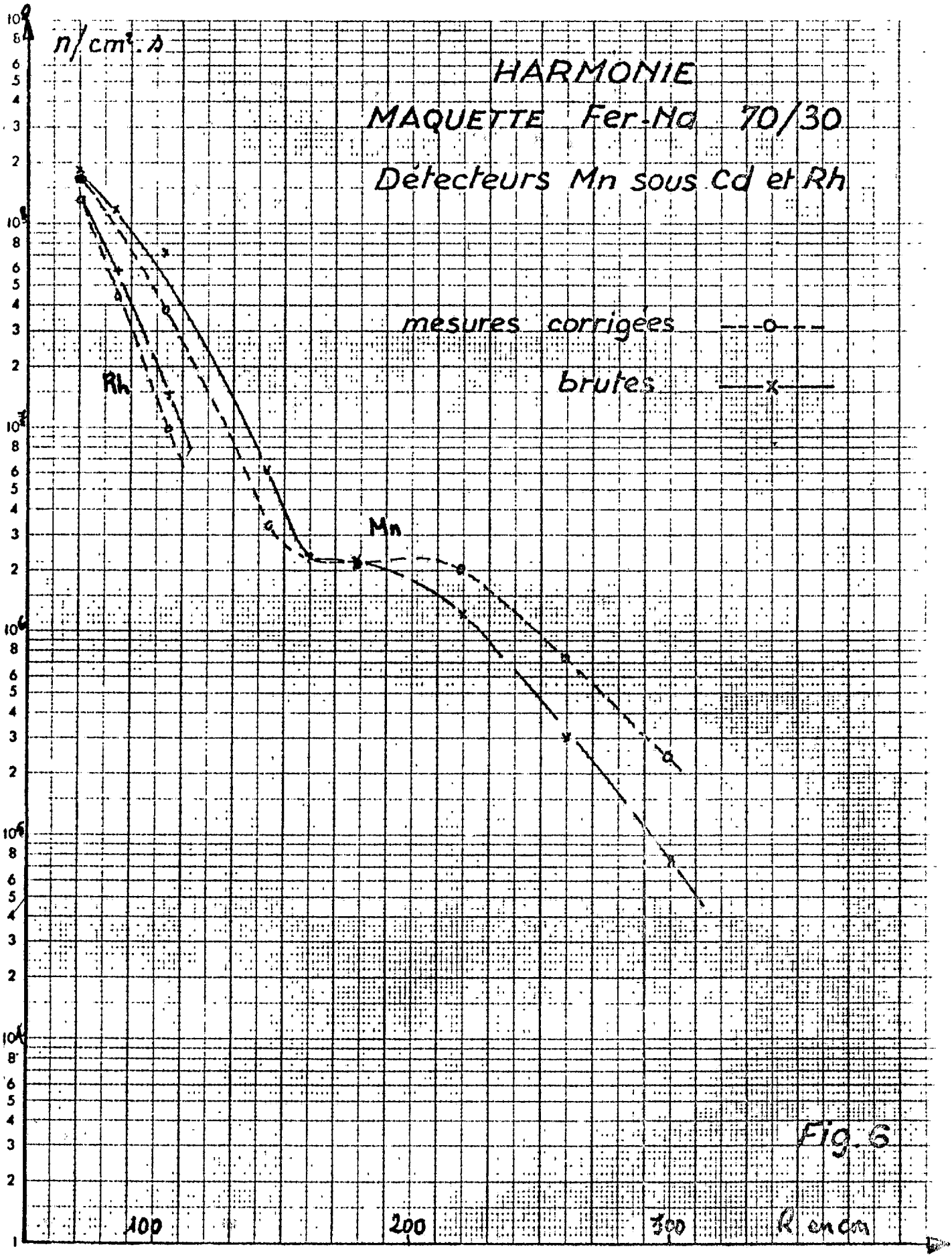
n/cm².s
HARMONIE
MAQUETTE Fer-Na 70/30
Détecteurs Mn sous Cd et Rh
mesures corrigées ---o---
brutes ——x——
Rh
Mn
100
200
300
R en cm

Fig. 6

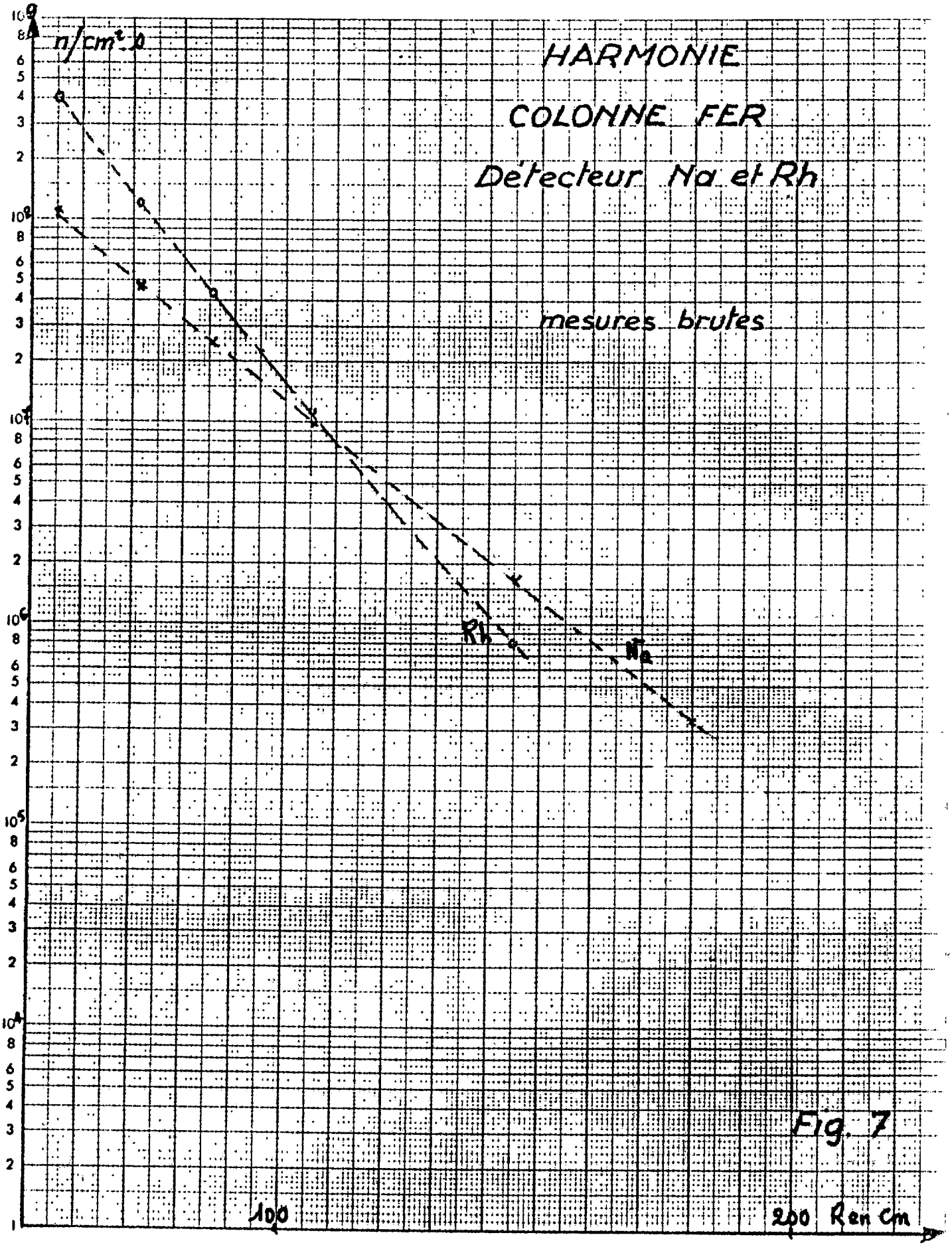
HARMONIE
COLONNE FER
Détecteur Na et Rh
mesures brutes
n/cm²-s
Rh
Na
100
200 Ren cm

Fig. 7

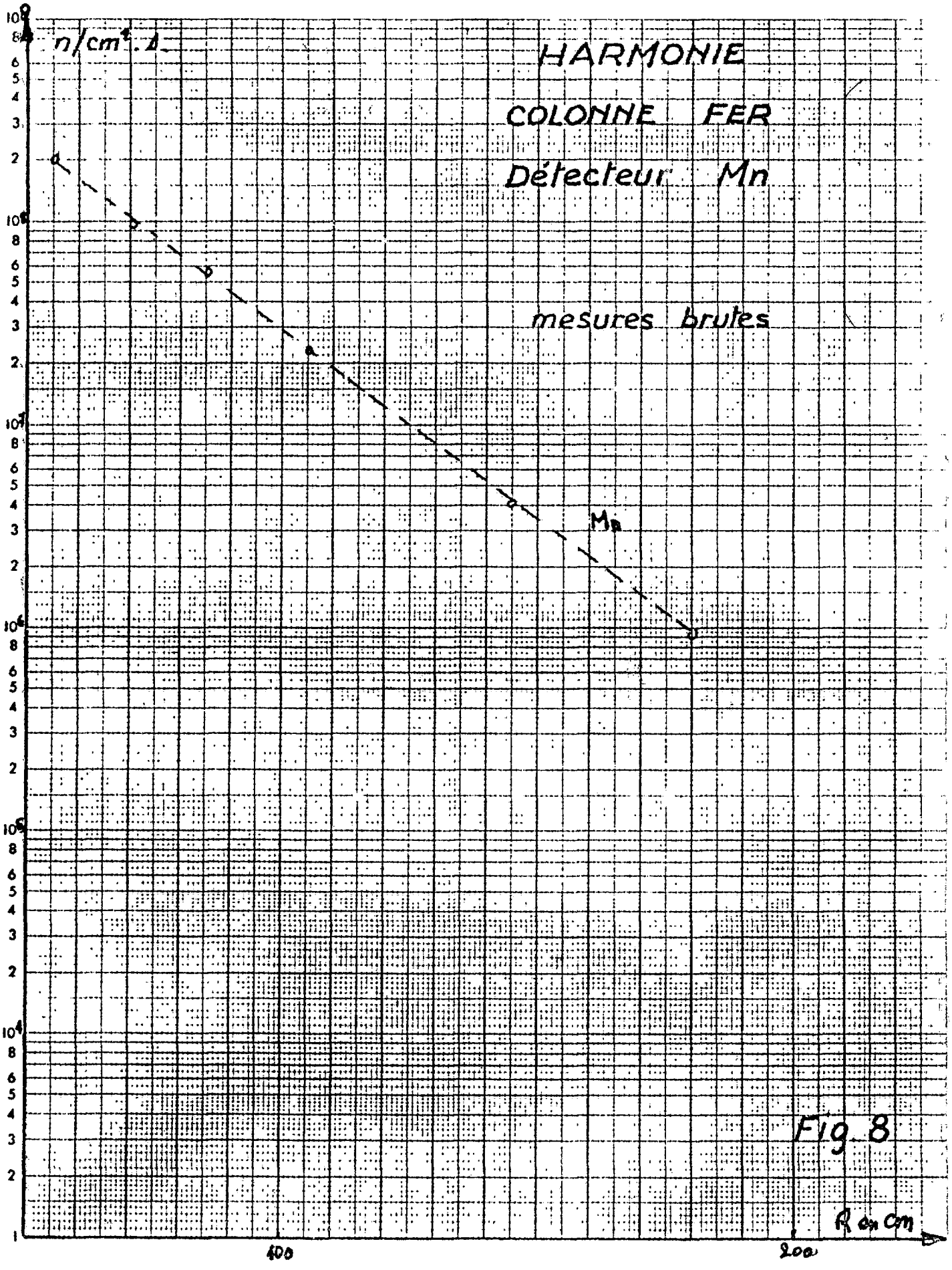
n/cm².Δ
HARMONIE
COLONNE FER
Détecteur Mn
mesures brutes
Mn
R en cm
400
200

Fig. 8

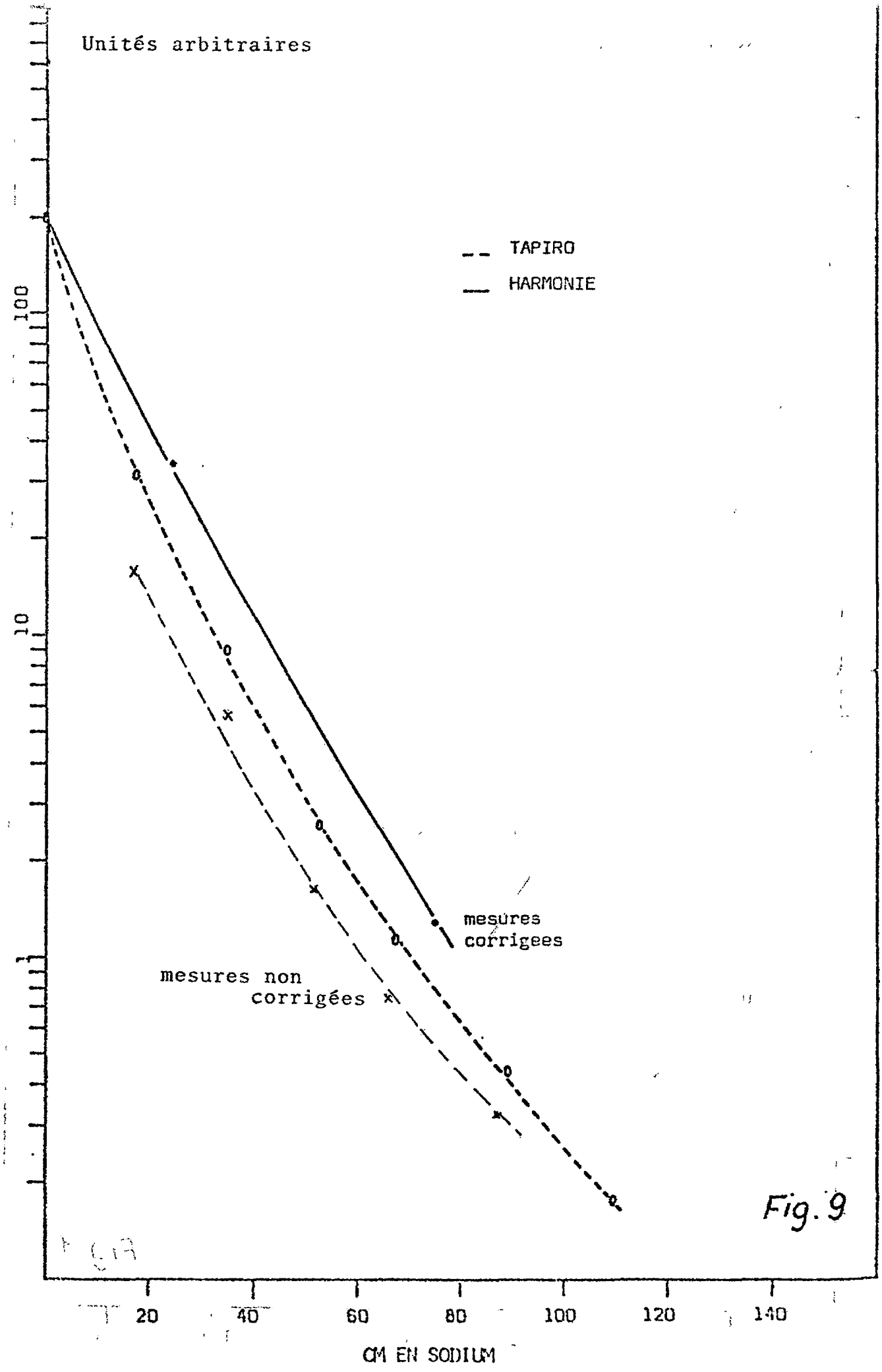
Unités arbitraires
100
10
1
TAPIRO
HARMONIE
mesures
corrigees
mesures non
corrigées
20
40
60
80
100
120
140
CM EN SODIUM

Fig. 9

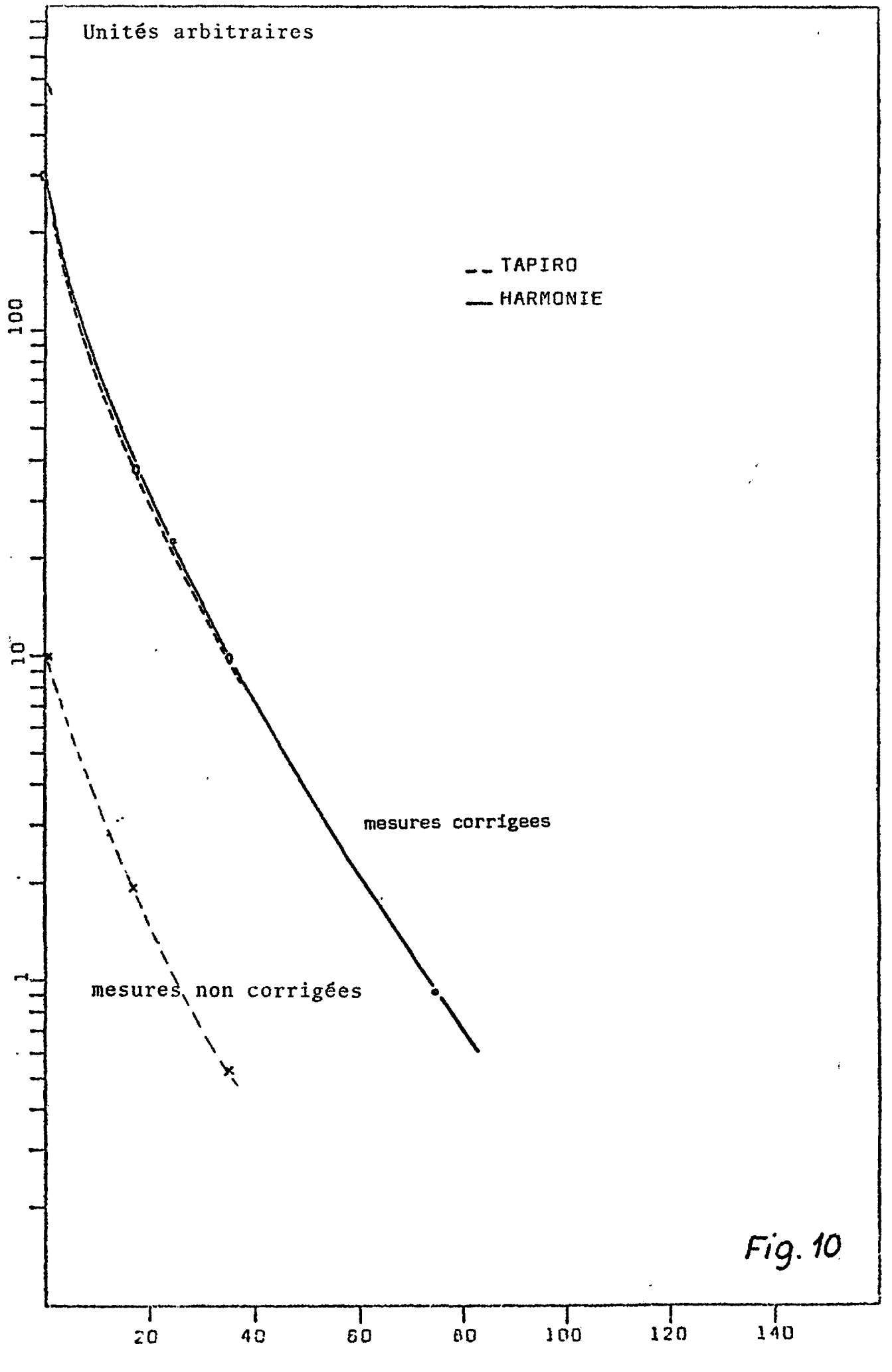
Unités arbitraires
TAPIRO
HARMONIE
100
10
1
mesures corrigees
mesures non corrigées
20
40
60
80
100
120
140
CM EN SODIUM

Fig. 10

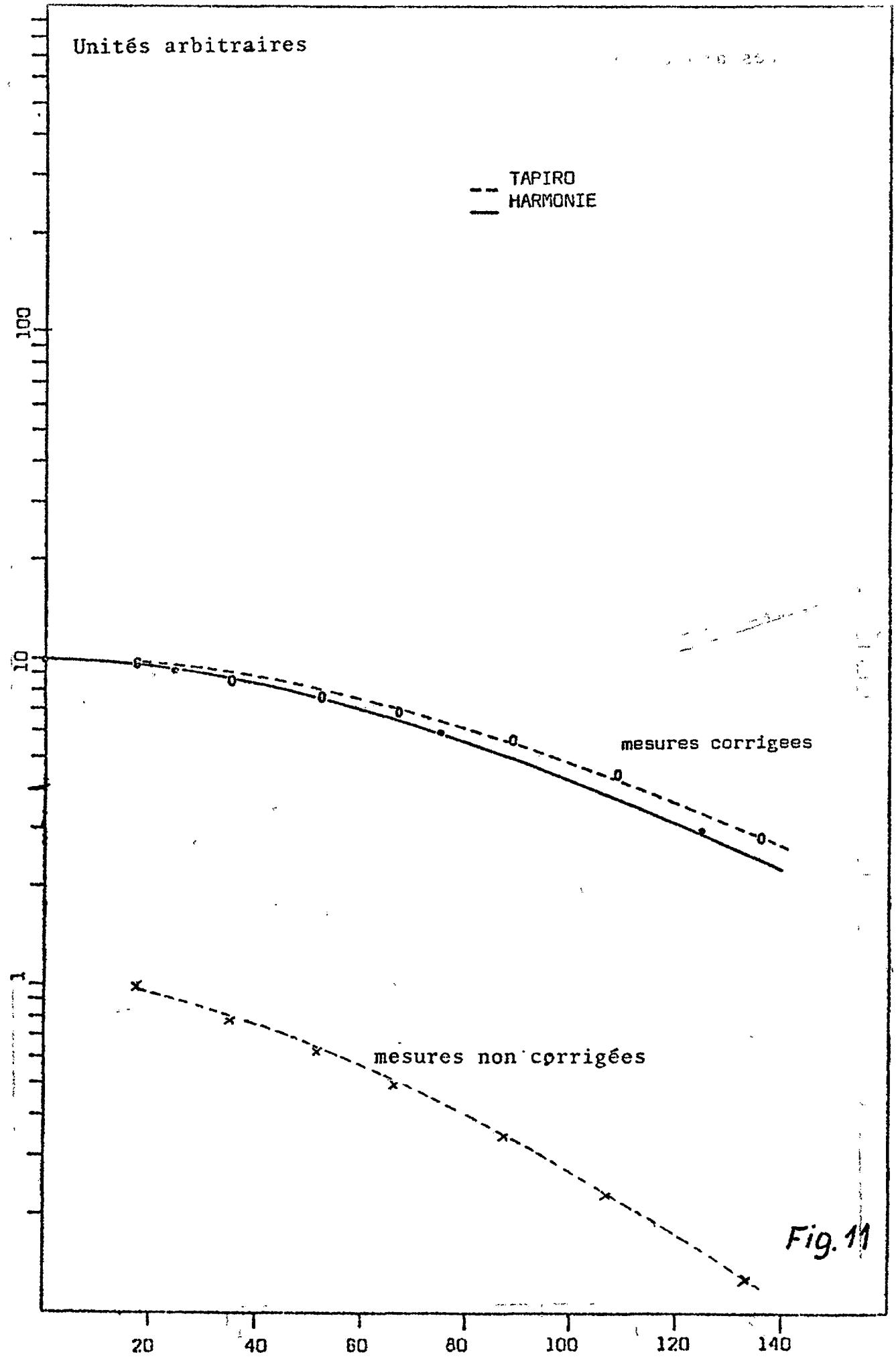

Fig. 11

CM EN SORTIE

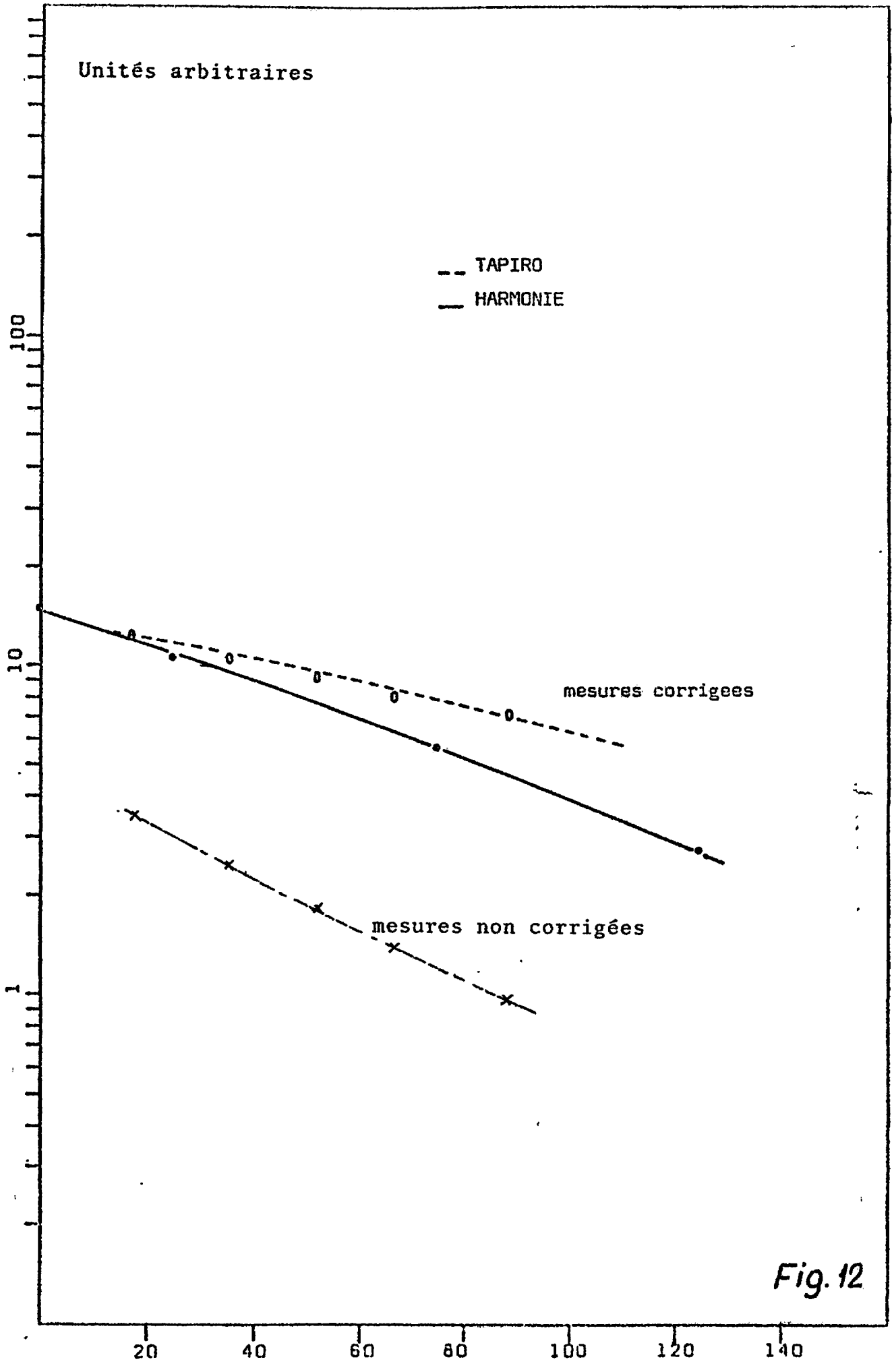
Unités arbitraires
TAPIRO
HARMONIE
100
10
1
mesures corrigees
mesures non corrigées
20
40
60
80
100
120
140
CM EN SODIUM

Fig. 12

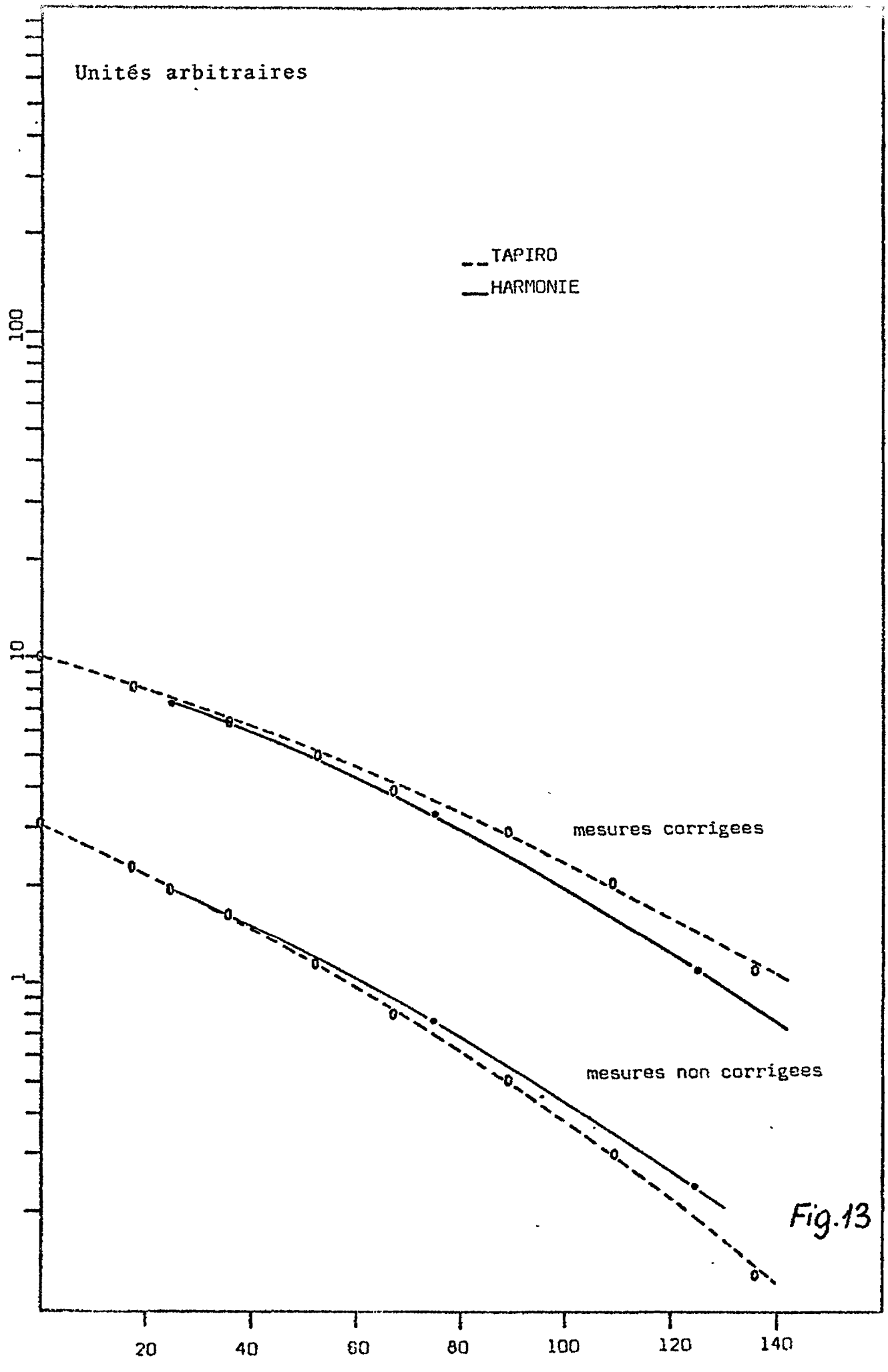
Unités arbitraires
TAPIRO
HARMONIE
100
10
1
mesures corrigees
mesures non corrigees
20
40
60
80
100
120
140
CM EN SODIUM

Fig.13

INTERPRETATION DES EXPERIENCES DE PROPAGATION DE NEUTRONS DANS DES MELANGES FER-SODIUM AVEC LE FORMULAIRE PROPANE O

J.C.ESTIOT, J.P.TRAPP*
M.SALVATORES, G.PALMIOTTI**

RESUME

PROPANE est le formulaire de calcul pour la propagation des neutrons dans la protection neutronique des réacteurs rapides. PROPANE O est la première version, non ajustée, de ce formulaire.

Les résultats d'expériences intégrales de propagation de neutrons dans le fer pur, le sodium pur et des mélanges de fer-sodium (HARMONIE-TAPIRO- et expériences ASPES) sont interprétés en utilisant PROPANE O. Les résultats expérimentaux sont, si nécessaire, corrigés des effets d'hétérogénéité et de fuite de manière à les convertir en résultats idéaux en géométrie homogène monodimensionnelle qui se prêtent mieux à des comparaisons avec des calculs.

Pour HARMONIE et TAPIRO, les calculs consistent à traiter la propagation des neutrons à partir d'une source de surface donnée à l'entrée des milieux étudiés. Le spectre de cette source est ajusté en tenant compte des mesures par protons de recul et d'indices de spectre expérimentaux.

La présente version de PROPANE O est qualifiée. Les causes possibles de désaccord entre calculs et mesures sont discutées à la lumière des études de sensibilité.

*CEA/CEN CADARACHE

**CNEN/CASACCIA

ABSTRACT

PROPANE is a calculationnal scheme for neutron propagation in the shield of fast reactors.PROPANE O is the first, non adjusted version of this scheme.

Results of integral neutron propagation experiments obtained in pure iron, pure sodium, and iron-sodium mixtures (HARMONIE-TAPIRO and ASPES experiments) are interpreted using PROPANE O. Experimental results are, when necessary, corrected for heterogeneity and leakage and converted into a simple homogeneous one dimensionnal model before comparison with calculations.

For HARMONIE and TAPIRO, the calculations consist of propagating a given surface source at the entry of the assemblies.

The spectrum of this source is adjusted using proton-recoil and spectral indices measurements.

The present version of PROPANE O is assessed. Possible source of discrepancies are discussed using essentially the results of sensitivity studies.

I - INTRODUCTION

PROPANE O est la version de départ du formulaire PROPANE pour le calcul des protections neutroniques des réacteurs rapides de puissance tels que SUPER-PHENIX. Ce formulaire, défini dans la référence /1/, est en cours de mise au point dans le cadre de l'accord de coopération entre le CEA et le CNEN.

L'interprétation des expériences de propagation de neutrons dans des mélanges de fer et de sodium a pour but d'effectuer un premier ajustement de ce formulaire, essentiellement pour ce qui concerne les sections efficaces du fer et

du sodium. Dans une deuxième étape le formulaire sera ajusté sur des expériences de propagation dans des mélanges d'acier et de sodium.

Dans la présente communication, on présente les résultats de l'interprétation, avec PROPANE O, d'expériences de propagation de neutrons effectuées sur HARMONIE, TAPIRO et ASPES. Les causes possibles de désaccord entre calculs et expériences sont discutées à la lumière de calculs de sensibilité.

II - EXPERIENCES INTEGRALES EFFECTUEES SUR LES REACTEURS HARMONIE ET TAPIRO

II-1. RAPPEL DES CONDITIONS EXPERIMENTALES POUR HARMONIE (figure 1)

- Cuve Na : hauteur 3 m, dimensions latérales 1,5 m. La cuve est entourée d'une protection de bois. Les mesures axiales sont effectuées tout les 50 cm.

- Massifs Fer-Na : cuve Fer-Na (hauteur 1,5 m, dimensions latérales 1 m) située sous une cuve de Na de 1,5 m de hauteur et de mêmes dimensions latérales.

L'ensemble est entouré d'une protection en bois.

Les mélanges étudiés correspondent aux proportions ci-dessous (en volume).

Fer	27.1 %	47.7%	70.4%
Na	72.9 %	52.3%	29.6%

- Massif Fer pur : il s'agit de la colonne intermédiaire du réacteur HARMONIE. La colonne mesure 1.77 m de long pour une section de 1.2 x 1.5 m. L'ensemble est entouré par une protection de béton lourd.

II-2. CONDITIONS EXPERIMENTALES POUR TAPIRO (figure 2)

Le massif est constitué de deux cuves remplies de Na pur. Les dimensions de chacune sont : 1 x 1 x 1 m.
Les parois sont en aluminium. Elles sont traversées horizontalement et verticalement par des canaux vides. Le fond de cuve s'adapte à la forme cylindrique du réfelcteur de cuivre du réacteur.

II-3. COMPARAISON ENTRE LES REACTEURS HARMONIE ET TAPIRO

Les 2 réacteurs HARMONIE et TAPIRO présentent des différences importantes en ce qui concerne :

.La puissance : HARMONIE : 2 KW
TAPIRO : 5 KW

.Le réflecteur: Fer pour HARMONIE, Cuivre pour TAPIRO.

Cela se traduit par des différences dans le spectre d'entrée des massifs, schématisés ci-dessous.

E (min)	3 Mev	800 Kev	100 Kev	1 Kev	30 ev	THERMIQUE
HARMONIE	$1.3\ 10^{-5}$	$2.19\ 10^{-3}$	$2.92\ 10^{-1}$	$4.78\ 10^{-1}$	$1.65\ 10^{-1}$	$6.2\ 10^{-2}$
TAPIRO	$4.5\ 10^{-5}$	$5.7\ 10^{-3}$	$1.84\ 10^{-1}$	$5.36\ 10^{-1}$	$2.21\ 10^{-1}$	$5.4\ 10^{-2}$

III - FORMULAIRE PROPANE O

Le formulaire de propagation PROPANE a essentiellement pour caractéristique, compte tenu des précisions souhaitées actuellement :

- de réduire le coût de la majeure partie des calculs de projets,
- de faciliter, grâce à la réduction des paramètres mis en jeu, l'adaptation de l'outil de calcul au problème étudié et son ajustement à partir des résultats de mesures intégrales dans des milieux Fer-Na (et ultérieurement acier-sodium) de compositions variables.

Ce formulaire comprend dans sa version initiale (non ajustée) PROPANE O :

- code de transport monodimensionnel ANISN
- découpage angulaire : S4 - développement en polynômes de Legendre ·P1.
- découpage spatial : pas de 3 cm pour Fer-Na et pas de 5 cm pour le Na pur.
- découpage du domaine énergétique : 26 groupes.
- sections efficaces : ce sont celles de la bande DLC2 100 groupes condensées en 26 groupes et pondérés par un flux provenant de milieux Fer-Na (50-50%) pour les différents mélanges et par un flux dans le Na pour le Na pur.

Ce formulaire est généralement utilisé en calcul de propagation avec source de surface.

IV - CONDITIONS DES CALCULS D'INTERPRETATION

Le formulaire PROPANE est utilisé ici en géométrie sphérique avec une source de surface. Les résultats expérimentaux sont convertis au préalable dans ce modèle.

IV-1. SOURCE DE SURFACE UTILISEE POUR L'INTERPRETATION DES EXPERIENCES HARMONIE

Cette dernière est ajustée sur les mesures faites à l'entrée des massifs. Elles sont de deux sortes :

- Protons de recul : permettent de déterminer le spectre de 9.6 à 1350 Kev,
- Mesures intégrales de taux de réaction qui permettent de compléter le spectre par ajustement dans la partie inférieure et supérieure du domaine énergétique, à partir d'une forme de spectre calculé.

Le tableau ci-dessous donne, une comparaison entre la source ajustée et la mesure par protons de recul.

		PROTONS DE RECUL	SOURCE AJUSTEE (*)	SOURCE AJUSTEE
	E 1.35 Mev			0.07 %
0.45	E 1.35 Mev	(8.20 $\pm$0.82) %	7.9 %	6.53 %
0.165	E 0.45 Mev	(26.53 $\pm$1.3) %	26.72 %	22.11 %
0.04	E 0.165 Mev	(36.79 $\pm$1.8) %	38.17 %	31.58 %
2	E 40 Kev	(28.48 $\pm$2.8) %	27.21 %	22.51 %
	E 2 Kev			17.20 %
TOTAL		100 %	100 %	100 %

* Les colonnes 2 et 3 contiennent la source ajustée, avec deux normalisations différentes.

IV-2. COEFFICIENTS CORRECTIFS D'HETEROGENEITE ET DE FUITE

Ces facteurs permettent de ramener les résultats expérimentaux à un équivalent monodimensionnel sphérique homogène ; ils sont définis par :

$$k = \frac{\text{Calcul monodimensionnel sphérique homogène ANISN}}{\text{Calcul bidimensionnel hétérogène DOT III}}$$

Le tableau I donne les facteurs de correction d'hétérogénéité et de fuites pour les maquettes Fer-Na, de fuite pour la maquette Na.
On remarque, pour les détecteurs Mn/Cd et Na, que ces facteurs deviennent très importants à partir de l'interface entre les 2 cuves superposées Fer-Na et Na.

La mauvaise connaissance de la précision de ces facteurs correctifs implique que les écarts calcul-expérience au-delà de cette interface seront difficilement interprétables.

V - COMPARAISON CALCUL-EXPERIENCE

V-1. EXPERIENCES HARMONIE

La comparaison est faite après correction des résultats expérimentaux bruts par les facteurs d'hétérogénéité et de fuite. Les calculs sont faits avec la source de surface ajustée.

V-1.1. Cuve Na-Tableau III - figures 5 et 6

Pour le détecteur Na, on observe un assez bon accord calcul/expérience (-5, +10%) sur l'ensemble de la cuve.

Pour le Mn/Cd l'accord est moins bon et atteint -43% au bout de 250 cm.

Pour le Rhodium, l'écart calcul-expérience croît rapidement avec la distance de pénétration mais la mesure est significative seulement sur 52 cm.

Pour le Soufre, les écarts sont très importants.

V-1.2. Massifs Fer-Na - Tableau IV à VI - Figures 7 à 12

Pour les détecteurs Rhodium et Soufre, l'écart calcul-expérience augmente fortement avec le pourcentage de Fer, comme le montre le tableau suivant :

RAPPORT C/E	DETECTEUR RHODIUM		SOUFRE	
	propagation 34 cm	74 cm	34 cm	74 cm
27% de Fer	0.87	pas mesuré	1.07	0.42
50% de Fer	0.6	0.61	0.57	0.33
73% de Fer	0.3	pas mesuré	0.25	0.02

Pour les détecteurs Na et Mn/Cd les écarts maximum entre calcul et expérience sont respectivement (-3, +12%) et (-28, +6%) sur toute la longueur du massif.

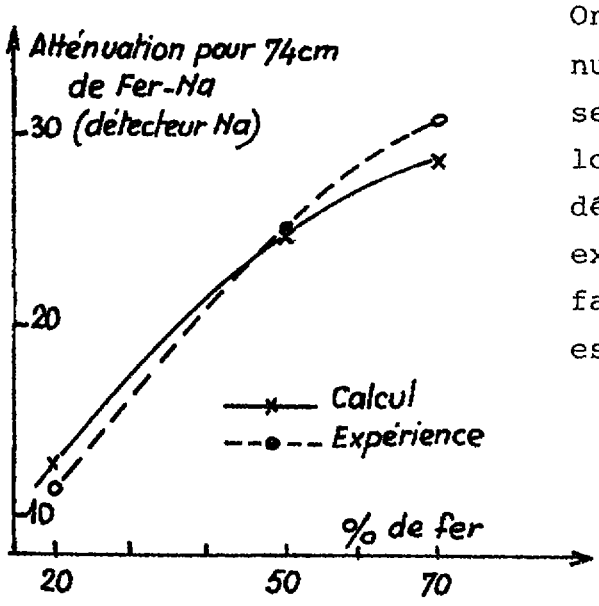

On remarque d'autre part que l'atténuation pour ces deux réponses présente une tendance à la saturation lorsque le pourcentage de Fer dépasse 50%. Les écarts calcul/ expérience étant relativement faibles, cet effet de saturation est bien rendu par le calcul.

V-1.3. Colonne Fer - Tableau VII - Figure 13

La comparaison est faite à partir des résultats non corrigés ; en effet le calcul complet des coefficients de correction au moyen du code DOT 3, dans une géométrie représentative demande un temps de calcul prohibitif. Il apparait cependant que, au moins pour les détecteurs Rh et S, ces facteurs sont proches de 1 à moins 10% près /2/, les calculs n'ont pas été poursuivis pour les détecteurs Na et Mn/Cd.

Les désaccords sont importants pour Rh.

Nous ne possédons pas de mesures significatives pour le Soufre.

Pour le Na, l'écart calcul-expérience brut croît jusqu'à 12 % pour 130 cm de parcours. L'écart est du même ordre que pour les autres massifs, ce qui laisse penser que le facteur correctif pour le Sodium est aussi proche de 1.

V-2. EXPERIENCES TAPIRO : MAQUETTE SODIUM

La comparaison entre les résultats expérimentaux et les calculs est présentée dans les figures 3 et 4 et dans le tableau IX.

Les résultats expérimentaux sont corrigés par des facteurs de fuite obtenus, point par point, et pour chaque détecteur,

par le rapport entre les taux calculés à 1D modèle plan et à 2D en géométrie RZ.

Les valeurs calculées sont obtenues par un calcul en géométrie plane. Le modèle plan a été choisi ici comme modèle de référence car il conduit pour le massif Na de TAPIRO, à des facteurs correctifs nettement plus proches de 1 que le modèle sphérique (cf Tableau II).

Les propagations sont évaluées à partir d'un calcul de Keff. Il faut noter que ces calculs sont préliminaires : la source, que l'on propage dans le sodium, est une source calculée, dont la distribution énergétique est différente du spectre mesuré. Tous les calculs sont faits avec la version du formulaire PROPANE O décrit au paragraphe III.

La comparaison entre les données calculées et mesurées, présentée aux points de mesure dans le tableau IX montre que :

- Pour le Mn et le Na, l'écart calcul-expérience croît rapidement avec la distance de pénétration et atteint 50% au bout de 150 cm ;
- Pour le Rhodium, il atteint environ 70% au bout de 100 cm.
- Pour le Soufre, les écarts sont très importants ; on observe un facteur 3 après 80 cm de propagation.

Les désaccords que nous constatons ne sont dus qu'en p artie aux données utilisées pour le calcul.

La source non ajustée sur le spectre mesuré est certainement une cause importante de désaccord.

V-3. EXPERIENCES ASPES /4/

Les facteurs correctifs de géométrie et de fuite sont calculés et utilisés dans un modèle plan.

Les facteurs de fuite, pour chaque région, sont introduits sous forme de pseudo-absorption à partir d'un calcul bidimensionnel cylindrique

$$\Sigma_a^9 = \frac{1}{r} \frac{\partial (r J_r^9)}{\partial r} / \phi^9$$

La comparaison entre l'expérience et le modèle équivalent monodimensionnel plan est donnée dans le tableau X.

Les calculs sont faits à la fois avec la version initiale du formulaire PROPANE O (section efficace du Fer provenant de ENDF/B2) et avec une version modifiée (section efficace du Fer provenant de ENDF/B4).

La comparaison de ces deux calculs avec l'expérience est donnée par les figures 14 à 17. On peut constater que l'utilisation de la section efficace du Fer ENDF/B4 amène à un meilleur accord calcul-expérience en particulier pour les détecteurs Rhodium et Soufre, c'est-à-dire pour les neutrons de hautes énergies.

V-4. COMPARAISON FER ENDF/B2 - ENDF/B4 DANS LA COLONNE DE FER HARMONIE

Pour étudier l'effet d'un changement de la bibliothèque du fer, on a comparé les résultats fournis par l'utilisation du fer issu de la bibliothèque ENDF/B2 à celui de la bibliothèque PROPANE (venant de ENDF/B2).

Le tableau VIII présente directement les écarts observés entre l'expérience et les 2 calculs, l'ensemble étant normé à 1 à la cote 71.5 cm.

On remarque que si pour les détecteurs sensibles aux neutrons de basse énergie, les écarts sont du même ordre de grandeur, pour le détecteur sensible aux neutrons de haute énergie, il y a amélioration très nette des résultats, d'un facteur 2 à 7 pour 1 m de propagation. La tendance est donc la même que celle observée sur ASPES.

VI - CALCULS DE SENSIBILITE

Les coefficients de sensibilités sont calculés à partir de la chaine de calcul : GIANT - SCOFF /5/, qui permet le calcul des coefficients de sensibilité correspondant à des fonctionnelles linéaires (taux de réaction) ou à des rapports de fonctionnelles linéaires.

Quelques résultats correspondants aux mélanges Fer-Na d'HARMONIE sont donnés aux tableau XI et XII. On présente les coefficient de sensibilité $(\delta R/R) / (\delta\sigma/\sigma)$, pour le rapport du taux de réaction S (n-p) en deux positions, aux section efficaces du Fer et du Na dans les 3 premiers groupes du découpage énergétique de PROPANE.

On voit que les sensibilités varient assez fortement en fonction de la proportion de Fer dans le mélange. Ainsi les sensibilités aux sections efficaces du Fer et du Na, presque comparables pour une proportion de Fer de 30%, deviennent très différentes (un facteur 10 en moyenne) quand cette proportion passe à 70%.

Dans une optique d'ajustement, on peut noter que quoique les sensibilités aux sections efficaces inélastiques soient nettement plus faibles qu'aux sections efficaces totales, leur importance est comparable, si l'on tient compte de leurs incertitudes admises (5 à 10% pour la totale 30 à 50% pour les inélastiques). Il faut ajouter enfin qu'une variation sur σ_{total} doit être considérée en liaison avec des variations sur les autres sections efficaces, telles que la section efficace élastique,ce qui tend à diminuer les sensibilités "effectives" aux sections efficaces totales.

VI - CONCLUSION

L'ensemble des résultats présentés permet de tirer les conclusions suivantes :

- L'interprétation des expériences effectuées sur HARMONIE et sur TAPIRO à l'aide du formulaire PROPANE O fait apparaitre un relativement bon accord calcul-expérience sur les détecteurs thermiques et épithermiques ; il existe un désaccord assez important pour les détecteurs rapides.

- L'interprétation des expériences ASPES et de la colonne de fer HARMONIE permettent de montrer que l'utilisation de la section efficace du fer provenant de ENDF/B4 rend mieux compte de la propagation des neutrons rapides. On peut noter

que les différences essentielles entre ce fer et celui de PROPANE O sont précisément dans les sections totales et inélastiques aux hautes énergies.

- Les calculs de sensibilités effectués à l'aide de la chaine GIANT-SCOFF montrent l'importance de la section efficace du Fer relativement à celle du Na pour de forts pourcentages de Fer dans le mélange.

Dès que le problème du calcul des facteurs correctifs de fuite aura été résolu /6/ on pourra passer à l'ajustement des diverses sections efficaces de fer et du sodium de PROPANE O sur les expériences intégrales.

/ REFERENCES /

/1/ F.BOUTEAU, P.CAUMETTE,C.DEVILLERS,A.KHAIRALLAH,Y.OCERAIES - Formulaire de propagation de neutrons dans les milieux acier-sodium pour les protections des réacteurs rapides. Communication à la réunion de spécialistes de PARIS - Octobre 1975.

/2/ C.DEVILLERS - Communication privée.

/3/ L.BOZZI,M.MARTINI,P.MOIOLI - Confronto HARMONIE-TAPIRO RIT/FIS-LNS (76)22

/4/ G.PALMIOTTI,M.SALVATORES - Towards Propane preliminary version 1 - Experimental analysis, sensitivity studies and related problems (June 76) RTJ/LTCR (76)3

/5/ G.PALMIOTTI, M.SALVATORES - Transport calculations of the generalized functions for sensitivity studies. Proceeding of the meeting on sensitivity studies and shielding benchmark Paris 1975.

/6/ F.BOUTEAU,D.CALAMAND, Y.OCERAIES,R.VIENOT,D.ANTONINI, L.BOZZI,M.MARTINI, P.MOIOLI - Résultats expérimentaux dans HARMONIE et TAPIRO sur la propagation des neutrons dans les mélanges Fe-Na. Communication VIENNE oct. 76.

TABLEAU I

FACTEUR CORRECTIFS D'HETEROGENEITE ET DE FUITE POUR LES MAQUETTES Na et Fer-Na d'HARMONIE

(le trait horizontal sépare les cuves Fer-Na de la cuve Na supérieure)

x (cm)	Distance de propagation	DETECTEUR SOUFRE				RHODIUM				Mn/Cd				Na			
		Na	Fer 27% Na 73%	Fer 50% Na 50%	Fer 70% Na 30%		Fer 27% Na 73%	Fer 50% Na 50%	Fer 70% Na 30%		Fer 27% Na 73%	Fer 50% Na 50%	Fer 70% Na 30%		Fer 27% Na 73%	Fer 50% Na 50%	Fer 70% Na 30%
71.5	18.5	0.75	0.77	0.85	0.80	0.99	1.1	1.10	1.12	1.2	1.71	1.54	1.38	1.32	1.7	1.52	1.36
85	32	0.64	0.71	0.79	0.62	0.96	1.1	1.08	1.07	1.7	1.65	1.47	1.20	1.42	1.7	1.49	1.27
105	52	0.5	0.64	0.56	0.365	0.93	1.1	1.05	1.	1.335	1.54	1.36	1.17	1.54	1.59	1.42	1.15
145	92	0.32	0.296	0.295	0.085		1.1	1.04	0.92	1.37	1.43	1.25	1.24	1.66	1.43	1.26	1.11
160	107	0.29	0.208	0.29	0.055		1.240	1.06	0.90	1.375	1.60	1.52	1.44	1.75	1.65	1.63	1.25
180	127	0.235	0.29	0.302	0.033		1.37	1.06	0.91	1.38	1.94	1.84	1.66	1.895	2.14	2.04	1.60
220	167			0.323	0.042		1.33		0.96	1.40	2.32	2.7	2.49	1.71	3.44	3.25	3.11
260	207			0.34	0.044		1.41		0.99	1.435	4.40	4.12	3.64	1.71	5.22	4.88	4.41
300	247			0.38	0.035		1.50			1.465	5.61	5.23	4.96	1.69	6.58	6.05	5.55

$$K = \frac{\text{ANISN sphérique homogène}}{\text{DOT cylindrique hétérogène}}$$

TABLEAU II

FACTEURS DE CORRECTION GEOMETRIQUE POUR TAPIRO

CALCUL PLAQUE 1D ANISN
CALCUL RZ DOT

CM DANS Na	DETECTEUR		
	Na	S	Rh
2.5	1.	1.	1.
22.5	.824	.907	1.10
27.5	.972	.891	1.14
42.5	.997	.798	1.08
57.5	1.01	.729	1.04
62.5	1.04	.710	.994
87.5	1.10	.611	.872
102.5	1.11	.556	.823
117.5	1.17	.509	.761
147.5	1.23	.417	.623
162.5	1.26	.370	.559
182.5	1.31	.321	.485
207.5	1.28		
237.5	1.26		
267.5	1.18		

TABLEAU III

MAQUETTE Na

DETECTEURS		Na				Mn/Cd				Rh				S			
POSITION	DISTANCE DE PROPAG. cm	EXP. BRUTE	EXP. CORRIGEE NORMEE	CALCUL NORME	C/E	EXP. BRUTE	EXP. CORRIGEE NORMEE	CALCUL NORME	C/E	EXP. BRUTE	EXP. CORRIGEE NORMEE	CALCUL NORME	C/E	EXP. BRUTE	EXP. CORRIGEE NORMEE	CALCUL NORME	C/E
1	18.5	$8.4\ 10^{7}$	1	1	1	$2.75\ 10^{8}$	1	1	1	$1.45\ 10^{8}$	1	1	1	$2.05\ 10^{6}$	1	1	1
2	32	$6.8\ 10^{7}$	0.87	0.88	1.01	2.3 -	0.86	0.895	1.04	$5.9\ 10^{7}$	0.304	0.43	1.09	1.01 -	0.42 ··	0.49	1.16
3	52	4.85 -	0.68	0.64	0.94	1.6 -	0.63	0.53	0.82	1.5 -	$9.68\ 10^{-2}$	0.13	1.34	$4.7\ 10^{5}$	0.15	0.158	1.05
4	92	2.35 -	0.35	0.36	1.03	$6.9\ 10^{7}$	0.28	0.25	0.87					$4.7\ 10^{4}$	$9.7\ 10^{-3}$	$3.1\ 10^{-3}$	0.32
5	127	1.2 -	$1.83\ 10^{-1}$	0.19	1.04	3. -	0.12	$9.02\ 10^{-2}$	0.75								
6	167	$5.5\ 10^{+6}$	$8.50\ 10^{-2}$	$8.3\ 10^{-2}$	0.98	$1.1\ 10^{7}$	$4.56\ 10^{-2}$	2.85 -	0.62								
7	207	2.2 -	3.40 -	3.72 -	1.09	$3.55\ 10^{6}$	1.51 -	$9.77\ 10^{-3}$	0.64								
8	247	$8.3\ 10^{5}$	1.2 -	1.29 -	1.02	1.3 -	0.56 -	3.3 -	0.57								

TABLEAU IV

MASSIF Fer-Na (27-73 %)

DETECTEURS		Na				Mn/Cd				Rh				S			
POSITION	DISTANCE DE PROPAG. cm	EXP. BRUTE	EXP. CORRIGEE NORMEE	CALCUL NORME	C/E	EXP. BRUTE	EXP. CORRIGEE NORMEE	CALCUL NORME	C/E	EXP. BRUTE	EXP. CORRIGEE NORMEE	CALCUL NORME	C/E	EXP.. BRUTE	EXP. CORRIGEE NORMEE	CALCUL NORME	C/E
1	18.5	$1.15\ 10^{8}$	1	1	1	$3.04\ 10^{8}$	1	1	1	$1.7\ 10^{8}$	1	1	1	$1.82\ 10^{6}$	1	1	1
2	32	$7.7\ 10^{7}$	0.67	0.75	1.12	2.4 -	0.72	0.718	1.	$5.44\ 10^{7}$	0.434	0.31	0.71	$4.7\ 10^{5}$	0.21	0.24	1
3	52	4.8 -	0.39	0.41	1.05	1.3 -	0.36	0.35	0.97	1.18 -	$6.94\ 10^{-2}$	$6\ 10^{-2}$	0.87	$6.8\ 10^{4}$	$3.1\ 10^{-2}$	$3.32\ 10^{-2}$	1.07
4	92	1. -	$7.31\ 10^{-2}$	$7.79\ 10^{-2}$	1.06	$2.8\ 10^{7}$	$7.38\ 10^{-2}$	$5.34\ 10^{-2}$	0.72					$4.4\ 10^{3}$	$1.72 10^{-3}$	$7.2\ 10^{-4}$	0.42
5	127	$4.\ 10^{6}$	4.37 -	3.57 -	0.81	$6.6\ 10^{6}$	2.34 -	1.26 -	0.53								
6	167	1.34 -	2.36 -	2.13 -	0.90	2.4 -	1.25 -	$4.53\ 10^{-3}$	0.36								
7	207	$5.4\ 10^{5}$	1.43 -	$9.9\ 10^{-3}$	0.67	$6.9\ 10^{5}$	$5.59\ 10^{-3}$	1.47 -	0.26								
8	247	1.64 -	$5.52\ 10^{-3}$	$1.48 10^{-3}$	0.27	1.7 -	$1.73\ 10^{-3}$	$4.42\ 10^{-4}$	0.26								

TABLEAU V

MASSIF FER Na (50 - 50 %)

DETECTEURS		Na				Mn/Cd				Rh				S			
POSITION	DISTANCE DE PROPAG. cm	EXP. BRUTE	EXP. CORRIGEE NORMEE	CALCUL NORME	C/E	EXP. BRUTE	EXP. CORRIGEE NORMEE	CALCUL NORME	C/E	EXP. BRUTE	EXP. CORRIGEE NORMEE	CALCUL NORME	C/E	EXP. BRUTE	EXP. CORRIGEE NORMEE	CALCUL NORME	C/E
1	18.5	$1.08\ 10^{8}$	1	1	1	$3.\ 10^{8}$	1	1	1	$1.7\ 10^{8}$	1	1	1	$1.76\ 10^{6}$	1	1	1
2	32	$6.9\ 10^{7}$	0.616	0.61	0.99	1.87 -	0.59	0.60	1.02	$5.2\ 10^{7}$	0.3	0.22	0.73	$3.03\ 10^{5}$	0.15	0.109	0.72
3	52	3.5 -	0.298	0.29	0.97	$8.45\ 10^{7}$	0.25	0.265	1.06	1.27 -	$6.9\ 10^{-2}$	$4.15\ 10^{-2}$	0.6	$5.1\ 10^{4}$	$1.74\ 10^{-2}$	$1.1\ 10^{-2}$	0.63
4	92	$5.2\ 10^{6}$	$3.9\ 10^{-2}$	$3.9\ 10^{-2}$	1	1.26 -	$3.41\ 10^{-2}$	$3.26\ 10^{-2}$	0.96	$3.3\ 10^{5}$	$1.85\ 10^{-3}$	$1.14\ 10^{-3}$	0.62	$1.07\ 10^{3}$	$1.94\ 10^{-4}$	$6.36\ 10^{-5}$	0.32
5	127	1.3 -	1.54 -	$8.08\ 10^{-3}$	0.52	$3.2\ 10^{6}$	1.26 -	$9.23\ 10^{-3}$	0.73								
6	167	$6.8\ 10^{5}$	1.32 -	5.72 -	0.43	1.3 -	$7.34\ 10^{-3}$	3.46	0.47								
7	207	2.3 -	$6.7\ 10^{-3}$	2.58 -	0.39	$3.9\ 10^{5}$	3.4 -	1.1	0.32								
8	247	$7.5\ 10^{4}$	2.72 -	$9.36\ 10^{-4}$	0.34	$9.3\ 10^{4}$	1.05 -	$3.26\ 10^{-4}$	0.31								

TABLEAU VI

MASSIF FER-Na (70-30 %)

DETECTEURS		Na				Mn/Cd				Rh				S			
POSITION	DISTANCE DE PROPAG. cm	EXP. BRUTE	EXP. CORRIGEE NORMEE	CALCUL NORME	C/E	EXP. BRUTE	EXP. CORRIGEE NORMEE	CALCUL NORME	C/E	EXP. BRUTE	EXP. CORRIGEE NORMEE	CALCUL NORME	C/E	EXP. BRUTE	EXP. CORRIGEE NORMEE	CALCUL NORME	C/E
1	18.5	$8.7\ 10^{7}$	1	1	1	$1.86\ 10^{8}$	1	1	1	$1.7\ 10^{8}$	1	1	1	8.10^{5}	1	1	1
2	32	5.5 -	0.59	0.61	1.02	1.18 -	0.6	0.615	1.02	$6.3\ 10^{7}$	0.36	0.25	0.70	$7.2\ 10^{4}$	$6.9\ 10^{-2}$	0.1	1.44
3	52	2.4 -	0.23	0.24	1.03	$4.99\ 10^{7}$	0.23	0.24	1.04	1.45	$7.63\ 10^{-2}$	$2.9\ 10^{-2}$	0.38	$7.8\ 10^{3}$	$4.461\bar{0}^{3}$	$2.8\ 10^{-3}$	0.63
4	92	$3.6\ 10^{6}$	$3.4\ 10^{-2}$	$3.29\ 10^{-2}$	0.97	$6.3\ 10^{6}$	$3.09\ 10^{-2}$	$3.271\bar{0}^{2}$	1.06					$1.4\ 10^{2}$	$1.9\ 10^{-5}$	$4.4\ 10^{-6}$	0.23
5	127	1.4 -	1.57 -	1.42 -	0.90	2.05 -	1.35 -	1.57 -	1.16								
6	167	$5.95\ 10^{5}$	1.54 -	$7.711\bar{0}^{3}$	0.48	1.25 -	1.23 -	$5.921\bar{0}^{3}$	0.48								
7	207	2.3 -	$8.4\ 10^{-3}$	3.63 -	0.43	3.10^{5}	$4.32\ 10^{-3}$	1.85 -	0.43								
8	247	$8.2\ 10^{4}$	3.83 -	1.36 -	0.35	$7.5\ 10^{4}$	1.47 -	$5.491\bar{0}^{4}$	0.37								

TABLEAU VII

COLONNE FER

DETECTEURS		Na				Mn/Cd				Rh			
POSITION	DISTANCE AU CENTRE cm	EXP. BRUTE	EXP. NORMEE	CALCUL NORME	C/E	EXP. BRUTE	EXP. NORMEE	CALCUL NORME	C/E	EXP. BRUTE	EXP. NORMEE	CALCUL NORME	C/E
1	71.5	$1. \ 10^{8}$	1	1	1	$1.05 \ 10^{8}$	1	1	1	$2.1 \ 10^{8}$	1	1	1
2	85	$5.3 \ 10^{7}$	0.53	0.52	0.98	$6. \ 10^{7}$	0.57	0.55	0.96	$7.5 \ 10^{7}$	0.36	0.20	0.56
	105	2.2 -	0.22	0.213	0.97	2.5 -	0.24	0.22	0.92	1.9 -	$9.04 \ 10^{-2}$	$2.1 \ 10^{-2}$	0.23
4	145	$3.6 \ 10^{6}$	$3.6 \ 10^{-2}$	$3.44 \ 10^{-2}$	0.96	$4.5 \ 10^{6}$	$4.2 \ 10^{-2}$	$3.7 \ 10^{-2}$	0.88	$1.35 \ 10^{6}$	$6.4 \ 10^{-3}$	$2.1 \ 10^{-4}$	0.03
5	180	$7.6 \ 10^{5}$	$7.5 \ 10^{-3}$	$6.81 \ 10^{-3}$	0.92	$9.5 \ 10^{5}$	$9. \ 10^{-3}$	$7.5 \ 10^{-3}$	0.83				

TABLEAU VIII

COMPARAISON DES RAPPORTS C/E DES 2 BIBLIOTHEQUES FER ENDF/BII et FER ENDF/BIV DANS LA COLONNE DE FER HARMONIE.

DETECTEURS		Na		Mn		Rh	
POSITION	DISTANCE AU CENTRE en cm	ENDF BII	ENDF BIV	ENDF BII	ENDF BIV	ENDF BII	ENDF BIV
1	71.5	1	1	1	1	1	1
2	85	0.98	1.08	0.96	1.04	0.56	0.76
3	105	0.97	1.1	0.92	1.09	0.23	0.5
4	145	0.96	0.91	0.88	0.82	0.03	0.19
5	180	0.92	0.67	0.83	0.59		

TABLEAU IX

MAQUETTE Na - TAPIRO

	Na			Mn		
POSITION CM Na	MESURES CORRIGEES	CALCUL PLAN	C/E	MESURES CORRIGEES	CALCUL PLAN	C/E
17.5	1.	1.	1.	1.	1.	1.
35.5	0.698	0.766	1.097	0.737	0.721	0.978
52.5	0.513	0.516	1.005	0.514	0.464	0.903
67.5	0.385	0.373	0.969	0.364	0.322	0.885
89.	0.264	0.224	0.847	0.231	0.160	0.69
109.	0.194	0.114	0.586	0.138	0.0869	0.629
136.				.0604	.341	0.565

	Rh			S		
POSITION CM Na	MESURES CORRIGEES	CALCUL PLAN	C/E	MESURES CORRIGEES	CALCUL PLAN	C/E
17.5	1.	1.	1.	1.	1.	1.
35.5	0.344	0.419	1.22	0.274	0.464	1.69
52.5	0.101	0.173	1.71	0.0897	0.239	2.66
67.5	0.0469	0.0806	1.72		0.131	
89.	0.020	0.0278	1.39			
109.		0.0102				

TABLEAU X

COMPARAISON CALCUL/EXPERIENCE - ASPES

a) réponse des détecteurs à la position 2 (normalisés à la position 1)

Position 1 : 142.24 cm (20.32 cm de Fer)
Position 2 :111,76 cm (50.80 cm de Fer)
Position 3 : 86.36 cm (76.6 cm de Fer)

b) Flux normalisés à la position 2

	S(n,p) a)	In(n,n^1) a)	Rh(n,n^1) a)	Au(n,) a)	Øint b) 820-302 Kev		Ø int b) 302 - 111 Kev		Øint b) 111-41 Kev	Ø int b) 41 - 15Kev
					Pos.1	Pos.3	Pos.1	Pos.3	Pos.3	Pos.3
Exp.	.369-2	.314-1	.934-1	.335	7.11	.192	3.87	.270	.313	.322
C/E Fe ENDF/B4	1.17	1.00	1.05	1.11	1.05	.79	1.12	.82	.88	1.07
C/E Fe PROPANE O	1.35	.89	.76	.97	1.52	.53	1.47	.58	.64	.124

TABLEAU XI

COEFFICIENTS DE SENSIBILITE DE LA REPONSE S (n,p) AUX VARIATIONS DES SECTIONS EFFICACES DU Fe.

(position 105. cm/position 71.5 cm)

Mélange Fe/Na	σ^{1}_{total}	σ^{2}_{total}	σ^{3}_{total}	$\sigma_{1\to 2}$	$\sigma_{2\to 3}$	$\sigma_{1\to 1}$	$\sigma_{2\to 2}$	$\sigma_{3\to 3}$
30/70	-1.531	-2.00	-.39	.35-1	.80-2	.72	1.08	.17
50/50	-1.79	-3.78	-1.12	.50-1	.28-1	.83	2.05	.59
70/30	-1.72	-5.67	-2.17	.56-1	.47-1	.78	3.03	1.14

TABLEAU XII

COEFFICIENTS DE SENSIBILITE DE LA REPONSE S (n,p) AUX SECTIONS EFFICACES DU Na (position 105. cm/position 71.5cm)

MELANGE Fe/Na	σ^{1}_{total}	σ^{2}_{total}	σ^{3}_{total}	$\sigma_{1\to 2}$	$\sigma_{2\to 3}$	$\sigma_{1\to 1}$	$\sigma_{2\to 2}$	$\sigma_{3\to 3}$
30/70	-.60	-1.29	-.29	.19-1	.64-2	.23	.71	.13
50/50	-.29	-1.00	-.35	.11-1	.89-2	.11	.55	.18
70/30	-.11	-.57	-.26	.48-2	.57-2	.04	.31	.13

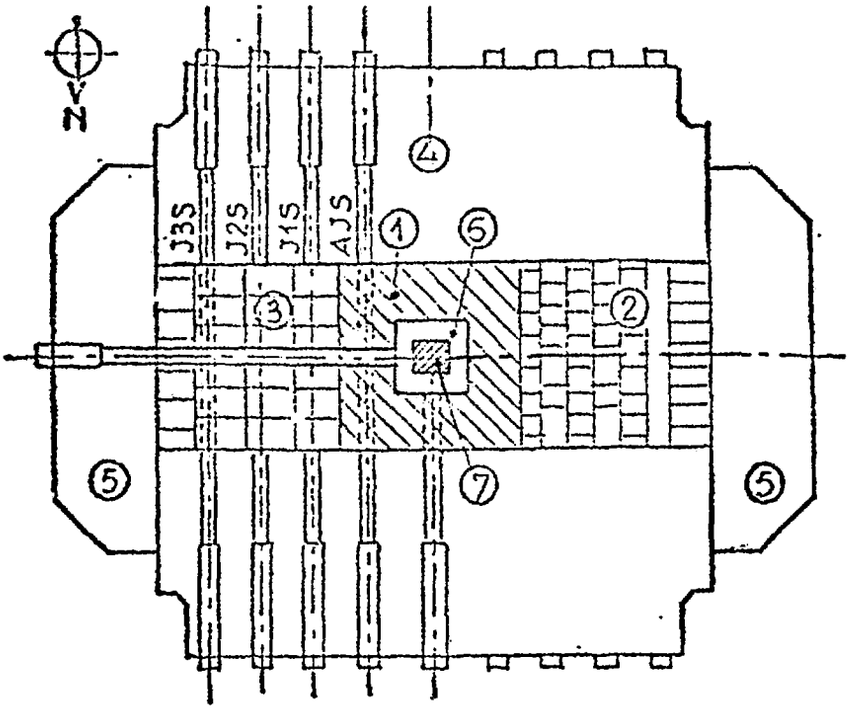

1-Bloc d'adaptation d'acier
2-Colonne Thermique
3-Colonne de Fer
4-5-Protection de béton lourd
6 -Couverture
7 -Coeur

SECTION HORIZONTALE D'HARMONIE MONTRANT LES CANAUX EXPERIMENTAUX DE LA COLONNE DE FER

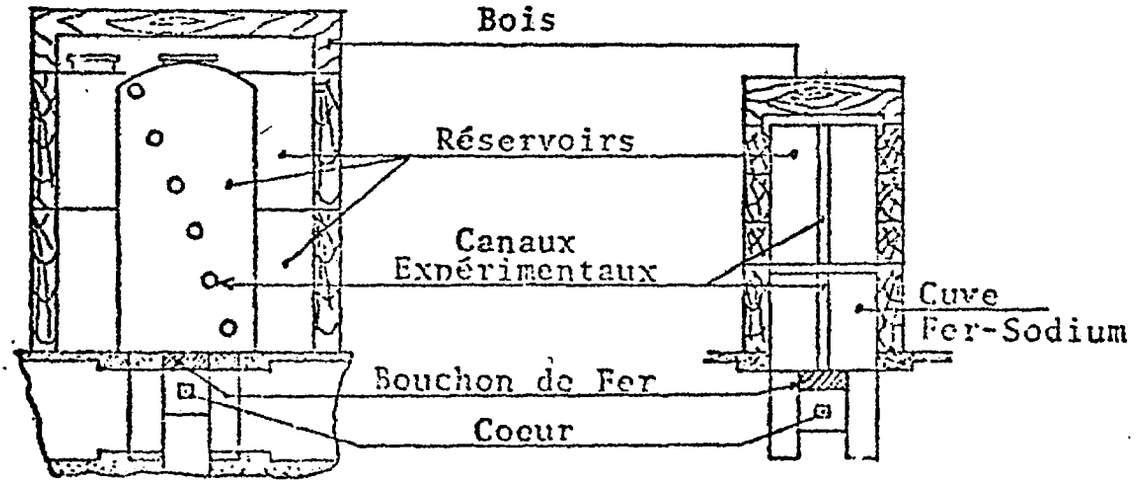

Assemblage Sodium

Assemblages Fer-Sodium

ASSEMBLAGES DISPOSÉS SUR LE REACTEUR HARMONIE

Schéma n° 1

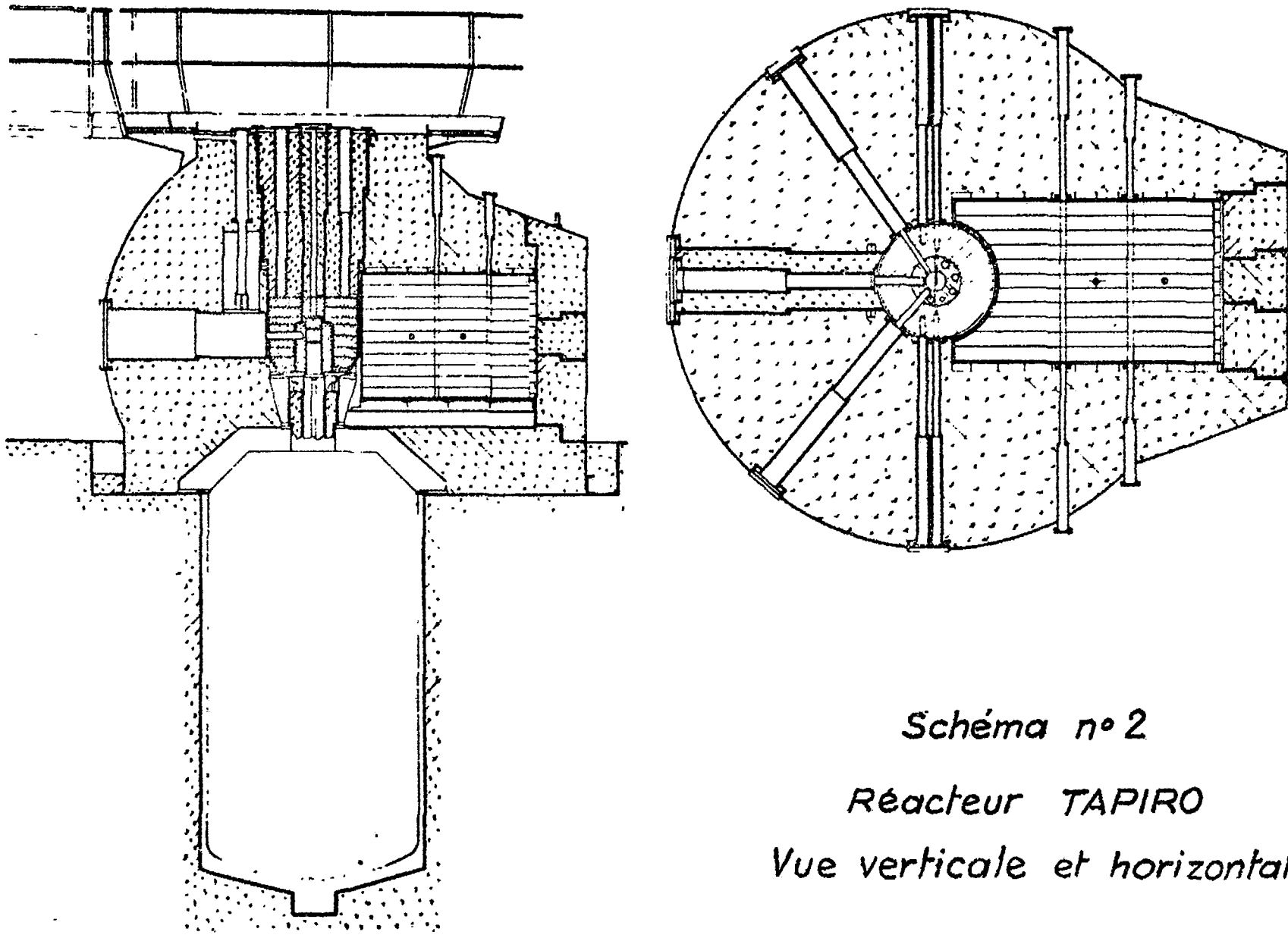

Schéma n° 2

Réacteur TAPIRO

Vue verticale et horizontale

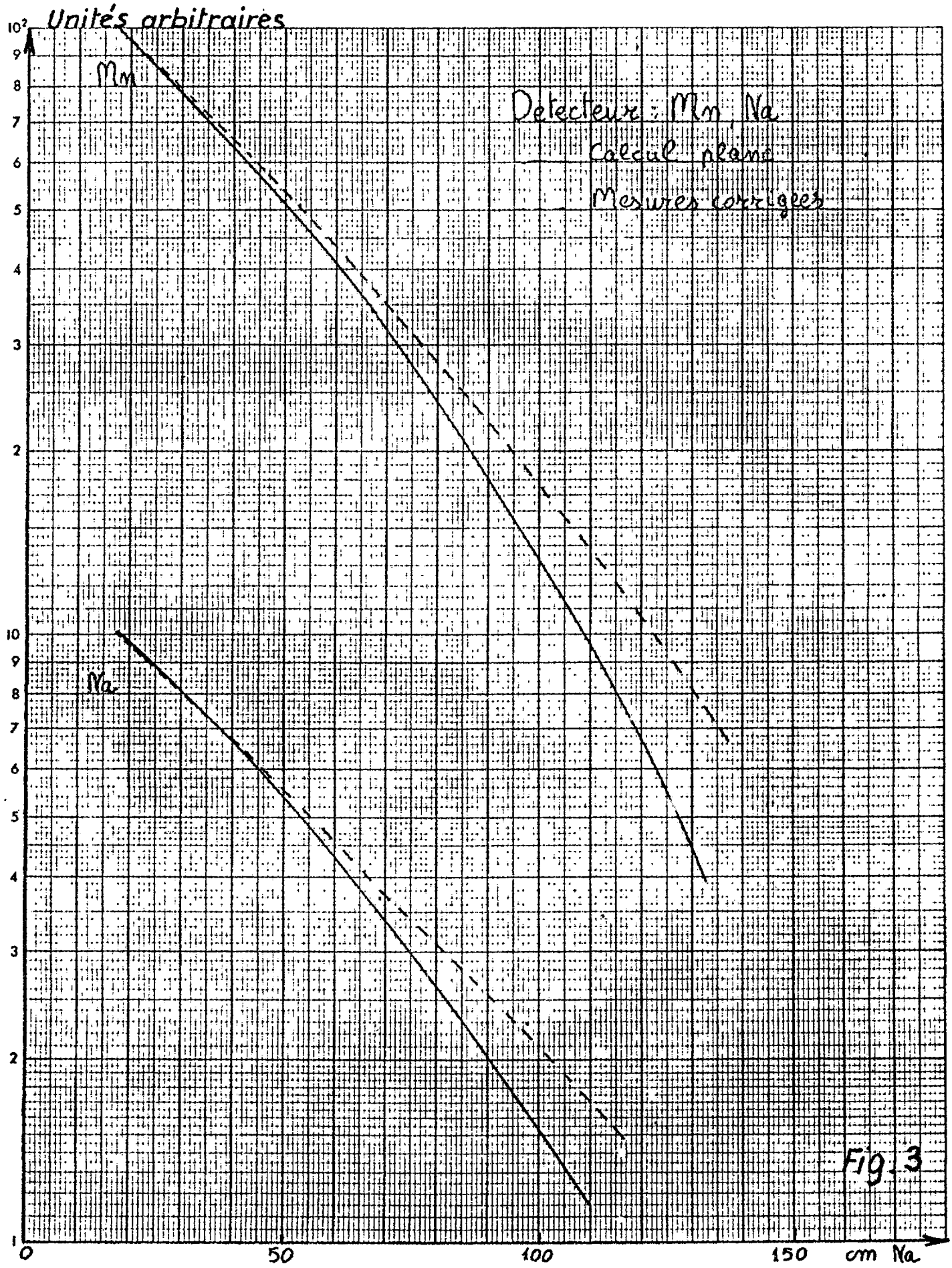
Unités arbitraires
Mn
Na
Détecteur : Mn, Na
Calcul plans
Mesures corrigées
cm Na
0
50
100
150

Fig. 3

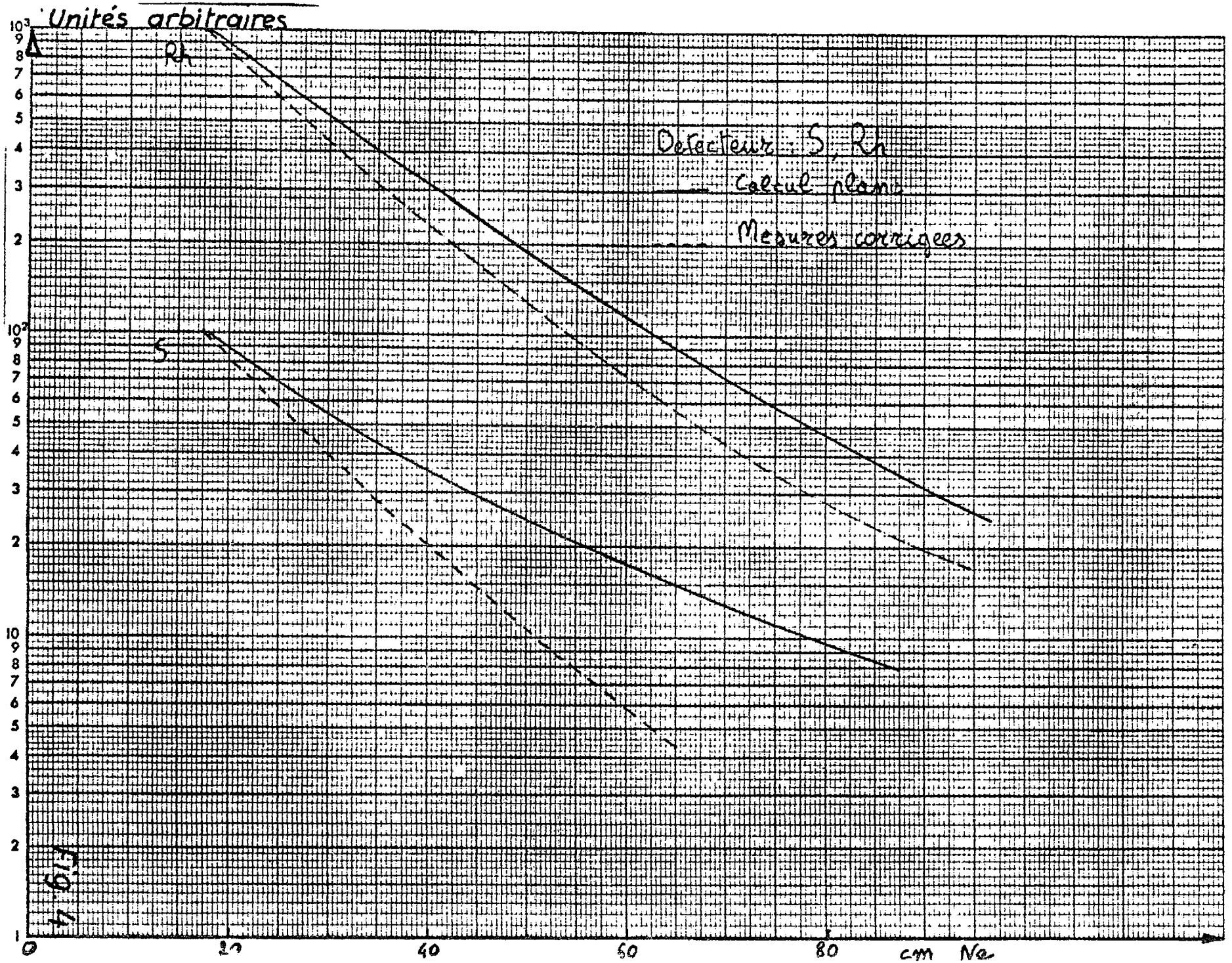
Unités arbitraires
Rh
S
Détecteur : S, Rh
Calcul plan
Mesures corrigées
cm Ne
0
10
40
50
80

Fig. 17

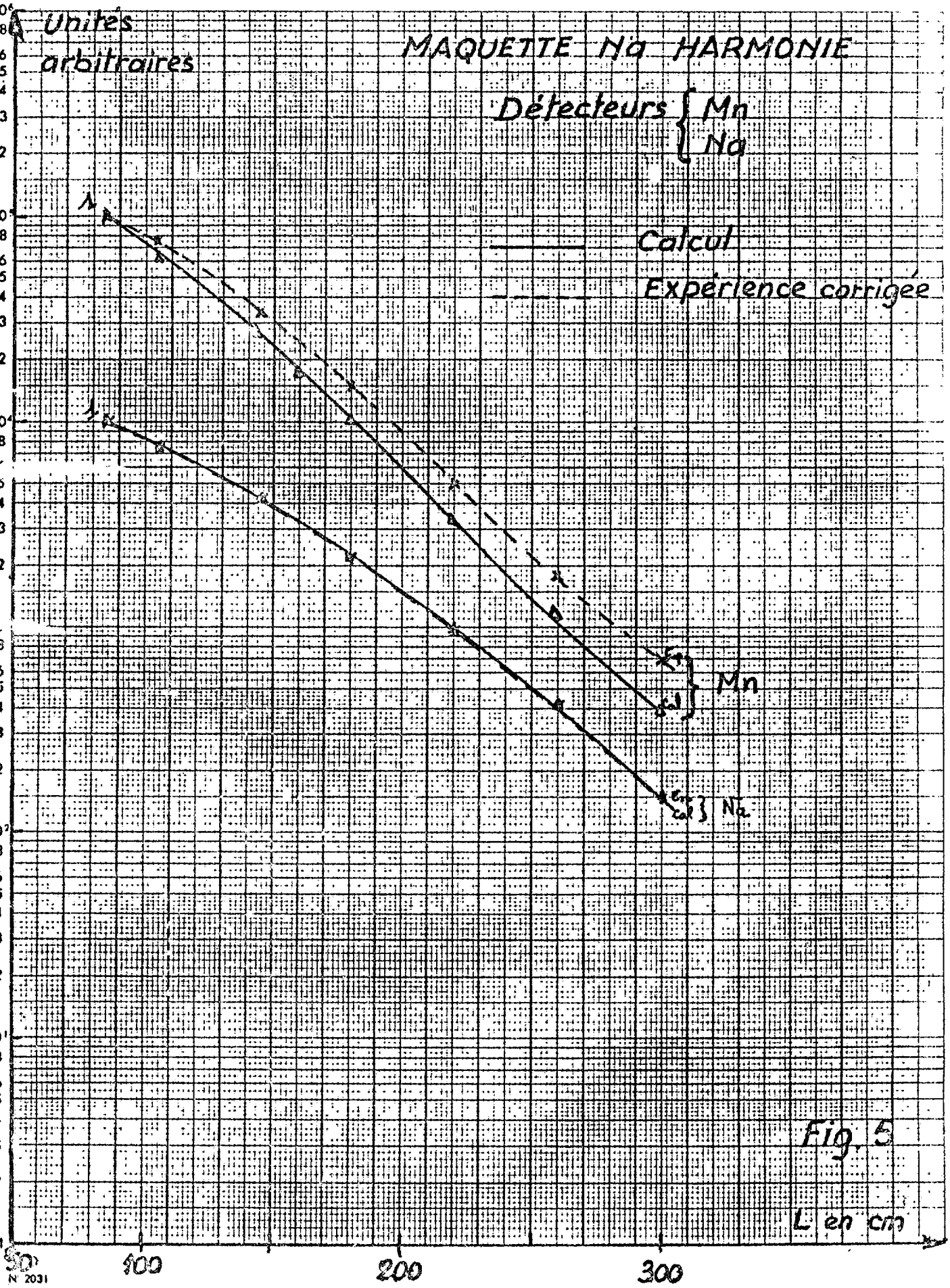
MAQUETTE Na HARMONIE
Détecteurs { Mn
Na
Calcul
Expérience corrigée
Unités arbitraires
Mn
N2
L en cm
50
100
200
300
N° 2031

Fig. 5

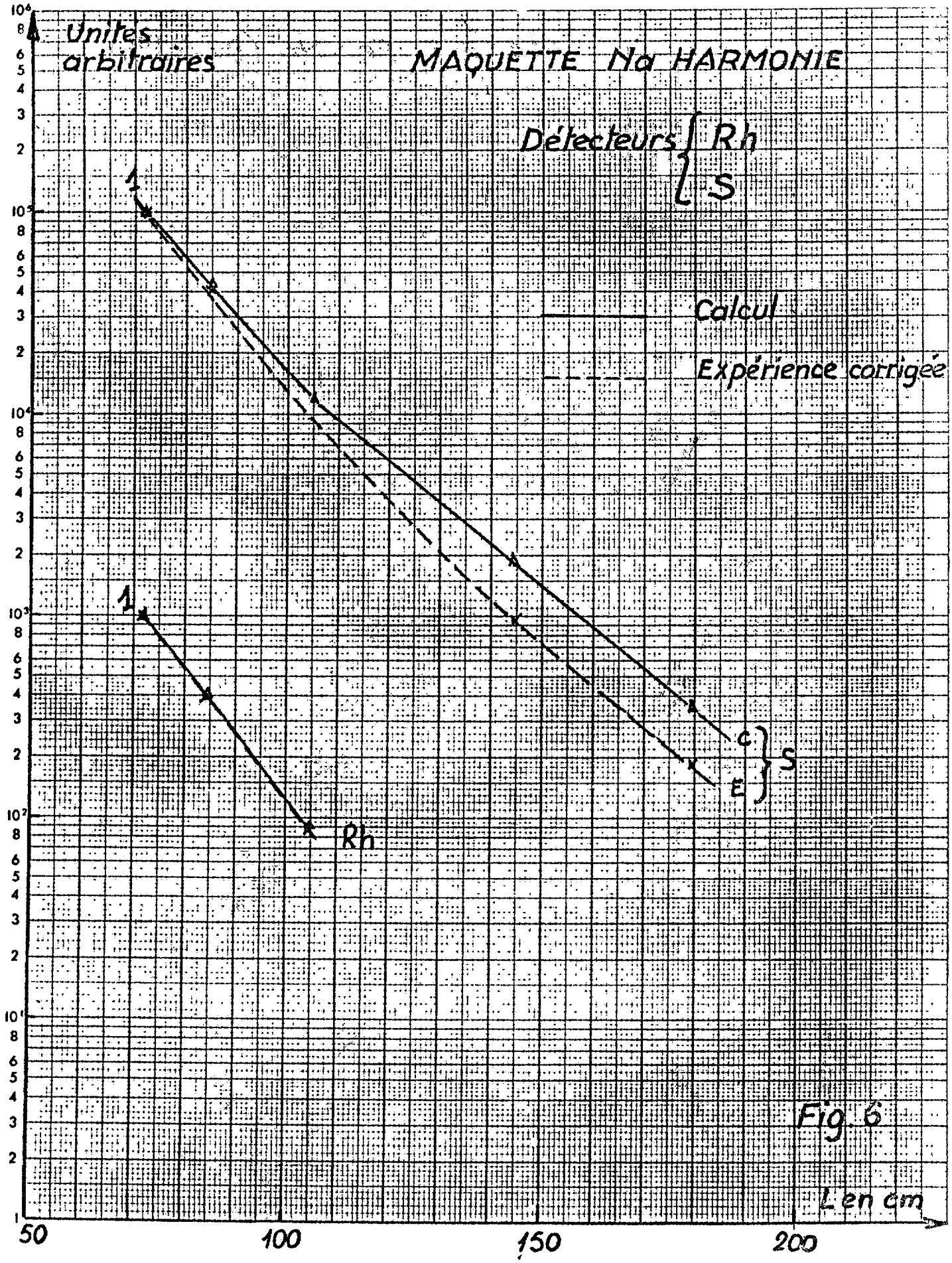
Unités arbitraires
MAQUETTE Na HARMONIE
Détecteurs { Rh
S
Calcul
Expérience corrigée
1
1
Rh
C
E
S
50
100
150
200
L en cm

Fig. 6

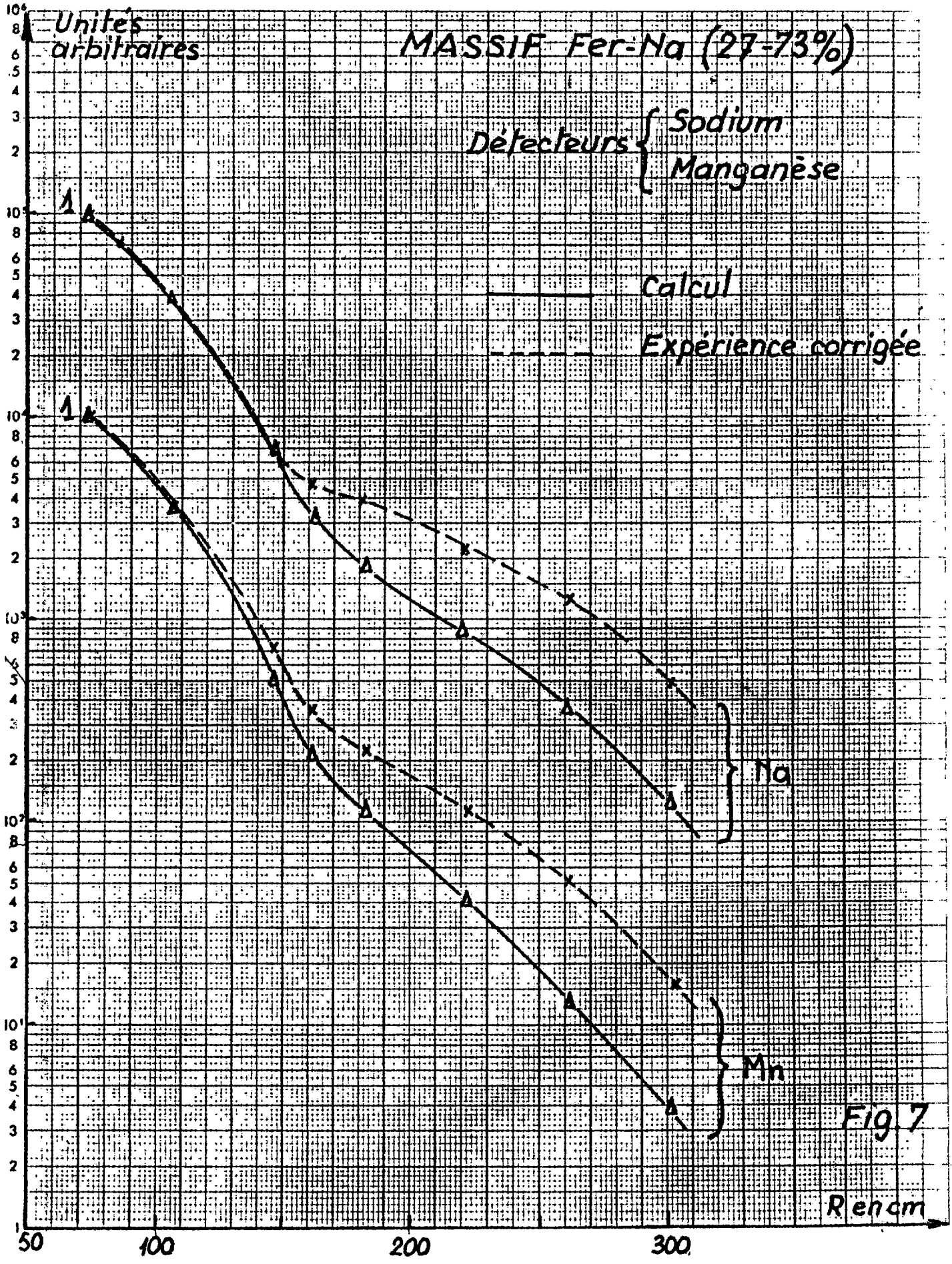
Unités arbitraires
MASSIF Fer-Na (27-73%)
Détecteurs { Sodium
Manganèse
Calcul
Expérience corrigée
1
1
Na
Mn
Fig 7
R en cm
50
100
200
300

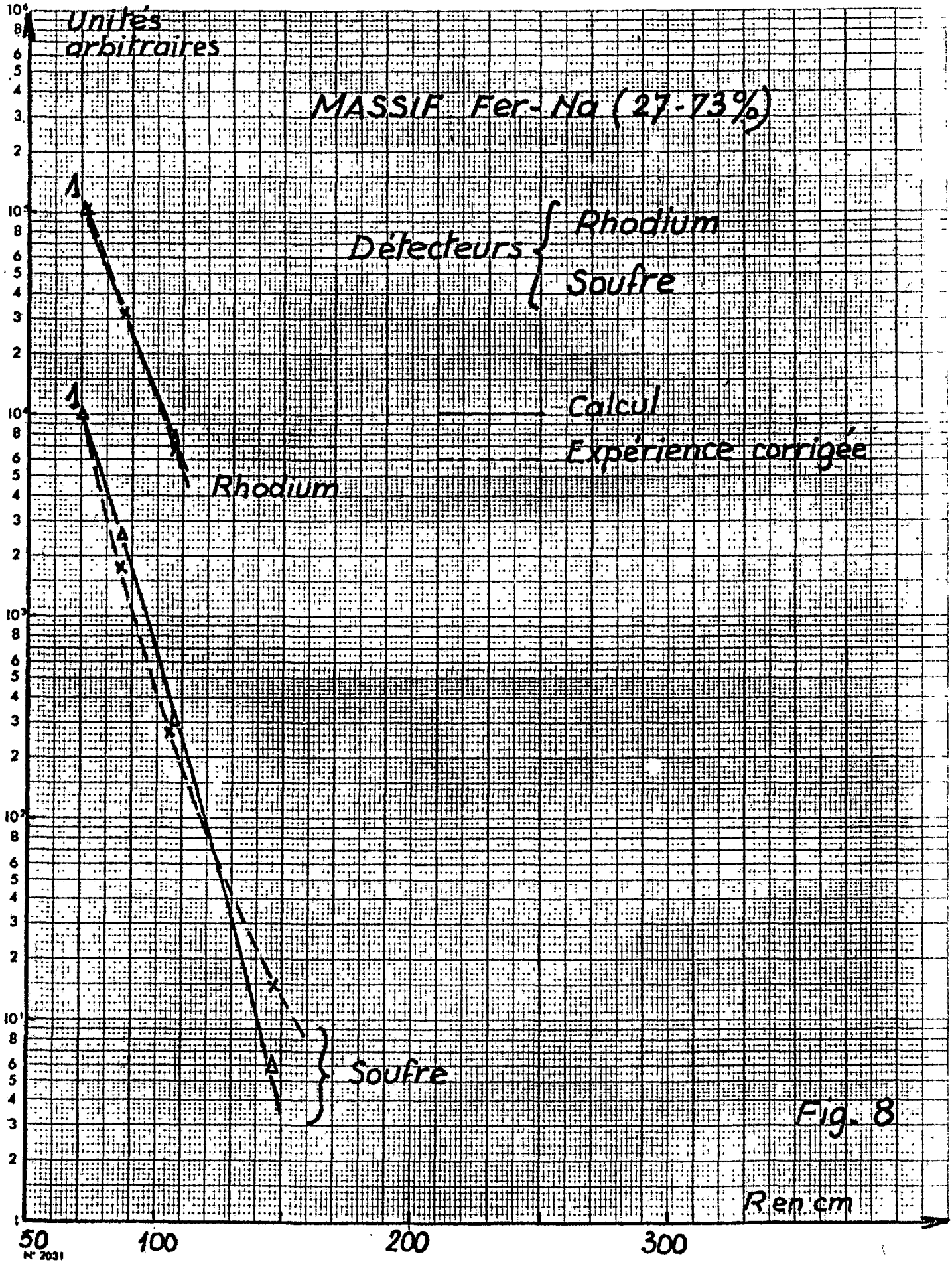
Unités arbitraires
MASSIF Fer-Na (27-73%)
Détecteurs
Rhodium
Soufre
Calcul
Expérience corrigée
Rhodium
Soufre
R en cm
50
100
200
300
N° 2031

Fig. 8

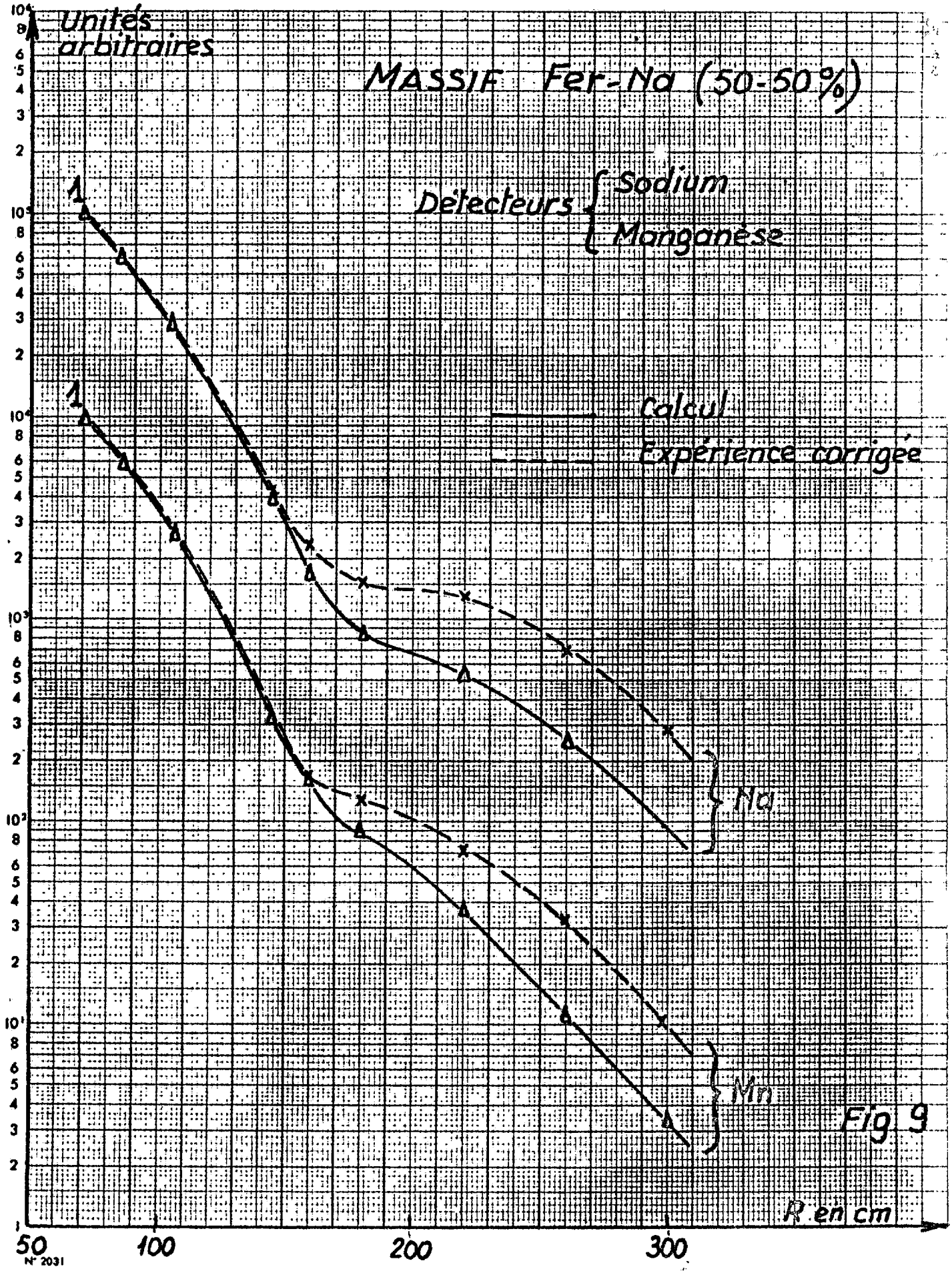
Unités arbitraires
MASSIF Fer-Na (50-50%)
Détecteurs { Sodium
Manganèse
Calcul
Expérience corrigée
1
1
Na
Mn
R en cm
50
100
200
300
N° 2031

Fig 9

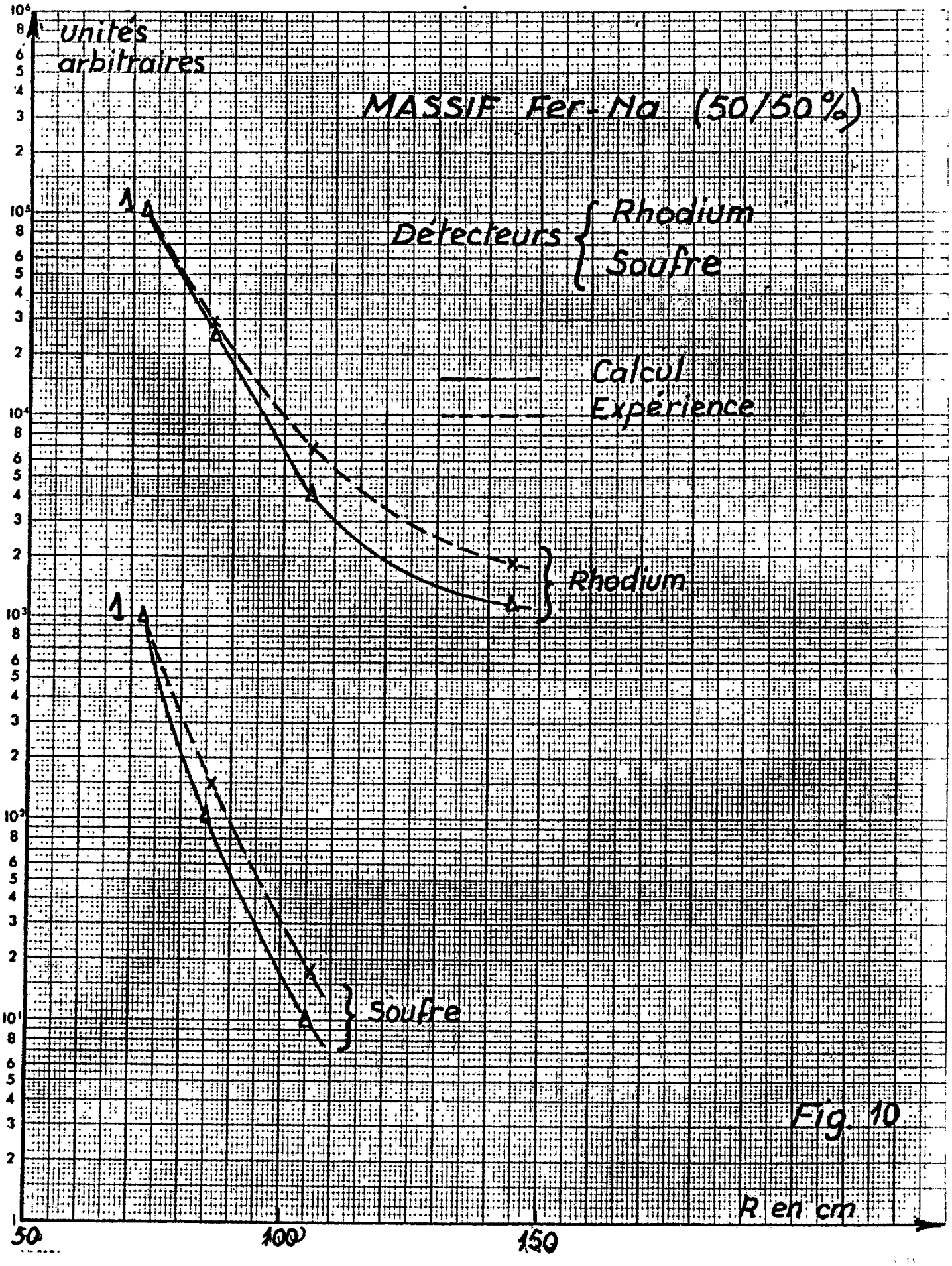
unités arbitraires
MASSIF Fer-Na (50/50 %)
Détecteurs { Rhodium
Soufre
Calcul
Expérience
Rhodium
Soufre
R en cm
50
100
150

Fig. 10

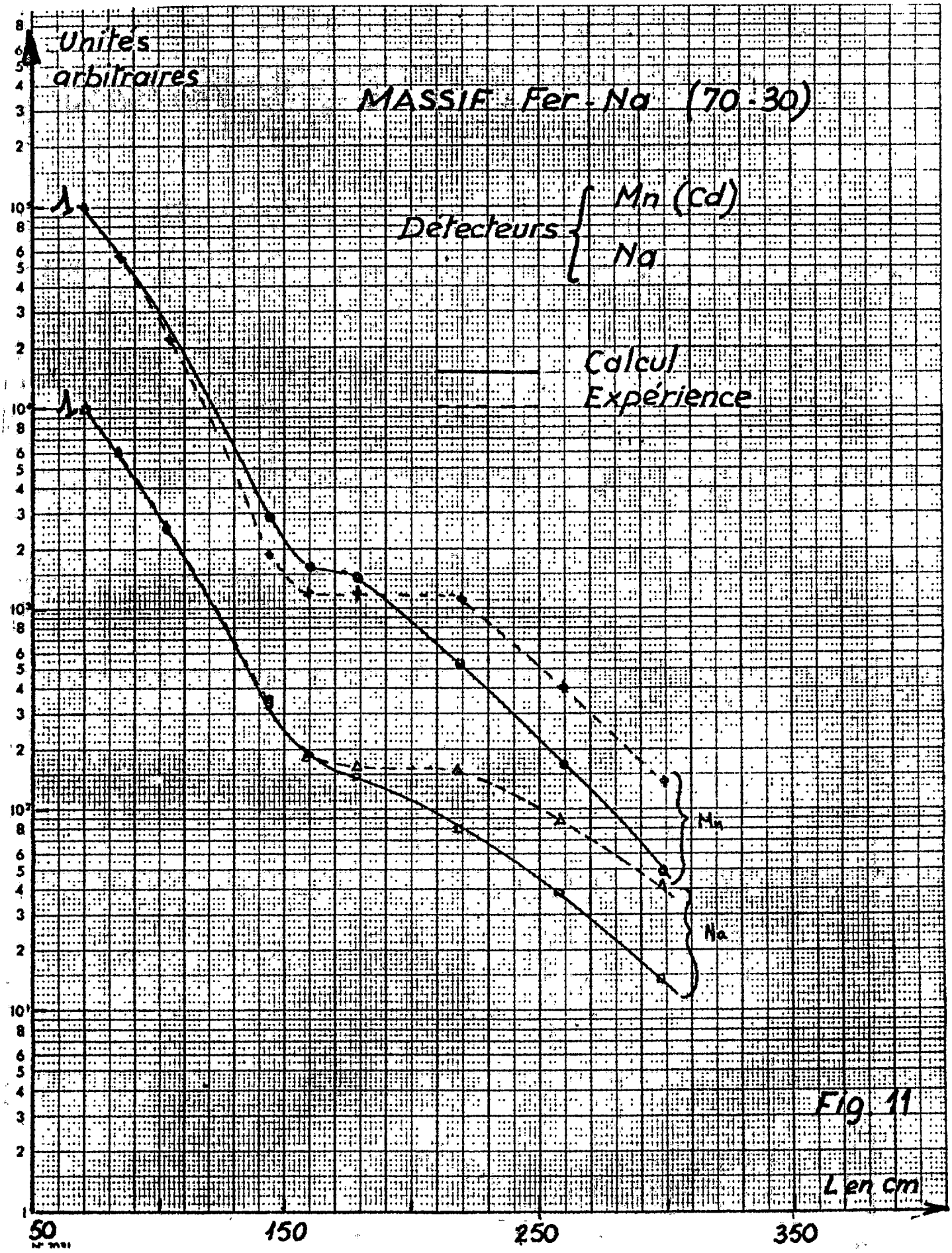
Unités arbitraires
MASSIF Fer - Na (70 - 30)
Détecteurs
Mn (Cd)
Na
Calcul
Expérience
Mn
Na
L en cm
50
150
250
350

Fig. 11

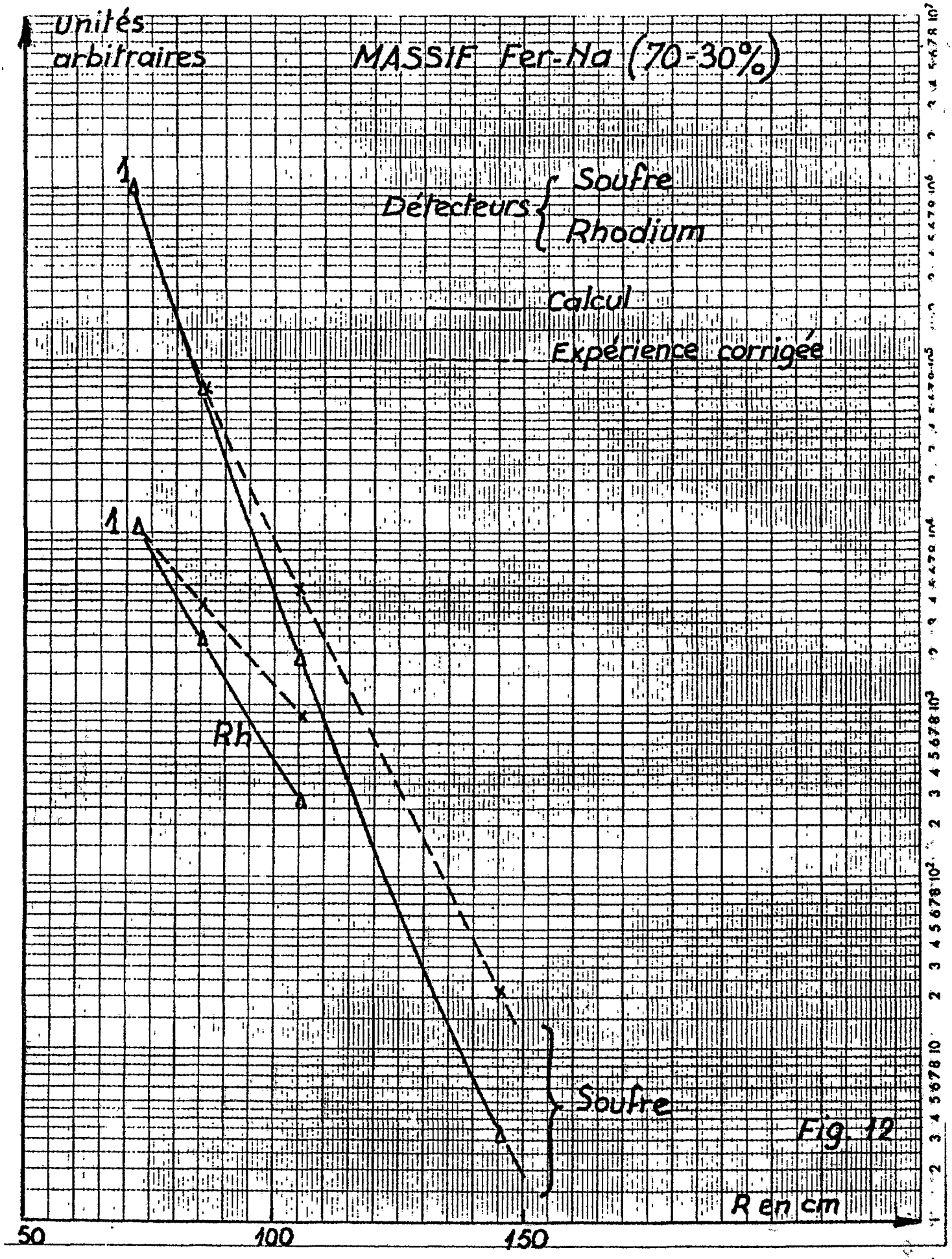
Unités arbitraires
MASSIF Fer-Ha (70-30%)
Détecteurs { Soufre
Rhodium
Calcul
Expérience corrigée
1
1
Rh
Soufre
R en cm
50
100
150

Fig. 12

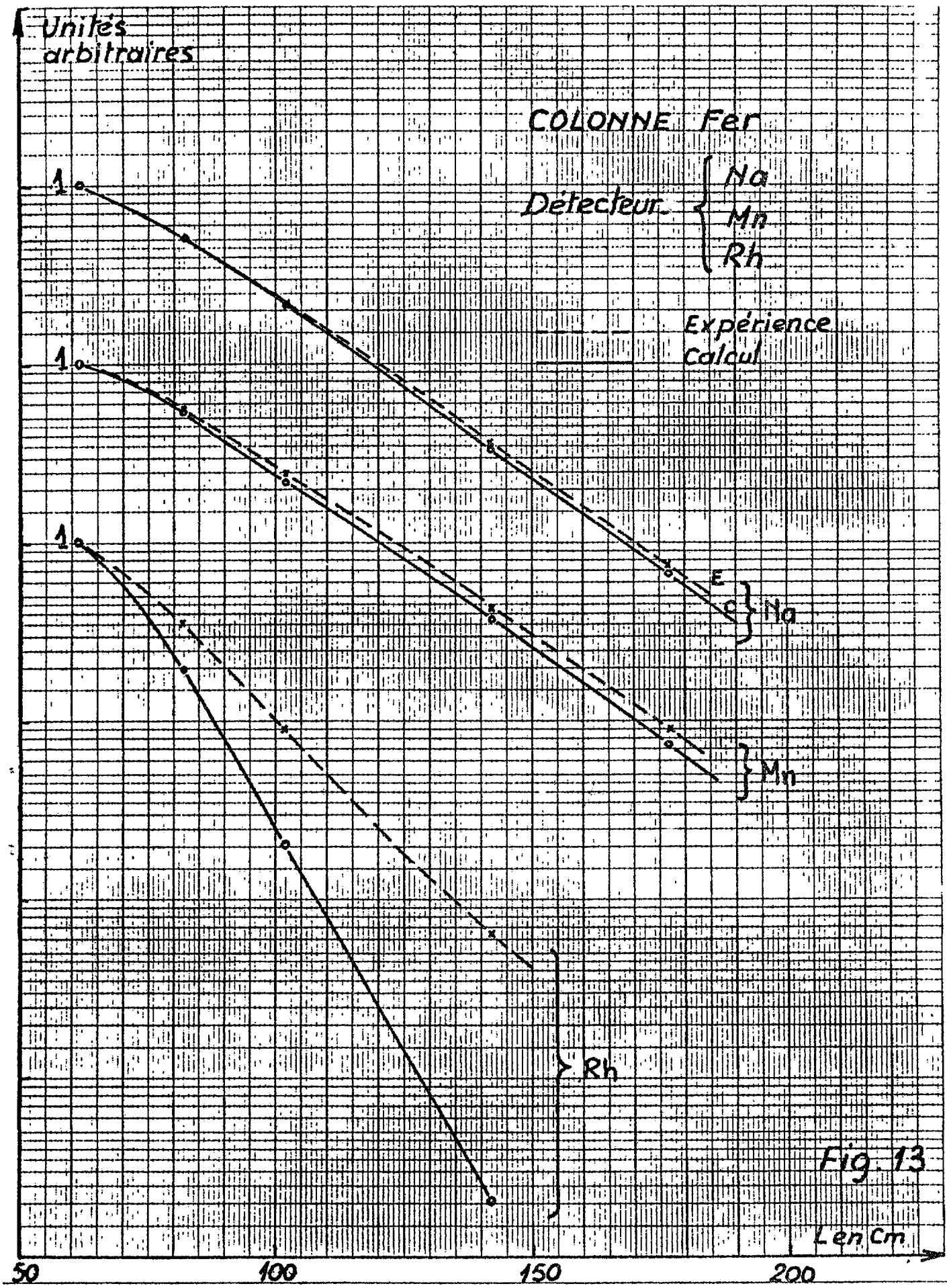
Unités arbitraires
COLONNE Fer
Détecteur { Na Mn Rh
Expérience
Calcul
1
1
1
E
C
Na
Mn
Rh
Fig. 13
Len cm
50
100
150
200

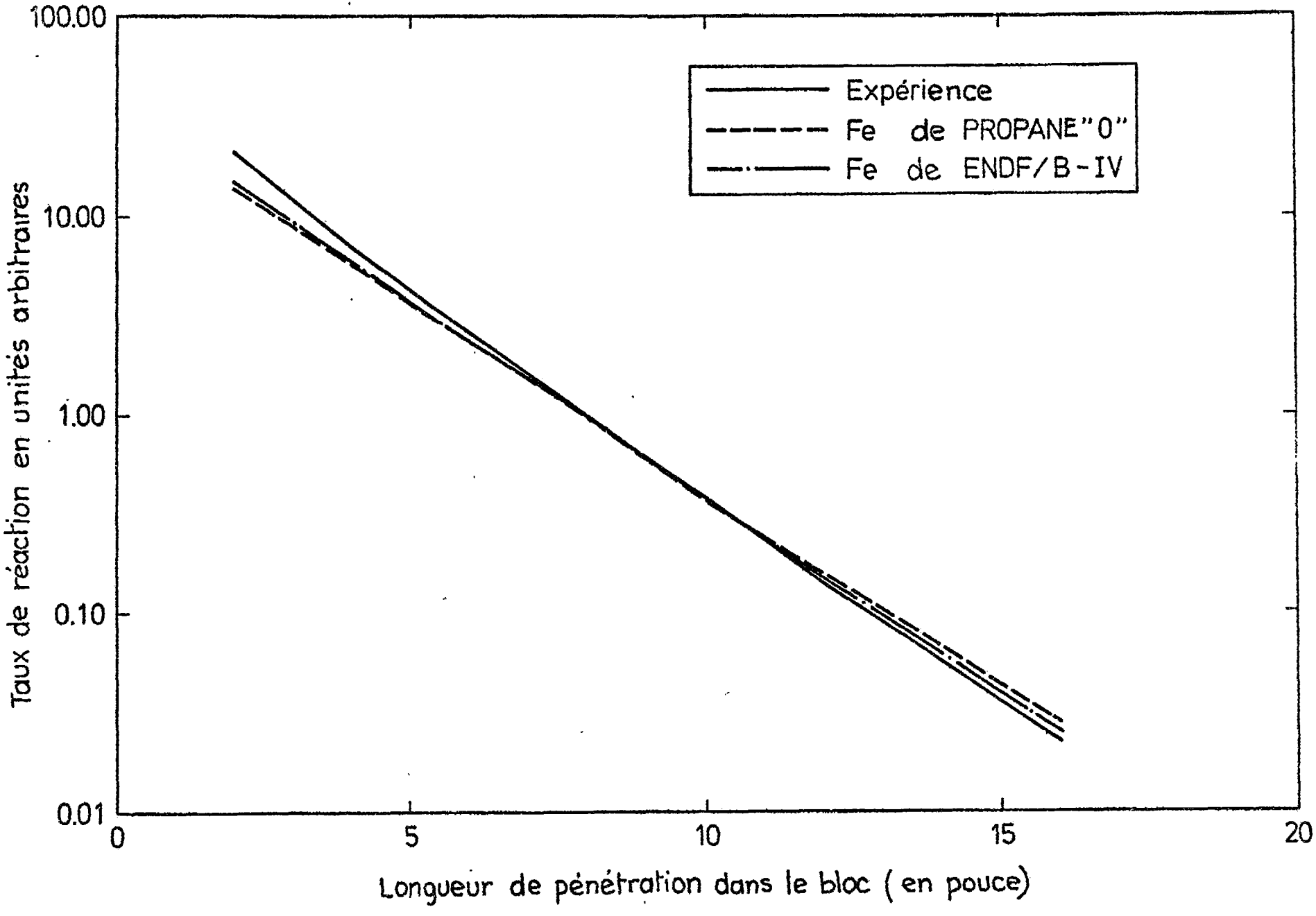

Fig.14 - *DISTRIBUTION DU TAUX DE REACTION DU SOUFRE (n,p) DANS LE BLOC DE FER ASPES*

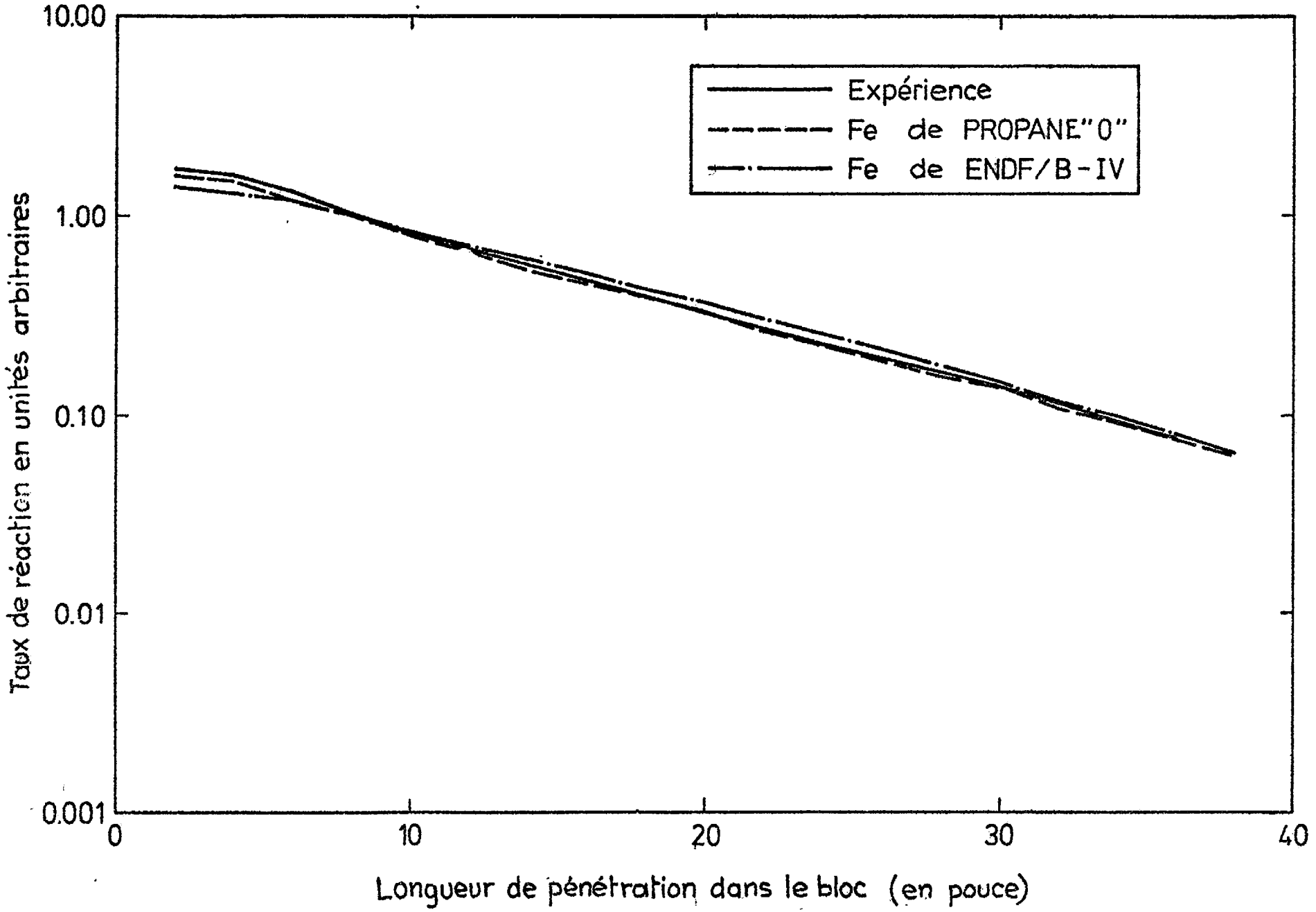

Fig. 15 : DISTRIBUTION DU TAUX DE REACTION DE L'OR(n,γ) DANS LE BLOC DE FER ASPES

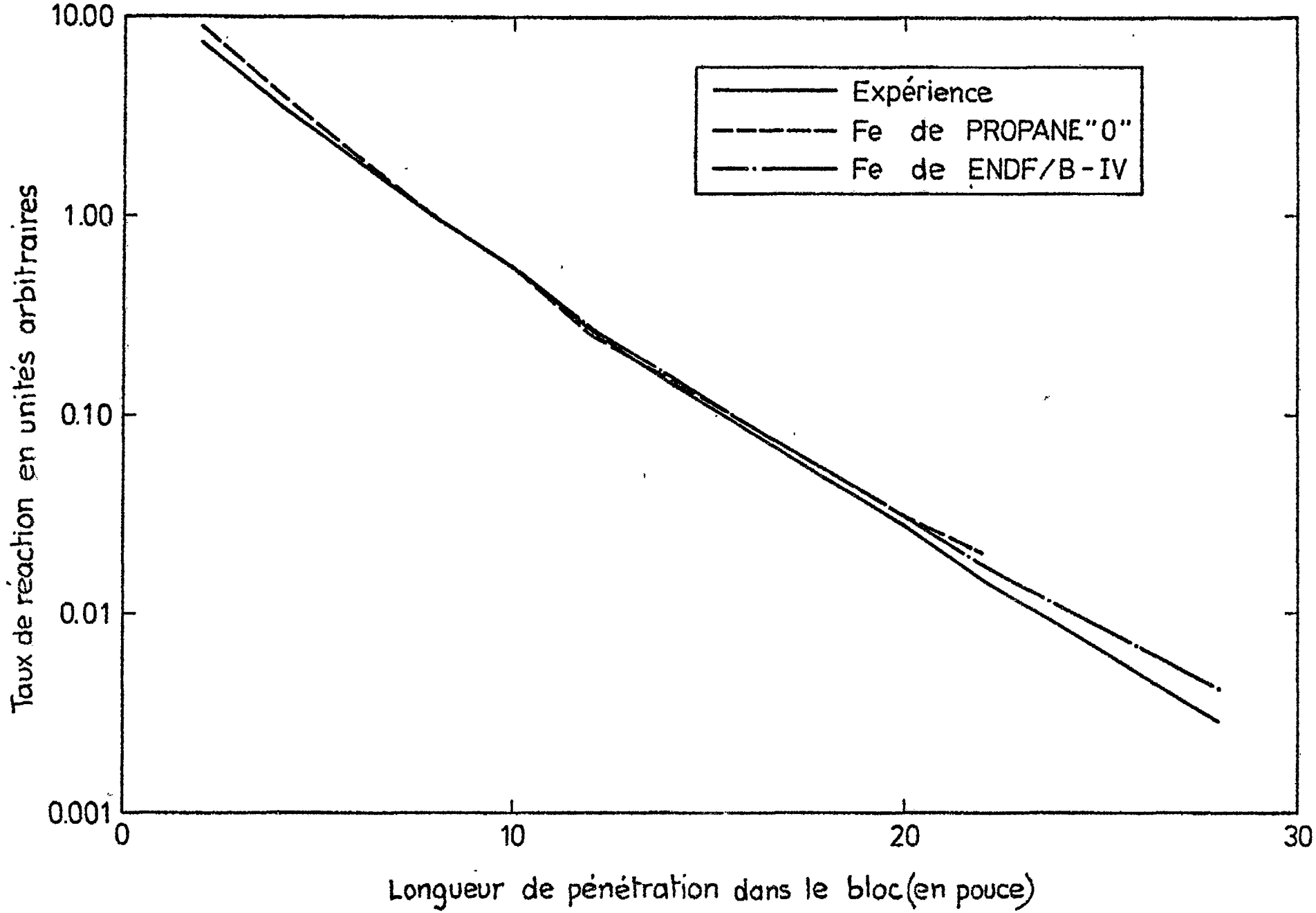

Fig. 16 - DISTRIBUTION DU TAUX DE REACTION DE L'INDIUM (n,n') DANS LE BLOC DE FER ASPES

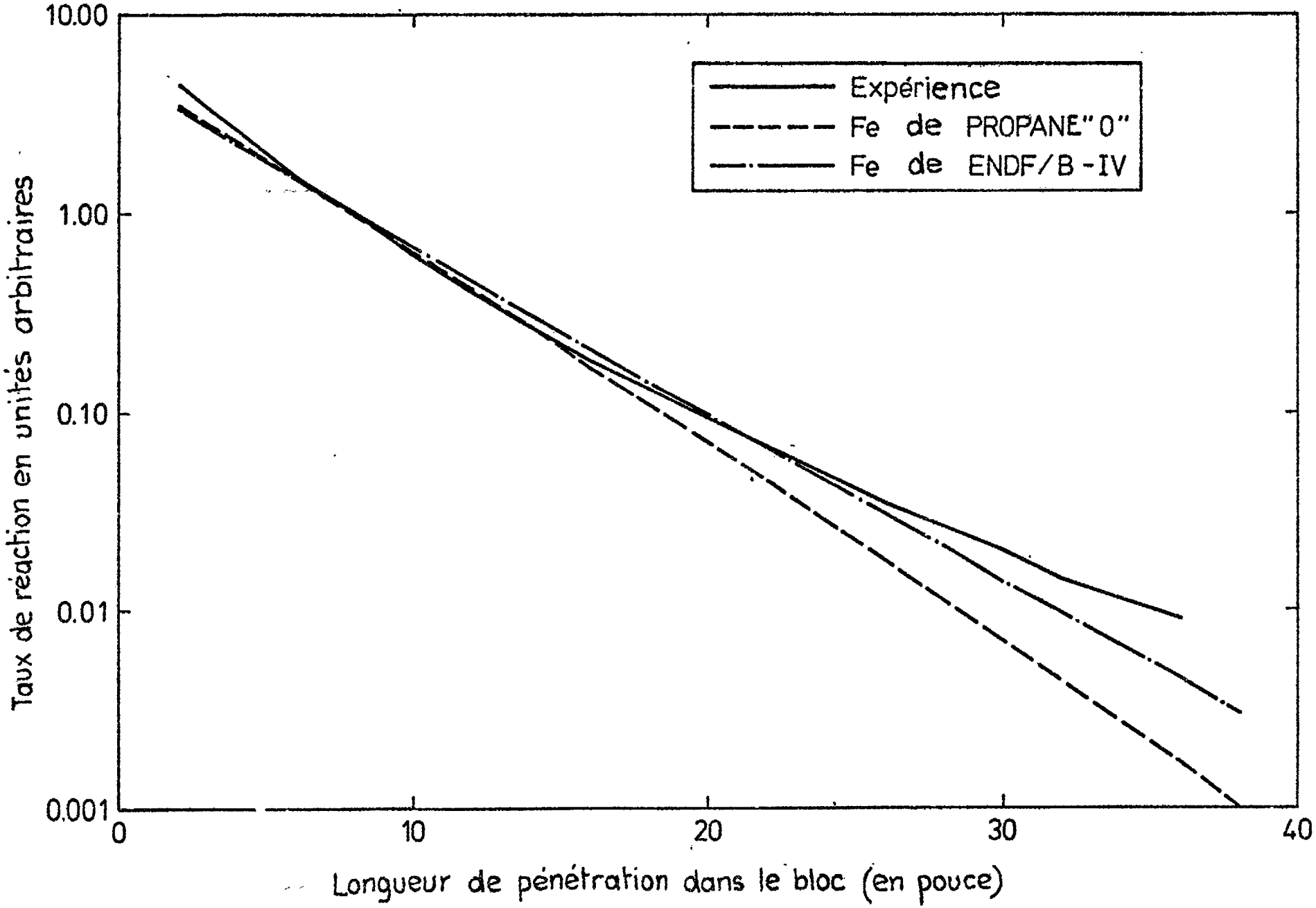

Fig. 17-*DISTRIBUTION DU TAUX DE RÉACTION DU RHODIUM (n, n') DANS LE BLOC DE FER ASPES*

Two-Dimensional Shielding Benchmarks for Iron at YAYOI (I)

Yoshiaki Oka, Shigehiro An, Shun-ichi Miyasaka*
Kinji Koyama*, Shigeru Kasai, Ryosuke Yoshii
Hiroyuki Hashikura, Masatsugu Akiyama
Tomonori Hyodo**

University of Tokyo
* Japan Atomic Energy Research Institute
Tokai-mura, Ibaraki, JAPAN
** Kyoto University
Kyoto, JAPAN

Abstract

The aim of this work is to assess the collapsed neutron and gamma multigroup cross sections for two dimensional discrete ordinate transport code.

Two dimensional distributions of neutron flux and gamma ray dose through a 70cm thick and 94cm square iron shield were measured at the fast neutron source reactor "YAYOI". The iron shield was placed over the lead reflector in the vertical experimental column surrounded by hearvy concrete wall. The detectors used in this experiment were threshold detectors In, Ni, Al, Mg, Fe and Zn, sandwitch resonance detectors Au, W and Co, activation foils Au for neutrons and thermoluminescence detectors for gamma ray dose.

The experimental results were compared with the calculated ones by the discrete ordinate transport code ANISN and TWOTRAN.

The region-wise, coupled neutron-gamma multigroup cross-sections (100n+20gamma, EURLIB structure) were generated from ENDF/B-IV library for neutrons and POPOP4 library for gamma-ray production cross-sections by using the code system RADHEAT. The effective microscopic neutron cross sections were obtained from the infinite dilution values applying ABBN type self-shielding factors. The gamma ray production multigroup cross-sections were calculated from these effective microscopic neutron cross-sections. For two-dimensional calculations the group constants were collapsed into 10 neutron groups and 3 gamma groups by using ANISN.

I. Introduction

In designing reactor shields of a liquid metal fast breeder reactor (LMFBR) the estimation of the neutrons and gamma-rays in the materials surrounding the core is very important for the assessment of neutron damage and heat generation. The calculations, however, are not reliable and accurate enough to satisfy the requirements of the design. The one and two dimensional discrete ordinate transport codes become now available in the design of the shields of LMFBRs. The accuracies of these transport calculations depend directly on those of the multigroup cross sections used in the calculations. In order to evaluate the accuracy of the two dimensional transport code and its cross sections, the present experiments were performed in a geometry suitable to that study. The experiments were performed in the vertical experimental column of the fast neutron source reactor YAYOI of University of Tokyo. A 70cm thick and about 94cm square iron shield was used. The shield was settled on the outer lead reflector of the core and was closely surrounded by heavy concrete wall of the vertical column. The iron is used because it is a basic material constituting reactor shields.

The distributions of neutrons and gamma-rays in the iron shield were measured by threshold detectors In, Ni, Al, Mg, Fe and Zn, sandwitch resonance foils Au, W and Co, activation foils Au for neutrons and thermo-luminescence detectors (TLDs) for gamma ray dose. The analysis of the experiments were performed by the one and two dimensional discrete ordinate transport code ANISN[1] and TWOTRAN[2]. The coupled neutron and gamma ray cross sections were generated by RADHEAT[3] system. Self shielding effect was taken into consideration in generating those cross sections. For two dimensional calculations a few group cross sections were collapsed by ANISN.

II. Experimental

The experimental configuration is presented in Fig. 1. The core of the fast neutron source reactor YAYOI is a horizontal cylinder of a 93% enriched uranium metal fuel of 125mm diam and 150mm long, which is surrounded by a 0.4% depleted uranium metal blanket and by the inner and outer reflector of lead. It is possible to move the core in the guide wall and to operate it at six stations. The present experiments were performed at the station B. Over the outer reflector is situated the vertical experimental column where the experiments were performed. The iron shield consists of seven iron plates each of which is 10cm thick and 88cm square. As seven plates are piled up, the iron shield becomes 70cm thick. This shield is contained in a support box and is setlled in the bottom of the vertical experimental column. Since the support box is made of iron plates of 3cm thickness except a bottom plate of stainless steel, the total width of the iron is about 94cm. The iron is closely surrounded by the heavy concrete wall of the vertical column.

The neutrons and gamma-rays in the iron shield were measured by using the threshold detectors, sandwitch resonance foils of Au, W and Co, activation foils Au for neutrons and thermo-luminescence detectors (TLD) for gamma ray dose. The threshold reactions were $^{115}In(n,n')$, $^{58}Ni(n,p)$, $^{27}Al(n,p)$, $^{27}Al(n,\alpha)$, $^{24}Mg(n,p)$, $^{54}Fe(n,p)$, $^{56}Fe(n,p)$ and $^{64}Zn(n,p)$. These threshold reactions except indium could be detected only at the inner

surface of the iron shield due to the lack of the integral irradiating power and also due to the weak activities. The distributions of the reaction rates in the iron shield were measured with indium pellets using 115In(n,n') reactions for fast neutrons and with gold foils and cadmium covered gold foils. The two dimensional distributions of these reactions were obtained at 0, 20, 40 and 60cm from the inner surface of the iron shield. The sizes of the detectors are as follows. The threshold detectors were the pellets of about 30mm in diam and 6mm thick. The sandwitch foils were thin foils of 12.7mm in diam and activation foils were about 0.05mm thick and about 7mm square. These foils or pellets were inserted and irradiated in small holes caved in the iron shield. The radioactivities were measured with a 77cc coaxial Ge(Li) semiconductor detector. The efficiency of this detector was calibrated with a point-like CEA standard gamma-ray source. This efficiency was used for foils. The efficiencies for the pellets were experimentally obtained by comparing the detected activities of a pellet with that of a foil both of which were simulaneously irradiated in the same neutron field.

Thulium activated $CaSO_4$ TLDs that were contained in rod-type glass capsules were used for the measurements of gamma-ray dose. These TLDs were the products of Matsushita Electric Industrial Co., Ltd. The reader of the TLDs is the type UD-502A of the same company. The calibration of the reader was performed by a Co-60 standard source. The additional measurement with a Mg_2SiO_4 TLD in a polyethylene capsule agreed with that of $CaSO_4$ TLDs within 20% in absolute value. The measurement by 7-LiF TLDs in glass capsules gave about 10% larger values than the $CaSO_4$ TLDs. The results by BeO TLDs showed about two times larger value than the value of the $CaSO_4$ TLDs. These differences seem to be due to the effect of neutrons.

III. Calculation

One and two dimensional discrete ordinate transport codes ANISN[1] and TWOTRAN-II[2] were used in the analysis of the experiments. In order to approximate the real reactor-shield configuration as precisely as passible, a slab model shown in

Fig. 2 and r-z model in Fig. 3 were used as calculational geometries for ANISN and TWOTRAN respectively. The atomic member densities at any region of these models are shown in Table I. The region-wise coupled neutron-gamma multigroup cross sections were generated by using the code system RADHEAT-V3[3], with which the following calculations were performed.

(1) The infinite dilution microscopic neutron cross section for each material was calculated by SUPERTOG-JR[3] using the ENDF/B-IV[4] library as basic cross sections.

(2) The effective region-wise macroscopic cross sections were generated by multiplying the ABBN type self shielding factors taken from the JAERI fast sets[5]. For the cross sections of Pb, H, Si, Ca and Al in Table I this factor cannot be multiplied because the JAERI fast sets do not contain the factors for these nuclides.

(3) The neutron-induced gamma-ray production cross sections and yield data were calculated based on the POPOP4[6] library. The gamma-ray transport cross sections were generated by the GAMLEG-JR[3] code. The material members of the ENDF/B-IV file and identification numbers of the POPOP-4 library used in the calculations are summarized in Table II.

(4) The EURLIB structure was used as the energy group structure for the one dimensional calculations. The P5 approximations was used as the Legendre expansion coefficient.

The EURLIB structure of the coupled 100 neutron groups and 20 gamma groups is presented in Table III. For two dimensional calculation a few group macroscopic cross sections were collapsed with the region dependent spectrum by P5-S8 ANISN calculation. The few group energy structure is shown in Table IV. This structure was chosen considering the calculated neutron spectrum in the iron shield by ANISN. The calculation by the TWOTRAN code is on only preliminary stage. The P1-S6 approximation is chosen in the present report.

The detector responses for one dimensioanl calculations are shown in Table V. These threshold neutron cross sections were taken from the OECD/NEA compilation of threshold neutron cross sections[7] published in Feb. 1974. The cross section for gold foils was calculated from the ENDF/B-IV file. The dose

conversion factor was calculated based on the formula of X-ray attenvation coeffecients. The detector responses for two dimensional calculations were also collspsed in the same way as the region wise macroscopic cross sections described in the above. The collapsed detector responses are shown in Table VI.

IV. Results and Discussions

The calculated total flux incident to the center of the inner surface of the iron shield is presented in Table VII(a). The calculated neutron spectra at 0, 20, 40 and 60cm from the inner surface of the iron shield are shown in Fig. 4(a). These are the results calculated by the ANISN code with a P5-S8 slab model with the buckling of 60cm plane height and 60cm plane depth, The calculated result without buckling effect are shown in Table VII(a) for total flux and Fig. 4(b) for the spectra. The effect of buckling is extremely strong at low energy region. The results without buckling are about from ten to fifty times larger than those with buckling effect. The spectra by the TWOTRAN code are presented in Fig. 5. Comparing Fig. 4(a), Fig. 4(b) and Fig. 5, we observe that the spectrum by TWOTRAN exists between that by ANISN without buckling and that with buckling.

The measured and calculated reaction rates at the inner surface of the iron shield are presented in Table VIII. The values are given in absolute reaction rates at 2kw power level. The detector cross sections used in the calculation have already presented in Table V and VI. The C/E values of threshold reactions are best for the ANISN calculation without buckling effect. The measurement of these threshold reactions and the measurement of the efficiencies for pellets were repeated more than three times. Based on the measured threshold reaction rates in Table VIII, the unfolding to neutron spectrum was performed by SAND-II code[8]. The result above 0.2MeV is presented in Fig. 6(a) together with the calculated spectrum by ANISN with buckling effect. Both results are shown in absolute spectra at 2kw power level and no other normalization is performed. This figure shows that at the source point of

the iron shield the calculated spectrum above 1MeV agrees fairly well with the experiment. Below 1MeV the measured value overestimates the calculated one about factor two. The comparison with the calculation of without buckling effect is shown in Fig. 6(b). The disagreement below 1MeV is small in this figure. In Fig. 7(a) the neutron spectra obtained by the sandwitch resonance foils are compared with the calculated results by ANISN. In this figure the calculation is normalized to the experimental result at 4.9eV of the gold sandwitch foils at the inner surface of the iron shield. In absolute comparison the calculation is about twenty six times smaller than the measurement at this energy. In Fig. 7(b) The comparison with the calculation without buckling effect is shown. In this figure the differences between the calculation and the measurements are small. The resonance integrals for these foils are based on the values presented in the report KFK-718[9].

The distributions of In(n,n') reaction rates in the iron shield are shown in Table IX. The comparison with the calculations by the ANISN and the TWOTRAN code are presented in Fig. 8 on the centerline of the iron shield. The results shows the absolute reaction rates at 2kw and no normalization is performed. The calculation by ANISN without buckling is the best in the calculations, but the difference from the experimental value is large at 60cm thick iron shield or 110cm from the core center. In Fig. 9 the measured two-dimensional distributions are compared with the results by TWOTRAN. In this figure the calculated value is normalized to the experiment at the center of the inner surface of the iron shield. As for the shapes of the calculated distributions the calculation agrees well with the measurement.

The distributions of the measured Au(n,gamma) reaction rates in the iron shield are shown in Table X. The uncertainties are estimated to be below 3% for relative comparison and below 10% for absolute values. The latter is mainly due to the error in calculating photo peak counts. The error due to the statistics of the counts is below 1%. The cadmium ratio is nearly 1.0 this is affirmed by the decrease in the neutron spectrum in low energy region shown in Fig. 6. The comparison with the calculation is shown in Fig.10. In absolute values the result by TWOTRAN shows

rather good agreement with the measurement, but in relative comparison the calculation by ANISN without buckling is the best. In Fig.11 the distributions are compared with calculated results by TWOTRAN. The shape of the distribution agrees fairly well with the measurement except at iron shield 60cm. Also at 40cm distance from the centerline the calculation shows about 40% larger value than the measurement. This is the effect of the boundary between the iron and the surrounding heavy concrete wall.

The distributions of the measured gamma ray dose in the iron shield are shown in Table XI. The uncertainties are estimated to be within 25%, which is obtained by the repeated measurements. The comparison with the calculed ones are presented in Fig.12. The calculation by ANISN without buckling overestimates the measurements, while the calculation by TWOTRAN shows underestimation. In Fig.13 the two dimensional distributions are compared with the experiments. At the inner surface of the iron shield the calculation shows good agreement with the measurement. The rise at 40cm distance from the centerline is due to the capture gamma ray by the thermal neutrons produced in the neighbouring heavy concrete. At 60cm iron shield the distribution does not agree with the measurement. Comparing Fig.13 and Fig.11, we observe that the distribution of the gamma-rays is similar to that of the gold foil reaction rates except at the point 40cm from the centerline. Since the gamma rays detected by TLDs are almost capture gamma rays in the iron, which was proved by the measurement of the gamma ray spectrum with a NE213 scintillator by Hyodo et.al.,[10] the disagreement in the gamma ray dose is due to the inadequate treatment of slowing down neutrons in the calculation.

V. Conclusions

The following conclusions are obtained about the difference between the calculation by TWOTRAN and that by ANISN. The P1-S6 approximation is taken for TWOTRAN, while P5-S8 approximation for ANISN. For TWOTRAN the components of forward scattering may be underestimated in higher energy range due to P1 approximations, so the threshold reaction rates of indium are underestimated. On the contrary in lower energy range this effect may be decreased and the TWOTRAN code gives the rather good results with the

measurement by the gold foils and the TLDs. For ANISN the P5-S8 approximation is good in higher energy range and the calculated spectrum agrees with the measurements. In the lower energy range the disagreement with the measurements by the gold foils, the TLDs and the sandwitch resonance foils may be due to the overestimation of the buckling for the case of the calculation including buckling H=Y=60cm and due to the underestimation of buckling for that of the calculation without buckling.

The analysis by TWOTRAN code is only on a preliminary stage. The followings will be considered in the forthcoming study.

(1) The effect of the order of scattering.

(2) The evaluation of the present region-wise macroscopic cross sections including the self shielding effect.

(3) The geometrical effect including mesh interval.

Acknowledgement

The authors wish to express thanks to Mr. M. Nakazawa of Univ. of Tokyo for his advice in the analysis of the sandwich foils and also express gratitudes to Messrs. K. Minami and K. Puruta and H. Natsume of JAERI for their helps in the calculations.

References

(1) R. G. Soltesz, : Revised WANL ANISN program user's manual, WANL-TMI-1967, (1969)

(2) K. D. Lathrop and F. W. Brinkley, : TWOTRAN-II LA-4848-MS, (1973)

(3) K. Koyama, : JAERI-report to be published.

(4) M. K. Drake, editor : Data formats and procedures for the ENDF neutron cross section library, BNL-50274, (1970)

(5) S. Katsuragi, : JAERI fast reactor group constants system part II-1, JAERI 1199, (1970)

(6) W. E. Ford, : The POPOP-4 library of neutron induced secondary gamma-ray yield and cross section data, CTC-42, (1970)

(7) A. Schetl, et. al. : Compilation of threshold neutron cross-sections, OECD/NEA, (1974)

(8) S. Berg and W. N. McElroy, : SAND-II and associated codes, AFWL-TR-67-41, vol II (1967)

(9) T. J. Connolly and F. de Kruizf, : An analysis of twenty four isotopes for use in multiple foil measurements of neutron spectra below 10keV, KFK-718 (1968)

(10) K. Shin, et. al. : Measurement of gamma rays by a liquid scintillator, submitted to Fifth international conference on reactor shielding

Table I. Atomic number densities in each region of YAYOI

(unit 10^{24} n/cc)

material region / element	(1) fuel	(2) blanket	(3) blanket	(4) blanket	(5) SUS+void	(6) lead reflector	(7) SUS+void	(8) SUS+void
U-235	3.5020-2*	1.4238-4	1.3672-4	1.1176-4	0.0	0.0	4.8760-6	0.0
U-238	7.1067-3	3.4369-2	3.3003-2	2.6977-2	0.0	0.0	1.1770-3	0.0
Cr	1.3092-3	3.6663-4	8.1659-4	4.1662-4	1.3882-2	2.6664-4	1.1082-2	1.6665-2
Fe	4.9888-3	1.4019-3	2.9337-3	1.4967-3	4.9873-2	9.5794-4	3.9814-2	5.9871-2
Ni	5.4464-4	1.5444-4	3.4397-4	1.7550-4	5.8476-3	1.1232-4	4.6682-3	7.0199-3
N	2.3478-7	9.4303-6	2.1522-6	7.2782-6	6.5347-6	2.0348-6	1.2130-5	0.0
O	6.2916-8	2.5271-6	5.7673-7	1.9504-6	1.7512-6	5.4527-6	3.2507-6	0.0
Pb	7.5806-4	1.6480-4	6.4600-3	7.0862-3	0.0	3.0718-2	0.0	0.0
C	2.3361-5	2.3308-5	3.0040-5	2.0419-5	2.2883-4	4.3954-6	1.8327-4	2.7471-4
H	0.0	0.0	0.0	0.0	0.0	0.0	0.0	0.0
Si	8.0283-5	2.3240-5	5.1761-5	2.6409-5	8.7994-4	1.6902-5	7.0248-4	1.0564-3
Ca	0.0	0.0	0.0	0.0	0.0	0.0	0.0	0.0
Al	0.0	0.0	0.0	0.0	0.0	0.0	0.0	0.0
Mn	7.8192-5	2.2634-5	5.0431-5	2.5721-5	8.5702-4	1.6461-5	6.8418-4	1.0288-3

material / element	(9) SUS+void	(10) iron	(11) lead	(12) iron+void	(13) SUS	(14) iron shield	(15) lead	(16) heavy concrete
U-235	0.0	0.0	0.0	0.0	0.0	0.0	0.0	0.0
U-238	0.0	0.0	0.0	0.0	0.0	0.0	0.0	0.0
Cr	1.4699-2	0.0	0.0	0.0	1.6665-2	0.0	0.0	0.0
Fe	5.2806-2	8.4604-2	0.0	5.9730-2	5.9871-2	8.4757-2	0.0	2.5522-2
Ni	6.1915-3	0.0	0.0	0.0	7.0199-3	0.0	0.0	0.0
N	4.6173-6	0.0	7.826 -7	1.1504-5	0.0	0.0	1.5652-6	0.0
O	1.2374-6	0.0	2.0097-7	3.0829-6	0.0	0.0	4.1944-7	4.678 -2
Pb	0.0	0.0	3.2300-2	0.0	0.0	0.0	3.1641-2	0.0
C	2.4230-4	7.1000-4	0.0	5.0126-4	2.7471-4	0.0	0.0	0.0
H	0.0	0.0	0.0	0.0	0.0	0.0	0.0	1.0973-2
Si	9.3170-4	0.0	0.0	0.0	1.0564-3	0.0	0.0	1.0430-3
Ca	0.0	0.0	0.0	0.0	0.0	0.0	0.0	2.202 -3
Al	0.0	0.0	0.0	0.0	0.0	0.0	0.0	1.890 -4
Mn	9.0744-4	8.6120-4	0.0	6.0801-4	1.0288-3	0.0	0.0	0.0

* read as 3.5020×10^{-2}

Table II. Material numbers of ENDF/B-IV and Identification numbers of POPOP-4 Library used in the calculations

material	ENDF/B-IV MAT. no.	POPOP-4 identification no.		
1- H- 1	1269	10101		
6- C- 12	1274	60103		
7- N- 14	1275	70102		
8- O- 16	1276	80201	86301	86601
13-Al- 27	1193	130101	130302	
14-Si	1194	140104	140302	140601
20-Ca	1195	200102	200301	200701
24-Cr	1191	240104	240301	
25-Mn- 55	1197	250101		
26-Fe	1192	260106	260301	
28-Ni	1190	280103	280301	
82-Pb	1288	820102	820301	
92- U-235	1261	925101	925301	925801
92- U-238	1262	928112	928301	

Table III. EURLIB energy group structure (eV)

--- NEUTRON GROUP ---						--- GAMMA GROUP ---		
GROUP	ENERGY	RANGE	GROUP	ENERGY	RANGE	GROUP	ENERGY	RANGE
1	1.4918E+07*	1.349 E+07	51	1.4996E+05	1.3569E+05	1	1.4000E+07	1.2000E+07
2	1.3499E+07	1.221 E+07	52	1.3569E+05	1.2277E+05	2	1.2000E+07	1.0000E+07
3	1.2214E+07	1.105 E+07	53	1.2277E+05	1.1109E+05	3	1.0000E+07	8.0000E+06
4	1.1052E+07	1.0000E+07	54	1.1109E+05	8.6517E+04	4	8.0000E+06	6.5000E+06
5	1.0000E+07	9.0484E+06	55	8.6517E+04	6.7379E+04	5	6.5000E+06	5.0000E+06
6	9.0484E+06	8.1873E+06	56	6.7379E+04	5.2475E+04	6	5.0000E+06	4.0000E+06
7	8.1873E+06	7.4082E+06	57	5.2475E+04	4.0868E+04	7	4.0000E+06	3.0000E+06
8	7.4082E+06	7.0469E+06	58	4.0868E+04	3.1828E+04	8	3.0000E+06	2.5000E+06
9	7.0469E+06	6.7032E+06	59	3.1828E+04	2.6050E+04	9	2.5000E+06	2.0000E+06
10	6.7032E+06	6.3763E+06	60	2.6050E+04	2.4788E+04	10	2.0000E+06	1.6600E+06
11	6.3763E+06	6.0653E+06	61	2.4788E+04	2.3570E+04	11	1.6600E+06	1.3300E+06
12	6.0653E+06	5.4881E+06	62	2.3570E+04	2.1870E+04	12	1.3300E+06	1.0000E+06
13	5.4881E+06	4.9659E+06	63	2.1870E+04	1.9305E+04	13	1.0000E+06	8.0000E+05
14	4.9659E+06	4.7240E+06	64	1.9305E+04	1.5034E+04	14	8.0000E+05	6.0000E+05
15	4.7240E+06	4.4933E+06	65	1.5034E+04	1.1709E+04	15	6.0000E+05	4.0000E+05
16	4.4933E+06	4.0657E+06	66	1.1709E+04	9.1188E+03	16	4.0000E+05	3.0000E+05
17	4.0657E+06	3.6788E+06	67	9.1188E+03	7.1017E+03	17	3.0000E+05	2.0000E+05
18	3.6788E+06	3.3287E+06	68	7.1017E+03	5.5308E+03	18	2.0000E+05	1.0000E+05
19	3.3287E+06	3.0112E+06	69	5.5308E+03	4.3074E+03	19	1.0000E+05	5.0000E+04
20	3.0112E+06	2.7253E+06	70	4.3074E+03	3.3546E+03	20	5.0000E+04	2.0000E+04
21	2.7253E+06	2.4660E+06	71	3.3546E+03	2.6126E+03			
22	2.4660E+06	2.3460E+06	72	2.6126E+03	2.0347E+03			
23	2.3460E+06	2.2313E+06	73	2.0347E+03	1.5846E+03			
24	2.2313E+06	2.0190E+06	74	1.5846E+03	1.2341E+03			
25	2.0190E+06	1.8268E+06	75	1.2341E+03	9.6112E+02			
26	1.8268E+06	1.6530E+06	76	9.6112E+02	7.4852E+02			
27	1.6530E+06	1.4957E+06	77	7.4852E+02	5.8295E+02			
28	1.4957E+06	1.3524E+06	78	5.8295E+02	4.5400E+02			
29	1.3524E+06	1.2246E+06	79	4.5400E+02	3.5357E+02			
30	1.2246E+06	1.1080E+06	80	3.5357E+02	2.7536E+02			
31	1.1080E+06	1.0026E+06	81	2.7536E+02	2.1445E+02			
32	1.0026E+06	9.0718E+05	82	2.1445E+02	1.6702E+02			
33	9.0718E+05	8.2085E+05	83	1.6702E+02	1.3007E+02			
34	8.2085E+05	7.4274E+05	84	1.3007E+02	1.0130E+02			
35	7.4274E+05	6.7206E+05	85	1.0130E+02	7.8893E+01			
36	6.7206E+05	6.0810E+05	86	7.8893E+01	6.1442E+01			
37	6.0810E+05	5.5023E+05	87	6.1442E+01	4.7851E+01			
38	5.5023E+05	4.9787E+05	88	4.7851E+01	3.7267E+01			
39	4.9787E+05	4.5049E+05	89	3.7267E+01	2.9023E+01			
40	4.5049E+05	4.0762E+05	90	2.9023E+01	2.2603E+01			
41	4.0762E+05	3.6883E+05	91	2.2603E+01	1.7603E+01			
42	3.6883E+05	3.3373E+05	92	1.7603E+01	1.0577E+01			
43	3.3373E+05	3.0197E+05	93	1.0677E+01	8.3153E+00			
44	3.0197E+05	2.7324E+05	94	8.3153E+00	5.0435E+00			
45	2.7324E+05	2.4724E+05	95	5.0435E+00	3.0592E+00			
46	2.4724E+05	2.2371E+05	96	3.0592E+00	1.8554E+00			
47	2.2371E+05	2.0242E+05	97	1.8554E+00	1.1254E+00			
48	2.0242E+05	1.8316E+05	98	1.1254E+00	6.2500E-01			
49	1.8316E+05	1.6573E+05	99	6.2500E-01	4.1399E-01			
50	1.6573E+05	1.4996E+05	100	4.1399E-01	1.0000E-03			

*read as 1.4918×10^7

Table IV. Energy group structure for two dimensional S_N calculation

Neutron		gamma	
Group	Energy range (eV)	Group	Energy range (MeV)
1	1.4918E 07*- 7.0469E 06	1	14.0 - 5.0
2	7.0469E 06 - 2.4660E 06	2	5.0 - 1.33
3	2.4660E 06 - 9.0718E 05	3	1.33 - 0.02
4	9.0718E 05 - 3.3373E 05		
5	3.3373E 05 - 6.7379E 04		
6	6.7379E 04 - 1.5034E 04		
7	1.5034E 04 - 3.3546E 03		
8	3.3546E 03 - 3.7267E 01		
9	3.7267E 01 - 4.1399E-01		
10	4.1399E-01 - 1.0000E-03		

* read as 1.4918×10^7

Table V. Detector responses for one dimensional calculation

Group	cross section (barn)								
	Energy(MeV)	115 In(n,n')	58 Ni(n,p)	64 Zn(n,p)	54 Fe(n,p)	27 Al(n,p)	56 Fe(n,p)	27 Al(n,a)	24 Mg(n,p)
1	14.4	0.0828	0.4000	0.1925	0.3285	0.0833	0.1054	0.1187	0.2201
2	13.0	0.0984	0.5187	0.2481	0.4209	0.0993	0.1110	0.1277	0.2110
3	11.6	0.1337	0.6473	0.2842	0.4000	0.1033	0.0968	0.1156	0.1703
4	10.5	0.1802	0.6698	0.3000	0.5541	0.1000	0.0812	0.1013	0.1599
5	9.52	0.2012	0.6698	0.2927	0.5674	0.0937	0.0681	0.0839	0.1269
6	8.62	0.2012	0.6584	0.2821	0.5765	0.0895	0.0552	0.0613	0.1208
7	7.80	0.2012	0.6418	0.2660	0.5674	0.0822	0.0423	0.0350	0.1000
8	7.06	0.2012	0.6400	0.2540	0.5629	0.0634	0.0295	0.0183	0.0427
9	6.54	0.2070	0.6360	0.2435	0.5324	0.0521	0.0235	0.0066	0.0267
10	6.22	0.2126	0.6200	0.2382	0.5157	0.0500	0.0169	0.0029	0.007
11	5.77	0.2194	0.6000	0.2181	0.4806	0.0528	0.0086	0.0	0.0
12	5.22	0.2282	0.5500	0.1953	0.4407	0.0257	0.0024		
13	4.84	0.2670	0.5000	0.1762	0.4000	0.0144	0.0		
14	4.61	0.2777	0.4720	0.1661	0.3696	0.0200			
15	4.30	0.2981	0.4220	0.1466	0.3158	0.0098			
16	3.87	0.3000	0.3385	0.1210	0.2437	0.0094			
17	3.50	0.3225	0.2100	0.1022	0.1669	0.0090			
18	3.21	0.3350	0.2080	0.0838	0.1180	0.0029			
19	2.87	0.3628	0.2000	0.0580	0.0674	0.0023			
20	2.60	0.3715	0.1370	0.0448	0.0420	0.0			
21	2.41	0.3301	0.0992	0.0346	0.0300				
22	2.29	0.3174	0.0828	0.0229	0.0230				
23	2.16	0.3000	0.0653	0.0176	0.0176				
24	1.92	0.2520	0.0388	0.0088	0.0094				
25	1.73	0.2246	0.0276	0.0027	0.0060				
26	1.57	0.1788	0.0161	0.0014	0.0037				
27	1.42	0.1348	0.0090	0.0	0.0				
28	1.29	0.1116	0.0058						
29	1.17	0.0730	0.0036						
30	1.05	0.0700	0.0013						
31	0.955	0.0455	0.0						
32	0.864	0.0389							
33	0.782	0.0249							
34	0.707	0.0179							
35	0.640	0.0116							
36	0.579	0.0090							
37	0.524	0.0050							
38	0.474	0.0030							
39	0.429	0.0024							
40	0.388	0.0017							
41	0.351	0.0							

Conversion factor for gamma dose R/h	
group	factor
101	1.35-5
102	1.18-5
103	1.02-5
104	8.05-6
105	7.27-6
106	5.97-6
107	5.11-6
108	4.16-6
109	3.65-6
110	3.11-6
111	2.73-6
112	2.31-6
113	1.84-6
114	1.51-6
115	1.17-6
116	7.75-7
117	5.67-7
118	3.54-7
119	1.53-7
120	4.0 -7

Table VI. Detector cross sections for two dimensional calculation

iron shield 0cm

reaction (barn)

group	energy	197Au(n,g)	115In(n,n')	58Ni(n,p)	54Fe(n,p)	64Zn(n,p)	27Al(n,a)	24Mg(n,p)
1	1.4918+7	1.244-2	1.937-1	6.458-1	5.554-1	2.723-1	5.421-2	1.068-1
2	7.0469+6	2.780-2	3.300-1	2.105-1	1.210-1	7.529-2	1.044-4	3.620-4
3	2.4460+6	7.841-2	8.469-2	5.879-3	1.058-3	8.056-4	0.0	0.0
4	9.0718+5	1.432-1	4.539-3	0.0	0.0	0.0	0.0	0.0
5	3.3373+5	2.764-1	0.0					
6	6.7379+4	5.672-1	0.0					
7	1.5034+4	1.560+0	0.0					
8	3.3546+3	1.078+1	0.0					
9	3.7267+1	2.793+2	0.0					
10	4.1399-1	1.565+2	0.0					
	1.0000-3							

* read as 1.4918×10^7

group	27Al(n,p)	56Fe(n,p)
1	8.386-2	5.277-2
2	5.401-3	6.385-4
3	0.0	0.0
4	0.0	0.0

gamma ray

group	energy	dose factor R/h
11	14.0 MeV	8.201-6
12	5.0	4.128-6
13	1.33	1.060-6
	0.02	

iron shield 20cm

reaction (barn)

group	energy	197Au(n,g)	115In(n,n')	58Ni(n,p)	54Fe(n,p)	64Zn(n,p)	27Al(n,a)	24Mg(n,p)
1	1.4918+7	1.242-2	1.932-1	6.456-1	5.546-1	2.726-1	5.511-2	1.079-1
2	7.0469+6	2.785-2	3.299-1	2.109-1	1.213-1	7.536-2	1.118-4	3.887-4
3	2.4460+6	7.962-2	7.717-2	4.717-3	8.265-4	6.226-4	0.0	0.0
4	9.0718+5	1.458-1	4.096-3	0.0	0.0	0.0	0.0	0.0
5	3.3373+5	2.797-1	0.0					
6	6.7379+4	5.810-1	0.0					
7	1.5034+4	1.624+0	0.0					
8	3.3546+3	1.223+1	0.0					
9	3.7267+1	3.018+2	0.0					
10	4.1399-1	1.565+2	0.0					
	1.0000-3							

group	27Al(n,p)	56Fe(n,p)
1	8.417-2	5.335-2
2	5.470-3	6.760-4
3	0.0	0.0
4	0.0	0.0

gamma ray

group	energy	dose factor R/h
11	14.0 MeV	7.992-6
12	5.0	4.222-6
13	1.33	1.040-6
	0.02	

iron shield 40cm

reaction (barn)

group	energy	197Au(n,g)	115In(n,n')	58Ni(n,p)	54Fe(n,p)	64Zn(n,p)	27Al(n,a)	24Mg(n,p)
1	1.4918+7	1.233-2	1.911-1	6.447-1	5.510-1	2.735-1	5.891-2	1.126-1
2	7.0469+6	2.823-2	3.306-1	2.074-1	1.177-1	7.390-2	1.262-4	4.416-4
3	2.4460+6	8.226-2	6.122-2	2.393-3	3.794-4	2.762-4	0.0	0.0
4	9.0718+5	1.493-1	3.448-3	0.0	0.0	0.0	0.0	0.0
5	3.3373+5	2.867-1	0.0					
6	6.7379+4	6.039-1	0.0					
7	1.5034+4	1.622+0	0.0					
8	3.3546+3	1.319+1	0.0					
9	3.7267+1	3.248+2	0.0					
10	4.1399-1	1.565+2	0.0					
	1.0000-3							

group	27Al(n,p)	56Fe(n,p)
1	8.540-2	5.585-2
2	5.385-3	7.389-4
3	0.0	0 0
4	0.0	0.0

gamma ray

group	energy	dose factor R/h
11	14.0 MeV	7.956-6
12	5.0	4.261-6
13	1.33	1.039-6
	0.02	

iron shield 60cm

reaction (barn)

group	energy	197Au(n,g)	115In(n,n')	58Ni(n,p)	54Fe(n,p)	64Zn(n,p)	27Al(n,a)	24Mg(n,p)
1	1.4918+7	1.222-2	1.881-1	6.429-1	5.457-1	2.741-1	6.336-2	1.180-1
2	7.0469+6	2.851-2	3.310-1	2.050-1	1.153-1	7.291-2	1.406-4	4.949-4
3	2.4460+6	8.392-2	5.172-2	1.163-3	1.614-4	1.131-4	0.0	0.0
4	9.0718+5	1.516-1	2.995-3	0.0	0.0	0.0	0.0	0.0
5	3.3373+5	2.946-1	0.0					
6	6.7379+4	6.250-1	0.0					
7	1.5034+4	1.592+0	0.0					
8	3.3546+3	1.281+1	0.0					
9	3.7267+1	3.253+2	0.0					
10	4.1399-1	1.565+2	0.0					
	1.0000-3							

group	27Al(n,p)	56Fe(n,p)
1	8.674-2	5.884-2
2	5.359-3	8.009-4
3	0.0	0.0
4	0.0	0.0

gamma ray

group	energy	dose factor R/h
11	14.0 MeV	7.956-6
12	5.0	4.265-6
13	1.33	1.039-6
	0.02	

Table VII(a) Total flux at the inner surface of the iron shield calculated by the ANISN code (with buckling effect H=Y=60cm)

(at 2kw)

Neutron flux ($n \cdot cm^{-2} \cdot sec^{-1}$)						photon flux ($p \cdot cm^{-2} \cdot sec^{-1}$)	
group	total flux	group	total flux	group	total flux	group	total flux
1	3.081+3*	36	1.409+8	71	3.077+7	101	0.0
2	6.474+3	37	1.540+8	72	2.709+7	102	2.553+5
3	1.209+4	38	1.494+8	73	2.648+7	103	2.519+5
4	2.300+4	39	1.790+8	74	2.367+7	104	1.054+7
5	3.997+4	40	1.169+8	75	1.525+7	105	4.773+6
6	6.391+4	41	1.999+8	76	1.371+7	106	2.713+6
7	9.743+4	42	2.407+8	77	1.241+7	107	3.577+6
8	6.273+4	43	3.091+8	78	1.118+7	108	2.222+6
9	7.288+4	44	1.575+8	79	7.916+6	109	2.421+6
10	8.303+4	45	1.961+8	80	9.133+6	110	3.127+6
11	9.420+4	46	1.701+8	81	8.687+6	111	2.945+6
12	2.139+5	47	1.606+8	82	8.062+6	112	4.838+6
13	2.416+5	48	1.498+8	83	7.486+6	113	4.806+6
14	1.274+5	49	1.956+8	84	6.956+6	114	5.742+6
15	1.402+5	50	1.860+8	85	6.457+6	115	8.017+6
16	3.471+5	51	1.611+8	86	5.929+6	116	6.068+6
17	4.602+5	52	2.390+8	87	5.516+6	117	9.556+6
18	6.846+5	53	1.589+8	88	5.068+6	118	9.293+6
19	9.088+5	54	2.614+8	89	4.636+6	119	5.143+5
20	1.378+6	55	4.847+8	90	4.218+6	120	
21	2.115+6	56	2.174+8	91	3.814+6		
22	1.444+6	57	1.957+8	92	6.178+6		
23	1.755+6	58	1.333+8	93	2.730+6		
24	3.824+6	59	1.130+8	94	4.212+6		
25	5.677+6	60	1.636+8	95	3.113+6		
26	7.352+6	61	8.999+7	96	2.184+6		
27	8.869+6	62	6.653+7	97	1.437+6		
28	1.294+7	63	5.839+7	98	9.571+5		
29	1.417+7	64	6.016+7	99	4.018+5		
30	2.564+7	65	6.693+7	100	8.465+4		
31	2.891+7	66	4.540+7				
32	4.534+7	67	2.446+7				
33	4.674+7	68	3.449+7				
34	4.643+7	69	3.652+7				
35	8.456+7	70	3.758+7				

* read as 3.081×10^3

Table VII(b) Total flux at the inner surface of the iron shield calculated by the ANISN code (without buckling)

(at 2kw)

Neutron flux ($n \cdot cm^{-2} \cdot sec^{-1}$)						photon flux ($p \cdot cm^{-2} \cdot sec^{-1}$)	
group	total flux	group	total flux	group	total flux	group	total flux
1	4.340+3	36	3.411+8	71	5.260+8	101	0.0
2	9.098+3	37	3.938+8	72	4.792+8	102	3.419+6
3	1.692+4	38	3.991+8	73	4.877+8	103	3.289+7
4	3.201+4	39	5.004+8	74	4.540+8	104	1.395+8
5	5.533+4	40	3.348+8	75	3.018+8	105	6.487+7
6	8.673+4	41	5.945+8	76	2.815+8	106	3.721+7
7	1.098+5	42	7.637+8	77	2.645+8	107	4.675+7
8	6.990+4	43	1.056+9	78	2.467+8	108	2.807+7
9	9.720+4	44	5.474+8	79	1.786+8	109	3.107+7
10	1.099+5	45	7.205+8	80	2.109+8	110	3.780+7
11	1.241+5	46	6.366+8	81	2.087+8	111	3.368+7
12	2.791+5	47	6.121+8	82	2.007+8	112	3.672+7
13	3.129+5	48	5.790+8	83	1.929+8	113	3.360+7
14	1.644+5	49	8.045+8	84	1.853+8	114	4.013+7
15	1.810+5	50	7.879+8	85	1.778+8	115	5.781+7
16	4.500+5	51	7.157+8	86	1.701+8	116	4.554+7
17	6.023+5	52	1.203+9	87	1.621+8	117	7.377+7
18	9.094+5	53	8.232+8	88	1.538+8	118	6.600+7
19	1.225+6	54	1.372+9	89	1.453+8	119	3.462+6
20	1.900+6	55	2.938+9	90	1.365+8	120	
21	2.997+6	56	1.331+9	91	1.274+8		
22	2.088+6	57	3.073+9	92	2.178+8		
23	2.577+6	58	2.101+9	93	9.937+7		
24	1.147+7	59	7.196+8	94	1.617+8		
25	8.812+6	60	1.678+9	95	1.258+8		
26	1.172+7	61	1.387+9	96	9.285+7		
27	1.457+7	62	1.091+9	97	6.415+7		
28	2.202+7	63	8.077+8	98	4.490+7		
29	2.451+7	64	8.377+8	99	1.962+7		
30	4.675+7	65	9.505+8	100	4.196+6		
31	5.484+7	66	6.580+8				
32	9.124+7	67	3.572+8				
33	9.633+7	68	5.222+8				
34	9.741+7	69	5.777+8				
35	1.858+8	70	6.170+8				

Table VIII. Measured and calculated reaction rates at the inner surface of the iron shield

(at 2kw)

reaction	Experiment sec^{-1}	Calculation sec^{-1}			C/E		
		ANISN with buckling	ANISN without buckling	TWOTRAN	ANISN with buckling	ANISN without buckling	TWOTRAN
$^{54}Fe(n,p)$	2.36 x10^{-18} ±0.295	1.16x10^{-18}	1.58x10^{-18}	6.88x10^{-19}	0.492	0.670	0.291
$^{58}Ni(n,p)$	3.32 x10^{-18} ±0.225	2.54x10^{-18}	3.61x10^{-18}	1.56x10^{-18}	0.765	1.09	0.470
$^{24}Mg(n,p)$	3.04 x10^{-20} ±0.108	3.54x10^{-20}	4.86x10^{-20}	2.09x10^{-20}	1.16	1.59	0.687
$^{115}In(n,n')$	4.41 x10^{-17} ±0.288	2.15x10^{-17}	4.00x10^{-17}	1.78x10^{-17}	0.488	0.907	0.403
$^{27}Al(n,\alpha)$	1.465x10^{-20} ±0.042	1.74x10^{-20}	2.40x10^{-20}	1.03x10^{-20}	1.19	1.63	0.709
$^{27}Al(n,p)$	7.76 x10^{-20} ±1.869	6.31x10^{-20}	8.44x10^{-20}	3.65x10^{-20}	0.813	1.08	0.470
$^{64}Zn(n,p)$	1.18 x10^{-18} ±0.259	7.23x10^{-19}	9.90x10^{-19}	4.31x10^{-19}	0.613	0.839	0.365
$^{197}Au(n,\gamma)$	1.21 x10^{-13} ±0.1	1.42x10^{-14}	4.59x10^{-13}	1.09x10^{-13}	0.117	3.79	0.898
$^{197}Au(Cd)(n,\gamma)$	1.21 x10^{-13} ±0.1	1.42x10^{-14}	4.58x10^{-13}	1.09x10^{-13}	0.117	3.78	0.898
TLD	1.65 x10^{3}R/h ±0.132	2.72x10^{+2}	3.25x10^{3}	9.31x10^{2}	0.164	1.97	0.564

Table IX. Measured reaction rates of $^{115}In(n,n')$ ^{115m}In reaction in the iron shield

(sec^{-1} at 2kw)

thickness of the iron shield	measured direction	distance from the centerline				
		0cm	10cm	20cm	30cm	40cm
0cm	North	4.41 x10^{-17}	4.20	2.95	1.68	0.860
	South		4.05	2.75	1.55	1.02
	East		3.78	2.83	1.78	0.736
	West		4.07	3.12	2.03	0.769
20cm	North	3.73 x10^{-18}	3.30	2.79	1.86	1.18
	East		3.25	2.53	1.80	0.946
40cm	North	4.48 x10^{-19}	4.53	3.74	2.66	1.71
	East		3.99	3.29	2.58	1.71
60cm	North	9.04 x10^{-20}	7.82	5.49	4.85	3.02
	East		5.71	3.34	3.42	2.38

Table X. Measured reaction rates of $^{197}Au(n,gamma)$ and the value of cadmium ratio in the iron shield

(sec^{-1} at 2kw)

thickness of the iron shield	measured direction	distance from the centerline				
		0cm	10cm	20cm	30cm	40cm
0cm	North (Cd ratio)*	1.21 x10^{-13} (1.011)*	1.15 (1.017)	1.07 (1.031)	0.935 (1.017)	0.835 (1.077)
	South		1.13 (1.010)	1.05 (1.019)	0.872 ( )	0.745 (1.056)
	East		1.14 (1.001)	1.05 (1.059)	0.857 (1.005)	0.732 (1.063)
20cm	North	4.41 x10^{-14} (1.037)	4.11 (1.038)	3.59 (1.021)	2.94 (1.038)	2.35 (1.009)
	South		4.20 (1.048)	3.59 (1.022)	2.86 (1.031)	2.24 (1.069)
	East		4.11 (1.025)	3.58 (1.020)	2.85 ( )	2.42 (1.034)
40cm	North	1.50 x10^{-14} (1.070)	1.37 (1.017)	1.22 (1.053)	0.961 ( )	0.842 (1.028)
	South		1.34 (1.032)	1.19 (1.020)	0.942 ( )	0.789 (1.044)
	East		1.44 (1.115)	1.19 (1.033)	0.977 (1.052)	0.851 (1.042)
60cm	North	4.45 x10^{-15} (1.081)	4.10 (1.041)	3.44 ( )	2.79 ( )	2.30 (1.027)
	South		3.77 ( )	3.45 (1.031)	2.88 (1.020)	2.11 ( )
	East		4.04 (1.081)	3.47 (1.007)	2.97 (1.022)	2.20 ( )

* The value of cadmium ratio is presented in parenthesis.

Table XI. Gamma dose rates in the iron shield measured with $CaSO_4$·Tm thermo-luminescence detectors

(R/h at 2kw)

thickness of the iron shield	measured direction	distance from the centerline				
		0cm	10cm	20cm	30cm	40cm
0cm	North	1.64x10^{3}	1.63	1.51	1.26	1.51
	South		1.62	1.46	1.19	1.34
	East		1.62	1.46	1.58	1.17
20cm	North	5.41x10^{2}	5.23	4.30	3.80	3.69
	South		5.08	4.32	3.58	3.52
	East		4.99	4.54	3.84	4.03
40cm	North	1.73x10^{2}	1.64	1.47	1.20	1.31
	South		1.72	1.43	1.11	1.26
	East		1.62	1.45	1.15	1.46
60cm	North	4.84x10^{1}	4.74	4.21	3.51	3.62
	South		4.72	4.85	3.88	3.20
	East		4.63	4.27	3.47	3.59

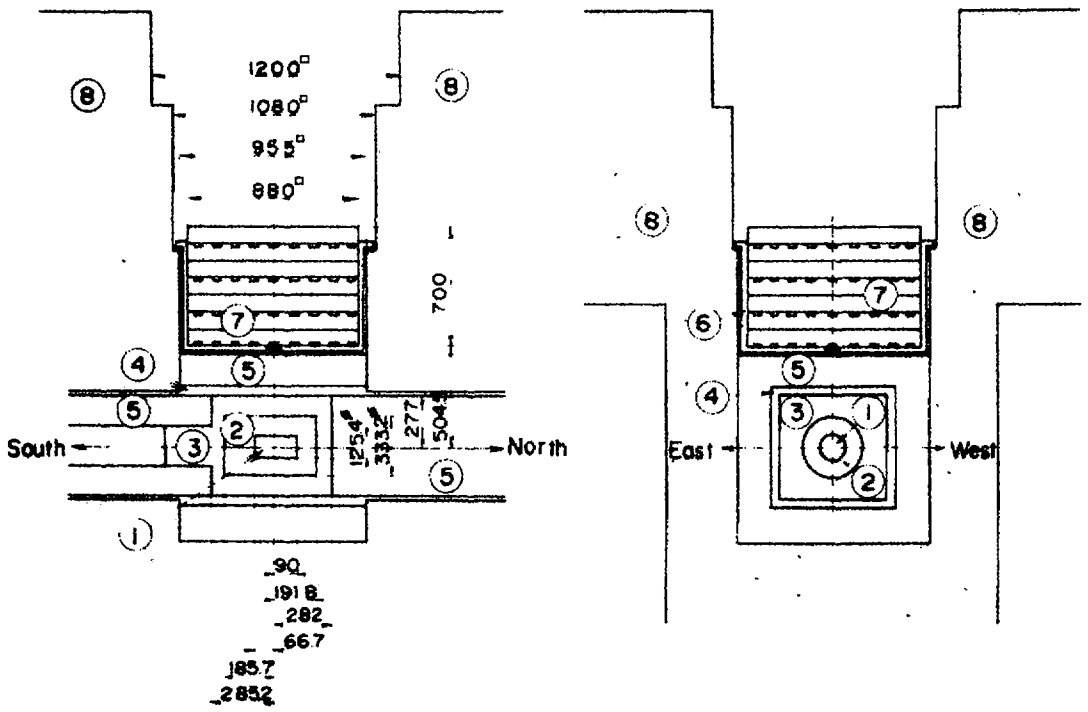

Fig.1 Experimental Configuration (dimensions in millimeter)

1. core 2 blanket 3 inner reflector(lead) 4 guide wall(iron)
5 outer reflector(lead) 6 support box(bottom·SUS, side.iron)
7 iron shield(test section) 8 heavy concrete

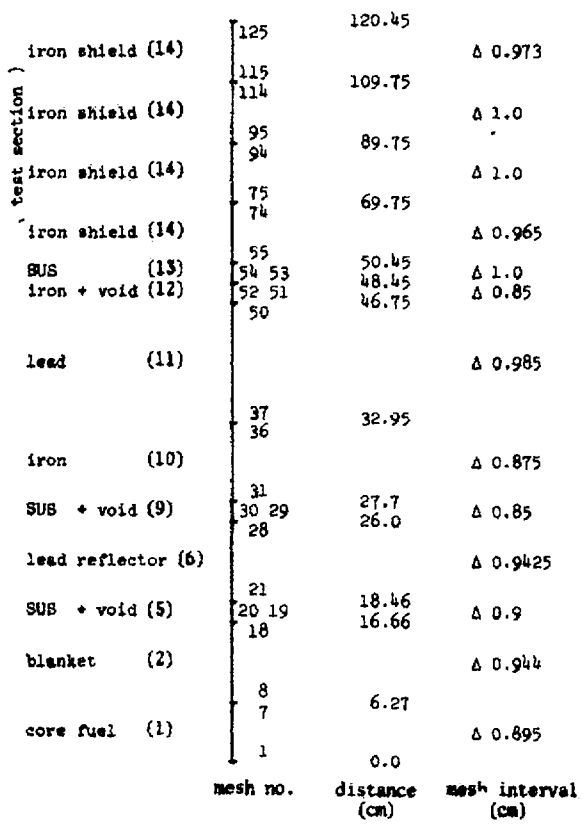

Fig.2. One dimensional Sn calculation model
( ) shows the material identification number shown in Table I.

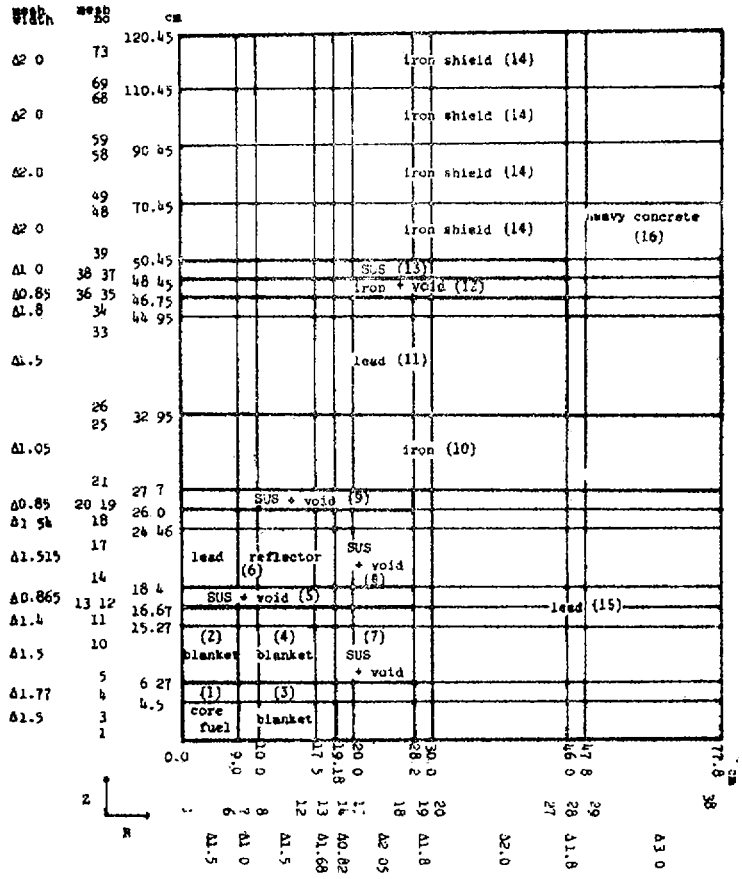

Fig 3. Two dimensional S_N calculation model (north direction)
( ) shows the material identification number shown in Table I

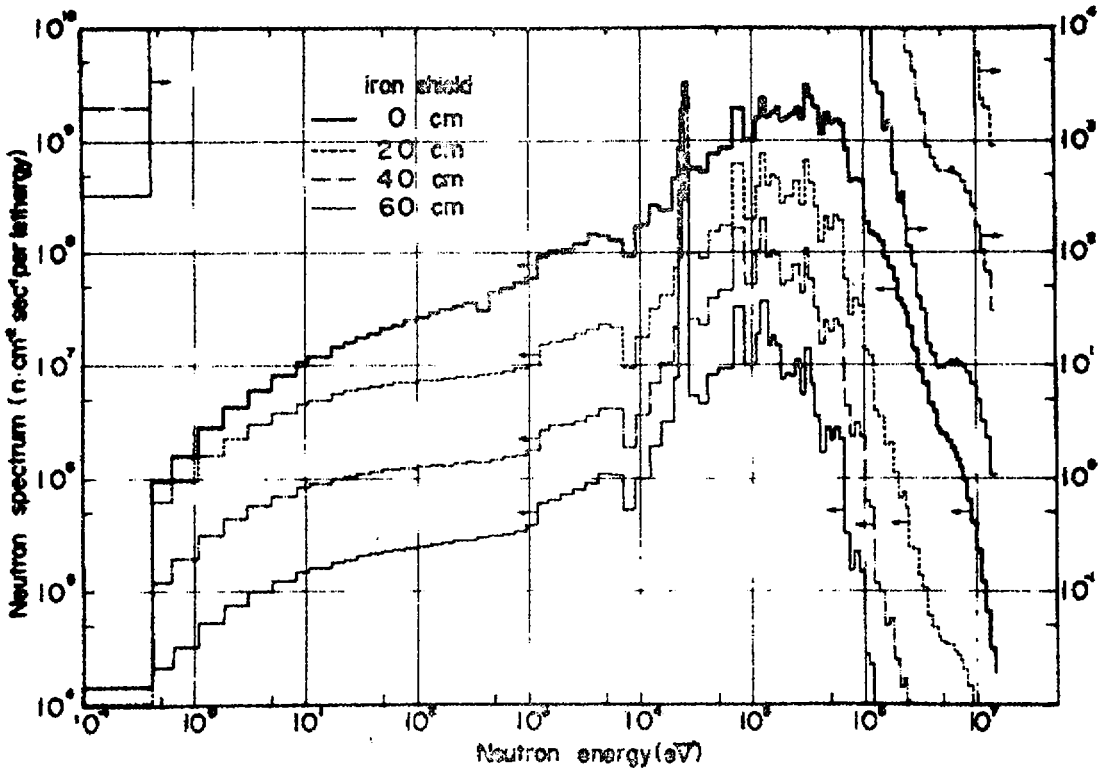

Fig.4(a) Neutron spectra at 0, 20, 40, 60 cm from the inner surface of the iron shield (calcurated by ANISN with buckling H=V=60 cm)

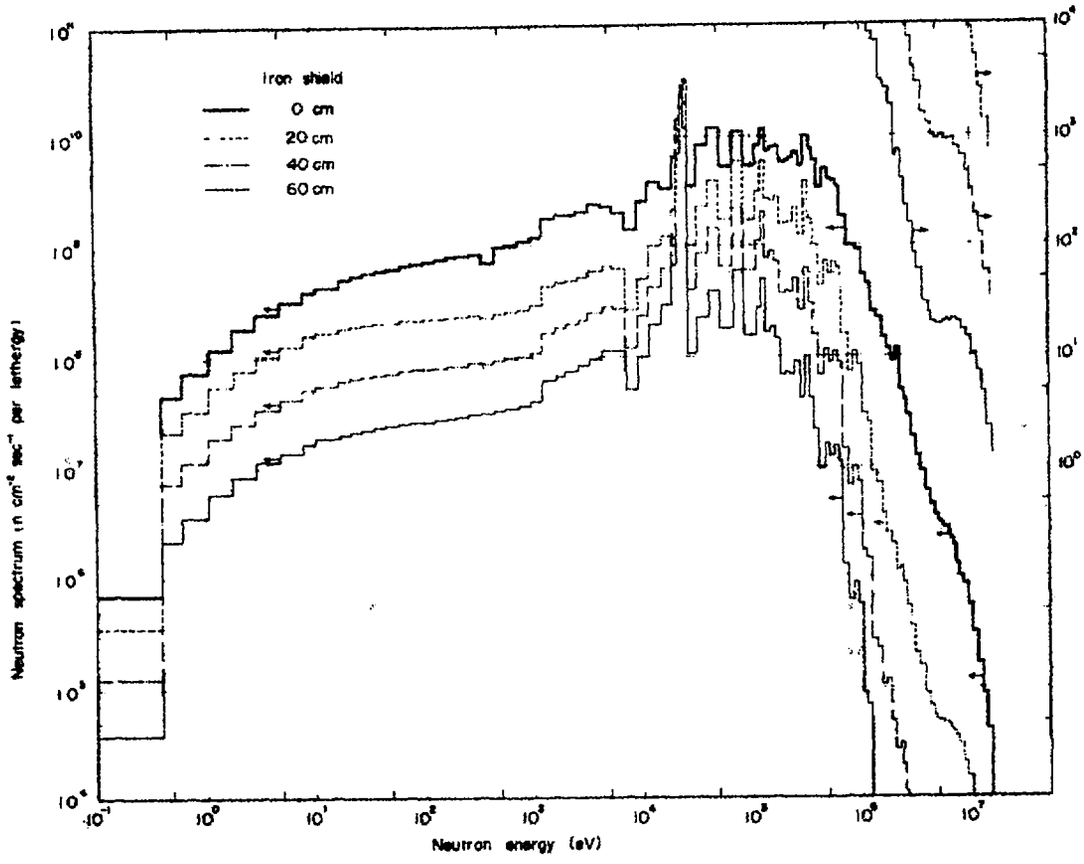

Fig 4(b) Neutron spectra at 0, 20, 40 and 60cm from the inner surface of the iron shield (calculated by ANISN, without buckling)

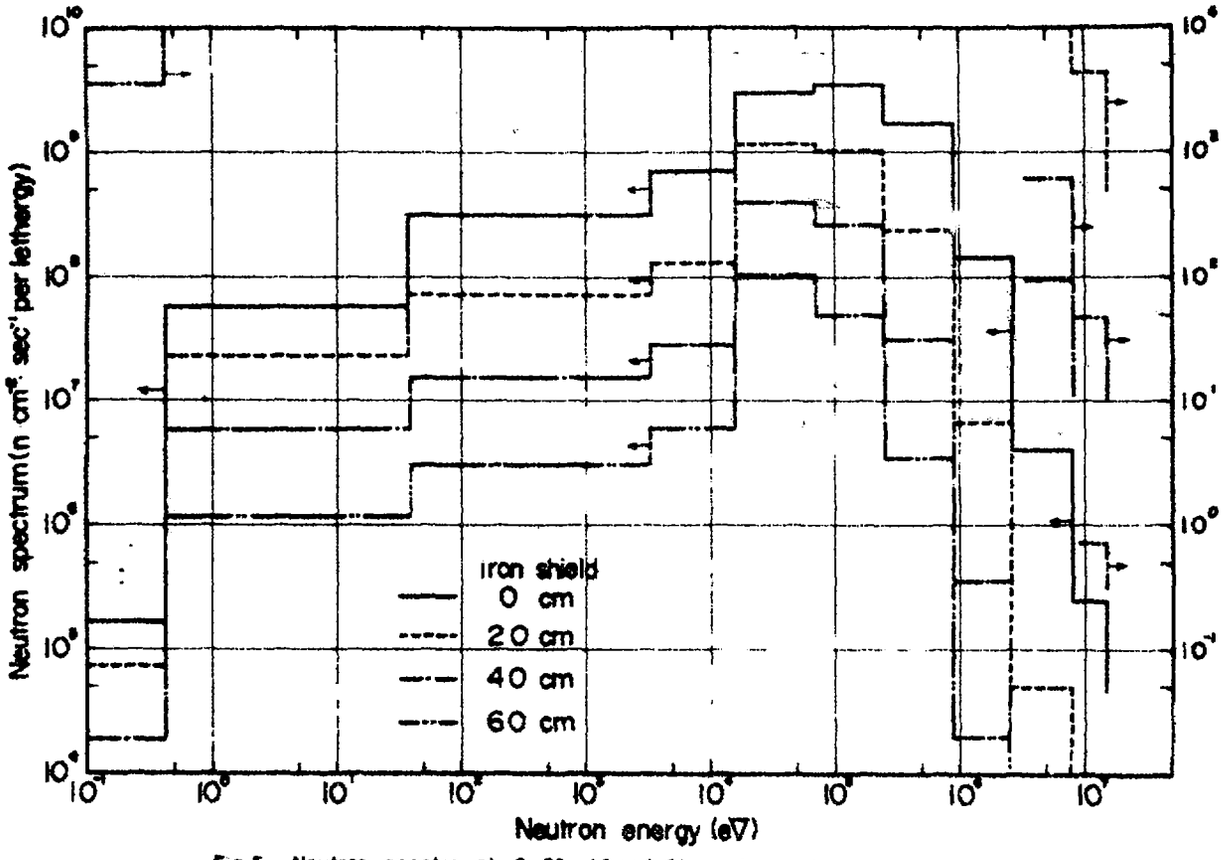

Fig 5 Neutron spectra at 0, 20, 40 and 60 cm from the inner surface of the iron shield (calcurated by TWOTRAN)

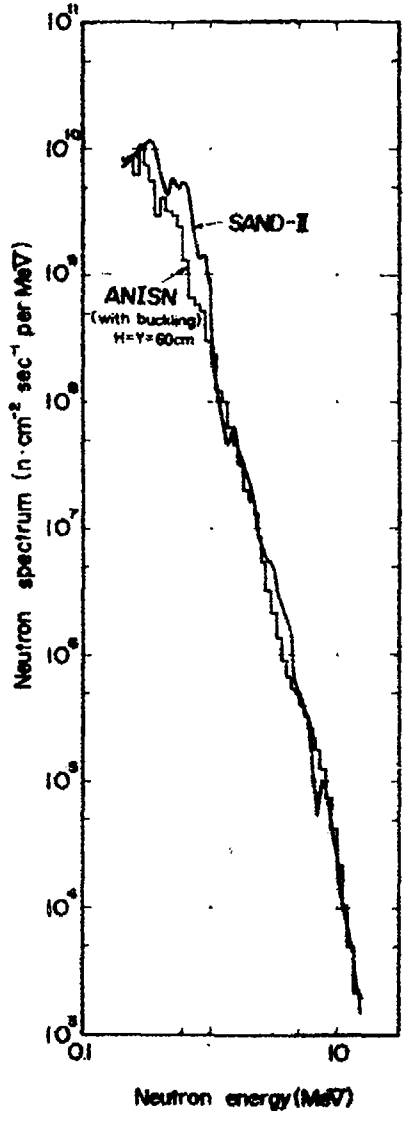

Fig 6(a) Comparison of fast neutron energy spectrum calculated by ANISN with the experimental result at the inner surface of the iron shield (unfolded by SAND-II)

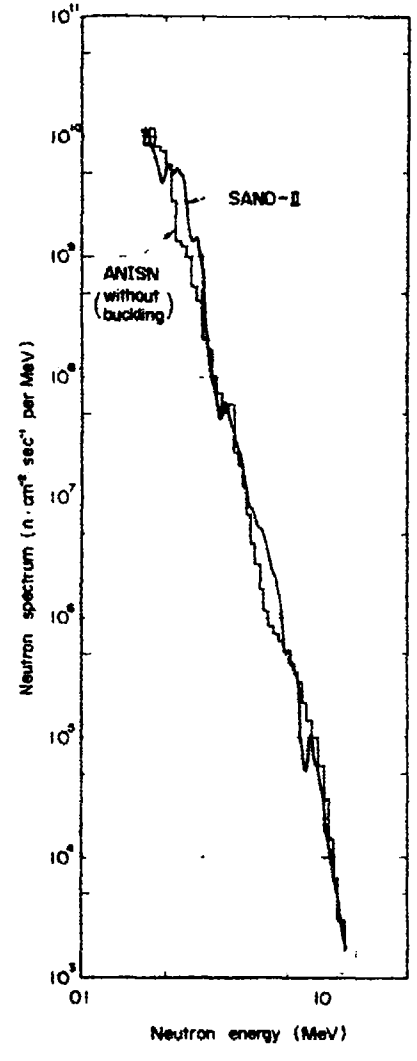

Fig 6(b) Comparison of the fast neutron energy spectrum at the inner surface of the iron shield unfolded by SAND-II and the calculation by ANISN without buckling effect

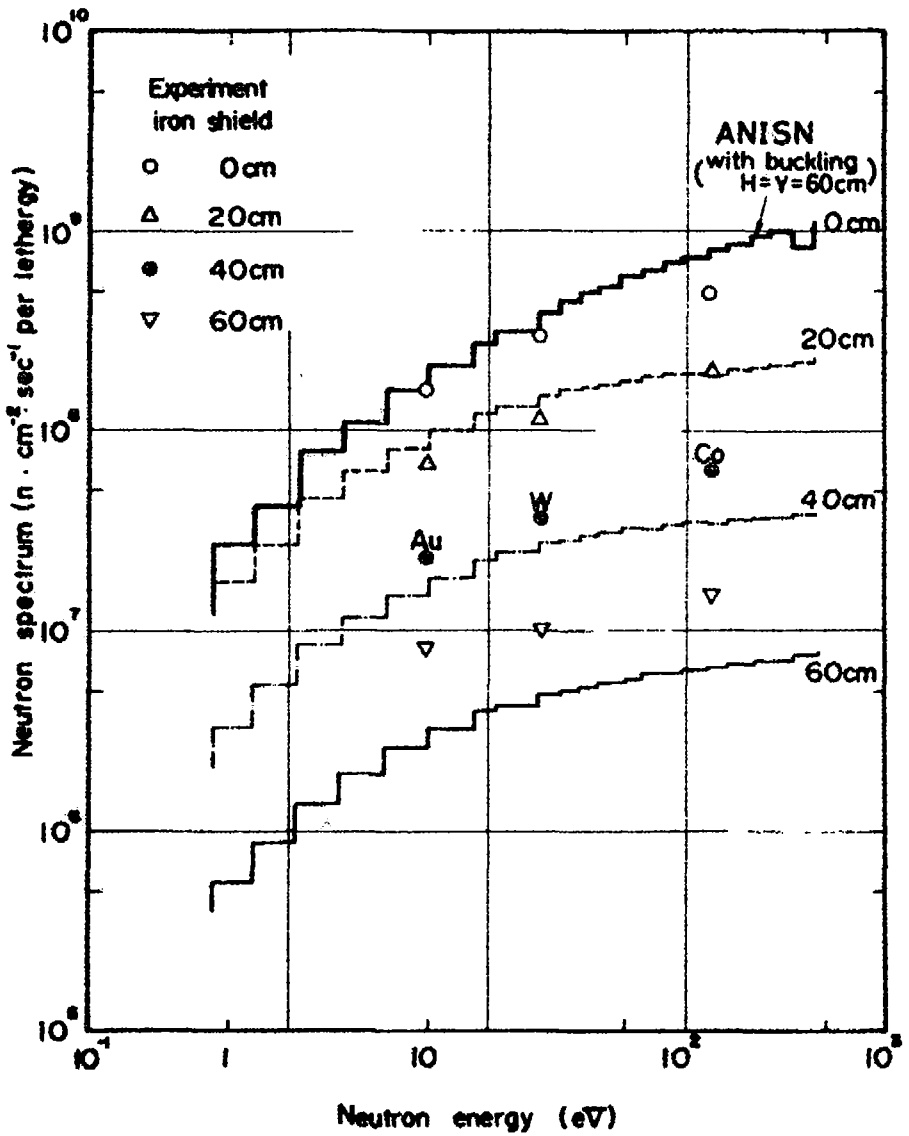

Fig. 7-a Comparison of the neutron spectrum by sandwitch resonance foil with the calculated results by ANISN.

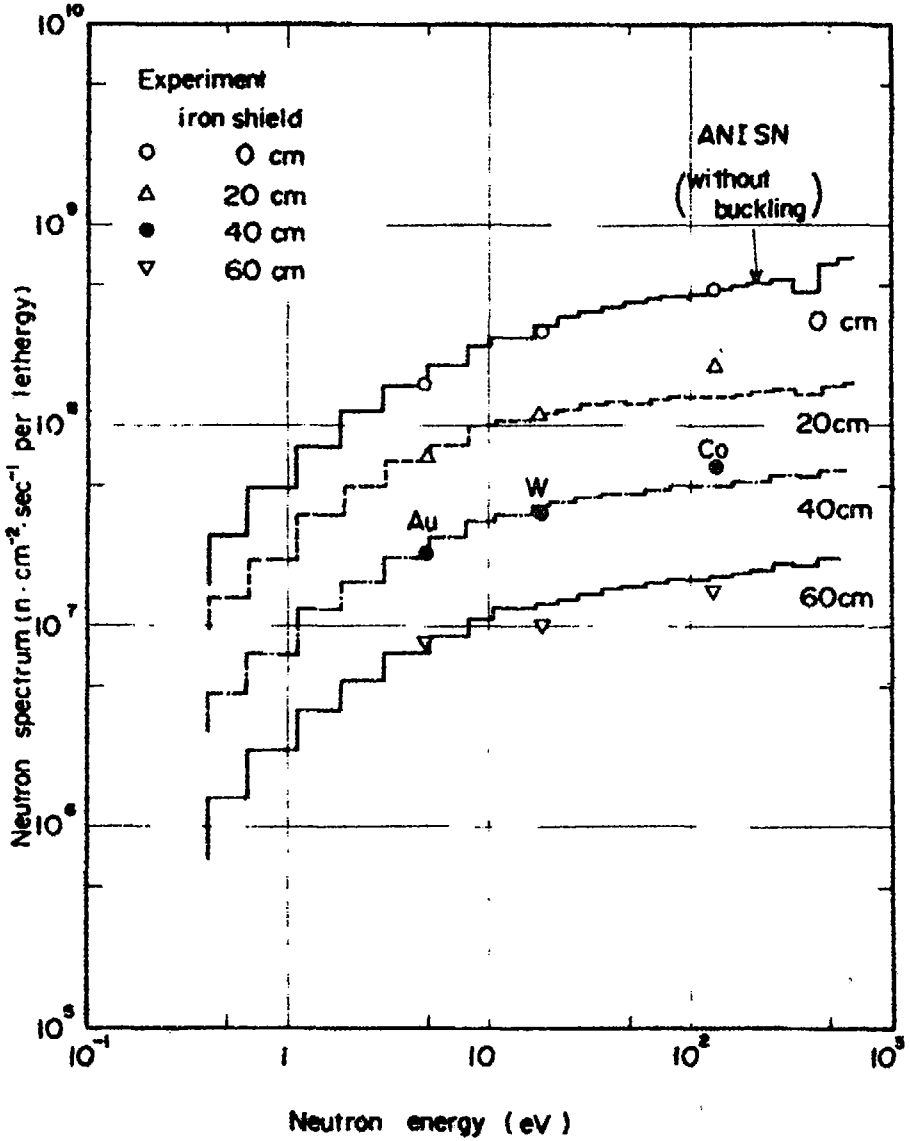

Fig 7 (b) Comparison of the neutron spectrum by sandwitch resonance foils with the calculated results by ANISN (without buckling)

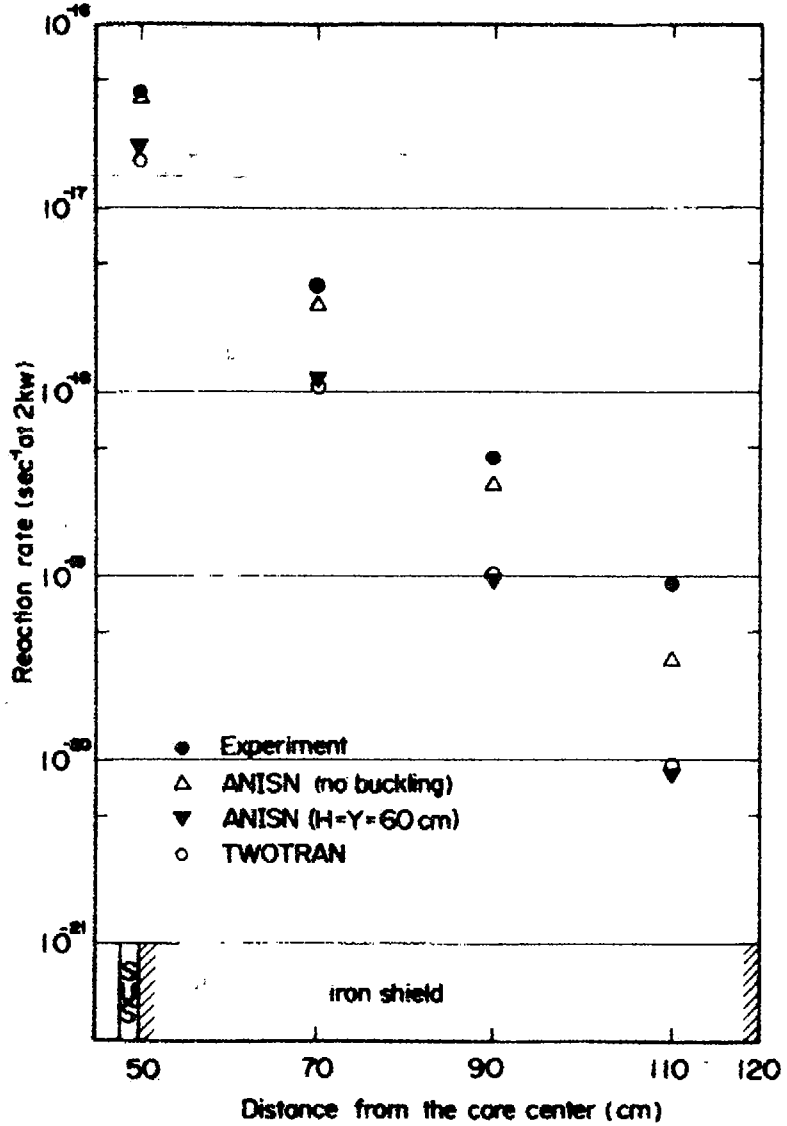

Fig 8 Axial distribution of $^{115}In(n,n')$ reaction in the iron shield

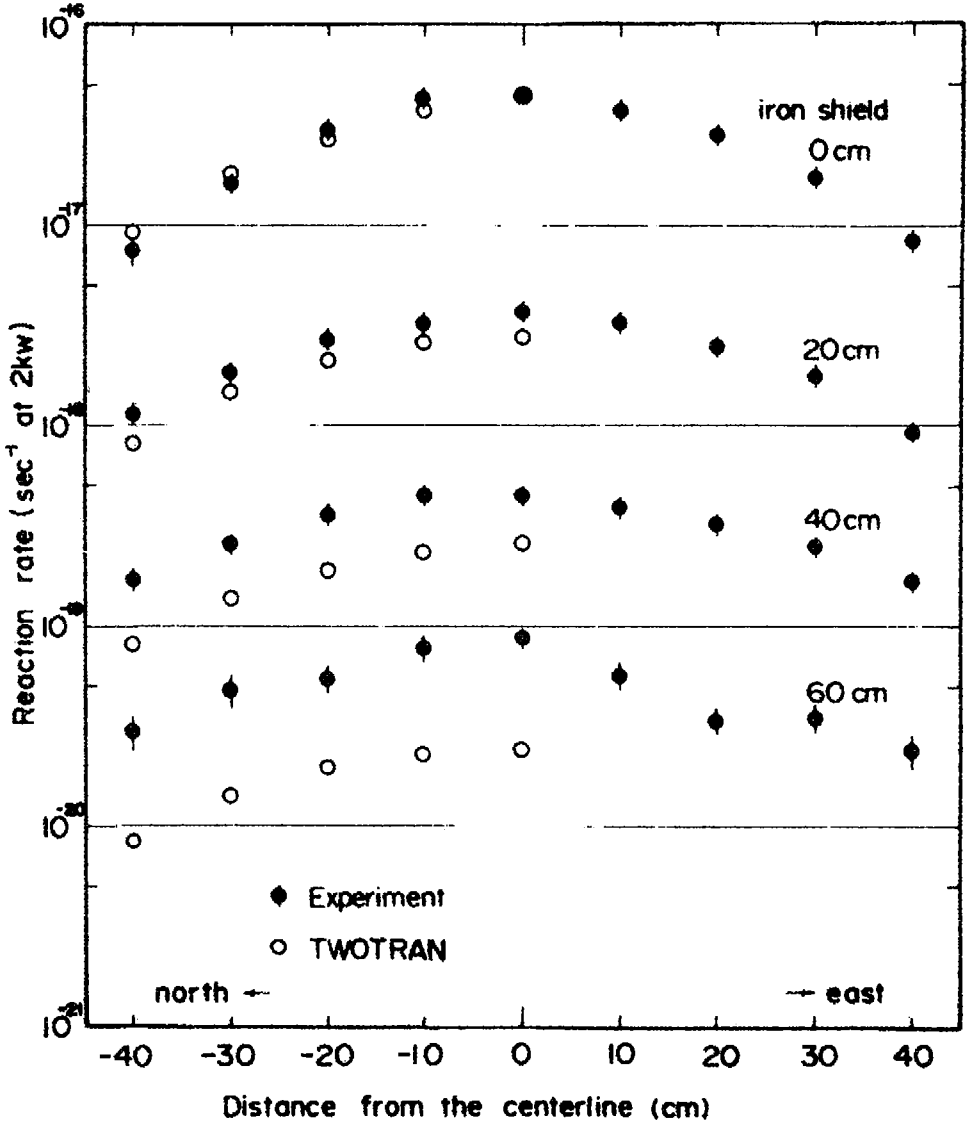

Fig. 9 Two dimensional distribution of $^{115}In(n,n')$ reaction in the iron shield

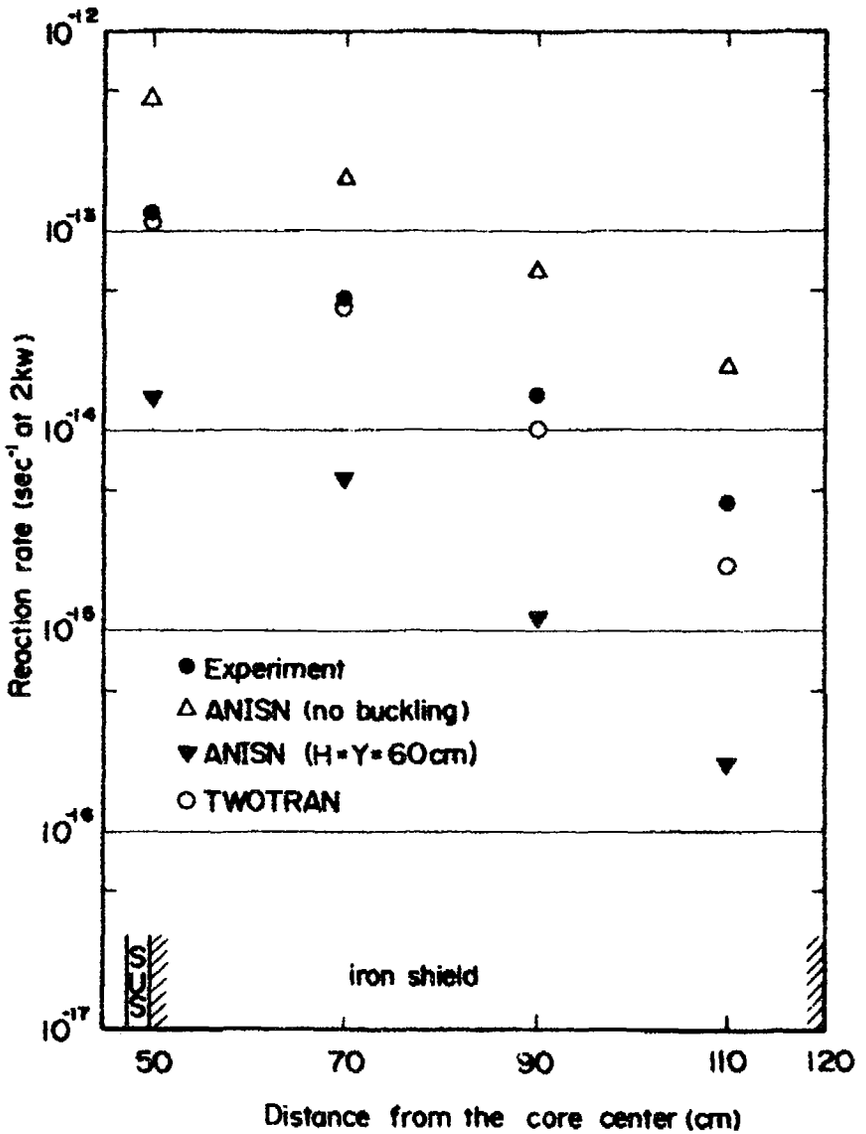

Fig.10 Axial distribution of $^{197}Au(n, gamma)$ reaction in the iron shield

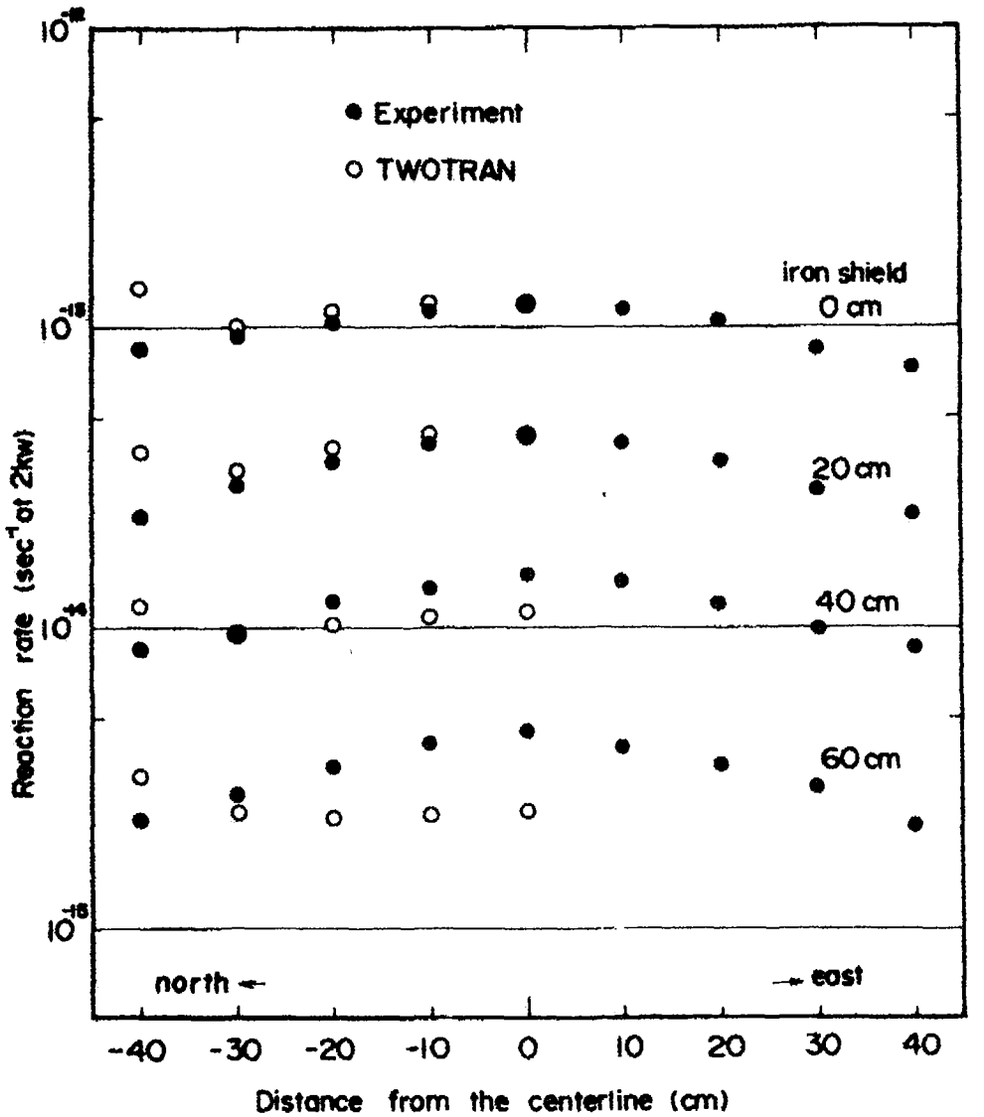

Fig.11 Two dimensional distribution of $^{197}Au(n,gamma)$ reaction in the iron shield

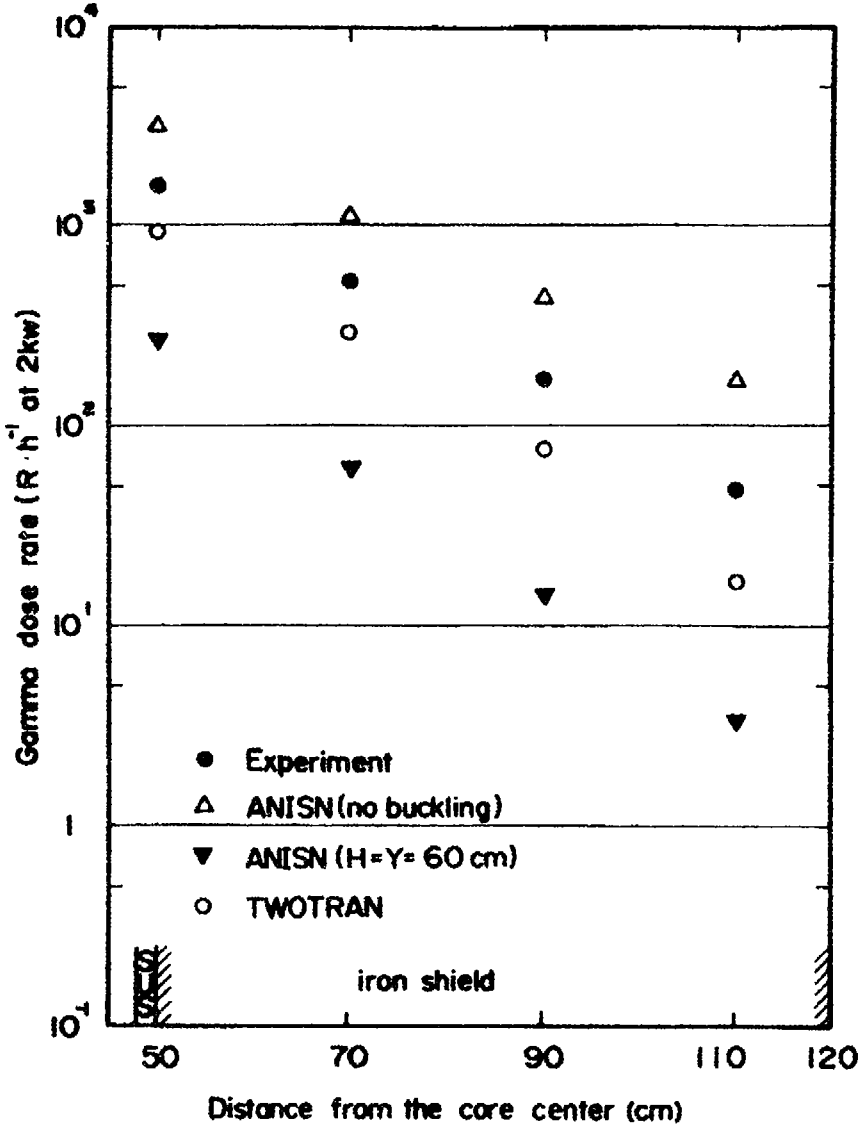

Fig.12 Axial distribution of gamma ray dose measured by $CaSO_4$ TLD in the iron shield

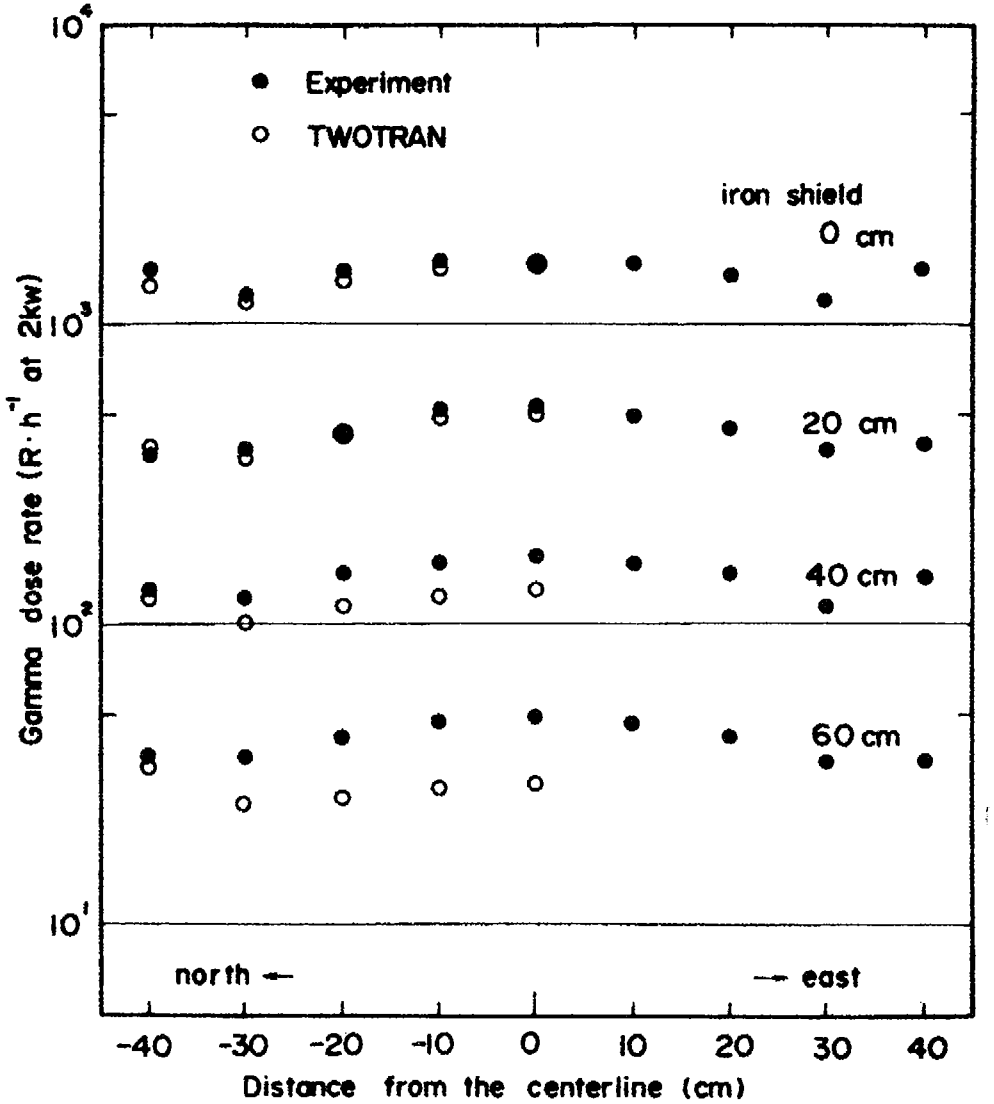

Fig.13 Two dimensional distribution of gamma ray dose measured by $CaSO_4$ TLD in the iron shield

100-GROUP, 2-D CALCULATION OF THE WINFRITH IRON BENCHMARK EXPERIMENT

(K. Burn, U. Canali, R. Nicks)

EURATOM - CCR - Ispra

Abstract

The neutron flux measured in the integral iron benchmark experiment at the ASPIS facility (Winfrith) has been calculed by means of the 2-Dimensional DOT Code, using the 100-group EURLIB standard library (based on ENDFB/III).

The calculation has been done in a P3/S4 approximation.
The results are compared with the experimental ones concerning the neutron spectra at four penetrations into the iron block.
For large depths the calculation appreciably underestimates the fast component above 0.8 MeV, indicating possibly an inadequacy of the fast neutron cross-sections for iron in EURLIB.

The results of these 100-group calculations are reduced to the agreed 15 group structure and are compared with those using a 15-group library obtained by collapsing EURLIB. Both calculations severely underestimate the flux above 0.1 MeV, at depths greater than 50 cm; the finer group structure does not significantly reduce this discrepancy The 100 group calculation has been repeated with the EURLIB-3 library, based on ENDF/B-IV, and the differences are discussed.

1. Introduction

The experiment analysed in this paper is part of a collaborative effort in the framework of the Common Shielding Benchmark Experimental Programme launched by NEACRP some years ago.

A full description of the experimental and shielding mock-up may be found in references (1), (2) and (3). Measurements of spectra were made at four positions in the iron shield corresponding to

equivalent thicknesses of 20.3 cm, 50.8 cm, 76.2 cm and 101.6 cm. At each of these positions measurements were made with hydrogen filled proportional-counters covering a neutron energy range of approximately 10 KeV to 2 MeV. The upper energy range was extended up to 5 MeV by liquid scintillator measurements.
The fast neutron source for this experiment was provided by a natural uranium convertor plate installed at the thermal column of the source reactor NESTOR. The iron shield consisted of 24 mild steel plates each 1830 mm wide, 1910 mm high and 50.8 mm thick.

The measured spectra were obtained from unfolding all the experimental data using the RADAK code (4). According to the recommendations issued at the Ispra Meeting on April 1973, the main codes used for the calculations are the discrete ordinates programmes ANISN and DOT. The data sets used are the 100-neutron group EURLIB based on ENDF/B3 and the new 120 (neutron plus gamma) group EURLIB-III based on ENDF/B4; only the first 67 groups were used, the lowest energy was 7 KeV.

2. The calculations with ANISN and DOT

2.1 The EURLIB library

Detailed information about this library may be obtained in references (5) and (6). It contains 14 elements, in a 100 group structure and in the P3 approximation. Weighting functions are 1/E (E ≤ 0.82 MeV) and (E) (E 0.82 MeV); for iron narrow resonance weighting is used.

2.2 The EURLIB-III coupled neutron-gamma library

For the neutrons, the 100 group structure of EURLIB was chosen. The elements and isotopes are H,C,O,Na, Al, Si, Ca, Cr, Mn, Fe, Ni, Zr, U-235, U-238, all in P3 approximation in the neutron and gamma parts. The weighting functions used in EURLIB were also applied to the new library. More information on EURLIB-III may be found in reference (7). Fig. 1 shows the relative differences between EURLIB and EURLIB-III.

2.3 Preliminary ANISN calculations

Some test cases were run in order to determine the influence of collapsing the data sets from 100 groups to 15 groups. The first line of Table I represents the summation of the ANISN 100 group fluxes into the agreed 15 group structure (ANISN 100/15). The calculations were performed with the old EURLIB library.

The second line gives the flux obtained by an ANISN run with the condensed 15 group structure, the third line gives the ratio of the two results; the fourth line represents the DOT 100/15 summations (taken from Table II) to be compared with the ANISN 100/15 values (line 1). The collapsing process introduces errors up to 30%, in the first 6 groups. On the other hand, a 15 group calculation ignores much of the structure of the spectrum; it was decided therefore to continue the investigation in a 100 group scheme, even at the expense of large computing time.

2.4 DOT-calculations

Two series of DOT calculations have been performed, the first one using the EURLIB-library, the second one with EURLIB-III, both runs were made in a P3, S4 approximation. The details of the geometrical 2D configuration are given in reference (1).

In a previous preliminary 15 group DOT analysis A.K.McCracken and M.J. Grimstone concluded that at small penetrations (20.3 cm) calculations with EURLIB are in excellent agreement with experiments at all energies between 50 KeV and 5 MeV. This conclusion is substantially confirmed by the 100 group EURLIB calculations, though there seems to exist a slight systematic overprediction of DOT in the energy range 200 KeV and below. The same authors attribute a satisfactory agreement of calculations and experiments at 50.8 cm; this is also confirmed by the present investigation in which an underprediction appears in the energy range 0.8 MeV - 1.5 MeV. At 70.6 cm penetration the agreement in the low energy range from 30 KeV to 300 KeV is excellent (contrary to the conclusion given in reference (3) concerning the calculations with the EURLIB library collapsed to 15 groups), whereas the tendency of underestimating the fluxes above 800 KeV is clearly confirmed. This underestimate becomes even more alarming at 101.6 cm where it may reach a factor larger than 50 at 1 MeV.

Apparently the EURLIB-III DOT calculations do not invalidate the above deduced conclusions. Inspection of figure 2 shows that the marked underpredictions in the high energy region exist for penetrations greater than 50 cm of iron. Furthermore also EURLIB-III (like EURLIB) progressively appears to underestimate fluxes in the energy region 30 KeV to 300 KeV. However a closer examination shows that EURLIB-III gives significantly better results than its precursor in the energy range

around 1 MeV; in fact at 1 MeV and 101 cm penetration the maximum discrepancy is inferior to a factor of 10 for the last EURLIB-III version, whereas it is superior to 50 for the previous one.
Table II permits a numerical comparison of 100 group calculations summed up into the agreed 15 group structure, for EURLIB and for EURLIB-III (DOT 100/15). The same table also contains experimental results reduced to the same energy structure. Table III shows the C/E values (ratio of calculated values to experimental results)deduced from Table I.
One clearly sees that EURLIB-III leads even to a lower prediction than EURLIB in the high energy range, whereas it gives a better agreement in group IV corresponding to 1.83 MeV - 0.82 MeV. The same table permits a comparison with the DOT calculations performed in ref.(3); figures 3, 4, 5, 6, taken from the reference (3) show that the effect of group collapsing may be significant at deep penetrations.

3. Conclusions and future work

Figure 2 shows quite clearly that something is wrong above 0.7 MeV for EURLIB and above 1.2 MeV for EURLIB-III.
EURLIB-III gives significantly better results in the range 0.8 MeV up to 1.2 MeV. This might be due to an improved elastic scattering treatment in EURLIB-III.

One could incriminate the low order of the angular quadrature used in the preceding calculation for the high energy underprediction. Preliminary calculations performed in reference (3) indicate that the order 4 seems to be adequate. Thus new differential measurements of inelastic scattering in the region above some MeV would appear to be justified. However, before making a final statement, it might be worthwhile to further investigate the influence of the higher order of quadrature in DOT calculations (S8, S12) as well as a higher Pn approximation; these calculations could be limited to the higher energy groups in order to make sure that the highly anisotropic fast fluxes are treated adequately.

The 17 experimental group fluxes of Table II have been reduced to 1D geometry by multiplication with the geometry factor(calculation ANISN)/(calculation DOT),in order to compensate for geometrical effects. It is foreseen to analyse these data by the linear regression technique described in reference (8). For this purpose a special code, CROCO,

has been established and will be applied for adjusting the 6 first total cross sections of the 15 group structure. The input data for CROCO are the partial derivatives(with respect to the total cross sections) of the 17 responses (17 group fluxes); these derivatives are deduced from a series of 17 SWANLAKE calculations based on one direct and 17 adjoint ANISN runs.

References

1. M.D. CARTER, A. PACKWOOD[+] - The Winfrith Benchmark Experiment in Iron - Experimental Results
2. R. NICKS - Results of the First Four Single Material Experiments in Iron - NEACRP - U - 73
3. A.K. McCRACKEN, M.J. GRIMSTONE[+] - Preliminary Analysis of the Winfrith Iron Benchmark Experiment
4. A.K. McCRACKEN, M.J.GRIMSTONE[+] - The experimental Data Processing Program RADAK
5. G. HEHN[+] - Experience with the group Cross-Section Library EURLIB-IV
6. G. GONANO et al. - Standard Neutron Energy Group Structure for Shielding Benchmark Experiments - ESIS Newsletter n. 12, Jan. 1975
7. G. GONANO et al. - The development of the coupled shielding standard library EURLIB-III - ESIS-Newsletter, N. 19, Oct. 1976
8. W. MATTHES[+] - Multigroup Cross-Section Adjustment by Linear Regression

[+] Proceedings of the Specialists'Meeting on Sensitivity Studies and Shielding Benchmarks, Paris 1975, NEA - IAEA

Table I: ANISN - Results

Group	I	II	III	IV	V	VI
	14.92-6.70 MeV	6.70-3.33 MeV	3.33-1.83 MeV	1.83-0.82 MeV	0.82-0.11 MeV	0.11-0.03 MeV
Penetration (cm)						
20.3	7.68(-1)	8.14	4.83(1)	3.85(2)	8.35(3)	3.82(3)
	7.4 (-1)	8.22	4.98(1)	3.86(2)	8.54(3)	3.81(3)
	1.04	0.99	0.97	1.00	0.98	1.00
	7.16(-1)	8.00	4.48(1)	3.33(2)	6.15(3)	2.54(3)
50.8	2.89(-3)	1.92(-2)	1.95(-1)	7.81	1.58(3)	1.05(3)
	2.64(-3)	1.89(-2)	2.01(-1)	7.68	1.43(3)	9.74(2)
	1.09	1.02	0.97	1.02	1.10	1.08
	2.36(-3)	1.59(-2)	1.59(-1)	5.79	8.43(2)	5.47(2)
76.2	3.13(-5)	1.32(-4)	1.82(-3)	3.11(-1)	2.91(2)	2.68(2)
	2.68(-5)	1.26(-4)	1.89(-3)	3.09(-1)	2.56(2)	2.28(2)
	1.17	1.05	0.95	1.01	1.14	1.18
	2.26(-5)	9.80(-5)	1.36(-3)	2.00(-1)	1.37(2)	1.18(2)
101.6	3.74(-7)	9.18(-7)	1.64(-5)	1.27(-2)	5.08(1)	5.66(1)
	2.98(-7)	8.99(-7)	1.69(-5)	1.21(-2)	3.90(1)	4.25(1)
	1.26	1.02	0.97	1.05	1.30	1.30
	2.27(-7)	6.37(-7)	1.12(-5)	6.94(-3)	2.04(1)	2.14(1)

Table II: DOT Calculations and Measurements

Penetration (cm)	Group	I 14.92-6.70 MeV	II 6.70-3.33 MeV	III 3.33-1.83 MeV	IV 1.83-0.82 MeV	V 0.82-0.11 MeV	VI 0.11-0.03 MeV
20.3	EURLIB	0.71	8.00	4.48(1)	3.33(2)	6.15(3)	2.54(3)
	EURLIB-III	0.68	6.44	4.03(1)	4.52(2)	6.13(3)	2.51(3)
	ASPIS	----	7.71	4.39(1)	3.68(2)	4.12(3)	1.45(3)
50.8	EURLIB	2.36(-3)	1.59(-2)	1.59(-1)	5.79(0)	8.43(2)	5.47(2)
	EURLIB-III	2.09(-3)	1.03(-2)	1.26(-1)	1.18(1)	8.67(2)	5.57(2)
	ASPIS	----	1.57(-2)	2.48(-1)	1.39(1)	8.42(2)	4.07(2)
76.2	EURLIB	2.26(-5)	9.80(-5)	1.36(-3)	2.00(-1)	1.37(2)	1.18(2)
	EURLIB-III	1.79(-5)	5.38(-5)	9.72(-4)	5.76(-1)	1.41(2)	1.21(2)
	ASPIS	----	----	8.16(-3)	1.29(0)	2.07(2)	1.27(2)
101.6	EURLIB	2.27(-7)	6.37(-7)	1.12(-5)	6.94(-3)	2.04(1)	2.14(1)
	EURLIB-III	1.57(-7)	2.91(-7)	6.95(-6)	2.80(-2)	2.00(1)	2.18(1)
	ASPIS	----	----	----	1.32(-1)	5.40(1)	4.19(1)

Table III : $\frac{C}{E}$ values

Group / Penetration (cm)		I 14.92-6.70 MeV	II 6.70-3.33 MeV	III 3.33-1.83 MeV	IV 1.83-0.82 MeV	V 0.82-0.11 MeV	VI 0.11-0.03 MeV
20.3	EURLIB/ASPIS	-----	1.04	1.02	0.90	1.49	1.75
	EURLIB-III/ASPIS	-----	0.84	0.92	1.23	1.49	1.73
50.8	EURLIB/ASPIS	-----	1.01	0.64	0.42	1.00	1.34
	EURLIB-III/ASPIS	-----	0.66	0.51	0.85	1.03	1.37
76.2	EURLIB/ASPIS	-----	-----	0.17	0.16	0.66	0.93
	EURLIB-III	-----	-----	0.12	0.45	0.68	0.95
101.6	EURLIB/ASPIS	-----	-----	-----	0.05	0.38	0.51
	EURLIB-III/ASPIS	-----	-----	-----	0.21	0.37	0.52

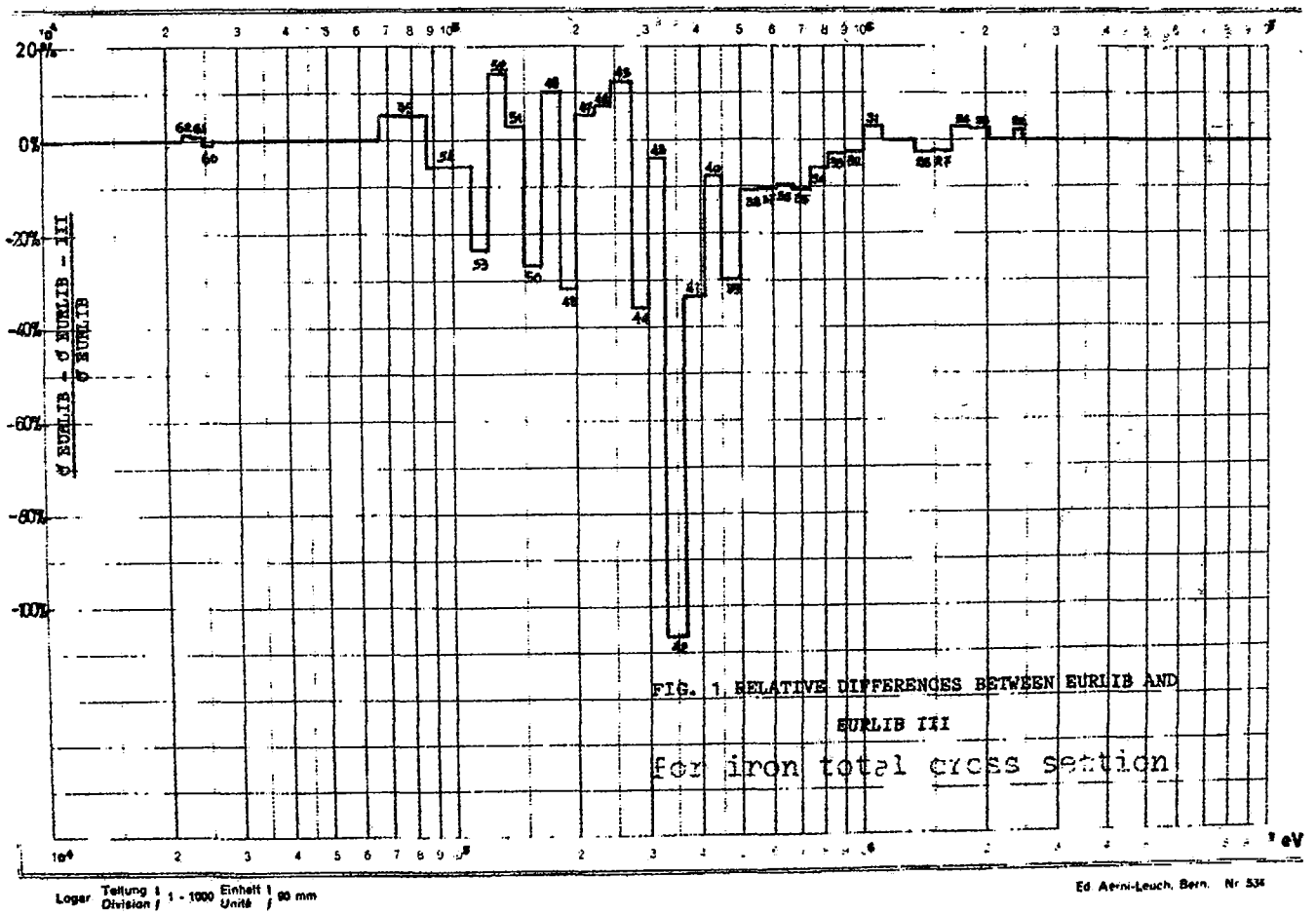

FIG. 1 RELATIVE DIFFERENCES BETWEEN EURLIB AND EURLIB III

for iron total cross section

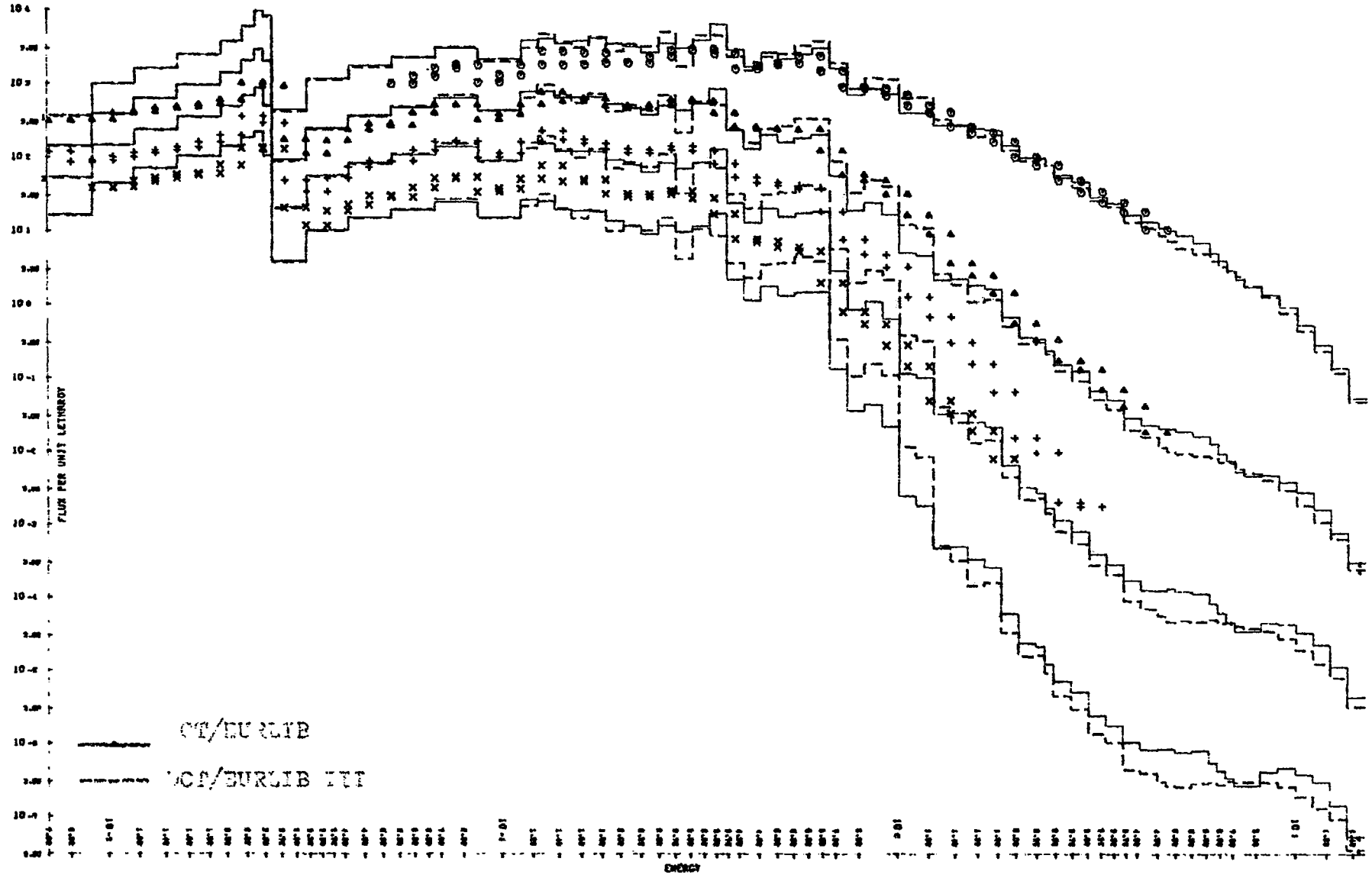

FIG. 2

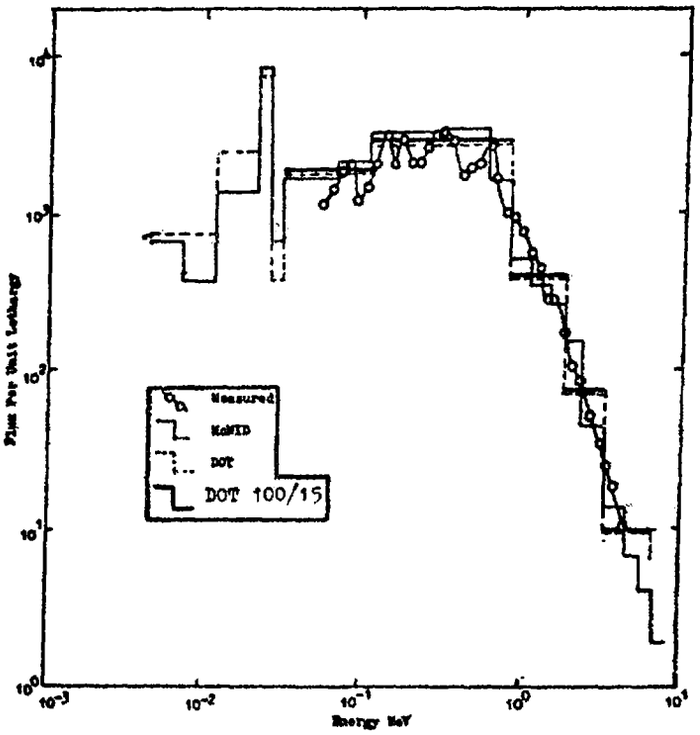

FIG. 3 Comparison of Measured and Calculated Spectrum at 20.1 cm Penetration in Iron

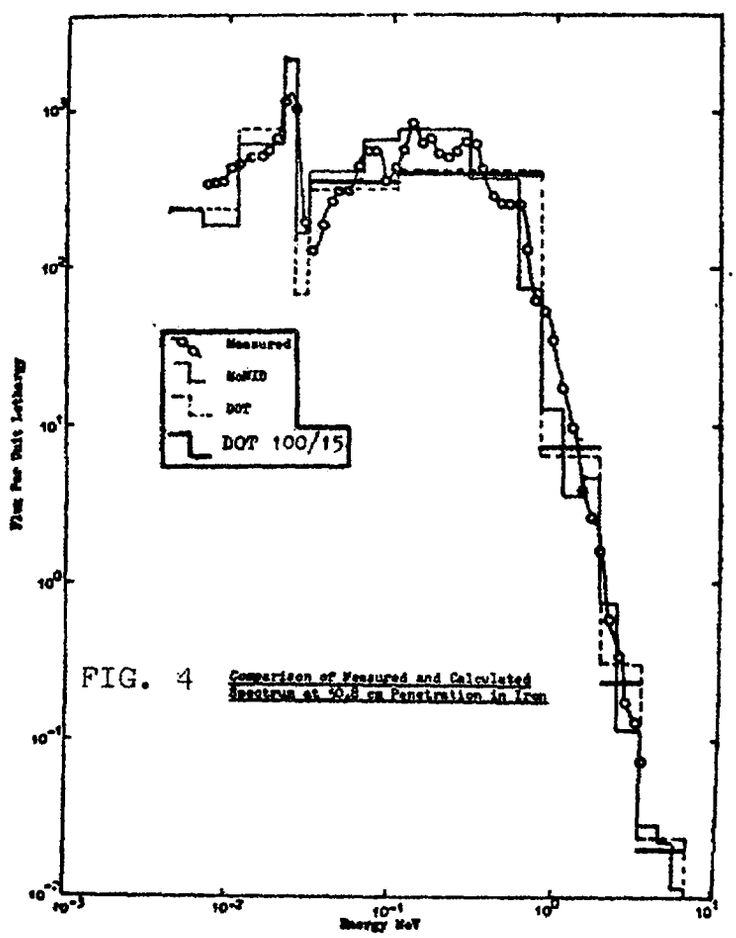

FIG. 4 Comparison of Measured and Calculated Spectrum at 30.8 cm Penetration in Iron

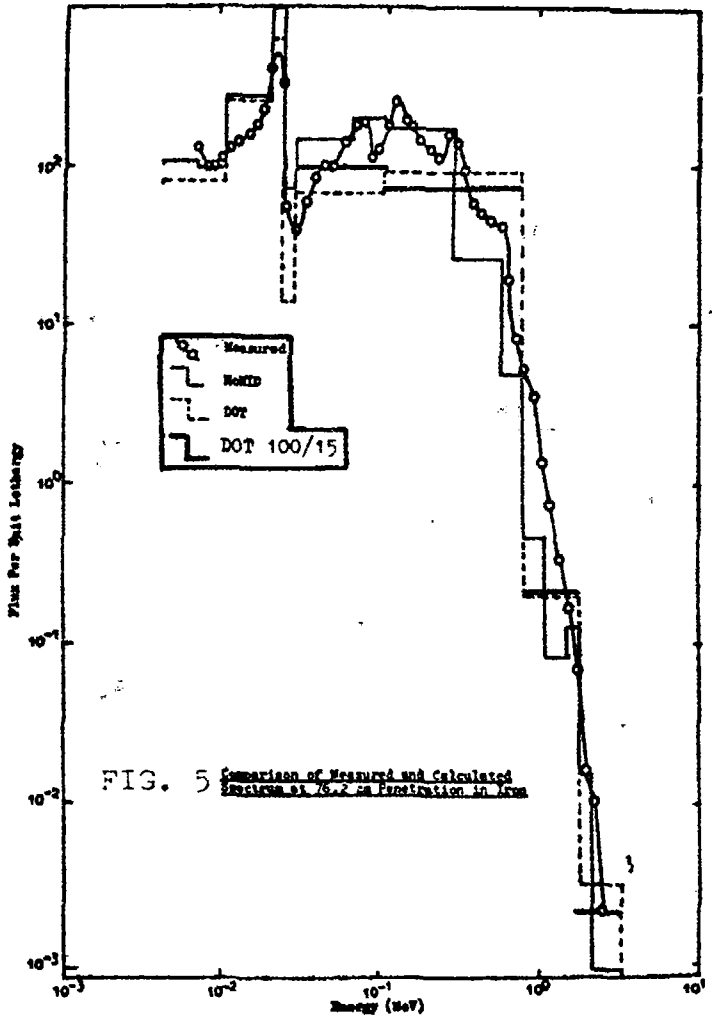

FIG. 5 Comparison of Measured and Calculated Spectrum at 76.2 cm Penetration in Iron

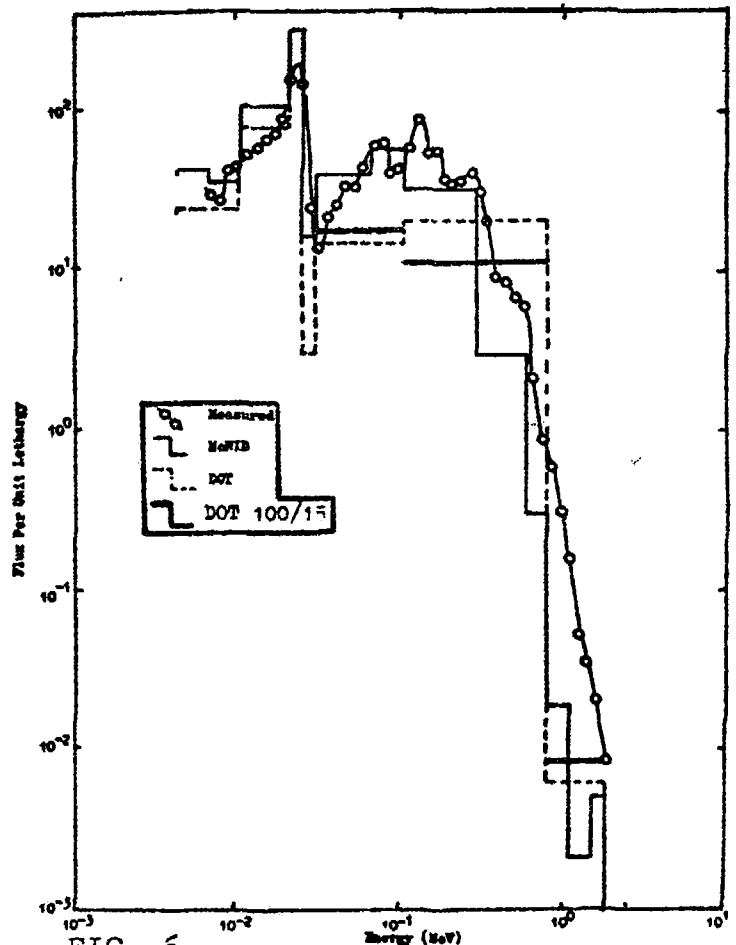

FIG. 6 Comparison of Measured and Calculated Spectrum at 101.6 cm Penetration in Iron

The design and analysis of integral assembly experiments for CTR neutronics

T.D. Beynon, R.H. Curtis and C. Lambert
Department of Physics
University of Birmingham
U.K.

Abstract

The use of simple-geometry integral assemblies of lithium metal or lithium compounds for the study of the neutronics of various CTR designs is considered and four recent experiments are analysed. The relatively long mean free path of neutrons in these assemblies produces significantly different design problems from those encountered in similar experiments for fission reactor design. By considering sensitivity profiles for various parameters it is suggested that experiments can be designed to be optimised for data adjustments.

1. Introduction

Most designs for the first generation of controlled thermonuclear reactors (CTR's) are based on the deuterium-tritium cycle

$$D + T \rightarrow \alpha\,(3.5\ \text{MeV}) + n\,(14.1\ \text{MeV})$$

with tritium breeding occurring in a suitably designed lithium blanket with the reactions

$$^{7}\text{Li} + n \rightarrow \alpha + T + n' - 2.5\ \text{MeV}$$

$$^{6}\text{Li} + n \rightarrow \alpha + T + 4.5\ \text{MeV}$$

A detailed neutronic analysis of such a system must consider interactions in the first wall (niobium or steel), the breeding blanket (lithium metal or lithium compounds) and a steel reflector, together with any associated structural material. In some designs it may be necessary to account for neutron multiplying regions

(beryllium or lead, for example) and a graphite thermalizing region. The energy range of interest is therefore about 15 MeV down to thermal energies.

The role of the CTR integral experiment in support of these designs is seen as twofold. First there is the traditional role of comparing measurements and calculations of neutron flux and reaction rate distributions in a relatively simple geometry with the aim of isolating gross uncertainties in neutron cross section data and in establishing minimum accuracy requirements for various neutron transport codes. With this philosophy in mind we present an analysis of four major integral experiments on lithium assemblies.

The second role of the integral assembly is seen as a more exploratory one. We can pose the following problem: can we design an experiment which is capable of answering a specific question? For example can we measure a tritium breeding ratio in an integral experiment so that comparisons with a calculated value could lead to data adjustments directly relevant to a particular CTR design? Using the ANISN - SWANLAKE programme for this particular design we can obtain the sensitivity of the tritium breeding ratio to changes in each energy group of a given cross section, that is we can obtain a sensitivity profile. The profiles for tritium breeding in our integral experiment and our CTR design should be similar if we wish to make optimal data adjustments to bring calculated and measured breeding values into agreement. Of course we now have no guarantee that the experiment, optimised for this particular profile, is anywhere near to being optimised for a profile for a different cross section. In this paper we consider integral experiments to measure tritium breeding via the ^{7}Li and ^{6}Li components of natural lithium where we may need to introduce reflected assemblies to optimise the ^{6}Li contribution. Similar analyses are made to investigate the sensitivity of tritium breeding to first wall interactions and the use of integral assemblies for this purpose.

2. Simple-geometry lithium assemblies: measurement and analysis

Ideally, integral assemblies should be in as simple a geometry as possible to allow one- or two-dimensional transport codes to be

used effectively. Consequently, experiments to date have been made with spheres or cylinders of lithium metal or lithium compounds driven by a centrally placed D-T source. The relatively long neutron mean free paths (Σ_t^{-1} = 14 cm for 14 MeV neutrons in natural lithium) results in values of the flux-weighted neutron energy well in excess of 1 or 2 MeV, which tends to limit the range of measuring techniques which can be made easily. The following methods could be or have been used:

i) reaction rate measurements in (n,p), (n,α) and (n,2n) threshold indicators,

ii) fission reaction rates and reaction rate ratios in fertile and fissile nuclides (^{238}U, ^{235}U, ^{237}Np, ^{232}Th, ^{239}Pu),

iii) spectrum measurements using nuclear emulsions, proton recoil (liquid scintillation, gas proportional), ^{6}Li scintillation spectrometers and time-of-flight,

iv) spatial distribution of tritium production rates using β - counting techniques, including estimates of production in each lithium isotope by using samples highly enriched in either ^{6}Li or ^{7}Li.

The four major integral experiments which have been reported in the literature /1-5/ are summarised below. A number of others are presently under construction or being planned.

a) <u>The AWRE lithium metal cylinder /1/</u>

A cylinder, 102 cm high and diameter 99 cm, was constructed from lithium metal rods and driven centrally by a 210 kV D^{+}-T source. Measurements were made of tritium production distributions in ^{6}Li, ^{7}Li and natural lithium, threshold reaction rates and fission reaction rates, neutron energy distributions using nuclear emulsions and NE213 organic scintillators, with long counter measurements of the leakage spectrum. Little analysis has previously been published of these measurements.

b) <u>The JAERI lithium metal sphere /2,3/</u>

Using a pseudo-sphere of mean diameter 110 cm constructed from lithium metal blocks and driven centrally by a 300 kV

D^+-T source, measurements have been made of the spatial distributions of $^{238}U/^{235}U$ fission rate ratios, fission rates in ^{232}Th, ^{238}U, ^{237}Np and ^{235}U. Penetration of 14 MeV neutrons has been measured by a ^{6}Li I scintillation counter and the fission rate measurements were repeated using a 20 cm thick graphite reflector.

c) The Julich lithium metal cylinder /4/

This experiment concentrated on the measurement and calculation of the tritium production rate in a hollow cylinder of homogeneous lithium metal, inner radius 10 cm and height and outer diameter 120 cm, centrally driven by a D^+-T source. Monte Carlo (MORSE) and SN(DOT-II) calculations were compared with the measured values of the tritium production using data from the ENDF/BIII file.

d) The Karlsruhe lithium metal sphere /5/

In a metal sphere of diameter 1 m, driven centrally by a D^+-T source, measurements at two radial positions have been made of the energy distribution of the angular and scalar fluxes using time-of-flight and proportional counters respectively.

Figure 1 summarises the geometries of these four experiments.

Two codes have been used to analyse the measurements made above. The ANISN code /6/ with the ENDF/BIII 100 group DLC library has been used for one dimensional analysis whilst the UKAEA Monte Carlo programme SPECIFIC II /7/ using the UKAEA Nuclear Data File has been used for a realistic representation of the geometries.

Figures 2-7 are some representative results for our comparisons with the Aldermaston measurements. All computations have been made using SPECIFIC II. Figures 2(a) and 2(b) show measured flux distributions at two positions in the central plane: the normalisation is absolute. The agreement is generally good except in the top energy group where the calculation is significantly higher than the measured value. This over-estimation has been noted by the investigators in the other integral experiments where fluxes have been

measured and more recently /8/ in a series of time-of-flight measurements with a 14 MeV neutron source in materials of interest to CTR design. Two possible explanations are suggested. First, the assumption in the calculations of a monoenergetic neutron source at 14 MeV will not be accurate enough. For example, 400 kV D^+ ions on a tritiated target will produce an energy spread from 15.6 MeV to 12.9 MeV. Secondly, we should look carefully at the assumptions which may be used in a spectrum unfolding code regarding the group 1 or estimated flux in the unfolding procedure. Since the flux deep into the assembly will still contain a large component of uncollided neutrons an accurate representation of the source energy distribution will need to be used in unfolding the flux.

Figures 3(a) and 3(b) are the comparisons with the ^6Li and ^7Li tritium production rates. These were measured using samples highly enriched in either isotope whereas the calculations are the reaction rates in the isotope in their natural abundance in lithium metal (^6Li 7.4%, ^7Li 92.6%). However the differences in the self shielding effects in each case are negligible. It is evident that whereas there is reasonable agreement between the calculations and measurements in the case of ^7Li, the calculation significantly underestimates the tritium production in ^6Li near the edge of the cylinder. It is believed /1/ that in this experiment there was a significant contribution from room return of thermal and epithermal neutrons.

Figures 4-7 show respectively comparisons with the reaction rate distributions of $^{27}Al(n,p)$, $^{239}Pu\ (n,f)$, $^{235}U(n,f)$ and $^{238}U(n,f)$. The calculations are for unshielded spectra and would need to be repeated with shielding included before any statement regarding a data evaluation in the high MeV range could be made. Once more room return neutrons would seem to be of some importance.

Our analyses of the JAERI, Julich and Karlsruhe experiments are essentially complementary to the computations made by the original investigators and no significant differences from these calculations have been found. Figure 8 shows the agreement between the Birmingham and JAERI ANISN calculations for various reaction rate distributions. Particular attention should be paid to the need for accurate spectrum weighting in the graphite reflector (cf fig 8(b)).

Figure 9 illustrates the Julich measurements of the tritium production distribution compared with the Birmingham ANISN (P3, S8) and SPECIFIC II calculations. Although not shown on this figure the Julich MORSE computations gave somewhat better agreement than the SPECIFIC II code.

Figure 10 shows the comparisons between the measurements and calculations of the scalar and angular flux distributions at two positions in the Karlsruhe sphere. One point is immediately obvious: neither set of calculations accurately reproduces the measured behaviour in the vicinity of the 265 keV resonance in ^{6}Li.

Finally we plot in figure 11 the behaviour of the flux-weighted neutron energy $\bar{E}$ across different integral assemblies. We see that $\bar{E} \gtrsim 4$ MeV in the unreflected assemblies and $\bar{E} \gtrsim 1$ MeV in the reflected system. This serves to show a major difference in the energy range of interest between the CTR integral assemblies and those assemblies usually used for fission reactor work.

3. Optimally designed assemblies

Once it has been demonstrated that the calculational ability exists to analyse the flux and reaction rate measurements of the type discussed above we must then decide on a scheme for cross section adjustments to improve the agreement between calculation and measurement. However, since the object of these measurements and the subsequent data adjustment is presumably to produce a data file optimised for CTR design, we must determine whether the experiment is suitably designed to give relevant information.

To define this relevance we use the concept of a sensitivity profile S(E) / 9 /. For a given parameter R, total tritium breeding for example, we can use first order perturbation theory to obtain the dependence of ΔR on a perturbation $\Delta X(E)$ in a parameter X(E) so that $S(E) = (\Delta R/R) / (\Delta X(E) / X(E))$. We now have a quantitative technique of determining in which energy region of X(E) R is most sensitive to a change $\Delta X(E)$. Unless S(E) for a CTR design is similar in shape to S(E) for the design of a proposed integral experiment for a given R and X(E) the experiment will not be tuned to give data adjustments to minimise the uncertainties in R in the engineering design.

To illustrate this idea we present a selection of results for a series of computations based on the ANISN-SWANLAKE programme /10/. These results compare sensitivity profiles for an integral experiment currently being made at Birmingham with a design for a stainless steel - liquid lithium - helium cooled Tokamak reactor. The Birmingham experiment is a 1 m diameter sphere of LiF driven centrally by a D-T source, in which measurements of neutron energy spectra and tritium production distributions are being made. The Harwell-Culham (HC) conceptual Tokamak blanket design is illustrated in figure 12.

Figure 13 shows the sensitivity of the breeding in ^{6}Li (T^{6}) to the ^{6}Li (n, α)T cross section for both the HC blanket and the Birmingham sphere. We see that apart from additional structure in the case of the integral experiment, due to resonance structure in ^{19}F, the shapes of S(E) are essentially the same. This means that the integral assembly is tuned in the sense that adjustments that we would need to make to the ^{6}Li (n, α)T cross section to bring the measured and calculated T^{6} values into agreement will be appropriate to the HC design.

To illustrate how an integral experiment is not tuned we consider the following examples. Suppose we were to modify the LiF integral experiment by placing a 0.5 cm thick spherical shell of steel around our D-T source in an attempt to simulate the effects of the first-wall interactions of neutrons leaving a plasma. In figure 14 we plot the sensitivity of the total tritium production (in ^{6}Li and ^{7}Li) to the total cross section of natural iron. We see that there is no similarity in the sensitivity profiles, the HC design being sensitive to uncertainties down to about 500 eV whereas the measured value in the experiment is only sensitive to changes down to about 500 keV. We can appreciate the reason for this by referring to figure 11. It is obvious that the 6 percent of stainless steel in the blanket region (representing structural materials) would not be properly represented in this modified experiment simply by including this steel shell. It should also be pointed out that the HC design used in these calculations contains no steel reflector region, the inclusion of which would significantly modify the HC profile in figure 14.

We conclude these illustrations of a poorly designed experiment with figures 15-17 in which we examine the relative sensitivities of total breeding to $\bar{\mu}$ (the average cosine of scattering angle in the L system) for elastic scattering in Fe, Ni and Cr. In none of the cases considered are the profiles seen to be similar for the reasons discussed above. From this examination we conclude that measurements of total tritium production in this modified experiment could not lead to data adjustments of the anisotropy of elastic scattering in these materials which would be of importance in this particular CTR design. Moreover, and perhaps more importantly, these integral measurements should not be used as the basis of recommendations for measurements of differential cross sections in Fe, Ni and Cr. A major re-design of the experiment would first need to be made to produce profiles similar to the HC profiles shown in figures 15-17.

Acknowledgements

The work reported in this paper is part of a programme supported by AERE Harwell under agreement no. H4B/2694 EMR. One of us (CL) wishes to thank the Science Research Council, London, for a research studentship.

References

1. Benjamin P.W., Goodfellow H., Gray J. and Weale J.W., (1964), AWRE rep. no. AWRE NR 4/64.

2. Hiraoka T., Maekawa H., Seki Y. and Hirota J., (1974), Nucl. Fusion, Spec. Supp. Proc. Symp. Fusion Reactor Design Problems, (IAEA) p. 363.

3. Maekawa H., Seki Y. and Hiraoka T., (1975) Nucl. Sci. Eng. 57, 335.

4. Herzing R., Kuypers L., Cloth P., Filges D., Hecker R. and Kirch N., (1976), Nucl. Sci. Eng. 60, 169.

5. Kappler F., Rusch D., Werle H. and Wiese H.W., (1974) 8th Symp. Fusion Technology (SOFT) Noordwijkerhout, The Netherlands.

6. Engle W.W., (1967), USAEC rep. K-1693.

7. Holbrough D.W. and Lipscombe B.A., (1971), UKAEA rep. no. AERE-R 6622.

8. Hansen L.F., Wong C., Komoto T. and Anderson J.D., (1976), Nucl. Sci. Eng., 60, 27.

9. Bartine D.E., Alsmiller R.G., Oblow E.M. and Mynatt F.R., (1974), Nucl. Sci. Eng., 53, 304.

10. Bartine D.E., Mynatt F.R., Oblow E.M., (1974), Oak Ridge National Laboratory report no. ORNL-TM-3809.

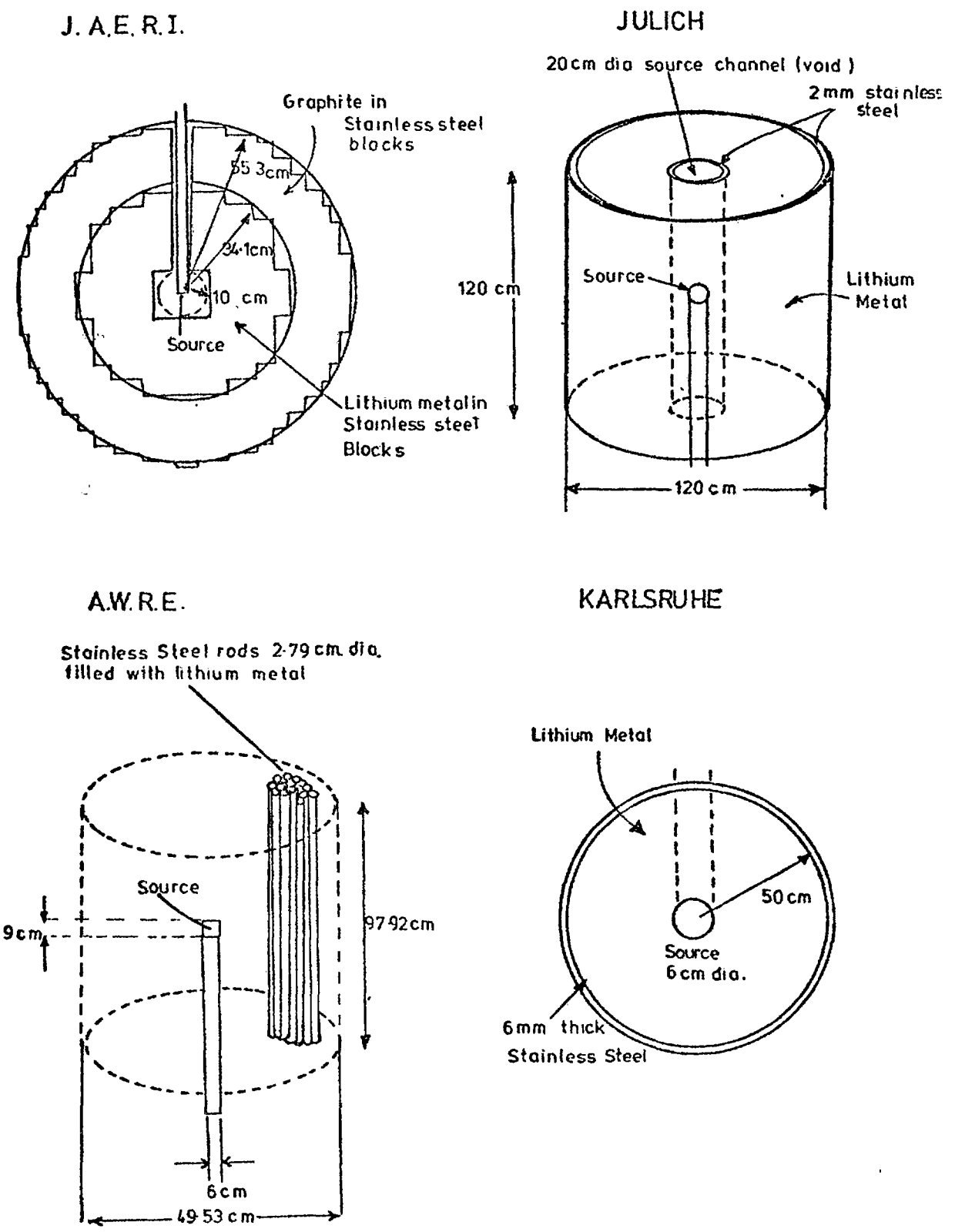

Figure 1. Summary of geometries of various lithium integral assemblies analysed.

Fig 2(a)

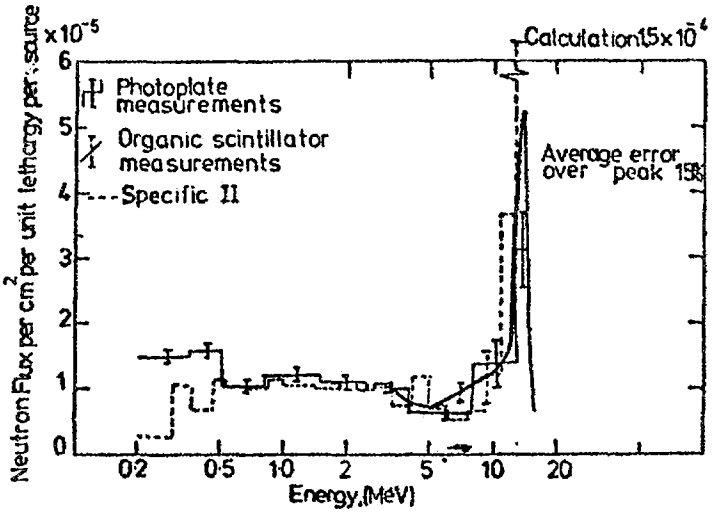

Fig .2(b)

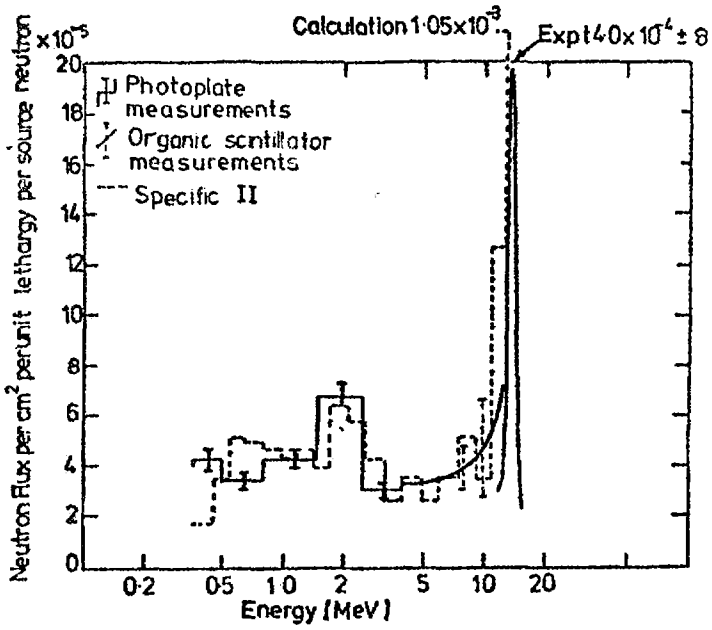

Figure 2. Comparison of measured and calculated neutron energy spectra in the AWRE cylinder at r = 25.86 cm, (Fig 2a) and r = 46.54 cm (Fig 2b).

Fig 3(a)

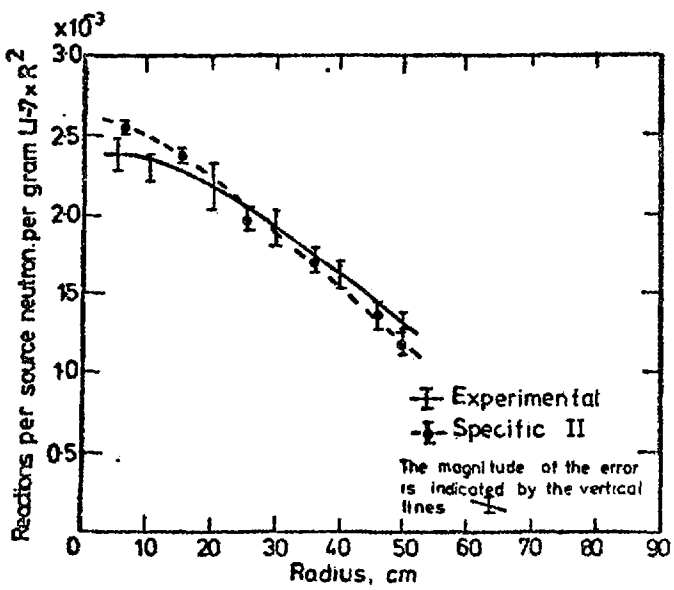

Fig 3(b)

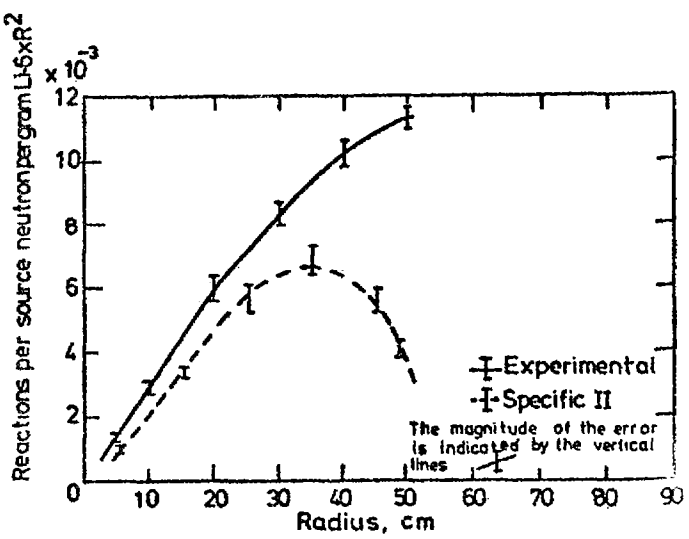

Figure 3. Comparison of measured and calculated tritium production distribution via Li-7 (Fig 3a) and Li-6 (Fig 3b) in the AWRE lithium metal cylinder. The broken curves through the Monte-Carlo results are eye-guides.

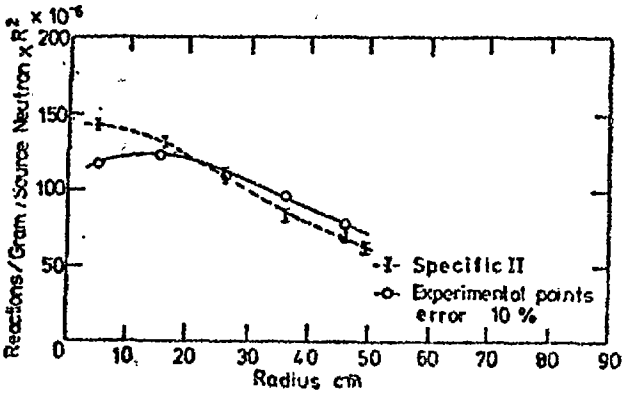

Figure 4. Comparison of the measured and calculated spatial distribution of Al-27 (n,p) reaction rates in the AWRE lithium metal cylinder. The broken line through the Monte-Carlo results is an eye-guide.

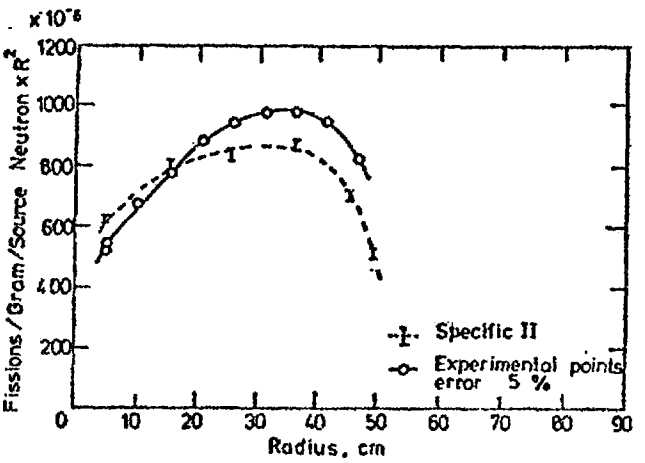

Figure 5. Comparison of the measured and calculated spatial distribution of Pu-239 (n,f) reaction rates in the AWRE lithium metal cylinder. The broken line through the Monte-Carlo results is an eye-guide.

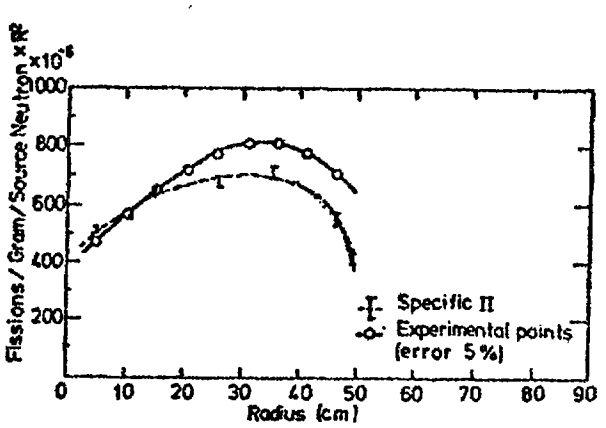

Figure 6. Comparison of the measured and calculated distribution of U-235 (n,f) reaction rates in the AWRE lithium metal cylinder. The broken line through the Monte-Carlo results is an eye-guide.

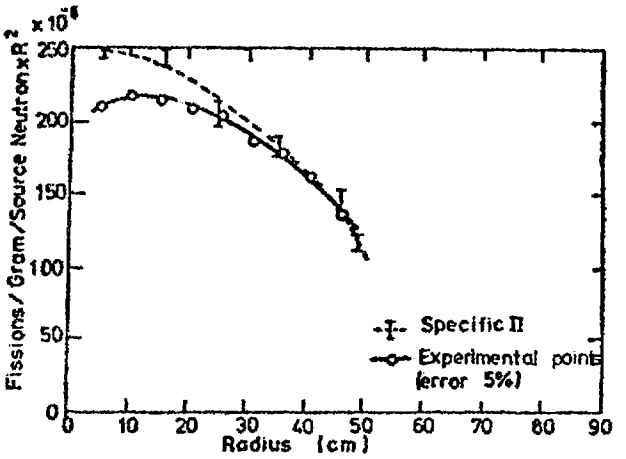

Figure 7. Comparison of the measured and calculated distribution of U-238 (n,f) reaction rates in the AWRE lithium metal cylinder. The broken line through the Monte-Carlo results is an eye-guide.

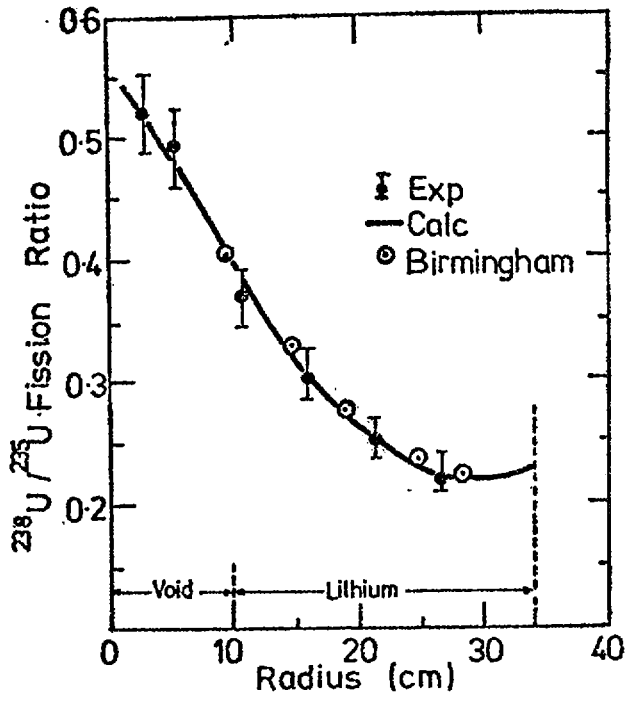

(a) Fission ratio distribution in the spherical lithium-metal assembly.

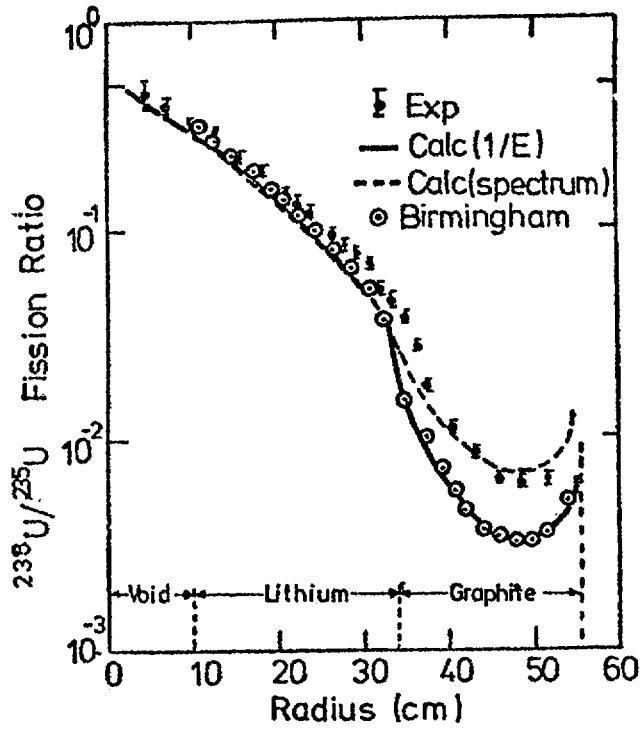

(b) Fission ratio distribution in the spherical lithium-metal assembly with a graphite reflector.

(c) Fission rate distributions of Th-232, U-238, and U-235 in the spherical lithium-metal assembly.

(d) Fission rate distributions of Th-232, U-238, and U-235 in the spherical lithium metal assembly with a graphite reflector.

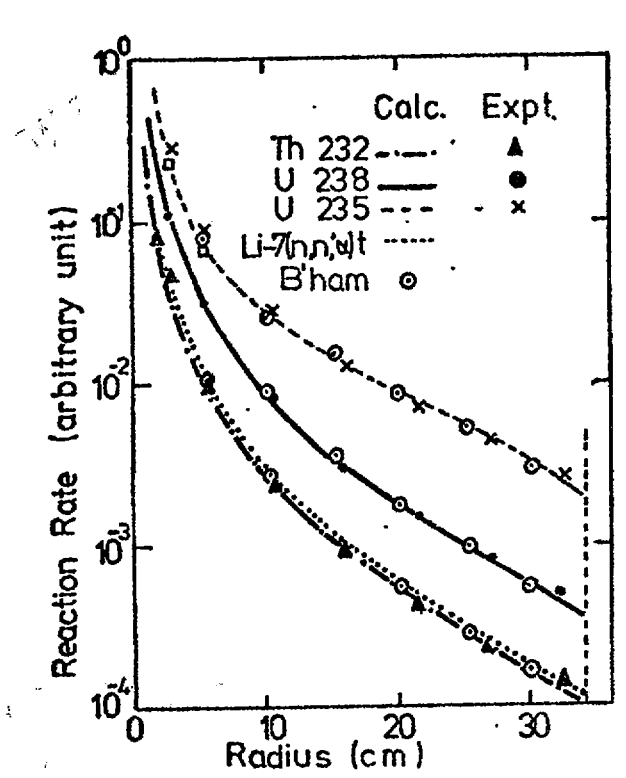

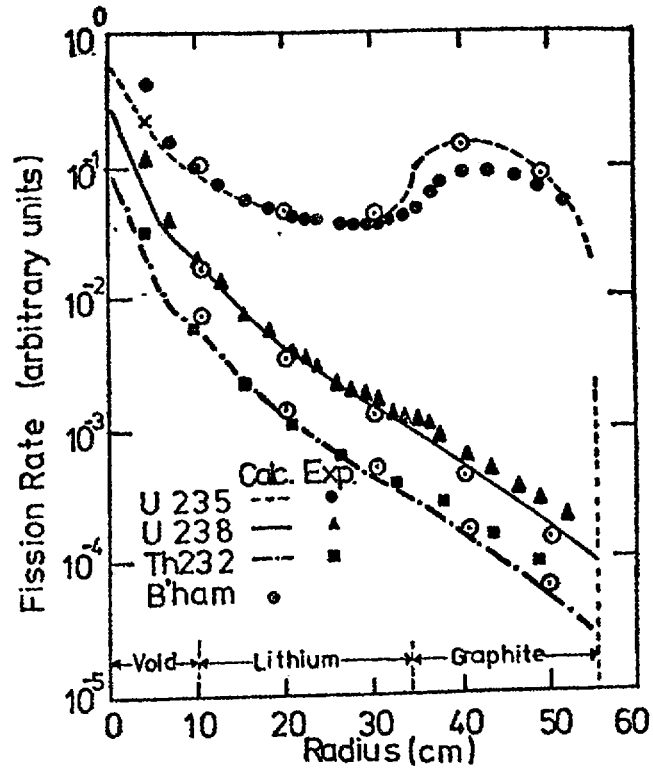

Figure 8. Comparisons of measurements and calculations of various reaction rates in the JAERI spheres. The JAERI calculations are from S8 P5 42 group ANISN calculations, and the Birmingham results are from S8 P3 100 group computations, both using ENDF/B III data.

In Figs. (c) and (d) the computed and measured reaction rates have been normalised at 15.9 cm and 15.6 cm respectively from the centre.

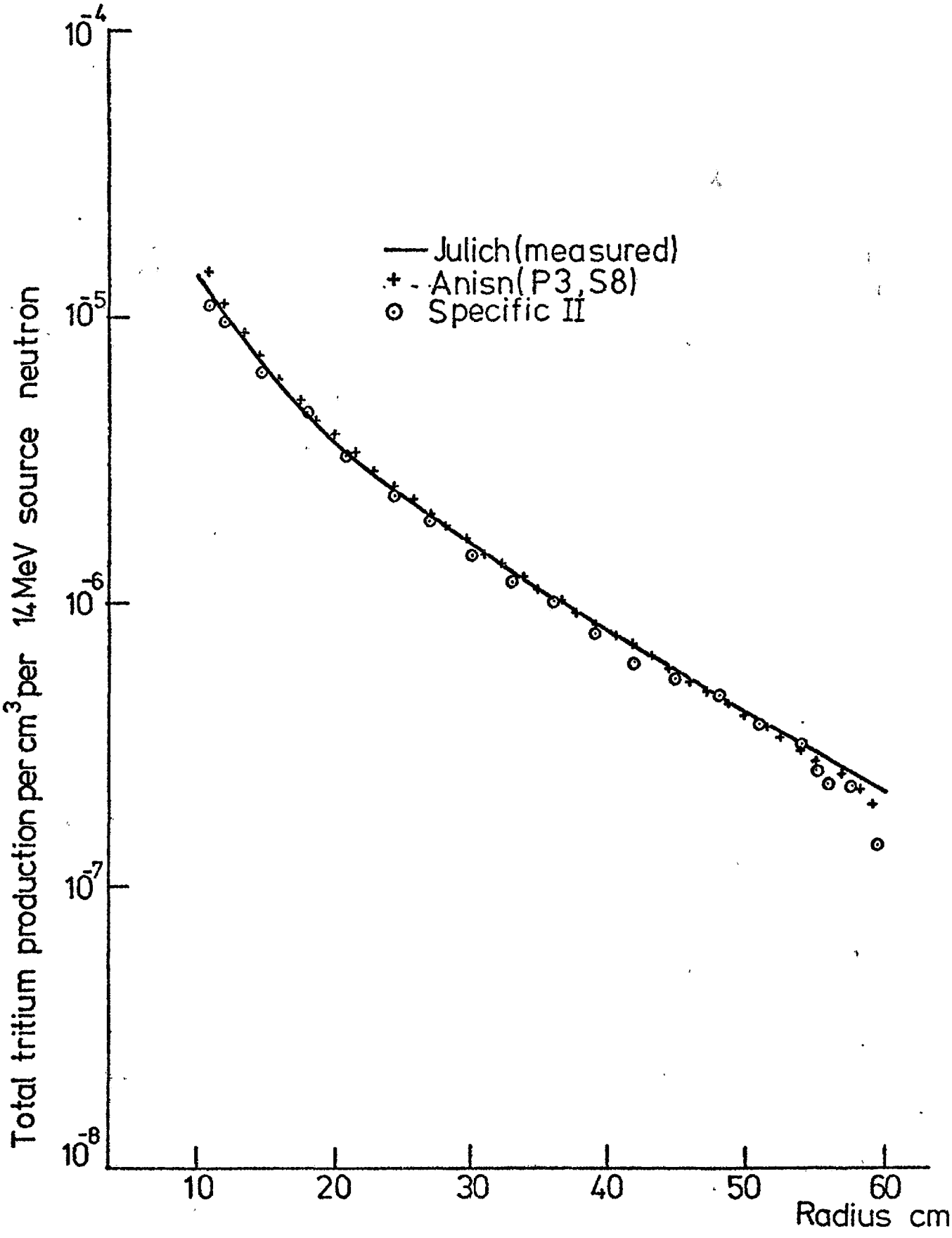

Figure 9. Comparison of the Julich tritium production measurements with Birmingham calculations.

Figure 10. Comparison of the Karsruhe measurements of the angular flux energy distribution in the radial (0 degrees) direction (Fig 10a) and the scalar flux distribution (Fig 10b) at positions inside the lithium metal sphere. The Karlsruhe calculation used the DTK code with 26 energy groups and P1 S16, and the Birmingham computation is for the ANISN code with 100 groups at P3 S8. In both cases ENDF/B III data was used.

Fig 10(a)

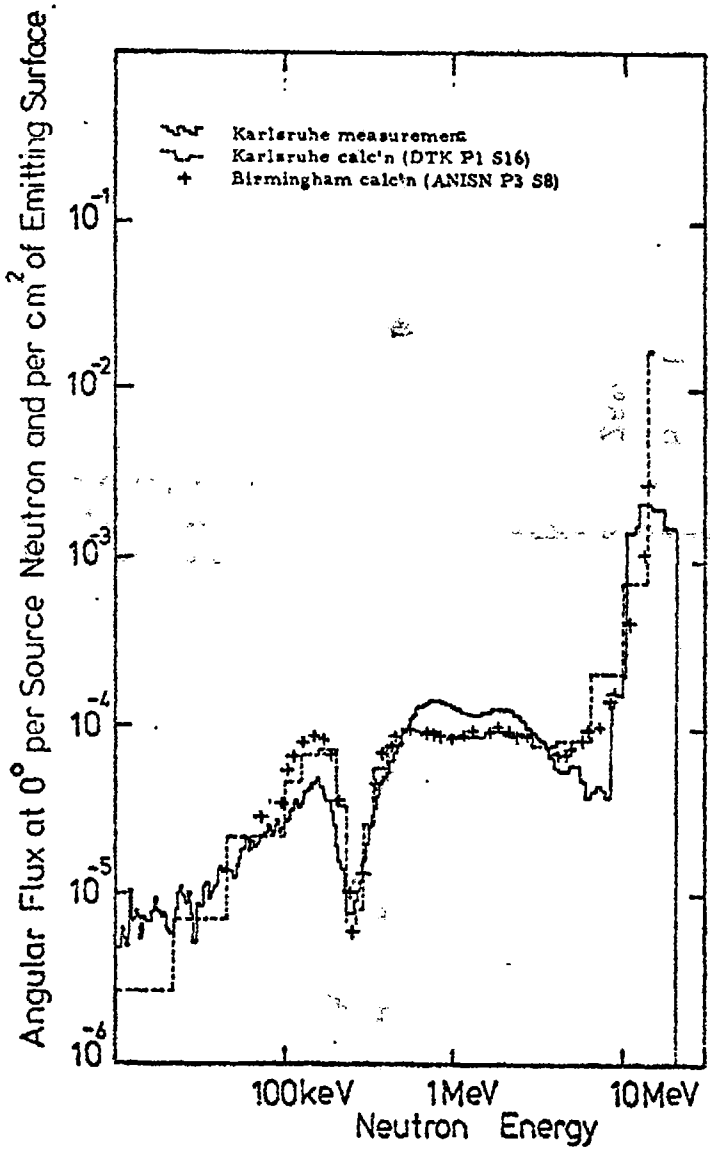

Fig 10 (b)

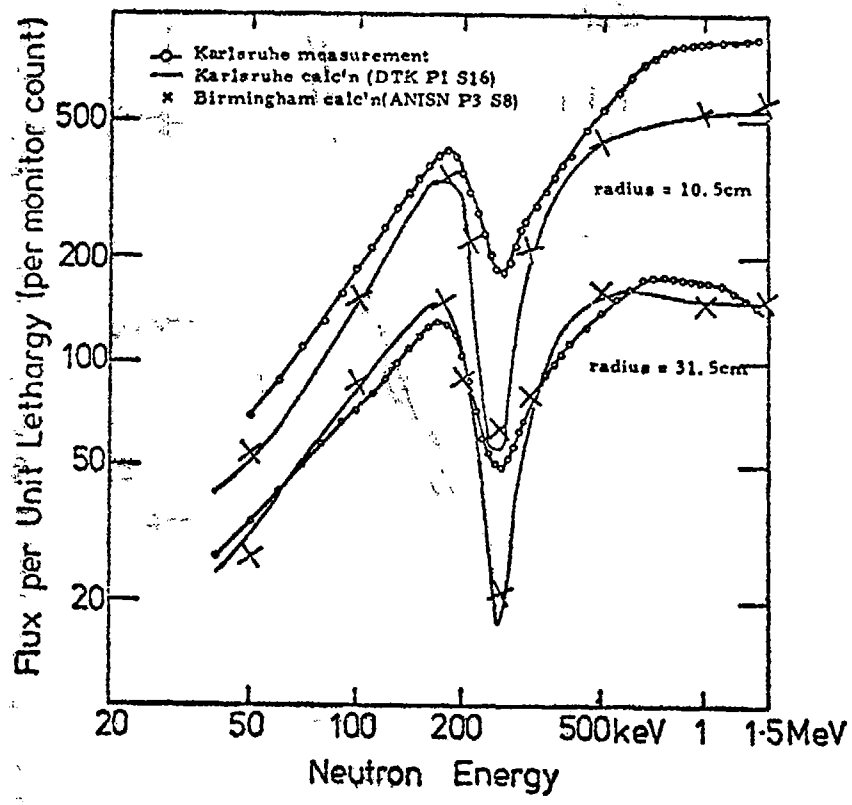

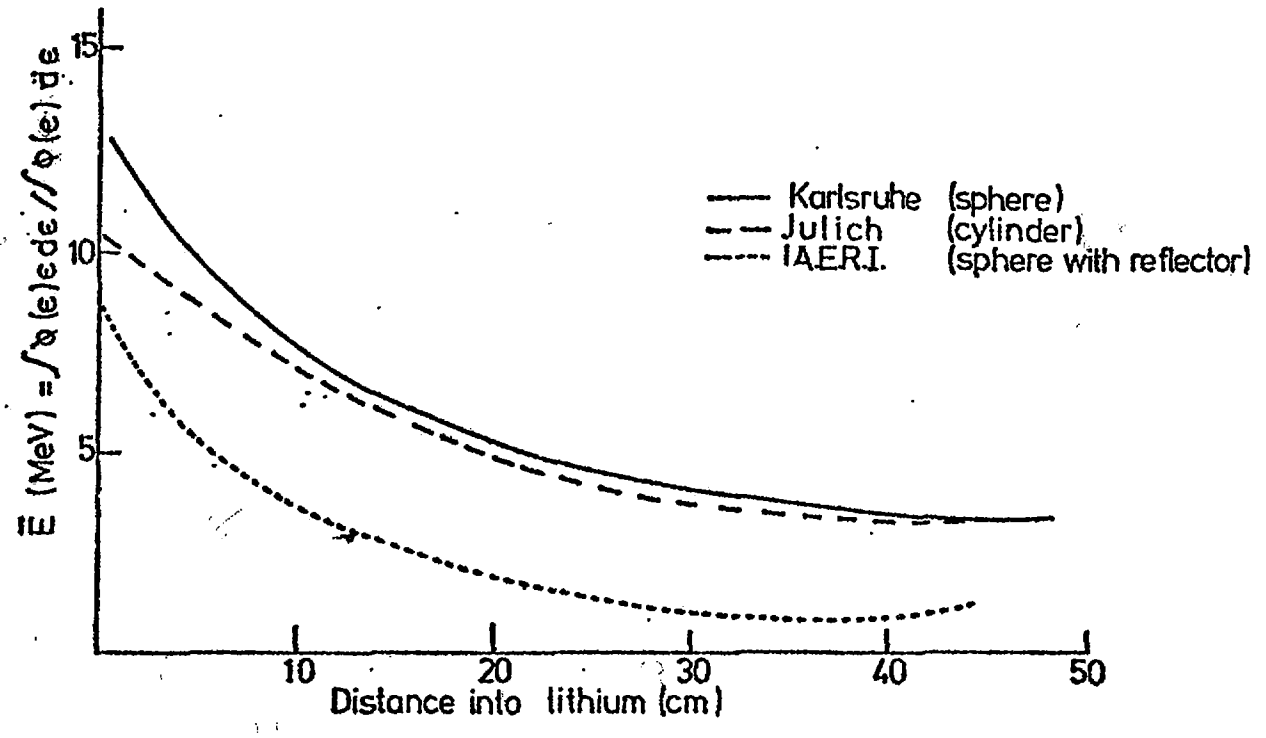

Figure 11. Spatial variation of the mean energy $\bar{E}$ in each of three integral lithium assemblies.

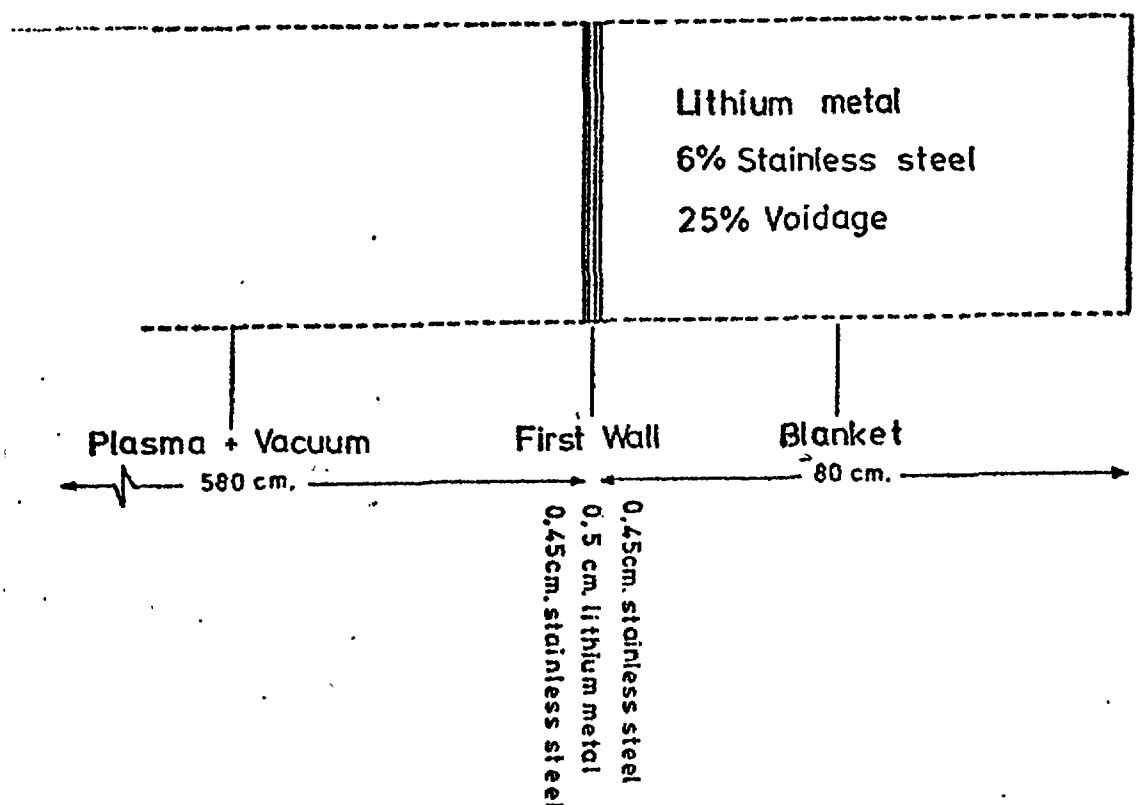

Figure 12. The Harwell-Culham conceptual design for a breeder blanket.

Figure 13. Comparisons of sensitivity profiles of breeding in ^{6}Li to the $^{6}Li(n, \alpha)T$ reaction for the Birmingham LiF experiment and a Harwell-Culham conceptual design.

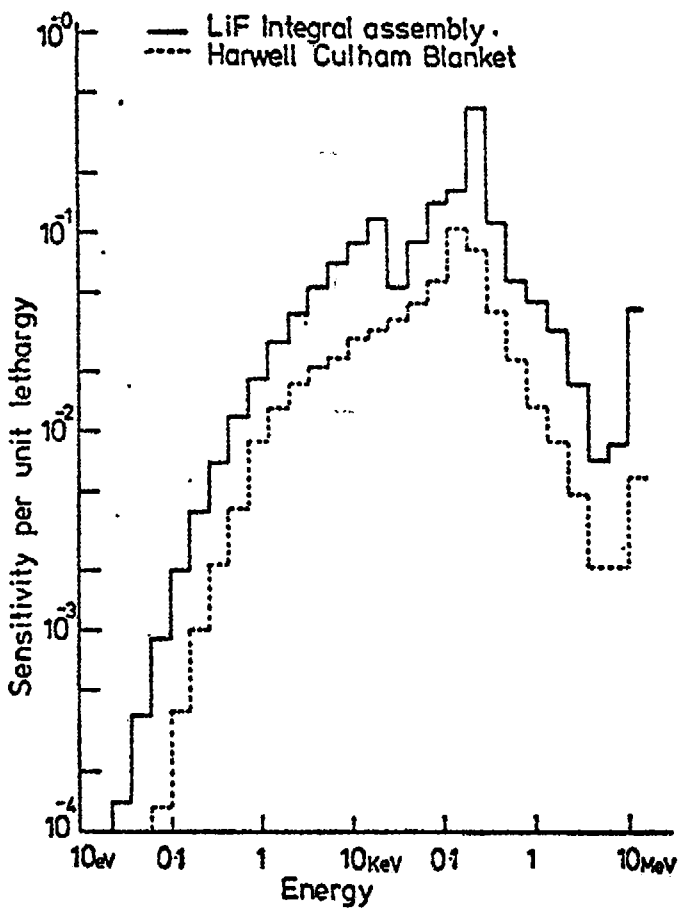

Figure 14. Sensitivity of the total tritium breeding to iron total cross sections in the HC design and in the Birmingham LiF experiment.

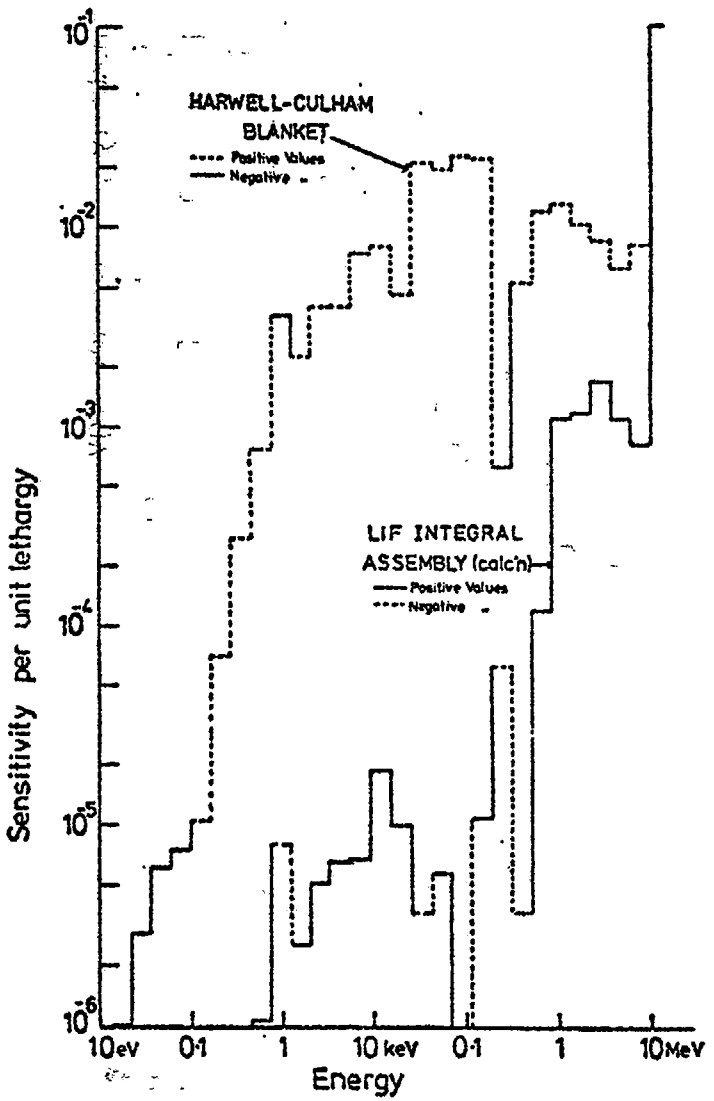

Figure 15. Sensitivity of total tritium breeding to $\bar{\mu}$ in elastic scattering in Fe in (a) the Birmingham LiF assembly and (b) the HC conceptual design.

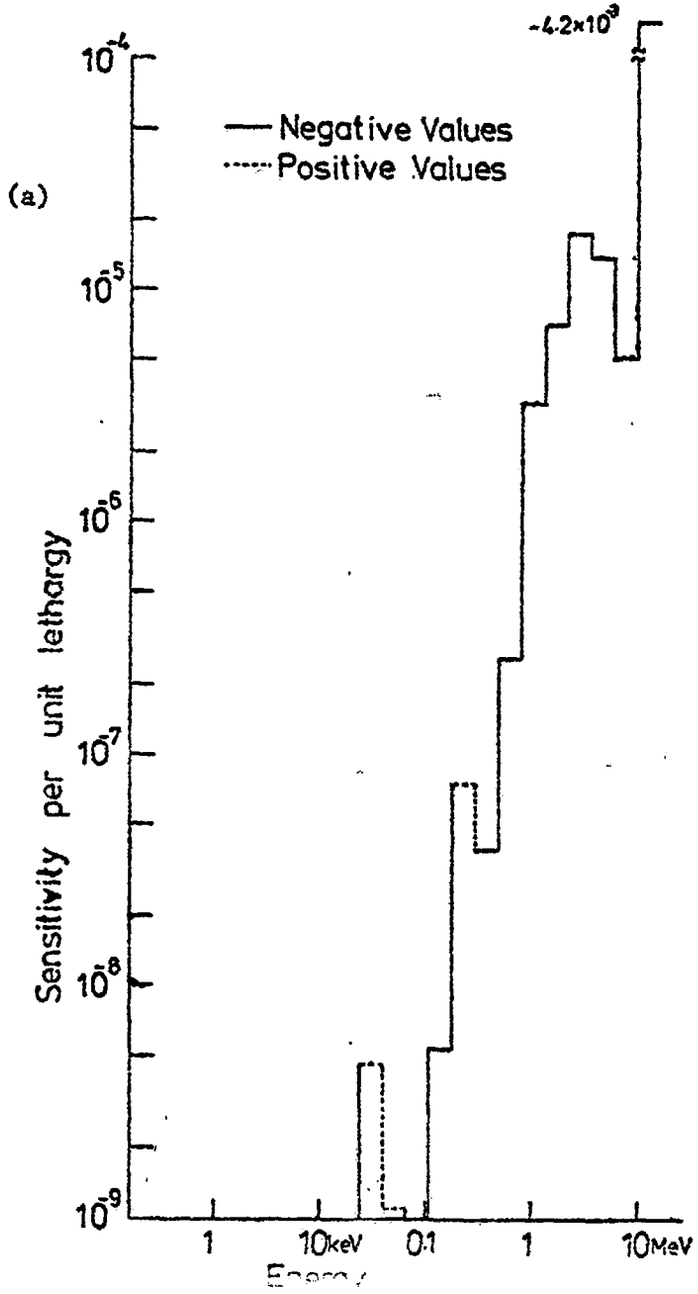

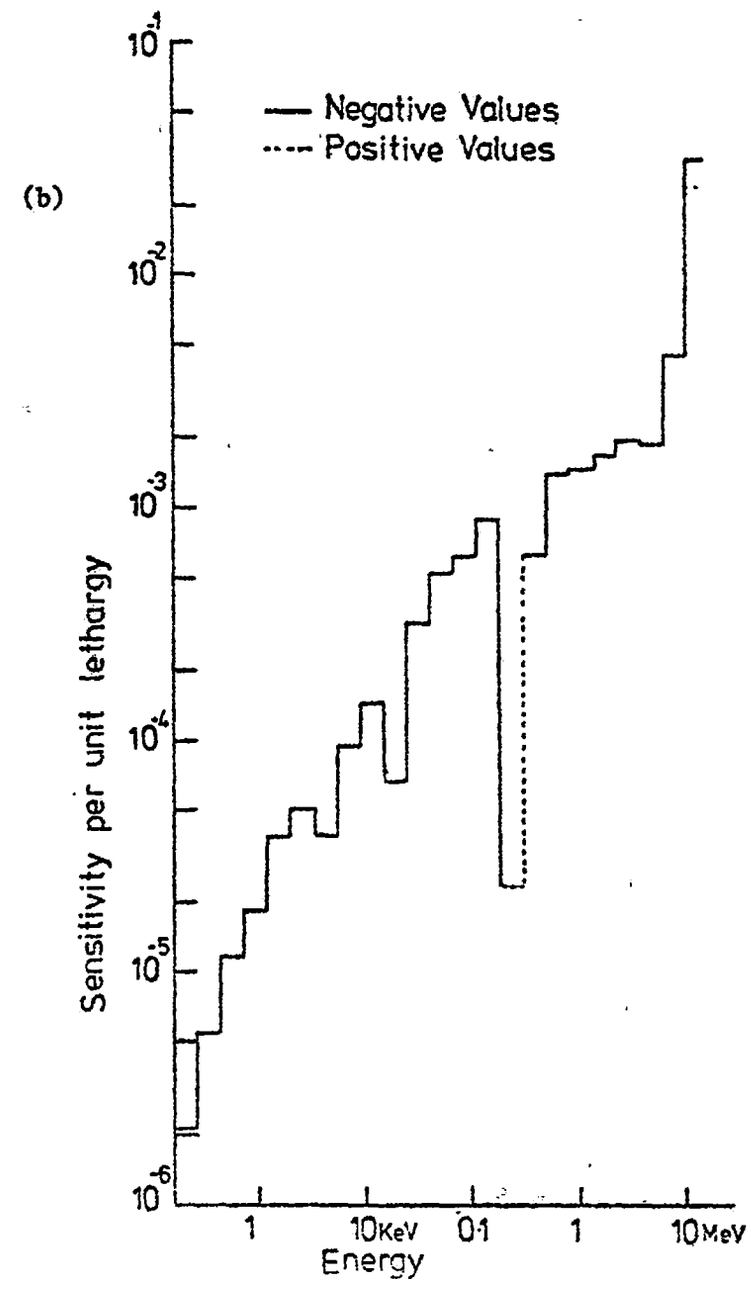

Figure 16. Sensitivity of total tritium breeding to $\bar{\mu}$ for elastic scattering in Cr in (a) the Birmingham LiF assembly and (b) the HC conceptual design.

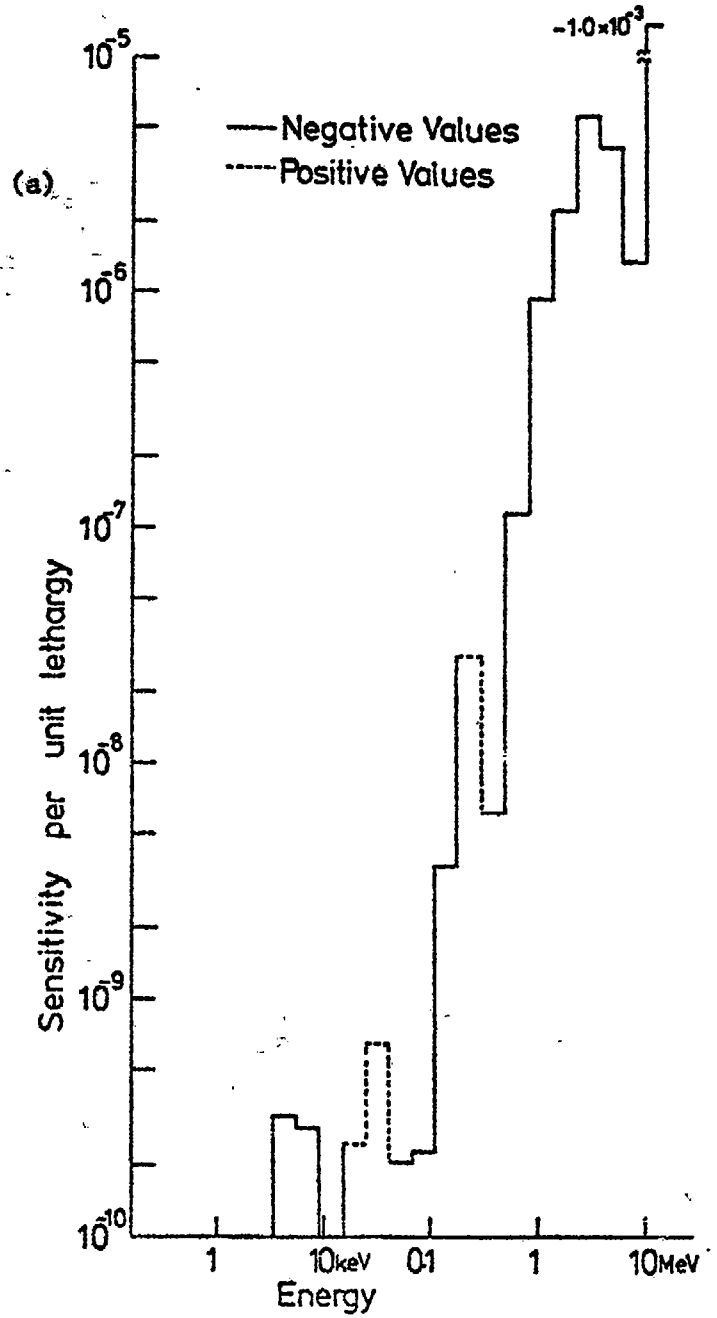

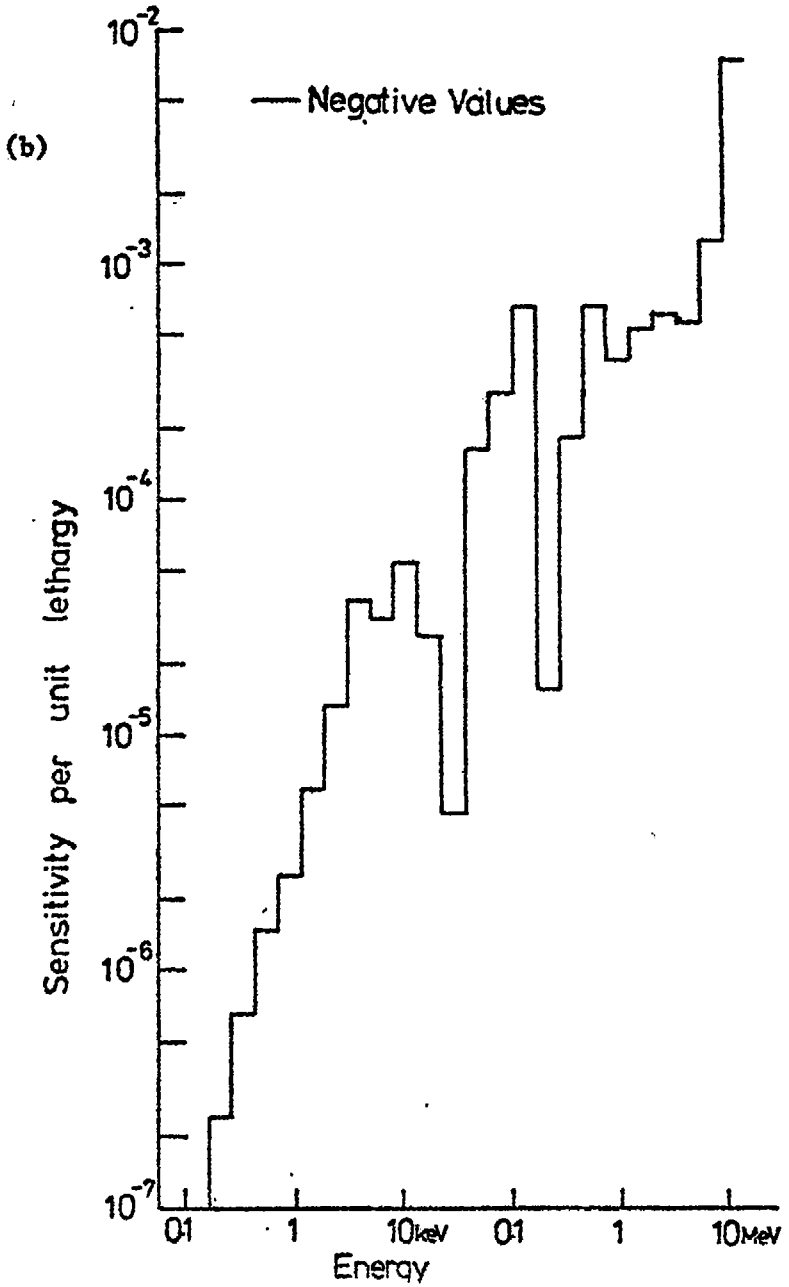

Figure 17. Sensitivity of total tritium breeding to $\bar{\mu}$ for elastic scattering in Ni in (a) the Birmingham LiF assembly and (b) the HC conceptual design.

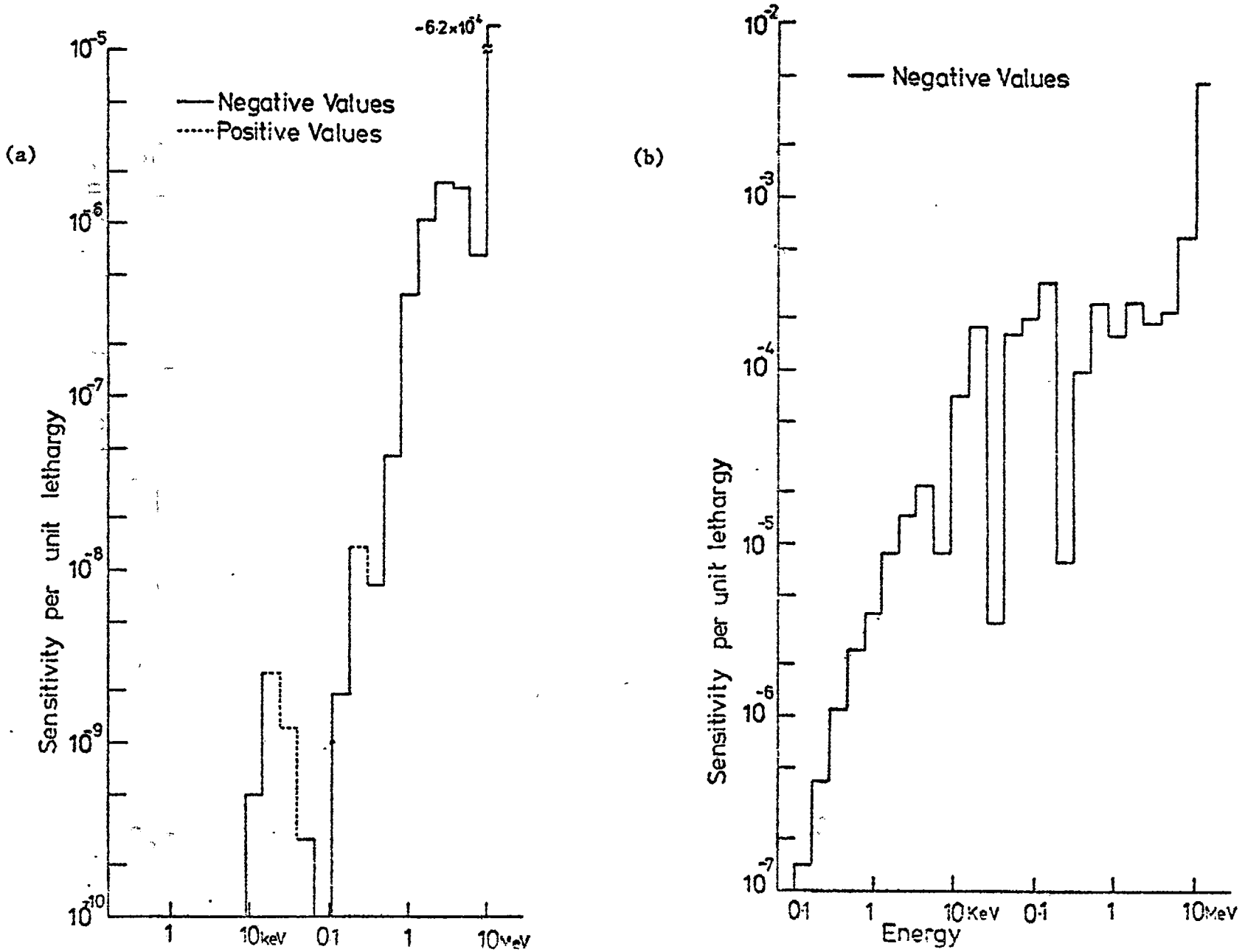

EVALUATION OF THE EFFECT OF ERRORS IN GROUP CONSTANTS ON CALCULATIONS OF NEUTRON FIELDS IN SHIELDING

T.A. Germogenova, A.P. Suvorov, V.A. Utkin
USSR

Abstract

Analytical expressions for the asymptotic neutron flux sensitivity function in an infinite homogeneous medium (plate geometry, isotopic scattering) to the neutron cross-section uncertainties were derived for the one-dimensional problem of neutron propagation in a shield. The results were compared with calculations performed by the discrete ordinate code ROZ-5.

Investigation of the sensitivity function for Fe-H_2O two-layer shields was made for the multigroup problem. Accuracy of neutron flux calculation results behind the shield was estimated.

Analysis of the sensitivity of the results of a calculation of radiation shielding to uncertainties in the nuclear data used in the calculations is a very important stage in the investigation of the requisite accuracy of measurement of nuclear constants and the correction of existing systems of constants to obtain an optimum description of macroexperiments. Such information is also useful for determining the uncertainty in the results of calculations and thus for establishing their reliability.

The object of this paper is to estimate the sensitivity of the calculated neutron flux in shielding to the uncertainty of the group cross-sections for interaction of neutrons with matter. For this we use the well known small perturbation formula of the radiation transport theory. For the functional $J = \int F(y)d(y)dy$, where $y = (r,E,\vec{\Omega})$ is a set of variables and F is the neutron flux density (see, for example, Ref. [1]), one can write the magnitude of its perturbation as

$$\delta J = -\int dr \int d\vec{\Omega} \int dE\, F^* [\delta\Sigma F - \int d\vec{\Omega}' \int dE' \delta\Sigma_s(E' \to E, \mu_s) F(r, E', \vec{\Omega}')]. \qquad (1)$$

Here $\delta\Sigma$ and $\delta\Sigma_s$ are the perturbations of the parameters of the problem and F* is the solution of the adjoint transport equation. In writing formula (1) we assumed that the sources in the direct and adjoint transport equations q and d are not perturbed. Therefore, in this paper the treatment is restricted to the case of neutron radiation, and the neutron sources (for example, their distribution in the core) are considered rigidly fixed.

It should be noted that correct use of the linear perturbation theory requires a check to be performed for each specific problem and depends on the degree of uncertainty of the constants used in the calculations.

In practice, in evaluations of systems of constants and their fitting to macroexperiments wide use is made of the concept of the function of the sensitivity of the calculated functionals to the uncertainty of the cross-sections. For the cross-section Σ_α (for example Σ or Σ_s) this function takes the form [2]

$$P_\alpha = \frac{\partial J}{\partial \Sigma_\alpha} \cdot \frac{\Sigma_\alpha}{J} . \tag{2}$$

In the case of small uncertainties of the cross-sections $\delta\Sigma_\alpha$

$$P_\alpha = \frac{\delta J_\alpha}{J} \Big/ \frac{\delta \Sigma_\alpha}{\Sigma_\alpha} , \tag{3}$$

where δJ_α is the uncertainty of the functional J due to the uncertainty of the cross-section $\delta\Sigma_\alpha$.

Let us now perform a Legendre polynomial expansion of the scattering cross-section

$$\Sigma_s(E' \to E, \mu_s) = \sum_{\ell=0}^{\infty} \frac{2\ell+1}{4\pi} \Sigma_{s,\ell}(E' \to E) P_\ell(\mu_s) \tag{4}$$

and similar expansions for the functions $F(\vec{\Omega})$ and $F^*(\vec{\Omega})$. Then with the aid of formula (1) we obtain

$$P_\Sigma = -\frac{1}{J} \int dr \int dE \int d\vec{\Omega}\, F^*(r,E,\vec{\Omega}) F(r,E,\vec{\Omega}) \Sigma(r,E) , \tag{5}$$

$$P_{\Sigma_{s\ell}} = \frac{(2\ell+1)}{J} \int dr \int dE\, F_\ell^*(r,E) \int dE' \Sigma_{s,\ell}(E' \to E) F_\ell(r,E) \tag{6}$$

In order to study the qualitative laws applicable to the problem, we first of all considered a one-velocity problem. For simplicity we took the case of a homogeneous medium with isotropic scattering in plane geometry. The solutions of the transport equation $F(x,\mu)$ and its adjoint $F^*(x,\mu)$ were

determined by the discrete ordinate method with the ROZ-5 programme in the $2D_7P_0$-approximation [1]. A homogeneous shield with a thickness of $\Sigma h = 20$ free path lengths was irradiated with an isotropic neutron beam (single power). The boundary conditions took the form

$$\left.\begin{aligned} F(0,\mu) &= I \quad \text{when} \quad \mu>0 \\ F^*(\Sigma h,\mu) &= \frac{1}{\mu} \quad \text{when} \quad \mu<0 \end{aligned}\right\} \tag{7}$$

Thus the calculated functional is the flux density $F_0(x) = 2\pi\int d\mu F(x,\mu)$ at 20 paths from the source. Table 1 shows the results of calculations of P_Σ and $P_{\Sigma_s} \equiv P_{\Sigma_{s,0}}$ performed with a special sub-program of the ROZ-5 program, which uses formulae of the type (5-6), for different values of $c = \frac{\Sigma_s}{\Sigma}$.

Table 1

Functions of the sensitivity of neutron flux density at 20 paths from the source to the uncertainty of the cross-sections

c	$F_0(\Sigma x=20)$		P_Σ		P_{Σ_s}		φ
	ROZ -5 ($\Sigma h=20$)	Asymptotic ($\Sigma h=\infty$)	ROZ -5	Asymptotic	ROZ-5	Asymptotic	
0,5	$0,18\cdot10^{-8}$	$0,28\cdot10^{-8}$	- 25,2	- 25,3	5,6	3,4	I,26
0,7	$0,37\cdot10^{-7}$	$0,58\cdot10^{-7}$	- 31,6	- 32,0	I4,7	6,6	I,56
0,9	$0,17\cdot10^{-4}$	$0,46\cdot10^{-4}$	- 53,5	- 57,9	42,8	II,2	2,7

The table also gives the results of calculation of the functions P_Σ and P_{Σ_s} with analytical formulae for the asymptotic distribution of the neutron flux density in the one-velocity problem with plane geometry for an infinite homogeneous medium with isotropic scattering. Using the expression for the asymptotic part of Green's function of the transport equation in an infinite homogeneous medium [3] for the angular neutron flux from a plane unidirectional source $\delta(\mu-\mu_0)$, one can obtain an asymptotic expression for the flux density G_0^{ac} from this source

$$G_0^{ac}(x,\mu_0) = \frac{\kappa}{\left(\frac{\Sigma_s\Sigma}{\Sigma^2-\kappa^2}-1\right)(\Sigma-\kappa\mu_0)}\, e^{-\kappa x}, \tag{8}$$

where k is a root of the equation

$$\frac{\Sigma_s}{2\kappa} \ln \frac{\Sigma+\kappa}{\Sigma-\kappa} = 1. \tag{9}$$

Assuming the above case of a problem with the boundary condition $F(o,\mu) = 1$ to be similar to the case of a surface source with angular distribution $q(\mu) = \mu$ (cf. Ref. [3]), we obtain a formula for the asymptotic value for a cosinusoidal source.

$$F_0^{ac}(x) = \int_0^1 \mu_0 G_0^{ac}(x,\mu_0)\, d\mu_0 = \frac{\frac{\Sigma}{\kappa}\ln\frac{\Sigma}{\Sigma-\kappa} - 1}{\frac{\Sigma_s \Sigma}{\Sigma^2-\kappa^2} - 1}\, e^{-\kappa x} \tag{10}$$

Taking into account that, when the functional is expressed analytically, the sensitivity function can be calculated directly from formula (2) without using the perturbation theory, we can obtain the following expressions on the basis of formula (10)

$$P_{\Sigma}^{ac}(x) = \frac{\partial F_0}{\partial \Sigma} \cdot \frac{\Sigma}{F_0} = -\frac{\kappa \Sigma \Sigma_s}{\kappa^2 - \Sigma\Sigma_a} x - \beta\,, \tag{11}$$

$$P_{\Sigma_s}^{ac}(x) = \frac{\partial F_0}{\partial \Sigma_s} \cdot \frac{\Sigma_s}{F_0} = t\kappa x + \delta,$$

where

$$\beta = \frac{2\Sigma\Sigma_s \kappa^2}{(\kappa^2 - \Sigma\Sigma_a)^2} - \frac{m\Sigma\Sigma_s}{\kappa^2 - \Sigma\Sigma_a} - 1\,; \tag{12}$$

$$\delta = t - m + \frac{2\kappa^2 - \Sigma\Sigma_s}{\kappa^2 - \Sigma\Sigma_a}\,;$$

$$t = \frac{\Sigma^2 - \kappa^2}{\Sigma\Sigma_s}\,;\quad m = \frac{\kappa(\Sigma+\kappa)}{\Sigma\Sigma_s\left(\frac{\Sigma}{\kappa}\ln\frac{\Sigma}{\Sigma-\kappa} - 1\right)}\,;\quad \Sigma_a = \Sigma - \Sigma_s\,.$$

Analysis of the data in Table 1 and the above formulae reveals the operation of the following laws:

1. The sensitivity of the neutron flux to a variation in the total cross-section is negative, i.e. an increase in Σ leads to a reduction in the flux density F_0. A variation in the scattering cross-section Σ_s has the opposite effect, i.e. $\frac{\partial F}{\partial \Sigma_s} > 0$.

2. The sensitivity of the flux to a variation in the cross-sections increasesmonotonically with the distance from the source. It is interesting that at a distance of one free path length away each one per cent variation in Σ results in F_0 changing by more than 1% in the cases considered. The dependence on $\delta\Sigma_s$ is somewhat weaker.

3. Despite the difference in geometry (bounded and infinite media) the results of the calculations of P_Σ using the asymptotic theory proved quite similar to the results of the numerical calculations, whereas the calculations of $P\Sigma_s$ differed appreciably (by up to several factors). This is explained by the marked effect of leakage on the neutron field in bounded, weakly absorbing (and weakly moderating) media. Table 1 also gives the values of the leakage factor φ - the ratio of the flux in infinite and bounded ($\Sigma h = 20$) media at a distance of $\Sigma x = 20$, obtained by comparing the results of calculations (for a plane unidirectional source) in a bounded ($\Sigma h = 20$) and a practically semi-infinite ($\Sigma h = 30$) medium, performed with the ROZ-5 program, and the results of calculations for an infinite medium performed in Ref. [4]. As can be seen, the effect of radiation leakage from the medium depends greatly on the degree of "transparency" of the medium $C = \frac{\Sigma_s}{\Sigma}$. Allowance for the leakage in accordance with formula (12) must increase the values of $P\Sigma_s$ (in particular on account of the reduction in F_0). If the values of the factor φ from Table 1 are used, it can be roughly estimated that an asymptotic treatment will lead to results for $P\Sigma_s$ about 30% too low compared with the numerical results in the same geometry, which is quite acceptable for estimations.

Thus the analytical results obtained satisfactorily describe the qualitative laws to which the problem conforms - the dependence on the variation of Σ and Σ_s and on the distance from the source. Generalization to the case of anisotropic scattering is quite clear.

In view of the laboriousness of the numerical calculations, it is worth noting the usefulness of analytical treatments of the sensitivity functions by which the main features of the behaviour of these functions

can be established, if only in simple geometries. It should be possible to generalize analytical treatments, including those involving the use of semi-empirical methods, to the case of more complex geometry. For this it is necessary to express clearly the relations of the macroparameters used in these methods and those of the neutron constants contained in the transport equation. An example of such a relation is that of the removal cross-section with the nuclear constants [1], which is obtained by applying the perturbation theory:

$$\delta_{rem}=\frac{\int dE\,\delta(E)\int d\vec{\Omega}\,F^{*}F-\int dE\int d\vec{\Omega}\,F^{*}(x,E,\vec{\Omega})\int dE'\int d\vec{\Omega}'\,\delta_{s}(E'\to E,\mu_{s})\,F(x,E',\vec{\Omega}')}{\int dE\int d\vec{\Omega}\,F^{*}F} \tag{13}$$

The data obtained by means of the sensitivity functions provide a means of estimating the error in the calculated neutron flux density. From formula (3) it can be established that the (relative) uncertainty of the functional due to the uncertainty Σ is equal to

$$\frac{\delta J_{\Sigma}}{J}=P_{\Sigma}\cdot\frac{\delta\Sigma}{\Sigma}\,, \tag{14}$$

and the uncertainty due to $\delta\Sigma_s$ is equal to

$$\frac{\delta J_{\Sigma_s}}{J}=P_{\Sigma_s}\cdot\frac{\delta\Sigma_s}{\Sigma_s}\,. \tag{14a}$$

On the basis of the law of summation of independent random errors, the total uncertainty of the functional can be estimated as follows:

$$\frac{\delta J}{J}\simeq\sqrt{P_{\Sigma}^{2}\cdot\left(\frac{\delta\Sigma}{\Sigma}\right)^{2}+P_{\Sigma_s}^{2}\cdot\left(\frac{\delta\Sigma_s}{\Sigma_s}\right)^{2}} \tag{15}$$

Taking the uncertainty Σ equal to 2%, and Σ_s equal to 5%, we can estimate from the data in Table 1 that at 20 paths from the source $\frac{\delta J}{J}\simeq 0.6$ when $c = 0.5$, $\frac{\delta J}{J}\simeq 0.9$ when $c = 0.7$ and $\frac{\delta J}{J}\simeq 2.4$ when $c = 0.9$.

Analysis of the sensitivity in multigroup problems is more complex. In the group approach expressions (5-6) are converted to the following form (i, j are the numbers of the energy groups)

$$P_{\Sigma^{i}}=-\frac{\int d\tau\int d\vec{\Omega}\,F^{*i}(\tau,\vec{\Omega})F^{i}(\tau,\vec{\Omega})\Sigma^{i}(\tau)}{\int d\tau\int d\vec{\Omega}\sum_{i}F^{i}(\tau,\vec{\Omega})\alpha^{i}(\tau,\vec{\Omega})}\,, \tag{16}$$

$$P_{\Sigma_s^{i\to j}} = \frac{\int d\tau\, F_0^{*j}(\tau)\, F_0^{i}(\tau)\, \Sigma_s^{i\to j}(\tau)}{\int d\tau \int d\vec{\Omega} \sum_i F^i(\tau,\vec{\Omega}) d^i(\tau,\vec{\Omega})} . \qquad (17)$$

(Integration over the spatial variable in the numerators of these formulae is performed for that part of the shielding where the material in question is located.)

For simplicity we shall not enter here into an analysis of the effect of the uncertainty of the neutron scattering anisotropy parameters, although this is a very important factor in radiation transport. The aim of this paper is simply to make an approximate estimate of the sensitivity and the error of the calculations.

On the example of the five-group problem, calculations based on expressions (16-17) were performed for plane one-dimensional shielding. We considered the transmission of fast neutrons with energy $E > 1.4$ MeV in a two-layer iron-water shield irradiated with a wide isotropic beam of fast neutrons from the spectrum of a water-cooled, water-moderated reactor. The thickness of the layer of water behind the iron shield was 30 cm in all cases. The thickness of the layer of iron varied from 10 to 100 cm. The calculated functional was the total fast neutron flux ($E > 1.4$ MeV) behind the shield. Solution of the direct and adjoint transport equations was performed in the $2D_5P_7$-approximation using the ROZ-5 program. For this purpose the group constants for iron and water given in Ref. [1] were employed. These constants are a refinement of the system of constants supplied in Ref. [5] with the addition of a group of neutrons with $E > 10.5$ MeV and data on scattering anisotropy [6]. The use of these constants was given experimental validity by an evaluation of experiments on the transmission of fast neutrons from a plane unidirectional source through shielding [1].

The functions of the sensitivity of a fast neutron flux behind a shield to the uncertainty of the iron nuclei cross-sections were calculated. The results of the calculations are given in Table 2 where, to simplify the estimations, the relative uncertainties of the elastic and inelastic scattering cross-sections were assumed to be identical. The function of the sensitivity to the total neutron scattering cross-section of each group can then be written

$$P_{\Sigma_s^i} = \sum_j P_{\Sigma_s^{i\to s}} \qquad (18)$$

As can be seen from Table 2, the sensitivity $P_{\Sigma}i$ and $P_{\Sigma_s}i$ increases with the thickness of the shielding and correspondingly with the attenuation of the neutron flux. It is characteristic that, as in the one-velocity problem, $P_{\Sigma}i < 0$ and $P_{\Sigma_s}i > 0$ for all groups, in which case $P_{\Sigma_s}i < |P_{\Sigma}i|$.

Table 2 also includes data on the neutron spectrum behind shields of different thickness. There is a definite correlation between the neutron spectrum and the sensitivity of the fast neutron flux to the cross-sections of different energy groups. In the example considered the neutron spectrum softens considerably when the thickness of the shielding is increased, i.e. there is an increase in the fraction of neutrons of lower groups. The total fast neutron flux is in fact most sensitive to a variation in the cross-sections of neutrons in the lower groups. For attenuations of $\sim 10^3$ characteristic of shielding located within the vessel of water-cooled, water-moderated reactors (thermal and radiation shielding of the vessel) the most significant uncertainty from the point of view of the effect on the fast neutron flux is that of the iron nuclei cross-sections in the 1-6 MeV neutron energy range.

On the basis of the data in Table 2 it can also be assumed that in the case of iron-water shields with a small water content (less than 20-30%) giving attenuations of $\sim 10^7$-10^8 (characteristic of the shielding of plant unattended during reactor operation) the uncertainty in the 1-4 MeV energy range has the greatest effect on the fast neutron flux in the iron nuclei cross-sections.

It is of interest to estimate the error in the sensitivity functions obtained. A number of direct calculations of the variation of the functional with variation of the cross-sections and comparison with calculations performed with expression (1) for the shields in question showed that the error in δJ and P increases with the thickness of the shield and can be quite high. It should be noted that calculations based on the theory of small perturbations give too high values for δJ and P. Variations of Σ of less than 3-5% and of Σ_s of less than 7-10% for the shielding investigated lead to an error in expression (1) of not more than 40-50%.

The results of calculations of the sensitivity functions shown in Table 2 can be used for estimating the uncertainty of the calculated fast neutron flux behind the iron-water shielding considered. If one neglects the correlation of the uncertainties of the cross-sections with each other and assumes the relative uncertainty of the total iron nuclei cross-sections

Table 2

Functions of the sensitivity P_{Σ}^{i} and $P_{\Sigma_s}^{i}$ of the fast neutron flux density behind an iron-water shield to the uncertainty in the iron nuclei cross-sections and the neutron spectrum behind the shield F^i/F

ΔE_i, MeV	h_{Fe}, cm	10	20	40	60	80	100
10,5–14	$-P_{\Sigma}^{1}$	0,04	0,07	0,15	0,21	0,27	0,32
6,5–10,5	$-P_{\Sigma}^{2}$	0,65	1,30	2,63	3,80	4,68	5,26
4 – 6,5	$-P_{\Sigma}^{3}$	1,63	2,73	3,87	4,13	3,99	3,72
2,5–4	$-P_{\Sigma}^{4}$	1,19	2,47	5,02	7,27	9,08	10,4
1,4–2,5	$-P_{\Sigma}^{5}$	0,49	1,37	4,19	8,40	13,9	20,3
10,5–14	$P_{\Sigma_s}^{1}$	0,01	0,02	0,03	0,03	0,04	0,05
6,5–10,5	$P_{\Sigma_s}^{2}$	0,18	0 34	0,64	0,89	1,09	1,20
4 – 6,5	$P_{\Sigma_s}^{3}$	0,52	0,86	1,22	1,34	1,34	1,30
2,5 – 4	$P_{\Sigma_s}^{4}$	0,51	1,08	2,21	3,23	4,07	4,71
1,4–2,5	$P_{\Sigma_s}^{5}$	0,27	0,76	2,31	4,60	7,56	11,0
10,5–14	F^1/F, %	0,4	0,4	0,4	0,3	0,3	0,2
6,5–10,5	F^2/F, %	5,4	5,4	5,2	4,7	4,1	3,5
4 – 6,5	F^3/F, %	19,8	17,4	13,2	10	7,6	5,9
2,5 – 4	F^4/F, %	29,2	27,4	23,2	19	15	11,8
1,4–2,5	F^5/F, %	45,2	49,4	58	66	73	78,6
Attenuation of flux by shielding		$5\cdot10^2$	$2,7\cdot10^3$	$8,8\cdot10^4$	$2,3\cdot10^6$	$6,2\cdot10^7$	$1,6\cdot10^9$

to be identical for all groups (in which case the sensitivies to the cross-sections of different groups can simply be added) and equal to 3%, and that of the scattering cross-sections to be identical and equal to 10%, one obtains, on the basis of expression (15), an uncertainty for the fast neutron flux behind the shielding of $\delta J/J \simeq 0.19$ for $h_{Fe} = 10$ cm, $\delta J/J \simeq 0.4$ for $h_{Fe} = 20$ cm, $\delta J/J \simeq 0.8$ for $h_{Fe} = 40$ cm, $\delta J/J \simeq 1.2$ for $h_{Fe} = 60$ cm, $\delta J/J \simeq 1.8$ for $h_{Fe} = 80$ cm, and $\delta J/J \simeq 2.2$ for $h_{Fe} = 100$ cm.

The results obtained for the uncertainty of the calculated neutron flux have an estimative character because several factors are not allowed for, namely the uncertainty in the scattering anisotropy parameters, the correlations of the uncertainties of the cross-sections, the approximate nature of the theory of small perturbations, and the uncertainty in the cross-sections of oxygen and hydrogen nuclei. Therefore it is still too early to draw a final conclusion about the degree of uncertainty of the calculated functional, let alone formulate requirements for cross-sections. None the less the results obtained enable us to draw certain conclusions, in particular, regarding the dependence of the sensitivity to the cross-sections of different groups on shielding thickness.

To formulate requirements for the accuracy of cross-sections, it is necessary to perform an analysis of sensitivity for a number of specific compositions of reactor shielding. Since the complexity of real geometry makes it difficult to perform such an analysis, it is important to study the laws involved and to gain experience of analysing the sensitivity problem in simple geometries.

REFERENCES

[1] GERMOGENOVA, T.A., DEGTYAREV, S.F., ORLOV, V.V., SUVOROV, A.P., TIKHONOV, V.K., TSYPIN, S.G., Perenos bystriykh nejtronov v ploskikh zashchitakh (Fast neutron transport in plane shielding), Moscow, Atomizdat (1971).

[2] GERSTL, S.A.W., Sensitivity analysis in shielding - an overview, Trans. ANS, Vol. 22 (1975) 791.

[3] CASE, K.M., ZWEIFEL, P.F., Linear transport theory. Addison-Wesley Series in Nuclear Engineering, 1967.

[4] BEACH, L.A., SHAPIRO, P., O'ROURKE, R.C., FAUST, W.R., LEPSON, B., Solutions of the constant velocity transport problem, Nucl. Sci. Eng., Vol. 6 (1959) 66.

[5] ABAGYAN, L.P., BAZAZYANTS, N.O., BONDARENKO, I.I., NIKOLAEV, M.N., Gruppovye konstanty dlya rascheta yadernykh reaktorov (Group constants for the design of nuclear reactors), Moscow, Atomizdat (1964).

[6] GOLDBERG, M.D., MAY, V.M., STEHN, J.P., Angular distributions in neutron-induced reactors, Report BNL-400 (1962).

List of Participants

AUSTRIA	G. Kamelander Institut für Reaktorsicherheit Sobieskigasse 21/III A-1090 Wien
BELGIUM	G. Minsart C.E.N/S.C.K- Boeretang 200 B-2400 Mol
GERMANY, Fed. Rep.	J. Koban Kraftwerkunion Hammerbacher Str. 12-14 8520 Erlangen
	G. Hehn Institut für Kernenergetik der Universität Stuttgart Pfaffenwaldring 31 7000 Stuttgart 80
	A. Scholz Hochtemperatur-Reaktorbau GmbH Gottlieb-Daimler-Strasse 8 D-6800 Mannheim 1
	M. Spicka BBR-Reaktor-GmbH 6800 Mannheim Heppenheimer Str. 27-29
	M. Mattes Institut für Kernergetik der Universität Stuttgart Pfaffenwaldring 31 7000 Stuttgart 80
FRANCE	C. Devillers DRE/SERMA -Centre d'études nucléaires de Saclay B.P. No. 2 91190 Gif-sur-Yvette
	J. P. Trapp DRE/SERMA - Centre d'études nucléaires de Cadar B.P. No. 1 13115 Saint Paul lez Durance
	J. Moreau Département des Réacteurs à Neutrons Rapides C.E.N. Cadarache, B.P. No. 1 13115 Saint Paul lez Durance

List of Participants (contd)

FRANCE	A. Khairallah DRE/SPNR - Centre d'études nucléaires de Cadarache B.P. No. 1 13115 Saint Paul lez Durance
	R. Pannetier Centre d'études de Limeil B.P. No. 27 F-94190-Villeneuve St. Georges
ISRAEL	A. Dubi Ben Gurion University of the Negev Faculty of Natural Sciences Dept. of Physics P.O. Box 653, Beersheva 84120
ITALY	U. Farinelli RIT-CNEN, CSN Casaccia 0060 Rome, Santa Maria Di Galeria
	M. Martini RIT-CNEN, CSN Casaccia 0060 Rome, Santa Maria Di Galeria
	M. Salvatores RIT/FIS-CSN Casaccia 0060 Rome, Santa Maria Di Galeria
	A. Boioli N.I.R.A. c/o. DRNR/ISEDC C.E.N. Cadarache, B.B. No. 1 13115 Saint Paul lez Durance France
JAPAN	S. An Department of Nuclear Engineering Faculty of Engineering University of Tokyo, 3-1 Hongo 7-Chome Bunkyo-ku, Tokyo
	S. Miyasaka Japan Atomic Energy Research Institute Tokai-mura, Ibaraki-Ken
SPAIN	A. Rovira Junta de Energia Nuclear Unidad Operativa de Teoria y Calculo de Reactors, Avda. Complutense Madrid-3
SWEDEN	T. Lefvert Research Institute of National Defence FOA 212, Fack, 10450 Stockholm 80

List of Participants (contd.)

SWITZERLAND	V. Herrmberger Institut fédéral de recherches en matière de réacteurs 5303 Würenlingen
USSR	M. Ja. Kulakovski Institute of Physics and Power Engineering Obninsk Kaluzskaja Region
	A. P. Suvorov Insitute of Physics and Power Engineering Obninsk Kaluzskaja Region
UNITED KINGDOM	J. Butler UKAEA Radiation Physics & Shielding Group AEE, Winfrith, Dorchester Dorset DT2 8DH
	T. D. Beynon Department of Physics University of Birmingham Birmingham B15 2TT
	A. K. McCracken UKAEA, AEE Winfrith, Dorchester Dorset, DT2 8DH
	A. F. Avery UKAEA, AEE Winfrith, Dorchester Dorset DT2 8DH
	B. H. Patrick Nuclear Physics Division, B-418 A.E.R.E. Harwell
UNITED STATES OF AMERICA	D. J. Dudziak Theoretical Division, P.O. Box 1663, MS-269 Los Alamos Scientific Laboratory New Mexico 87545
	F. C. J. Perey Neutron Physics Division Oak Ridge National Laboratory Tennessee 37830
	E. M. Oblow Oak Ridge National Laboratory Tennessee 37830

List of Participants (contd.)

CEC	H. Rief C.C.R. EURATOM Ispra, Varese, Italy
	U. Canali C.C.R. EURATOM Ispra, Varese, Italy
	R. Nicks C.C.R. EURATOM, Ispra, Varese, Italy
OECD/NEA	N. A. Tubbs OECD Nuclear Energy Agency 38, boulevard Suchet F-75016 Paris
	L. Edvardson OECD Nuclear Energy Agency CCDN, BP 9 (Bât. 45) 91190 Gif-sur-Yvette (F)
	J. Guasp OECD Nuclear Energy Agency CCDN, BP 9 (Bât. 45) F-91190 Gif-sur-Yvette
IAEA	J. Rátøj CZE/7502, IAEA Fellow at the University of Stuttgart
	J. A. Larrimore Division of Nuclear Power & Reactors
	R. Lessler Division of Research & Laboratories Nuclear Data Section
	I. Neamu Division of Nuclear Power & Reactors
	J. Schmidt Division of Research and Laboratories Nuclear Data Section
OBSERVERS	N. McDonald Permanent Mission of Australia to the IAEA Mattiellistrasse 2-4/III A-1040 Vienna
OBSERVERS (IAEA)	M. Vlasov K. Okamoto A. Lorenz H. Lemmel O. Schwerer P. Smith
	Mrs. P. Attree G. Lammer F. Hirschbichler